eCAM
Evidence-Based Complementary and Alternative Medicine

Translational Research in Complementary and Alternative Medicine

Guest Editors: Wei Jia, Martin Kohlmeier, Aiping Lu, and Rong Zeng

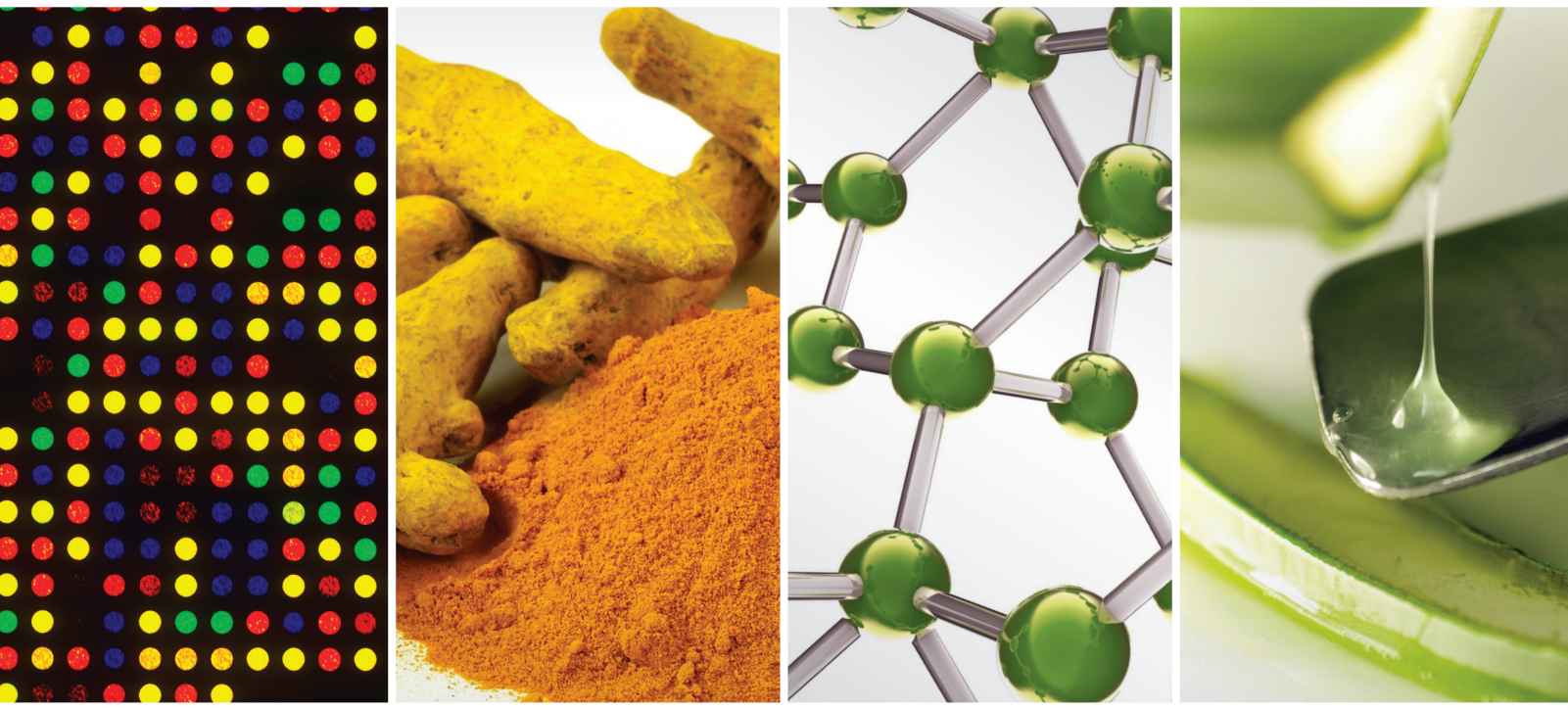

Translational Research in Complementary and Alternative Medicine

Evidence-Based Complementary and Alternative Medicine

Translational Research in Complementary and Alternative Medicine

Guest Editors: Wei Jia, Martin Kohlmeier, Aiping Lu, and Rong Zeng

Editorial Board

Contents

Hindawi Publishing Corporation
Evidence-Based Complementary and Alternative Medicine
Volume 2013, Article ID 296817, 2 pages
http://dx.doi.org/10.1155/2013/296817

Editorial

Translational Research in Complementary and Alternative Medicine

Wei Jia,[1] Martin Kohlmeier,[2] Aiping Lu,[3] and Rong Zeng[4]

[1] *Cancer Epidemiology, University of Hawaii Cancer Center, Honolulu, HI 96813, USA*
[2] *UNC Nutrition Research Institute, University of North Carolina Schools of Medicine and Public Health, North Carolina Research Campus, Kannapolis, NC 28081, USA*
[3] *School of Chinese Medicine, Hong Kong Baptist University, Kowloon Tong, Hong Kong*
[4] *Institute of Biochemistry and Cell Biology, Shanghai Institutes for Biological Sciences, Chinese Academy of Sciences, 320 Yue Yang Road, Shanghai 200031, China*

Correspondence should be addressed to Wei Jia; wjia@cc.hawaii.edu

Received 22 August 2013; Accepted 22 August 2013

Due to the compartmentalization within scientific disciplines and the fact that modern scientific methods are extensively used in CAM research, it appears that there has been a huge disconnect between clinical studies and preclinical studies including authentication, quality control, pharmacology, and toxicology of CAM agents. In this special issue, we would like to promote a concept of "translation" in CAM research by bringing a cluster of translational work (25 papers) that utilized multidisciplinary teams and approaches towards a clear clinical goal.

One of the highlights in this special issue is that there are a number of articles describing or summarizing novel approaches that may address bottleneck issues in CAM research. K. Lan et al. propose a novel strategy to determine the pharmacokinetics of multicomponent pharmaceuticals, termed as polypharmacokinetics, where the dynamic concentration profile of bioavailable xenobiotics and metabolic response profile in animals are integrated. The application of this strategy may lead to the direct elucidation of the pharmacological and molecular mechanisms of the multicomponent herbal medicines. L. Wang et al. propose an expert consensus approach that can be applied in the clinical treatment of complex diseases using traditional Chinese medicine (TCM). In their study, a group of clinical experts were consulted three times with the use of TCMs to treat hypertension, which enables investigators to take advantage of both research and clinical experience of the experts while using a standard "typical symptoms" instead of classical pattern differentiation methods. To the same goal but with differ rent approaches, J. Dai et al. introduce a macro-micro approach that combines pattern differentiation, clinical indicators, and metabolite markers to diagnose HBV-induced chronic hepatitis and nonalcoholic fatty liver disease.

More novel approaches are presented by Y. Gu et al., who propose a network flux model, using multitarget docking and network analysis, to screen molecules for antiplatelet aggregation, and X. Li et al., who provide a metabolomics-based approach to enhance the current quality control techniques for multicomponent herbal medicines.

T. Chen et al. evaluate various bioinformatics classifiers that are currently used in clinical-metabolomics studies and provide an expert opinion on the selection of classification tools based on their experimental evidence. Meanwhile, B. Zhao et al. introduce a novel strategy, in which stable-isotope labeled amino acids in cell culture were used as internal standards for clinical proteomic study, to achieve accurate quantitation of serum or urinary proteins.

Another unique feature of this issue is the extensive use of omics technologies in clinical and preclinical studies, highlighting the promise of dynamic and multiparametric profiling approach in CAM research. C. Lu et al. report a metabolomics study of hand-foot-and-mouth disease (n = 18), which reveals perturbation in lipid metabolism and inflammatory response in patients and showed beneficial

effect of a combination therapy. Y. Zhang et al. report a metabolomics study of human aromatherapy (n = 31) which has, for the first time, captured the subtle metabolic changes resulting from exposure to essential oils. X. Xin et al. conduct a metabolomics study which assess the holistic efficacy of a TCM agent, compound Danshen dripping pills, for myocardial infarction in male Sprague-Dawley rats. X. Gao et al. present a urinary metabolomics study which reveals novel antipyretic mechanisms of a TCM drug, Qingkailing injection, in a rat model of yeast-induced pyrexia.

In the paper by G. Hegyi et al., the evidence and challenges of hyperthermia, overheating of a part of or the whole body, and oncothermia, which is a "spin-off" of the hyperthermia as a specialized complementary therapeutic modality, are discussed for clinical oncology.

M. G. Porpora et al. introduce an observational cohort study on ovarian endometrioma with 92 Italian women using an alternative therapeutic agent, N-acetylcysteine, and suggest a clinically effective and feasible treatment of endometriosis based on the positive results observed.

S. Subenthiran et al. conduct a clinical CAM study on 228 patients with dengue fever with juice prepared from *Carica papaya* leaves and report that man platelet count in the treatment group (n = 111) was significantly higher than controls after 40 and 48 hours of admission.

Y. Gu et al. report an effective 8-week dietary intervention study of 53 healthy obese volunteers with very low carbohydrate diet. They conclude that the enhanced hepatic and whole-body lipolysis and oxidation may be associated with the clinical beneficial effects (weight loss and improved metabolic profile).

Two *in vitro* studies are included which test plant-derived extracts and compounds for bioactivities and/or therapeutic mechanisms. R. P. Samy et al. find most of the methanol extracts of 78 medicinal plants containing phenolic and polyphenolic compounds exhibit activity against the multidrug resistant Gram-negative and Gram-positive bacteria. J. G. Chung et al. report the antimetastatic activity of cantharidin, a derivative of Blister Beetles, on the adhesion, migration and invasion of human bladder cancer TSGH-8301 cells.

M. Zhang et al. observe the differential effects of two isoforms of alkylglycerols on obesity and insulin resistance in high fat diet fed mice, including significantly decreased bodyweight, serum levels of triglyceride, cholesterol, fasting glucose, insulin, and leptin by one form of alkylglycerols, and selachyl alcohol, but increased fasting insulin level by administration of the other form, batyl alcohol.

M. Wang et al. evaluate a TCM preparation, *Jiang-Zhi Granule*, on high fat diet induced steatosis in Sprague-Dawley rats and report an antisteatotic effect with a molecular mechanism through inhibiting LXRa-mediated SEBP-1c transcription and the maturation of SREBP-1c independent of LXRa.

N. Zheng et al. provide an overview of an ancient TCM, *Xiao Chai Hu Tang*, and each single herb used in the formula, for the treatment of chronic liver disease with a focus on hepatocarcinoma.

C.-J. Lin et al. report a significant preventive effect of an ancient TCM, *Bai-Hu-Tang*, in an experimental model of sepsis in male Sprague-Dawley rats, highlighting the complementary treatment option with this TCM agent for clinical sepsis.

Several studies are included in this issue evaluating traditional medicines for improving neurological conditions. E.-Y. Jung et al. report a neuroprotective effect of a traditional herbal preparation, *Gugijihwang Tang*, in a trimethyltin-induced memory dysfunction rat model. Z.-G. Yao et al. report the significant therapeutic effect of an ancient TCM preparation, PN-1, the name and the ingredients of which are not released, on the learning and memory in a transgenic mouse model of Alzheimer's disease. D. Wan et al. use a phytochemical compound, catalpol, an iridoid glycosides compound extracted from *Rehmannia glutinosa* Libosch, to treat permanent middle cerebral artery occlusion mice model and report significant neuroprotective and memory enhancement effects of this molecule. E. J. Yang and S.-Mi. Choi found that bee venom treatment attenuates the dysfunction of the ubiquitin-proteasomal system in a symptomatic $hSOD1^{G93A}$ mice model of amyotrophic lateral sclerosis and suggest that this treatment may reduce motor neuron loss caused by misfolded protein aggregates in the mouse model.

In summary, these 25 papers represent exciting CAM research activities with translational strategies embedded in design and context. The articles cover a wide variety of topics, from novel modalities used for clinical studies to omics technologies and bioinformatics that will contribute to an improved understanding of mechanisms and pharmacology of the CAM treatments. We would like to thank all the authors and reviewers.

Wei Jia
Martin Kohlmeier
Aiping Lu
Rong Zeng

Hindawi Publishing Corporation
Evidence-Based Complementary and Alternative Medicine
Volume 2013, Article ID 525613, 17 pages
http://dx.doi.org/10.1155/2013/525613

Research Article

Evaluation of Aromatic Plants and Compounds Used to Fight Multidrug Resistant Infections

Ramar Perumal Samy,[1] Jayapal Manikandan,[2,3] and Mohammed Al Qahtani[2]

[1] *Infectious Diseases Programme, MD4, 5 Science Drive 2, Department of Microbiology, Yong Loo Lin School of Medicine, National University Health System (NUHS), National University of Singapore, Singapore 117597*
[2] *Center of Excellence in Genomic Medicine Research, King Abdulaziz University, P.O. Box 80216, Jeddah 21589, Saudi Arabia*
[3] *School of Anatomy, Physiology and Human Biology, The University of Western Australia, 35 Stirling Highway, Crawley, WA 6009, Australia*

Correspondence should be addressed to Ramar Perumal Samy; rperumalsamy@yahoo.co.uk
and Mohammed Al Qahtani; mhalqahtani@kau.edu.sa

Received 29 November 2012; Revised 7 May 2013; Accepted 23 May 2013

Academic Editor: Rong Zeng

Traditional medicine plays a vital role for primary health care in India, where it is widely practiced to treat various ailments. Among those obtained from the healers, 78 medicinal plants were scientifically evaluated for antibacterial activity. Methanol extract of plants (100 μg of residue) was tested against the multidrug resistant (MDR) Gram-negative and Gram-positive bacteria. Forty-seven plants showed strong activity against *Burkholderia pseudomallei* (strain TES and KHW) and *Staphylococcus aureus*, of which *Tragia involucrata* L., *Citrus acida* Roxb. Hook.f., and *Aegle marmelos* (L.) Correa ex Roxb. showed powerful inhibition of bacteria. Eighteen plants displayed only a moderate effect, while six plants failed to provide any evidence of inhibition against the tested bacteria. Purified compounds showed higher antimicrobial activity than crude extracts. The compounds showed less toxic effect to the human skin fibroblasts (HEPK) cells than their corresponding aromatic fractions. Phytochemical screening indicates that the presence of various secondary metabolites may be responsible for this activity. Most of the plant extracts contained high levels of phenolic or polyphenolic compounds and exhibited activity against MDR pathogens. In conclusion, plants are promising agents that deserve further exploration. Lead molecules available from such extracts may serve as potential antimicrobial agents for future drug development to combat diseases caused by the MDR bacterial strains as reported in this study.

1. Introduction

Treatment of infections is compromised worldwide by the emergence of bacteria that are resistant to multiple antibiotics [1]. New and emerging drug resistance bacteria strains, particularly methicillin-resistant *Staphylococcus aureus* (MRSA), vancomycin-resistant enterococci (VRE), *Mycobacterium tuberculosis* (MTB), and multidrug resistance (MDR) Gram-negative bacteria, are increasing worldwide and add to the gravity of the situation [2]. *S. aureus* cause a variety of syndromes such as food poisoning, toxic shock syndrome, skin lesions [3], hyperproliferative skin disease [4], and atopic dermatitis [5, 6]. Community-acquired pneumonia caused by *Streptococcus pneumoniae, Klebsiella pneumonia,* and *S. aureus* accounts for significant mortality in Southeast Asia [7]. Melioidosis has been recognized as an important human infection caused by *Burkholderia pseudomallei* in Singapore, Malaysia, Thailand, and Northern Australia [8, 9]. Cases have also been reported from some other tropical and subtropical regions like Africa and America, and a number of cases in man has recently been reported to increase in China, Taiwan, and South India [10, 11]. Infection with antibiotic resistant bacteria negatively impacts on public health, due to an increased incidence of treatment failure and severity of diseases. Development of resistant bacteria due to the chromosomal mutations is more commonly associated with the horizontal transfer of resistance determinants borne on mobile genetic elements [12]. *B. pseudomallei* is intrinsically

resistant to many antibiotics [13, 14]. Considering the higher cost for producing synthetic drugs and the various side effects associated with their use, the need to search for alternative agents from medicinal plants and essential oils used in folklore medicine is further justified to overcome these issues. In India, there are about 550 tribal communities covered under 227 ethnic groups residing in about 5000 villages throughout different forest and vegetation regions [15]. India is one of the world's 12 megabiodiversity countries [16, 17]. Plant derived medicines have played a major role in human societies throughout the history and prehistory of mankind [18]. The traditional healers (traditional physicians) or medicinemen have a long history of their own diagnostic and treatment system, which they have acquired from their ancestors [19]. Approximately 80% of the world population still relies on traditional medicine for the treatment of common diseases [20–22]. Medicinal plants thus offer significant potential for the development of novel antibacterial therapies and adjunct treatments [23]. Plant derived drugs serve as a prototype to develop more effective and less toxic medicines. In previous studies, few attempts were made to confirm the antimicrobial activity of some indigenous medicinal plants [24, 25]. Not only extracts of various medicinal plants but also essential oils and their constituents have been investigated for their antimicrobial properties against bacteria and fungi [26–28].

The principal compounds from the leaves showed a better antibacterial activity against *P. aeruginosa* and *B. subtilis* bacteria and a significant antifungal activity on *C. albicans* [29]. The essential oil from *R. officinalis* (alpha pinene/verbenone/bornyl acetate) was found to be more sensitive to the Gram-positive bacteria (MIC 2.5–4 mg/mL) than to the Gram-negative bacteria [30]. Several essential oils kill bacteria by damaging the cell membrane structure and inhibiting their membrane function [31]. Because of the antimicrobial potency of plant extracts and oils, they become a rich source of raw materials for many biotechnological and pharmaceutical industries for the development of therapeutic drugs. The increasing trend in the use of aromatic plants and essential oils in food, cosmetic, and pharmaceutical industries suggests that a systematic study of traditional medicinal plants is very important in order to find active compounds from such sources [32–34]. The purpose of this study is to survey and investigate popular medicinal aromatic plants and their essential oils with a view to fight against multidrug resistant human pathogens. In the present study, 71 plant species were selected on the basis of the available medicinal information and screened for their *in vitro* antimicrobial efficacy against bacteria.

2. Materials and Methods

2.1. Ethnomedicinal Survey and Collection of Plants. Ethnomedicinal surveys were conducted during March 1998 and July 2001 from various tribal localities (Kolli hills, Kalrayan hills, Pachamalai, Javadi hills, Mundanthurai) of Eastern and Western Ghats, Tamil Nadu, India. For ethnobotanical studies, questioners were used to collect the general information on the tribes, and the key information on medicinal details was collected through interviews. The medicinal plants were identified by a taxonomist using the standard Flora of Tamil Nadu Carnatic [35], and the voucher specimens were deposited in the department's herbarium at the Entomology Research Institute, Loyola College, Chennai, India.

2.2. Preparation of Plant Extracts. Using a Soxhlet apparatus, the shade-dried and powdered plant materials (200 g of each) were extracted with 1000 mL of methanol (CH_3OH) for 10 h. The collected methanol extracts were filtered (Whatman no. 1 filter paper) and evaporated with a rotary evaporator and freeze dryer (lyophilized) to obtain the crude extracts (Buchi, Labortechnik AG, Switzerland). The dried crude extracts were stored at 4°C for antimicrobial assays [34].

2.3. Culture of Microorganisms. The following Gram-negative: *Burkholderia pseudomallei* (TES21), *Burkholderia pseudomallei* (KHW22), *Klebsiella pneumoniae* (ATCC15380), *Klebsiella pneumoniae*, *Pseudomonas aeruginosa* (ATCC2-7853), *Vibrio damsela*, and *Salmonella typhi* (ATCC51812) and Gram-positive: *Staphylococcus aureus* (ATCC 29213), *Streptococcus pyogenes*, and *Streptococcus pneumoniae* (ATCC49619) microorganisms were used for cultures. *B. pseudomallei* bacterial strains such as KHW and TES were isolated from the patient samples obtained from the Department of Microbiology, NUS, Singapore. The strains were subcultured on 20 mL Tryptic Soy (TS) and Mueller Hinton (MH) agar plates (pH 7.4) and incubated overnight at 37°C before use.

2.4. Antimicrobial Activity. The standard bacterial cultures were stored at −70°C, subcultured on 20 mL MH and TS agar plates (pH 7.4), and incubated overnight at 37°C prior to use. The antimicrobial property was tested using the disc-diffusion method [36]. Five young colonies of each strain of bacteria taken from their respective cultures grown overnight on TS agar plates (Oxoid limited, Wode Road, Basingstoke, Hants, England, UK) were suspended in 5 mL of sterile saline (0.9%), and the density of the suspension was adjusted to approximately 3×10^8 colony forming unit (CFU). The swab was used to inoculate the dried surface of TS agar plate by streaking four times over the surface of the agar and rotating the plate approximately 90°C to ensure an even distribution of the inoculums. The medium was allowed to dry for about 3 min before adding a 6 millimeter in diameter (mm) sterile paper disc (Becton Dickinson, USA) on the surface. Each disc was tapped gently down onto the agar to provide a uniform contact. Lyophilized residue (100 μg/mL) of each plant extracts and purified fractions was weighed and dissolved in 1 mL of water, and 20 μL of the extracts and oils (containing 100 μg of residue) were applied on each disc (3 replicates), while the sterile blank disc served as a normal control. The antimicrobial effect of the extracts on the clinical isolates was determined in comparison with the reference antibiotics (chloramphenicol 30 μg/disc and ceftazidime 30 μg/disc), which were used as positive controls. The plates were incubated at 37°C for 24 h, and the inhibition zones were measured and calculated.

2.5. Minimum Inhibitory Concentrations (MICs) Assay. MICs were evaluated based on the *in vitro* screening of 16 purified fractions that were found to have potent antimicrobial activity. Broth dilution method was used for the MIC assay with some slight modifications as recommend by the NCCLS [37]. Two-fold serial dilutions of all the fractionated compounds were made with MH and TS broth in microtiter plate wells to adjust the final concentration from 7.8 to 250 μg/mL, while wells containing the broth alone without any sample served as a control. Three replicates ($n = 3$) were used for each dilution and culture containing approximately 1×10^5 CFU/mL. The plates were incubated at 37°C for 24 h, and the absorbance was measured at 560 nm.

2.6. Cytotoxicity Assay. The cytotoxic effects of various extracts were tested by MTT assay [38] using human skin fibroblast HEPK cells. The toxic effect of plant extracts and essential oils was assayed on human skin fibroblast (HEPK) cell proliferation in 96-well microtitre plates. Confluent cells (5×10^6 cells per well) were incubated with extracts and oils for 24 h, and the percentage inhibitory concentration (IC_{50}) was determined.

2.7. Phytochemical Analysis of Plant Extracts. The most active extracts were used for purification of antimicrobial compounds [39]. 100 g each of the plant powder was percolated with 500 mL of 4% aqueous HCl (adjusted to pH 2) and heated at 50°C for 3 h. The extract was washed with 2×250 mL of diethyl ether, and the organic phase evaporated to dryness using vacuum rotary evaporator. The dark brown gummy residues obtained by acid hydrolysis were chromatographed on silica gel column 60 × 3.2 cm (60–120 mesh, pH 7, Merck) by gradually eluting with n-hexane/ethyl acetate (8 : 2; 6 : 4; 3 : 7 and 1 : 1) and chloroform/methanol (3 : 2). The aliquots of each fraction were subjected to thin layer chromatography (TLC) on silica gel coated TLC plate (1 mm Merck) using the solvent system consisting of 20% (v/v) n-hexane/ethyl acetate. The chromatograms were detected using 50% H_2SO_4 solution as a spray reagent [34]. The individual fractions were collected and concentrated by vacuum rotary evaporator at 40°C. All the purified compounds recovered from the silica gel column were monitored by reading the absorbance at 190–350 nm (UV spectrophotometer, Hitachi, Japan). The active fractions were further purified, and the final yields of the compounds were recorded. The lyophilized pooled concentrated compounds were then assayed (100 μg/mL) against bacteria. The phytochemical screening was done on the pure compounds using the chemical method previously reported for the detection of secondary metabolites [40]. The different chemical constituents tested include alkaloids, flavonoids, glycosides, polyphenols, saponin, sterols, triterpenes, tannins, reducing sugars, gallic acid, catechol, and aglycones.

2.8. Statistical Analysis. The bacterial growth inhibitory activity (inhibition zones millimeter in diameter) was compared for significant differences within the bacterial strains. One way analysis of variance was performed (mean ± SD, $n = 3$ replicates) using GraphPad Prism 4, USA. $^*P < 0.01$ was considered statistically significant (inhibition zones of extracts/fractions versus antibiotic drugs).

3. Results

3.1. Study Area for the Collection of Aromatic Medicinal Plants. The Western and Eastern Ghats were selected for the present study with the cite map showing the landmarks (Figures 1(a)-1(b)). Kalrayan hills are situated north of Attur taluk (Salem district), one of the major range of hills in the Eastern Ghats of Tamil Nadu (Figure 1(c)). Pachamalai hills are situated to the north of Thuraiyur taluk of Tiruchirappalli district. The rich biodiversity part of Eastern Ghats lies between latitudes 11°09′ 00″ to 11° 27′ 00″ N and longitudes 78°28′ 00″ to 78° 49′ 00″ E, and occupies an area of about 527.61 square km. It is located near 11° 11′N 78°21E/11.18°N 78.35°E/11.18; 78.35 (Figure 1(d)). Mundanthurai is located nearly 45 km west of Tirunelveli district, TN, between latitude 8° 25′ and 8° 53′ N and longitude 77° 10′ and 77° 35′ E. This is the only area of Western Ghats that has the longest raining period of about 8 months and forms the catchment area for 14 rivers and streams (Figure 1(e)). Kolli Malai is a small mountain range located in Namakkal district. The mountains are about 1000–1300 m in height and cover an area of approximately 280 km. The Kolli hills are part of the Eastern Ghats, which is a mountain range that runs mostly parallel to the east coast of Tamil Nadu in South India (Figure 1(f)). Javadi hills are one of the largest in the Eastern Ghats in Vellore district in the northern part of the state of Tamil Nadu. They consist of bluish gray hills, with peaks averaging 3600–3800 feet or 1100–1150 meter (Figure 1(g)). Based on the vegetation type (Figures 2(a)–2(d)), the study area consists of (i) dry, deciduous, (ii) moist deciduous, and (iii) rain forests and diverse proportion of plant parts in abundance (Figures 2(e)-2(f)). Three different types of tribes (i.e., Kani, Malayali and Paliyan tribes) inhabit in the hill ranges. The Kani tribes, located at Mundanthurai, raise different types of vegetables in their own fields, while the Malayali tribes cultivate rice. They all engage not only in the agricultural work but also are involved in silvicultural work assigned by the forest department, Government of TN, India.

3.2. Medicinal Plants Glory. Western Ghats (Mundanthurai) and Eastern Ghats (Kolli hills, Javadi hills, Kalrayan hills, Pachamalai hills) possess a rich diversity of medicinal plants that are used as food and drug by different groups of tribal communities. Urbanization, habitat degradation, and fragmentation of these forests have resulted in the depletion of natural resources on which these tribes used to depend for their livelihoods. It has become increasingly difficult for them to live in their traditional way. In addition, the impact of modernization and urbanization has encroached in and around tribal settlements, thus changing their lifestyles.

3.3. Plants Valued as Edibles. Various types of plant parts are collected during different seasons, cooked, and eaten along with boiled rice (Table 1). For example, *Solanum nigrum* leaf is most commonly used in all the four regions. There are

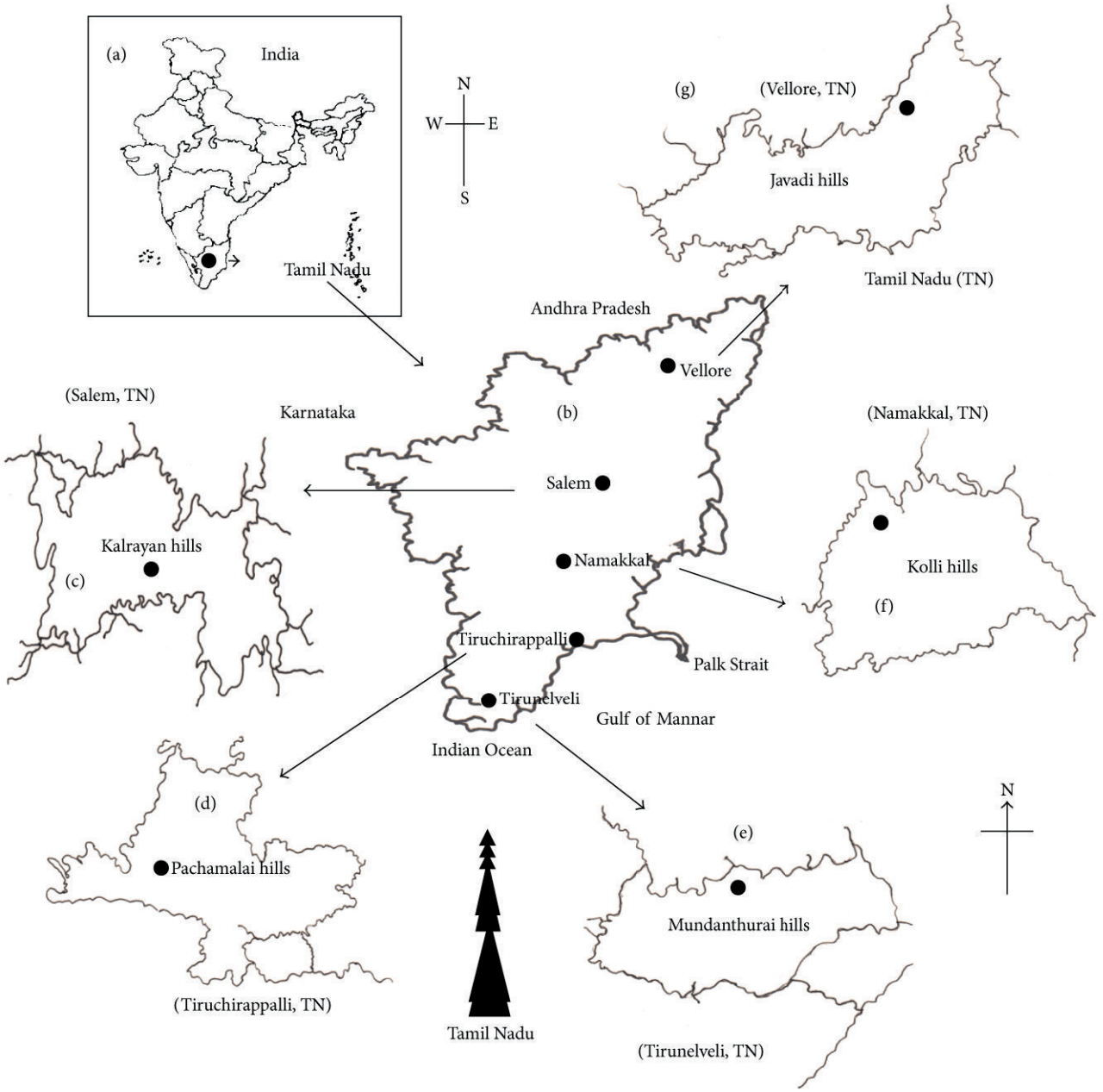

Figure 1: (a) The site for collection of medicinal plants in Western and Eastern Ghats of Tamil Nadu. (b) The landmark (map) of traditional medicine distribution and collection of different types of plants. (c) District map showing the collection site of plants from Kalrayan hills (Salem), (d) Pachamalai hills (Thiruchirappalli), and (e) Mundanthurai (Tirunelveli) rich biodiversity hot-spot of the Western Ghats. (f) Kolli hills (Namakkal), (g) Javadi hills (Vellore), part of the Eastern Ghats, which is a mountain range that runs mostly parallel to the east coast of South India.

a large number of wild edible fruits, including yielding plants such as *Citrus acida, Ficus benghalensis, Ficus microcarpa*, *Ficus racemosa, Phyllanthus emblica*, *Solanum trilobatum,* and *Syzygium cumini* are popularly used by the tribes.

3.4. Plants Used for Snakebite Treatment. Thirty-four plants used for snakebite treatment are documented (Table 1). Snakebite is a major health hazard that leads to high mortality in tribal settlements. The majority of the antidotes are prepared freshly from plant materials frequently collected from the leaves of *A. paniculata, A. echioides, Aristolochia indica, E. alba*, *E. prostrata, M. pudica, O. sanctum, T. involucrata*, and *Cleistanthus collinus* (Oduvanthalai); the whole plants of *Achyranthes aspera* and *Wedelia calendulacea*; the stem-barks and nuts of *Strychnos nux-vomica*; the roots of *Hemidesmus indicus, Tephrosia purpurea, Rauwolfia serpentina, C. roseus,* and so forth, and the tubers of *Gloriosa superba*. The tuber paste is usually applied externally on

Table 1: Some of the important traditional medicinal plant species, families, voucher specimens, parts used, yield of extracts, phytochemical screening, and toxicity on human macrophage cells.

Scientific name	Family	Voucher specimen	Plant parts	Yield (gm)	Phytochemical analysis
Adhatoda vasica Nees	Acanthaceae	D2020	Leaf	6.4	Vasicine
Aegle marmelos (L.) Correa ex Roxb.	Rutaceae	D2018	Root-bark	5.8	Alkaloids
Alangium salvifolium (L.) f. Wangerin.	Alangiaceae	0140	Leaf	6.3	Phenolic
Andrographis paniculata Wallich ex Nees	Acanthaceae	0061	Leaf	6.8	Andrographolide
Andrographis echioides Nees	Acanthaceae	0116	Leaf	7.0	Terpenoids,
Acalypha indica L.	Euphorbiaceae	29644	Leaf	6.1	Acalyphe
Acalypha lanceolata L.	Euphorbiaceae	15791	Leaf	7.1	Alkaloids
Achyranthes aspera L.	Amaranthaceae	2666	Leaf	2.7	Betaine
Ageratum conyzoides L.	Asteraceae	4812	Leaf	3.7	Essential oils
Asteracantha longifolia L.	Acanthaceae	0234	Stem	7.4	Glycosides
Azadirachta indica A. Juss.	Meliaceae	D0204	Leaf, bark	6.7	Tannins
Borassus flabellifer L.	Arecaceae	D0202	Root	0.8	Flavonoids, phenolics
Boerhavia erecta L.	Nyctaginaceae	10897	Whole plant	2.8	Phenolics
Calotropis procera (Ait.) Ait. f.	Asclepiadaceae	D073	Root-bark	1.3	Terpenoids
Calotropis gigantea (L.) R.Br.ex Ait	Asclepiadaceae	D070	Milky latex	4.8	Alkaloids
Cassia auriculata L.	Caesalpiniaceae	0141	Leaf	4.9	Saponins
Cassia occidentalis L.	Caesalpiniaceae	0111	Root	9.5	Flavonoids, saponins
Cassia tora L.	Caesalpiniaceae	0100	Stem, bark	6.9	Saponins
Cassia fistula L.	Caesalpiniaceae	037	Whole plant	7.9	Saponins
Cardiospermum halicacabum L.	Sapindaceae	0125	Whole plant	5.8	Flavonoids
Catharanthus roseus (L.) G.Don.	Apocynaceae	0029	Leaf, root	1.4 0.7	Alkaloids
Cinnamomum zeylanicum Garcin ex Blume	Lauraceae	00209	Bark	3.1	Essential oil, Tannin
Cinnamomum iners Reinw. ex Blume	Lauraceae	043-c	Leaf, bark		Alkaloids
Cissus quadrangularis Roxb.	Vitaceae	D02023	Leaf	6.8	Glycosides
Citrus acida Roxb. Hook.f.	Rutaceae	0213	Leaf	5.2	Saponins, Terpenoids
Centella asiatica (L.)	Umbelliferae	0138	Whole plant	8.9	Flavonoids, Alkaloids
Clerodendrum inerme (L.) Gaertn.	Verbenaceae	D02043	Stem	7.8	Sterols, diterpenes
Clitoria ternatea L.	Papilionaceae	D02026	Seed	9.8	Protein
Cleistanthus collinus (Roxb.) Benth. and Hook.f.	Euphorbiaceae	0011	Whole plant	0.03	Cleistanthin, collinusin
Cleome gynandropsis L.	Capparidaceae	12247	Leaf	6.2	Glycosides
Cleome viscose L.	Capparidaceae	29999	Leaf	2.7	Phenolics

Table 1: Continued.

Scientific name	Family	Voucher specimen	Plant parts	Yield (gm)	Phytochemical analysis
Coccinia grandis W & A	Cucurbitaceae	D02030	Leaf, root	0.9	Glycosides
Cymbopogon citratus (DC.)	Gramineae	D012	Root	0.25	Essential oil
Datura metel L.	Solanaceae	D02038	Leaf, stem	3.9	Steroids
Eucalyptus globulus Labill.	Myrtaceae	D0220	Leaf	1.2	Terpenoids
Eclipta alba (L.) Hassk	Asteraceae	D028	Whole plant	0.7	Phenolic
Euphorbia hirta Linn	Euphorbiaceae	0018-c	Whole plant	0.12	—
Eclipta prostrata (L.)	Asteraceae	D210	Leaf	1.10	Triterpenoid, saponin
Eugenia caryophyllus (Sprengel) Bullock & Harrison	Myrtaceae	0025	Flower buds	1.16	Essential oils
Elettaria cardamomum White et Mason	Zingiberaceae	0009	Fruit pods	3.17	Essential oils
Gloriosa superba L.	Liliaceae	020-S	Tuber	1.08	Alkaloids, phenol
Jatropha curcas L.	Euphorbiaceae	015	Whole plant	5.3	Alkaloids, flavonoids
Hyptis suaveolens (L.) Poit.	Lamiaceae	24688	Leaf	6.3	Essential oil
Hemidesmus indicus L.	Asclepiadaceae	D-009	Roots		Coumarins
Ichnocarpus frutescens (L.) R.Br.	Apocynaceae	0110	Root, flower	7.3	Terpenoids
Leucas aspera (Willd.) Link	Labiatae	0114	Leaf	8.3	Triterpenes
Lawsonia inermis L.	Lythraceae	T261	Leaf	0.9	Glycosides, phenolic
Madhuca longifolia (L.) JF Macbr	Sapotaceae	D01415	Nut	9.3	Sitosterol
Merremia hastate L. (Desr.) Hallier.f.	Convolvulaceae	10894	Whole plant	4.0	Alkaloids
Mentha piperita L.	Lamiaceae	0217-c	Whole plant	0.7	Essential oils
Morinda tinctoria Roxb	Rubiaceae	0122	Leaf	1.4	Glycosides
Mimosa pudica L.	Mimosaceae	0071	Whole plant	0.6	—
Oldenlandia umbellata L.	Rubiaceae	D02047	Leaf	4.4	Alkaloids
Ocimum sanctum L.	Lamiaceae	0016	Whole plant	3.0	Alkaloids
Piper attenuatum Buch. Hamex Miq.	Piperaceae	007	Flower	4.6	Alkaloids
Plumbago zeylanica (L.) Cav	Plumbaginaceae	0121	Root	4.8	*Plumbagin*
Plectranthus amboinicus (L.) *Spreng.*	Lamiaceae	0410	Whole plant	1.2	Essential oils, terpenoids
Phyllanthus debilis L. (Klein ex Willd)	Euphorbiaceae	0120	Whole plant	4.9	Polyphenol
Phyllanthus madraspatensis L.	Euphorbiaceae	0117	Whole plant	5.0	Polyphenol
Premna tomentosa Willd.	Verbenaceae	0129	Leaf	5.3	Diterpenes
Rosmarinus officinalis L.	Lamiaceae	0017	Root	0.23	Essential oils
Rauwolfia serpentine L.	Apocynaceae	020-S	Root	1.15	Alkaloid
Sebastiania chamaelea (L.) Muell Arg.	Euphorbiaceae	0034	Leaf	1.1	Polyphenol
Solanum trilobatum L.	Solanaceae	D02054	Leaf, flower	4.0	Tannins

Table 1: Continued.

Scientific name	Family	Voucher specimen	Plant parts	Yield (gm)	Phytochemical analysis
Sphaeranthus indicus L.	Asteraceae	D02060	Whole plant	1.0	Essential oil
Swertia chirata (L.) Ham.	Gentianaceae	D0540	Whole plant	1.6	Glycodises
Strychnos nux-vomica L.	Loganiaceae	S-22	Nuts	0.36	Alkaloids
Tragia involucrata L.	Euphorbiaceae	D068	Leaves	1.6	Shellsol
Tinospora cordifolia (Willd.) Miers ex Hoof.f & Thoms	Menispermaceae	0118	Leaf, root, stem	5.0	Glycosides, tannins
Tridax procumbens L.	Compositae	10649	Leaf	1.8	Flavonoids
Terminalia arjuna (DC) W & A	Combretaceae	033-c	Bark	8.0	Phenolics
Tephrosia purpurea (L.) Pers	Fabaceae	S-43	Whole plant	0.8	Isoflavone
Vitex negundo L.	Verbenaceae	0031	Leaf	2.4	Terpineol
Vetiveria zizanioides L.	Gramineae	0051	Root	1.03	Essential oil
Withania somnifera (L.) Dunal	Solanaceae	D02063	Root	2.1	Alkaloids
Wedelia calendulacea Less	Asteraceae	S-24	Leaves		Flavonoids
Zingiber officinale Rosc.	Zingiberaceae	0327	Rhizome	2.3	Tannins
Zanthoxylum limonella (Dennst.) Alston	Rutaceae	009	Bark	1.9	Alkaloids, essential oil

Class of chemical compounds: A: alkaloids, S: saponins, T: tannins, St: steroids, G: glycosides, T: terpenoids, P: polyphenol, P: phenolics, Sh: shellsol, H: hydrocarbon esters.

the site of snakebite, and decoction is given orally for treatment by indigenous people. Besides, these tribes rely on the medicinal plants as ingredients for fabricating a kind of medicated stone for health management. "Vishakallu" (poison stone) is used by the indigenous groups called Kani in Kerala, India, to treat a snakebite. When the stone is placed directly on the bitten area, it sticks to the body to absorb the poison and then become detached when absorption seems to be complete. The ingredients of Vishakallu stones are made with leaves of *Ocimum sanctum, Anisomeles malabarica, Leucas aspera*, Piper betle, *Santalum album,* and the pebbles collected from the river bank.

3.5. Survey of Medicinal Plants and Their Health Care Values. The present study is an attempt to provide scientific basis and obtain justification for the traditional beliefs of reliance on a rich diversity of ethnomedicinal plants, along with the rich heritage of traditional medicine practices related to health care system made available by the primitive tribal communities located at different settlements. The native traditional practitioners called "vaidyars" have a good knowledge about the traditional plants locally available for treatment of various diseases (Figures 3(a)–3(p)). Such traditional medical knowledge is used for preparing home remedies, ill health prevention, and routine health maintenance. This knowledge is also applicable to cover other sectors of social life. During the ethnobotanical survey, the wealth of 78 medicinal plant species used by the indigenous tribal community for various types of health treatment was documented. The botanical names, family names, parts used, chemical constituents, and their application are provided (Table 1).

3.6. Antimicrobial Activity of Crude Extracts. In this study, we reported the antimicrobial screening of methanolic crude extracts of 78 medicinal plants (Table 2). Results revealed that 68 plant extracts displayed potent activities against one or more Gram-positive and -negative bacteria. Of which, *Tragia involucrata, Citrus acida, Aegle marmelos, Adhatoda vasica, Calotropis procera, Andrographis paniculata* and *Mentha piperita, Azadirachta indica, Sphaeranthus indicus,* and *Elettaria cardamomum* showed the highest antibacterial activity against the multidrug resistant *B. pseudomallei* (KHW and TES) and *S. aureus* at 100 μg/mL concentration. The extracts showed pronounced antibacterial activity with their inhibitory zones ranging from 20 to 31 mm in diameter as compared to the standard drugs chloramphenicol and ceftazidime (29–33 mm). The majority of the plants demonstrated a powerful antimicrobial potency against the multidrug resistant strains of *B. pseudomallei* (KHW and TES), *K. pneumonia,* and *S. aureus.* Approximately, twenty-one plant extracts exerted only a weak or moderate effect against the tested bacteria, while the crude extract of 13 plants failed to show any effect at all. Except for the plant extracts of *T. involucrata, A. lanceolata, A. vasica*, and *S. indicus* extracts, the majority of the plant extracts were ineffective against the *V. damsela* infection, fascinatingly, only 11 plants exhibited activity against *P. aeruginosa,* of which *S. indicus, M. piperita,* and *C. procera* were found to have very strong inhibition of bacteria at the tested concentrations.

Table 2: Antimicrobial activity of methanol extract of aromatic medicinal plants and essential oils evaluated against multidrug resistant (MDR) human pathogens at 100 μg/mL concentration.

Scientific name	Microorganisms; growth inhibition zones (6 millimeter in diameters)									
	KHW	*TES*	*K.p*	*K.pr*	*P.a*	*S.a*	*St.p*	*S.p*	*V.d*	*V.d*
Adhatoda vasica Nees	28	19	22	18	12	—	10	17	16	—
Aegle marmelos (L.) Correa ex Roxb.	29	17	9	10	—	15	—	—	—	—
Alangium salvifolium (L.) f. Wangerin.	15	10	8	8	—	12	9	10	—	—
Andrographis echioides L.	12	9	—	—	—	17	8	9	—	—
Andrographis paniculata Wallich ex Nees	26	21	19	13	—	25	8	16	12	—
Acalypha indica L.	—	—	—	—	—	18	—	—	—	—
Acalypha lanceolata L.	—	—	12	13	—	10	—	—	21	—
Achyranthes aspera L.	—	—	7	14	—	15	12	11	—	—
Ageratum conyzoides L.	10	8	—	—	—	—	—	—	—	—
Asteracantha longifolia L.	16	12	—	—	—	15	—	—	—	—
Azadirachta indica A. Juss.	15	17	21	16	14	23	12	14	—	—
Borassus flabellifer L.	9	10	17	8	—	—	9	10	—	—
Boerhavia erecta L.	—	—	8	9	7	16	—	—	—	—
Calotropis procera (L.)	—	—	15	—	18	28	9	—	—	—
Calotropis gigantea (L.) R.Br.ex Ait	11	9	—	—	—	20	—	—	9	8
Cardiospermum halicacabum L.	23	—	—	14	—	9	19	—	—	—
Catharanthus roseus (L.) G.Don.	13	7	12	9	—	15	11	8	—	—
Cassia auriculata L.	17	13	12	—	—	19	13	—	—	—
Cassia occidentalis L.	18	—	—	—	—	—	—	—	—	—
Cassia tora L.	—	—	—	—	—	—	—	—	—	—
Cassia fistula L.	—	—	—	—	—	—	—	—	—	—
Citrus acida Roxb. Hook.f.	26	22	—	12		29	9	13	8	—
Cissus quadrangularis L.	—	—	—	—	—	—	—	—	—	—
Cinnamomum zeylanicum Garcin ex Blume	14	16	7	20	—	22	19	7	—	—
Cinnamomum iners Reinw. ex Blume	20	16	—	15	—	16	12	—	—	—
Rosmarinus officinalis L.	—	9	—	10	—	7	—	8	—	—
Centella asiatica (L.)	9	8	—	—	—	11	—	—	—	—
Clerodendrum inerme (L.) Gaertn.	13	7	12	—	—	15	11	8	—	—
Clitoria ternatea L.	—	—	—	—	—	—	—	—	—	—
Clitoria ternatea L.	16	12	—	13	—	8	10	—	—	—
Cleome gynandropsis L.	—	—	12	19	11	—	9	15	12	—
Cleome viscose L.	—	—	8	10	14	20	—	—	—	—
Coccinia grandis W & A	9	10	17	8	—	—	9	10	—	—
Cymbopogon citratus (DC.)	16	18	—	17	—	14	—	—	—	—
Datura metel L.	—	—	—	—	—	—	—	—	—	—
Eclipta alba (L.) Hassk	20	—	—	9	—	—	10	—	—	—
Euphorbia hirta Linn	11	—	—	—	—	16	—	—	—	—
Eucalyptus globulus Labill.	—	—	—	7	—	—	—	7	—	—
Eugenia caryophyllus Bullock & Harrison	—	7	—	11	—	9	—	8	—	—
Elettaria cardamomum White et Mason	21	20	7	14	—	22	12	17	—	—
Hyptis suaveolens (L.) Poit.	8	10	8	7	—	—	—	—	—	—
Ichnocarpus frutescens (L.) W.J. Aiton	—	—	—	—	—	—	—	—	—	—
Jatropha curcas L.	—	—	—	8	—	11	—	12	—	7
Leucas aspera (Willd.) Link	9	10	17	8	—	12	9	10	—	—
Lawsonia inermis L.	—	—	—	—	—	—	—	—	—	—
Madhuca longifolia (L.) JF Macbr	18	16	14	19	12	—	8	7	9	—

Table 2: Continued.

Scientific name	Microorganisms; growth inhibition zones (6 millimeter in diameters)									
	KHW	*TES*	*K.p*	*K.pr*	*P.a*	*S.a*	*St.p*	*S.p*	*V.d*	*V.d*
Merremia hastate L. (Desr.) Hallier.f.	—	—	—	—	—	—	—	—	—	—
Morinda tinctoria Roxb	—	—	—	—	—	—	—	—	—	—
Mentha piperita L.	23	17	26	12	20	25	19	—	—	—
Ocimum sanctum L.	12	9	11	7	—	15	7	8	—	—
Oldenlandia umbellata L.	—	—	—	—	—	17	—	—	—	—
Piper attenuatum Buch. Hamex Miq.	13	7	12	21	—	17	11	8	—	—
Plumbago zeylanica (L.) Cav	9	10	17	8	—	12	9	10	—	—
Plectranthus amboinicus (L.) Spreng.	—	—	—	8	11	15	—	—	—	—
Phyllanthus debilis L. (Klein ex Willd)	7	8	—	9	—	9	18	7	—	—
Phyllanthus maderaspatensis L.	17	—	—	—	—	—	—	—	—	—
Premna tomentosa Willd.	13	10	—	15	—	9	10	—	—	—
Gloriosa superba L.	17	16	7	8	—	15	—	—	—	8
Sebastiania chamaelea (L.) Muell Arg.	19	12	—	17	—	13	19	8	—	—
Solanum trilobatum L.	—	—	13	9	—	8	—	—	—	—
Sphaeranthus indicus L.	20	18	21	7	22	—	11	9	—	16
Swertia chirata (L.) Ham.	—	—	—	—	—	—	—	—	—	—
Terminalia arjuna (W. & A)	—	—	—	—	—	16	—	—	—	—
Tinospora cordifolia (Willd.) Miers ex Hoof.f & Thoms	—	—	23	16	—	12	15	—	—	—
Tridax procumbens L.	9	8	7	—	—	14	—	—	—	—
Tragia involucrata L.	25	23	20	—	—	31	28	22	19	—
Vitex negundo L.	—	—	—	—	—	14	—	—	—	—
Vetiveria zizanioides (L.)	11	9	7	7	—	16	—	—		8
Withania somnifera (L.) Dunal	12	20	—	—	—	15	12	—	—	—
Zingiber officinale Rosc.	14	11	7	15	—	7	12	7	—	—
Zanthoxylum limonella (Dennst.) Alston	13	7	12	9	—	—	11	8	—	—
Chloramphenicol (30 μg/disc)	21	12	15	17	29	16	15	18	13	11
Ceftazidime (30 μg/disc)	33	16	22	19	16	25	21	20	12	15

*Bacteria (+/−). Results obtained in the disc diffusion assay; antibacterial activity is expressed as the mean ± SD ($n = 3$), of the inhibition by the extract and its diameter around the discs. One way analysis of variance was performed (mean ± SD, $n = 3$ replicates). Size of inhibition zones were including the sterile blank discs 6 millimeter (mm) in diameters. Absence of bacterial inhibition indicates (—), antibiotic disc (30 μg/disc).

Interestingly, sixteen plants such as *Andrographis echioides, C. auriculata, C. viscose, C. gigantea, T. arjuna, Oldenlandia umbellata, Boerhavia erecta,* and *E. hirta* exerted a strong activity against the Gram-positive *S. aureus* bacteria.

3.7. Phytochemical Screening of Plants. The results obtained from the phytochemical screening as shown in Table 1 indicate the presence of various types of secondary metabolites such as polyphenols, tannins, saponins, alkaloids, and glycosides/polysaccharides. Most of the plant extracts relatively rich in alkaloids, phenols, flavonoids, polyphenols, tannins, sterols, and terpenoids were found to inhibit the growth of organisms.

3.8. Antimicrobial Activity of Fractioned Compounds. Active components were purified from the most active extracts for further testing. The compound shellsol of *T. involucrata* and *C. acida* exhibited the most potent action against the antibiotic resistant strains of *B. pseudomallei* (KHW), *S. aureus, B. pseudomallei* (TES), and *K. pneumoniae. A. marmelos* was also found to inhibit the growth of *B. pseudomallei* (KHW) more effectively than other tested bacteria. *A. vasica* showed the broad spectrum growth inhibitory activity on *B. pseudomallei* (KHW), *K. pneumoniae, K. pneumoniae,* resistant *B. pseudomallei* (TES), *S. pyogenes,* and *V. damsela.* However, *E. cardamomum* displayed antimicrobial activity on some of the *B. pseudomallei* (KHW), *S. pyogenes, B. pseudomallei* (TES), and *S. typhi* strains. Similarly, *A. indica* exerted the growth inhibition on *K. pneumoniae* and *S. aureus.* Remarkably, *Sebastiania chamaelea* was more active against *K. pneumoniae, K. pneumoniae,* and *S. pyogenes.* The compound from *S. indicus* inhibited the growth of *K. pneumoniae, K. pneumoniae, B. pseudomallei* (KHW and TES), and *S. typhi* strains, as compared to the activity shown

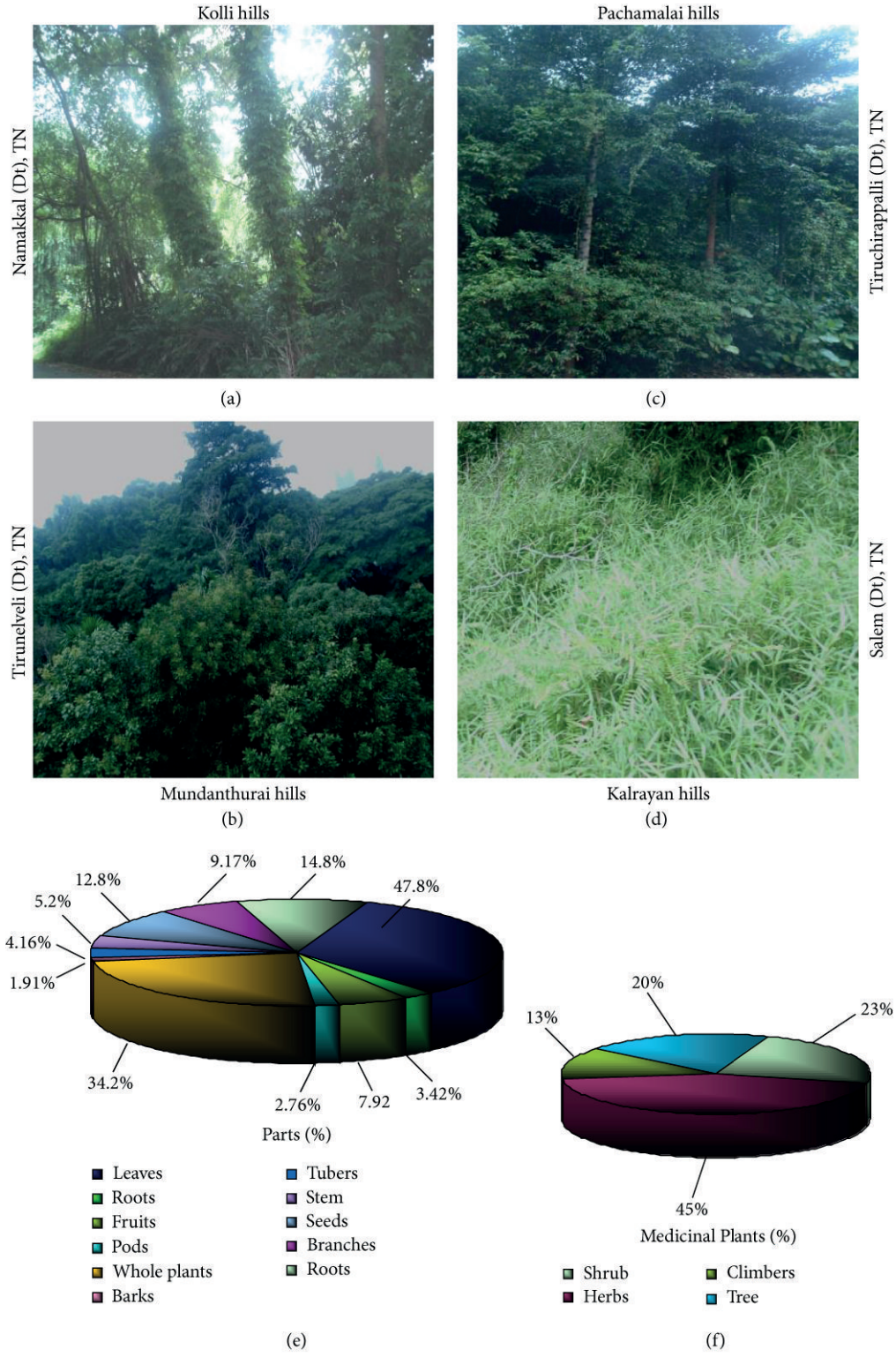

Figure 2: Diverse biodiversity richness of medicinal plants in Western and Eastern Ghats. (a) Topography of plant covering area in Kolli hills (Namakkal district, Tamil Nadu). (b) Aerial view of occurrence of medicinal plants in Mundanthurai hills (Tirunelveli district, TN). (c) Pachamalai hills (Trichy district) and its natural vegetation inhabitants for Malaiyali tribes. (d) Deforestation of natural herbal resources due to urbanization in Kalrayan hills (Salem district) in the Eastern Ghats of TN. (e) Medicinal plants and its various parts used by the natives (traditional healers) for the treatment of diverse human illness with a very high percentage of leaves and whole plants often used for herbal drug preparation by the local practitioners. (f) Various category of plants like shrub, herb, climbers and tree, and the parts used in medicine.

FIGURE 3: Medicinal aromatic herbs, spices, and toxic plants were collected from the tribal areas of the Western and Eastern Ghats region in Tamil Nadu, India. (a) *A. vasica* Nees (leaf), (b) *Eclipta alba* (L.) Hassk. (whole plant), (c) *Mimosa pudica* L. (whole plant), (d) *P. amboinicus* (L.) *Spreng.* (whole plant), (e) *T. procumbens* (L.) (whole plant), (f) *Euphorbia hirta* Linn (whole plant), (g) *A. paniculata* Wallich ex Nees, (H) *C. roseus* (L.) G.Don. (whole plant) used for therapy. (i) *Cinnamomum iners* Reinw. ex Blume (leaf) (j) *E. globulus* Labill. (leaf and bark), (k) *Z. officinale Rosc.* (Rhizome), (l) *E. caryophyllus (Sprengel) Bullock and Harrison* (flower buds), (m) *M. piperita* L. (whole plant), (n) *C. citratus* (DC.) *Clitoria ternatea* L. (whole plant), (o) *C. zeylanicum Garcin ex Blume* (bark), (p) *Elettaria cardamomum* White et Mason (fruit pod) used for medicine and food preparation.

by the crude extracts (Figure 4). The antimicrobial efficacy of fractions collected from the oil yielding plants was also compared with that of the tested compounds. *C. zeylanicum* and *R. officinalis* were the most sensitive in controlling the growth of *B. pseudomallei* (KHW), *S. aureus, K. pneumonia,* and *S. pneumoniae*. Fascinatingly, all the compounds obtained from aromatic plants, except those from *E. globules,* were found to be very effective against the multidrug resistant human pathogen *B. pseudomallei* (KHW) that causes melioidosis. On the other hand, compounds from *C citrates, O. sanctum, E. caryophyllus,* and *Z. zizanioide,* showed some promising effect only against *S. aureus* (Figure 5). The activity of the compounds were pronounced more than that of the oil yielding plant fractions.

3.9. Minimum Inhibitory Concentrations (MICs). The antibiotic potential of the purified fractions was obtained from the MIC determination. The hydrocarbon ester shellsol

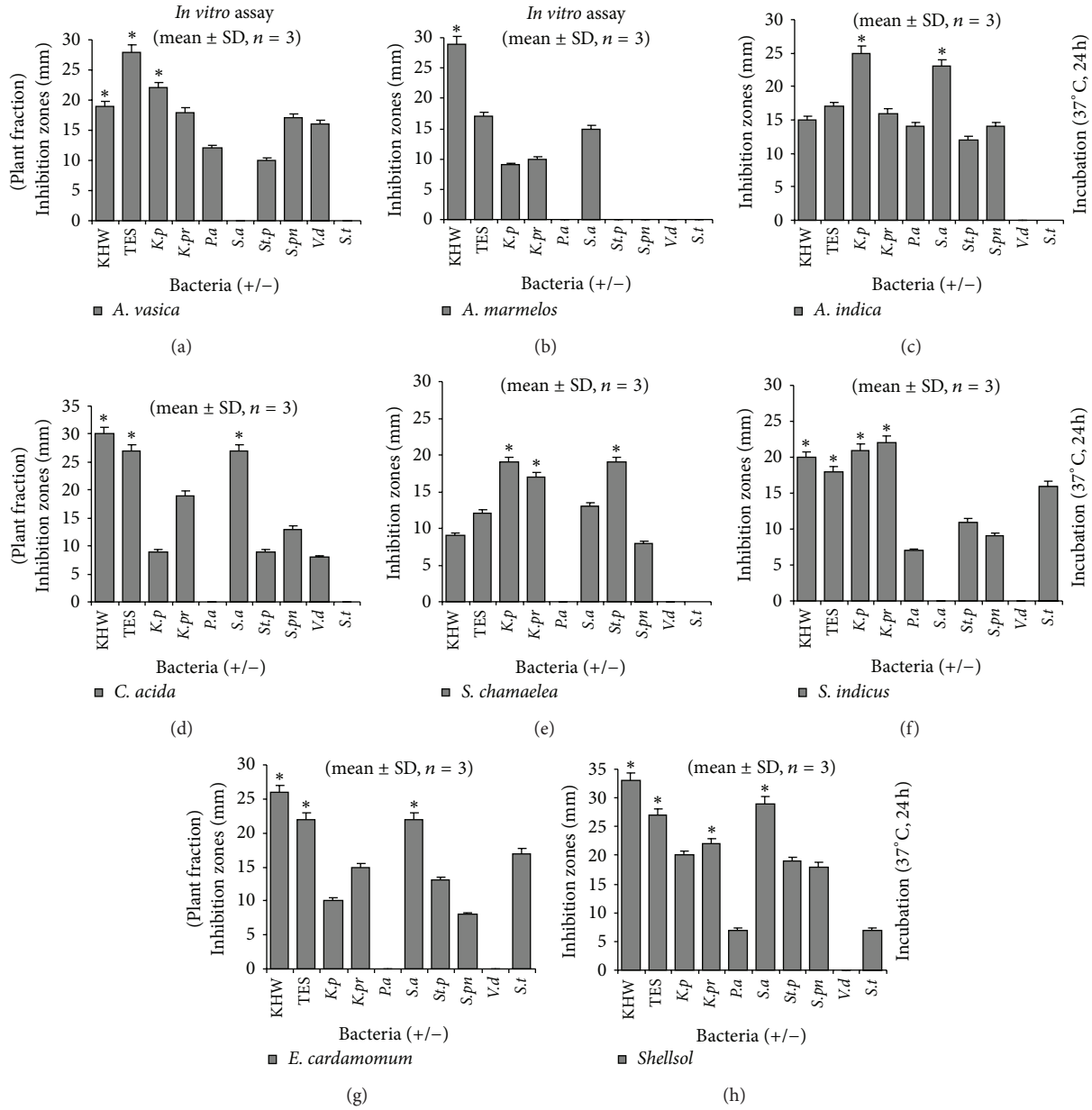

Figure 4: *In vitro* antimicrobial activity of purified fractions from the most active plant extracts tested against bacteria. Growth inhibition zones were measured and analyzed with mean ± standard deviation (SD), ($n = 3$) using one way analysis of variance. Level of significance at ($^*P > 0.01$). Most of the fractions exerted a potent inhibitory effect against multidrug resistant Gram-negative bacteria (*B. pseudomallei* strains KHW and TES), *K. pneumonia,* and Gram-positive bacteria *S. aureus*.

(*T. involucrata*) and *C. acida* showed an interesting inhibitory potential against *S. aureus* (MIC of 7.8 μg/mL) and *B. pseudomallei* strain of KHW (MIC of 15.6 μg/mL). *A. vasica* showed an MIC of 15.6 μg/mL against *B. pseudomallei* (KHW) and an MIC of 31.25 μg/mL against *K. pneumoniae, K. pneumoniae, S. pyogenes,* and *V. damsela* strains. Fractions from *A. marmelos* and terpenoid from *A. indica* exerted bacteriostatic effect with MIC values of 31.25 μg/mL on some selected bacteria including *B. pseudomallei* of KHW, *S. aureus,* and *B. pseudomallei* of TES. The MIC of 31.25 μg/mL was found for *E. cardamomum* against *S. aureus*, *K. pneumonia,* and *S. pyogenes*. *S. indicus* displayed a very strong inhibition against MDR *K. pneumoniae* (MIC of 15.6 μg/mL), and against *B. pseudomallei* (KHW and TES) at MIC of 31.25 μg/mL. When the antimicrobial efficacies of purified fractions from aromatic plants were compared, the *C. zeylanicum* fraction displayed an important antimicrobial effect against *S. aureus* (MIC of 7.8 μg/mL), MDR *B. pseudomallei* of KHW (MIC of 15.6 μg/mL), and *S. pneumoniae* (MIC of 31.25 μg/mL). The essential oil from *M. piperatea* showed MIC value of 31.25 μg/mL against *K. pneumoniae, S. aureus,* and *B. pseudomallei* (KHW), respectively. *O. sanctum*

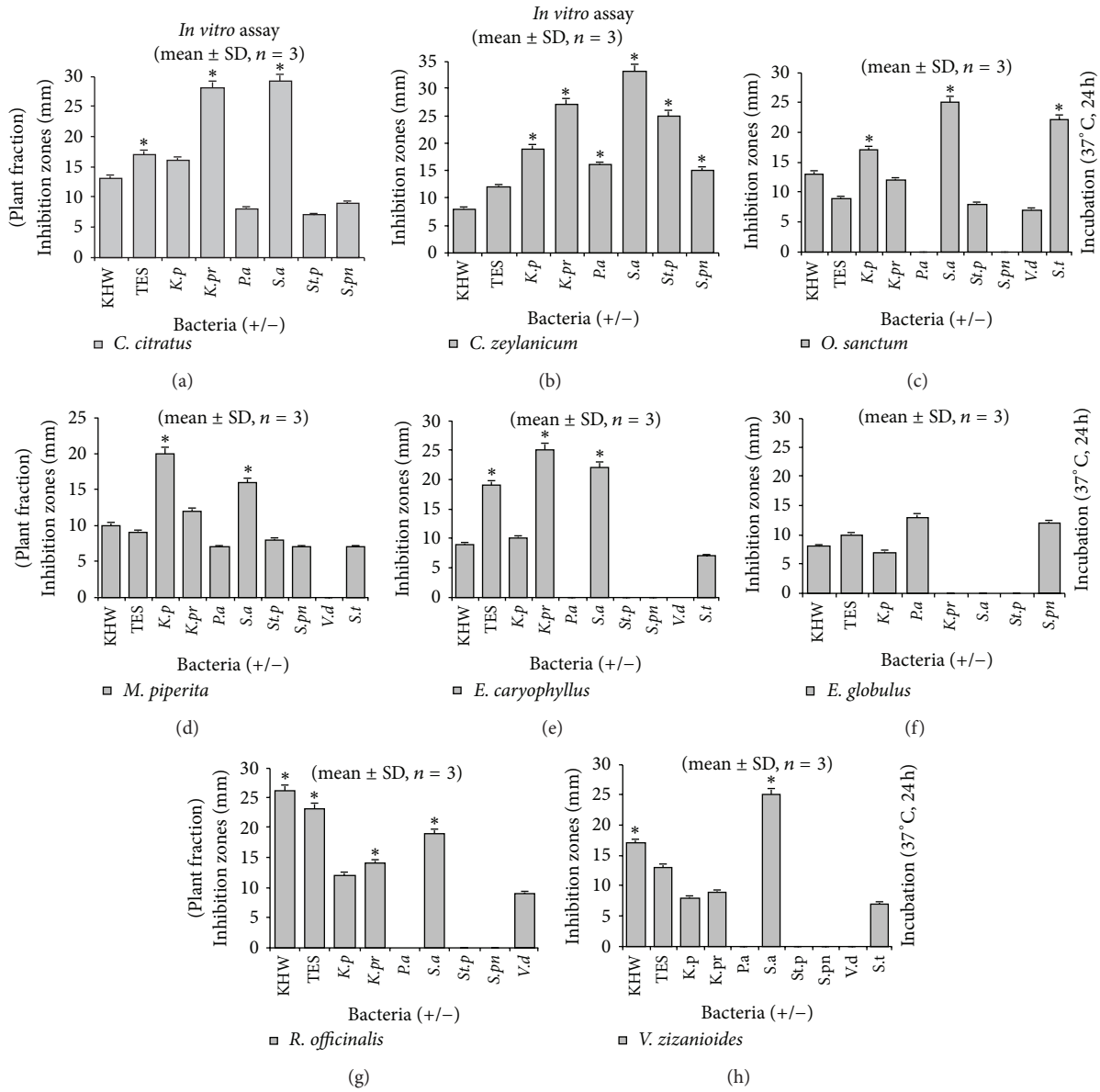

Figure 5: Comparison of antimicrobial effect of plant compounds obtained from the most popularly used sources of essential oils as assayed by the disc-diffusion method *in vitro*. It displayed a powerful activity against *B. pseudomallei* and *S. aureus* than the other bacteria strains. Other compounds showed only a moderate or weak action against the tested bacteria. Values for zone of bacterial growth inhibition were presented as mean ± SD, ($n = 3$) with level of significance at ($^{*}P > 0.01$).

and *C. citratus* fractions also showed antimicrobial activity (MICs of 31.25–125 μg/mL) only at higher concentrations against the tested bacteria. In addition to that, higher concentrations (>250 μg/mL) (of *Vetiveria* fractions) were required to inhibit *Vibro species,* and others (including *E. globulus* fractions) failed to show any effect at tested concentrations (7.8–125 μg/mL). However, the purified fractions (from most active medicinal plants) showed strong bacteriostatic inhibition against the tested organisms (Table 3).

3.10. Cytotoxic Effects of Plants. When the components were assayed for cytotoxicity against the normal human skin fibroblasts (HEPK) cells, the compounds obtained from *E. cardamomum*, *T. involucrata*, *S. indicus*, *C. acida*, *A. vasica*, *A. marmelos*, *A. indica,* and *A. paniculata* did not show toxicity up to 1000 μg/mL (see Figures S1 and S2 in Supplementary Material available online at http://dx.doi.org/10.1155/2013/525613). A slight reduction of cell proliferation was noted only at higher doses (2000 μg/mL). In contrast, cell proliferation was markedly reduced after exposure of HEPK cells to *O. sanctum*, *E. globulus*, *V. zizanioides*, *C. citratus,* and *E. globulus* compounds. There was no gradual reduction in skin cell proliferation seen after exposure to *C. zeylanicum*, *R. officinalis,* and *M. piperita* (see Figures S3 and S4) compounds. The toxicity was found to be concentration-dependent when the skin fibroblasts (HEPK) cells were

Table 3: Minimum inhibitory concentrations (MICs) of purified plant fractions and essential oils against antibiotic resistant bacteria.

Botanical name	Family	Parts used	Gram-positive and -negative bacteria (MICs μg/mL)								
			KHW	*TES*	*K.p*	*K.Pr*	*S.a*	*St.p*	*S.p*	*V.d*	*S.t*
A. indica Juss.	Meliaceae	Seed (fraction)	31.25	62.5	125	<250	31.25	—	—	—	—
A. marmelos (L.)	Rutaceae	Root-bark (F)	31.25	31.25	—	—	31.25	62.5	125	250	—
A. paniculata Nees	Acanthaceae	Leaf (fraction)	250	—	125	—	62.5	—	—	125	—
A. vasica Nees	Acanthaceae	Fraction (Stem)	15.6	31.25	31.25	62.5	—	<250	31.25	31.25	—
C. acida Roxb.	Rutaceae	Leaf (fraction)	15.6	62.5	—	—	7.8	—	31.25	—	—
E. cardamomum White et Mason	Acanthaceae	Fraction (WP)	62.5	—	31.25	—	31.25	250	62.5	—	—
S. indicus (L.)	Euphorbiaceae	Whole plant (F)	31.25	125	15.6	—	62.5	—	—	<250	—
T. involucrata (L.)	Euphorbiaceae	Shellosol (leaf)	15.6	31.25	—	—	7.8	62.5	—	—	—
Cinnamomum zeylanicum (L.)	Lauraceae	Bark (fraction)	15.6	62.5	—	—	7.8	31.25	—	—	125
Cymbopogon citratus (L.)	Graminae	Leaf (fraction)	250	<250	62.5	—	62.5	125	—	—	—
Eugenia caryophyllus (L.)	Myrtaceae	Flower buds (F)	62.5	125	—	—	62.5	—	—	—	—
Eucalyptus globulus (L.)	Myrtaceae	Fraction (leaf)	—	—	—	—	—	—	<250	—	<250
Mentha piperita (L.)	Labiatae	Fraction (WP)	—	62.5	31.25	—	31.25	—	<250	—	—
Ocimum sanctum (L.)	Labiatae	Leaf (fraction)	62.5	125	—	31.25	62.5	—	125	<250	—
Rosmarinus officinalis (L.)	Labiatae	Rosemary oil	31.25	—	—	—	31.25	—	—	—	—
Vetiveria zizanioides (L.)	Graminae	Root (fraction)		—	125	125	—	—	—	>250	>250

The bacterial growth inhibitory activity was compared for significant differences within the bacterial strains by broth-dilution method at 250, 125, 62.5, 31.25, 15.6, and 7.8 μg/mL. F: fractions.

exposed to various compounds. The cell proliferation was increased by the influence of the plant components at the lower concentrations. Whereas the oil yielding plant compounds showed inhibition of cell proliferation and toxicity at higher doses 250–1000 μg/mL.

4. Discussion

The Western Ghats is considered as one of the richest biodiversity hotspots in the world [41]. In this survey, we collected nearly 78 medicinal plants from Western and Eastern Ghats that are edible and popularly used for curing various ailments including snakebite. Traditional remedies have a long-standing history in many tribal settlements in TN, India, and they continue to provide useful and applicable tools for treating ailments [42]. The ingredients that make up the "Vishakallu" stone, which is used as an antidote for snakebite, are different herbs and pebbles available from the river banks. Likewise, aqueous paste and decoction obtained from the leaves of *A. paniculata* are widely used for snakebite treatment by indigenous people [43]. Previous studies have reported that ethnomedicine plays major roles in conserving the disappearing knowledge of tribal communities [44–47]. The traditional beliefs of reliance on a rich diversity of ethnomedicinal plants located at different settlements have also been confirmed in another study [48, 49]. Herein, we explored the various types of traditional practices reported by the primitive tribal communities with a view to gain further knowledge from such studies.

In the present investigation, potentially rich sources of tribal medicine (71 plants) were scientifically evaluated for their antibacterial activity against the MDR bacteria, and the accumulated data was disseminated for the first time to the scientific community. Out of the 71 medicinal plants screened for the antibacterial activity, 10 of them (*T. involucrata, C. acida, A. marmelos, A. vasica, C. procera, A. paniculata* and *M. piperita, A. indica, S. indicus,* and *E. cardamomum*) displayed the highest antibacterial activity against the multidrug resistant *B. pseudomallei* (KHW and TES) and *S. aureus* strains. The antibacterial activity of those crude plant extracts was as equally effective as that of the standard drugs. Our findings corroborated with the previous reports made on the *antistaphylococcal* activity of tribal medicinal plants [34, 50, 51]. On the other hand, isolated components from the most active extracts of *T. involucrata*, shellsol, and *C. acida* exhibited the most potent action against the antibiotic resistant *B. pseudomallei* (KHW), *K. pneumoniae*, and *S. aureus* strains. These results further confirmed our previous findings on the leaves of *T. involucrata* and its compounds hydrocarbon ester-like shellsol, which displayed a high antibacterial effect against the different bacterial strains, especially that of *S. aureus* [34]. Eugenol and caryophyllene are the active agents contained in the *M. piperita* [52] and *O. sanctum* plants, which are believed to be mainly responsible for the antimicrobial properties of these plants [53]. Interestingly, the compounds obtained from the aromatic plants such as *C. zeylanicum* and *R. officinalis* were also found to be very effective against the multidrug resistant human pathogen *K. pneumoniae, S. aureus*, *S. typhi,* and *B. pseudomallei* (KHW) that causes melioidosis.

The inhibitory potential determined for the shellsol (*T. involucrata*), vaseline (*A. vasica*), *C. acida,* and *C. zeylanicum* indicates that the MIC of 7.8–31.25 μg/mL found against the *B. pseudomallei* of KHW, *K. pneumoniae, K. pneumoniae, S. pyogenes,* and *V. damsel,* and S. *pneumoniae* was quite low. Similarly, lower MIC values were found for

M. piperita (MIC of 1.13–2.25 mg/mL) against the above bacterial strains [52]. MIC was found for the most active alcohol extracts of *A. salvifolium* (MIC 0.034–0.263 mg/mL) on *S. aureus* [54], and the MIC for *S. trilobatum* aqueous extracts determined against the tested organisms ranged from 0.06 to 0.5 mg/mL [55]. *C. zeylanicum* was found to have an effective antibacterial activity (MIC 64 μg/mL) against *P. aeruginosa, E. coli, B. subtilis,* and *S. aureus* [56]. Previously, several investigators have demonstrated that active agents exert interesting activity against bacteria even at lower concentrations tested [57, 58]. The bacteriostatic mechanism involves damage to the cell walls of bacteria, followed by inhibition of protein synthesis that ultimately leads to bacterial death [59]. The most active plants are widely used by various tribes as traditional treatment (i.e., cut wounds, skin infection, and scabies), thus indicating the potential for further development into promising drugs. In order to ascertain the safety and efficacy of the most active compounds, their effect on human skin fibroblast cells was evaluated. Chemical constituents of *E. cardamomum, T. involucrata, S. indicus, C. acida, A. vasica, A. marmelos, A. indica,* and *A. paniculata* plants failed to produce any noticeable toxicity up to 1000 μg/mL. Although some of the tested compounds exhibited a slight reduction of cell proliferation and some minor morphological changes, such changes were insignificant at lower doses and became evident only at higher doses. However, certain aromatic compounds of *O. sanctum, E. globulus, V. zizanioides, C. citratus,* and *E. globulus* plants showed reduction of cell proliferation against HEPK cells.

Our phytochemical screening also provides evidence of the presence of several types of compounds that are mainly responsible for the remarkable antibacterial effect of these plants. The differences noted for the bactericidal activity of various plant extracts in this study appears to be directly related to the diversity of compounds (shown in parentheses) that are accumulated in the following plants (e.g., *A. marmelos* and *O. umbellate*) [60–62]. Compounds like tannins, phenol, and polyphenols can bind the Gram-negative bacteria to form a heavy soluble complex on the cell surface, which subsequently disturbs the availability of receptor on cells and kills the bacteria [63]. Several species having wide spectra of antimicrobial activity mainly due to the active constituents such as essential oil, phenolic compounds like thymol, carvacrol in oregano and thyme, eugenol in clove, and cinnamon were also identified previously [64, 65]. Essential oils degrade the cell wall, interact with the cell components, and then disrupt the cytoplasmic membrane [66]. The antimicrobial effect of phenolic compounds may involve multiple modes of action, including damage to the membrane protein, interference with membrane integrated enzymes [67], causing leakage of cellular components, coagulation of cytoplasm, depletion of the proton motive force, alteration of fatty acid and phospholipid constituents, impairment of enzymatic mechanisms for production and metabolism, alteration of nutrient uptake and electron transport [68], influencing the synthesis of DNA and RNA, and destroying protein translation and the function of the mitochondrion in eukaryotes [69]. The mode of action of antimicrobial agents depends on the type of microorganism and is mainly related to their cell wall structure and the outer membrane arrangement. Most of the plant spices and herbs contain complex phenolics (i.e., phenolic acids, flavonoids, tannins, lignans, coumarins, quinines). In addition, the mechanisms of action of each phenolic compound against various bacteria are also very complicated [26, 70]. Further investigation is therefore required to understand the relationship between the antimicrobial action and the chemical structure of every phenolic compound in the tested extracts. The information available from previous pharmacological sources combined with the findings herein reported on the medicinal plant extracts may serve as essential data for future drug development to combat diseases caused by the MDR bacterial strains.

Abbreviations

MDR: Multidrug resistant bacteria
TES: Strain of *Burkholderia pseudomallei*
MRSA: Methicillin-resistant *Staphylococcus aureus*
VRE: Vancomycin-resistant enterococci
MTB: *Mycobacterium tuberculosis*
CH_3OH: Methanol
CFU: Colony forming unit
HCl: Hydrochloric acid
TLC: Thin layer chromatography
H_2SO_4: Sulphuric acids
UV: Ultraviolet spectrophotometer
HEPK: Human skin fibroblasts.

Acknowledgments

The authors are thankful to the ERI, Loyola College, Chennai, India, for his support during the survey. The authors also thank the Department of Microbiology, NUHS, NUS for the bacterial cultures used in this investigation. The authors are thankful to the tribal people for sharing their healing knowledge on medicinal aromatic plants.

References

[1] M. N. Alekshun and S. B. Levy, "Molecular mechanisms of antibacterial multidrug resistance," *Cell*, vol. 128, no. 6, pp. 1037–1050, 2007.

[2] A. D. Russell, "Antibiotic and biocide resistance in bacteria: introduction," *Symposium Series Society for Applied Microbiology*, vol. 31, no. 92, pp. 1S–3S, 2002.

[3] D. R. Guay, "Treatment of bacterial skin and skin structure infections," *Expert Opinion on Pharmacotherapy*, vol. 4, no. 8, pp. 1259–1275, 2003.

[4] A. J. Brosnahan and P. M. Schlievert, "Gram-positive bacterial superantigen outside-in signaling causes toxic shock syndrome," *FEBS Journal*, vol. 278, no. 23, pp. 4649–4667, 2011.

[5] K. Fellermann, J. Wehkamp, K. R. Herrlinger, and E. F. Stange, "Crohn's disease: a defensin deficiency syndrome?" *European Journal of Gastroenterology and Hepatology*, vol. 15, no. 6, pp. 627–634, 2003.

[6] L. Chen, S. Lin, R. Agha-Majzoub, L. Overbergh, C. Mathieu, and L. S. Chan, "CCL27 is a critical factor for the development of atopic dermatitis in the keratin-14 IL-4 transgenic mouse model," *International Immunology*, vol. 18, no. 8, pp. 1233–1242, 2006.

[7] J. H. Song, V. Thamlikitkul, and P. R. Hsueh, "Clinical and economic burden of community-acquired pneumonia amongst adults in the Asia-Pacific region," *International Journal of Antimicrobial Agents*, vol. 38, no. 2, pp. 108–117, 2011.

[8] D. A. B. Dance, "Melioidosis," *Current Opinion in Infectious Diseases*, vol. 15, no. 2, pp. 127–132, 2002.

[9] N. J. White, "Melioidosis," *The Lancet*, vol. 361, no. 9370, pp. 1715–1722, 2003.

[10] S. Yang, "Melioidosis research in China," *Acta Tropica*, vol. 77, no. 2, pp. 157–165, 2000.

[11] P. R. Hsueh, L. J. Teng, L. N. Lee et al., "Melioidosis: an emerging infection in Taiwan?" *Emerging Infectious Diseases*, vol. 7, no. 3, pp. 428–433, 2001.

[12] C. Walsh and S. Fanning, "Antimicrobial resistance in food-borne pathogens—a cause for concern?" *Current Drug Targets*, vol. 9, no. 9, pp. 808–815, 2008.

[13] M. Vorachit, P. Chongtrakool, S. Arkomsean, and S. Boonsong, "Antimicrobial resistance in *Burkholderia pseudomallei*," *Acta Tropica*, vol. 74, no. 2-3, pp. 139–144, 2000.

[14] F. M. Thibault, E. Hernandez, D. R. Vidal, M. Girardet, and J. D. Cavallo, "Antibiotic susceptibility of 65 isolates of *Burkholderia pseudomallei* and *Burkholderia mallei* to 35 antimicrobial agents," *Journal of Antimicrobial Chemotherapy*, vol. 54, no. 6, pp. 1134–1138, 2004.

[15] R. L. S. Sikarwar, "Ethnogynaecological uses of plants new to India," *Ethnobotany*, vol. 12, no. 1-2, pp. 112–115, 2002.

[16] R. Siva, "Status of natural dyes and dye-yielding plants in India," *Current Science*, vol. 92, no. 7, pp. 916–925, 2007.

[17] P. Kumar Singh, V. Kumar, R. K. Tiwari, A. Sharma, Ch. V. Rao, and R. H. Singh, "Medico-ethnobotany of 'chatara' block of district sonebhadra, Uttar Pradesh, India," *Advances in Biological Research*, vol. 4, no. 1, pp. 65–80, 2010.

[18] W. H. Lewis and M. P. Elwin-Lewis, *Medical Botany: Plants Affecting Human Health*, John Wiley & Sons, New York, NY, USA, 2003.

[19] R. Perumal Samy, P. N. Pushparaj, and P. Gopalakrishnakone, "A compilation of bioactive compounds from Ayurveda," *Bioinformation*, vol. 3, no. 3, pp. 100–110, 2008.

[20] World Health Organization (WHO), *Traditional Medicine Strategy 2002–2005*, Genera: World Health Organization, Geneva, Switzerland, 2002.

[21] P. S. Haddad, G. A. Azar, S. Groom, and M. Boivin, "Natural health products, modulation of immune function and prevention of chronic diseases," *Evidence Based Complementary and Alternative Medicine*, vol. 2, no. 4, pp. 513–520, 2005.

[22] K. Poonam and G. S. Singh, "Ethnobotanical study of medicinal plants used by the Taungya community in Terai Arc Landscape, India," *Journal of Ethnopharmacology*, vol. 123, no. 1, pp. 167–176, 2009.

[23] G. B. Mahady, "Medicinal plants for the prevention and treatment of bacterial infections," *Current Pharmaceutical Design*, vol. 11, no. 19, pp. 2405–2427, 2005.

[24] V. P. Kumar, N. S. Chauhan, H. Padh, and M. Rajani, "Search for antibacterial and antifungal agents from selected Indian medicinal plants," *Journal of Ethnopharmacology*, vol. 107, no. 2, pp. 182–188, 2006.

[25] R. Nair, T. Kalariya, and S. Chanda, "Antibacterial activity of some plant extracts used in folk medicine," *Journal of Herbal Pharmacotherapy*, vol. 7, no. 3-4, pp. 191–201, 2007.

[26] D. Kalemba and A. Kunicka, "Antibacterial and antifungal properties of essential oils," *Current Medicinal Chemistry*, vol. 10, no. 10, pp. 813–829, 2003.

[27] A. H. Ashour, "Antibacterial, antifungal, and anticancer activities of volatile oils and extracts from stems, leaves, and flowers of *Eucalyptus sideroxylon* and *Eucalyptus torquata*," *Cancer Biology and Therapy*, vol. 7, no. 3, pp. 399–403, 2008.

[28] M. J. Abad, L. M. Bedoya, L. Apaza, and P. Bermejo, "The *Artemisia* L. genus: a review of bioactive essential oils," *Molecules*, vol. 17, no. 3, pp. 2542–2566, 2012.

[29] H. N. Marzoug, M. Romdhane, A. Lebrihi et al., "*Eucalyptus oleosa* essential oils: chemical composition and antimicrobial and antioxidant activities of the oils from different plant parts (stems, leaves, flowers and fruits)," *Molecules*, vol. 16, no. 2, pp. 1695–1709, 2011.

[30] C. Proestos, D. Sereli, and M. Komaitis, "Determination of phenolic compounds in aromatic plants by RP-HPLC and GC-MS," *Food Chemistry*, vol. 95, no. 1, pp. 44–52, 2006.

[31] S. Chao, G. Young, C. Oberg, and K. Nakaoka, "Inhibition of methicillin-resistant *Staphylococcus aureus* (MRSA) by essential oils," *Flavour and Fragrance Journal*, vol. 23, no. 6, pp. 444–449, 2008.

[32] M. Akin, D. Oguz, and H. T. Saracoglu, "Antibacterial effects of some plant extracts from Labiatae (Lamiaceae) growing naturally around Sirnak-Silopi, Turkey," *International Journal of Pharmaceutical and Applied Sciences*, vol. 1, no. 1, pp. 4–47, 2010.

[33] K. Bayoub, T. Baibai, D. Mountassif, A. Retmane, and A. Soukri, "Antibacterial activities of the crude ethanol extracts of medicinal plants against *Listeria monocytogenes* and some other pathogenic strains," *African Journal of Biotechnology*, vol. 9, no. 27, pp. 4251–4258, 2010.

[34] R. P. Samy, P. Gopalakrishnakone, M. Sarumathi, P. Houghton, and S. Ignacimuthu, "Purification of antibacterial agents from *Tragia involucrata*—a popular tribal medicine for wound healing," *Journal of Ethnopharmacology*, vol. 107, no. 1, pp. 99–106, 2006.

[35] K. M. Matthew, *The Flora of Tamil Nadu Carnatic*, Part I–III printed at the Diocesan Press, Madras, India, 1981–1983.

[36] A. W. Bauer, W. M. Kirby, J. C. Sherris, and M. Turck, "Antibiotic susceptibility testing by a standardized single disk method," *American Journal of Clinical Pathology*, vol. 45, no. 4, pp. 493–496, 1966.

[37] National Committee for Clinical Laboratory Standards, *Performance Standards For Antimicrobial Susceptibility Testing, 12th Informational Supplement*, Approved standard M100-S12, National Committee for Clinical Laboratory Standards, Wayne, Pa, USA, 2002.

[38] E. A. Elsinghorst, "Measurement of invasion by gentamicin resistance," *Methods in Enzymology*, vol. 236, pp. 405–420, 1994.

[39] J. B. Harborne, *Phytochemical Methods*, Chapman and Hall, New York, NY, USA, 1976.

[40] H. Wagner, S. Bladt, and E. M. Zgairski, *Plant Drug Analysis*, Springer, New York, NY, USA, 1984.

[41] N. Myers, R. A. Mittermeler, C. G. Mittermeler, G. A. B. da Fonseca, and J. Kent, "Biodiversity hotspots for conservation priorities," *Nature*, vol. 403, no. 6772, pp. 853–858, 2000.

[42] R. Perumal Samy and S. Ignacimuthu, "Antibacterial activity of some folklore medicinal plants used by tribals in Western Ghats

of India," *Journal of Ethnopharmacology*, vol. 69, no. 1, pp. 63–71, 2000.

[43] K. Nampoothiri, A. Chrispal, A. Begum, S. Jasmine, K. G. Gopinath, and A. Zachariah, "A clinical study of renal tubular dysfunction in *Cleistanthus collinus* (Oduvanthalai) poisoning," *Clinical Toxicology*, vol. 48, no. 3, pp. 193–197, 2010.

[44] M. Strathern, *UsefulKnowledge*, The Isiah Berlin Lecture. University of Manchester, Brunswick, UK.

[45] C. N. Sunil and A. K. Pradeep, "(2001) Another new species of *Tripogon* (Poaceae) from India," *Sida*, vol. 19, pp. 803–806, 2005.

[46] S. Biber-Klemm and T. Cottier, *Right To Plant Genetic Resources and Traditional Knowledge: Basic Issues and Prospective*, Oxfordshire, Nosworthy Way, UK, 2006.

[47] V. S. Ramachandran, S. Shijo Joseph, and R. Aruna, "Ethnobotanical studies from amaravathy range of Indira Gandhi Wildlife Sanctuary, Western Ghats, Coimbatore District, Southern India," *Ethnobotanical Leaflets*, vol. 13, pp. 1069–1087, 2009.

[48] A. H. Rajasab and I. Mohamad, "Documentation of folk knowledge on edible wild plants of North Karnataka," *Indian Journal of Traditional Knowledge*, vol. 3, no. 4, pp. 419–429, 2004.

[49] M. Rajadurai, V. G. Vidhya, M. Ramya, and A. Bhaskar, "Ethnomedicinal plants used by the traditional healers of pachamalai hills, Tamilnadu, India," *Studies on Ethno-Medicine*, vol. 3, no. 1, pp. 39–41, 2009.

[50] S. K. Adesina, O. Idowu, A. O. Ogundaini et al., "Antimicrobial constituents of the leaves of *Acalypha wilkesiana* and *Acalypha hispida*," *Phytotherapy Research*, vol. 14, no. 5, pp. 371–374, 2000.

[51] M. T. Gutierrez-Lugo, M. P. Singh, W. M. Maiese, and B. N. Timmermann, "New antimicrobial cycloartane triterpenes from *Acalypha communis*," *Journal of Natural Products*, vol. 65, no. 6, pp. 872–875, 2002.

[52] A. K. Tyagi and A. Malik, "Antimicrobial potential and chemical composition of *Mentha piperita* oil in liquid and vapour phase against food spoiling microorganisms," *Food Control*, vol. 22, no. 11, pp. 1707–1714, 2011.

[53] G. Devendran and U. Balasubramanian, "Qualitative phytochemical screening and GC-MS analysis of *Ocimum sanctum* L. leaves," *Asian Journal of Plant Science and Research*, vol. 1, no. 4, pp. 44–48, 2011.

[54] V. C. Jain, N. M. Patel, D. P. Shah, P. K. Patel, and B. H. Joshi, "Antioxidant and antimicrobial activities of *Alangium salvifolium* (L.f.) Wang root," *Global Journal of Pharmacology*, vol. 4, no. 1, pp. 13–18, 2010.

[55] P. Swapna Latha and K. Kannabiran, "Antimicrobial activity and phytochemicals of *Solanum trilobatum* Linn," *African Journal of Biotechnology*, vol. 5, no. 23, pp. 2402–2404, 2006.

[56] M. Usha1, S. Ragini, and S. M. A. Naqvi, "Antibacterial activity of acetone and ethanol extracts of Cinnamon (*Cinnamomum zeylanicum*) and Ajowan (*Trachyspermum ammi*) on four food spoilage bacteria," *International Research Journal of Biological Sciences*, vol. 1, no. 4, pp. 7–11, 2012.

[57] S. Prabuseenivasan, M. Jayakumar, and S. Ignacimuthu, "*In vitro* antibacterial activity of some plant essential oils," *BMC Complementary and Alternative Medicine*, vol. 6, article 39, pp. 1–8, 2006.

[58] G. A. Ayoola, F. M. Lawore, T. Adelowotan et al., "Chemical analysis and antimicrobial activity of the essential oil of *Syzigium aromaticum* (clove)," *African Journal of Biotechnology*, vol. 7, no. 13, pp. 2227–2231, 2008.

[59] Y. J. Fu, L. Chen, Y. Zu et al., "The antibacterial activity of clove essential oil against *Propionibacterium acnes* and its mechanism of action," *Archives of Dermatology*, vol. 145, no. 1, pp. 86–88, 2009.

[60] D. Venkatesan, C. M. Karrunakarn, S. Selva Kumar, and P. T. Palani Swamy, "Identification of phytochemical constituents of *Aegle marmelos* responsible for antimicrobial activity against selected pathogenic organisms," *Ethnobotanical Leaflets*, vol. 13, pp. 1362–1372, 2009.

[61] P. Arun, K. G. Purushotham, J. Johnsy jayarani, and V. Kumari, "*In vitro* Antibacterial Activity of *Oldenlandia umbellata* an Indian medicinal Plant," *Journal of Pharmaceutical Science and Technology*, vol. 2, no. 4, pp. 198–201, 2010.

[62] A. Manjamalai, R. Sardar Sathyajith Singh, C. Guruvayoorappan, and V. M. Berlin Grace, "Analysis of phytochemical constituents and antimicrobial activity of some medicinal plants in Taminadu, India," *Global Journal of Biotechnology and Biochemistry*, vol. 5, no. 2, pp. 120–128, 2010.

[63] E. Haslam, "Natural polyphenols (vegetable tannins) as drugs: Possible modes of action," *Journal of Natural Products*, vol. 59, no. 2, pp. 205–215, 1996.

[64] Y. Cai, Q. Luo, M. Sun, and H. Corke, "Antioxidant activity and phenolic compounds of 112 traditional Chinese medicinal plants associated with anticancer," *Life Sciences*, vol. 74, no. 17, pp. 2157–2184, 2004.

[65] B. Shan, Y. Z. Cai, M. Sun, and H. Corke, "Antioxidant capacity of 26 spice extracts and characterization of their phenolic constituents," *Journal of Agricultural and Food Chemistry*, vol. 53, no. 20, pp. 7749–7759, 2005.

[66] R. J. W. Lambert, P. N. Skandamis, P. J. Coote, and G.-J. E. Nychas, "A study of the minimum inhibitory concentration and mode of action of oregano essential oil, thymol and carvacrol," *Journal of Applied Microbiology*, vol. 91, no. 3, pp. 453–462, 2001.

[67] M. Raccach, "The antimicrobial activity of phenolic antioxidants in food: a review," *Journal of Food Safety*, vol. 6, no. 3, pp. 141–170, 1984.

[68] M. Taniguchi, Y. Yano, E. Tada et al., "Mode of action of polygodial, an antifungal sesquiterpene dialdehyde," *Agricultural and Biological Chemistry*, vol. 52, no. 6, pp. 1409–1414, 1988.

[69] G. J. E. Nychas, "Natural antimicrobials from plants," in *New Methods of Food Preservation*, G. W. Gould, Ed., pp. 58–89, Blackie Academic, London, UK, 1995.

[70] S. Burt, "Essential oils: their antibacterial properties and potential applications in foods—a review," *International Journal of Food Microbiology*, vol. 94, no. 3, pp. 223–253, 2004.

Hindawi Publishing Corporation
Evidence-Based Complementary and Alternative Medicine
Volume 2013, Article ID 134852, 9 pages
http://dx.doi.org/10.1155/2013/134852

Research Article

Catalpol Induces Neuroprotection and Prevents Memory Dysfunction through the Cholinergic System and BDNF

Dong Wan,[1] LiJun Xue,[2] HuiFeng Zhu,[3,4] and Yong Luo[5]

[1] *Department of Emergency, The First Affiliated Hospital of Chongqing Medical University, Chongqing 400016, China*
[2] *Chongqing Chemical Industry Vocational College, 400020, China*
[3] *College of Pharmaceutical Sciences and Traditional Chinese Medicine, Southwest University, Chongqing 400715, China*
[4] *Chongqing Engineering Research Center for Pharmacological Evaluation, Chongqing 400715, China*
[5] *Department of Neurology, The First Affiliated Hospital of Chongqing Medical University, Chongqing 400016, China*

Correspondence should be addressed to HuiFeng Zhu; zhfbsci@126.com

Received 7 January 2013; Revised 19 June 2013; Accepted 25 July 2013

Academic Editor: Wei Jia

To investigate the role and mechanism of catalpol on neuroprotective effects and memory enhancing effects simultaneously, neuroprotective effects of catalpol were assessed by neurological deficits score, TTC staining, and cerebral blood flow detecting. Morris water maze was employed to investigate its effects on learning and memory and then clarify its possible mechanisms relating the central cholinergic system and BDNF. Edaravone and oxiracetam were used for positive control drugs based on its different action. Results showed that catalpol and edaravone significantly facilitated neurological function recovery, reduced infarction volume, and increased cerebral blood flow in stroke mice. Catalpol and oxiracetam decreased the escape latency significantly and increased the numbers of crossing platform obviously. The levels of ACh, ChAT, and BDNF in catalpol group were increased in a dose-dependent manner, and AChE declined with a U-shaped dose-response curve. Moreover, the levels of muscarinic AChR subtypes M_1 and M_2 in hippocampus were considerably raised by catalpol. These results demonstrated that catalpol may be useful for neuroprotection and memory enhancement, and the mechanism may be related to the central cholinergic system.

1. Introduction

Ischemic stroke remains a leading cause of mortality and long-term disability worldwide in adults. Tissue plasminogen activator (tPA) is the only approved drug for acute ischemic stroke, approved by the Food and Drug Administration for ischemic stroke treatment since 1996 [1]. However, only 1-2% of patients can receive thrombolytic therapy mainly due to the short time window (no more than 3–6 h after stroke) and the possible complication such as hemorrhagic transformation (HT) and brain edema [2]. Although edaravone, a free radical scavenger [3, 4], has been used in Asian countries for many years, it is still not approved by the United States and Europe because of its side effects in liver and kidney and only a small clinical trial found that edaravone might improve outcomes [5–7]. Thus, additional effective new drugs are urgently needed.

Cognitive impairment is a common consequence of stroke affecting one to three quarters of the patients [8, 9], slowing down physical functional recovery [10, 11]. Therefore, targeting cognitive impairments could be a viable approach to facilitate the physical and mental functional recoveries [12, 13]. To date, oxiracetam is shown to improve cognitive ability through increasing brain ACh concentration [14], but its neuroprotective effects on stroke are still not known. In fact, there is a general lack of effective drugs in clinic against cerebral ischemic damage and cognitive deficits simultaneously. So it becomes very important to find out a new drug to treat stroke and improve their cognitive impairment.

Cholinergic signaling is involved in central cognitive processes such as learning and memory [15, 16]; cholinergic deficit is a major neuropathological feature that is associated with memory loss and closely correlated with the severity of cognitive dysfunction in AD [16] and poststroke cognitive

impairments [17, 18]. Cholinergic transmission is terminated mainly by ACh hydrolysis through the acetylcholinesterase (AChE) which is responsible for degradation of ACh to acetate and choline in the synaptic cleft [19]. Thus, modulation of the cholinergic signaling pathway, such as inhibition of AChE, activation of ChAT, and promotion of ACh synthesis, may serve as strategies for the treatment of memory dysfunction due to AD [20] or poststroke cognitive impairments [17, 18].

Catalpol is an important iridoid glycosides compound purified from *Rehmannia glutinosa Libosch* which has been widely used as a traditional Chinese herbal medicine for the treatment of aging diseases and stroke. Our previous research revealed that catalpol can cross BBB into the brain [21] and promote angiogenesis but not aggravate blood-brain barrier leakage in the ischemic brain. Electron microscopic analysis demonstrated that catalpol reduces the edema of microvessels endothelia [22]. Moreover, catalpol can increase the number of synapses [23] and enhance the neuronal axon growth [24], which indicate that catalpol may be a potential protection drug for neurovascular unit. Besides, some researchers reported that catalpol is effective in Alzheimer's disease (AD) [25] and Parkinson's disease (PD) and can improve memory [26]. We also found that stroke rats treated with catalpol are more easily and more quickly to find and grasp the sunflower seeds in the small plate when these rats performed skilled reaching task (data not shown). Evidence above has converged to suggest that catalpol may be a potential agent reducing ischemic damage and enhancing memory. However, the mechanism(s) for these actions has not been well defined.

The present study was aimed at exploring the effects of catalpol on stroke mice and SCOP-induced memory deficits mice, compared with edaravone and oxiracetam. To further study mechanisms of catalpol on stroke and cognitive impairment, ACh, AChE, ChAT, and BDNF in central cholinergic system in hippocampus were investigated.

2. Material and Methods

2.1. Reagent and Drugs. Catalpol was purchased from Liu-bo-bainiao Biotechnology Co., Ltd. (Shijiazhuang, China). The purity of the compound was 99% as assayed by high-performance liquid chromatography analysis. ACh and BDNF (brain-derived neurotrophic factor) ELISA kits (R&D system) were purchased from Beijing Dingguochangsheng Biotechnology Co., Ltd. (Beijing, China). TTC (Sigma), Oxiracetam (Guangdong Sencee Pharmaceutical Co., Ltd.), edaravone (Jilin Province Huinan Changlong Bio-pharmacy Co., Ltd.), and SCOP (Hainan Shuangcheng Pharmaceutical Co., Ltd.) were dissolved in 0.9% physiological saline.

2.2. Animals. 120 Kunming mice were purchased from the Animal Centre, Chongqing Medical University. They (equal numbers of males and females, weighing 25~30 g) were allowed access to water and food ad libitum and maintained at constant temperature (25 ± 1°C) and humidity (55 ± 5%) under a 12 h light/dark cycle (07:00 on to 19:00 off).

2.3. The pMCAO Model and Drug Administration. Except for sham group, all groups established a model of permanent middle cerebral artery occlusion (pMCAO) with introducing a suture into the left internal carotid artery (ICA) through the external left carotid artery (ECA) and occluding the middle cerebral artery (MCA). Sham (0.9% saline), model (0.9% saline), edaravone (7.9 mg/kg), oxiracetam (105 mg/kg), and catalpol (9 mg/kg) were administered intraperitoneally 24 h after stroke and then daily for 3 days.

For the Morris water maze test and biochemical analysis, mice were divided into 7 groups: normal control (normal + 0.9% saline), model (SCOP + 0.9% saline), edaravone (7.9 mg/kg + SCOP) and oxiracetam (105 mg/kg + SCOP) as two positive control groups, three doses of catalpol (1, 3 and 9 mg/kg + SCOP, resp.) as treatment group. Drugs were injected intraperitoneally for three days. In all groups, except for the normal control, learning and memory dysfunction in mice was induced by SCOP (2 mg/kg) intraperitoneal injection 30 min before behavioral testing.

2.4. Zea Longa's Score. After operation, the neurological function of all animals was evaluated daily with a 5-point scale as previously described [27]: (0) no neurologic deficit, (1) failure to extend right forepaw fully, (2) circling to the right, (3) falling to the right, and (4) unable to walk spontaneously and had a depressed level of consciousness.

2.5. Cerebral Blood Flow Ratios. Three days later, blood flow ratio was measured using a laser Doppler blood flow imager (FLPI, Moor Instruments). The ratio was calculated using the following formula:

$$\text{Blood flow ratios} = \frac{[\text{normal (right)} - \text{ischemic (left)}]}{\text{normal (right) brain}}. \quad (1)$$

2.6. TTC Staining. Five mice were taken from each of groups to have a TTC staining 3 days after treatment. The brains were taken and cut into coronal sections. Four sections in each brain were obtained and then put in 0.5% TTC PBS solution for 10 min at 37°C without light exposure and then in 4% paraform PBS to fix. The normal brain tissue stained red and infarction area stained white. BI2000 medical image analysis system was used to count the infarction area after the picture was taken.

2.7. Morris Water Maze Test. The behavioural procedure of Morris water maze was the same as previously described [28, 29]. The maze was a circular pool (80 cm in diameter and 30 cm in height) filled with water and a nontoxic water-soluble black ink. The black platform (10 cm in diameter and 28 cm in height) was centered in one of the four quadrants of the pool and placed 2 cm beneath the surface of the water. Water temperature was maintained at 25 ± 1°C. The numbers of platform-crossing and escape latencies to find the platform were recorded with a video tracking system. During the test, mice were given four trials per day for 3 days with an intertrial interval 2 min. Once the mice reached the platform, it was permitted to remain on it for 10 s. If mouse failed to reach

the platform within 120 s, the escape latencies regarded as 120 s and mice were placed on the platform for 10 s to be induced learning. On the fourth day, the mice were placed in the water at a random point with the platform removed, and the numbers of crossing platform areas were recorded over 120 s. Thirty minutes before the test, mice were injected with SCOP (2 mg/kg) or saline intraperitoneally.

2.8. Biochemical Analysis. Following the Morris water maze test, brains were removed after decapitation. The hippocampi were dissected and homogenized containing 10 volumes of cold physiologic saline. The homogenate (10%) was centrifuged at 4000 ×g for 10 min at 4°C. The contents of ACh and BDNF in the hippocampus were measured by ELISA.

2.9. Western Blot Analysis. After transcardially perfused with 0.9% NaCl solution to rinse out the blood, mice's hippocampus (0.1 g per brain) in each group was separated and weighed for detecting M_1, M_2, AChE, and ChAT by western blot. According to our past reference [22], hippocampus was lysed on ice in lysis buffer (50 mm Tris-HCl (pH 8.2), 0.5 M saccharose, 10 mM HEPES (pH 7.9), 1.5 mM $MgCl_2$, 10 mM KCl, 1 mM EDTA, 10% (v/v) glycerine, 1 mM DTT, 1 mM PMSF, 10 μg/mL Aprotinin, and 5 μg/mL Leupeptin), after centrifugation at 12,000 rpm for 5 minutes. Protein content in cleared lysate was determined by Bradford Assay. Lysate samples containing 40 μg of protein were fractionated by SDS-5% polyacrylamide gel electrophoresis and then electroblotted onto PVDF membranes (Millipore, IPVH00010). The membranes were probed with primary antibodies as rabbit anti-mouse- M_1 (1 : 500, Santa, sc-9106), M_2 (1 : 2000, Abcam, ab109226), AChE (1 : 500, Santa, sc-11409) and ChAT (1 : 500, Millipore, AB143) polyclonal antibody, and mice anti-rabbit β-actin (1 : 1000, Santa, SC-1616R) and then incubated with the horseradish peroxidase-conjugated goat anti-rabbit IgG (1 : 3000; KPL, 074-1506); the PVDF membrane was put into ECL solution. Immunoreactivity was digitally scanned by ScanMaker E6 system and quantified using Alpha Imager Mini (Alpha, American) software. β-actin was used as an internal control for all western blotting.

2.10. Statistical Analysis. Data were expressed as mean ± SEM All data were analyzed by two-way analysis of variance (ANOVA) using the SPSS 11.5 software. Statistical significance was set at $P < 0.05$.

3. Results

3.1. Catalpol but Not Oxiracetam Improves Functional Outcome after pMCAO by Zea Longa's Score. Zea Longa's score of the model group was significantly higher than that of the sham group on days 1, 2, and 3 (Figure 1, $P < 0.01$). Compared to the model group, the edaravone group had significantly decreased Zea Longa's score on days 2 and 3 (Figure 1, $P < 0.01$). The catalpol (9 mg/kg) group had significantly decreased score on day 3 (Figure 1, $P < 0.01$). There was no group difference between the oxiracetam and model groups.

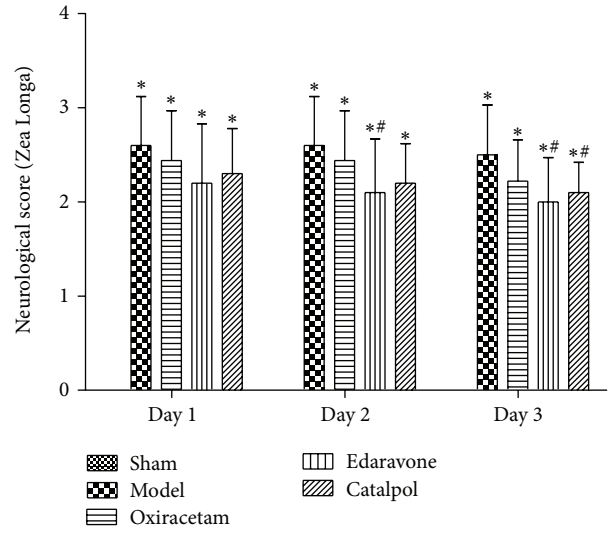

Figure 1: Effect of catalpol on Zea Longa's score at days 1, 2, and 3. The data reported as mean ± SEM ($n = 10$). $^*P < 0.01$ versus sham group. $^\#P < 0.01$ versus model group.

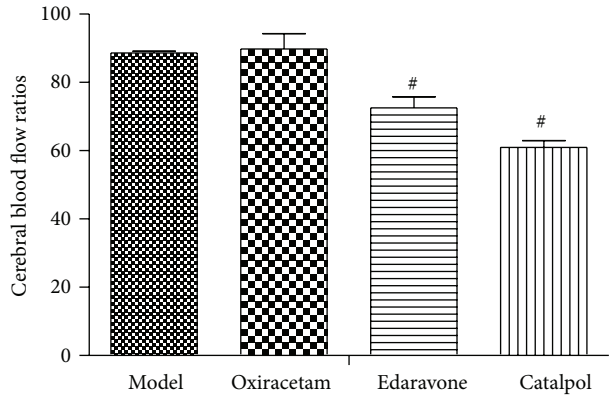

Figure 2: Effect of catalpol on the cerebral blood flow ratios at day 3. The data reported as mean ± SEM ($n = 10$). $^\#P < 0.05$ versus model group.

3.2. Catalpol but Not Oxiracetam Increases the Cerebral Blood Flow. Compared to the model group, the edaravone and catalpol groups significantly decreased cerebral blood flow ratios and increased cerebral blood flow in infarct brain (Figure 2, $P < 0.05$). There was no difference between oxiracetam and model group.

3.3. Catalpol but Not Oxiracetam Reduces Infarct Volume after pMCAO. Treatments with catalpol at 9 mg/kg reduced the total infarct volumes in the permanent model of stroke significantly (Figure 3, $P < 0.05$), and edaravone 7.9 mg/kg also diminished brain damage significantly (Figure 3, $P < 0.05$). However, compared with model group, oxiracetam 105 mg/kg did not reduce the lesion volume in stroke animals (Figure 3, $P > 0.05$).

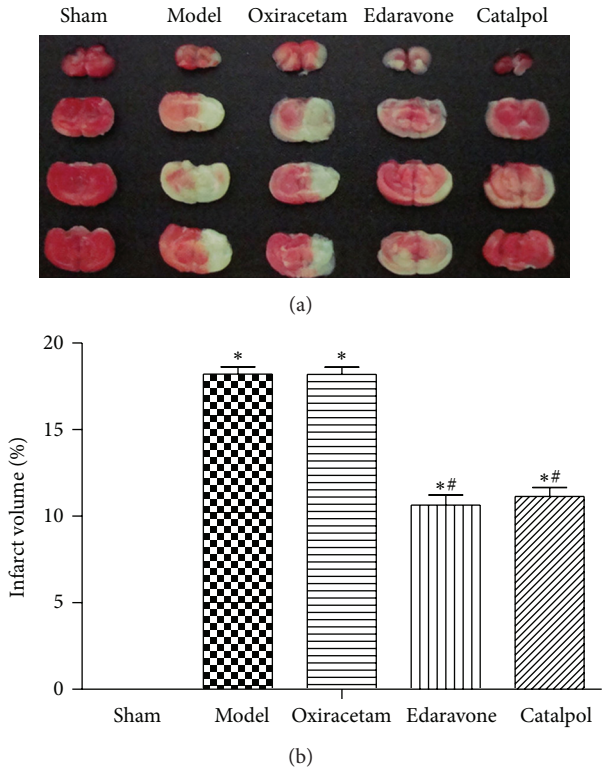

Figure 3: Effect of catalpol on TTC-stained mice brain slice (a) and the infarct volume (b). The data reported as mean ± SEM ($n = 5$). $^{*}P < 0.01$ versus sham group. $^{\#}P < 0.05$ versus model group.

3.4. Catalpol but Not Edaravone Attenuates the Memory Impairments Induced by Scopolamine in the Morris Water Maze Test. The effect of catalpol on spatial learning and memory was investigated in the Morris water maze test (shown in Figure 4). The normal control group rapidly learned the location of the platform. The escape latency of the model group was significantly longer than that of the normal control group on days 2 and 3 (Figure 4(a), $P < 0.05$). As compared with the model group, the oxiracetam and catalpol (9 mg/kg) group significantly decreased the escape latency on days 2 and 3 (Figure 4(a), $P < 0.05$) and the catalpol (3 mg/kg) group also significantly decreased it on day 3 (Figure 4(a), $P < 0.05$). Oxiracetam group and catalpol (1, 3 or 9 mg/kg) significantly increased the numbers of crossing platform areas (Figure 4(b), $P < 0.05$). There was no difference between model group and edaravone group (Figure 4(b), $P > 0.05$).

3.5. Catalpol but Not Edaravone Increases ACh and BDNF Contents in the Hippocampus. As compared with model group (0.199 ± 0.013 ng/L), the ACh level in the hippocampus significantly increased in the normal control group (0.232 ± 0.008 ng/L), the catalpol (3 or 9 mg/kg, 0.254 ± 0.019 or 0.260 ± 0.026 ng/L), and the oxiracetam groups (0.241 ± 0.033 ng/L) (Figure 5(a), $P < 0.01$). But edaravone group was only 0.208 ± 0.020 ng/L; there was no significant difference with model group ($P > 0.05$). The level of BDNF in the hippocampus of the normal control group (0.325 ± 0.011 ng/L) was significantly higher as compared with the model group (0.293 ± 0.032 ng/L) (Figure 5(a), $P < 0.05$). Oxiracetam (0.353 ± 0.034 ng/L) and catalpol (3 or 9 mg/kg, 0.331 ± 0.035 or 0.360 ± 0.023) significantly increased in the BDNF level (Figure 5(a), $P < 0.01$ versus model group). But BDNF level in edaravone group was only 0.298 ± 0.022 ng/L ($P > 0.05$ versus model). Furthermore, the level of BDNF was positively correlated with the ACh level in the hippocampus (Figure 5(b); $r = 0.859$, $P < 0.01$).

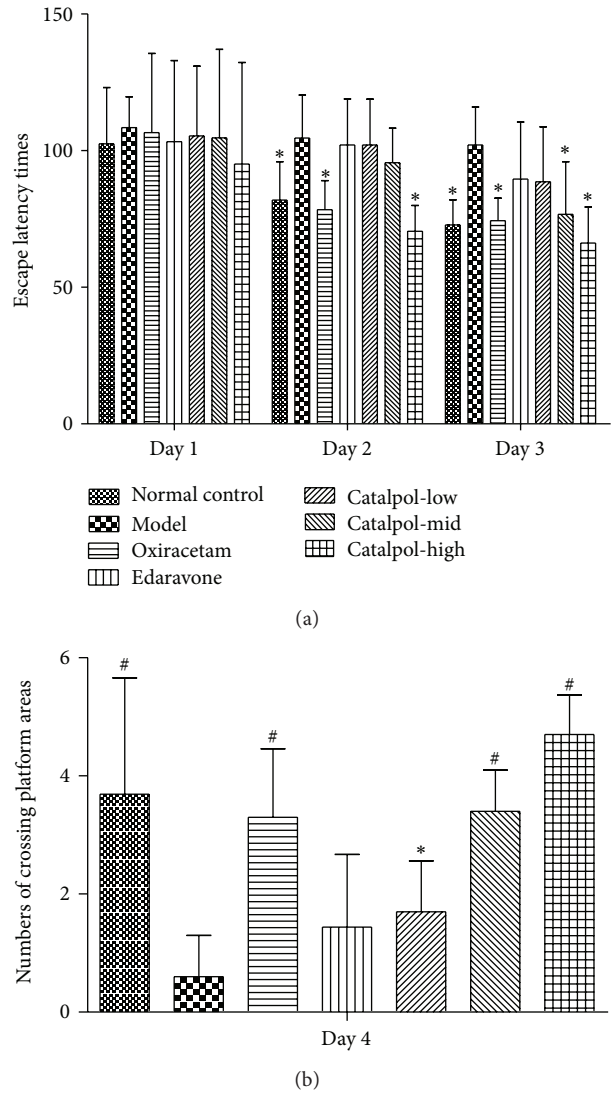

Figure 4: Effect of catalpol on escape latency time (a) and the numbers of crossing platform areas (b). The mice were treated with scopolamine (2 mg/kg i.p.) 30 mins before Morris water maze except for the normal control group. The data represent mean ± SEM ($n = 10$). $^{*}P < 0.05$ versus model group. $^{\#}P < 0.01$ versus model group.

3.6. Catalpol Upregulates ChAT Expression and the Ach Receptor M_1, M_2 Level but Reduces AchE Expression in Hippocampus. Catalpol at 1, 3, 9 mg/kg increased M_1, M_2 expression in a dose-dependent manner. Compared with normal

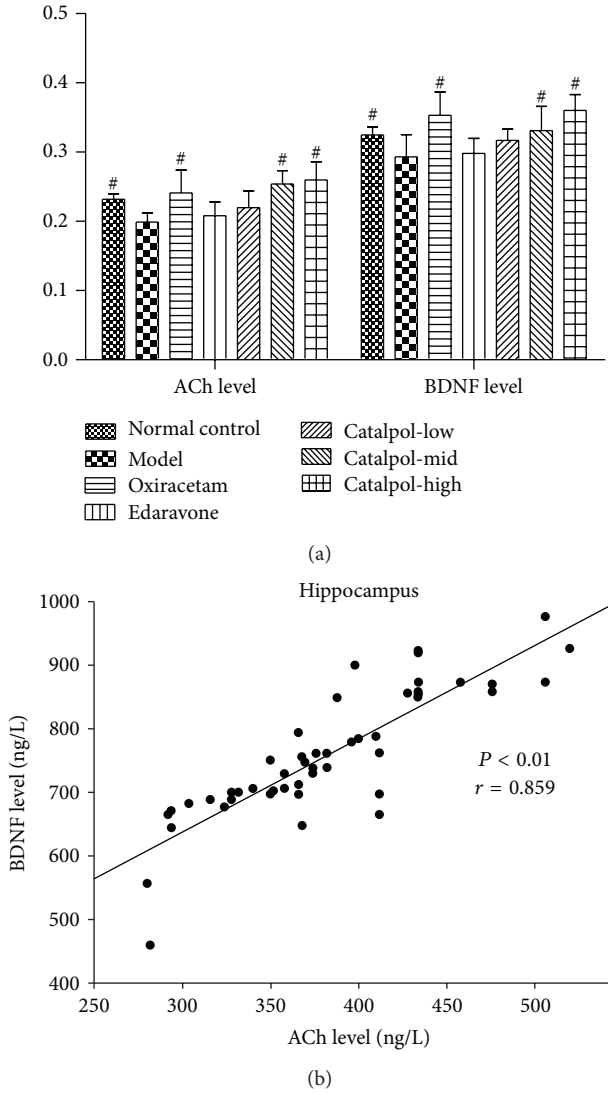

Figure 5: Effect of catalpol on the ACh level (a) and the BDNF level (b), correlations between the ACh level and the BDNF level (b) in hippocampus of mice. The data represent mean ± S.E.M. ($n = 10$). $^{*}P < 0.05$ versus model group. $^{\#}P < 0.01$ versus model group.

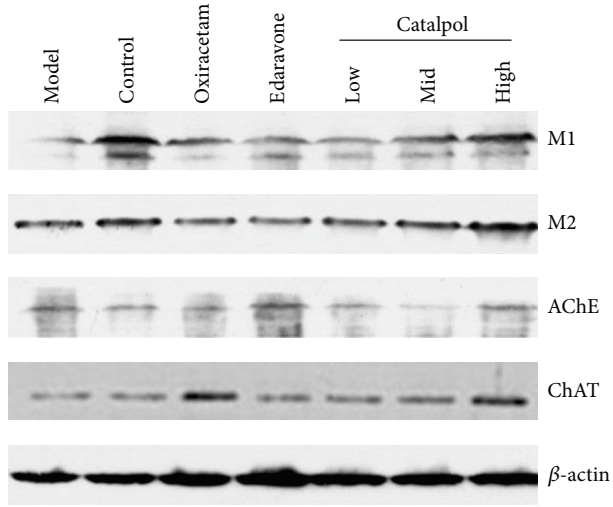

Figure 6: The expression of receptor M_1, M_2, AChE, and ChAT in hippocampus (western blot $n = 5$).

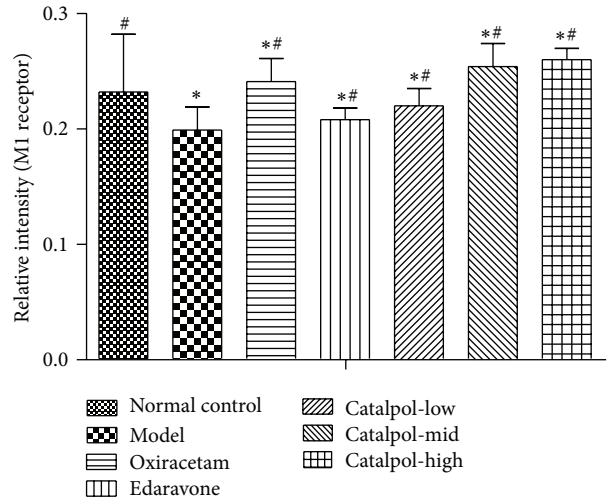

Figure 7: Western blot analysis of the effect of catalpol on the expression of M_1 in hippocampus ($x \pm s, n = 5$). $^{*}P < 0.01$ versus normal group. $^{\#}P < 0.01$ versus the model group.

group, the Ach receptor M_1, M_2 level in the model hippocampus was significantly decreased (Figure 6, $P < 0.01$). This effect was reversed by catalpol and oxiracetam (Figure 6, $P < 0.01$).

As for AChE, although catalpol showed bidirectional regulation on AChE expression, each dose of catalpol decreased AChE expression significantly in hippocampus of mice (Figure 6, $P < 0.01$). Compared with the model group, catalpol at dose of 1, 3 mg/kg reduced AChE expression significantly in a dose-dependent way (Figure 6, $P < 0.01$), but compared with catalpol at dose of 1, 3 mg/kg, catalpol at dose of 9 mg/kg increased the AChE expression, nearing the level of normal group.

But for ChAT, Catalpol significantly upregulated ChAT level at doses of 1, 3, 9 and mg/kg (Figure 6, $P < 0.01$), respectively. Oxiracetam also significantly reduced AChE and upregulated ChAT levels. However, edaravone increased both AChE and ChAT significantly (Figure 6, $P < 0.01$).

The statistical graph of expression of receptor M_1, M_2, AChE, and ChAT in hippocampus is shown in Figures 7, 8, 9, and 10, respectively.

4. Discussion

Cognitive impairment is a common consequence of stroke and impacts on recovery of sensorimotor functions after stroke [8]. However, there is a lack of drugs that not only improve cognitive status effectively but also promote function recovery after stroke. The dilemma has raised the discovery of new drugs to an issue of major importance.

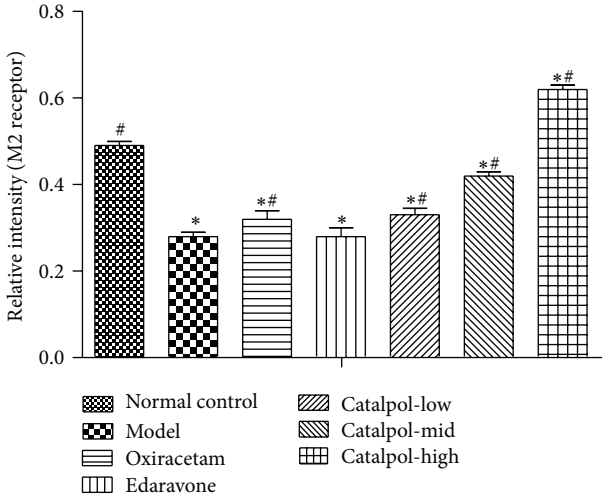

Figure 8: Western blot analysis of the effect of Catalpol on the expression of M_2 in hippocampus ($x \pm s$, $n = 5$). $^{*}P < 0.01$ versus normal group. $^{\#}P < 0.01$ versus model group.

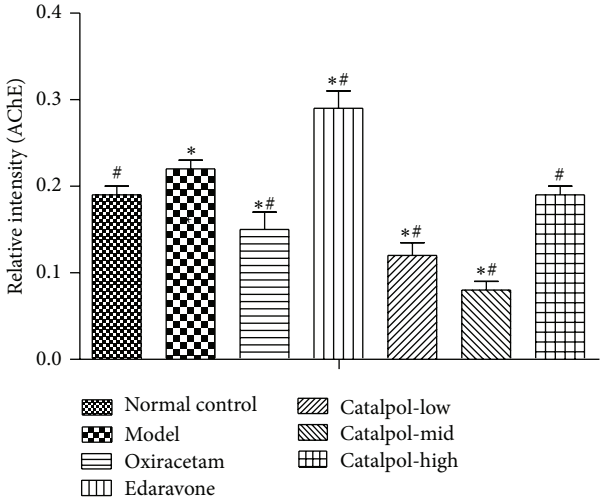

Figure 9: Western blot analysis of the effect of Catalpol on the expression of AChE in hippocampus ($x \pm s$, $n = 5$). $^{*}P < 0.01$ versus normal group. $^{\#}P < 0.01$ versus model group.

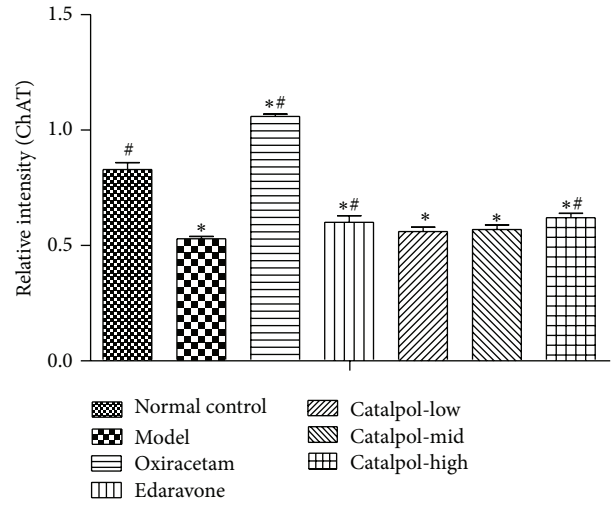

Figure 10: Western blot analysis of the effect of Catalpol on the expression of ChAT in hippocampus ($x \pm s$, $n = 5$). $^{*}P < 0.01$ versus normal group. $^{\#}P < 0.01$ versus model group.

The present work revealed that catalpol has a neuroprotective effect against cerebral ischemic damage and memory-enhancing effects and disclosed a novel mechanism; that is, catalpol could improve memory function via mediating Cholinergic signaling pathway.

In our study, we employed cerebral ischemic stroke model to confirm catalpol's neuroprotective effects. As expected, an obvious improvement of neurological function was found in ischemic mice treatment with catalpol, a marked reduction in the infarction volume validated the catalpol's neuroprotection against cerebral ischemic damage. Further studies demonstrated that catalpol facilitated cerebral blood flow restoration, which would be in accordance with infarct volume reduction. However, oxiracetam, a nootropic agent, which is known to improve both learning and memory processes and used for treatment of various cognitive disorders, did not reduce the infarction volume. The experimental results presented here, in line with previous observations [30, 31], supported that catalpol may be a promising candidate as a treatment of choice for neuroprotection after stroke.

Scopolamine (SCOP), a blocker of muscarinic acetylcholine receptor (mAChR), induces cognitive deficit in various animals [32]. Acute and systemic administration of SCOP in young animals provides the appropriate memory deficits related to the cholinergic deficit in AD, senile CNS dysfunction, or poststroke cognitive impairment. So SCOP-induced amnesic model has been widely used to provide a pharmacological model of memory dysfunction for screening potential cognition enhancing agents [33, 34]. In the present study, the effect of improving memory deficit of catalpol was evaluated using the amnesic mouse model induced by SCOP using Morris water maze test and biochemical assessments. In the Morris water maze test, if the animals spent more time and swam a longer distance in the pool quadrant where the platform had previously been placed during the training session, this would indicate that the animals learned from prior experience with the Morris water maze test, showing the spatial memory improvement [31, 35]. Mice treated with SCOP showed a more prolonged escape latency than mice in the normal control group. Catalpol and oxiracetam, but not edaravone, lowered the escape latency and significantly increased the number of times of crossing over the platform site comparable to the control group. It is important to notice that the Morris water maze test investigating spatial learning and memory has been used in detecting changes of the central cholinergic system [33, 36]. Therefore, these results suggested that catalpol can improve the long-term memory in SCOP-induced memory impairments and may be involved in mediation of the cholinergic nervous system.

Previous studies suggested that the central cholinergic system plays an important role in learning and memory [37].

Damage to the cholinergic system (acetylcholine producing) in the brain has been shown to be plausibly associated with the memory deficits associated with Alzheimer's disease [38] and poststroke dementia (PSD) [17, 18]. After release from the nerve terminal, ACh may bind with cholinoceptors or split into choline and acetate by acetylcholinesterase (AChE). In an in vivo study as a model of dementia treated with SCOP, cholinergic neurotransmission was obstructed leading to an increase of the AChE and impaired cognition [19]. The cholinesterase inhibitors act primarily where ACh is released and work as an amplifier of endogenous ACh. ChAT, the biosynthetic enzyme for ACh, is presently the most specific cholinergic marker for checking the functional state of cholinergic neurons in the CNS and peripheral nervous system [39, 40]. According to the cholinergic hypothesis, memory impairments in patients with senile dementia are due to a selective and irreversible deficiency in the cholinergic functions in the brain [41, 42]. Therefore, downregulation of AChE and upregulation of ChAT may compensate for reduced ACh levels in brains with AD disease or stroke and may facilitate ischemia-induced memory functional recovery.

To elucidate the underlying mechanisms of memory enhancing effects of catalpol, contents of ACh, AChE, ChAT, and muscarinic ACh receptors M_1 and M_2 as cholinergic markers were assessed using hippocampus homogenates. The current work displayed that catalpol and oxiracetam both significantly increased the ACh concentration in the hippocampus. Further examinations demonstrated that catalpol treatment mainly upregulated the expression of ChAT in a dose-dependent manner but did not show dose dependently downregulated expression of AChE in hippocampus. Although each dose of catalpol significantly reduced AChE expression compared with the model group, middle (3 mg/kg) dose of catalpol induced the lowest expression level in AChE compared to the high (9 mg/kg) dose, which may be a negative feedback from the higher dose. This phenomenon may be in part explained by that high concentration of neurotransmitters such as acetylcholine or glutamate would suppress the synaptic transmission by an action at a presynaptic autoreceptor and activate its degrading enzyme production such as AChE, which results in a U-shaped dose-response curve [43]. Further studies would be needed to explore the interesting dosage effects and its exact mechanism(s). Oxiracetam treatment not only significantly reduced AChE but also increased ChAT. However, edaravone obviously increased both AChE and ChAT. It is well known that AChE accelerates ACh degradation, which neutralizes ChAT action on ACh production, and this finding well explained why edaravone fails to improve learning or memory behaviour in our study. In fact, partly in consistent with our result, scopolamine caused impairment in memory associated with reduced acetylcholine (ACh) level and elevated acetylcholinesterase (AChE) activity previously [44]. Oxiracetam (100 mg/kg, ip) significantly prevented the SCOP-induced memory impairment in mice [14], and edaravone (6 mg/kg) gave no protection to the learning and memory capability in a rat model of neonatal hypoxic-ischemic encephalopathy; 9 mg/kg edaravone has no amelioration on learning and memory deficit at 5 d or 10 d [45]. Doses of Oxiracetam and edaravone were chosen in our study on the basis of previously conducted behavioral studies that produced differential effects in cognitive performance, when the body surface area normalization method was used. Thus, modification of cholinergic systems via modulation of AChE, ChAT protein expressions, and elevation of ACh level was, at least in part, linked closely with the antiamnesic effect of catalpol on SCOP-induced impairment of learning and memory.

Muscarinic acetylcholine receptors (mAChR) control the time course of evoked ACh release [46] and play essential role in memory formation. Until now, at least five well-characterized subtypes of mAChR (M_1–M_5) have been found in the brain, in which M_1 and M_2 are mainly expressed in the hippocampus and cortex [47, 48]. M_1 has a close relation with motor and memory; M_2 has a relation to ACh release; antagonism of M_2 will worsen memory impairment [48]. Our results showed that SCOP-induced mice had lower level of M_1 and M_2 in the hippocampus than mice from the normal control group. Catalpol and oxiracetam reversed the effects partly. Notably, Catalpol upregulated the M_1 and M_2 expression in a dose-dependent manner, and even more, the M_2 level in catalpol groups (except for 1 mg/kg) was significantly higher than that of the normal control group. Thus, it could be deduced that catalpol-induced cognitive ameliorative effects may be related to controlling ACh release via regulating the expression of muscarinic ACh receptors, which implies that catalpol has multiple action sites in the cholinergic pathway.

Brain-derived neurotrophic factor (BDNF) is a key regulator in the formation of memory [49], and there are positive feedbacks between ACh and BDNF in the rat hippocampus [50]. BDNF interaction with tropomyosin-related kinase B receptors and presynaptic muscarinic receptors modulates transmitter release in adult rodent motor nerve terminal, which can improve stroke motor function recovery [51]. Previous studies reported that catalpol increased the hippocampal neuroplasticity in the aged rats [52] and attenuated MPTP-induced neuronal degeneration of nigral-striatal dopaminergic pathway in mice [53] partly attributed to BDNF upregulation. At the same time, higher BDNF level, together with ACh, is beneficial to brain plasticity and the induction of specific, associative detail behavioral memory [54, 55] and synaptogenesis [56]. In line with previous studies, our results showed that catalpol can upregulate BDNF level and here existed the strong positive correlation between the ACh level and the BDNF level in the hippocampus ($r = 0.859$, $P < 0.01$), which are together beneficial to memory improvement and to explain from another side why catalpol ameliorated memory impairments in the SCOP-induced amnesic mice.

In summary, we report in this experiment that advantage of catalpol is its ability not only to protect ischemic damage but also improve memory through multiple mechanisms of action, including increasing ACh production by the promotion of ChAT, inhibition of AChE, and upregulating M_1 and M_2 expression together with increasing BDNF generation.

The development of such herbal medicines capable of targeting multiple sites could be useful for future drug discovery and the potential management of stroke diseases.

Authors' Contribution

Dong Wan and LiJun Xue contributed equally to this work.

Acknowledgments

This work was supported by the National Natural Science Foundation of China (81073084), Natural Science Foundation Project of CQ CSTC (2010BB5127), and Fundamental Research Funds for the Central Universities (XDJK2012B010, XDJK2009C081). The authors gratefully acknowledge Ming Li, Ph.D. in Department of Psychology University of Nebraska-Lincoln for his review and helpful comments regarding this paper.

References

[1] W.-H. Chen, H.-S. Lin, C.-I. Chen, M.-S. Chou, C.-W. Liou, and S.-S. Chen, "The medicolegal issue of tissue plasminogen activator in ischemic stroke: a review of judiciary decrees in Taiwan," *Acta Neurologica Taiwanica*, vol. 20, no. 3, pp. 163–171, 2011.

[2] K. Birmingham, "Future of neuroprotective drugs in doubt," *Nature Medicine*, vol. 8, no. 1, p. 5, 2002.

[3] H. Yoshida, H. Yanai, Y. Namiki, K. Fukatsu-Sasaki, N. Furutani, and N. Tada, "Neuroprotective effects of edaravone: a novel free radical scavenger in cerebrovascular injury," *CNS Drug Reviews*, vol. 12, no. 1, pp. 9–20, 2006.

[4] K. Kikuchi, H. Uchikado, N. Miyagi et al., "Beyond neurological disease: new targets for edaravone (Review)," *International Journal of Molecular Medicine*, vol. 28, no. 6, pp. 899–906, 2011.

[5] S. Feng, Q. Yang, M. Liu et al., "Edaravone for acute ischaemic stroke," *Cochrane Database of Systematic Reviews*, vol. 12, Article ID CD007230, 2011.

[6] H. P. Adams Jr., G. Del Zoppo, M. J. Alberts et al., "Guidelines for the early management of adults with ischemic stroke: a guideline from the American heart association/American stroke association stroke council, clinical cardiology council, cardiovascular radiology and intervention council, and the atherosclerotic peripheral vascular disease and quality of care outcomes in research interdisciplinary working groups: the American Academy of Neurology affirms the value of this guideline as an educational tool for neurologists," *Stroke*, vol. 38, no. 5, pp. 1655–1711, 2007.

[7] E. C. Jauch, J. L. Saver, H. P. Adams Jr. et al., "Guidelines for the early management of patients with acute ischemic stroke: a guideline for healthcare professionals from the American Heart Association/American Stroke Association," *Stroke*, vol. 44, no. 3, pp. 870–947, 2013.

[8] H.-P. Haring, "Cognitive impairment after stroke," *Current Opinion in Neurology*, vol. 15, no. 1, pp. 79–84, 2002.

[9] S. D. Makin, S. Turpin, M. S. Dennis et al., "Cognitive impairment after lacunar stroke: systematic review and meta-analysis of incidence, prevalence and comparison with other stroke subtypes," *Journal of Neurology, Neurosurgery & Psychiatry*, vol. 84, pp. 893–900, 2013.

[10] P. A. Celnik and L. G. Cohen, "Modulation of motor function and cortical plasticity in health and disease," *Restorative Neurology and Neuroscience*, vol. 22, no. 3-4, pp. 261–268, 2004.

[11] C. M. Cirstea, A. Ptito, and M. F. Levin, "Feedback and cognition in arm motor skill reacquisition after stroke," *Stroke*, vol. 37, no. 5, pp. 1237–1242, 2006.

[12] A. J. Orrell, F. F. Eves, and R. S. W. Masters, "Motor learning of a dynamic balancing task after stroke: Implicit implications for stroke rehabilitation," *Physical Therapy*, vol. 86, no. 3, pp. 369–380, 2006.

[13] M. Cao, M. Ferrari, R. Patella, C. Marra, and M. Rasura, "Neuropsychological findings in young-adult stroke patients," *Archives of Clinical Neuropsychology*, vol. 22, no. 2, pp. 133–142, 2007.

[14] L. de Angelis and C. Furlan, "The effects of ascorbic acid and oxiracetam on scopolamine-induced amnesia in a habituation test in aged mice," *Neurobiology of Learning and Memory*, vol. 64, no. 2, pp. 119–124, 1995.

[15] P. E. Gold, "Acetylcholine modulation of neural systems involved in learning and memory," *Neurobiology of Learning and Memory*, vol. 80, no. 3, pp. 194–210, 2003.

[16] M. E. Hasselmo, "The role of acetylcholine in learning and memory," *Current Opinion in Neurobiology*, vol. 16, no. 6, pp. 710–715, 2006.

[17] R. N. Kalaria and C. Ballard, "Stroke and cognition," *Current Atherosclerosis Reports*, vol. 3, no. 4, pp. 334–339, 2001.

[18] K. Ofek and H. Soreq, "Cholinergic involvement and manipulation approaches in multiple system disorders," *Chemico-Biological Interactions*, vol. 203, no. 1, pp. 113–119, 2013.

[19] C. G. Ballard, N. H. Greig, A. L. Guillozet-Bongaarts, A. Enz, and S. Darvesh, "Cholinesterases: roles in the brain during health and disease," *Current Alzheimer Research*, vol. 2, no. 3, pp. 307–318, 2005.

[20] M. Heinrich and H. L. Teoh, "Galanthamine from snowdrop—the development of a modern drug against Alzheimer's disease from local Caucasian knowledge," *Journal of Ethnopharmacology*, vol. 92, no. 2-3, pp. 147–162, 2004.

[21] Y. He, H. Zhu, W. Li, G. Chen, Z. Li, and X. Xu, "HPLC determination of catalpol in cerebrospinal fluid of rats," *Zhongguo Zhongyao Zazhi*, vol. 34, no. 13, pp. 1717–1719, 2009.

[22] H.-F. Zhu, D. Wan, Y. Luo, J.-L. Zhou, L. Chen, and X.-Y. Xu, "Catalpol increases brain angiogenesis and up-regulates VEGF and EPO in the rat after permanent middle cerebral artery occlusion," *International Journal of Biological Sciences*, vol. 6, no. 5, pp. 443–453, 2010.

[23] D. Wan, H. Zhu, Y. Luo, and P. Xie, "Changes in synapse quantity and growth associated protein 43 expression in the motor cortex of focal cerebral ischemic rats following catalpol treatment," *Neural Regeneration Research*, vol. 6, no. 18, pp. 1380–1385, 2011.

[24] D. Wan, H.-F. Zhu, Y. Luo, P. Xie, and X.-Y. Xu, "Study of catalpol promoting axonal growth for cultured cortical neurons from rats," *China Journal of Chinese Materia Medica*, vol. 32, no. 17, pp. 1771–1774, 2007.

[25] Z. Xia, R. Zhang, P. Wu, Z. Xia, and Y. Hu, "Memory defect induced by beta-amyloid plus glutamate receptor agonist is alleviated by catalpol and donepezil through different mechanisms," *Brain Research*, vol. 1441, pp. 27–37, 2012.

[26] X.-L. Zhang, L.-J. An, Y.-M. Bao, J.-Y. Wang, and B. Jiang, "d-galactose administration induces memory loss and energy metabolism disturbance in mice: protective effects of catalpol," *Food and Chemical Toxicology*, vol. 46, no. 8, pp. 2888–2894, 2008.

[27] E. Z. Longa, P. R. Weinstein, S. Carlson, and R. Cummins, "Reversible middle cerebral artery occlusion without craniectomy in rats," *Stroke*, vol. 20, no. 1, pp. 84–91, 1989.

[28] M. M. McClure, S. W. Threlkeld, and R. H. Fitch, "Auditory processing and learning/memory following erythropoietin administration in neonatally hypoxic-ischemic injured rats," *Brain Research*, vol. 1132, no. 1, pp. 203–209, 2007.

[29] M. Onozuka, K. Watanabe, S. M. Mirbod et al., "Reduced mastication stimulates impairment of spatial memory and degeneration of hippocampal neurons in aged SAMP8 mice," *Brain Research*, vol. 826, no. 1, pp. 148–153, 1999.

[30] D.-Q. Li, Y. Li, Y. Liu, Y.-M. Bao, B. Hu, and L.-J. An, "Catalpol prevents the loss of CA1 hippocampal neurons and reduces working errors in gerbils after ischemia-reperfusion injury," *Toxicon*, vol. 46, no. 8, pp. 845–851, 2005.

[31] A. Blokland, E. Geraerts, and M. Been, "A detailed analysis of rats' spatial memory in a probe trial of a Morris task," *Behavioural Brain Research*, vol. 154, no. 1, pp. 71–75, 2004.

[32] W. W. Beatty, N. Butters, and D. S. Janowsky, "Patterns of memory failure after scopolamine treatment: implications for cholinergic hypotheses of dementia," *Behavioral and Neural Biology*, vol. 45, no. 2, pp. 196–211, 1986.

[33] M.-R. Lee, B.-S. Yun, S.-Y. Park et al., "Anti-amnesic effect of Chong-Myung-Tang on scopolamine-induced memory impairments in mice," *Journal of Ethnopharmacology*, vol. 132, no. 1, pp. 70–74, 2010.

[34] U. Ebert and W. Kirch, "Scopolamine model of dementia: electroencephalogram findings and cognitive performance," *European Journal of Clinical Investigation*, vol. 28, no. 11, pp. 944–949, 1998.

[35] A. Blokland, A. Şik, and F. J. van der Staay, "Delayed nonmatching to position performance in aged hybrid Fischer 344 × Brown Norway rats: a longitudinal study," *Brain Research Bulletin*, vol. 64, no. 1, pp. 39–46, 2004.

[36] R. D'Hooge and P. P. De Deyn, "Applications of the Morris water maze in the study of learning and memory," *Brain Research Reviews*, vol. 36, no. 1, pp. 60–90, 2001.

[37] A. Blokland, "Acetylcholine: a neurotransmitter for learning and memory?" *Brain Research Reviews*, vol. 21, no. 3, pp. 285–300, 1995.

[38] P. T. Francis, A. M. Palmer, M. Snape, and G. K. Wilcock, "The cholinergic hypothesis of Alzheimer's disease: a review of progress," *Journal of Neurology Neurosurgery and Psychiatry*, vol. 66, no. 2, pp. 137–147, 1999.

[39] Y. Oda, "Choline acetyltransferase: the structure, distribution and pathologic changes in the central nervous system," *Pathology International*, vol. 49, no. 11, pp. 921–937, 1999.

[40] S. Kasashima, A. Kawashima, Y. Muroishi, H. Futakuchi, I. Nakanishi, and Y. Oda, "Neurons with choline acetyltransferase immunoreactivity and mRNA are present in the human cerebral cortex," *Histochemistry and Cell Biology*, vol. 111, no. 3, pp. 197–207, 1999.

[41] A. Giraldi, P. Alm, V. Werkström, L. Myllymäki, G. Wagner, and K. E. Andersson, "Morphological and functional characterization of a rat vaginal smooth muscle sphincter," *International Journal of Impotence Research*, vol. 14, no. 4, pp. 271–282, 2002.

[42] R. Galani, O. Lehmann, T. Bolmont et al., "Selective immunolesions of CH4 cholinergic neurons do not disrupt spatial memory in rats," *Physiology and Behavior*, vol. 76, no. 1, pp. 75–90, 2002.

[43] E. J. Calabrese, "U-shaped dose response in behavioral pharmacology: historical foundations," *Critical Reviews in Toxicology*, vol. 38, no. 7, pp. 591–598, 2008.

[44] S. Tota, C. Nath, A. K. Najmi, R. Shukla, and K. Hanif, "Inhibition of central angiotensin converting enzyme ameliorates scopolamine induced memory impairment in mice: role of cholinergic neurotransmission, cerebral blood flow and brain energy metabolism," *Behavioural Brain Research*, vol. 232, no. 1, pp. 66–76, 2012.

[45] J. I. Noor, T. Ikeda, K. Mishima et al., "Short-term administration of a new free radical scavenger, edaravone, is more effective than its long-term administration for the treatment of neonatal hypoxic-ischemic encephalopathy," *Stroke*, vol. 36, no. 11, pp. 2468–2474, 2005.

[46] D. A. Brown, "Muscarinic acetylcholine receptors (mAChRs) in the nervous system: some functions and mechanisms," *Journal of Molecular Neuroscience*, vol. 41, no. 3, pp. 340–346, 2010.

[47] A. I. Levey, "Muscarinic acetylcholine receptor expression in memory circuits: implications for treatment of Alzheimer disease," *Proceedings of the National Academy of Sciences of the United States of America*, vol. 93, no. 24, pp. 13541–13546, 1996.

[48] L. AI, "Immunological localization of M1-M5 muscarinic acetyleheline recertors in periphraltissues and brain," *Life Sciences*, vol. 52, no. 5-6, pp. 441–448, 1993.

[49] P. Barnes and K. L. Thomas, "Proteolysis of proBDNF is a key regulator in the formation of memory," *PLoS ONE*, vol. 3, no. 9, Article ID e3248, 2008.

[50] M. Knipper, M. De Penha Berzaghi, A. Blochl, H. Breer, H. Thoenen, and D. Lindholm, "Positive feedback between acetylcholine and the neurotrophins nerve growth factor and brain-derived neurotrophic factor in the rat hippocampus," *European Journal of Neuroscience*, vol. 6, no. 4, pp. 668–671, 1994.

[51] N. Garcia, M. Tomàs, M. M. Santafé, N. Besalduch, M. A. Lanuza, and J. Tomàs, "The interaction between tropomyosin-related kinase B receptors and presynaptic muscarinic receptors modulates transmitter release in adult rodent motor nerve terminals," *Journal of Neuroscience*, vol. 30, no. 49, pp. 16514–16522, 2010.

[52] J. Liu, Q.-J. He, W. Zou et al., "Catalpol increases hippocampal neuroplasticity and up-regulates PKC and BDNF in the aged rats," *Brain Research*, vol. 1123, no. 1, pp. 68–79, 2006.

[53] G. Xu, Z. Xiong, Y. Yong et al., "Catalpol attenuates MPTP induced neuronal degeneration of nigral-striatal dopaminergic pathway in mice through elevating glial cell derived neurotrophic factor in striatum," *Neuroscience*, vol. 167, no. 1, pp. 174–184, 2010.

[54] N. M. Weinberger, A. A. Miasnikov, and J. C. Chen, "Sensory memory consolidation observed: increased specificity of detail over days," *Neurobiology of Learning and Memory*, vol. 91, no. 3, pp. 273–286, 2009.

[55] N. M. Weinberger, "The nucleus basalis and memory codes: auditory cortical plasticity and the induction of specific, associative behavioral memory," *Neurobiology of Learning and Memory*, vol. 80, no. 3, pp. 268–284, 2003.

[56] H. B. Peng, J.-F. Yang, Z. Dai et al., "Differential effects of neurotrophins and Schwann cell-derived signals on neuronal survival/growth and synaptogenesis," *Journal of Neuroscience*, vol. 23, no. 12, pp. 5050–5060, 2003.

Hindawi Publishing Corporation
Evidence-Based Complementary and Alternative Medicine
Volume 2013, Article ID 834027, 11 pages
http://dx.doi.org/10.1155/2013/834027

Research Article

Oral Administration of Alkylglycerols Differentially Modulates High-Fat Diet-Induced Obesity and Insulin Resistance in Mice

Mingshun Zhang,[1,2] Shuna Sun,[3] Ning Tang,[1] Wei Cai,[1,4] and Linxi Qian[1,4]

[1] *Xinhua Hospital, Shanghai Institute for Pediatric Research, Shanghai Jiao Tong University, School of Medicine, Shanghai 200092, China*
[2] *Department of Immunology, Nanjing Medical University, Nanjing 210029, China*
[3] *Fudan Children's Hospital, Fudan University, School of Medicine, Shanghai 201102, China*
[4] *Shanghai Key Laboratory of Pediatric Gastroenterology and Nutrition, Shanghai 200092, China*

Correspondence should be addressed to Wei Cai; caiw204@yahoo.com.cn and Linxi Qian; microtuble@gmail.com

Received 1 January 2013; Accepted 5 June 2013

Academic Editor: Wei Jia

Alkylglycerols (AKGs) from shark liver oil (SLO) were demonstrated to have strong potency to stimulate immune response. However, no study has been conducted on the effects of AKGs on diet-induced obesity and metabolic inflammatory disorder. The purpose of the present study was to investigate the effect of two AKGs isoforms on obesity and insulin resistance in mice fed high-fat (HF) diet. Forty-eight C57BL/6 mice were divided into normal, HF, HF + 20 mg/kg selachyl alcohol (SA), HF + 200 mg/kg SA, HF + 20 mg/kg batyl alcohol (BA), and HF + 200 mg/kg BA groups. Body weight, fasting glucose, lipids, insulin and leptin levels, serum IL-1β, and TNF-α levels were compared among different groups. Our results showed that high-dose SA decreased body weight, serum triglyceride, cholesterol, fasting glucose level, insulin level, and serum leptin level of the HF fed mice, while high-dose BA increased fasting insulin level of the HF fed mice. Pretreatment of primary adipocytes with 10 μM SA or BA differentially modulates LPS-mediated MAPK and NF-κB signaling. Our study demonstrated that oral administration of AKGs has differential effects on HF-induced obesity and metabolic inflammatory disorder in mice.

1. Introduction

Obesity has become a common public health issue with a cluster of metabolic abnormalities. The incidence of obesity-related chronic diseases is increasing rapidly worldwide [1]. Evidence has accumulated indicating that obesity is closely associated with a state of systematic, low-grade inflammation characterized by activation of inflammatory signaling pathways and abnormal cytokine production in adipose tissue [2, 3]. The cytokines produced by adipocytes include several inflammatory markers such as interleukin (IL)-6, tumor necrosis factor (TNF)-α, and monocyte chemoattractant protein (MCP)-1 [4]. These cytokines are elevated in patients with obesity and insulin resistance and are highly associated with the development of cardiovascular diseases and type 2 diabetes mellitus.

Recently, dietary supplements have been used for prevention of obesity and diabetes mellitus due to their high compliance and low toxicity. Shark liver oil (SLO), a well-known dietary supplement, contains alkylglycerols (AKGs), squalene, and essential fatty acids [5]. It has recently been shown that SLO has various pharmacological benefits such as chemoprotective properties against reactive oxygen species as well as anti-inflammatory, antibacterial, antifungal, and anticancer potency [6]. AKGs, the major component of SLO, are glycerol ether lipids that have structural characteristics of an ether linkage between fatty acid and α-position of the glycerol backbone. According to the fatty acid chain length and the number of double bonds, several derivatives of AKGs have been identified. They include such substances as batyl alcohol (BA), chimyl alcohol (CA), and selachyl alcohol (SA) [7]. SA, the predominant component of bioactive AKGs in the

SLO (accounting for 59.4%), contains an unsaturated bond in the long hydrocarbon chain (18C:1). CA and BA, which are saturated in their hydrocarbon chains (16C:0 CA, 18C:0 BA), account for a minor proportion of SLO (9.1% CA, 2.8% BA) [6]. AKGs are also found in immune organs such as bone marrow and spleen, indicating their important role in human immune activity [8]. AKGs mainly function by stimulating immune response to enhance the human defense against inflammation [9]. AKGs can also be applied to treat leukemia and solid tumor as well [10]. It was demonstrated that AKGs can inhibit the growth, vascularization, and dissemination of lung carcinoma tumors in mice [11, 12].

The antidiabetic effects of various bioactive food components have gained widespread attention. However, it was also demonstrated that some nutrients such as selenium have side-effect on energy metabolism if they are supplemented inappropriately [13]. AKGs have been shown to have capability of activating cytotoxic macrophages leading to an enhanced phagocytosis and elevating Th-1 cytokines such as TNF-α which are required for macrophage activation [14]. Adipose tissue macrophages play a key role in obesity-induced inflammation and insulin resistance [15]. However, no study has been conducted on the effects of AKGs on diet-induced obesity and metabolic inflammatory disorder. It is interesting to explore how AKGs affect energy metabolism if consumed daily as a nutrition supplement. Therefore, we examined the effect of AKGs on lipopolysaccharide- (LPS-) mediated insulin resistance and induction of inflammatory genes in high-fat (HF) fed mice.

2. Materials and Methods

2.1. Chemicals. SA was purchased from NIKKO Chemicals (Tokyo, Japan). BA was purchased from Bachem (Bubendorf, Switzerland). Escherichia coli LPS 0111:B6 was purchased from Sigma-Aldrich (St. Louis, MO). Glucose, cholesterol, and triglyceride kits were obtained from Kinghawk Pharmaceutical (Beijing, China). Insulin, leptin, IL-1β, and TNF-α ELISA kits were purchased from R&D systems (Minneapolis, MN). Antiphospho- (Thr183/Tyr185) and total JNK, antiphospho- (Thr202/Tyr204) and total ERK, and anti-IκBα were purchased from Santa Cruz (Santa Cruz, CA). All other chemical reagents used in the present study were of analytical grade.

2.2. Animals and Facilities. The study was approved by the Animal Ethics Committee of Xinhua Hospital. Forty-eight, 4-week old male C57BL/6 mice were purchased from SLAC Laboratories (Shanghai, China). All mice were housed in stainless steel cages with bedding (6 mice/cage). Sufficient bedding was used to keep mice dry and clean. All the mice were exposed to a 12-hour light and dark cycle. Frequent bedding changes and cage cleaning were performed as often as necessary.

2.3. Animal Study Design. After arrival, mice were acclimatized for 4 days. After acclimatation, forty-eight mice were randomly divided into six groups of 8 mice each. Both normal chow and high-fat diets were purchased from Shanghai Slac Laboratory Animal Co., Ltd. Normal chow diets contained 20.5% crude protein, 4.62% crude fat, 52.5% nitrogen-free extract, and 4.35% crude fibers (total calories 3.45 Kcal/g, 12% calories in fat). High-fat diets contained 18.8% crude protein, 16.2% crude fat, 45.2% nitrogen-free extract, and 3.98% crude fibers (total calories 3.79 Kcal/g, 38% calories in fat) [16]. For 8 weeks, groups 1 and 2 received the normal diets (ND) and high-fat diets (HF), respectively; groups 3 and 4 were fed the HF supplemented with 20 and 200 mg/kg SA, respectively; groups 5 and 6 were fed the HF supplemented with 20 and 200 mg/kg BA, respectively. Body weight was monitored weekly. At the end of the experiment, blood samples were collected after overnight fasting. Following 4 days recovery, all groups were fasted for 5 hours and then challenged with 100 ng LPS intraperitoneally. After 2 hours, animals were then euthanized and blood samples, liver, and epididymal fat were collected. Liver tissues and visceral adipose were immediately weighted after removal [17]. Serum was isolated by centrifugation at 1500 g at 4°C for 10 min and stored at −80°C until it was used for blood biochemical assays.

2.4. Culturing of Primary Adipocytes. Abdominal white adipose tissue was obtained from 4- to 5-week-old, wild-type mice. After blood washing, the adipose tissues were minced and digested with 1 mg/mL collagenase type I (Sigma-Aldrich, St. Louis, MO) for 30 min at 37°C. Cells were filtered through 200-μm pore size nylon meshes. The stromal vascular cells (SVCs) were separated from adipocytes by centrifugation and washed with DMEM (Invitrogen, Carlsbad, CA) supplemented with 10% fetal bovine serum (FBS). SVCs were plated and propagated to confluence in DMEM supplemented with 10% FBS, 50 μg/mL streptomycin, and 50 U/mL penicillin [18]. After attachment, the medium was replaced by induction medium containing 10 μg/mL insulin (INS), 1 μm dexamethasone (DEX), and 0.5 mm 3-isobutyl-1-methylxanthine (MIX) with 10% FBS and continued differentiation for 12 days. On day 12, cultures were pretreated with DMSO vehicle, or different concentrations of SA or BA for 24 hrs, and then treated with 10 μg/L LPS for 6 hrs.

2.5. Immunoblotting Analysis. Following treatment, cultures were harvested and protein was extracted with RIPA buffer. Immunoblotting analysis was performed as described previously [19].

2.6. Biochemical Analysis. Concentrations of insulin, leptin, IL-1β, and TNF-α were measured using ELISA kit. Glucose, total cholesterol, and triglyceride were tested using enzymatic methods. Homeostatic Model Assessment-Insulin Resistance (HOMA-IR) was calculated from glucose and insulin concentrations (fasting glucose (mmol/L) × fasting insulin (μU/mL)/22.5) [20].

2.7. Statistical Analysis. Data are shown as means with their standard errors. Statistical significance was evaluated using one-way ANOVA followed by Duncan's multiple range test. P value < 0.05 was considered statistically significant.

3. Results

3.1. Effects of AKGs Diets on Body and Organ Weights. Daily food intake during the experimental period was not significantly different among groups. No changes of end-point body weight and net weight gain were observed between HF diet group and low-dose (20 mg/kg) AKGs (SA or BA) supplemented groups during the 60-day period. High-dose SA (200 mg/kg) supplementation significantly decreased the end-point body weight and net weight gain of the HF fed mice during the 60-day dietary intervention. Weights of epididymal white adipose tissue and liver were compared among the different dietary treatments. Epididymal fat was significantly decreased as percent body weight in mice that received 200 mg/kg SA supplementation (Table 1).

3.2. Effects of AKGs Diets on Serum Triglyceride and Cholesterol. There was a significant (110%) increase in the serum triglyceride level of the HF group compared with the ND group, whereas a 25% decrease of serum triglyceride was observed in the 200 mg/kg SA group relative to the HF group ($P < 0.01$) (Figure 1(a)). HF feeding caused a significant (50%) increase in the total cholesterol level. 200 mg/kg SA treatment; however, had reduced the serum cholesterol level by 30% as compared to the HF group ($P < 0.001$) (Figure 1(b)). There was no significant difference in triglyceride or cholesterol level between the HF group and the HF plus low-dose SA group. No significant change in triglyceride or cholesterol level was observed in HF plus BA diet group as compared with HF group.

3.3. Effects of AKGs Diets on Glucose, Insulin, and HOMA-IR. To investigate the impact of different AKGs supplemented HF diets in comparison with HF diet on glucose metabolism, we examined blood glucose concentrations before and after LPS challenge in different dietary groups. HF diet group had significantly higher fasting blood glucose concentration as compared to ND diet group (9.84 mmol/L versus 7.62 mmol/L; $P < 0.001$) (Table 2). Fasting blood glucose was significantly lower in mice fed HF diet plus 20 or 200 mg/kg SA than that in mice fed HF diet ($P < 0.001$). After intraperitoneal injection of LPS, a drop of blood glucose concentration was observed in all groups. HF diet plus 200 mg/kg SA caused lower blood glucose concentration after LPS challenge as compared to HF diet group (5.05 mmol/L versus 5.71 mmol/L; $P < 0.05$) (Table 2).

The impact of different forms of AKGs on insulin resistance induced by HF diet was also assessed. The plasma insulin concentrations were examined before and after LPS challenge in different dietary groups. As expected, HF diet group had significantly higher fasting insulin concentrations as compared to ND diet group (27.81 μIU/mL versus 13.49 μIU/mL; $P < 0.001$) (Table 2). It was noted that fasting insulin concentration was decreased in mice fed HF diet plus 200 mg/kg SA relative to mice fed HF diet (20.92 μIU/mL versus 27.81 μIU/mL; $P < 0.05$), whereas insulin concentration was increased in mice fed HF diet plus 200 mg/kg BA ($P < 0.05$). After intraperitoneal injection of LPS, mice fed HF plus 200 mg/kg SA showed lower insulin increase compared to mice fed HF diet (22.92 μIU/mL versus 37.13 μIU/mL; $P < 0.05$). No effects of low-dose AKGs (SA or BA) supplementation were observed on fasting insulin concentrations at pre- and post-LPS challenge (Table 2). The HOMA-IR score was calculated from fasting blood glucose and insulin concentration to assess whether AKGs diet protected mice from insulin resistance. In fact, mice that received 20 or 200 mg/kg SA supplementation had significantly lower HOMA-IR scores ($P < 0.001$), however, mice received 200 mg/kg BA supplementation had significantly higher HOMA-IR scores as compared to mice that received HF diet at pre-LPS challenge ($P < 0.05$). After intraperitoneal injection of LPS, only 200 mg/kg SA supplementation showed

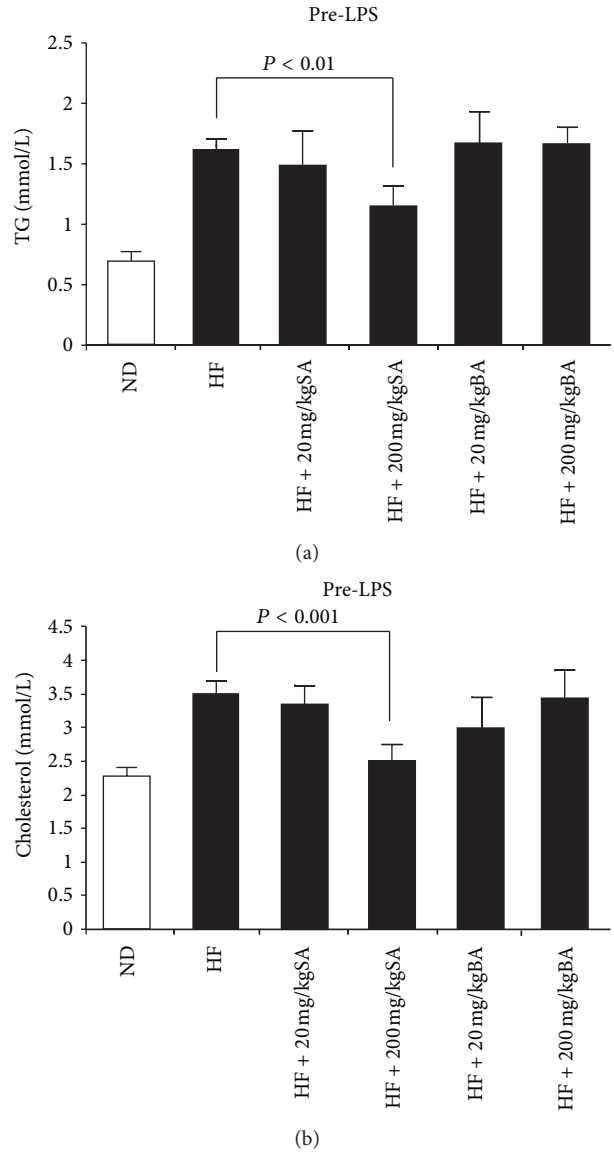

Figure 1: The effect of selachyl alcohol (SA) or batyl alcohol (BA) supplementation on serum triglycerides (a) and cholesterol (b). Data were presented as mean ± SE. Significant differences were tested with two-way ANOVA. Only significant comparisons are presented.

Table 1: The effect of selachyl alcohol (SA) or batyl alcohol (BA) supplementation on body weights, tissue weights, and food consumption.

	Treatment[1]								
Item	ND	HF	HF + 20 mg/kg SA	HF + 200 mg/kg SA	HF + 20 mg/kg BA	HF + 200 mg/kg BA	*P* value[6] (HF)	*P* value (SA)	*P* value (BA)
Initial body wt[2] (g)	14.05 ± 0.18[5]	14.27 ± 0.21	14.38 ± 0.23	14.36 ± 0.27	14.22 ± 0.29	14.33 ± 0.23	0.299	0. 943	0.950
End-point body wt[3] (g)	25.92 ± 0.56	35.21 ± 0.57	36.48 ± 0.59	32.80 ± 0.54*	36.35 ± 0.44	36.17 ± 0.39	<0.001	<0.001	0.087
Net weight gain[4] (g)	11.87 ± 0.63	20.93 ± 0.51	22.10 ± 0.67	18.43 ± 0.57*	22.12 ± 0.55	21.83 ± 0.54	<0.001	<0.001	0.062
Epididymal fat[3] (%)	1.76 ± 0.29	2.39 ± 0.09	2.20 ± 0.05	2.02 ± 0.10*	2.48 ± 0.08	2.64 ± 0.07	<0.001	0.019	0.130
Liver weight[3] (%)	3.86 ± 0.04	3.29 ± 0.05	3.42 ± 0.07	3.49 ± 0.08	3.37 ± 0.02	3.18 ± 0.03†	<0.001	0.150	0.011
Food intake (g/mouse/day)	2.80 ± 0.05	2.64 ± 0.04	2.57 ± 0.04	2.58 ± 0.05	2.64 ± 0.06	2.69 ± 0.05	0.005	0.563	0.729

[1]ND: normal diet; HF: high-fat diet; SA: selachyl alcohol; BA: batyl alcohol.[2]Measured before dietary intervention. [3]Measured after 8-week feeding period. [4]Difference between end-point body weight and initial body weight. [5]Values are mean ± SEM. Means with a mark (*) in HF + 20 mg/kg SA or HF + 200 mg/kg SA group differ significantly from the HF diet group. Means with a mark (†) in HF + 20 mg/kg BA or HF + 200 mg/kg BA group differ significantly from the HF diet group. [6]*P* value (HF) indicates the effect of HF treatment. *P* value (SA) indicates the effect of different doses of SA supplements on HF fed mice. *P* value (BA) indicates the effect of different doses of BA supplements on HF fed mice.

significant protective effect on insulin resistance which was indicated by HOMA-IR scores ($P < 0.005$) (Table 2).

3.4. Effect of AKGs on Serum Cytokines and Leptin. The proinflammatory cytokines such as IL-1β and TNF-α were elevated after LPS challenge. Interestingly, high-dose SA or BA showed differential effects on serum IL-1β and TNF-α production after 100 ng LPS challenge (Table 3). 200 mg/kg SA supplementation suppressed serum IL-1β and TNF-α level induced by LPS challenge ($P < 0.05$), whereas 200 mg/kg BA supplementation significantly enhanced serum IL-1β and TNF-α level induced by LPS challenge ($P < 0.05$). However, there was no significant effect on IL-1β and TNF-α response to LPS challenge by low-dose AKGs (SA or BA) supplementation.

As for serum leptin, mice that received HF diet had significantly higher serum leptin concentration compared to those received ND diet (16.55 ng/mL versus 7.26 ng/mL; $P < 0.05$). We found that serum leptin concentration was significantly decreased in mice that received 200 mg/kg SA supplementation as compared to mice that received HF diet at pre-LPS challenge (13.57 ng/mL versus 16.55 ng/mL; $P < 0.05$) (Table 3).

3.5. Effect of AKGs on LPS-Mediated MAPK and NF-κB Activation. Given the role of MAPK pathway in inducing inflammatory gene expression via Toll-like-receptor-(TLR-) 4 activation, we examined the effects of AKGs on MAPK phosphorylation. Pretreatment of mice adipocyte cultures with 10 μM SA modestly decreased LPS-mediated phosphorylation of JNK and ERK (Figure 2). However, pretreatment of mice adipocyte cultures with 10 μM BA increased LPS-mediated phosphorylation of JNK and ERK. In the absence of LPS, AKGs treatment did not enhance the MAPK activation. Because the activation of NF-κB also plays a crucial role in the transcriptional activation of inflammation-responsive genes, the effects of AKGs on NF-κB activation were examined by detecting IκBα degradation via immunoblot. We found that the pretreatment with SA attenuated IκBα degradation by LPS (Figure 2). However, BA did not present effect on LPS-induced NF-κB activation in our experiments.

4. Discussion

SLO has been widely used in the past years in the Scandinavian medicine because of its properties as immunity boosters and a remedy against radiation therapy and cancer [21]. AKGs are the major components in SLO which could stimulate immunity both *in vitro* and *in vivo* [22, 23]. Daily consumption of AKGs-rich SLO showed benefits to the immune system. Despite widespread intake of AKGs, safety studies on AKGs extract were poor. The acute and repeated (28 days) oral toxicity has been evaluated for oral AKGs administration in rats at doses of 200 and 1000 times the maximum recommended dose in humans [24]. In that study, AKGs administration showed no adverse effects on mortality at either acute or subchronic dose. However, the correlation between long-term AKGs supplement and HF-induced obesity has not been shown. In previous studies, AKGs were demonstrated to have potency to activate cytotoxic macrophages and increase humoral immune response [22]. AKGs could also stimulate the IL-12 and IFN-gamma production and elicit Th1 response [25, 26]. As we know, adipose infiltrated macrophage and secreted cytokines play important roles in obesity and insulin resistance [27–29]. Thus, the potency of AKGs to stimulate immunity spurred our interest to examine the AKGs effect on HF-induced obesity and insulin resistance.

Studies have shown that HF diets induce adipose tissue inflammation and stimulate TLR-4 expression [30]. TLR-4, a subclass of the TLR family, plays a critical role in activating innate immune and inflammation response in mammals by recognizing bacterial LPS [31, 32]. Activation of TLR-4 in adipocytes leads to the activation of MAPK and NF-κB signaling pathways, and induction of many inflammatory cytokines [33, 34]. These cytokines are involved in inducing glucose intolerance, insulin resistance, and infiltration of macrophages into adipose tissue. Recent study showed that TLR-4 responds to nonbacterial ligands such as fatty acids [35–37]. It was demonstrated that saturated fatty acids such as lauric acid and palmitic acid are able to induce cyclooxygenase-2 (COX-2) expression; however, unsaturated fatty acids such as docosahexaenoic acid (DHA) and eicosapentaenoic acid (EPA) are able to inhibit saturated fatty acid-induced COX-2 expression [38]. In present study, we demonstrated that AKGs with saturated chain increased LPS-mediated activation of the MAPK signaling, which could cause the expression of inflammatory genes and insulin resistance in adipocytes. AKGs with unsaturated chain decreased LPS-mediated activation of the MAPK and NF-κB signaling, thus ameliorated insulin resistance. However, both AKGs with saturated and unsaturated chain did not activate MAPK or NF-κB signaling in the absence of LPS. Accordingly, it was indicated that both AKGs with saturated chain and unsaturated chain modulated TLR-4 signaling and insulin response in the hyperinflammatory environment such as high-fat diet feeding or LPS treatment but did not show direct effect in the hypoinflammatory environment. This result was also noticed by Ocaña et al., who showed that BA activated the expression of IL-1β and IL-6 genes only in TNF-α-induced adipocytes but not in the nonstimulated cells [39].

Several studies have demonstrated that different forms of AKGs have differential biological effects. The unsaturated AKGs with 16 or 18 carbon alkyl chains showed strong anti-tumor and antimetastasis activities in mice model [40]. By contrast, the saturated AKGs with 16 or 18 carbon alkyl chains showed less antitumor effect or even tumor-promoting activity. Previous studies also demonstrated that proinflammatory responses were enhanced by most saturated fatty acids but reduced by most unsaturated fatty acids. In metabolic experiments, rats fed saturated fatty acids had higher triacylglycerol, cholesterol, and low-density lipoprotein cholesterol, whereas rats fed unsaturated fatty acids had lower triacylglycerol, cholesterol, and low-density lipoprotein cholesterol as compared with control rats [41, 42]. Moreover, the increased ratio of P/S (polyunsaturated/saturated) fatty

Table 2: The effect of selachyl alcohol (SA) or batyl alcohol (BA) supplementation on serum glucose, insulin, and Homeostatic Model Assessment-Insulin Resistance (HOMA-IR) before and after 100 ng lipopolysaccharide (LPS) challenge.

				Pre-LPS[1]					
Item	ND[2]	HF	HF + 20 mg/kg SA	HF + 200 mg/kg SA	HF + 20 mg/kg BA	HF + 200 mg/kg BA	*P* value[4] (HF)	*P* value (SA)	*P* value (BA)
Glucose (mmol/L)	7.62 ± 0.30[3]	9.84 ± 0.34	8.69 ± 0.20*	7.47 ± 0.29*	10.03 ± 0.37	10.06 ± 0.54	<0.001	<0.001	0.761
Insulin (μIU/mL)	13.49 ± 1.14	27.81 ± 1.85	25.05 ± 2.03	20.92 ± 1.5*	25.33 ± 2.73	34.41 ± 2.03†	<0.001	0.043	0.025
HOMA-IR	4.63 ± 0.54	12.11 ± 0.78	9.71 ± 0.86*	7.00 ± 0.69*	11.12 ± 1.02	15.39 ± 1.17†	<0.001	<0.001	0.017
				Post-LPS					
Glucose (mmol/L)	6.19 ± 0.30	5.71 ± 0.16	5.73 ± 0.21	5.05 ± 0.22*	5.16 ± 0.15	5.88 ± 0.30	0.182	0.038	0.062
Insulin (μIU/mL)	21.20 ± 3.35	37.13 ± 2.86	33.03 ± 3.65	22.99 ± 3.08*	33.86 ± 2.42	39.92 ± 2.33	<0.005	0.018	0.246
HOMA-IR	5.71 ± 0.79	9.48 ± 0.91	8.35 ± 0.91	5.11 ± 0.70*	7.80 ± 0.62	10.62 ± 1.08	0.008	0.004	0.096

[1]Serum glucose and insulin were measured before LPS challenge (Pre-LPS) and 2 hours following 100 ng LPS challenge (Post-LPS). [2]ND: normal diet; HF: high-fat diet; SA: selachyl alcohol; BA: batyl alcohol. [3]Values are mean ± SEM. Means with a mark (*) in HF + 20 mg/kg SA or HF + 200 mg/kg SA group differ significantly from the HF diet group. Means with a mark (†) in HF + 20 mg/kg BA or HF + 200 mg/kg BA group differ significantly from the HF diet group. [4]*P* value (HF) indicates the effect of HF treatment. *P* value (SA) indicates the effect of different doses of SA supplements on HF fed mice. *P* value (BA) indicates the effect of different doses of BA supplements on HF fed mice.

Table 3: The effect of selachyl alcohol (SA) or batyl alcohol (BA) supplementation on serum cytokines and leptin before and after 100 ng lipopolysaccharide (LPS) challenge.

				Pre-LPS[1]					
Item	ND[2]	HF	HF + 20 mg/kg SA	HF + 200 mg/kg SA	HF + 20 mg/kg BA	HF + 200 mg/kg BA	*P* value[4] (HF)	*P* value (SA)	*P* value (BA)
IL-1β (pg/mL)	2.3 ± 0.19[3]	8.8 ± 0.70	8.25 ± 1.09	7.1 ± 0.82	8.18 ± 0.59	10.47 ± 1.37	<0.001	0.404	0.074
TNF-α (pg/mL)	4.83 ± 0.56	5.83 ± 0.29	5.5 ± 0.44	5.95 ± 0.25	5.07 ± 0.39	5.68 ± 0.36	0.138	0.625	0.289
Leptin (ng/mL)	7.26 ± 0.50	16.55 ± 0.60	16.18 ± 0.59	13.57 ± 0.49*	16.52 ± 0.42	16.13 ± 0.55	<0.001	0.005	0.837
				Post-LPS					
IL-1β (pg/mL)	100.85 ± 9.2	196.2 ± 15.4	187.1 ± 10.1	149.6 ± 6.7*	204.5 ± 10.8	253.1 ± 8.7†	<0.001	0.016	0.005
TNF-α (pg/mL)	231 ± 8.78	347 ± 10.23	320.75 ± 13.06	288.87 ± 9.49*	370.25 ± 14.44	476.79 ± 19.28†	<0.001	0.004	<0.001
Leptin (ng/mL)	9.18 ± 0.32	18.16 ± 0.83	16.74 ± 0.76	16.27 ± 0.78	16.37 ± 0.8	16.81 ± 0.68	<0.001	0.063	0.238

[1]Serum cytokines and leptin were measured before LPS challenge (Pre-LPS) and 2 hours following 100 ng LPS challenge (Post-LPS). [2]ND: normal diet; HF: high-fat diet; SA: selachyl alcohol; BA: batyl alcohol. [3]Values are mean ± SEM. Means with a mark (*) in HF + 20 mg/kg SA or HF + 200 mg/kg SA group differ significantly from the HF diet group. Means with a mark (†) in HF + 20 mg/kg BA or HF + 200 mg/kg BA group differ significantly from the HF diet group. [4]*P* value (HF) indicates the effect of HF treatment. *P* value (SA) indicates the effect of different doses of SA supplements on HF fed mice. *P* value (BA) indicates the effect of different doses of BA supplements on HF fed mice.

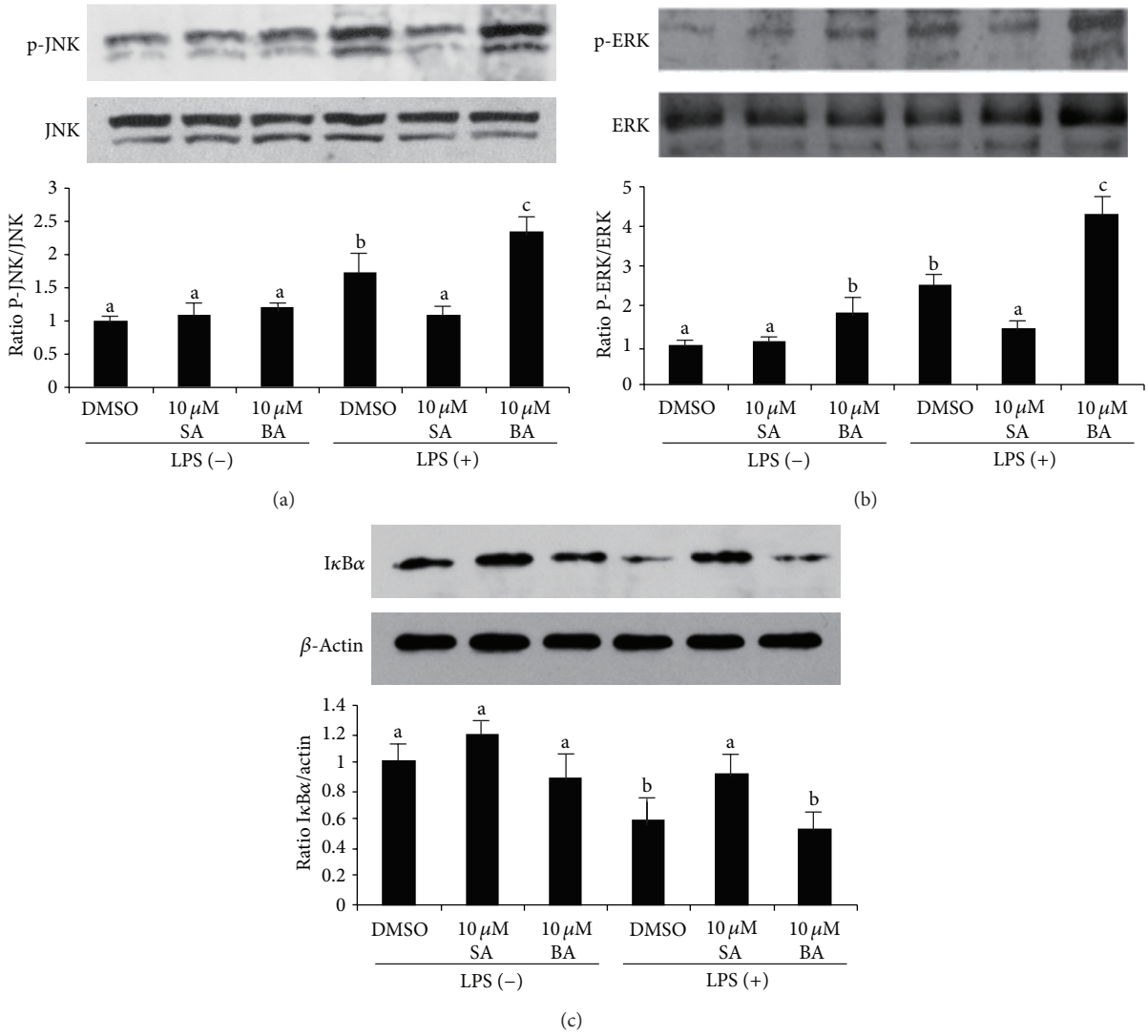

Figure 2: The effect of selachyl alcohol (SA) or batyl alcohol (BA) on TLR-4 signaling activated by LPS in mice primary adipocytes. Newly differentiated cells were pretreated with DMSO vehicle (−) or 10 μM SA or 10 μM BA for 24 h and then treated with 10 μg/L LPS for 6 h. (a) Phosphorylation of JNK (P-JNK-to-JNK ratio). (b) Phosphorylation of ERK (P-ERK-to-ERK ratio). (c) Expression of IκBα (IκBα-to-actin ratio). Levels of protein were measured by western blotting. Data are a mean of ± SE and corrected for loading. Significant differences between each group are indicated by different letters.

acids was beneficial in depleting white adipose tissue accumulation and improved the metabolic status in diet-induced obese hamster [43]. The controlled clinical trials have also indicated that replacing saturated fat with unsaturated fat was more effective in lowering risk of metabolic disorder than simply reducing total fat consumption [44, 45]. Our studies showed that AKGs had the similar effects on metabolic and inflammatory status as free fatty acids in spite of their ether bond with glycerol. As we know, SLO and human breast milk are both good sources of AKGs, with unsaturated forms as the predominant components. In clinical studies, SLO showed beneficial effect on lipid metabolism in patients with hypertension [46]. Breast milk has also been demonstrated to be protective against the development of childhood overweight and obesity [47]. Thus, we postulated that the predominant unsaturated AKGs in SLO and breast milk would neutralize the adverse effects of saturated AKGs on metabolism and play a prominent role of preventing metabolic syndrome.

Increasing studies have indicated that dietary supplementation of oils extracted from marine species can alter the metabolic and immunologic status which is highly associated with the incidence of obesity and type 2 diabetes. Different marine oils have distinct lipid profiles, which result in potential differences in their effects on inflammation and metabolism. Fish oil, the typical marine oil product, was demonstrated to have protective effect on LPS-induced inflammation and insulin resistance [17]. It was also shown that dietary fish oil supplementation could reduce body weight gain in HF-induced obese mice [48]. The anti-inflammation and antiobesity effects of fish oil were attributed to its richness of ($n-3$) PUFA [49]. SLO, which was also rich of ($n-3$) PUFA, was known to contain high

proportion of squalene and AKGs. Both squalene and AKGs have potent immunological activity, thus eliciting people's interest of investigating their impact on metabolic balance. Squalene has already been demonstrated to be able to elevate the body weight and serum cholesterol in high-fat fed hamsters due to its involvement in hepatic cholesterol metabolism [50]. However, little is known about the association between AKGs intake and metabolic alteration. Our results showed that AKGs differentially modulated HF-induced obesity and insulin resistance in mice, which gave us indication that more attention should be paid to the impact of these immune-stimulating chemicals on metabolism.

Actually, it has already been noticed that oral SLO intake has adverse effect on liver function if supplemented at high dosage [51]. Therefore, it is important to use AKGs in animal experiment at the dosage comparable to that of human supplementation for nutritional purpose. The Biomare Immuno which is manufactured by Hankintatukku (Finland) contains 60 mg AKGs per capsule. On the label, it recommends six capsules daily, which equals to 7.2 mg AKGs/kg^{weight} ($60\,mg \times 6/50\,kg^{weight}$) provided that a male adult weighs 50 kg on average. In the present study, AKGs at 20 mg/kg^{diet} and 200 mg/kg^{diet} dietary supplementation corresponded to 4 mg/kg^{weight} ($20\,mg/kg^{diet} \times 0.005\,kg^{diet}/0.025\,kg^{weight}$) and 40 mg/$kg^{weight}$ ($200\,mg/kg^{diet} \times 0.005\,kg^{diet}/0.025\,kg^{weight}$), respectively, assuming that a male adult mouse weighs 25 g and expends 5 g diet on average. Thus, the amount of 20 mg/kg^{diet} AKGs dietary supplement was comparable to that commonly consumed by a SLO-supplement consumer. The results obtained from rodents showed that the 20 mg/kg^{diet} dietary AKGs supplementation did not have significant effect on body weight but only showed minor effect on glucose metabolism. Nevertheless, 200 mg/kg^{diet} dietary AKGs supplementation showed obvious effects not only on body weight but also on lipid, glucose metabolism, and pro-inflammatory cytokine production. Although these results were not directly applicable to humans, they provided some implications for individuals who routinely consume AKGs supplement or AKGs-rich SLO. Taken together, our results provided novel insights into differential effects of saturated- and unsaturated-chain AKGs on adipose tissue inflammation, which suggested that routine consumption of SLO consisting of different isoforms of AKGs is safe at normal dosage and shows balanced effect on obesity and insulin resistance.

5. Conclusion

Collectively, these data demonstrate that the unsaturated AKGs (SA) have potency to decrease the HF-induced obesity at high dosage and ameliorate insulin resistance at normal or high dosage. The saturated AKGs (BA) can increase insulin resistance at high dosage. Our data also suggest that AKGs show differential effects on LPS-induced inflammation in adipocytes. The effect of SLO rich for AKGs on adipose metabolism and insulin response should be evaluated in the future, to warrant supplementing SLO products at a safe dosage and prevent its potential hazardous effects on metabolism.

Abbreviations

AKGs:	alkylglycerols
SA:	Selachyl alcohol
BA:	Batyl alcohol
HF:	High fat
ND:	Normal diets
LPS:	Lipopolysaccharides
IL:	Interleukin
TNF:	Tumor necrosis factor
SLO:	Shark liver oil
SVCs:	Stromal vascular cells
HOMA-IR:	Model assessment-insulin resistance
TLR:	Toll-like-receptor
PUFAs:	Polyunsaturated fatty acids.

Acknowledgments

This research was supported by Grants 81000242, 30901472, 30772270, and 30972427 from the National Natural Science Foundation of China (to Linxi Qian, Wei Cai, and Shuna Sun), Program for Innovative Research Team of Shanghai Municipal Education Commission (to Wei Cai), 11QA1405400 Hesper Foundation of Shanghai Scientific Bureau (to Linxi Qian), 2010Y157 Junior Scientist Foundation of Shanghai Health Bureau (to Linxi Qian), and 11DZ2260500 Shanghai Key Laboratory of Pediatric Gastroenterology and Nutrition (to Wei Cai).

References

[1] H. Tilg and A. R. Moschen, "Adipocytokines: mediators linking adipose tissue, inflammation and immunity," *Nature Reviews Immunology*, vol. 6, no. 10, pp. 772–783, 2006.

[2] H. Xu, G. T. Barnes, Q. Yang et al., "Chronic inflammation in fat plays a crucial role in the development of obesity-related insulin resistance," *Journal of Clinical Investigation*, vol. 112, no. 12, pp. 1821–1830, 2003.

[3] H. Wu, S. Ghosh, X. D. Perrard et al., "T-cell accumulation and regulated on activation, normal T cell expressed and secreted upregulation in adipose tissue in obesity," *Circulation*, vol. 115, no. 8, pp. 1029–1038, 2007.

[4] G. S. Hotamisligil, "Inflammation and metabolic disorders," *Nature*, vol. 444, no. 7121, pp. 860–867, 2006.

[5] C. G. Bordier, N. Sellier, A. P. Foucault, and F. le Goffic, "Purification and characterization of deep sea shark Centrophorus squamosus liver oil 1-O-alkylglycerol ether lipids," *Lipids*, vol. 31, no. 5, pp. 521–528, 1996.

[6] T. Iannitti and B. Palmieri, "An update on the therapeutic role of alkylglycerols," *Marine Drugs*, vol. 8, no. 8, pp. 2267–2300, 2010.

[7] A. Brohult, J. Brohult, and S. Brohult, "Biochemical effects of alkoxyglycerols and their use in cancer therapy," *Acta chemica Scandinavica*, vol. 24, no. 2, p. 730, 1970.

[8] B. Hallgren, A. Niklasson, G. Ställberg, and H. Thorin, "On the occurrence of 1-O-alkylglycerols and 1-O-(2-methoxyalkyl)glycerols in human colostrum, human milk, cow's milk, sheep's milk, human red bone marrow, red

cells, blood plasma and a uterine carcinoma," *Acta chemica Scandinavica B*, vol. 28, no. 9, pp. 1029–1034, 1974.

[9] D. G. Osmond, P. J. Roylance, A. J. Webb, and J. M. Yoffey, "The action of batyl alcohol and selachyl alcohol on the bone marrow of the guinea pig," *Acta haematologica*, vol. 29, pp. 180–186, 1963.

[10] P. Langen, H. Brachwitz, and J. Schildt, "Inhibition of proliferation of Ehrlich ascites carcinoma cells in vitro and in vivo by halogeno analogues of long chain acyl- and alkylglycerols," *Acta Biologica et Medica Germanica*, vol. 38, no. 7, pp. 965–974, 1979.

[11] F. Pédrono, B. Martin, C. Leduc et al., "Natural alkylglycerols restrain growth and metastasis of grafted tumors in mice," *Nutrition and Cancer*, vol. 48, no. 1, pp. 64–69, 2004.

[12] E. Skopińska-Rózewska, J. Chorostowska-Wynimko, M. Krotkiewski et al., "Inhibitory effect of Greenland shark liver oil combined with squalen and arctic birch ashes on angiogenesis and L-1 sarcoma growth in Balb/c mice," *Polish Journal of Veterinary Sciences*, vol. 6, supplement 3, pp. 54–56, 2003.

[13] M.-S. Zeng, X. Li, Y. Liu et al., "A high-selenium diet induces insulin resistance in gestating rats and their offspring," *Free Radical Biology and Medicine*, vol. 52, no. 8, pp. 1335–1342, 2012.

[14] W. E. Berdel, W. R. Bausert, and H. U. Weltzien, "The influence of alkyl-lysophospholipids and lysophospholipid-activated macrophages on the development of metastasis of 3-Lewis lung carcinoma," *European Journal of Cancer and Clinical Oncology*, vol. 16, no. 9, pp. 1199–1204, 1980.

[15] E. Ortega Martinez de Victoria, X. Xu, J. Koska et al., "Macrophage content in subcutaneous adipose tissue: associations with adiposity, age, inflammatory markers, and whole-body insulin action in healthy pima Indians," *Diabetes*, vol. 58, no. 2, pp. 385–393, 2009.

[16] W. Xie, D. Gu, J. Li, K. Cui, and Y. Zhang, "Effects and action mechanisms of berberine and rhizoma coptidis on gut microbes and obesity in high-fat diet-fed C57BL/6J mice," *PLoS One*, vol. 6, no. 9, Article ID e24520, 2011.

[17] M. Vijay-Kumar, S. M. Vanegas, N. Patel, J. D. Aitken, T. R. Ziegler, and V. Ganji, "Fish oil rich diet in comparison to saturated fat rich diet offered protection against lipopolysaccharide-induced inflammation and insulin resistance in mice," *Nutrition and Metabolism*, vol. 8, no. 1, article 16, 2011.

[18] M. Masaki, T. Kurisaki, K. Shirakawa, and A. Sehara-Fujisawa, "Role of meltrin α (ADAM12) in obesity induced by high-fat diet," *Endocrinology*, vol. 146, no. 4, pp. 1752–1763, 2005.

[19] D. Hwang, B. C. Jang, G. Yu, and M. Boudreau, "Expression of mitogen-inducible cyclooxygenase induced by lipopolysaccharide: mediation through both mitogen-activated protein kinase and NF-κB signaling pathways in macrophages," *Biochemical Pharmacology*, vol. 54, no. 1, pp. 87–96, 1997.

[20] M. J. Holness, G. K. Greenwood, N. D. Smith, and M. C. Sugden, "PPARα activation and increased dietary lipid oppose thyroid hormone signaling and rescue impaired glucose-stimulated insulin secretion in hyperthyroidism," *American Journal of Physiology—Endocrinology and Metabolism*, vol. 295, no. 6, pp. E1380–E1389, 2008.

[21] A. Brohult, J. Brohult, S. Brohult, and I. Joelsson, "Effect of alkoxyglycerols on the frequency of fistulas following radiation therapy for carcinoma of the uterine cervix," *Acta Obstetricia et Gynecologica Scandinavica*, vol. 58, no. 2, pp. 203–207, 1979.

[22] S. Homma, I. Millman, and N. Yamamoto, "A serum factor for macrophage activation after in vitro dodecylglycerol treatment of mouse lymphocytes," *Immunology and Cell Biology*, vol. 68, part 2, pp. 137–142, 1990.

[23] S. Y. Oh and L. S. Jadhav, "Effects of dietary alkylglycerols in lactating rats on immune responses in pups," *Pediatric Research*, vol. 36, no. 3, pp. 300–305, 1994.

[24] A. Anadón, M. A. Martínez, I. Ares et al., "Acute and repeated dose (28 days) oral safety studies of an alkoxyglycerol extract from shark liver oil in rats," *Journal of Agricultural and Food Chemistry*, vol. 58, no. 3, pp. 2040–2046, 2010.

[25] P. Lewkowicz, M. Banasik, E. Głowacka, N. Lewkowicz, and H. Tchórzewski, "Effect of high doses of shark liver oil supplementation on T cell polarization and peripheral blood polymorphonuclear cell function," *Polski Merkuriusz Lekarski*, vol. 18, no. 108, pp. 686–692, 2005.

[26] R. Ziegler, W. Jobst, H. Minne, and J. D. Faulhaber, "Calciotropic hormones and lipolysis of human adipose tissue: role of extracellular calcium as conditioning but not regulating factor," *Endokrinologie*, vol. 75, no. 1, pp. 77–88, 1980.

[27] M. E. Rausch, S. Weisberg, P. Vardhana, and D. V. Tortoriello, "Obesity in C57BL/6J mice is characterized by adipose tissue hypoxia and cytotoxic T-cell infiltration," *International Journal of Obesity*, vol. 32, no. 3, pp. 451–463, 2008.

[28] J. Jager, T. Grémeaux, M. Cormont, Y. le Marchand-Brustel, and J.-F. Tanti, "Interleukin-1β-induced insulin resistance in adipocytes through down-regulation of insulin receptor substrate-1 expression," *Endocrinology*, vol. 148, no. 1, pp. 241–251, 2007.

[29] G. S. Hotamisligil, D. L. Murray, L. N. Choy, and B. M. Spiegelman, "Tumor necrosis factor α inhibits signaling from the insulin receptor," *Proceedings of the National Academy of Sciences of the United States of America*, vol. 91, no. 11, pp. 4854–4858, 1994.

[30] E. Gäbele, K. Dostert, C. Dorn, E. Patsenker, F. Stickel, and C. Hellerbrand, "A new model of interactive effects of alcohol and high-fat diet on hepatic fibrosis," *Alcoholism*, vol. 35, no. 7, pp. 1361–1367, 2011.

[31] B. Beutler, "Inferences, questions and possibilities in Toll-like receptor signalling," *Nature*, vol. 430, no. 6996, pp. 257–263, 2004.

[32] S. Akira, "Toll-like receptors and innate immunity," *Advances in Immunology*, vol. 78, pp. 1–56, 2001.

[33] E. Faure, L. Thomas, H. Xu, A. E. Medvedev, O. Equils, and M. Arditi, "Bacterial lipopolysaccharide and IFN-γ induce toll-like receptor 2 and toll-like receptor 4 expression in human endothelial cells: role of NF-κB activation," *Journal of Immunology*, vol. 166, no. 3, pp. 2018–2024, 2001.

[34] M. J. Song, K. H. Kim, J. M. Yoon, and J. B. Kim, "Activation of Toll-like receptor 4 is associated with insulin resistance in adipocytes," *Biochemical and Biophysical Research Communications*, vol. 346, no. 3, pp. 739–745, 2006.

[35] D. Hwang, "Modulation of the expression of cyclooxygenase-2 by fatty acids mediated through Toll-like receptor 4-derived signaling pathways," *The FASEB Journal*, vol. 15, no. 14, pp. 2556–2564, 2001.

[36] J. Y. Lee, K. H. Sohn, S. H. Rhee, and D. Hwang, "Saturated fatty acids, but not unsaturated fatty acids, induce the expression of cyclooxygenase-2 mediated through Toll-like receptor 4," *Journal of Biological Chemistry*, vol. 276, no. 20, pp. 16683–16689, 2001.

[37] J. Y. Lee, A. Plakidas, W. H. Lee et al., "Differential modulation of Toll-like receptors by fatty acids: preferential inhibition by n-3 polyunsaturated fatty acids," *Journal of Lipid Research*, vol. 44, no. 3, pp. 479–486, 2003.

[38] S. A. Lee, H. J. Kim, K. C. Chang et al., "DHA and EPA down-regulate COX-2 expression through suppression of NF-κB activity in LPS-treated human umbilical vein endothelial cells," *Korean Journal of Physiology and Pharmacology*, vol. 13, no. 4, pp. 301–307, 2009.

[39] A. Ocaña, C. Gómez-Asensio, E. Arranz-Gutiérrez, C. Torres, F. J. Señoráns, and G. Reglero, "In vitro study of the effect of diesterified alkoxyglycerols with conjugated linoleic acid on adipocyte inflammatory mediators," *Lipids in Health and Disease*, vol. 9, article 36, 2010.

[40] A.-L. Deniau, P. Mosset, F. Pédrono, R. Mitre, D. le Bot, and A. B. Legrand, "Multiple beneficial health effects of natural alkylglycerols from shark liver oil," *Marine Drugs*, vol. 8, no. 7, pp. 2175–2184, 2010.

[41] N. W. Chang and P. C. Huang, "Effects of the ratio of polyunsaturated and monounsaturated fatty acid to saturated fatty acid on rat plasma and liver lipid concentrations," *Lipids*, vol. 33, no. 5, pp. 481–487, 1998.

[42] Y. S. Diniz, A. C. Cicogna, C. R. Padovani, L. S. Santana, L. A. Faine, and E. L. B. Novelli, "Diets rich in saturated and polyunsaturated fatty acids: metabolic shifting and cardiac health," *Nutrition*, vol. 20, no. 2, pp. 230–234, 2004.

[43] F.-H. Liao, T.-H. Liou, W.-C. Chiu, M.-J. Shieh, and Y.-W. Chien, "Differential effects of high MUFA with high or low P/S ratio (polyunsaturated to saturated fatty acids) on improving hepatic lipolytic enzymes and mediating PPARγ related with lipoprotein lipase and hormone-sensitive lipase of white adipose tissue in diet-induced obese hamster," *International Journal of Obesity*, vol. 34, no. 11, pp. 1608–1617, 2010.

[44] F. B. Hu, J. E. Manson, and W. C. Willett, "Types of dietary fat and risk of coronary heart disease: a critical review," *Journal of the American College of Nutrition*, vol. 20, no. 1, pp. 5–19, 2001.

[45] J. Salmerón, F. B. Hu, J. E. Manson et al., "Dietary fat intake and risk of type 2 diabetes in women," *American Journal of Clinical Nutrition*, vol. 73, no. 6, pp. 1019–1026, 2001.

[46] A. V. Pogozheva, S. A. Derbeneva, N. V. Anykina et al., "The clinical and experimental research of metabolic effects of shark liver oil," *Voprosy Pitaniia*, vol. 76, no. 6, pp. 28–32, 2007.

[47] C. McCrory and R. Layte, "Breastfeeding and risk of overweight and obesity at nine-years of age," *Social Science and Medicine*, vol. 75, no. 2, pp. 323–330, 2012.

[48] T. Mori, H. Kondo, T. Hase, I. Tokimitsu, and T. Murase, "Dietary fish oil upregulates intestinal lipid metabolism and reduces body weight gain in C57BL/6J mice," *Journal of Nutrition*, vol. 137, no. 12, pp. 2629–2634, 2007.

[49] F. Belzung, T. Raclot, and R. Groscolas, "Fish oil n-3 fatty acids selectively limit the hypertrophy of abdominal fat depots in growing rats fed high-fat diets," *American Journal of Physiology—Regulatory Integrative and Comparative Physiology*, vol. 264, no. 6, part 2, pp. R1111–R1118, 1993.

[50] Z. Zhang, W. K. Yeung, Y. Huang, and Z.-Y. Chen, "Effect of squalene and shark liver oil on serum cholesterol level in hamsters," *International Journal of Food Sciences and Nutrition*, vol. 53, no. 5, pp. 411–418, 2002.

[51] S. Kilincalp, M. Deveci, O. Basar, F. Ekiz, S. Coban, and O. Yuksel, "Shark liver oil: hidden dangers," *Annals of Hepatology*, vol. 11, no. 5, pp. 728–730.

Hindawi Publishing Corporation
Evidence-Based Complementary and Alternative Medicine
Volume 2013, Article ID 529458, 14 pages
http://dx.doi.org/10.1155/2013/529458

Review Article

Current Understanding on Antihepatocarcinoma Effects of Xiao Chai Hu Tang and Its Constituents

Ningning Zheng,[1] Jianye Dai,[1] Huijuan Cao,[1] Shujun Sun,[1] Junwei Fang,[1] Qianhua Li,[1] Shibing Su,[2] Yongyu Zhang,[1] Mingfeng Qiu,[3] and Shuang Huang[4]

[1] *Center for Traditional Chinese Medicine and Systems Biology, Shanghai University of Traditional Chinese Medicine, Shanghai 201203, China*
[2] *Research Center for Traditional Chinese Medicine Complexity System, Shanghai University of Traditional Chinese Medicine, Shanghai 201203, China*
[3] *School of Pharmacy, Shanghai Jiao Tong University, Shanghai 200240, China*
[4] *Department of Biochemistry and Molecular Biology, Medical College of Georgia, Georgia Health Sciences University, Augusta, GA 30907, USA*

Correspondence should be addressed to Yongyu Zhang; dryyz@sina.com and Mingfeng Qiu; mfqiu@sjtu.edu.cn

Received 3 January 2013; Revised 25 April 2013; Accepted 27 May 2013

Academic Editor: Rong Zeng

Xiao Chai Hu Tang (XCHT), a compound formula originally recorded in an ancient Chinese medical book *Shanghanlun*, has been used to treat chronic liver diseases for a long period of time in China. Although extensive studies have been demonstrated the efficacy of this formula to treat chronic hepatitis, hepatic fibrosis, and hepatocarcinoma, how it works against these diseases still awaits full understanding. Here, we firstly present an overview arranging from the entire formula to mechanism studies of single herb in XCHT and their active components, from a new perspective of "separation study," and we tried our best to both detailedly and systematically organize the antihepatocarcinoma effects of it, hoping that the review will facilitate the strive on elucidating how XCHT elicits its antihepatocarcinoma role.

1. Introduction

The American Cancer Society's estimation for primary liver and bile duct cancers in the United States for 2013 is about 30,640 new cases and 21,670 deaths from these cancers. Liver cancer is even more common in sub-Saharan Africa and Southeast Asia and currently is the most common type of cancers in many countries in these regions [1]. Among various types of liver cancer, hepatocellular carcinoma (HCC) is the most common one, and the majority of them are associated with chronic hepatitis B virus (HBV) or hepatitis C virus (HCV) infections [2, 3]. Chronic viral hepatitis, chemical-induced liver damage, could cause liver fibrosis and cirrhosis, finally leading to liver cancer.

Compound herbal formulas have been used to treat cancers, and many of them have shown the promise to improve the life of cancer patients [4–6]. These compound formulas are usually made of several Chinese medicinal herbs and suppress tumor progression by multiple mechanisms [7]. One of them is called Xiao Chai Hu Tang (XCHT, Sho-saiko-to, in Japanese) that was originally recorded in ancient Chinese medical book *Shanghanlun*. It consists of seven medicinal herbs (*Bupleurum falcatum*, *Scutellaria baicalensis*, *Panax ginseng*, *Zizyphus jujube*, *Pinellia ternate*, *Zingiber officinale*, *and Glycyrrhiza glabra*) and is currently used to treat chronic liver diseases especially chronic hepatitis [8–11]. Data from recent clinical trials convincingly show that XCHT can prevent the development of HCC in patients with cirrhosis, particularly those without HBs antigen [9]. Experimental studies further indicate that XCHT may achieve its effect by reducing hepatocyte necrosis and enhancing liver function. Moreover, XCHT has also been shown to exhibit various anticarcinogenic properties such as induction of apoptosis and suppression of invasion [12, 13].

Table 1: Some clinical trials of XCHT.

Author; year	Cases	Research design	Results
Hirayama et al. [8]; 1989	222 chronic hepatitis subjects	Double-blind, multicenter	The difference of the mean value of AST and ALT between the XCHT group and placebo group was significant; a tendency towards a decrease of HBeAg and an increase of anti-HBe antibodies was also observed in patients with chronic active type B hepatitis
Oka et al. [9]; 1995	260 cirrhotic subjects	Randomized, controlled	The cumulative incidence curve for 5 years of the trial group (XCHT combined with conventional drugs) was lower while the survival curve for 5 years of the trial group was higher compared with control group (conventional drugs). The difference was significant for patients without HBs antigen
Deng et al. [11]; 2011	24 chronic hepatitis C subjects	A single arm phase II study	Improvement of AST (16 subjects) and ALT (18 subjects) was observed; 9 subjects showed improvement in histology activity index scores
Bo and Du [14]; 2006	96 chronic hepatitis B subjects	Randomized, controlled	Experiment group (XCHT combined with α-interferon) showed better effect in aspects of ALT improvement and HBeAg negative transform than α-interferon treatment group
Li et al. [15]; 2001	110 chronic hepatitis B subjects	Randomized, controlled	ALT, total bilirubin, and serum liver fibrosis indexes were decreased in combination treatment group (XCHT and γ-interferon) and the difference was significant compared with γ-interferon treatment group
Sun et al. [16]; 2003	94 chronic hepatitis B with fibrosis subjects	Randomized, controlled	The liver function was improved and serum liver fibrosis indexes were decreased; the difference was significant between combination treatment group (XCHT and oxymatrine) and controlled group (reduced glutathione and vitamin treatment)
Wu [17]; 2009	142 chronic hepatitis B with cirrhosis subjects	Randomized, controlled	The liver function was improved and serum liver fibrosis indexes were decreased; the difference was significant between XCHT treatment group and controlled group (hepatic protective drug and antifibrosis drug treatment)

Chinese herbal medicines are usually used to counteract tumor progression by a formula of multiple herbs rather than a single one. Unfortunately, studies have been mainly focused on defining the mechanism of a single herb or its ingredients. As each herb in XCHT can potentially exert its effect in a distinct mechanism, a formula of seven herbs is expected to reach its full effect by targeting multipathways and multitargets. So we firstly introduce a new perspective of "separation study," that is, from the entire formula to single herb and their active components, both detailedly and systematically organize the antihepatocarcinoma effects of XCHT. We hope that this review will help XCHT to receive its well-deserved global recognition and to be better appreciated for its clinical use to treat liver cancers.

2. Xiao Chai Hu Tang (XCHT)

2.1. Clinical Trials of XCHT. XCHT has long been used in clinical trials for the study and treatment of liver diseases. Some XCHT clinical trials (including the clinical trials mentioned above and some other trials [14–17] conducted in China) are summarized in Table 1.

2.2. Experimental Studies of XCHT. The potential tumor-suppressing effect of XCHT was reported in 1994, in which XCHT was found capable of inhibiting the proliferation of KIM-1, a human hepatocellular carcinoma cell line and KMC-1, a cholangiocarcinoma cell line [18]. Later on, XCHT was shown to diminish not only the growth of various cancer cell lines but also in vivo tumor outgrowth in xenograft model [19–21].

In addition to its tumor-suppressing role, Chang et al. studied the effect of XCHT on HBV replication in HepG2 2.2.15 cell model [22]. Their study showed that XCHT reduced HBV production and HBeAg expression without altering the level of HBsAg. Although XCHT can also block Coxsackie B type 1 virus infection in CCFS-1 cells through the induction of Type I interferon expression [23], the mechanism responsible for XCHT-mediated suppression of HBV production awaits being defined.

Hepatic fibrosis and liver cirrhosis result from wound healing of ongoing hepatocellular damage caused by chronic liver injuries [13]. Most of HCCs ensue in a cirrhotic liver [24]. Kusunose et al. created an animal model that reflected various stage-liver injuries and used this model to determine under what condition XCHT extract could improve hepatic inflammation and fibrosis [25]. Their study found that the ability of XCHT extract was limited to a certain degree which was expressed by levels of respective parameters (AST, ALT, TGF-β, hydroxyproline, and the ratio of liver fibrosis

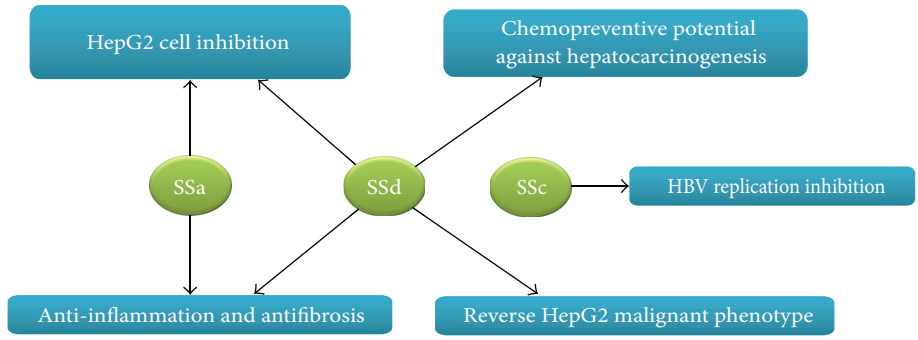

Figure 1: Antitumorigenesis effect of active components in *Bupleuri* radix.

area). Chen et al. later elucidated the mechanism pertinent to XCHT's antifibrosis capability by assessing its effect on the expression of those growth factors and cytokines important for the activation of hepatic stellate cells (HSCs) [26]. They showed that XCHT downregulated the levels of stellate cell activation-essential TGFβ1, platelet derived growth factor (PDGF), and IL-1β while stimulated the production of stellate cell activation-inhibitory TNFα.

3. Individual Herbs and Active Components in XCHT

In TCM, XCHT is a classical formula to treat the typhoid lesser yang syndrome. The compound prescription has its formulating principle. Among the seven herbs included in XCHT, *Bupleurum falcatum* is the "monarch" and *Scutellaria baicalensis* is the "minister," which are the principal herbs in this formula. *Panax ginseng*, *Zizyphus jujube*, *Pinellia ternate*, and *Zingiber officinale* are the "assistant" while *Glycyrrhiza glabra* is the "guide" [27]. *Bupleurum* has the effect of upraising and dispersing the pathogen and soothing the meridian Qi. *Scutellaria* has the effect of clearing and down-sending heat with bitter-cold, as well as eliminating the heat. *Panax ginseng* and *Zizyphus jujube* work compatibly to tonify Qi and fortify the spleen, thus strengthening the body and eliminate pathogens; *Pinellia ternate* and *Zingiber officinale* work together to regulate the stomach Qi and prevent vomit; and the "guide" *Glycyrrhiza glabra* is used to harmonize the other herbs. Nowadays, XCHT is used to treat common cold, chronic hepatitis, hepatic cirrhosis, bile reflux gastritis, cholecystitis, acute pancreatitis, and so forth, which belong to lesser yang syndrome.

3.1. Bupleurum falcatum. The root of *Bupleurum falcatum* L. (Umbelliferae), especially *B. chinense* from mainland China and *B. falcatum* from Japan [28, 29], is also called Bupleuri Radix ((BR) Chaihu, in Chinese and Saiko in Japanese) and is one of the principal herbs in XCHT. Early study examined the hepatoprotective effect of several BR extracts with dimethylnitrosamine- (DMN-) induced hepatic fibrosis rat model and these extracts appeared to prevent fibrosis by improving liver function and modulating the levels of relevant cytokines [29]. Recent studies also suggest BR extracts as potent antioxidant agents because they are able to decrease L-thyroxine-induced hypothyroidism and to enhance the liver antioxidant defense systems [30].

Some saikosaponins, which are the active ingredients of BR, have been found to suppress hepatic fibrosis [31, 32], hepatocarcinoma [33–36], and HBV infection [37] and improve chemotherapy [38]. The different mechanisms through which saikosaponins suppressed hepatocarcinoma were summarized in Figure 1. Saikosaponin a (SSa) was shown to effectively inhibit CCl_4-induced liver inflammation and fibrosis in SD rats by simultaneously blocking the production of hepatic proinflammatory cytokines/growth factors (TGFβ1 and hydroxyproline) and increasing the expression of anti-inflammatory cytokine IL-10 [31]. Saikosaponin d (SSd) was found to suppress hepatic fibrosis through the downregulation of TNF-α, IL-6, and NF-κB activities [32]. SSa may inhibit HepG2 growth by increasing the levels of p-15INK4a and p-16INK4b (cyclin-dependent kinase inhibitors) in a protein kinase C (PKC) [33] and/or extracellular signal-regulated kinase (ERK) signaling pathway-dependent manner [34]. SSd markedly reduced the liver nodule, tumor cell invasion while increased cellular atypia in xenograft model [35]. It appeared that SSd exerted its action by diminishing the expression of highly expressed cyclooxygenase 2 (COX-2) and CCAAT/enhancer-binding protein β (C/EBPβ) in tumor cells and macrophages of liver tumors [35]. In a study reported by Zhu et al. [36], SSd was shown capable of reversing the malignant phenotype of HepG2 cells. SSd-treated HepG2 cells grew and migrated at slower rate, had decreased volume ratios of nucleus to plasma and small round cell shape. At molecular level, SSd decreased the level of alpha-fetoprotein (AFP) and enhanced the expression of cell cycle inhibitor p27. Moreover, Chiang et al. showed that HBV-containing human hepatoma cells (2.2.15 cells) treated with saikosaponin c (SSc) secreted significantly less HBeAg into culture medium and had reduced HBV DNA replication [37]. Although not directly using liver cancer cells, SSa and SSd were also shown to sensitize cervical (HeLa and Siha), ovarian (SKOV3), and lung cancer cells (A549) to cisplatin-induced cell death by inducing the production of reactive oxygen species (ROS) and activation of caspases [38].

3.2. Scutellaria baicalensis. The dry root of *Scutellaria baicalensis*, Scutellaria radix ((SR) Hangqin, in Chinese) is

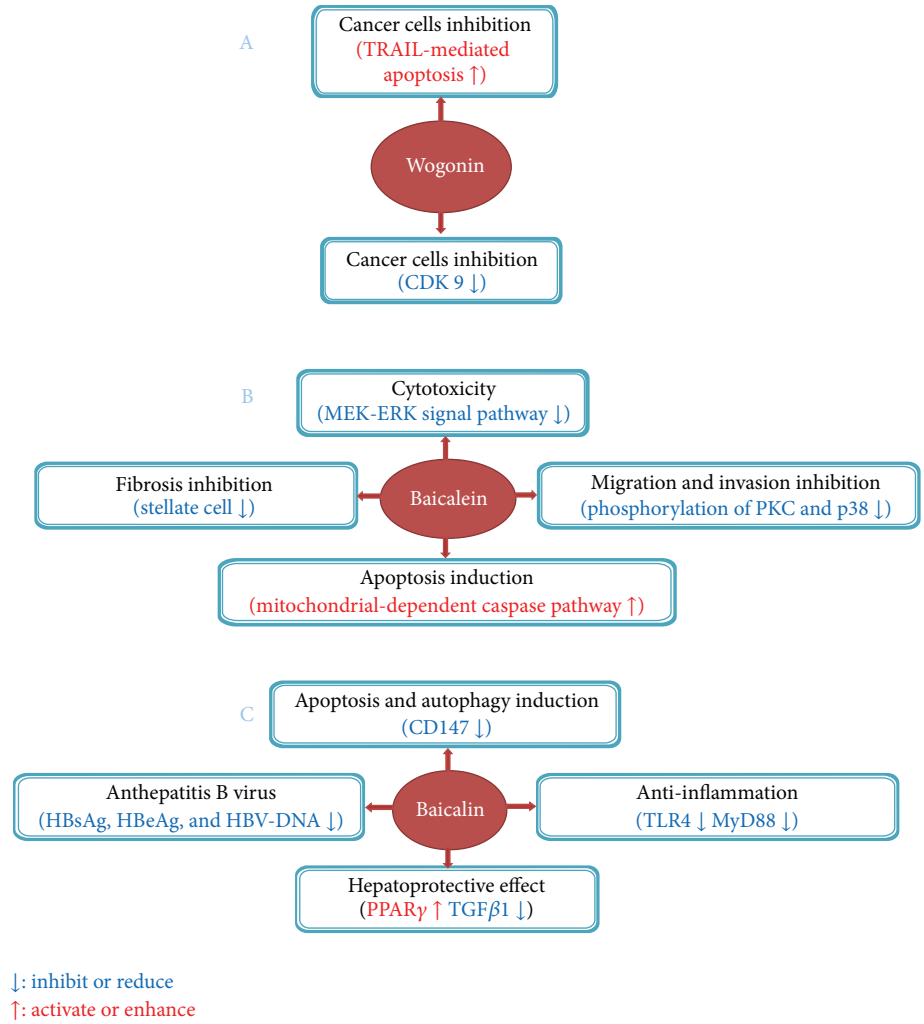

Figure 2: Suppressive effect of active components of *Scutellaria* radix on liver tumorigenesis and fibrosis.

another principal herb in XCHT. Accumulating evidences indicate that wogonin, baicalein, and baicalin are the principal active components in SR [39]. SR has been widely used to treat hyperlipemia, atherosclerosis, and hypertension. Recent studies with various model systems suggest that SR also possesses a potent cytostatic [40–42], anti-inflammatory [43] and antiviral capabilities [44, 45].

Antitumorigenesis ability of SR was reported by Gao et al. in human lung cancer cells (SK-MES-1, SK-LU-1, and A549) [42]. Their study showed that the absolute ethanol extracts of *Scutellaria baicalensis*, baicalin, baicalein, and wogonin all displayed a concentration- and time-dependent cytotoxicity to lung cancer cells while were only weakly cytotoxic to the normal human lung fibroblasts. Jung et al. later discovered that *Scutellaria baicalensis* is an anti-inflammatory agent because it decreases histamine release and inhibits the passive cutaneous anaphylaxis reaction in SD rats [43]. Antiviral effect of *Scutellaria baicalensis* was shown by Tang et al., in which it was shown to significantly inhibit the replication of HCV RNA in HCV-infected nude mice [44]. Later study revealed that the aqueous extract of *Scutellaria baicalensis* was also able to suppress the replication of lamivudine-resistant HBV mutant in human hepatoma cells by suppressing HBV core promoter activity [45].

Besides the studies performed with *Scutellaria baicalensis*, active components of it have also been extensively investigated (Figure 2). TNF-related apoptosis-inducing ligand (TRAIL) has been recognized as a promising anticancer agent because it kills tumor cells without damaging normal tissues [46, 47]. However, resistance to TRAIL is frequently seen in various tumor types. Ding et al. found that wogonin and structurally related natural flavones apigenin and chrysin overcame TRAIL resistance by downregulating the level of c-FLIP (a key inhibitor of death receptor signaling) and up-regulating TRAIL receptor 2 (TRAIL-R2) expression in human T-cell leukemia virus type 1- (HTLV-1-) associated adult T leukemia/lymphoma (ATL) cells [48]. They further showed that these flavones could enhance TRAIL-mediated apoptosis in a wide variety of cancer cell types including hepatocellular carcinomas (HepG2), breast (MDA-MB-231), colon (HT-29), and pancreatic cancer cells (Capan-1) as well as melanoma cells (SK-MEL-37) [48], implicating the use

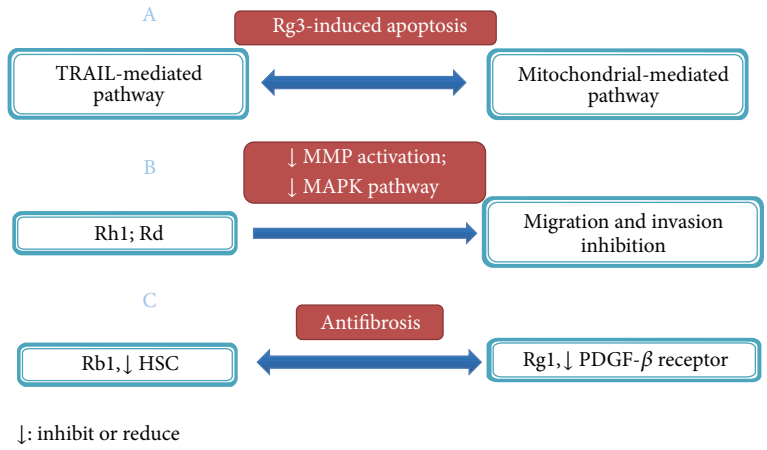

Figure 3: Antitumorigenesis effect of active components in ginseng.

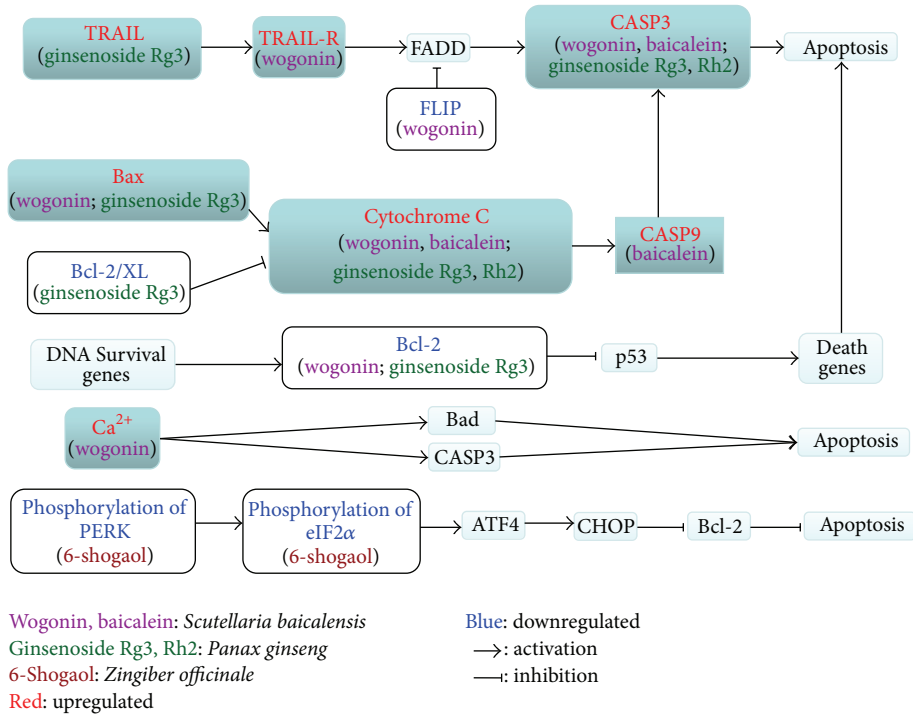

Figure 4: Tumor cell apoptosis-related pathways targeted by active components.

of flavones as an adjuvant for TRAIL-mediated anticancer therapy. In another study, Polier et al. initially showed that wogonin and flavones are inhibitors of cyclin-dependent kinase 9 (CDK9) and can effectively block phosphorylation of the carboxy-terminal domain of RNA polymerase II at Ser2, which in turn reduces RNA synthesis and subsequent down-regulation of antiapoptotic protein myeloid cell leukemia 1 (Mcl-1), leading to significant apoptosis in a variety of human cancer cells [49]. However, wogonin-induced apoptosis of human hepatocarcinoma cells was found to be accompanied with Bax increase and Bcl-2 decrease [50, 51]. Anti-HBV effect of wogonin was also found in vitro and in vivo [52], with the HBV antigen and HBV DNA level reduction.

Baicalein, a flavonoid extracted from SR, has been shown to possess potent antitumorigenesis capability toward liver cancer cells. For example, baicalein is highly cytotoxic to HCC cell lines and exerts its cytotoxicity by reducing mitochondrial transmembrane potential and subsequent cytochrome c release and caspase-3/9 activation. Disruption of MEK-ERK signaling pathway is at least partially responsible for baicalein-induced cytotoxicity [53, 54]. When used in vivo, baicalein can significantly inhibit tumor growth of HCC xenografts [53]. In another study, baicalein was reported to block cell migration and invasion of human hepatoma cells through multiple mechanisms including the suppression of MMP-2, MMP-9, and uPA expressions, blockage of NF-κB

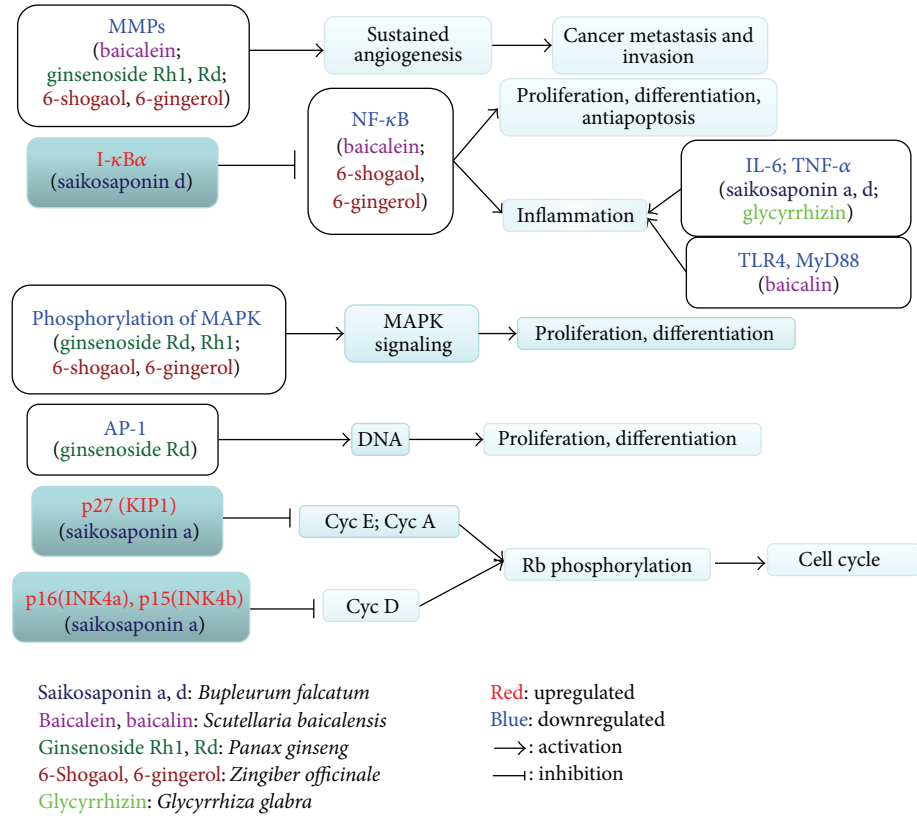

Figure 5: Tumor- and fibrosis-related pathways targeted by active components.

activation, and decreasing the phosphorylation levels of PKCα and p38 MAPK activities [55]. In a recent study, Sun et al. showed that baicalein dose dependently decreased AST, ALT, hyaluronic acid, laminin, and procollagen type III (PCIII) in serum as well as hydroxyproline and MMPs in liver in CCl_4-induced liver fibrosis model [56]. Moreover, baicalein also alleviated inflammation, destruction of liver architecture, collagen accumulation and expression of PDGFβ receptor, thus preventing the activation of stellate cells and liver fibrosis [56].

Baicalin is also an important active component included in SR. Zhang et al. [57] found that baicalin induced apoptosis with downregulation of glycosylated immunoglobulin superfamily transmembrane protein CD147 expression in SMMC-7721 cells, and interestingly, this effect was accompanied with cell autophagy. This study firstly suggested that baicalin induced autophagy cell death in SMMC-7721 cells and revealed a new mechanism for the anticancer effects of baicalin. Qiao et al. [58] studied the antihepatic fibrosis effect of baicalin and found that transplantation with baicalin-treated mesenchymal stem cells in combination with baicalin administration had the best therapeutic effect for hepatic fibrosis. This may further introduce a new therapeutic regimen for some liver diseases. Baicalin combined with oxymatrine showed better effect against HBV replication than oxymatrine in vitro, which was proved by Cheng et al. [59]. In aspects of the potential protective effect on liver injury, baicalin was also researched in many experiments [60–62]. Activation of peroxisome proliferator-activated receptor (PPARγ) signaling pathway, and Toll-like receptor 4- (TLR4-) mediated inflammatory responses were involved in the protective effect.

3.3. Panax ginseng. Ginseng products are regularly consumed worldwide for the purpose of increasing vitality [63]. Recently, many studies have shown the chemopreventive or adjuvant effect of it [64]. A study involving two cases of control (905 pairs and 1987 pairs, resp.) and a cohort (4675 subjects) demonstrated the benefit of ginseng use for cancer prevention as ginseng use was found to be nonorgan-specific cancer preventive, and its effect depends on the frequency of ginseng intake [65].

In addition to ginseng's preventive effect toward cancer, evidences from experimental studies also suggest its direct role to suppress liver tumorigenesis. Wu et al. showed that ginseng lowered the rate of hepatoma development and prolonged life span on diethylnitrosamine (DEN) rat liver cancer model [66]. Kwon et al. found that oral administration of ginseng decreased the levels of AST and ALT, number of degenerative cells, and area of connective tissue in the liver of dogs during liver regeneration after partial hepatectomy [67]. Bak et al. showed that the use of ginsengs' essential oil diminished the production of ROS and restored both the activities and expression of antioxidant enzymes including superoxide dismutase (SOD), glutathione peroxidase (GPx) and catalase (CAT) in H_2O_2-treated HepG2 cells or CCl_4-treated

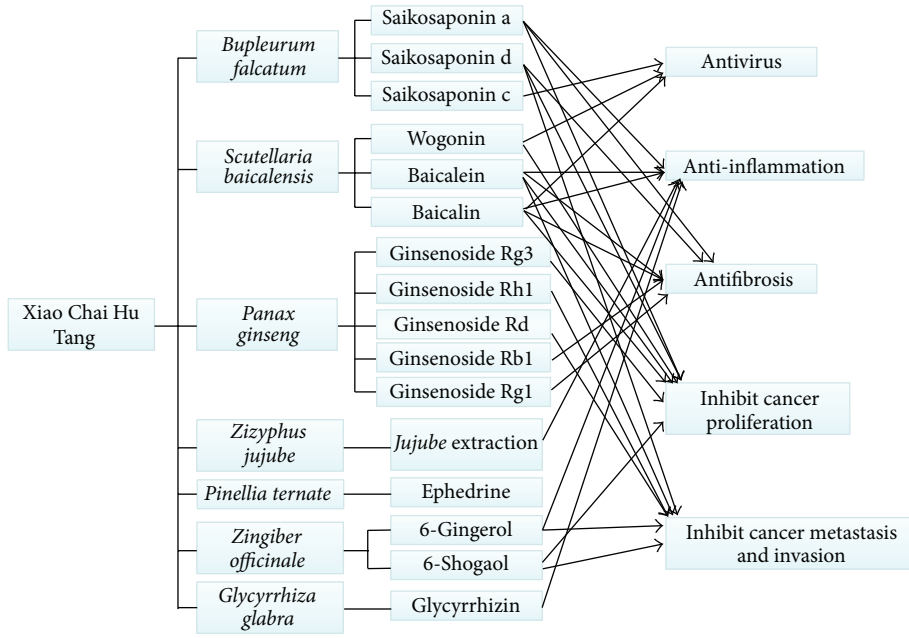

Figure 6: Antihepatocarcinoma effects of XCHT.

mice [68]. The effect of ginseng appears to be mediated by a simultaneous inhibition of JNK, ERK, and p38 activities and upregulated expression of antioxidant enzyme expression in the liver.

Components of ginseng have also been investigated for their inhibitory effect on liver tumorigenesis (Figure 3). Lee et al. showed that 20(S)-ginsenoside Rg3, a steroidal saponin was able to sensitize HCCs, but not normal hepatocytes to TRAIL-induced cell death [69]. Importantly, Rg3 was found to be well tolerated in animals and significantly enhance the therapeutic efficacy of TRAIL in xenograft models [69]. And other studies [70, 71] suggested that intrinsic apoptotic pathway may be involved in the inhibitory effect of Rg3 on hepatocellular carcinoma cell lines. To elucidate the mechanism associated with ginseng extract-induced cell death, Park et al. showed that primary ginsenosides Rg3 and Rh2 are mainly responsible for ginseng's effect and they act by directly activating mitochondrial-dependent apoptotic pathway and inducing the production of intracellular ROS [72].

Components of ginseng also exhibit their tumor-suppressing capability by blocking cell migration and invasion. Yoon et al. found that ginsenoside Rh1 inhibited HepG2 cell migration and invasion by abrogating MAPK-dependent MMP-1 expression [73]. Similar effect was also observed with ginsenoside Rd in HepG2 cells [74]. As excess production of extracellular matrix by activated hepatic stellate cells (HSCs) is the major cause of liver fibrosis, Lo et al. determined the potential protective effect of ginseng components toward liver fibrosis. They revealed that ginsenoside Rb1 exerted an antifibrotic effect under H_2O_2 oxidative stress by inhibiting HSC activation/proliferation [75]. Another ginsenoside, Rg1, has also been shown to prevent thioacetamide-induced hepatic fibrosis in rats by intercepting NF-κB-mediated PDGFβ receptor expression [76].

3.4. Other Herbs in XCHT. Besides the three herbs that have been described above, the remaining herbs in XCHT are *Zizyphus jujube*, *Pinellia ternate*, *Zingiber officinale*, *and Glycyrrhiza glabra* and act as adjuvant herbs in this compound formula. *Zizyphus jujube* in XCHT is prescribed by Traditional Chinese Medicine doctors to calm mind based on its ability to invigorate the spleen and nourish the blood. Recent experimental evidences showed that it was able to attenuate chemical-induced liver injury in rats [77, 78]. *Pinellia ternate* is another herb in XCHT while the mechanism study about its antihepatocarcinoma effect is rare. Although it appears to boost the efficacy of XCHT, how it does this awaits being further explored. *Zingiber officinale*, a species used for over thousand years, appears to display anticancer, anti-inflammatory, and chemopreventive effects in both in vitro and in vivo models [79, 80]. 6-shogaol and 6-gingerol are the two active compounds of ginger, and their effects of apoptosis induction [81], hepatocarcinoma invasion inhibition [82] and anti-hepatoxicity [83] were also studied. Licorice is the dried root of *Glycyrrhiza uralensis* Fisch, and both the extract [84, 85] and its active component glycyrrhizin [86, 87] were explored for their hepatoprotective capability. Though these adjuvant herbs are also essential in XCHT from the view point of TCM, modern mechanism studies about their anti-hepatocarcinoma effects are relatively less than *Bupleurum falcatum*, *Scutellaria baicalensis,* and *Panax ginseng*. So we did not summarize the antihepatocarcinoma-related effects of these adjuvant herbs as detailedly as the former three herbs here.

4. Summary and Prospect

Besides the summary above, experimental studies of the active components in the herbs on antihepatocarcinoma-related effects are further summarized in Tables 2, 3, 4,

Table 2: Apoptosis-inducing effects of active components.

Author; year	Animal or cell	Active components	Factors and pathways
Wu and Hsu [33]; 2001	HepG2 cells	Saikosaponin a	PKC signaling pathway involved; CDK inhibitor p-15^{INK4a} and p-16^{INK4b} mRNA and protein↑
Wu [34]; 2003	HepG2 cells	Saikosaponin a	ERK signaling pathway involved; CDK inhibitor p-15^{INK4a} and p-16^{INK4b} mRNA and protein↑
Wang et al. [38]; 2010	Cervical cancer (HeLa and Siha); ovarian cancer (SKOV3); non-small-cell lung cancer (A549) cell lines	Saikosaponin a, d	ROS↑; caspase pathway activation
Ding et al. [48]; 2012	HTLV-1-associated ATL	Wogonin	c-FLIP↓; TRAIL-R2 expression↑
Polier et al. [49]; 2011	The human colorectal carcinoma (HCT116); the human leukemic T-cell line (CEM); the adult T-cell leukemic cell line (SP)	Wogonin	CDK9↓; antiapoptotic protein Mcl-1↓
Wang et al. [50]; 2006	Human hepatoma cell line (SMMC-7721)	Wogonin	Bax↑Bcl-2↓
Lin et al. [51]; 2011	Human osteosarcoma cell line (U-2 OS)	Wogonin	ROS↑ intracellular $Ca2^{+}$ ↑ caspase-3 activity↑; Bad, Bax, cytochrome c↑; mitochondrial membrane potential↓
Liang et al. [53]; 2012	HCC cell lines; mice with HCC xenografts	Baicalein	Mitochondrial transmembrane potential↓; caspase-9, caspase-3↑; phosphorylation of MEK1, ERK1/2, and Bad↓
Kuo et al. [54]; 2009	Human hepatoma J5 cells	Baicalein	Mitochondrial-dependent caspase activation pathway involved (mitochondrial cytochrome c release; activation of caspase-9 and -3; the ratio of Bax/Bcl-2↑)
Zhang et al. [57]; 2012	HCC cell line (SMMC-7721)	Baicalin	CD147↓ cell apoptosis and autophagy were induced
Lee et al. [69]; 2012	HepG2, SK-Hep1, Huh-7, and Hep3B cell lines; mouse xenograft model	Ginsenoside Rg3	Promoting TRAIL-induced apoptosis
Zhang et al. [70]; 2012	Human hepatocellular carcinoma cell lines (SMMC-7721; HepG2)	Ginsenoside Rg3	Gene expression of caspase-3; Bax↑; Bcl-2↓
Jiang et al. [71]; 2011	Hep1-6 and HepG2 cells; liver tumor-bearing C57Bl6 mice	Ginsenoside Rg3	Mitochondrial pathway involved (mitochondria membrane potential↓; caspase-3 activation↑; Bax↑ Bcl-2 and Bcl-XL↓)
Park et al. [72]; 2012	Human hepatocellular carcinoma cells (Hep3B)	Ginsenoside Rg3, Rh2	Activating the mitochondrial pathway (ROS↑; Bax↑ Bcl-2↓; cytochrome c↑; activation of caspase-3)
Hu et al. [81]; 2012	SMMC-7721, BEL-7404, HL-7702 cells; SMMC-7721 xenograft-bearing mouse	6-Shogaol	Unfolded protein response (UPR)↑; PERK/eIF2α pathway↑; eIF2α phosphorylation↓; caspase 3↑

and 5 based on their distinct cellular aspects, and some other carcinoma cell lines were also included in Tables 2–5 to better elucidate the mechanism. What is more, to systematically organize the mechanism, we searched Kyoto Encyclopedia of Genes and Genomes (KEGG) database (http://www.genome.jp/kegg/) to connect the factors and pathways together which were targeted by the active components, as presented in Figures 4 and 5. Though the two

Table 3: Metastasis and invasion-inhibitory effects of active components.

Author; year	Animal or cell	Active components	Factors and pathways
Zhu et al. [36]; 2011	HepG2 cells	Saikosaponin d	Cell growth↓ cell migration↓; AFP↓; p27 mRNA expression↑
Chiu et al. [55]; 2011	human hepatoma cell lines (HA22T/VGH and SK-Hep1)	Baicalein	The gelatinolytic activities of MMP-2, MMP-9, uPA↓; NF-κB activation↓; phosphorylation of PKCα and p38 proteins↓
Yoon et al. [73]; 2012	HepG2 cells	Ginsenoside Rh1	Inactivation of MAPKs; MMP-1 gene expression↓
Yoon et al. [74]; 2012	HepG2 cells	Ginsenoside Rd	MAPK signaling↓; activation of AP-1↓; expression of MMP-1, MMP-2, and MMP-7↓
Weng et al. [82]; 2012	Hep3B cells	6-Shogaol; 6-gingerol	MMP-2 and MMP-9↓; uPA↓; the phosphorylation of MAPK↓; PI3K/Akt signaling↓; NF-κB activation↓

Table 4: Inflammation and fibrosis inhibitory effects of active components.

Author; year	Animal or cell	Active components	Factors and pathways
Wu et al. [31]; 2010	CCl_4-induced liver inflammation and fibrosis rats	Saikosaponin a	Proinflammatory cytokines TNF-α, IL-1β, IL-6↓; anti-inflammatory cytokine IL-10↑; TGF-β1 and hydroxyproline↓; NF-κB↓
Dang et al. [32]; 2007	Liver fibrotic rats	Saikosaponin d	TNF-α, IL-6 and NF-κBp65 expression↓; I-κBα activity↑
Sun et al. [56]; 2010	CCl_4-induced liver fibrosis rats	Baicalein	AST, ALT, hyaluronic acid, laminin, and PDGF-β receptor↓; hydroxyproline, MMPs↓
Qiao et al. [60]; 2011	CCl_4-induced liver injury rats	Baicalin	PPARγ↑; TGFβ1↓
Kim and Lee [62]; 2012	Ischemia/reperfusion injured rats with alcoholic fatty liver	Baicalin	Toll-like receptor 4 (TLR4)↓; myeloid differentiation primary response protein My88↓
Lo et al. [75]; 2011	HSCs	Ginsenoside Rb1	HSCs activation and proliferation↓; expression of collagen, TGF-β1, MMP-2, and TIMP-1↓
Geng et al. [76]; 2010	Thioacetamide-treated rats; HSCs	Ginsenoside Rg1	AST, ALT, hydroxyproline↓; HSCs↓; PDGF-β receptor expression↓
Sabina et al. [83]; 2011	Acetaminophen-treated mice	6-gingerol	The hepatic marker enzymes (AST, ALT, and ALP) and total bilirubin in serum↓; hepatic malondialdehyde formation↓; liver antioxidant status↑
Gumpricht et al. [86]; 2005	Rat hepatocytes exposed to GCDC	Glycyrrhizin; 18-beta-glycyrrhetinic acid	Glycyrrhizin-enhanced GCDC induced cell apoptosis; 18-beta-glycyrrhetinic acid reduced cell necrosis and protected against GCDC-induced cell apoptosis
Lee et al. [87]; 2007	CCl_4-induced liver injury rats	Glycyrrhizin	Liver function improvement; proinflammatory mediators (TNF-α, inducible nitric oxide synthase, and COX-2)↓; heme oxygenase-1↑;

Table 5: Antiviral effect of active components.

Author; year	Animal or cell	Active components	Factors and pathways
Chiang et al. [37]; 2003	HBV-transfected human hepatoma cells	Saikosaponin c	HBeAg↓; HBV DNA↓
Guo et al. [52]; 2007	HepG2.2.15; HBV-infected ducks; HBV-transgenic mice	Wogonin	HBsAg and HBeAg↓; HBV DNA↓
Cheng et al. [59]; 2006	HepG2.2.15 cells	Baicalin	HBsAg and HBeAg↓; HBV DNA↓

figures cannot present all the targets summarized in our paper, they still could illustrate the mechanism from a more systematical aspect. On the basis of Figures 1 to 5, we depicted Figure 6 to better display the antihepatocarcinoma effects at three different levels of formula, herbs, and components. From them, it is apparent that components of XCHT possess a broad spectrum of activities ranging from antitumor, anti-inflammation to fibrosis-protective effects. Some of the components directly target on tumor growth, metastasis, and invasion, while others act on inflammation and fibrosis related pathways or antiviral process to prevent further virus-facilitated tumorigenesis. Particularly, many of these components share analogous factors and pathways.

Besides tumor growth, metastasis and invasion, angiogenesis is also an essential pathological component of cancer. Antiangiogenic therapy is considered to limit tumor progression [88]. Research about the anti-angiogenic effect on hepatocarcinoma of XCHT has not been seen, while some reseachers have studied the effect of herbs and active compounds in it on the angiogenic action [89–91]. Interestingly, different compounds in ginseng (ginsenoside Rg3 and Rg1) possessed contrary angiogenic action (antiangiogenic and angiogenic effects) [89, 90]. What is more, as we summarized in our review, components of XCHT may affect various biochemical pathways, many of which are related to angiogenesis [92]. So it is also worthy to deeply study XCHT's effect on the angiogenic action for tumor treatment.

Our overview is based on a perspective of "separation study," that is, arranging from the entire formula to each herb and their active components. This method may comprehensively utilize and deeply excavate the existing researches. It is difficult to directly elucidate a complex formula, while it will be easier when we separately study the constituents in it. Currently, to unequivocally interpret the antihepatocarcinoma effect of XCHT and the active ingredients contained in it is still difficult. The underlying reasons are severalfold. The first is that the knowledge on how each component works is still not sufficient and their respective targets are still needed to be identified. The second is how these components work in concert to achieve therapeutic effect is not understood. As the philosophy of Traditional Chinese Medicine, compound herbal formulas are used to treat disease by regulating human body globally, targeting multiple pathways and targets. This characteristic may be better coincident with cancer which may be induced by multiple factors. Tumor growth, metastasis, and invasion are the final features that we notice, but the underlying mechanism may be related with many factors. The method of "separation study" should be combined with bioinformatics, meaning that we may use bioinformatics to integrate these separated studies. So more innovative researches and novel strategies will have to be employed to fully understand the mechanisms responsible for XCHT's therapeutic effects.

Abbreviations

ATL: Adult T-cell leukemia/lymphoma
ALP: Alkaline phosphatase
AFP: Alpha-fetoprotein
AP-1: Activator protein-1
ATF4: Cyclic AMP-dependent transcription factor
c-FLIP: Cellular FLICE inhibitory protein (CASP8 and FADD-like apoptosis regulator)
CASP: Caspase
CycD: Cyclin D
CDK9: Cyclin-dependent kinase 9
COX-2: Cyclooxygenase 2
C/EBPβ: CCAAT/enhancer-binding protein β
CD147: Glycosylated immunoglobulin superfamily transmembrane protein
CHOP: C/EBP homologous protein
DEN: Diethylnitrosamine
ERK: Extracellular signal-regulated kinase
eIF2α: Translation initiation factor
FADD: FAS-associated death domain protein
GCDC: Glycochenodeoxycholic acid
HTLV-1: Human T-cell leukemia virus type1
HSCs: Hepatic stellate cells
HBsAg: Hepatitis B surface antigen
HBeAg: Hepatitis B e antigen
I-κBα: NF-kappa-B inhibitor alpha
Mcl-1: Myeloid cell leukemia-1
MMP: Matrix metalloproteinase
MAPK: Mitogen-activated protein kinase
My88: Myeloid differentiation primary response protein
PKC: Protein kinase C
PDGF: Platelet derived growth factor
PERK: PKR-like endoplasmic reticulum associated kinase (eukaryotic translation initiation factor kinase)
PPARγ: Peroxisome proliferator-activated receptor γ
ROS: Reactive oxygen species
Rb: Retinoblastoma-associated protein
TRAIL-R2: TNF-related apoptosis-inducing ligand receptor 2
TIMP: Tissue inhibitor of metalloproteinase
TGFβ1: Tumor growth factor β1
TLR4: Toll-like receptor 4
uPA: Urokinase plasminogen activator.

Authors' Contribution

Ningning Zheng, Jianye Dai, and Huijuan Cao have contributed equally to this work and should be considered as co-first authors.

Acknowledgments

This paper was supported by Shanghai Interdisciplinary Cultivation Platform of Outstanding and Innovative Postgraduates and Shanghai "085" Science and Technology Innovation Supporting Project for Top-Grade Discipline Construction.

References

[1] http://www.cancer.org/cancer/livercancer/overviewguide/liver-cancer-overview-key-statistics.

[2] H. B. El-Serag, "Epidemiology of viral hepatitis and hepatocellular carcinoma," *Gastroenterology*, vol. 142, no. 6, pp. 1264–1273, 2012.

[3] E. A. Akriviadis, J. M. Llovet, S. C. Efremidis et al., "Hepatocellular carcinoma," *British Journal of Surgery*, vol. 85, no. 10, pp. 1319–1331, 1998.

[4] I. Hyodo, N. Amano, K. Eguchi et al., "Nationwide survey on complementary and alternative medicine in cancer patients in Japan," *Journal of Clinical Oncology*, vol. 23, no. 12, pp. 2645–2654, 2005.

[5] X. Q. Li and C. Q. Ling, "Chinese herbal medicine for side effects of transarterial chemoembolization in liver cancer patients: a systematic review and meta-analysis," *Zhong Xi Yi Jie He Xue Bao*, vol. 10, no. 12, pp. 1341–1362, 2012.

[6] J. L. McQuade, Z. Meng, Z. Chen et al., "Utilization of and attitudes towards traditional Chinese medicine therapies in a Chinese cancer hospital: a survey of patients and physicians," *Evidence-Based Complementary and Alternative Medicine*, vol. 2012, Article ID 504507, 11 pages, 2012.

[7] W.-J. Ruan, M.-D. Lai, and J.-G. Zhou, "Anticancer effects of Chinese herbal medicine, science or myth?" *Journal of Zhejiang University. Science. B*, vol. 7, no. 12, pp. 1006–1014, 2006.

[8] C. Hirayama, M. Okumura, K. Tanikawa, M. Yano, M. Mizuta, and N. Ogawa, "A multicenter randomized controlled clinical trial of Shosaiko-to in chronic active hepatitis," *Gastroenterologia Japonica*, vol. 24, no. 6, pp. 715–719, 1989.

[9] H. Oka, A. Yamamoto, T. Kuroki et al., "Prospective study of chemoprevention of hepatocellular carcinoma with Shosaiko-to (TJ-9)," *Cancer*, vol. 76, no. 5, pp. 743–749, 1995.

[10] X.-K. Qin, P. Li, M. Han, and J.-P. Liu, "Xiaochaihu Tang for treatment of chronic hepatitis B: a systematic review of randomized trials," *Journal of Chinese Integrative Medicine*, vol. 8, no. 4, pp. 312–320, 2010.

[11] G. Deng, R. C. Kurtz, A. Vickers et al., "A single arm phase II study of a Far-Eastern traditional herbal formulation (shosai-ko-to or xiao-chai-hu-tang) in chronic hepatitis C patients," *Journal of Ethnopharmacology*, vol. 136, no. 1, pp. 83–87, 2011.

[12] I. Shimizu, "Sho-saiko-to: Japanese herbal medicine for protection against hepatic fibrosis and carcinoma," *Journal of Gastroenterology and Hepatology*, vol. 15, supplement, pp. D84–D90, 2000.

[13] J.-K. Lee, J.-H. Kim, and H. K. Shin, "Therapeutic effects of the oriental herbal medicine Sho-saiko-to on liver cirrhosis and carcinoma," *Hepatology Research*, vol. 41, no. 9, pp. 825–837, 2011.

[14] Q. L. Bo and W. W. Du, "Effect observation of fifty chronic hepatitis B patients under the treatment of interferon combined with xiaochaihu tang," *Shandong Medical Journal*, vol. 46, no. 8, pp. 82–83, 2006 (Chinese).

[15] Z. Li, H. H. Liao, M. J. Wu, and Z. H. Lin, "Study on the combination treatment of γ-interferon and xiaochaihu tang on liver fibrosis," *Chinese Journal of Integrated Traditional and Western Medicine on Liver Diseases*, vol. 11, supplement, p. 95, 2001 (Chinese).

[16] W. H. Sun, M. Q. Song, and Z. J. Liu, "Study on the combination treatment of xiaochaihu tang and oxymatrine on hepatitis and hepato-fibrosis," *Chinese Journal of Integrated Traditional and Western Medicine on Liver Diseases*, vol. 13, no. 1, pp. 41–42, 2003 (Chinese).

[17] Q. Q. Wu, "Clinical observation on the effect of xiaochaihu tang on chronic hepatitis B with cirrhosis patients," *Journal of Zhejiang College of Traditional Chinese Medicine*, vol. 33, no. 4, pp. 517–518, 2009 (Chinese).

[18] H. Yano, A. Mizoguchi, K. Fukuda et al., "The herbal medicine sho-saiko-to inhibits proliferation of cancer cell lines by inducing apoptosis and arrest at the G0/G1 phase," *Cancer Research*, vol. 54, no. 2, pp. 448–454, 1994.

[19] T. Makino, R. Tsubouchi, K. Murakami, M. Haneda, and M. Yoshino, "Generation of reactive oxygen species and induction of apoptosis of HL60 cells by ingredients of traditional herbal medicine, Sho-saiko-to," *Basic and Clinical Pharmacology and Toxicology*, vol. 98, no. 4, pp. 401–405, 2006.

[20] K. Zhu, I. Fukasawa, M. Furuno et al., "Inhibitory effects of herbal drugs on the growth of human ovarian cancer cell lines through the induction of apoptosis," *Gynecologic Oncology*, vol. 97, no. 2, pp. 405–409, 2005.

[21] J. Li, M. Xie, and Y. Gan, "Effect of Xiaochaihu decoction and different herbal formulation of component on inhibiting H22 liver cancer in mice and enhancing immune function," *Zhongguo Zhongyao Zazhi*, vol. 33, no. 9, pp. 1039–1044, 2008 (Chinese).

[22] J.-S. Chang, K.-C. Wang, H.-W. Liu, M.-C. Chen, L.-C. Chiang, and C.-C. Lin, "Sho-saiko-to (Xiao-Chai-Hu-Tang) and crude saikosaponins inhibit Hepatitis B virus in a stable HBV-producing cell line," *American Journal of Chinese Medicine*, vol. 35, no. 2, pp. 341–351, 2007.

[23] P.-W. Cheng, L.-T. Ng, and C.-C. Lin, "Xiao Chai Hu Tang inhibits CVB1 virus infection of CCFS-1 cells through the induction of type I interferon expression," *International Immunopharmacology*, vol. 6, no. 6, pp. 1003–1012, 2006.

[24] A. Cucchetti, M. Cescon, F. Trevisani, and A. D. Pinna, "Current concepts in hepatic resection for hepatocellular carcinoma in cirrhotic patients," *World Journal of Gastroenterology*, vol. 18, no. 44, pp. 6398–6408, 2012.

[25] M. Kusunose, B. Qiu, T. Cui et al., "Effect of Sho-saiko-to extract on hepatic inflammation and fibrosis in dimethylnitrosamine induced liver injury rats," *Biological and Pharmaceutical Bulletin*, vol. 25, no. 11, pp. 1417–1421, 2002.

[26] M.-H. Chen, J.-C. Chen, C.-C. Tsai et al., "The role of TGF-β1 and cytokines in the modulation of liver fibrosis by Sho-saiko-to in rat's bile duct ligated model," *Journal of Ethnopharmacology*, vol. 97, no. 1, pp. 7–13, 2005.

[27] B. S. Dun, *Fang Ji Xue*, Xi'an Jiaotong University Press, Xi'an, China, 2nd edition, 2011.

[28] B. Lee, I. Shim, H. Lee, and D.-H. Hahm, "Effect of Bupleurum falcatum on the stress-induced impairment of spatial working memory in rats," *Biological and Pharmaceutical Bulletin*, vol. 32, no. 8, pp. 1392–1398, 2009.

[29] M.-H. Yen, T.-C. Weng, S.-Y. Liu, C.-Y. Chai, and C.-C. Lin, "The hepatoprotective effect of Bupleurum kaoi, an endemic plant to Taiwan, against dimethylnitrosamine-induced hepatic fibrosis in rats," *Biological and Pharmaceutical Bulletin*, vol. 28, no. 3, pp. 442–448, 2005.

[30] S. M. Kim, S. C. Kim, I. K. Chung, W. H. Cheon, and S. K. Ku, "Antioxidant and protective effects of Bupleurum falcatum on the L-thyroxine-induced hyperthyroidism in rats," *Evidence-Based Complementary and Alternative Medicine*, vol. 2012, Article ID 578497, 12 pages, 2012.

[31] S.-J. Wu, K.-W. Tam, Y.-H. Tsai, C.-C. Chang, and J. C.-J. Chao, "Curcumin and saikosaponin a inhibit chemical-induced liver inflammation and fibrosis in rats," *American Journal of Chinese Medicine*, vol. 38, no. 1, pp. 99–111, 2010.

[32] S.-S. Dang, B.-F. Wang, Y.-A. Cheng, P. Song, Z.-G. Liu, and Z.-F. Li, "Inhibitory effects of saikosaponin-d on CCl_4-induced hepatic fibrogenesis in rats," *World Journal of Gastroenterology*, vol. 13, no. 4, pp. 557–563, 2007.

[33] W.-S. Wu and H.-Y. Hsu, "Involvement of p-15^{INK4b} and p-16^{INK4a} gene expression in saikosaponin a and TPA-induced growth inhibition of HepG2 cells," *Biochemical and Biophysical Research Communications*, vol. 285, no. 2, pp. 183–187, 2001.

[34] W.-S. Wu, "ERK signaling pathway is involved in $p15^{INK4b}$/$p16^{INK4a}$ expression and HepG2 growth inhibition triggered by TPA and Saikosaponin a," *Oncogene*, vol. 22, no. 7, pp. 955–963, 2003.

[35] X.-L. Lu, S.-X. He, M.-D. Ren, Y.-L. Wang, Y.-X. Zhang, and E.-Q. Liu, "Chemopreventive effect of saikosaponin-d on diethylinitrosamine-induced hepatocarcinogenesis: involvement of CCAAT/enhancer binding protein β and cyclooxygenase-2," *Molecular Medicine Reports*, vol. 5, no. 3, pp. 637–644, 2012.

[36] B. H. Zhu, R. Pu, G. P. Zhang, M. Y. Li, L. T. Wang, and J. K. Yuan, "Effect of Saikosaponins-d on reversing malignant phenotype of HepG2 cells in vitro," *Zhonghua Gan Zang Bing Za Zhi*, vol. 19, no. 10, pp. 764–767, 2011 (Chinese).

[37] L.-C. Chiang, L. T. Ng, L.-T. Liu, D.-E. Shieh, and C.-C. Lin, "Cytotoxicity and anti-hepatitis B virus activities of saikosaponins from Bupleurum species," *Planta Medica*, vol. 69, no. 8, pp. 705–709, 2003.

[38] Q. Wang, X.-L. Zheng, L. Yang et al., "Reactive oxygen species-mediated apoptosis contributes to chemosensitization effect of saikosaponins on cisplatin-induced cytotoxicity in cancer cells," *Journal of Experimental and Clinical Cancer Research*, vol. 29, no. 1, article 159, 2010.

[39] M. Li-Weber, "New therapeutic aspects of flavones: the anticancer properties of Scutellaria and its main active constituents Wogonin, Baicalein and Baicalin," *Cancer Treatment Reviews*, vol. 35, no. 1, pp. 57–68, 2009.

[40] S. Ikemoto, K. Sugimura, N. Yoshida et al., "Antitumor effects of Scutellariae radix and its components baicalein, baicalin, and wogonin on bladder cancer cell lines," *Urology*, vol. 55, no. 6, pp. 951–955, 2000.

[41] D. Y. Zhang, J. Wu, F. Ye et al., "Inhibition of cancer cell proliferation and prostaglandin E2 synthesis by Scutellaria baicalensis," *Cancer Research*, vol. 63, no. 14, pp. 4037–4043, 2003.

[42] J. Gao, W. A. Morgan, A. Sanchez-Medina, and O. Corcoran, "The ethanol extract of Scutellaria baicalensis and the active compounds induce cell cycle arrest and apoptosis including upregulation of p53 and Bax in human lung cancer cells," *Toxicology and Applied Pharmacology*, vol. 254, no. 3, pp. 221–228, 2011.

[43] H.-S. Jung, M. H. Kim, N.-G. Gwak et al., "Antiallergic effects of Scutellaria baicalensis on inflammation in vivo and in vitro," *Journal of Ethnopharmacology*, vol. 141, no. 1, pp. 345–349, 2012.

[44] Z.-M. Tang, M. Peng, and C.-J. Zhan, "Screening 20 Chinese herbs often used for clearing heat and dissipating toxin with nude mice model of hepatitis C viral infection," *Zhongguo Zhong Xi Yi Jie He Za Zhi*, vol. 23, no. 6, pp. 447–448, 2003 (Chinese).

[45] Y. P. Tseng, Y. C. Wu, Y. L. Leu, S. F. Yeh, and C. K. Chou, "Scutellariae radix suppresses hepatitis B virus production in human hepatoma cells," *Frontiers in Bioscience*, vol. 2, pp. 1538–1547, 2010.

[46] S. R. Wiley, K. Schooley, P. J. Smolak et al., "Identification and characterization of a new member of the TNF family that induces apoptosis," *Immunity*, vol. 3, no. 6, pp. 673–682, 1995.

[47] B. R. James and T. S. Griffith, "Activation of systemic antitumor immunity via TRAIL-induced apoptosis," *Oncoimmunology*, vol. 1, no. 7, pp. 1178–1180, 2012.

[48] J. Ding, G. Polier, R. Köhler, M. Giaisi, P. H. Krammer, and M. Li-Weber, "Wogonin and related natural flavones overcome tumor necrosis factor-related apoptosis-inducing ligand (TRAIL) protein resistance of tumors by down-regulation of c-FLIP protein and up-regulation of TRAIL receptor 2 expression," *The Journal of Biological Chemistry*, vol. 287, no. 1, pp. 641–649, 2012.

[49] G. Polier, J. Ding, B. V. Konkimalla et al., "Wogonin and related natural flavones are inhibitors of CDK9 that induce apoptosis in cancer cells by transcriptional suppression of Mcl-1," *Cell Death & Disease*, vol. 2, no. 7, article e182, 2011.

[50] W. Wang, Q. Guo, Q. You et al., "Involvement of bax/bcl-2 in wogonin-induced apoptosis of human hepatoma cell line SMMC-7721," *Anti-Cancer Drugs*, vol. 17, no. 7, pp. 797–805, 2006.

[51] C.-C. Lin, C.-L. Kuo, M.-H. Lee et al., "Wogonin triggers apoptosis in human osteosarcoma U-2 OS cells through the endoplasmic reticulum stress, mitochondrial dysfunction and caspase-3-dependent signaling pathways," *International Journal of Oncology*, vol. 39, no. 1, pp. 217–224, 2011.

[52] Q. Guo, L. Zhao, Q. You et al., "Anti-hepatitis B virus activity of wogonin in vitro and in vivo," *Antiviral Research*, vol. 74, no. 1, pp. 16–24, 2007.

[53] R. R. Liang, S. Zhang, J. A. Qi et al., "Preferential inhibition of hepatocellular carcinoma by the flavonoid Baicalein through blocking MEK-ERK signaling," *International Journal of Oncology*, vol. 41, no. 3, pp. 969–978, 2012.

[54] H.-M. Kuo, H.-C. Tsai, Y.-L. Lin et al., "Mitochondrial-dependent caspase activation pathway is involved in baicalein-induced apoptosis in human hepatoma J5 cells," *International Journal of Oncology*, vol. 35, no. 4, pp. 717–724, 2009.

[55] Y.-W. Chiu, T.-H. Lin, W.-S. Huang et al., "Baicalein inhibits the migration and invasive properties of human hepatoma cells," *Toxicology and Applied Pharmacology*, vol. 255, no. 3, pp. 316–326, 2011.

[56] H. Sun, Q.-M. Che, X. Zhao, and X.-P. Pu, "Antifibrotic effects of chronic baicalein administration in a CCl_4 liver fibrosis model in rats," *European Journal of Pharmacology*, vol. 631, no. 1–3, pp. 53–60, 2010.

[57] X. Zhang, X. Tang, H. Liu, L. Li, Q. Hou, and J. Gao, "Autophagy induced by baicalin involves downregulation of CD147 in SMMC-7721 cells in vitro," *Oncology Reports*, vol. 27, no. 4, pp. 1128–1134, 2012.

[58] H. Qiao, Y. Tong, H. Han et al., "A novel therapeutic regimen for hepatic fibrosis using the combination of mesenchymal stem cells and baicalin," *Pharmazie*, vol. 66, no. 1, pp. 37–43, 2011.

[59] Y. Cheng, J. Ping, H.-D. Xu, H.-J. Fu, and Z.-H. Zhou, "Synergistic effect of a noval oxymatrine-baicalin combination against hepatitis B virus replication, α smooth muscle actin expression and type I collagen synthesis in vitro," *World Journal of Gastroenterology*, vol. 12, no. 32, pp. 5153–5159, 2006.

[60] H. Qiao, H. Han, D. Hong, Z. Ren, Y. Chen, and C. Zhou, "Protective effects of baicalin on carbon tetrachloride induced liver injury by activating PPARγ and inhibiting TGFβ1," *Pharmaceutical Biology*, vol. 49, no. 1, pp. 38–45, 2011.

[61] S.-W. Park, C.-H. Lee, Y. S. Kim et al., "Protective effect of baicalin against carbon tetrachloride-induced acute hepatic injury in mice," *Journal of Pharmacological Sciences*, vol. 106, no. 1, pp. 136–143, 2008.

[62] S.-J. Kim and S.-M. Lee, "Effect of baicalin on toll-like receptor 4-mediated ischemia/reperfusion inflammatory responses in alcoholic fatty liver condition," *Toxicology and Applied Pharmacology*, vol. 258, no. 1, pp. 43–50, 2012.

[63] L. Jia, Y. Zhao, and X.-J. Liang, "Current evaluation of the millennium phytomedicine—ginseng (II): collected chemical entities, modern pharmacology, and clinical applications emanated from traditional chinese medicine," *Current Medicinal Chemistry*, vol. 16, no. 22, pp. 2924–2942, 2009.

[64] S. Helms, "Cancer prevention and therapeutics: Panax ginseng," *Alternative Medicine Review*, vol. 9, no. 3, pp. 259–274, 2004.

[65] T. K. Yun, S. Y. Choi, and H. Y. Yun, "Epidemiological study on cancer prevention by ginseng: are all kinds of cancers preventable by ginseng?" *Journal of Korean Medical Science*, vol. 16, supplement, pp. S19–S27, 2001.

[66] X. G. Wu, D. H. Zhu, and X. Li, "Anticarcinogenic effect of red ginseng on the development of liver cancer induced by diethylnitrosamine in rats," *Journal of Korean Medical Science*, vol. 16, supplement, pp. S61–S65, 2001.

[67] Y.-S. Kwon, K.-H. Jang, and I.-H. Jang, "The effects of Korean red ginseng (ginseng radix rubra) on liver regeneration after partial hepatectomy in dogs," *Journal of Veterinary Science*, vol. 4, no. 1, pp. 83–92, 2003.

[68] M.-J. Bak, M. Jun, and W.-S. Jeong, "Antioxidant and hepatoprotective effects of the red ginseng essential oil in H_2O_2-treated HepG2 cells and CCl_4-treated mice," *International Journal of Molecular Sciences*, vol. 13, no. 2, pp. 2314–2330, 2012.

[69] J. Y. Lee, K. H. Jung, M. J. Morgan et al., "Sensitization of TRAIL-induced cell death by 20S-Ginsenoside Rg3 via CHOP-mediated DR5 upregulation in human hepatocellular carcinoma cells," *Molecular Cancer Therapeutics*, 2012.

[70] C. Zhang, L. Liu, Y. Yu, B. Chen, C. Tang, and X. Li, "Antitumor effects of ginsenoside Rg3 on human hepatocellular carcinoma cells," *Molecular Medicine Reports*, vol. 5, no. 5, pp. 1295–1298, 2012.

[71] J.-W. Jiang, X.-M. Chen, X.-H. Chen, and S.-S. Zheng, "Ginsenoside Rg3 inhibit hepatocellular carcinoma growth via intrinsic apoptotic pathway," *World Journal of Gastroenterology*, vol. 17, no. 31, pp. 3605–3613, 2011.

[72] H. M. Park, S. J. Kim, J. S. Kim, and H. S. Kang, "Reactive oxygen species mediated ginsenoside Rg3-and Rh2-induced apoptosis in hepatoma cells through mitochondrial signaling pathways," *Food and Chemical Toxicology*, vol. 50, no. 8, pp. 2736–2741, 2012.

[73] J.-H. Yoon, Y.-J. Choi, and S.-G. Lee, "Ginsenoside Rh1 suppresses matrix metalloproteinase-1 expression through inhibition of activator protein-1 and mitogen-activated protein kinase signaling pathway in human hepatocellular carcinoma cells," *European Journal of Pharmacology*, vol. 679, no. 1–3, pp. 24–33, 2012.

[74] J.-H. Yoon, Y.-J. Choi, S.-W. Cha, and S.-G. Lee, "Anti-metastatic effects of ginsenoside Rd via inactivation of MAPK signaling and induction of focal adhesion formation," *Phytomedicine*, vol. 19, no. 3-4, pp. 284–292, 2012.

[75] Y.-T. Lo, Y.-H. Tsai, S.-J. Wu, J.-R. Chen, and J. C.-J. Chao, "Ginsenoside Rb1 inhibits cell activation and liver fibrosis in rat hepatic stellate cells," *Journal of Medicinal Food*, vol. 14, no. 10, pp. 1135–1143, 2011.

[76] J. Geng, W. Peng, Y. Huang, H. Fan, and S. Li, "Ginsenoside-Rg1 from Panax notoginseng prevents hepatic fibrosis induced by thioacetamide in rats," *European Journal of Pharmacology*, vol. 634, no. 1–3, pp. 162–169, 2010.

[77] C. F. Chen, J. F. Lee, D. Wang, C. Y. Shen, K. L. Shen, and M. H. Lin, "Water extract of Zizyphus Jujube attenuates ischemia/reperfusion-induced liver injury in rats (PP106)," *Transplantation Proceedings*, vol. 42, no. 3, pp. 741–743, 2010.

[78] X. Shen, Y. Tang, R. Yang, L. Yu, T. Fang, and J.-A. Duan, "The protective effect of Zizyphus jujube fruit on carbon tetrachloride-induced hepatic injury in mice by anti-oxidative activities," *Journal of Ethnopharmacology*, vol. 122, no. 3, pp. 555–560, 2009.

[79] S. H. M. Habib, S. Makpol, N. A. A. Hamid, S. Das, W. Z. W. Ngah, and Y. A. M. Yusof, "Ginger extract (Zingiber officinale) has anti-cancer and anti-inflammatory effects on ethionine-induced hepatoma rats," *Clinics*, vol. 63, no. 6, pp. 807–813, 2008.

[80] Y. A. M. Yusof, N. Ahmad, S. Das, S. Sulaiman, and N. A. Murad, "Chemopreventive efficacy of ginger (Zingiber officinale) in ethionine induced rat hepatocarcinogenesis," *African Journal of Traditional, Complementary and Alternative Medicines*, vol. 6, no. 1, pp. 87–93, 2008.

[81] R. Hu, P. Zhou, Y. B. Peng et al., "6-Shogaol induces apoptosis in human hepatocellular carcinoma cells and exhibits anti-tumor activity in vivo through endoplasmic reticulum stress," *Plos One*, vol. 7, no. 6, Article ID e39664, 2012.

[82] C. J. Weng, C. P. Chou, C. T. Ho, and G. C. Yen, "Molecular mechanism inhibiting human hepatocarcinoma cell invasion by 6-shogaol and 6-gingerol," *Molecular Nutrition and Food Research*, vol. 56, no. 8, pp. 1304–1314, 2012.

[83] E. P. Sabina, S. J. Pragasam, S. Kumar, and M. Rasool, "6-gingerol, an active ingredient of ginger, protects acetaminophen-induced hepatotoxicity in mice," *Journal of Chinese Integrative Medicine*, vol. 9, no. 11, pp. 1264–1269, 2011.

[84] H. Z. Huo, B. Wang, Y. K. Liang, Y. Y. Bao, and Y. Gu, "Hepatoprotective and antioxidant effects of licorice extract against CCl_4-induced oxidative damage in rats," *International Journal of Molecular Sciences*, vol. 12, no. 10, pp. 6529–6543, 2011.

[85] A. Sharma and H. S. Rathore, "Prevention of acetaminophen induced hepatorenal damage in mice with rhizomes of Glycyrrhiza glabra. A histophysiological study," *Ancient Science of Life*, vol. 30, no. 3, pp. 72–77, 2011.

[86] E. Gumpricht, R. Dahl, M. W. Devereaux, and R. J. Sokol, "Licorice compounds glycyrrhizin and 18β-glycyrrhetinic acid are potent modulators of bile acid-induced cytotoxicity in rat hepatocytes," *The Journal of Biological Chemistry*, vol. 280, no. 11, pp. 10556–10563, 2005.

[87] C.-H. Lee, S.-W. Park, Y. S. Kim et al., "Protective mechanism of glycyrrhizin on acute liver injury induced by carbon tetrachloride in mice," *Biological and Pharmaceutical Bulletin*, vol. 30, no. 10, pp. 1898–1904, 2007.

[88] J. Folkman, "Angiogenesis: an organizing principle for drug discovery?" *Nature Reviews Drug Discovery*, vol. 6, no. 4, pp. 273–286, 2007.

[89] P. Y. K. Yue, D. Y. L. Wong, P. K. Wu et al., "The angiosuppressive effects of 20(R)- ginsenoside Rg3," *Biochemical Pharmacology*, vol. 72, no. 4, pp. 437–445, 2006.

[90] P. Y. K. Yue, D. Y. L. Wong, W. Y. Ha et al., "Elucidation of the mechanisms underlying the angiogenic effects of ginsenoside Rg1 in vivo and in vitro," *Angiogenesis*, vol. 8, no. 3, pp. 205–216, 2005.

[91] K. Zhang, J. Lu, T. Mori et al., "Baicalin increases VEGF expression and angiogenesis by activating the ERRα/PGC-1α pathway," *Cardiovascular Research*, vol. 89, no. 2, pp. 426–435, 2011.

[92] S. M. Sagar, D. Yance, and R. K. Wong, "Natural health products that inhibit angiogenesis: a potential source for investigational new agents to treat cancer—part 2," *Current Oncology*, vol. 13, no. 3, pp. 99–107, 2006.

Hindawi Publishing Corporation
Evidence-Based Complementary and Alternative Medicine
Volume 2013, Article ID 864747, 8 pages
http://dx.doi.org/10.1155/2013/864747

Research Article

UPLC Q-TOF/MS-Based Metabolic Profiling of Urine Reveals the Novel Antipyretic Mechanisms of Qingkailing Injection in a Rat Model of Yeast-Induced Pyrexia

Xiaoyan Gao,[1] Mingxing Guo,[1] Long Peng,[1] Baosheng Zhao,[1] Jiankun Su,[1] Haiyu Liu,[1] Li Zhang,[1] Xu Bai,[2] and Yanjiang Qiao[3]

[1] *Science Experiment Center for Traditional Chinese Medicine, Beijing University of Chinese Medicine, No. 11 North Third Ring Road, Chaoyang District, Beijing 100029, China*
[2] *Waters Technologies (Shanghai) Ltd., No. 1378 Zhangdong Road, Shanghai 201203, China*
[3] *Key Laboratory of TCM-Information Engineering of State Administration of TCM, Beijing Key Laboratory for Basic and Development Research on Chinese Medicine, Beijing University of Chinese Medicine, No. 6 Zhonghuan South Road, Wangjing, Chaoyang District, Beijing 100102, China*

Correspondence should be addressed to Yanjiang Qiao; yanjiangqiao@sina.cn

Received 4 February 2013; Accepted 27 May 2013

Academic Editor: Rong Zeng

Fever is one of the most common clinical symptoms of many diseases. Qingkailing (QKL) injection is widely used in China as a clinical emergency medicine due to its good antipyretic effects. It is a herbal formula which is composed by eight kinds of traditional Chinese medicines (TCM). As a kind of typical multiple constituents and multiple actions of TCM, it is very difficult to elaborate the antipyretic mechanism by conventional pharmacological method. Metabonomics technique provides beneficial tool for this challenge. In this study, an ultra performance liquid chromatography quadrupole time-of-flight mass spectrometry (UPLC Q-TOF/MS) metabonomics method was developed to explore the changing process of biochemical substances in rats of yeast-induced pyrexia. Partial least squares discriminate analysis (PLS-DA) was used to distinguish the normal control group, the pyrexia model group, and the pyrexia model group treated by QKL injection. The potential biomarkers related to pyrexia were confirmed and identified. MetPA was used to find the possible metabolic pathways. The results indicated that the antipyretic effect of QKL injection on yeast-induced pyrexia rats was performed by repairing the perturbed metabolism of amino acids.

1. Introduction

Fever is one of the most common clinical symptoms of many diseases, such as infection, inflammation, trauma, and metabolic disorders. Fever was defined as a state of elevated core temperature, which is often, but not necessarily, part of the defensive responses of multicellular organisms (host) to the invasion of live (microorganisms) or inanimate matter recognized as pathogenic or alien by the host [1]. Although some kinds of fever were beneficial to the host, it is not without its ill-effects, especially in cases of very high fevers, or when high fever is associated with comorbidities such as severe sepsis and preexisting cardiopulmonary disease [2]. So, antipyretic is still necessary in these situations. The ordinary antipyretic medications, the nonsteroidal anti-inflammatory drugs (NSAIDs), for example, ibuprofen, aspirin, and acetaminophen, are used primarily as pain relievers or anti-inflammatory. More and more debates over the appropriate use of such medications with the serious side effects of NSAIDs have been increasingly reported [3–8].

Traditionally, plants/herbs with antipyretic properties are commonly used in China. More than one thousand years ago, fever was discussed in *Shanghanlun*, a classic book about the basic theory of TCM, written by Zhongjing Zhang, a medical sage respected by the Chinese. Since then, Chinese medicines

are still in use as antipyretic. In the large number of Chinese medicine preparations with antipyretic action, QKL injection is focused on for its significant effect of antipyretic action and larger market share. QKL injection is prepared from eight medicinal materials or their extracts, including *Radix Isatidis*, *Flos Lonicerae*, Fructus Gardeniae, Cornu Bubali, *Concha Margaritifera*, Baicalin, Cholic acid and Hyodeoxycholic acid [9]. It is commonly used in clinical practice for the treatment of high fever, upper respiratory inflammation, viral encephalitis, hepatitis, stoke, cerebral thrombosis, tonsillitis, tracheitis [10, 11]. Though QKL injection has been widely used to treat the fever patients in clinic in China, few literatures have reported about the detailed antipyretic mechanism. For one reason, TCM and preparation complexity and variability present challenges for researchers. For another reason, the conventional studies on TCM pharmacological mechanism have faced many difficulties.

Metabonomics is a new platform of systems biology, defined as the quantitative measurement of the dynamic multiparametric metabolic responses of living systems to pathophysiological stimuli or genetic modifications [12]. Metabonomics makes an impact at several points in the drug mechanism research: multitarget validation, multiple mechanism integration, and comprehensive evaluation [13–15]. The application of metabonomics has dramatically increased in the fields of explanation of medicines mechanism and evaluation of drug efficacy and toxicity [16–18]. Published results indicated that metabonomics presented the potential capability to improve our understanding of TCM like QKL injection [19–22]. Recently, some advanced instruments and bio-information analysis techniques enable us to perform the simultaneous analysis of a large number of metabolites [23–26]. UPLC-Q-TOF/MS system can provide accurate mass of fragments, precursor ions, and neutral loss information, and it has a larger peak capacity and better resolution and sensitivity. Metabonomics technique combined with advanced instruments and appropriate data processing method provides support to us for explaining the antipyretic mechanism of QKL injection.

In the present study, yeast-induced fever is adopted as pathogenic fever model [27]. This type of fever leads to an intense inflammatory reaction caused by ulceration at the injection site. This model is suitable for studying the effects of some antipyretic medicines such as QKL injection [28–31]. In this paper, a metabonomics method was employed to explore the mechanism of the antipyretic effects of QKL injection.

2. Materials and Methods

2.1. Chemicals and Reagents. QKL injection was purchased from Yabao Beizhongda (Beijing) Pharmaceutical Co., Ltd. (no. 012907A, China). Yeast was obtained from Mauri Food Co., Ltd. (Heibei, China). LC-grade methanol and acetonitrile were acquired from Baker Company (Baker Inc., USA). Ultra high-purity water was prepared by Millipore-Q SAS 67120MOLSHEIM (France). Formic acid (no. 7000027413) was obtained from Sigma Chemical Co., Ltd. (St. Louis, MO, USA).

2.2. Animals and Sample Collection. The protocol of the study was approved by the Ethics Committee of Beijing University of Chinese Medicine. All procedures and care of the rats were in accordance with the institutional guidelines for animal use in research. Male Sprague-Dawley rats (200 ± 20 g) were obtained from Beijing Weitonglihua Laboratory Animal Technology Co., Ltd. (Beijing, China). Before use in the study, all the rats were acclimated for five days in a controlled room with temperature (23 ± 2°C), humidity (60 ± 5%), and a light/dark cycle of 12 h. Then they were transferred to individual metabolism cages and allowed to acclimatize for an additional three days. During that time, the rats' rectal temperatures were measured three times per day using a digital thermometer for the regular rhythm of body temperatures. The rats with a temperature difference that was greater than 0.5°C were excluded. Twenty-four qualified rats were selected and divided into three groups randomly: the normal control group (CG), the pyrexia model group (PG), and the pyrexia model group treated by QKL injection (TG). After the start of the experiment, the rats of PG and TG were subcutaneously injected with a 20% aqueous suspension of yeast (15 mL/kg) in the back of rats. The rats of CG were similarly given an equal volume of 0.9% saline. One hour later, the rats of TG were injected with 4.2 mL/kg QKL injection in the tail vein. The rats of CG and PG were similarly injected with an equal volume of 0.9% saline in the tail vein. Urine was collected before yeast was injected and at different time-points, including 4 h, 8 h, 12 h, 24 h, 36 h, 48 h, 60 h, and 72 h after QKL was injected. The rectal temperature was also measured during that time. Urine was centrifuged at 14000 rpm for 10 min at 4°C, and the supernatant was collected and stored at −20°C.

2.3. Urine Sample Preparation. The urine samples were thawed at room temperature. The supernatant was diluted at a ratio of 2 : 1 with distilled water, vortex mixed and filtered through a 0.22 μm filter membrane. A 2 μL sample was injected into the UPLC Q-TOF/MS system for analysis.

2.4. UPLC-Q-TOF/MS Analysis. Waters Acquity Ultra Performance LC system (Waters Corp., Milford, MA, USA) was performed to separate the metabolites, which was equipped with an HSS T3 column (2.1 mm × 100 mm, 1.7 μm, UK). The column temperature was set to 45°C and the gradient elution program started with 99% solvent A and 1% solvent B (solvent A: 0.1% formic acid in water; solvent B: acetonitrile modified by the addition of 0.1% formic acid). The column was eluted with a linear gradient of 99%–60% A over 0.5 to 10 min, 60%–1% A over 10 to 11 min, 1% A was held for 1 min and then returned to 99% A over 12.0 to 15.0 min at a flow rate of 0.45 mL/min.

A Xevo G2-Q-TOF (Waters MS Technologies, Manchester, UK) was performed on mass spectrometry with an electrospray ionisation source. The positive ion mode was performed. Data were collected from m/z 50 to m/z 1200. The capillary and cone voltage were set at 3.0 kV and 45 V, respectively. The desolvation gas was set at 800 L/h at a temperature of 450°C, the cone gas was set at 30 L/h, and the source

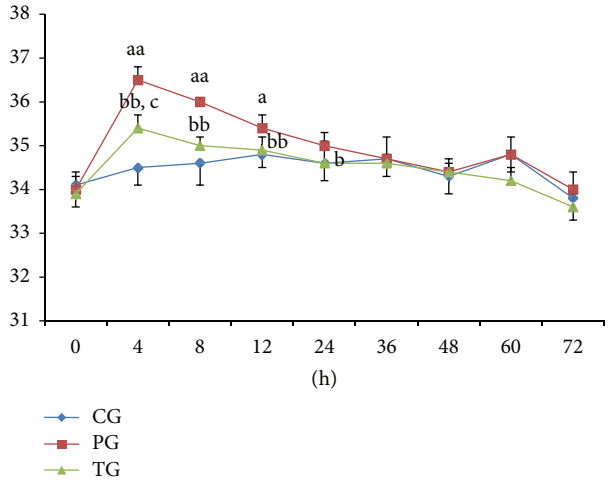

Figure 1: Results of rectal temperature in CG, PG, and TG. Data were expressed by independent sample t-test. $^{aa}P < 0.01$, $^{a}P < 0.05$ compared with CG. $^{bb}P < 0.01$, $^{b}P < 0.05$ compared with PG. $^{c}P < 0.05$ compared with CG.

temperature was set at 120°C. The Leucine enkephalin was used as the lock mass solution in accurate mass measurement.

2.5. Data Analysis. The statistical analysis of the rectal temperature was performed by SPSS 17.0 (SPSS Inc., Chicago, IL, USA).

Mass spectrometry data was processed using Waters Markerlynx XS software. The UPLC-MS data were detected and noise-reduced in both the UPLC and MS domains such that only true analytical peaks were further processed by the software. A list of intensities (chromatographic peak areas) of the peaks detected was then generated for the first chromatogram, using the t_R-m/z data pairs as identifiers. The data was analyzed further with PLS-DA. For the identification of potential biomarkers, the following databases had been used: HMDB (http://www.hmdb.ca/), KEGG (http://www.genome.jp/kegg/), Massbank (http://www.massbank.jp/), Chemspider (http://www.chemspider.com/), and METLIN (http://metlin.scripps.edu/). Ingenuity pathway analysis (IPA) was performed with MetPA (http://metpa.metabolomics.ca./MetPA/faces/Home.jsp) based on database sources including the KEGG, HMDB, SMPD (http://www.smpdb.ca/), and METLIN to identify the affected metabolic pathways analysis and visualization.

3. Results and Discussion

3.1. Efficacy of QKL Injection as Antipyretic. To monitor the temperature changes, the rectal temperatures of the rats in each group before and after QKL injection administrated were tested. As showed in Figure 1, at the time-point of 4 h, the body temperature was elevated by 2.0 ± 0.5°C ($P < 0.01$, versus CG) in PG, indicating that the yeast-induced pyrexia model was succeed. At the same time-point, for TG, the body temperature dropped by 1.1 ± 0.4°C ($P < 0.01$, versus PG) after QKL injecting, demonstrating that QKL injection had significant antipyretic effects on yeast-induced fever rats. At the time-point of 8 h after QKL was injected, the body temperature reached the normal level ($P > 0.05$, versus CG).

3.2. Multivariate Data Analysis. UPLC Q-TOF/MS was used to collect the urine information. The detailed information of the UPLC-Q-TOF/MS analysis and validation was shown in Supplementary Materials (Text S1 and Figure S1) available online at http://dx.doi.org/10.1155/2013/864747.

A method of PCA was used for unsupervised multivariate data analysis. It is well known that drug-induced ingredients will affect the results of the cluster analysis, even deceptively. In the previous study of our laboratory, more than 40 organic ingredients were found in QKL injection, among which, bile acid, hyodeoxycholic acid, baicalin, and geniposide were higher-content compounds [32, 33]. In this paper, the high contents of drug-induced components and their metabolites were deducted before using the multivariate data analysis (see Supplementary Materials, Table S1). All of these ingredients were also verified by Thermo Accela HPLC-LTQ/Orbitrap coupled LC-MS system (Thermo Fisher Scientific, Bremen, Germany) (see Supplementary Materials, Figure S2). Figure 2 showed the PLS-DA score plot among CG, PG, and TG at the time-points of 4 h and 8 h. The result demonstrated that the metabolites in the pyrexia model rats were disturbed by the fever pathological state (PG versus CG) and the treatment rats which were gradually returned to normal based on the plots of TG were gradually close to the plots of CG (8 h versus 4 h). Interestingly, the results were almost in accordance with the variation of body temperature. We could speculate that the changes of body temperature were highly related to the disturbance of the endogenous components. Accordingly, the time-point of 4 h after QKL injection was administered was selected to reveal the antipyretic mechanism of QKL injection due to the plots separated clearly among the three groups.

3.3. Detection and Elucidation of Biomarker Candidates. To reveal the antipyretic mechanism of QKL injection, a PLS-DA loading plot was used to find potential biomarkers among CG, PG, and TG (see Supplementary Materials, Figure S3). The potential biomarkers were chosen based on two rules: for one rule, the VIP values (variable importance in the projection) from the PLS-DA model must be higher than 2; for the other rule, the compound changing trends of TG and PG must be opposite. Twenty-one metabolites were selected as potential biomarkers to characterize the antipyretic mechanism of QKL injection (Table 1). The structural elucidation of biomarker candidates is a challenging task. The detailed identification procedure of the biomarkers was shown in Supplementary Materials (Text S2 and Figure S4).

3.4. Explore the Antipyretic Mechanism of QKL Injection. The twenty-one biomarkers were listed in Table 1. As we expected, the changing trends of TG and PG were opposite. After QKL injection was administrated, these differences of metabolites may denote their potential as targeted biomarkers for the antipyretic mechanism of QKL injection. More detailed analysis of pathways and networks influenced by

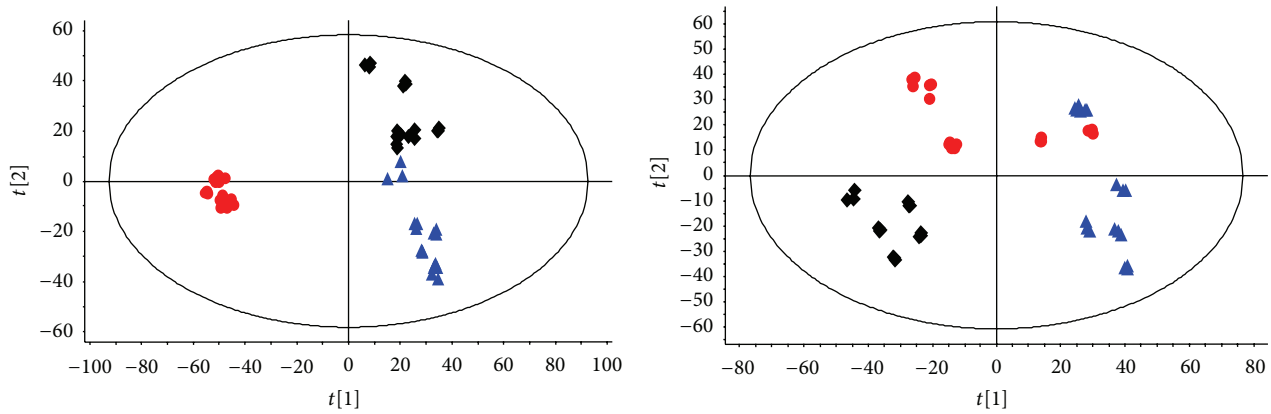

(a) Scores comp[1] versus comp[2] colored by sample group

(b) Scores comp[1] versus comp[2] colored by sample group

Figure 2: PLS-DA score plot obtained from CG (▲), PG (◆), and TG (•) at 4 h (a) and 8 h (b).

Table 1: Metabolites selected as biomarkers characterized in urine profiles and their change trends.

No.	t_R (min)	m/z	Metabolites	Trend in PG[a]	Trend in TG[b]	VIP
1	0.5222	104.1074	4-Aminobutyric acid	$\uparrow^{***}$	$\downarrow^{***}$	4.73
2	0.5549	118.0867	Glycocyamine	$\uparrow^{***}$	$\downarrow^{**}$	5.08
3	0.5648	114.0667	Creatinine	$\uparrow$	$\downarrow^{**}$	4.66
4	0.6110	143.0819	Ectoine	$\uparrow^{*}$	$\downarrow^{*}$	5.14
5	0.6440	176.0978	Citrulline	$\uparrow^{***}$	$\downarrow^{***}$	3.51
6	0.6686	325.1131	Difructose anhydride I	$\uparrow^{**}$	$\downarrow$	3.95
7	0.6730	127.0478	Imidazoleacetic acid	$\uparrow^{***}$	$\downarrow^{***}$	3.54
8	0.6877	259.0931	3-Methyluridine	$\uparrow^{***}$	$\downarrow^{***}$	4.17
9	0.7837	130.0502	1-Pyrroline-4-hydroxy-2-carboxylate	$\downarrow$	$\uparrow^{***}$	3.98
10	1.2175	116.0709	Proline	$\downarrow^{**}$	$\uparrow^{*}$	3.38
11	1.5638	126.0666	5-Methylcytosine	$\uparrow^{*}$	$\downarrow^{***}$	3.07
12	2.6807	227.1029	3-Hydroxykynurenine	$\uparrow$	$\downarrow^{***}$	2.18
13	2.7929	220.1183	Pantothenic acid	$\uparrow$	$\downarrow^{*}$	5.10
14	2.8259	384.1149	Succinyladenosine	$\uparrow^{***}$	$\downarrow^{***}$	6.10
15	3.3189	205.0966	Tryptophan	$\uparrow^{***}$	$\downarrow^{***}$	4.84
16	3.4148	206.0452	Xanthurenate	$\downarrow^{***}$	$\uparrow^{***}$	6.88
17	3.6484	160.0971	Methylbutyrylglycine	$\downarrow^{***}$	$\uparrow$	3.10
18	4.2819	180.0658	Hippurate	$\downarrow^{*}$	$\uparrow$	3.53
19	4.8699	162.0553	Indole-3-carboxylic acid	$\uparrow$	$\downarrow^{**}$	2.38
20	10.8441	274.2741	Hexadecasphinganine	$\uparrow^{*}$	$\downarrow^{**}$	4.06
21	11.3671	812.4414	PE(22:6/20:4)	$\uparrow^{***}$	$\downarrow^{***}$	5.39

[a]Change trend compared with CG.

[b]Change trend compared with PG.

The levels of potential biomarkers were labeled with (↓) downregulated and (↑) upregulated ($^{*}P < 0.05$; $^{**}P < 0.01$; $^{***}P < 0.001$; one-way ANOVA followed by independent samples t-test).

QKL injection was performed by ingenuity network analysis (IPA). In order to identify possible pathways affected by QKL injection, biomarkers contributing to the separation of the CG, PG, and TG were analyzed using MetPA. MetPA is a free, web-based tool that combines result from powerful pathway enrichment analysis with the pathway topology analysis to help researchers identify the most relevant pathways involved in the conditions under study [34–36]. It is well known that repairing in more important positions of a network will arouse a more active impact on the pathway than repairing occurring in marginal or relatively isolated positions. Metabolic pathway analysis with MetPA revealed that these potential biomarkers, which were important for the antipyretic mechanism of QKL injection, were responsible for tryptophan metabolism; arginine and proline metabolism; alanine, aspartate, and glutamate metabolism, and so on.

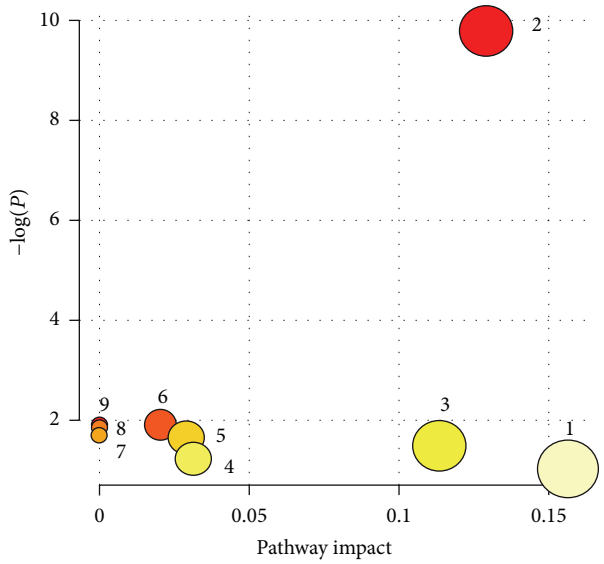

FIGURE 3: Summary of pathway analysis. (1) Tryptophan metabolism; (2) arginine and proline metabolism; (3) alanine, aspartate and glutamate metabolism; (4) glycine, serine, and threonine metabolism; (5) butanoate metabolism; (6) pantothenate and CoA biosynthesis; (7) histidine metabolism; (8) aminoacyl-tRNA biosynthesis; (9) beta-alanine metabolism.

MetPA generated 9 networks (Figure 3, Table S2 of Supplementary Materials), demonstrating that the repaired amino acids metabolism was the antipyretic mechanism of QKL injection (Figure 4).

3.4.1. Tryptophan Metabolism. 3-Hydroxykynurenine and xanthurenate were the metabolites of tryptophan. These three biomarkers were closely related to tryptophan metabolism. L-tryptophan is an essential amino acid in human body; it participates in the regulation of protein synthesis and metabolic networks. There are two main ways for the degradation of tryptophan, namely, the kynurenine pathway and 5-hydroxytryptamine (5-HT) pathway [37, 38]. Some studies have shown that the monoamine neurotransmitters in the centre participate in the regulation of body temperature [39]. When 5-HT was injected into the intraventricular, it could cause fever [40, 41]. The elevated tryptophan in PG might indirectly reflect the increasing of 5-HT in the central, which leads to fever. Meanwhile, 3-hydroxykynurenine was also increased in the pathway, but xanthurenate, the metabolite of 3-hydroxykynurenine, dropped in PG. The decrease might be caused by the change of enzyme activity between 3-hydroxykynurenine and xanthurenate, which led to generate a large number of 5-HT. After QKL injection was administrated, the content of tryptophan decreased significantly, indicating that by enhancing the activity of the enzyme between 3-hydroxykynurenine and xanthurenate, it regulated the hypothalamic thermoregulatory center.

3.4.2. Arginine and Proline Metabolism. Glycocyamine, citrulline, proline, 1-pyrroline-4-hydroxy-2-carboxylate, and 4-aminobutyric acid participated in arginine and proline metabolism. L-arginine is an amino acid that has numerous functions in body. It helps disposal of ammonia, which is used to generate compounds such as nitric oxide, creatine, L-glutamate, and L-proline, and it can be converted to glucose and glycogen if needed [42–44]. The pathway contains urea cycle and creatinine metabolism. Citrulline and glycocyamine were the intermediate and metabolite in urea cycle. In the urea cycle, it generates fumarate which associates with the Krebs cycle. The Krebs cycle is the final pathway of the three major nutrients and it is the hub of carbohydrates, lipids, and amino acid metabolites. As we all know, fever causes the three major nutrients' metabolism disorder. The disorder may be related to the perturbed of arginine metabolic pathway. Meanwhile, the elevated pantothenic acid which is the precursor substance of CoA also proved the enhancement of Krebs cycle.

Our study found that glycocyamine and citrulline in fevered rats were significantly increased. After QKL injection was administrated, these two substances significantly decreased, indicating that QKL injection had an active impact on the urea cycle. QKL injection might reduce the speed of the urea cycle thus further corrected the metabolic rate of the three major nutrients' metabolism. Studies have shown that arginine plays an important regulatory role in wound healing [45]. Yeast-induced fever is a severe inflammatory response. The increased arginine in administered rats would contribute to the healing of the wound.

Much or all of the pyrrole-2-carboxylate in human urine may be formed from labile precursors; the probable source of pyrrole-2-carboxylate is free hydroxy-L-proline [46]. Proline hydroxylation generates hydroxyproline. Hydroxyproline is the main component of collagen in body [47–49]. When the body's bones or skin is damaged, take yeast stimulation, for example, the collagen metabolism is affected. The decreased pyrrole-2-carboxylate and proline in fever rats demonstrated that collagen metabolism is inhibited. After QKL injection was administrated, the two substances were increased, meaning that QKL injection corrected collagen metabolism. The amount of the serum creatinine is an important indicator in measuring kidney function [50]. QKL injection also plays an important role in the treatment of acute renal failure and nephritis. We found that QKL injection could significantly reduce the amount of creatinine in fevered rats, which also confirmed the role of QKL injection in the treatment of nephritis.

3.4.3. Alanine, Aspartate, and Glutamate Metabolism. 4-Aminobutyric acid is an inhibitory neurotransmitter found in the nervous systems and has analgesic effect [51]. The mechanism was for mutual adjustment by $GABA_A$ receptor and $GABA_B$ receptor. Study found that giving $GABA_B$ receptor agonist in the myelin could produce significant analgesic effect. In the fevered rats, the body's stress effect was also reflected by the increasing of 4-aminobutyric acid. After QKL injection was administrated, the 4-aminobutyric acid had a clear downward trend compared with the PG, indicating

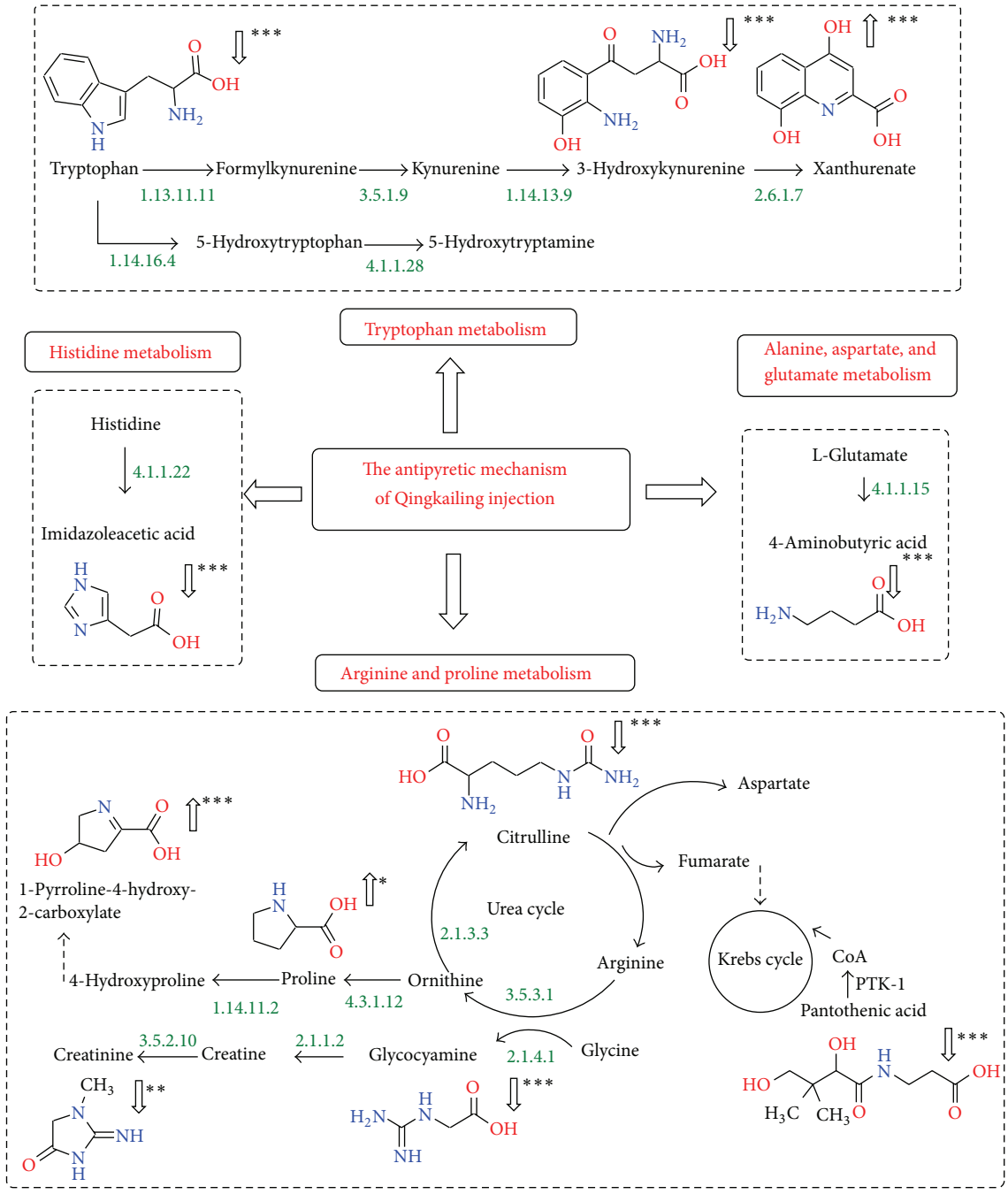

Figure 4: The perturbed metabolic pathways in response to the antipyretic mechanism of QKL injection.

that QKL injection played an important role in antipyretic and analgesic effects.

3.4.4. Histidine Metabolism. Imidazoleacetic acid is a metabolite of histamine metabolism. Histamine is one of the autacoids and is generated by histidine decarboxylase. When the body is stimulated by physical and chemical factors, the mast cells degranulate and release histamine. Histamine binds with histamine receptor and causes inflammation. Yeast-induced fever is a severe inflammatory reaction. The elevated imidazoleacetic acid in the urine of fevered rats indicated that histamine increased in body, which also proved the pathogenesis of yeast-induced fever. After QKL injection was administrated, imidazoleacetic acid significantly decreased, implying that the body immunity improved. It showed that QKL injection significantly affected the fever caused by inflammation.

4. Conclusion

In this paper, a metabonomics approach using UPLC Q-TOF/MS was successfully established to explore the antipyretic mechanism of QKL injection based on the variation of endogenous metabolites. Twenty-one representative biomarkers were found by PLS-DA. By metabolic pathway analysis with MetPA, the repaired amino acids metabolism was identified as the antipyretic mechanism of QKL injection. The antipyretic effect of QKL injection was performed by correcting perturbed metabolism of some metabolites such as tryptophan; arginine and proline; alanine, aspartate, and glutamate; histidine.

Conflict of Interests

The authors confirm that there is no conflict of interests.

Authors' Contribution

Xiaoyan Gao and Mingxing Guo equally contributed to this paper.

Acknowledgments

This study was supported in part by National Natural Science Foundation of China (81173649/H2817) and Foundation of Independent Topics in Beijing University of Chinese Medicine (0100601055).

References

[1] The Commission for Thermal Physiology of the International Union of Physiological Sciences, "Glossary of terms for thermal physiology 3rd edition," *Japanese Journal of Physiology*, vol. 51, no. 2, pp. 245–280, 2001.

[2] P. A. Mackowiak, "Fever: blessing or curse? A unifying hypothesis," *Annals of Internal Medicine*, vol. 120, no. 12, pp. 1037–1040, 1994.

[3] G. A. Balint, "A novel approach to reduce the unwanted gastric side-effects of orally administered non-steroidal anti-inflammatory drugs in rats," *Experimental and Toxicologic Pathology*, vol. 49, no. 1-2, pp. 61–63, 1997.

[4] S. Bancos, M. P. Bernard, D. J. Topham, and R. P. Phipps, "Ibuprofen and other widely used non-steroidal anti-inflammatory drugs inhibit antibody production in human cells," *Cellular Immunology*, vol. 258, no. 1, pp. 18–28, 2009.

[5] P. Purcell, D. Henry, and G. Melville, "Diclofenac hepatitis," *Gut*, vol. 32, no. 11, pp. 1381–1385, 1991.

[6] C. M. Fored, E. Ejerblad, P. Lindblad et al., "Acetaminophen, aspirin, and chronic renal failure," *The New England Journal of Medicine*, vol. 345, no. 25, pp. 1801–1808, 2001.

[7] H. T. V. Nguyen and D. N. Juurlink, "Recurrent ibuprofen-induced aseptic meningitis," *Annals of Pharmacotherapy*, vol. 38, no. 3, pp. 408–410, 2004.

[8] B. Cryer and M. B. Kimmey, "Gastrointestinal side effects of nonsteroidal anti-inflammatory drugs," *The American Journal of Medicine*, vol. 105, no. 1, pp. S20–S30, 1998.

[9] Chinese Pharmacopoeia Commission, *Pharmacopoeia of the People's Republic of China*, vol. 1, 2010.

[10] X. Chen, O. M. Z. Howard, X. Y. Yang, L. H. Wang, J. J. Oppenheim, and T. Krakauer, "Effects of Shuanghuanglian and Qingkailing, two multi-components of traditional Chinese medicinal preparations, on human leukocyte function," *Life Sciences*, vol. 70, no. 24, pp. 2897–2913, 2002.

[11] S. K. Yan, W. F. Xin, G. A. Luo, Y. M. Wang, and Y. Y. Cheng, "An approach to develop two-dimensional fingerprint for the quality control of Qingkailing injection by high-performance liquid chromatography with diode array detection," *Journal of Chromatography A*, vol. 1090, no. 1-2, pp. 90–97, 2005.

[12] J. K. Nicholson, J. C. Lindon, and E. Holmes, "'Metabonomics': understanding the metabolic responses of living systems to pathophysiological stimuli via multivariate statistical analysis of biological NMR spectroscopic data," *Xenobiotica*, vol. 29, no. 11, pp. 1181–1189, 1999.

[13] Y. M. Lao, J. G. Jiang, and L. Yan, "Application of metabonomic analytical techniques in the modernization and toxicology research of traditional chinese medicine," *The British Journal of Pharmacology*, vol. 157, no. 7, pp. 1128–1141, 2009.

[14] X. J. Wang, H. Sun, A. H. Zhang, W. J. Sun, P. Wang, and Z. G. Wang, "Potential role of metabolomics apporoaches in the area of traditional Chinese medicine: as pillars of the bridge between Chinese and Western medicine," *Journal of Pharmaceutical and Biomedical Analysis*, vol. 55, no. 5, pp. 859–868, 2011.

[15] P. Jonsson, E. S. Johansson, A. Wuolikainen et al., "Predictive metabolite profiling applying hierarchical multivariate curve resolution to GC-MS data—a potential tool for multi-parametric diagnosis," *Journal of Proteome Research*, vol. 5, no. 6, pp. 1407–1414, 2006.

[16] J. L. Griffin and M. E. Bollard, "Metabonomics: its potential as a tool in toxicology for safety assessment and data integration," *Current Drug Metabolism*, vol. 5, no. 5, pp. 389–398, 2004.

[17] M. Chen, M. Su, L. Zhao et al., "Metabonomic study of aristolochic acid-induced nephrotoxicity in rats," *Journal of Proteome Research*, vol. 5, no. 4, pp. 995–1002, 2006.

[18] H. B. He, X. B. Ren, X. Y. Wang et al., "Therapeutic effect of Yunnan Baiyao on rheumatoid arthritis was partially due to regulating arachidonic acid metabolism in osteoblasts," *Journal of Pharmaceutical and Biomedical Analysis*, vol. 59, no. 1, pp. 130–137, 2012.

[19] P. Li, L. W. Qi, E. H. Liu, J. L. Zhou, and X. D. Wen, "Analysis of Chinese herbal medicines with holistic approaches and integrated evaluation models," *Trends in Analytical Chemistry*, vol. 27, no. 1, pp. 66–77, 2008.

[20] Y. Gu, Y. F. Zhang, X. Z. Shi et al., "Effect of traditional Chinese medicine berberine on type 2 diabetes based on comprehensive metabonomics," *Talanta*, vol. 81, no. 3, pp. 766–772, 2010.

[21] Y. H. Lu, X. R. Liu, X. Liang, L. Xiang, and W. D. Zhang, "Metabolomic strategy to study therapeutic and synergistic effects of tanshinone IIA, salvianolic acid B and ginsenoside Rb1 in myocardial ischemia rats," *Journal of Ethnopharmacology*, vol. 134, no. 1, pp. 45–49, 2011.

[22] A. H. Zhang, H. Sun, Y. Yuan, W. J. Sun, G. Z. Jiao, and X. J. Wang, "An in vivo analysis of the therapeutic and synergistic properties of Chinese medicinal formula Yin-Chen-Hao-Tang based on its active constituents," *Fitoterapia*, vol. 82, no. 8, pp. 1160–1168, 2011.

[23] B. W. Tang, J. J. Ding, F. H. Wu, L. Chen, Y. X. Yang, and F. Y. Song, "^{1}H NMR-based metabonomics study of the urinary biochemical changes in Kansui treated rat," *Journal of Ethnopharmacology*, vol. 141, no. 1, pp. 134–142, 2012.

[24] E. Werner, J. F. Heilier, C. Ducruix, E. Ezan, C. Junot, and J. C. Tabet, "Mass spectrometry for the identification of the discriminating signals from metabolomics: current status and future trends," *Journal of Chromatography B*, vol. 871, no. 2, pp. 143–163, 2008.

[25] C. H. Grün, F. A. van Dorsten, D. M. Jacobs et al., "GC-MS methods for metabolic profiling of microbial fermentation products of dietary polyphenols in human and in vitro intervention studies," *Journal of Chromatography B*, vol. 871, no. 2, pp. 212–219, 2008.

[26] J. Godzien, M. Ciborowski, S. Angulo et al., "Metabolomic approach with LC-QTOF to study the effect of a nutraceutical treatment on urine of diabetic rats," *Journal of Proteome Research*, vol. 10, no. 2, pp. 837–844, 2011.

[27] L. O'Mahony, M. Akdis, and C. A. Akdis, "Regulation of the immune response and inflammation by histamine and histamine receptors," *Journal of Allergy and Clinical Immunology*, vol. 128, no. 6, pp. 1153–1162, 2011.

[28] F. Sui, M. J. Yan, N. Lin, Y. Q. Xiao, and L. Li, "Comparative study on the antipyretic effects and its mechanisms by four processed Rhei Radix et Rhizoma products," *Chinese Journal of Experimental Traditional Medical Formulae*, vol. 18, no. 15, pp. 155–158, 2012.

[29] A. Rajasekaran, R. Arivukkarasu, and S. Murugesh, "Evaluation of antipyretic activity of ethyl acetate extract of Adenema hyssopifolium G. Don in a rat model," *Asian Pacific Journal of Tropical Medicine*, vol. 3, no. 7, pp. 523–526, 2010.

[30] B. P. Devi, R. Boominathan, and S. C. Mandal, "Evaluation of antipyretic potential of *Cleome viscosa* Linn. (Capparidaceae) extract in rats," *Journal of Ethnopharmacology*, vol. 87, no. 1, pp. 11–13, 2003.

[31] L. S. Huang, "Study on antipyretic and anti-inflammatory effects of Qingkailing injection," *Clinical Rational Drug Use*, vol. 5, no. 1, pp. 6–7, 2012.

[32] X. Y. Gao, N. Li, Y. Wang, X. Y. Shi, and Y. J. Qiao, "Rapid quality control of *Fructus Gardeniae* extraction in the preparation of Qingkailing injection," *Chinese Journal of Pharmaceutical Analysis*, vol. 26, no. 3, pp. 336–338, 2006.

[33] N. Li, X. Y. Gao, Q. Fan, and Y. J. Qiao, "Rapid determination of chlorogenic acid in aqueous solution of *Flos Lonicerae Japonicae* extraction," *Zhongguo Zhongyao Zazhi*, vol. 32, no. 4, pp. 312–314, 2007.

[34] P. Scherp, N. Putluri, G. J. LeBlanc et al., "Proteomic analysis reveals cellular pathways regulating carbohydrate metabolism that are modulated in primary human skeletal muscle culture due to treatment with bioactives from *Artemisia dracunculus* L.," *Journal of Proteomics*, vol. 75, no. 11, pp. 3199–3210, 2012.

[35] X. Wang, Q. Wang, A. Zhang et al., "Metabolomics study of intervention effects of Wen-Xin-formula using ultra high-performance liquid chromatography/mass spectrometry coupled with pattern recognition approach," *Journal of Pharmaceutical and Biomedical Analysis*, vol. 74, pp. 22–30, 2013.

[36] S. Wu, Y. Gao, X. Dong et al., "Serum metabonomics coupled with ingenuity pathway analysis characterizes metabolic perturbations in response to hypothyroidism induced by propylthiouracil in rats," *Journal of Pharmaceutical and Biomedical Analysis*, vol. 72, pp. 109–114, 2013.

[37] G. Allegri, C. V. L. Costa, A. Bertazzo, M. Biasiolo, and E. Ragazzi, "Enzyme activities of tryptophan metabolism along the kynurenine pathway in various species of animals," *Farmaco*, vol. 58, no. 9, pp. 829–836, 2003.

[38] A. Bertazzo, E. Ragazzi, M. Biasiolo, C. V. L. Costa, and G. Allegri, "Enzyme activities involved in tryptophan metabolism along the kynurenine pathway in rabbits," *Biochimica et Biophysica Acta*, vol. 1527, no. 3, pp. 167–175, 2001.

[39] R. Peindaries and J. Jacob, "Interactions between 5-hydroxytryptamine and a purified bacterial pyrogen when injected into the lateral cerebral ventricle of the wake rabbit," *European Journal of Pharmacology*, vol. 13, no. 3, pp. 347–355, 1971.

[40] R. F. Hellon, "Monoamines, pyrogens and cations: their actions on central control of body temperature," *Pharmacological Reviews*, vol. 26, no. 4, pp. 289–321, 1974.

[41] E. Zeisberger, "The roles of monoaminergic neurotransmitters in thermoregulation," *Canadian Journal of Physiology and Pharmacology*, vol. 65, no. 6, pp. 1395–1401, 1987.

[42] R. M. J. Palmer, D. D. Rees, D. S. Ashton, and S. Moncada, "L-arginine is the physiological precursor for the formation of nitric oxide in endothelium-dependent relaxation," *Biochemical and Biophysical Research Communications*, vol. 153, no. 3, pp. 1251–1256, 1988.

[43] R. G. Knowles, M. Palacios, R. M. J. Palmer, and S. Moncada, "Formation of nitric oxide from L-arginine in the central nervous system: a transduction mechanism for stimulation of the soluble guanylate cyclase," *Proceedings of the National Academy of Sciences of the United States of America*, vol. 86, no. 13, pp. 5159–5162, 1989.

[44] B. Tan, Y. L. Yin, Z. Q. Liu et al., "Dietary L-arginine supplementation increases muscle gain and reduces body fat mass in growing-finishing pigs," *Amino Acids*, vol. 37, no. 1, pp. 169–175, 2009.

[45] A. Barbul, S. A. Lazarou, D. T. Efron, H. L. Wasserkrug, and G. Efron, "Arginine enhances wound healing and lymphocyte immune responses in humans," *Surgery*, vol. 108, no. 2, pp. 331–337, 1990.

[46] A. Hammershøi, R. M. Hartshorn, and A. M. Sargeson, "Conversion of chelated hydroxy-L-proline into pyrrole-2-carboxylate," *Journal of the Chemical Society, Chemical Communications*, no. 18, pp. 1267–1269, 1988.

[47] D. J. Prockop and K. Kivirikko, "Relationship of hydroxyproline excretion in urine to collagen metabolism: biochemistry and clinical applications," *Annals of Internal Medicine*, vol. 66, no. 6, pp. 1243–1266, 1967.

[48] T. A. Dull and P. H. Henneman, "Urinary hydroxyproline as an index of collagen turnover in bone," *The New England Journal of Medicine*, vol. 268, pp. 132–134, 1963.

[49] R. Hata, H. Sunada, K. Arai et al., "Regulation of collagen metabolism and cell growth by epidermal growth factor and ascorbate in cultured human skin fibroblasts," *European Journal of Biochemistry*, vol. 173, no. 2, pp. 261–267, 1988.

[50] T. H. Jafar, C. H. Schmid, and A. S. Levey, "Serum creatinine as marker of kidney function in South Asians: a study of reduced GFR in adults in Pakistan," *Journal of the American Society of Nephrology*, vol. 16, no. 5, pp. 1413–1419, 2005.

[51] P. Yogeeswari, J. V. Ragavendran, D. Sriram et al., "Discovery of 4-aminobutyric acid derivatives possessing anticonvulsant and antinociceptive activities: a hybrid pharmacophore approach," *Journal of Medicinal Chemistry*, vol. 50, no. 10, pp. 2459–2467, 2007.

Hindawi Publishing Corporation
Evidence-Based Complementary and Alternative Medicine
Volume 2013, Article ID 542081, 6 pages
http://dx.doi.org/10.1155/2013/542081

Research Article

The Neuroprotective Effect of Gugijihwang-Tang on Trimethyltin-Induced Memory Dysfunction in the Rat

Eun-Yee Jung,[1] Mi-Sook Lee,[1] Chang Joon Ahn,[1] Seung-Hun Cho,[2] Hyunsu Bae,[1] and Insop Shim[1,3]

[1] *Department of Basic Korean Medical Science, Acupuncture and Meridian Science Research Center, Kyung Hee University, Seoul 130-701, Republic of Korea*
[2] *Hospital of Korean Medicine, College of Korean Medicine, Kyung Hee University, Seoul 130-701, Republic of Korea*
[3] *Department of Basic Oriental Medical Science, College of Oriental Medicine, Kyung Hee University, Seoul 130-701, Republic of Korea*

Correspondence should be addressed to Insop Shim; ishim@khu.ac.kr

Received 21 November 2012; Revised 8 April 2013; Accepted 15 May 2013

Academic Editor: Rong Zeng

Gugijihwang-Tang (the herbal formula PM012), a decoction consisting of several herbs including *Rehmanniae Radix Preparata*, has been widely used as herbal treatment for dementia. In order to investigate the neuroprotective action of this prescription, we examined the effect of Gugijihwang-Tang on learning and memory using the Morris water maze and [F-18]FDG micro PET neuroimaging technique. After injection of trimethyltin (TMT, 8.0 mg/kg, i.p.), which is a potent toxicant that selectively kills cells in the central nervous system, rats were administered Gugijihwang-Tang (100 mg/kg, p.o.) daily for two weeks, followed by the Morris water maze tasks and [F-18]FDG micro PET neuroimaging. In Gugijihwang-Tang administered TMT-treated rats, they showed improved learning and memory abilities in water maze tasks and glucose metabolism, suggesting that Gugijihwang-Tang plays effectively positive role in the improvement of brain function including learning and memory after TMT-induced neurodegeneration. Taken together, our results suggested that the Gugijihwang-Tang should be useful for developing strategies protecting nervous system and improving brain function.

1. Introduction

Dementia is a brain disorder that seriously affects a person's ability to carry out daily activities and its causes generally include primary neurodegenerative disorders, with the most prevalent being Alzheimer's disease (AD) [1]. Trimethyltin (TMT) is an organotoxic compound with potent neurotoxicant effects which is regarded as being particularly useful for studying the response to injury on account of the distinct pattern of neuronal degeneration in rodent brain. When rat is treated with TMT, it causes a loss of pyramidal neurons predominantly in the rat hippocampal CA3 region starting 3-4 days later [2–4]. Behaviorally, TMT intoxication is characterized by seizure, self-biting, aggressive behavior, hyperactivity, and impairment of working memory [5–7]. The precise mechanism of selective and delayed neuronal death after TMT administration has not been clarified yet. Intoxication with TMT leads to profound neurodegeneration, behavioral and cognitive deficits in both humans and experimental animals [6]. In rats, TMT induced the loss of pyramidal neurons in the hippocampus at 4 days, which was robust at 14 days after TMT administration [8]. These anatomical and behavioral findings have made TMT-intoxicated rats an attractive model for degenerative diseases such as AD, the most common cause of dementia [9, 10]. Herbal medicines, such as *Ginkgo biloba, Ginseng*, or *Melissa officinalis*, have been commonly used as memory or cognition enhancers. The effects of these enhancers have been demonstrated scientifically [11, 12]. *Yukmi-jiwang gamibang* (YJG) has a significant effect on memory enhancement and the expression of genes associated with not only the prevention of neuronal degeneration but also neuronal growth events [13]. Recent double-blind, placebo-controlled trials have also demonstrated that *Yukmi-jiwang gamibang* significantly enhances cognitive abilities in normal human subjects [14].

Table 1: The contents of Gugijihwang-Tang and the amounts of standard materials.

Herbal Medicines	Ratio (%)
Rehmanniae radix Preparant	8 (28.6%)
Cornii fructus	4 (14.3%)
Lycium chinense	3 (10.7%)
Discoreae radix	4 (14.3%)
Hoelen	3 (10.7%)
Mountain Cortex radix	3 (10.7%)
Alismatis radix	3 (10.7%)

However, there have been few reported studies on accessing learning and memory enhancement triggered by treatment with YJG in dementia animal models. Gugijihwang-Tang (GJT), the herbal formula PM012, is another memory or cognition enhancer which is composed of 7 herbal medicines, including steamed *Rehmanniac radix Preparata*, *Lycium chinense, Dioscoreae radix, Corni fructus, Hoelen, Mountain cortex radix, and Alismatis radix*. GJT is composed of 7 herbal medicines which are 6 herbal medicines of *Yukmi-jiwang gamibang* and *Lycium chinense*. Thus, we examined the effect of GJT (YJG and *Lycium chinense*) on learning and memory ability in TMT-induced amnesia rats using the Morris water maze. Furthermore, we examined brain activity using the technique of positron emission tomography (PET) with ^{18}F-2 fluoro-2-deoxy-D-glucose ([F-18]FDG) that allows autoradiographic assessment of radiolabeled 2-deoxyglucose uptake. [F-18]FDG micro PET scan, a functional neuroimaging technique, PET brain imaging has been used for the diagnosis and assessment of cerebrovascular diseases, such as dementia. More recently, [F-18]FDG micro PET scan became available for visualizing brain activity in small rodents [15, 16]. We hypothesized applying this technique in TMT-induced dementia animal model and memory improving substance (GJT). Thus, we have attempted to measure brain activity changes with the technique in TMT-treated rats.

2. Materials and Method

2.1. Animals. Male Sprague-Dawley rats weighting 250–280 g each were purchased from Samtaco Animal Corp. (Kyungki-do, Republic of Korea). The animals were allowed to acclimatize themselves for at least 7 days prior to the experimentation. The animals were housed in individual cages under light-controlled conditions (12/12 hr light/dark cycle) and at 23°C room temperature. Food and water were available ad libitum.

2.2. Preparation of Gugijihwang-Tang (GJT). The contents and the ratio of each component in Gugijihwang-Tang are shown in Table 1.

2.3. Reagents. Trimethyltin chloride (TMT; Sigma-Aldrich Inc., St. Louis, MO, USA) or 0.9% saline (vehicle) was injected and Gugijihwang-Tang was administered into rats during 2 weeks.

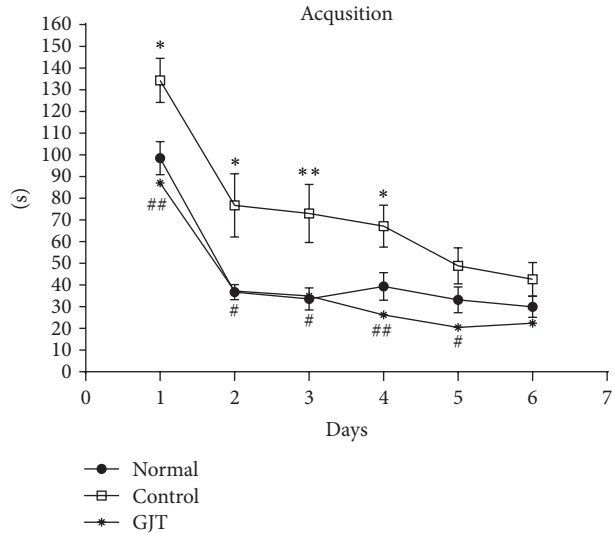

Figure 1: The latency to escape onto the hidden platform during the Morris water maze. The task was performed with 3 trials per day during 6 days for the acquisition test. The values are presented as means ± S.E.M. $^{*}P < 0.05$, $^{**}P < 0.01$, compared with the normal group; $^{\#}P < 0.05$, $^{\#\#}P < 0.01$, compared with the control group.

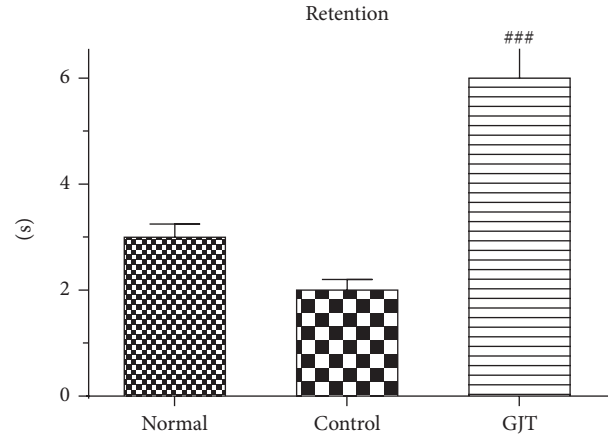

Figure 2: Retention performance was tested on the 7th day. The rats received a 1 min probe trial in which the platform was removed from the pool for retention testing. The values are presented as means ± S.E.M., $^{\#\#\#}P < 0.001$, compared with the control group.

2.4. Experimental Design. Rats were randomly assigned into three groups ($n = 10$ per group): the normal group (vehicle group), the TMT-lesioned + saline group (the control group), and TMT-lesioned + Gugijihwang-Tang (100 mg/kg treated animals, the GJT group). The rats were injected intraperitoneally (i.p.) with TMT (8.0 mg/kg, body weight) dissolved in 0.9% saline and then returned to their home cages. Gugijihwang-Tang (100 mg/kg, p.o.) was dissolved in saline and orally administered for two weeks after TMT-induced neurodegeneration. To verify that TMT causes damage to hippocampal neurons, Nissl staining was performed using a previously described procedure (see Supplementary

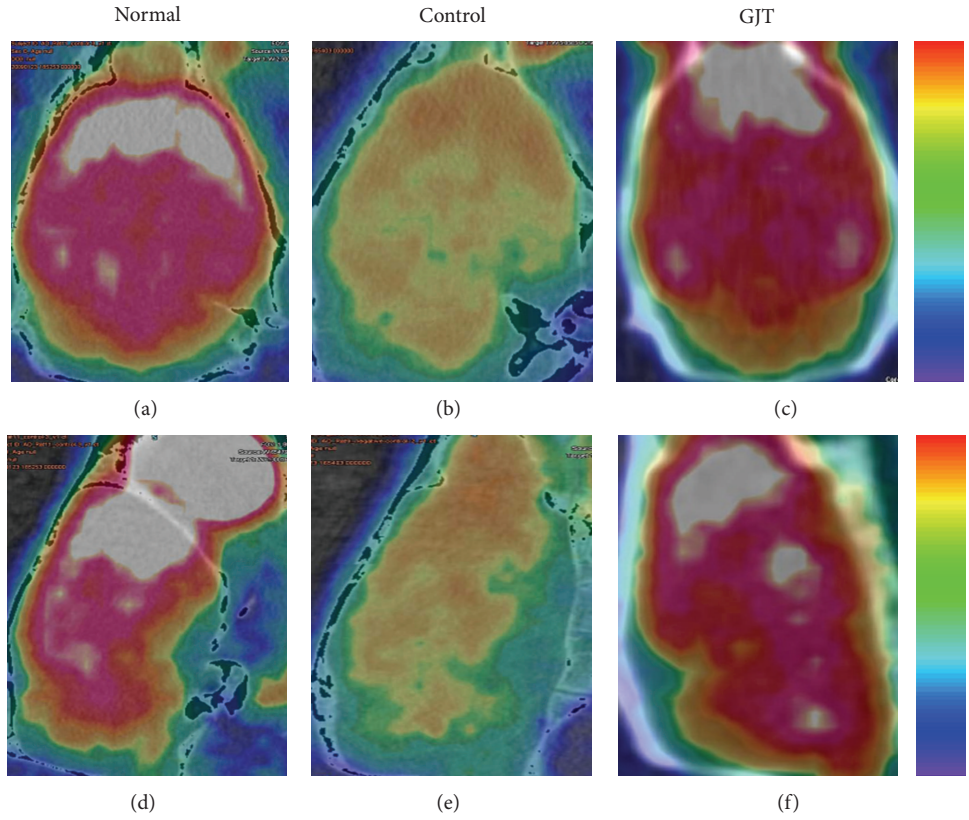

Figure 3: Changes in whole brain glucose metabolism in TMT-induced neurogeneration and treatment of GJT. (a and d) Normal, (b and e) control, and (c and f) GJT groups, (a to c) axial and (d to f) saggital section of the brain.

Figure 1 in the Supplementary Material available online at http://dx.doi.org/10.1155/2013/542081) [17].

The water maze test was performed for one week and [F-18] FDG micro PET neuroimaging from the 15th day after the injection of TMT.

2.5. Water Maze Test. The swimming pool of the Morris water maze was a circular water tank 200 cm in diameter and 35 cm deep. It was filled to a depth of 21 cm with water at $23 \pm 2^{\circ}$C. A platform 15 cm in diameter and 20 cm in height was placed inside the tank with its top surface being 1.5 cm below the surface of the water. The pool was surrounded by many cues that were external to the maze. A CCD camera was equipped with a personal computer for the behavioral analysis. Each rat received four daily trials. For 6 consecutive days, the rats were tested with three acquisition tests. They also received retention tests on the 7th day. For the acquisition test, the rat was allowed to search for the hidden platform for 180 s, and the latency to escape onto the platform was recorded. The animals were trained to find the platform that was in a fixed position during 6 days for the acquisition test, and, then for the retention test, they received a 1 min probe trial in which the platform was removed from the pool. The interval time was 1 min. Performance of the test animals in each water maze trial was assessed by a personal computer for the behavioral analysis (S-mart program, Spain).

2.6. [F-18]FDG Micro PET Scan. All rats were deprived of food for 12–15 h before the experiments to enhance [F-18]FDG uptake in the brain. Each animal was placed on a heating pad in a cage and warmed for at least 30 min before the [F-18]FDG injection. The temperature of the cages was kept at 30°C throughout the uptake period in accordance with an optimized [F-18]FDG uptake protocol [18]. [F-18]FDG (500 μCi/100 g body weight) was injected through tail vein. After [F-18]FDG injection, radioactivity in rat brain tissue initially rises rapidly. During [F-18]FDG micro PET scans, the animals were kept under isoflurane inhalation anesthesia (2% in 100% oxygen; IsoFlo; Abbott Laboratories).

2.7. Voxel-Based Statistical Analysis. Voxel-based statistical analysis was performed to compare the cerebral glucose metabolism of the group's datasets. The procedure used for SPM analysis of the animal PET data was as previously described in our previous study [18]. Briefly, for efficient spatial normalization, only the brain region was extracted. A study-specific template was then constructed using all the datasets. The PET data was spatially normalized onto a rat brain template and smoothed using a 3 mm Gaussian kernel. Count normalization was performed. A voxelwise t-test between the group's datasets was performed using the Statistical Parametric Mapping 5 program ($P < 0.05$, $K > 50$).

2.8. Behavioral Data Analysis. The data were presented as means ± S.E.M. Behavioral data (acquisition and retention data) were statistically analyzed by ANOVA testing with repeated measures on the time factor. The origin of the significant effects was further examined by posthoc comparisons using the LSD technique. The criterion for statistical significance was considered to be P values <0.05.

3. Results

3.1. Effect of Gugijihwang-Tang on Performance in Water Maze Task. The latency to escape onto the hidden platform during the acquisition trial of the water maze was recorded, and the results are depicted in Figure 1. The escape latency differed among the groups when the results were averaged over all the session. The latency to find the hidden platform of the normal and GJT groups was significantly decreased compared with the control group. TMT severely impaired spatial cognition in the water maze test, and the GJT group ameliorated TMT-induced learning and memory deficits in the water maze.

The total time spent on the platform was used to evaluate the spatial performance of the rat during retention trials. The results of the retention test at the 7th day are depicted in Figure 2. The time spent around platform among the groups differed. The time spent around the platform was 3.3 ± 0.84 in the normal group, 2.3 ± 0.53 in the control group, and 6.2 ± 2.2 in the GJT group. The normal and GJT groups spent more time around the platform than did the control group. The GJT group showed a significant increase ($P < 0.001$) in retention time compared to the control group (Figure 2).

3.2. [F-18]FDG Micro PET Neuroimaging in the Brain Changes in the Whole Brain Glucose Metabolism in TMT-Induced Neurodegeneration and Treatment of GJT. Figure 3 shows changes in glucose metabolism of each group in axial and saggital section of the whole brain. Figure 4 summarizes these changes in graph indicating statistical difference between groups.

Figure 5 shows changes in glucose metabolism of each group in coronal section of the region of the hippocampus. Figure 6 summarizes these changes in graph indicating statistical difference between groups. The control group significantly reduced glucose metabolism, exhibiting a 19% decrease in [F-18]FDG uptake in the whole brain ($P < 0.05$) and a 30% decrease in the hippocampus ($P < 0.05$) when compared to the normal group. Treatment with GJT can significantly reverse hypometabolism as shown by increasing [F-18]FDG uptake by 67% in the whole brain ($P < 0.05$) and 62% in the hippocampus ($P < 0.05$).

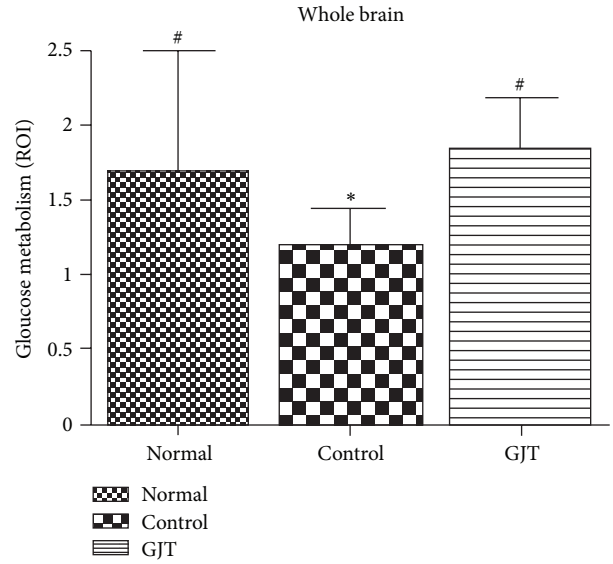

Figure 4: Changes in whole brain glucose metabolism in TMT-induced neurogeneration and treatment of GJT. The values are presented as means ± S.E.M. $^{*}P < 0.05$, compared with the normal group, $^{\#}P < 0.05$, compared with the control group.

4. Discussion

Several studies have demonstrated behavioral abnormalities such as increased seizure susceptibility, aggression, and learning impairment after TMT-induced neurodegeneration, which is consistent with results of this study [5, 19]. The present study confirms previous findings that TMT treatment induces learning impairment from Morris water maze test. This study thus strongly proposes TMT-treated rat to be a good model for studying neuronal degeneration. This model may be also useful for elucidating mechanisms underlying resistance to dementia and excite toxic injury in the hippocampus. Other many studies clearly exhibit the functional significance of the hippocampal neurodegeneration by TMT [2, 5, 19, 20]. The hippocampus possesses information derived from the associated brain regions that are involved in learning, memory, emotion, and motivation [20]. In TMT exposed rats, GJT treatment improved spatial learning and memory in Morris water maze, suggesting that GJT can reduce spatial deficits on the central nervous system after TMT-induced neurodegeneration. The latency of the GJT group to find the hidden platform was significantly decreased on the acquisition testing, suggesting that GJT could improve the acquisition and retention deficits on the Morris water maze testing. Although the precise mechanisms for recovery of such behavioral deficits following the administering of GJT are not clear, this present study collectively demonstrates that GJT ameliorated learning and memory deficits through its neuroprotective effects on the central nervous system, and thus may have beneficial effects on TMT-induced cognitive impairment.

Numerous studies from epidemiological [21, 22] and functional neuroimaging [23] studies indicate that the dysregulation of energy metabolism in the brain is an important causative factor in the developing dementia. PET imaging has been used for the assessment of dementia and can be used in the diagnosis of disease and new therapeutic searching. More recently, [F-18]FDG micro PET scan became available for visualizing brain activity in small rodents [15, 16]. [F-18]FDG micro PET neuroimaging effects from those components in GJT may have been responsible for the protection against TMT-induced neurodegeneration and cognitive deficits shown in the present study. Thus herbal medicine

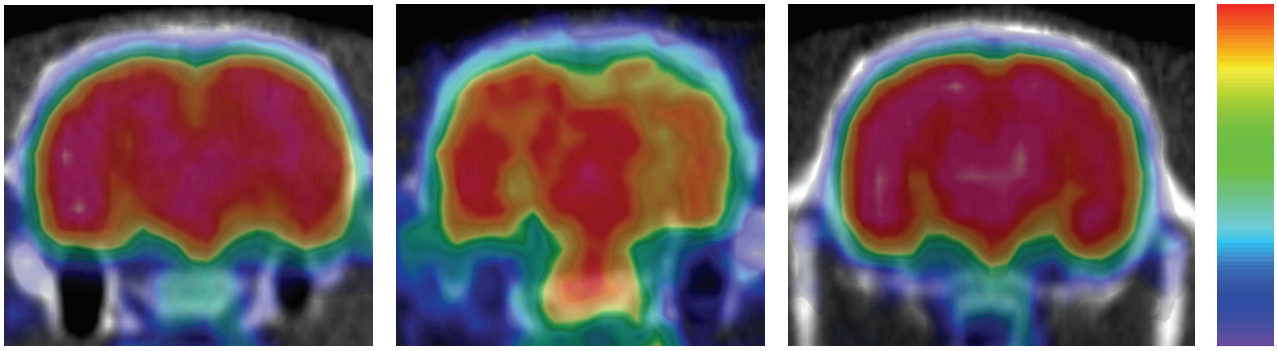

Figure 5: Changes in the region of the hippocampus glucose metabolism in TMT-induced neurodegeneration and treatment of GJT. (a to c) Coronal section of the brain.

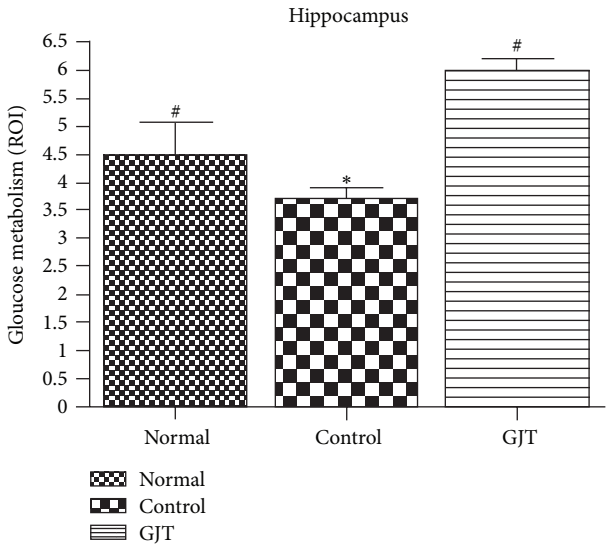

Figure 6: Changes in the region of the hippocampus glucose metabolism in TMT-induced neurodegeneration and treatment of GJT. (a to c) Coronal section of the brain. The value are presented as means ± S.E.M. $^{*}P < 0.05$, compared with the normal group, $^{\#}P < 0.05$, compared with the control group.

therapy using GJT in the TMT-induced neurodegeneration brain may have a solid therapeutic potential as a treatment for dementia and amnesia.

Authors' Contribution

Eun-Yee Jung and Mi-Sook Lee equally contribute to this work.

Acknowledgments

The authors thank the Korea Basic Science Institute (Chuncheon Center) for the use of facilities. This work was supported by a post-doctoral fellowship Grant from the Kyung Hee University in 2011 (KHU-20110693) and the Traditional Korean Medicine R&D Project, Ministry for Health & Welfare (Grant no. B110025), Republic of Korea.

References

[1] M. Di Carlo, D. Giacomazza, and P. L. San Biagio, "Alzheimer's disease: biological aspects, therapeutic perspectives and diagnostic tools," *Journal of Physics*, vol. 24, no. 24, Article ID 244102, 2012.

[2] L. W. Chang and R. S. Dyer, "A time-course study of trimethyltin induced neuropathology in rats," *Neurobehavioral Toxicology and Teratology*, vol. 5, no. 4, pp. 443–459, 1983.

[3] T. W. Bouldin, N. D. Goines, C. R. Bagnell, and M. R. Krigman, "Pathogenesis of trimethyltin neuronal toxicity," *American Journal of Pathology*, vol. 104, no. 3, pp. 237–249, 1981.

[4] D. G. Robertson, R. H. Gray, and F. A. De la Iglesia, "Quantitative assessment of trimethyltin induced pathology of the hippocampus," *Toxicologic Pathology*, vol. 15, no. 1, pp. 7–17, 1987.

[5] N. Ishida, M. Akaike, S. Tsutsumi et al., "Trimethyltin syndrome as a hippocampal degeneration model: temporal changes and neurochemical features of seizure susceptibility and learning impairment," *Neuroscience*, vol. 81, no. 4, pp. 1183–1191, 1997.

[6] R. S. Dyer, T. J. Walsh, W. F. Wonderlin, and M. Bercegeay, "The trimethyltin syndrome in rats," *Neurobehavioral Toxicology and Teratology*, vol. 4, no. 2, pp. 127–133, 1982.

[7] P. H. Ruppert, T. J. Walsh, L. W. Reiter, and R. S. Dyer, "Trimethyltin-induced hyperactivity: time course and pattern," *Neurobehavioral Toxicology and Teratology*, vol. 4, no. 2, pp. 135–139, 1982.

[8] Y. Liu, H. Imai, M. Sadamatsu, K. Tsunashima, and N. Kato, "Cytokines participate in neuronal death induced by trimethyltin in the rat hippocampus via type II glucocorticoid receptors," *Neuroscience Research*, vol. 51, no. 3, pp. 319–327, 2005.

[9] V. Corvino, E. Marchese, F. Michetti, and M. C. Geloso, "Neuroprotective strategies in hippocampal neurodegeneration induced by the neurotoxicant trimethyltin," *Neurochemical Research*, vol. 38, no. 2, pp. 240–253, 2013.

[10] M. C. Geloso, V. Corvino, and F. Michetti, "Trimethyltin-induced hippocampal degeneration as a tool to investigate neurodegenerative processes," *Neurochemistry International*, vol. 58, no. 7, pp. 729–738, 2011.

[11] J. Birks, E. V. Grimley, and M. Van Dongen, "Ginkgo biloba for cognitive impairment and dementia," *Cochrane Database of Systematic Reviews*, no. 4, Article ID CD003120, 2002.

[12] D. O. Kennedy, A. B. Scholey, L. Drewery, V. R. Marsh, B. Moore, and H. Ashton, "Electroencephalograph effects of single doses of Ginkgo biloba and Panax ginseng in healthy young volunteers," *Pharmacology Biochemistry and Behavior*, vol. 75, no. 3, pp. 701–709, 2003.

[13] S. Rho, M. Kang, B. Choi et al., "Effects of Yukmijihwang-tang derivatives (YMJd), a memory enhancing herbal extract, on the gene-expression profile in the rat hippocampus," *Biological and Pharmaceutical Bulletin*, vol. 28, no. 1, pp. 87–93, 2005.

[14] E. Park, M. Kang, J. Oh et al., "Yukmijihwang-tang derivatives enhance cognitive processing in normal young adults: a double-blinded, placebo-controlled trial," *American Journal of Chinese Medicine*, vol. 33, no. 1, pp. 107–115, 2005.

[15] M. M. Mirrione, W. K. Schiffer, M. Siddiq, S. L. Dewey, and S. E. Tsirka, "PET imaging of glucose metabolism in a mouse model of temporal lobe epilepsy," *Synapse*, vol. 59, no. 2, pp. 119–121, 2006.

[16] M. M. Mirrione, W. K. Schiffer, J. S. Fowler, D. L. Alexoff, S. L. Dewey, and S. E. Tsirka, "A novel approach for imaging brain-behavior relationships in mice reveals unexpected metabolic patterns during seizures in the absence of tissue plasminogen activator," *NeuroImage*, vol. 38, no. 1, pp. 34–42, 2007.

[17] J. Lee, D. Son, P. Lee et al., "Protective effect of methanol extract of Uncaria rhynchophylla against excitotoxicity induced by N-methyl-D-aspartate in rat hippocampus," *Journal Pharmacological Sciences*, vol. 92, no. 1, pp. 70–73, 2003.

[18] H. S. Swartzwelder, R. S. Dyer, W. Holahan, and R. D. Myers, "Activity changes in rats following acute trimethyltin exposure," *NeuroToxicology*, vol. 2, no. 3, pp. 589–593, 1981.

[19] B. Earley, M. Burke, and B. E. Leonard, "Behavioural, biochemical and histological effects of trimethyltin (TMT) induced brain damage in the rat," *Neurochemistry International*, vol. 21, no. 3, pp. 351–366, 1992.

[20] L. P. Lanier and R. L. Isaacson, "Activity changes related to the location of lesions in the hippocampus," *Behavioral Biology*, vol. 13, no. 1, pp. 59–69, 1975.

[21] J. A. Luchsinger, J. M. Noble, and N. Scarmeas, "Diet and Alzheimer's disease," *Current Neurology and Neuroscience Reports*, vol. 7, no. 5, pp. 366–372, 2007.

[22] P. Toro, P. Schönknecht, and J. Schröder, "Type II diabetes in mild cognitive impairment and Alzheimer's disease: results from a prospective population-based study in Germany," *Journal of Alzheimer's Disease*, vol. 16, no. 4, pp. 687–691, 2009.

[23] R. A. Sperling, B. C. Dickerson, M. Pihlajamaki et al., "Functional alterations in memory networks in early alzheimer's disease," *NeuroMolecular Medicine*, vol. 12, no. 1, pp. 27–43, 2010.

Hindawi Publishing Corporation
Evidence-Based Complementary and Alternative Medicine
Volume 2013, Article ID 584634, 10 pages
http://dx.doi.org/10.1155/2013/584634

Research Article

Inhibition of LXRα/SREBP-1c-Mediated Hepatic Steatosis by *Jiang-Zhi* Granule

Miao Wang,[1] Shanshan Sun,[1] Tao Wu,[1,2] Li Zhang,[1] Haiyan Song,[1] Weiwei Hao,[1] Peiyong Zheng,[1] Lianjun Xing,[1] and Guang Ji[1,3]

[1] *Institute of Digestive Disease, Longhua Hospital, Shanghai University of Traditional Chinese Medicine, Shanghai 200032, China*
[2] *Center of Chinese Medicine Therapy and Systems Biology, Shanghai University of Traditional Chinese Medicine, Shanghai 201203, China*
[3] *E-Institute of Shanghai Municipal Education Commission, Shanghai University of Traditional Chinese Medicine, Shanghai 201203, China*

Correspondence should be addressed to Guang Ji; jiliver@vip.sina.com

Received 3 January 2013; Accepted 22 April 2013

Academic Editor: Rong Zeng

Nonalcoholic fatty liver (NAFL) is increasingly recognized as one of the most common causes of chronic liver disease worldwide. Traditional Chinese medicine (TCM), as the alternative and complementary medicine, may provide some profound health benefit. "*Jiang-Zhi*" Granule (JZG) was composed based on TCM pathogenesis of NAFL: the retention of inner dampness, heat and blood stasis. This study investigated effects of JZG on liver X receptor-α (LXRα)/sterol regulatory element binding protein-1c (SREBP-1c) pathway in high-fat-diet-(HFD-)induced hepatic steatosis, as well as in free-fatty-acid-(FFA-)and T0901317-treated HepG2 cells. The results showed that JZG had an antisteatotic effect on HFD-fed rats. JZG decreased the activation of SREBP-1c through inhibiting LXRα-mediated SREBP-1c transcription, as well as through inhibiting the maturation of SREBP-1c independent of LXRα. These findings may provide molecular evidence for the use of JZG as a promising therapeutic option for NAFL and support us to continue JZG treatment in NAFL. For JZG treatment to be widely accepted, a randomized, double-blind, multicenter, placebo-controlled, phase III trial is ongoing.

1. Introduction

Nonalcoholic fatty liver (NAFL) includes a spectrum of clinic pathological conditions with the characteristic change of excessive triglyceride accumulation in hepatocytes. NAFL is increasingly recognized as one of the most common causes of chronic liver disease worldwide [1] with the prevalence of about 15%–30% in the general population of various countries [2] and approximately 20% in china [3, 4]. Although generally patients with NAFL can live for decades without any clinically significant symptoms, they are at high risk of progressing to nonalcoholic steatohepatitis (NASH), cirrhosis, and ultimately hepatocellular carcinoma [5, 6]. Therefore, an effective pharmacological intervention is entailed to prevent or delay the onset and progress of NAFL.

To date, no effective conventional western medicine is accepted as standard treatment to treat NAFL and its complications. Traditional Chinese medicine (TCM), as the alternative and complementary medicine, may provide some profound health benefit. In TCM algorithm, obesity-related diseases, including NAFL, are rooted in spleen Qi deficiency and inner phlegm retention; however, our previous study identified some limitations in treating NALF by method of spleen Qi-fortifying and phlegm resolving [7]. An appropriate and effective TCM treatment is based on a valid TCM theory. Epidemiological evidence [8] indicated that the crucial TCM pathogenesis of NAFL was the retention of inner dampness, heat and blood stasis. Thus a rationale NALF treatment should include the following elements: dampness-resolving, heat clearing, blood circulation activation, and stasis resolving. *Jiang-Zhi* Granule (JZG) was developed in accordance with the aforementioned TCM theory. It was composed of five herbs: Radix et Rhizoma Salviae Miltiorrhizae (24 g),

Folium Nelumbinis (6 g), Rhizoma Polygoni Cuspidati (60 g), Herba Artemisiae Scopariae (6 g), and Herba seu Radix Gynostemmatis Pentaphylli (60 g). The quality was controlled under ultra-performance liquid chromatography (UPLC) as previously described [9]. JZG showed positive drug safety evaluation and obtained approval by State Food and Drug Administration (SFDA) for clinical trials (the Authorized Number is Z10960082). Our preliminary study demonstrated that JZG was beneficial for improving hepatic fat accumulation in HFD-fed rats [10]. We therefore conducted this study to explore whether JZG exerts a protective effect in NAFL, as well as its underlying mechanism.

2. Materials and Methods

2.1. Animals and Interventions. Sprague-Dawley (200–250 g) rats were obtained from SLAC Laboratory Animals Co. (Shanghai, China). Rats were housed in a temperature of 22°C ± 2°C and humidity-controlled (50% ± 5%) room with a 12 hr light-dark cycle. Food (standard diet, STD, SLAC Laboratory Animals Co.) and drinking water were supplied ad libitum. Studies began after an acclimation period of one week. Animals were randomly divided into three groups: HFD+JZG group received 8-week high-fat diet (HFD consists of 10% lard oil, 2% cholesterol, and 88% STD) and then 4 weeks of HFD with JZG ($n = 10$), JZG was dissolved in saline and administered daily by oral gavage at a dose of 828 mg/kg/d, which was approximately 10 times of the standard dose in practice; HFD group received 8-week HFD and then 4 weeks of HFD with an equal volume of saline ($n = 10$); control group received 8-week STD and then 4 weeks of STD with an equal volume of saline ($n = 10$). We weighted the rats and recorded their food intake during the experimental period.

At the end of the experimental period, blood samples were obtained from the abdominal aorta while rats were under anesthesia, livers were excised and weighed, and samples were either immediately snap-frozen in liquid nitrogen (for real-time PCR, western blot and hepatic TG measurement) or fixed in 4% PFA (for histological examination).

All animal procedures were reviewed and approved by the Animal Experiment Ethics Committee of Shanghai University of Traditional Chinese Medicine.

2.2. Plasma Biochemical Analysis. Plasma levels of triglyceride (TG), total cholesterol (TC), alanine aminotransferase (ALT), and aspartate transaminase (AST) were analyzed by an automatic blood chemistry analyzer (HITACHI 7170S, Japan).

2.3. Determination of Hepatic and Intracellular Lipid Content. Liver samples were fixed in 4% PFA, processed, and embedded into paraffin blocks, and then routine Hematoxylin and Eosin (H&E) stains were performed. Cells were fixed in 4% PFA for 30 min, washed in PBS, stained in Oil Red O for 20 min at room temperature, and then rinsed with PBS. Images were acquired on an Olympus BX-50 microscope.

Total liver lipid extracts were prepared using Folch's method [11]. Briefly, liver tissues (~200 mg) were homogenized in 2 mL of PBS and extracted twice with 2 mL of a chloroform/methanol (v : v = 2 : 1) solution and then centrifuged at 6000 rpm for 10 min to obtain the organic substratum (lower phase), which was dried and then resolubilized in 1 mL of chloroform. The mixed solution was used for measurement of triglyceride in duplicate, using the triglyceride (GPO-Trinder) kit as described by the manufacturer (Sigma, St. Louis, MO, USA).

2.4. Cell Culture. HepG2 cells were obtained from the Cell Bank of the Chinese Academy of Sciences (Shanghai, China). HepG2 cells were cultured in DMEM supplemented with 10% fetal bovine serum, 100 U/mL penicillin, 100 μg/mL streptomycin, and 5.5 mmol/L D-glucose. Cells were incubated at 37°C in a 5% CO_2/95% air atmosphere on 100 mm diameter dishes, and analysis began after reaching 70% confluence.

For cell viability assay, cells were seeded in 96-well plates at a density of 1×10^4 cells/mL in 100 ul culture medium. After 24 hours incubation, cell adherence was observed and the medium was refreshed with different concentrations of JZG (0, 5, 10, 50, 100, 500, and 1000 μg/mL). Cell viability was determined by WST-1 assays (C0036, Beyotime, China) according to the manufacturers' instructions.

For experiments, cells were incubated on 12-well plates at a concentration of 1×10^5 cells/mL or on 6-well plates at a concentration of 5×10^5 cells/mL. Two HepG2-cell models were established: (1) HepG2 incubated in culture medium containing T0901317 (T090) (1 μM) and treated with or without JZG (100 μg/mL) for 24 hours [12]; (2) HepG2 cells incubated in culture medium containing palmitate (0.5 mM) and treated with or without JZG (100 μg/mL) for 24 hours [13]. All experiments were performed independently in triplicate.

2.5. Preparation of Freeze-Dried Serum Containing Drugs. Drug-containing serum was obtained to study the pharmacological activity of herbs *in vitro*. Ten SD (200–250 g) rats were randomly assigned to accept JZG treatment or saline treatment (oral gavage). JZG was dissolved in saline and administered daily for one week by oral gavage at a dose of 828 mg/kg/d. Saline group were administered with an equal volume of saline for one week. One hour after the final treatment, all animals were anesthetized, and blood samples were obtained from the abdominal aorta under aseptic condition blood samples were then centrifuged at 3000 rpm for 15 min. All serums were filtered through a 0.45 μm filter membrane and then concentrated and freeze-dried to achieve powder; all of these procedures were conducted by School of Pharmacy, East China University of Science and Technology (Shanghai, China). The powder was stored at −20°C until use.

2.6. Real-Time PCR. Total RNA was isolated from liver tissues and cells by the acid guanidinium thiocyanate/phenol/chloroform method, as described previously [14]. cDNA was prepared by 1 μg of total RNA (ReverTra Ace qPCR RT Kit, Toyobo, Japan). Real-time PCR was performed using an ABI step one plus, real-time PCR System (Applied Biosystems,

Table 1: List of primers used in the present study.

Gene	Forward primer	Reverse primer
Rat LXRα	TCAAGGGAGCACGCTATGTC	GTTCCTCTTCTTGCCGCTTC
Rat SREBP-1	GGTTTTGAACGACATCGAAGA	CGGGAAGTCACTGTCTTGGT
Rat FAS	GGCACTGACTGTCTGTTTTCCA	GTAAAAATGACACAGTCCAGACACTTC
Human LXRα	GAGTTTGCCTTGCTCATTGC	ATCCGTGGGAACATCAGTCG
Human SREBP-1	CAGCCCCACTTCATCAAGG	ACTGTTGCCAAGATGGTTCCG
Human FAS	ACTGTTGCCAAGATGGTTCCG	GGCATCAAACCTAGACAGGTC
siRNA human LXRα	CGGAACAACTGGGCATGATCGAGAA	CGGCAACTGGGCATGATCGAAAGAA

Table 2: Physiologic and hepatic parameters in rats.

Group	Body weight (g)			Liver weight (g)	Liver/body ratio (%)
	Initial	Final	Gain		
Control ($n = 10$)	209.9 ± 6.5	323.8 ± 19.7	113.8 ± 13.6	8.6 ± 0.74	2.65 ± 0.10
HFD ($n = 10$)	211.5 ± 9.1	349.8 ± 25.2*	138.3 ± 17.7**	13.1 ± 1.45**	3.75 ± 0.18**
HFD+JZG ($n = 10$)	212.1 ± 7.7	333.0 ± 23.4	120.9 ± 17.3$^{\#}$	11.7 ± 1.86$^{\#}$	3.48 ± 0.33$^{\#}$

HFD: high-fat diet, JZG: "*Jiang-Zhi*" Granule.
$^{*}P < 0.05$ and $^{**}P < 0.01$ versus the control group, $^{\#}P < 0.05$ versus the HFD group.

Foster City, CA, USA) with the SYBR Premix Ex Taq (SYBR Green Real-time PCR Master Mix,TOYOBO, Japan). The primers used were shown in Table 1.

2.7. Western Blot. Protein extraction (10 μg) from liver tissues and cells was separated by SDS-PAGE. Immunoblotting was performed as described previously [14]. Protein expression was quantified using the Fujifilm Image Reader LAS-3000 (Fuji Medical Systems, Stamford, CT, USA) and NIH ImageJ software (http://rsbweb.nih.gov/ij/). Monoclonal anti-LXRα, anti-SREBP-1, anti-FAS, and anti-Actin antibodies were purchased from abcam.

2.8. Transient Transfection with siRNA. siRNA transfection was performed using Lipofectamine-RNAiMAX reagent (Invitrogen, Carlsbad, CA, USA) according to the manufacturer's instructions. Reverse transfection of HepG2 cells with siRNA (15 pmol/1.9-cm dish) targeting LXRα (Table 1) or with nonsilencing control siRNA (Invitrogen, Carlsbad, CA, USA) was performed. Cells were harvested after transfection to determine the mRNA and protein expression.

2.9. Statistical Analyses. Data were expressed as mean ± SD unless otherwise specified and evaluated using One-way Analysis of Variance (ANOVA), followed by Bonferroni post hoc test if a significant difference was detected by ANOVA. P values < 0.05 were considered statistically significant. Statistical analyses were performed using SPSS 16.0 software (SPSS, Chicago, USA).

3. Results

3.1. Effects of JZG on HFD-Induced Body Weight and Liver Weight Gain. Rats were randomized by body weight. After 8 weeks of HFD feeding, body weight gain and liver/body weight ratio in the HFD group was higher than that in the control group (Table 2, $P < 0.01$). Four-week JZG treatment significantly reduced the body weight gain and liver/body weight ratio (Table 2, $P < 0.05$). Overall food intake did not differ among groups throughout this long-term experiment (data not shown). These results suggested that JZG could reduce HFD-induced body weight and liver weight gain in rats.

Table 3: Plasma biochemical parameters in rats.

	Control ($n = 10$)	HFD ($n = 10$)	HFD + JZG ($n = 10$)
TC (mmol/L)	1.44 ± 0.14	1.81 ± 0.81**	1.55 ± 0.55$^{\#\#}$
TG (mmol/L)	0.73 ± 0.09	1.43 ± 0.11**	1.01 ± 0.15$^{\#\#}$
ALT (U/L)	19.66 ± 1.50	30.01 ± 2.73**	25.50 ± 4.55$^{\#\#}$
AST (U/L)	6.62 ± 0.42	20.75 ± 2.59**	12.09 ± 1.69$^{\#\#}$

$^{**}P < 0.01$ versus the control group, $^{\#\#}P < 0.01$ versus the HFD group.

3.2. Effect of JZG on Plasma and Hepatic Lipid Levels. To determine whether JZG has an antisteatotic effect, we analyzed the plasma and hepatic lipid levels. As shown in Table 3, plasma levels of TC and TG in the HFD group were significantly increased compared to the control group; JZG treatment markedly relieved these increases ($P < 0.01$). In addition, compared to the control group, ALT and AST, which are sensitive indicators of liver damage, significantly elevated in the HFD group, and a decline was seen in the HFD+JZG group. These results indicated that HFD induced liver damage and JZG provided protective effect for the HFD-induced liver injury (Table 3).

Long-term HFD exposure induced not only increased plasma lipid, but also fat accumulation in the liver, leading to hepatic steatosis. Xu et al. showed that 8-week HFD induced more severe hepatic steatosis [15]. In this study, results from H&E staining showed that HFD feeding markedly increased

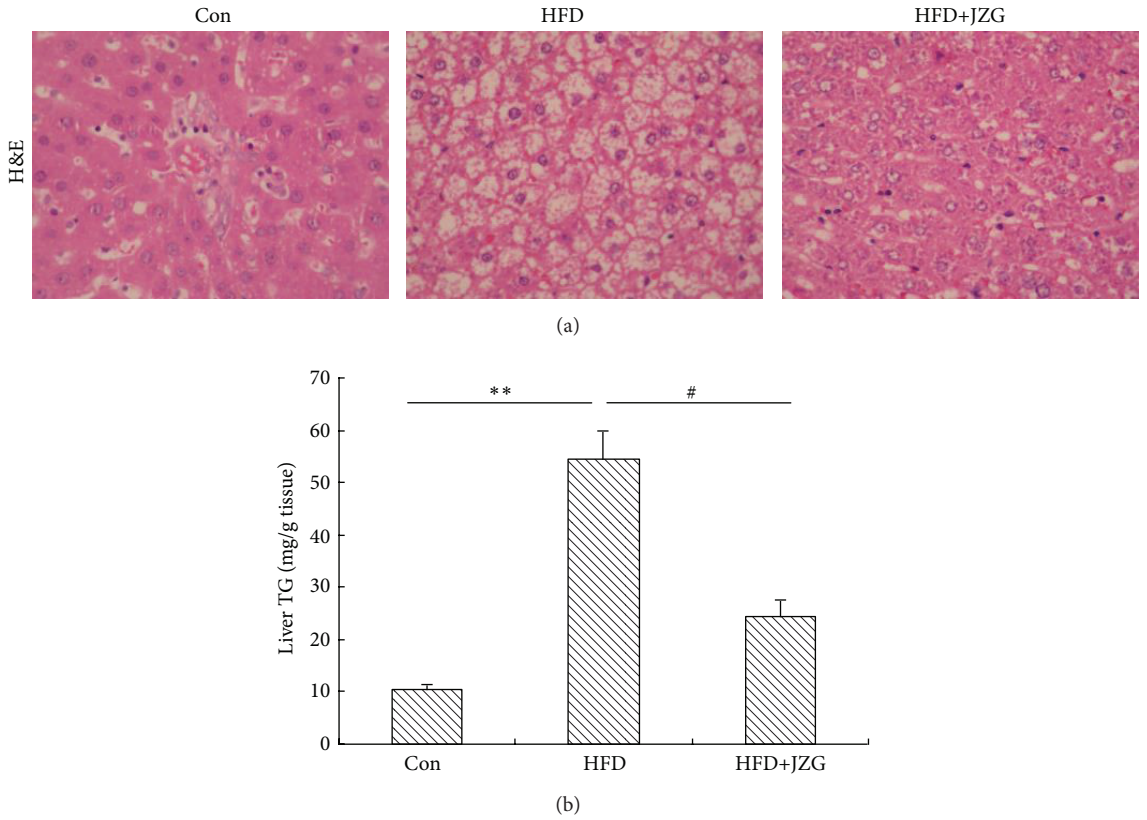

Figure 1: JZG reduced hepatic fat accumulation in the liver of HFD-fed rats. (a) Histological analysis of liver sections of HFD-fed rats treated with or without JZG and control group. Hematoxylin and eosin (H&E) staining. Original magnification ×400. (b) Triglyceride concentration in the liver. Data were presented as mean ± SEM. $^{**}P < 0.01$ versus the control group, $^{\#}P < 0.05$ versus the HFD group.

lipid accumulation as shown by increases in both the number and size of liver fat droplets (Figure 1(a)). Consistent with hepatic histology, hepatic triglyceride content increased by 5.5-fold compared to that of the control group (Figure 1(b)), suggesting the development of fatty liver. In contrast, JZG treatment resulted in decreases in the lipid accumulation to some extent, and hepatic triglyceride content was similar to that in control group by concomitant JZG treatment.

The evaluation of plasma and hepatic lipid demonstrated that JZG could decrease lipid accumulation and alleviate HFD-induced fatty liver in rats.

3.3. Effect of JZG on Expression of Lipogenesis-Related Genes and Proteins. It has been reported that LXRα/SREBP-1c pathway plays a critical role in the regulation of hepatic lipid metabolism. In HFD-fed rodents, hepatic fat accumulation is closely related to the LXRα/SREBP-1c pathway [16, 17]. Therefore, we assessed the effect of JZG on LXRα/SREBP-1c pathway activation in the liver of HFD-fed rats. The mRNA expression of LXRα, SREBP-1c, and FAS changes in liver was shown in Figure 2(a). Compared to the control group, mRNA expression of these genes was significantly upregulated in the HFD group; HFD-induced upregulation of these genes was decreased by concomitant JZG treatment (Figure 2(a)).

In accordance with the changes in the mRNA expression, protein expression levels of hepatic LXRα, SREBP-1c precursor (pSREBP-1c), mature SREBP-1c (mSREBP-1c), and FAS were significantly increased in the HFD group, compared to the control group. As expected, these increases were significantly attenuated by JZG treatment (Figure 2(b)).

Taken together, our results demonstrated that JZG suppressed hepatic steatosis through regulating the expression of genes and proteins related to lipogenesis.

3.4. Effects of JZG (Drug-Containing Serum) on FFA-Induced Lipid Accumulation in HepG2 Cells. For cell viability assay, JZG at 500 and 1000 μg/mL significantly decreased the cell viability, and concentration of 100 μg/mL displayed no cytotoxic effects on the cells (Sup Figure 1) (see Supplementary material available online at http://dx.doi.org/10.1155/2013/584634). Therefore, 100 μg/mL dose was selected for further study.

As shown in Figure 3, consistent with the in vivo results, JZG reduced intracellular lipid accumulation.

3.5. Inhibition of LXRα Activation by JZG (Drug-Containing Serum) in HepG2 Cells. SREBP-1c is a critical transcriptional factor which regulates hepatic lipogenic pathway, and

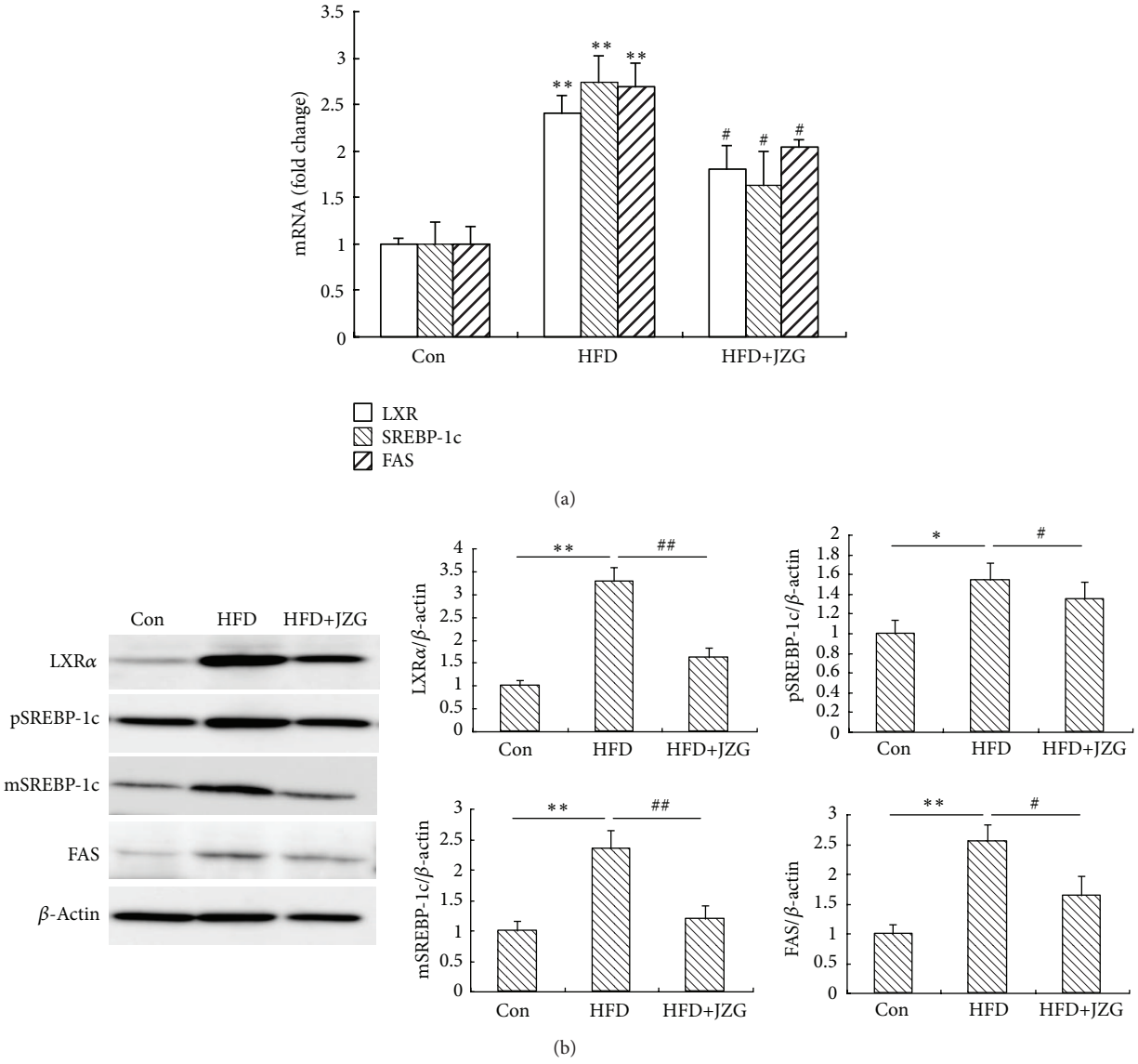

Figure 2: JZG reduced HFD-induced expression of lipogenesis-related genes and proteins. (a) The effect of JZG on HFD-induced LXRα, SREBP-1c, and FAS mRNA expression levels. (b) The effect of JZG on HFD-induced LXRα, pSREBP-1, mSREBP-1, and FAS protein expression levels. Data were presented as the mean ± SEM. $^{*}P < 0.05$ and $^{**}P < 0.01$ versus the control group, $^{\#}P < 0.05$ and $^{\#\#}P < 0.01$ versus the HFD group.

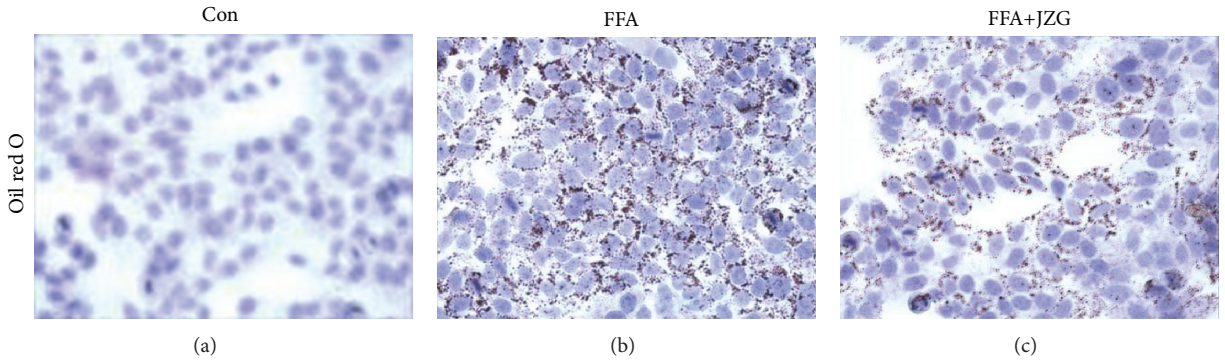

Figure 3: JZG decreased intracellular lipid content in HepG2 cells. Images showed lipid accumulation in cells stained by oil red O. Original magnification ×200.

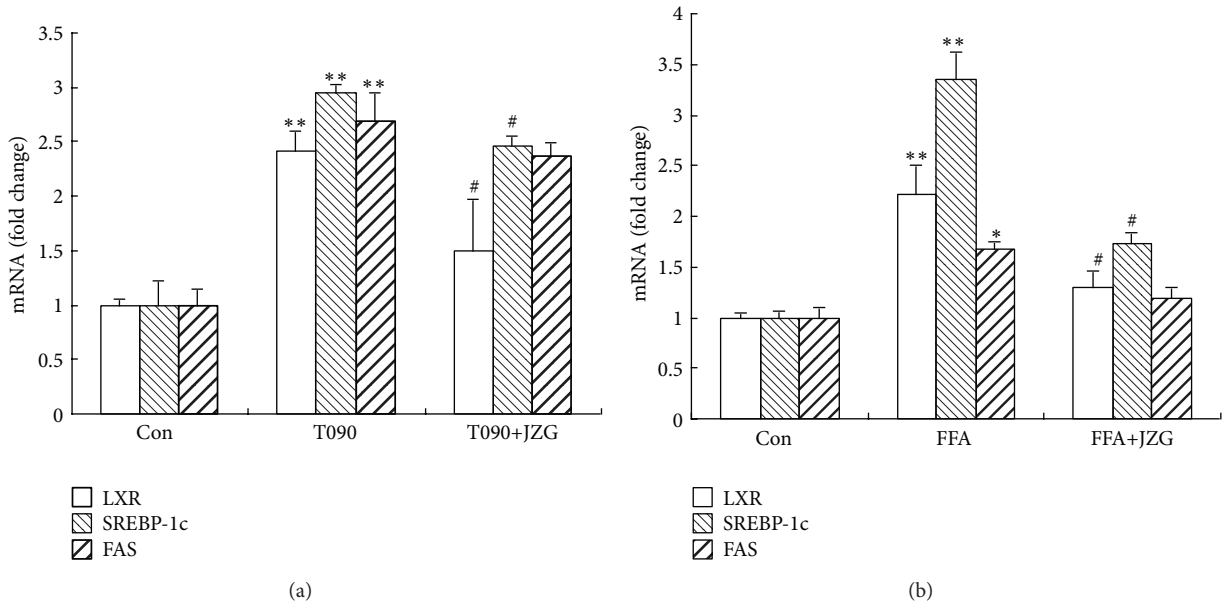

Figure 4: JZG reduced T090-mediated and FFA-induced expression of lipogenesis-related genes. (a) The effect of JZG on T090-mediated LXRα, SREBP-1c, and FAS mRNA expression levels. (b) The effect of JZG on FFA-induced LXRα, SREBP-1c, and FAS mRNA expression levels. The data represent the mean ± SEM of three separate measurements. $^{*}P < 0.05$ and $^{**}P < 0.01$ versus the control group, $^{\#}P < 0.05$ versus the FFA group.

LXRα is important in SREBP-1 expression and SREBP-1-mediated lipogenesis. We first investigated the effect of JZG on the T090-mediated and FFA-induced LXRα/SREBP-1c activation. The mRNA expression of LXRα, SREBP-1c, and FAS was significantly increased after treatment with T090 (1 μM) or palmitate (0.5 mM) for 24 hours; this induction was inhibited by concomitant JZG treatment (Figure 4).

Therefore, we speculated that JZG might inhibit the activation of LXRα and then decrease the expression of SREBP-1c and its target gene, FAS.

3.6. Inhibition of SREBP-1c Activation by JZG (Drug-Containing Serum) in siRNA Targeting LXRα HepG2 Cells. Some agents have little effect on the level of hepatic SREBP-1c precursor but significantly increase the level of hepatic mature SREBP-1c [18]. We have proved that LXRα-mediated elevation of SREBP-1c was alleviated by JZG treatment, but we had little knowledge about the effect of JZG on SREBP-1c activation independent of LXRα. Therefore, we introduced siRNA targeting LXRα in FFA-treated HepG2 cells to assess the activation of SREBP-1c. The siRNA targeting LXRα markedly reduced the levels of LXRα mRNA (sup Figure 2). As shown in Figure 5(a), in FFA-treated LXRα knockdown HepG2 cells, the mRNA levels of SREBP-1c and FAS were mildly increased compared to those in the control cells. However, these effects were blocked by concomitant JZG treatment. For protein examination, although JZG had little effect on the level of pSREBP-1c, the level of mSREBP-1c was significantly decreased (Figure 5(b)). Based on these results, we speculated that JGZ might not only decrease the expression of SREBP-1c through inhibiting LXRα activation, but also inhibit the maturation of SREBP-1c independent of LXRα.

4. Discussion

To determine the effects of JZG on hepatic steatosis, two approaches were employed in this study: (1) an *in vivo* model involving HFD-fed rats and (2) an *in vitro* model by treatment with FFA, LXRα agonist (T090), and siRNA targeting LXRα. These results suggested that JZG exerted an anti-fatty liver effect through inhibition of LXRα/SREBP-1c pathway.

TCM has been used in China for thousands of years. It is widely practiced nowadays to manage different diseases and is regarded as an important part of the current health care system. Five herbs in JZG formula are generally used in China and listed in the Chinese Pharmacopoeia (2005 edition). They have good biological activities in lowering lipid level and improving liver function, as well as anti-inflammatory properties [19–21]. Integration of several herbs in a certain proportion to form a formula is the unique feature of TCM. The efficacy of a formula derives from the complex interactions of herbs, and this surpasses a single drug while treating certain disease. Therefore, we expected that JZG formula would achieve a maximized efficacy though potential synergistic effects of the five herbs. In our previous Randomized Controlled Trail (RCT) [22], 144 eligible patients were randomized to treatment group (JZG combinated with behavioral intervention) or control group (behavioral intervention alone). The primary outcome was an improvement in hepatic steatosis. The liver fat content was measured by ultrasound and graded into normal, mild, moderate and

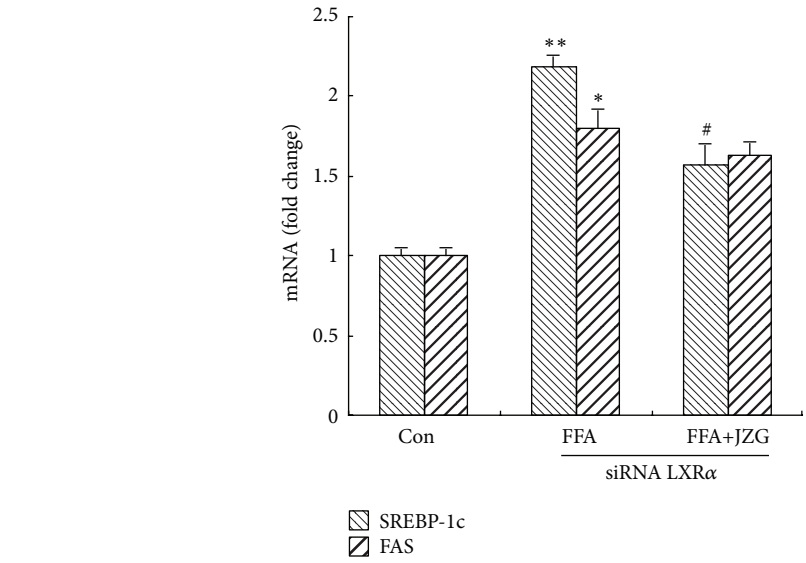

(a)

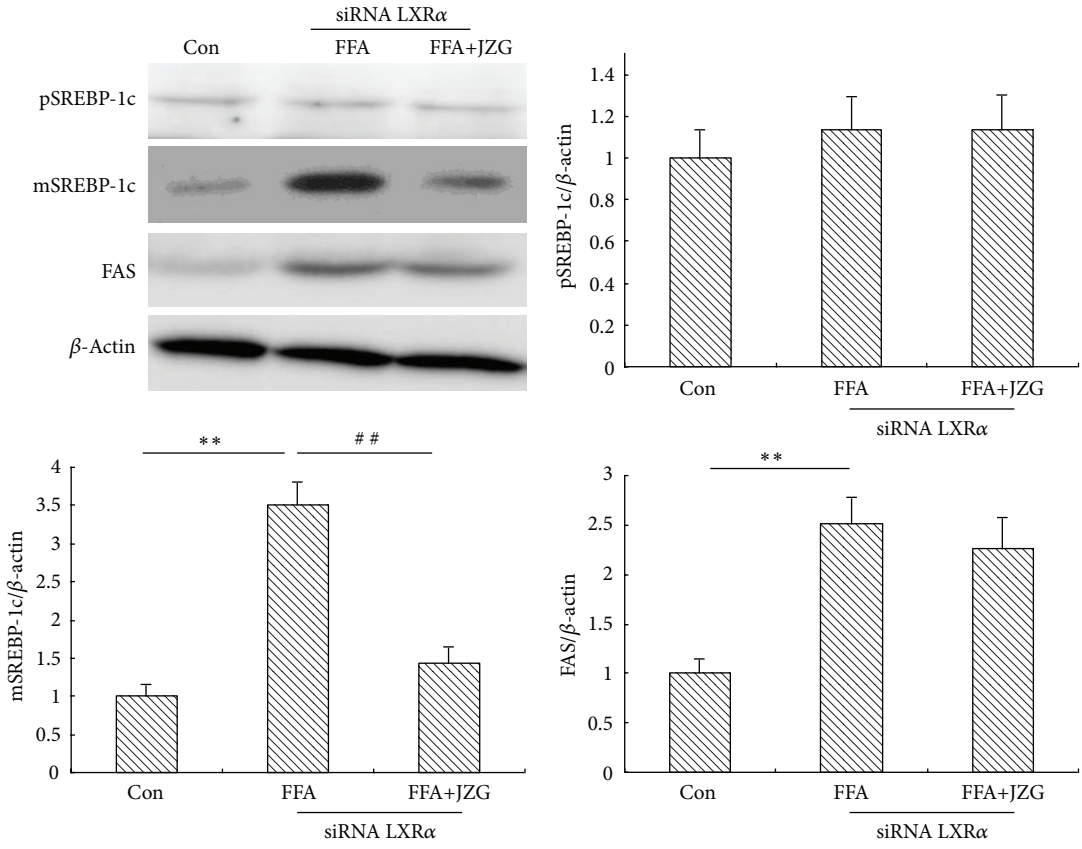

(b)

Figure 5: JZG reduced expression of SREBP-1c-related genes and proteins independent of LXRα. (a) The effect of JZG on FFA-induced SREBP-1c and FAS mRNA expression levels in LXRα knockdown HepG2 cells. (b) The effect of JZG on FFA-induced pSREBP-1c, mSREBP-1c, and FAS protein expression levels in LXRα knockdown HepG2 cells. The data represent the mean ± SEM of three separate measurements. $^{*}P < 0.05$ and $^{**}P < 0.01$ versus the control group, $^{\#}P < 0.05$ and $^{\#\#}P < 0.01$ versus the FFA group.

severe degrees [23]. The effective treatment was defined as one or more degrees decline in ultrasound grading after treatment. Our results demonstrated that a total effective rate was 76.56% in the treatment group versus 52.54% in the control group ($P < 0.01$). Nevertheless, further phytochemical studies elucidating its mechanisms are necessary for JZG treatment to be widely accepted into mainstream medical practice.

Dietary fat is one of the most important environmental factors associated with NAFL. It was previously shown that HFD is a good strategy for inducing a NAFL model [15]. The rat model in this study confirmed successful fat accumulation in the liver after HFD feeding for 8 weeks. The changes in body weight or liver weight, plasma levels of triglyceride and cholesterol, and hepatic fat accumulation were significantly lowered in the HFD+JZG group compared with the HFD group. Meanwhile, food consumption did not significantly differ between the two groups. These results suggested that energy intake did not contribute to the significant anti-fatty liver effects of JZG.

We speculated that the hypolipidemic effects of JZG came from the altered hepatic lipid metabolism. It was reported that dietary fat content, independent from caloric intake, is a crucial factor in the development of hepatic steatosis [24], and saturated fat intake can activate SREBP-1c and LXRα [25–27]. LXRα is a key regulator of fatty acid synthesis in NALF [18, 28] and a member of the nuclear receptor superfamily, which regulates the expression of key proteins involved in lipid metabolism [29]. LXRα agonist is primarily considered beneficial in the treatment of atherosclerosis [30], but the induction of fatty liver and hepatic dysfunction has limited their clinical development [31]. LXRα agonist also increases the expression of SREBP-1c, which leads to increased hepatic triglyceride synthesis [32]. Therefore, researchers consider the LXRα/SREBP-1c pathway an attractive target for the prevention and/or treatment of steatosis in hepatocytes [33], and several lines of evidence indicate that the suppression or disruption of LXRα leads to the reduction of hepatic triglyceride synthesis and accumulation [12, 34]. The present study found that the expression of LXRα and SREBP-1c was upregulated in HFD-fed rats, as well as FFA- and T090-treated HepG2 cells; JZG significantly alleviated the upregulation of LXRα and SREBP-1c in liver and cells.

SREBPs are a family of transcription factors that consist of SREBP-1a, SREBP-1c, and SREBP-2 [35]. SREBP-1c is the major isoform in liver and stimulates several lipogenic enzymes involved in liver fatty-acid synthesis [36], such as the gene that encodes FAS [37]. Increased SREBP-1c levels have been found in patients with histologically diagnosed NAFLD [38] and HFD-induced obese rats [39]. Transgenic mice overexpressing SREBP-1c produced massive fatty livers owing to increased accumulation of cholesteryl esters and triglycerides [40]. Several studies demonstrated that the mature form of hepatic SREBP-1c was significantly increased in fatty liver models [18, 41]. We therefore assessed whether JZG decreased hepatic steatosis through reducing SREBP-1c levels and/or activities independent of LXRα. We observed that JZG decreased the expression of SREBP-1c mRNA and mSREBP-1c protein in FFA-treated LXRα knockdown HepG2 cells. These results suggested that JZG could inhibit the maturation of SREBP-1c independent of LXRα.

The results from this study support us to continue JZG treatment in NAFL. JZG also has to withstand the rigorous scrutiny of research like other novel treatments. This required scientifically accepted research methodologies to avoid overstating study results. A randomized, double-blind, multicenter, placebo-controlled, phase III trial with 24 weeks followup is ongoing. The primary outcome is an alleviation in hepatic steatosis on the basis of computed tomography scans. Improvements in plasma biochemical parameters are secondary outcome measures. We expect that this confirmatory study will support JZG to be used in clinical treatment of NAFL.

5. Conclusion

We conclude that the effect of JZG on hepatic steatosis is likely to be multifactorial: JZG decreases the activation of SREBP-1c through inhibiting LXRα-mediated SREBP-1c transcription, as well as through inhibiting the maturation of SREBP-1c independent of LXRα. These findings may provide molecular evidence, at least partially, for the use of JZG as a promising therapeutic option for NAFL.

Authors' Contribution

Miao Wang, Shanshan Sun, and Tao Wu have equally contributed to this paper.

Acknowledgments

This study was supported by the National Nature Science Foundation of China (81001508 and 81273727), Leading Academic Discipline Project of Shanghai Municipal Education Commission (J50305 and E3008) and Innovative Research Team in Universities, Shanghai Municipal Education Commission, Longhua Hospital's Excellent Group, Longhua Hospital's Outstanding Scholar Project (no. D-09), and national TCM Clinical Research Base in Longhua Hospital. There is no conflict of interests involved in this paper.

References

[1] S. Chitturi, G. C. Farrell, and J. George, "Non-alcoholic steatohepatitis in the Asia-Pacific region: future shock?" *Journal of Gastroenterology and Hepatology*, vol. 19, no. 4, pp. 368–374, 2004.

[2] S. Bellentani and M. Marino, "Epidemiology and natural history of non-alcoholic fatty liver disease (NAFLD)," *Annals of Hepatology*, vol. 8, supplement 1, pp. S4–S8, 2009.

[3] H. Zhang, S. M. He, J. Sun et al., "Prevalence and etiology of abnormal liver tests in an adult population in Jilin, China," *International Journal of Medical Sciences*, vol. 8, no. 3, pp. 254–262, 2011.

[4] S. H. Chen, F. He, H. L. Zhou, H. R. Wu, C. Xia, and Y. M. Li, "Relationship between nonalcoholic fatty liver disease and

metabolic syndrome," *Journal of Digestive Diseases*, vol. 12, no. 2, pp. 25–130, 2011.

[5] M. R. Teli, O. F. W. James, A. D. Burt, M. K. Bennett, and C. P. Day, "The natural history of nonalcoholic fatty liver: a follow-up study," *Hepatology*, vol. 22, no. 6, pp. 1714–1719, 1995.

[6] P. Angulo, "Nonalcoholic fatty liver disease," *The New England Journal of Medicine*, vol. 346, no. 16, pp. 1221–1231, 2002.

[7] H. F. Wei and G. Ji, "Systematic review of treating nonalcoholic fatty liver with taking TCM orally: a clinical randomized controlled trial," *China Journal of Traditional Chinese Medicine and Pharmacy*, vol. 27, no. 5, pp. 1309–1314, 2012.

[8] H. F. Wei, T. Liu, L. J. Xing, P. Y. Zheng, and G. Ji, "Distribution pattern of traditional Chinese medicine syndromes in 793 patients with fatty liver disease," *Journal of Chinese Integrative Medicine*, vol. 7, no. 5, pp. 411–417, 2009.

[9] Y. L. Lu, M. Wang, L. Zhang et al., "Simultaneous determination of six components in the 'Jiang-Zhi' Granule by UPLC-MS analysis," *Chinese Journal of Natural Medicines*, vol. 8, no. 6, pp. 449–455, 2010.

[10] Z. S. Ma, T. Liu, P. Y. Zheng et al., "Effect of Chinese medicine Jiangzhi granula on hepaticlipid of nonalcoholic fatty liver disease rats," *Chinese Archives of Traditional Chinese Medicine*, vol. 25, no. 4, pp. 942–944, 2007.

[11] J. Folch, M. Lees, and G. H. Slane Stanley, "A simple method for the isolation and purification of total lipides from animal tissues," *The Journal of Biological Chemistry*, vol. 226, no. 1, pp. 497–509, 1957.

[12] K. G. Park, A. K. Min, E. H. Koh et al., "Alpha-lipoic acid decreases hepatic lipogenesis through adenosine monophosphate-activated protein kinase (AMPK)-dependent and AMPK-independent pathways," *Hepatology*, vol. 48, no. 5, pp. 1477–1486, 2008.

[13] Y. T. Kuo, T. H. Lin, W. L. Chen, and H. M. Lee, "Alpha-lipoic acid induces adipose triglyceride lipase expression and decreases intracellular lipid accumulation in HepG2 cells," *European Journal of Pharmacology*, vol. 692, no. 1–3, pp. 10–18, 2012.

[14] W. Cui, M. Wang, H. Maegawa et al., "Inhibition of the activation of hepatic stellate cells by arundic acid via the induction of cytoglobin," *Biochemical and Biophysical Research Communications*, vol. 425, no. 3, pp. 642–648, 2012.

[15] Z. J. Xu, J. G. Fan, X. D. Ding, L. Qiao, and G. L. Wang, "Characterization of high-fat, diet-induced, non-alcoholic steatohepatitis with fibrosis in rats," *Digestive Diseases and Sciences*, vol. 55, no. 4, pp. 931–940, 2010.

[16] J. R. Schultz, H. Tu, A. Luk et al., "Role of LXRs in control of lipogenesis," *Genes and Development*, vol. 14, no. 22, pp. 2831–2838, 2000.

[17] Z. L. Ai, C. H. Zhu, M. Min et al., "The role of hepatic liver X receptor alpha- and sterol regulatory element binding protein-1c-mediated lipid disorder in the pathogenesis of non-alcoholic steatohepatitis in rats," *Journal of International Medical Research*, vol. 39, no. 4, pp. 1219–1229, 2011.

[18] X. Chen, C. Zhang, M. Zhao et al., "Melatonin alleviates lipopolysaccharide-induced hepatic SREBP-1c activation and lipid accumulation in mice," *Journal of Pineal Research*, vol. 51, no. 4, pp. 416–425, 2011.

[19] Y. Wang, F. Catana, Y. Yang, R. Roderick, and R. B. Van Breemen, "An LC-MS method for analyzing total resveratrol in grape juice, cranberry juice, and in wine," *Journal of Agricultural and Food Chemistry*, vol. 50, no. 3, pp. 431–435, 2002.

[20] H. Du, J. S. You, X. Zhao, J. Y. Park, S. H. Kim, and K. J. Chang, "Antiobesity and hypolipidemic effects of lotus leaf hot water extract with taurine supplementation in rats fed a high fat diet," *Journal of Biomedical Science*, vol. 17, no. 1, article S42, 2010.

[21] W. Xie, Y. Zhao, and L. Du, "Emerging approaches of traditional Chinese medicine formulas for the treatment of hyperlipidemia," *Journal of Ethnopharmacology*, vol. 140, no. 2, pp. 345–367, 2012.

[22] M. Wang, T. Liu, H. F. Wei et al., "Clinical study of "Jiang zhi Granule" and behavioral intervention for nonalcoholic fatty liver disease of phlegm and blood-stasis syndrome," *Shanghai Zhong Yi Yao Za Zhi*, vol. 44, no. 4, pp. 11–13, 2010.

[23] Fatty Liver and Alcoholic Liver Disease Study Group of the Chinese Liver Disease Association, "Guidelines for diagnosis and treatment of nonalcoholic fatty liver diseases," *Chinese Journal of Hepatology*, vol. 14, no. 3, pp. 161–163, 2006.

[24] V. E. de Meijer, H. D. Le, J. A. Meisel et al., "Dietary fat intake promotes the development of hepatic steatosis independently from excess caloric consumption in a murine model," *Metabolism*, vol. 59, no. 8, pp. 1092–1105, 2010.

[25] J. Lin, R. Yang, P. T. Tarr et al., "Hyperlipidemic effects of dietary saturated fats mediated through PGC-1β coactivation of SREBP," *Cell*, vol. 120, no. 2, pp. 261–273, 2005.

[26] M. T. Flowers and J. M. Ntambi, "Role of stearoyl-coenzyme A desaturase in regulating lipid metabolism," *Current Opinion in Lipidology*, vol. 19, no. 3, pp. 248–256, 2008.

[27] H. X. Guo, D. H. Liu, Y. Ma et al., "Long-term baicalin administration ameliorates metabolic disorders and hepatic steatosis in rats given a high-fat diet," *Acta Pharmacologica Sinica*, vol. 30, no. 11, pp. 1505–1512, 2009.

[28] N. Higuchi, M. Kato, Y. Shundo et al., "Liver X receptor in cooperation with SREBP-1c is a major lipid synthesis regulator in nonalcoholic fatty liver disease," *Hepatology Research*, vol. 38, no. 11, pp. 1122–1129, 2008.

[29] N. Zelcer and P. Tontonoz, "Liver X receptors as integrators of metabolic and inflammatory signaling," *Journal of Clinical Investigation*, vol. 116, no. 3, pp. 607–614, 2006.

[30] S. B. Joseph, A. Castrillo, B. A. Laffitte, D. J. Mangelsdorf, and P. Tontonoz, "Reciprocal regulation of inflammation and lipid metabolism by liver X receptors," *Nature Medicine*, vol. 9, no. 2, pp. 213–219, 2003.

[31] A. Grefhorst, B. M. Elzinga, P. J. Voshol et al., "Stimulation of lipogenesis by pharmacological activation of the liver X receptor leads to production of large, triglyceride-rich very low density lipoprotein particles," *Journal of Biological Chemistry*, vol. 277, no. 37, pp. 34182–34190, 2002.

[32] A. I. Shulman and D. J. Mangelsdorf, "Retinoid X receptor heterodimers in the metabolic syndrome," *The New England Journal of Medicine*, vol. 353, no. 6, pp. 604–615, 2005.

[33] D. J. Peet, S. D. Turley, W. Ma et al., "Cholesterol and bile acid metabolism are impaired in mice lacking the nuclear oxysterol receptor LXRα," *Cell*, vol. 93, no. 5, pp. 693–704, 1998.

[34] H. Basciano, A. Miller, C. Baker, M. Naples, and K. Adeli, "LXRα activation perturbs hepatic insulin signaling and stimulates production of apolipoprotein B-containing lipoproteins," *The American Journal of Physiology*, vol. 297, no. 2, pp. G323–G332, 2009.

[35] T. C. Otto and M. D. Lane, "Adipose development: from stem cell to adipocyte," *Critical Reviews in Biochemistry and Molecular Biology*, vol. 40, no. 4, pp. 229–242, 2005.

[36] I. Shimomura, H. Shimano, J. D. Horton, J. L. Goldstein, and M. S. Brown, "Differential expression of exons 1a and 1c in mRNAs for sterol regulatory element binding protein-1 in human and mouse organs and cultured cells," *Journal of Clinical Investigation*, vol. 99, no. 5, pp. 838–845, 1997.

[37] L. W. Weber, M. Boll, and A. Stampfl, "Maintaining cholesterol homeostasis: sterol regulatory element-binding proteins," *World Journal of Gastroenterology*, vol. 10, no. 21, pp. 3081–3087, 2004.

[38] M. Kohjima, N. Higuchi, M. Kato et al., "SREBP-1c, regulated by the insulin and AMPK signaling pathways, plays a role in nonalcoholic fatty liver disease," *International Journal of Molecular Medicine*, vol. 21, no. 4, pp. 507–511, 2008.

[39] L. Madsen, R. K. Petersen, M. B. Sørensen et al., "Adipocyte differentiation of 3T3-L1 preadipocytes is dependent on lipoxygenase activity during the initial stages of the differentiation process," *Biochemical Journal*, vol. 375, no. 3, pp. 539–549, 2003.

[40] H. Shimano, J. D. Horton, R. E. Hammer, I. Shimomura, M. S. Brown, and J. L. Goldstein, "Overproduction of cholesterol and fatty acids causes massive liver enlargement in transgenic mice expressing truncated SREBP-1a," *Journal of Clinical Investigation*, vol. 98, no. 7, pp. 1575–1584, 1996.

[41] M. Sekiya, N. Yahagi, T. Matsuzaka et al., "Polyunsaturated fatty acids ameliorate hepatic steatosis in obese mice by SREBP-1 suppression," *Hepatology*, vol. 38, no. 6, pp. 1529–1539, 2003.

Hindawi Publishing Corporation
Evidence-Based Complementary and Alternative Medicine
Volume 2013, Article ID 193084, 8 pages
http://dx.doi.org/10.1155/2013/193084

Research Article

Bai-Hu-Tang, Ancient Chinese Medicine Formula, May Provide a New Complementary Treatment Option for Sepsis

Chien-Jung Lin,[1,2] Yi-Chang Su,[2,3] Cheng-Hung Lee,[2] Tsai-Chung Li,[4,5] Yun-An Chen,[3] and Sunny Jui-Shan Lin[2,3]

[1] *Department of Chinese Medicine, National Defense Medical Center, Tri-Service General Hospital, Taipei 11490, Taiwan*
[2] *Graduate Institute of Chinese Medicine, College of Chinese Medicine, China Medical University, No. 91 Hsueh-Shih Road, Taichung 40402, Taiwan*
[3] *School of Chinese Medicine, College of Chinese Medicine, China Medical University, Taichung 40402, Taiwan*
[4] *Graduate Institute of Biostatistics, College of Public Health, China Medical University, Taichung 40402, Taiwan*
[5] *Department of Healthcare Administration, College of Health Science, Asia University, Taichung 41354, Taiwan*

Correspondence should be addressed to Sunny Jui-Shan Lin; taco423@ms26.hinet.net

Received 7 January 2013; Revised 19 April 2013; Accepted 25 April 2013

Academic Editor: Martin Kohlmeier

Bai-Hu-Tang (BHT) has been broadly applied to treating the early stage of acute infection with systemic inflammation for two thousand years in Chinese medicine. We explore whether BHT is beneficial in treating sepsis and its effects on proinflammatory cytokine, interleukin-6, and anti-inflammatory cytokine interleukin-10, in which both play key roles in the progress of sepsis. Thirty-six male Sprague-Dawley rats were randomized into six groups, with cecal ligation and puncture (CLP) performed in all but the sham-control group. Rats in CLP + BHT-L_6 and CLP + BHT-H_6 groups, respectively, received a low (0.45 g/kg) and high doses (0.9 g/kg) of BHT, 6 hrs postoperatively. CLP + BHT-L_{12} and CLP + BHT-H_{12} groups, respectively, received low and high doses of BHT, 12 hrs postoperatively. Sham-control and sepsis-control groups received distilled water (1 mL) as vehicle, 6 hrs postoperatively. Serial blood samples were drawn before operation, as baseline, and at 4, 8, and 12 hrs postoperatively for IL-6 and IL-10 assay. All rats were monitored for 3 days for survival study. Rats in the CLP + BHT-H_6 group had significantly higher survival rate (80%) and significantly lower levels of both IL-6 and IL-10 at 12 hrs postoperatively than those in the sepsis-control group. Results suggested that BHT may be a new complementary treatment option for sepsis.

1. Introduction

The term "translational research" first appeared in PubMed in 1993, and it has cropped up in hundreds of articles each year after 2000. Relatively recent, a chasm has opened up between biomedical researchers and the patients who need their discoveries [1, 2]. Enormous resources have been thrown into biomedical research, but the resulting commensurate gains are not as expected [1]. To bridge the gap between basic and clinical research, thriving treasures recorded in the Chinese medicine literature are worthy to be refined to provide promising targets since series of theoretical systems and practical experience of Chinese medicine were constructed through fighting diseases in the past thousands of years.

Sepsis is the leading cause of death in intensive care patients, with a reported incidence of more than 750,000 people each year in North America and Europe [3, 4]. Despite major advances in the understanding of its pathogenesis, no satisfactory therapy has emerged [5, 6]; mortality from severe sepsis remains high at approximately 28% [3].

The most prominent pathological feature of sepsis is the exuberant, poorly regulated cytokine-mediated inflammatory response to microbial products [7]. Release of proinflammatory cytokines prolongs the inflammatory reaction [8] and leads to organ injury or dysfunction [9–12]. To prevent severe damage, anti-inflammatory cytokines are released. With overproduction of anti-inflammatory cytokines being occurred, the host becomes immunosuppressed, which can

Table 1: Study groups and their interventions.

Groups	Model	Administration (timing)
Sham-control ($n = 6$)	Sham operation	Distilled water 1 mL as vehicle (6 hrs after operation)
Sepsis-control ($n = 6$)	CLP	Distilled water 1 mL as vehicle (6 hrs after CLP)
CLP + BHT-L_6 (0.45 g/kg) ($n = 6$)	CLP	BHT 0.5 mL + distilled 0.5 mL (6 hrs after CLP)
CLP + BHT-H_6 (0.9 g/kg) ($n = 6$)	CLP	BHT 1 mL (6 hrs after CLP)
CLP + BHT-L_{12} (0.45 g/kg) ($n = 6$)	CLP	BHT 0.5 mL + distilled 0.5 mL (12 hrs after CLP)
CLP + BHT-H_{12} (0.9 g/kg) ($n = 6$)	CLP	BHT 1 mL (12 hrs after CLP)

CLP: rats received cecal ligation and puncture.
BHT-L_6: low dose of BHT was orally administered 6 hrs postoperatively.
BHT-H_6: high dose of BHT was orally administered 6 hrs postoperatively.
BHT-L_{12}: low dose of BHT was orally administered 12 hrs postoperatively.
BHT-H_{12}: high dose of BHT was orally administered 12 hrs postoperatively.

lead to death [13, 14]. A recent large observational study of sepsis revealed mortality highest when proinflammatory and anti-inflammatory cytokine levels are high [15]. These findings demonstrate that limiting both proinflammatory and anti-inflammatory cytokines should be considered in treating sepsis.

Bai-Hu-Tang (BHT, also known as *White Tiger Decoction*), a widely used Chinese medicine formula composed of *Shi-Gao* (*Gypsum Fibrosum*), *Zhi-Mu* (*Rhizoma Anemarrhenae*), *Zhi-Gan-Cao* (Radix Glycyrrhizae Preparata), and *Geng-Mi* (nonglutinous rice), has been extensively used in the early stage of acute infection with systemic inflammation for two thousand years in Chinese medicine [16–18], yet no empirical studies conducted. We explored treatment effects of BHT against cecal ligation and puncture- (CLP-) induced sepsis in rats. Since plasma levels of interleukin-6 (IL-6) and interleukin-10 (IL-10) were demonstrated as good parameters to predict the outcome of sepsis in our previous study [19], survival rate and plasma levels of IL-6 and IL-10 of rats were measured in the present study. Furthermore, mean arterial pressure (MAP) and heart rate (HR) were also measured to monitor the development and progression of sepsis.

2. Materials and Methods

2.1. Drugs and Preparation. *Bai-Hu-Tang* concentrated extract powder is composed of four ingredients: *Shi-Gao* (*Gypsum Fibrosum*), *Zhi-Mu* (*Rhizoma Anemarrhenae*), *Zhi-Gan-Cao* (Radix Glycyrrhizae Preparata), and *Geng-Mi* (nonglutinous rice) with the proportion of 3 : 8 : 1 : 4. We purchased the formula from a renowned GMP manufacturer of concentrated herbal extracts which conforms to international standards (*Sun-Ten* Pharmaceutical CO., Taipei; its products can be purchased in Asia, Europe, and North America.). When in use, BHT was prepared by mixing 1 gram of extract powder with 5 mL of warm sterile distilled water (30°C).

2.2. Animal Model. A total of 36 male Sprague-Dawley (SD) rats, weighing 250 to 300 g, were obtained from BioLASCO Taiwan Co. Ltd. and then maintained at a constant 25°C with free access to pelleted food and water in a room with 12 h light/dark cycle. Sepsis was induced by CLP as previously described [19, 20]. Briefly, rats were anesthetized with ether, with blood samples obtained from the tail artery. After that, a 2 cm midline incision was made, and then the cecum was exteriorized. Ligation was performed below the ileocecal valve without causing intestinal obstruction. Ligated cecum was punctured twice with a 20-gauge needle at the antimesenteric surface and then gently squeezed to extrude adequate amount of stool through two puncture wounds. The bowel was then replaced in the peritoneal cavity and abdomen closed in layers with 3-O silk sutures. Finally, warm saline (3 mL/100 g body weight, 37°C) was subcutaneously injected [20]. Sham-operated rats underwent the same treatment, except for ligation and puncture procedures.

The right carotid artery was then cannulated by PE-50 tubing (Clay Adams, Parsippany, NJ, USA) equipped with a heparin lock filled with heparin saline to permit blood pressure measurement, drawing of blood samples, and infusion of fluids. This catheter was passed through the subcutaneous tunnel to the back of the neck. Finally, rats were placed in cages with warm light and allowed to recover for half an hour; serial MAP and HR were measured and recorded by MP100 System (Biopac Inc., Santa Barbara, CA, USA) at 1, 4, 8, and 12 hrs postoperatively by inserting the probe into the catheter via the heparin lock. Experimental protocols were approved by the Animal Experiment Committee of China Medical University and conducted according to the American Physiological Society guiding principles for the care and use of laboratory animals.

2.3. Study Groups. Thirty-six rats were randomly divided into six experimental groups of six rats each. According to prior study, after being subjected to CLP, the hyperdynamic state developed within 10 hrs; rats became obviously ill looking 12 hrs postoperatively [20]. Timing of early oral administration of BHT was thus set at 6 hrs postoperatively within the progress of the hyperdynamic state in our study because BHT is applied clinically when the following symptoms developed in the early stage of infectious diseases: high fever, presence of sweating, thirst, and flooding big pulse [17]. The time points we defined as early and late interventions at 6 hrs and 12 hrs postoperatively, respectively, were consistent with current international opinions [21, 22]. This design was also aimed to compare the effects on survival between "early" and "late" administration of BHT. Table 1 details the intervention established in each group.

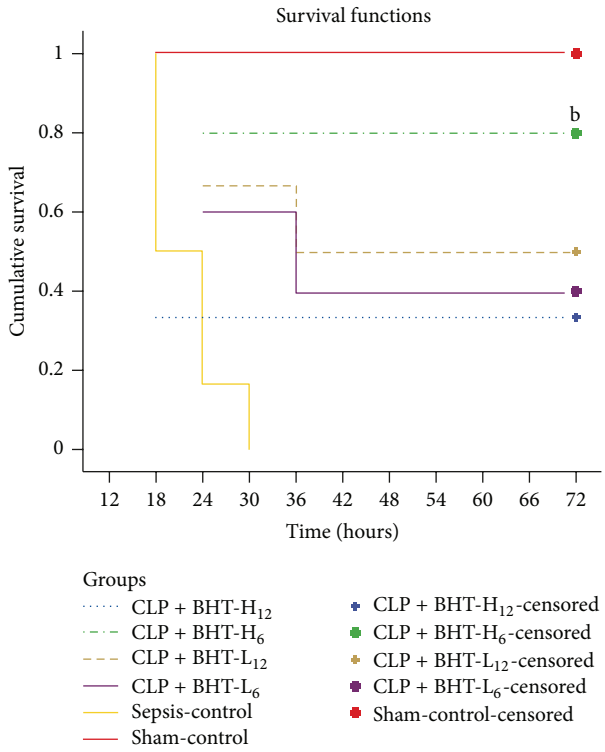

FIGURE 1: Kaplan-Meier survival curves of all groups. Sham-control group received sham operation and distilled water; the remaining groups received cecum ligation and puncture (CLP). All CLP rats received *Bai-Hu-Tang* (BHT), except for those in the sepsis-control group, which received distilled water. CLP + BHT-L_6: low dose of BHT (0.45 g/kg) administered 6 hrs postoperatively. CLP + BHT-H_6: high dose of BHT (0.9 g/kg) administered 6 hrs postoperatively. CLP + BHT-L_{12}: low dose BHT (0.45 g/kg) administered 12 hrs postoperatively. CLP + BHT-H_{12}: high-dose of BHT (0.9 g/kg) administered 12 hrs postoperatively. All rats were monitored for three days postoperatively for survival study. Notice that the survival was highest in the CLP + BHT-H_6 group. $^bP < 0.05$, compared to sepsis-control group.

2.4. Survival Studies. All rats were monitored for three days postoperatively, those surviving for more than three days categorized in the survival group and the remainder in the nonsurvival group.

2.5. Collection of Serum Samples and Cytokine Assay. Before CLP and catheterization, a 0.5 mL blood sample was drawn from the tail artery to establish baseline value measurement of cytokines. After CLP and catheterization, 0.5 mL blood samples were taken from the heparin lock of the carotid artery catheter 4, 8, and 12 hrs later. Normal saline (0.5 mL, 37°C) was injected into the artery to replace blood volume each time. The blood samples were placed in 1.5 mL microtubes and centrifuged at 9000 rpm for 5 min at 25°C to separate plasma. Serum samples were then removed and stored at −80°C for further cytokine assay. Serum levels of IL-6 and IL-10 were measured by the enzyme-linked immunosorbent assay (ELISA) via a commercially available kit (R&D systems, MN55413, Minneapolis, MN, USA) according to manufacturer's specifications.

2.6. Statistical Analysis. Log-rank test with Bonferroni adjustment for multiple comparisons analyzed differences in survival among all groups.

Comparisons of MAP, HR, and plasma levels of IL-6 and IL-10 were analyzed only among the sham-control, sepsis-control, CLP + BHT-L_6, and CLP + BHT-H_6 groups since we did not measure these four observation parameters in the CLP + BHT-L_{12} and CLP + BHT-H_{12} groups. Because MAP, HR, and plasma levels of IL-6 and IL-10 were not normally distributed, Kruskal-Wallis was used for overall comparison and then Mann-Whitney *U* with Bonferroni adjustment for multiple comparisons was adopted to detect the differences of these parameters at baseline, and at 4, 8, and 12 hrs postoperatively among groups.

To examine the dose effect of BHT on survival and cytokine changes, we first derived an ordinal variable by coding the sepsis-control group as "0," early administration of low-dose BHT (CLP + BHT-L_6) as "0.5," and early administration of high-dose BHT (CLP + BHT-H_6) as "1." Second, we defined changes of IL-6 and IL-10 by subtracting plasma levels of cytokines at baseline from those at 12 hrs postoperatively. All cytokine change values were natural log transformed. Then we applied simple linear regression to correlate doses of BHT with changes of IL-6 and IL-10. Finally, we adopted Cox proportional hazards models to explore how doses of BHT correlated with survival through modulating cytokines. Statistical analyses used SPSS version 14.0 for Windows (SPSS, Chicago, IL, USA); P value < 0.05 was considered statistically significant.

3. Results

Totally, 36 rats were observed. However, two were excluded due to catheter obstruction. Therefore, the study population comprised 34 rats.

3.1. Effects of BHT on Survival. No rats died until 18 hrs postoperatively. Overall test for comparing survival functions of each group was significant ($P < 0.05$). Kaplan-Meier survival curves are shown in Figure 1. The sham-control group had a 100% survival rate, the sepsis-control group 0% in survival. Survival rates were 40% for CLP + BHT-L_6, 80% for CLP + BHT-H_6, 50% for CLP + BHT-L_{12}, and 33% for CLP + BHT-H_{12}. Survival rate was significantly higher in the CLP + BHT-H_6 group (80%) than in the sepsis-control group ($P < 0.05$).

3.2. Effects of BHT on Plasma Levels of IL-6 and IL-10. Figure 2 illustrates changes in plasma levels of IL-6 and IL-10, that is, similar to all groups at baseline and both increasing significantly after CLP in the sepsis-control, CLP + BHT-L_6, and CLP + BHT-H_6 groups as compared with sham-control group ($^aP < 0.05$).

Early administration of high-dose BHT (CLP + BHT-H_6) significantly reduced elevations of IL-6 and IL-10 as compared with the sepsis-control group at 12 hrs postoperatively ($^bP < 0.05$, IL-6: 868.24 versus 3177.64 pg/mL; IL-10: 85.35 versus 229.45 pg/mL). Likewise, compared with low-dose BHT administration group, rats in the high-dose group

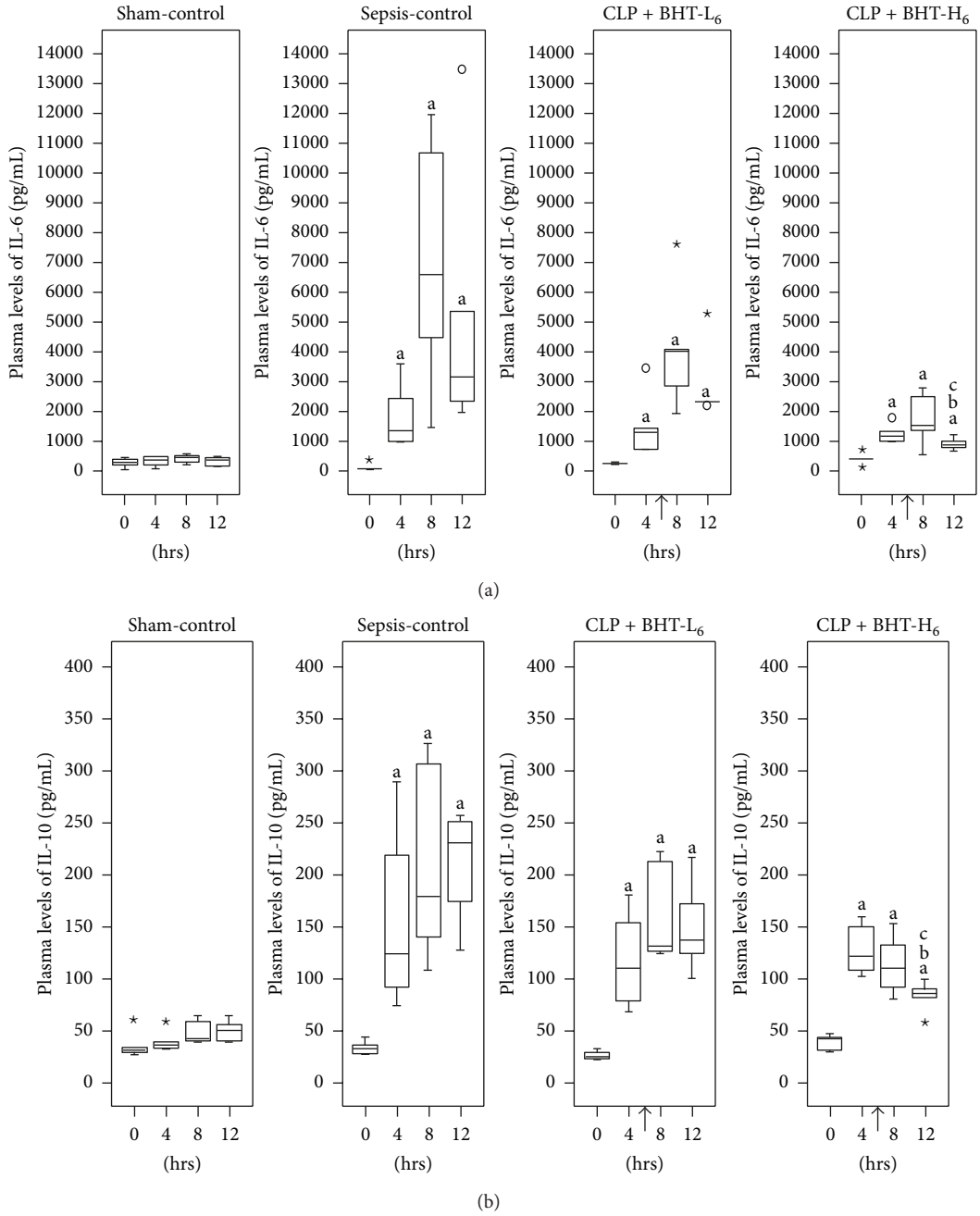

Figure 2: Effects of *Bai-Hu-Tang* on plasma levels of IL-6 (a) and IL-10 (b). Plasma levels of IL-6 and IL-10 in the sham-control, sepsis-control, CLP + BHT-L_6, and CLP + BHT-H_6 groups at 0, 4, 8, and 12 hours postoperatively were shown above. Boxes denote 25th and 75th percentile; horizontal lines in boxes indicate the median. Outliers are displayed as circles (○) and extreme values as stars (⋆). "↑": BHT was administered at 6 hrs postoperatively. Notice that the elevations of IL-6 and IL-10 levels were both reduced after the administration of BHT and it was most prominent in the CLP + BHT-H_6 group. [a]$P < 0.05$, compared with sham-control group. [b]$P < 0.05$, compared with sepsis-control group. [c]$P < 0.05$, compared with CLP + BHT-L_6 group.

had significantly lower plasma levels of IL-6 and IL-10 at 12 hrs postoperatively ([c]$P < 0.05$, IL-6 median: 868.24 versus 2346.94 pg/mL, IL-10 median: 85.35 versus 136.32 pg/mL).

3.3. Effect of BHT on MAP and HR. No significant difference in MAP arose among four groups at baseline and postoperatively (Figure 3). HR were similar in all groups at baseline and increased significantly after CLP, as compared with the sham-control group ([a]$P < 0.05$). No significant difference appeared for any BHT treatment group versus sepsis-control group (Figure 4).

3.4. Association among BHT, Cytokine Changes, and Survival Rate. Table 2 plots linear regression model for association

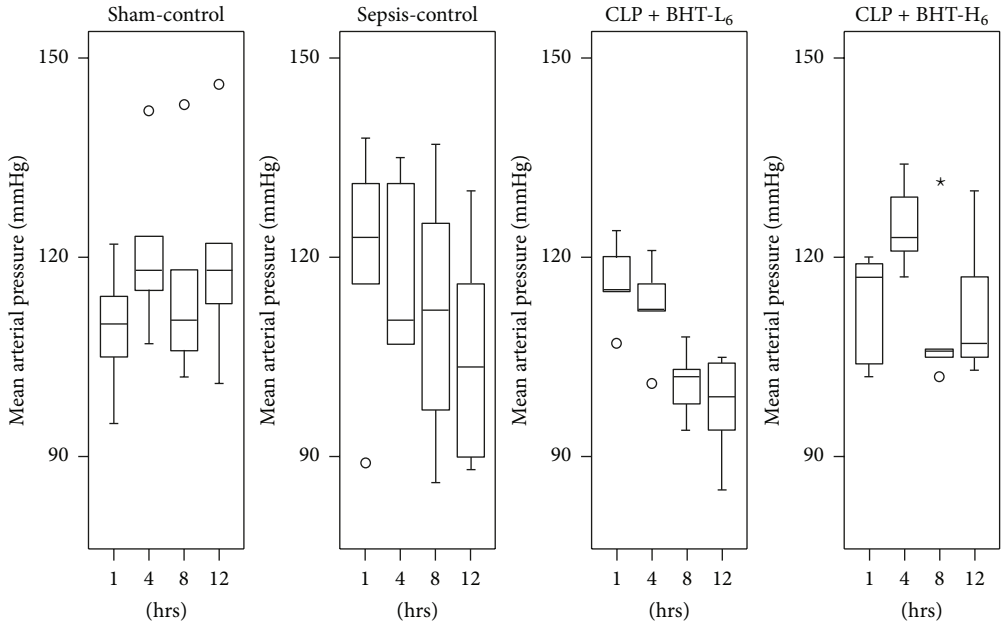

Figure 3: Effects of *Bai-Hu-Tang* on mean arterial pressure (MAP). MAP in sham-control, sepsis-control, CLP + BHT-L_6, and CLP + BHT-H_6 groups at 0, 4, 8, and 12 hours after operation were expressed as the box plots. Boxes denote the 25th and 75th percentile; horizontal lines in the box indicate the median. Outliers are displayed as circles (○) and extreme values as stars (⋆). No significant difference was noted at any time point among the four groups.

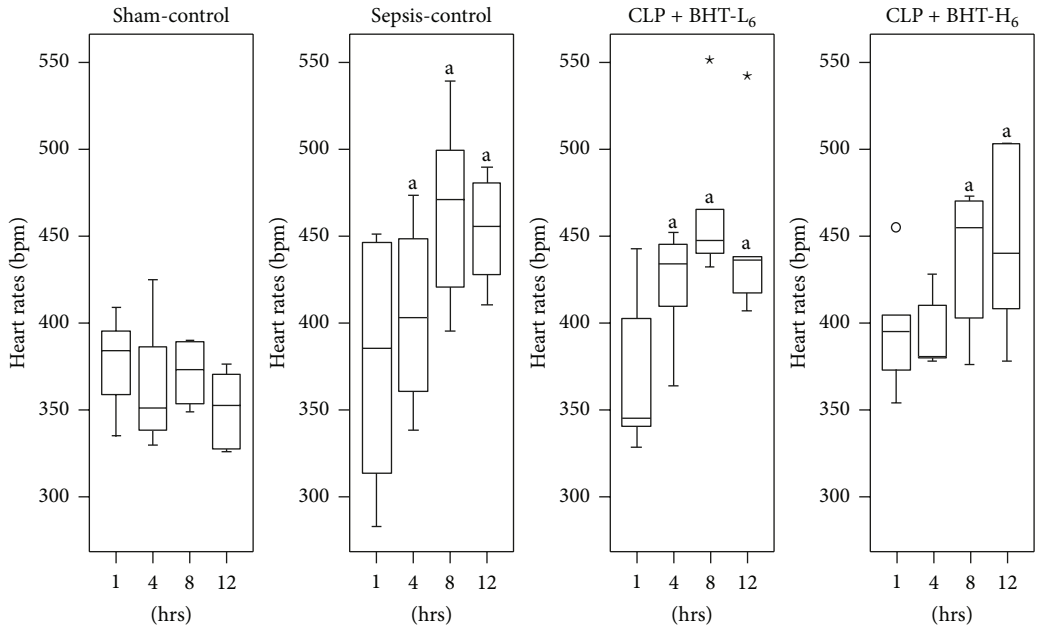

Figure 4: Effects of *Bai-Hu-Tang* on heart rates (HR). HR in the sham-control, sepsis-control, CLP + BHT-L_6, and CLP + BHT-H_6 groups at 0, 4, 8, and 12 hours after operation were shown above. Boxes denote 25th and 75th percentile; horizontal lines in the box indicate the median. Outliers are displayed as circles (○) and extreme values as stars (⋆). Notice that HR elevated in all groups after CLP. $^{a}P < 0.05$, compared with sham-control group.

between different doses of BHT and cytokine changes. We found significant negative correlation between a high dose of BHT and change in IL-6 and IL-10 ($\beta = -2.13$ and -1.41, resp., both $P < 0.001$). The model thus proved effects of BHT on changes of IL-6 and IL-10 as inverse and dose-dependent ($\beta = -2.09, -1.39$, P *for trend* < 0.001). Table 3 displays results of Cox regression models. Before adjustment, high dose BHT manifested negative correlation with risk of death (hazard ratio: 0.08; 95% confidence interval (CI): 0.01–0.73) ($P < 0.05$); changes in IL-6 and IL-10 both exhibited

Table 2: Linear regression model of association between different doses of BHT and cytokine changes.

	Change of IL-6[b]			Change of IL-10[b]		
	β	P value	P for trend	β	P value	P for trend
Dose of BHT	−2.09		<0.001*	−1.39		<0.001*
High dose (1)[a]	−2.13	<0.001*		−1.41	<0.001*	
Low dose (0.5)[a]	−0.39	0.295		−0.38	0.081	

[a]Ordinal variable: coding the early administration of high-dose BHT (CLP + BHT-H_6) as "1," and the early administration of low-dose BHT administration (CLP + BHT-L_6) as "0.5".
[b]changes of IL-6 and IL-10: subtracting the plasma levels of cytokines at baseline from those at 12 hrs postoperatively.
All cytokine changed values were natural log transformed.
*$P < 0.05$.

Table 3: Cox proportional hazards models of survival rates for different doses of BHT and changes of IL-6 and IL-10.

Covariate	Unadjusted		Adjusted+	
	HR (95% CI)	P value	HR (95% CI)	P value
Dose of BHT				
High dose (1)[a]	0.08 (0.01–0.73)	0.025*	0.56 (0.02–20.17)	0.751
Low dose (0.5)[a]	0.26 (0.06–1.19)	0.083	0.25 (0.05–1.40)	0.115
Sepsis control (0)[a]			Reference	
Cytokine changes				
Change of IL-6[b]	3.58 (1.50–8.56)	0.004*	3.87 (1.03–14.53)	0.045*
Change of IL-10[b]	4.56 (1.50–13.84)	0.007*	0.82 (0.10–6.91)	0.851

[a]Ordinal variable: coding the early administration of high-dose BHT (CLP + BHT-H_6) as "1," and the early administration of low-dose BHT administration (CLP + BHT-L_6) as "0.5".
[b]Changes of IL-6 and IL-10: subtracting the plasma levels of cytokines at baseline from those at 12 hrs postoperatively.
All values were natural log transformed.
Unadjusted: univariate Cox proportional hazards model.
Adjusted+: for different doses of BHT, changes of IL-6 and IL-10.
HR: hazard ratio, CI: confidence interval, *$P < 0.05$.

significant positive correlation with individual risk of death (hazard ratio: 3.58 and 4.56; 95% (CI): 1.50–8.56 and 1.50–13.84) ($P < 0.05$). Accounting for diverse BHT doses and cytokine changes, IL-6 variation was the sole predictor for survival, estimated at nearly fourfold greater risk of death (adjusted hazard ratio: 3.87; 95% (CI): 1.03–14.53) ($P < 0.05$).

4. Discussion

To our knowledge, this is the first study to explore treatment effects of BHT on survival and cytokine regulation in CLP-induced septic rats. Our results show early administration of high-dose BHT significantly improving survival by reducing IL-6 level. Although IL-10 was simultaneously reduced, modulating effects of BHT on IL-10 did not have significant effects on survival. In addition, we revealed effects of BHT on cytokine changes as dose dependent.

The study design of this study is based on our previous report [19], in which the prognosis of septic rats was followed up for 3 days after CLP, and IL-6 and IL-10 were found to be good predictors of sepsis mortality. Therefore, this time we adopted the same experiment protocol and administered BHT only one time after sepsis induction, in order to clearly evaluate the effects of BHT on both cytokines changes and survival rate. The protocol to monitor the septic rats for the first 3 days after sepsis induction is the same as the method reported in similar studies of sepsis [23, 24]. Besides, once the septic rats can survive more than 3 days, most of them will survive thereafter.

There has been no satisfying improvement in finding new therapies to decrease mortality of sepsis in the past 20 years. Many clinical trials and experiments suffered from design flows [25], for example, key biological information not accessed before initiating trial of an experimental agent [25]. Target biomarker should be present at the time of study entry. Serial measurement should better evaluate the immune status of sepsis [25]. Hence, our study measured baseline levels of cytokines before operation and obtained time serial plasma cytokines levels later, thus confirming IL-6 and IL-10 plasma levels as elevated already before BHT administration; their change patterns followed treatment intervention. These data lent insight into dynamic BHT immune-modulating effects. Simultaneously, time serial MAP and HR were measured, enabling us to gauge development and progression of sepsis in CLP rats.

Recently, both IL-6 and IL-10 elevations were found to be significantly correlated with mortality of sepsis [15, 26]. Peng et al. revealed hemoadsorption decreasing risk of death from sepsis by removal of both IL-6 and IL-10 [27]. Our results concurred with these findings, yet there were several key features in our study. First, oral BHT administration was not as invasive as hemoadsorption or hemofiltration. Second, unlike hemoadsorption or hemofiltration applied in treating late-stage sepsis, appropriate treatment timing

of BHT is at early stages of sepsis. Third, while proinflammatory cytokines, including IL-1, tumor necrosis factor alpha (TNF-α), and IL-6, have been shown to induce cardiac myocyte apoptosis and necrosis and may cause damage to other organs, expression of inflammatory cytokines during specific response is not entirely deleterious. Inflammatory cytokines are necessary for limiting and eliminating local infections and increasing host survival [28, 29], for example, IL-6 required for successful outcome in sepsis, given its ability to promote hepatocyte recovery and regeneration [30]. These findings point to appropriate downregulation, albeit not extreme suppression, of proinflammatory cytokines as beneficial in treating sepsis. Our study results showed that the BHT administration decreases elevation of IL-6 after CLP without totally blocking the expression of IL-6, which might not make the host suffer from immunosuppression.

On the other hand, magnitude of IL-10 response appears to correlate with both severity of inflammatory insult and plasma concentration of proinflammatory cytokines, such as TNF-α [31]. We found that IL-10 simultaneously reduced following early administration of high-dose BHT, but with no direct cause and effect between BHT administration and level of IL-10. These findings imply reduction of proinflammatory cytokine in early-stage sepsis as sequentially downregulating anti-inflammatory cytokine, IL-10. Hence, the mechanism by which BHT modulated IL-6 and whether BHT can modulate TNF-α or other proinflammatory cytokines should be evaluated in the future.

This study had several limitations. First, due to limited amount of blood volume we could draw from rats each time, we only observed plasma level of proinflammatory cytokine IL-6 and anti-inflammatory cytokine IL-10, with the main focus chosen from the literature review and based on results of our prior study [15, 19, 26, 32]. Second, to probe treatment effects of BHT, our intervention only included BHT administration with limited fluid supplement (Normal Saline, 3 mL/100 g body weight). Thus, we could not evaluate treatment effects of BHT applied in combination with current clinical therapies like antibiotics, fluid resuscitation, or inotropics. Third, before formally performing the experiment described in this manuscript, pilot studies were conducted to confirm the optimal dose of BHT adopted. The results of these pilot studies revealed the same trend that the group of septic rats which received BHT had higher survival rate in a dose-dependent manner. Due to the limitation of grant resources, the sample size of each group in this experiment only received the average number of animal experiments [23, 24]. The relative small sample size is a limitation of our study, but the dose-dependent effects of BHT on both the survival rate and circulating IL-6 and IL-10 still provide evidence of BHT as a new treatment option for sepsis.

5. Conclusions

For centuries, based on theories of traditional Chinese Medicine, BHT has been considered effective in treating early stage severe infection with systemic inflammation. Results of our study afforded scientific evidence for BHT in treating sepsis by a CLP model and its effects on cytokine modulation: early administration of high-dose BHT markedly improved survival by directly reducing plasma level of IL-6, and simultaneously decreased IL-10 was observed. Our results suggest BHT as a novel complementary therapeutic candidate in treating early sepsis besides antibiotic, fluid resuscitation, and inotropic therapy, though combined effects of BHT with these treatments still need further evaluation.

Conflict of Interests

All authors declare that there is no conflict of interests.

Acknowledgments

The authors would like to thank the Committee on Chinese Medicine and Pharmacy, Department of Health, Executive Yuan, Taiwan, for the Grants support (nos. CCMP95-RD-214 and CCMP96-RD-209).

References

[1] D. Butler, "Translational research: crossing the valley of death," *Nature*, vol. 453, no. 7197, pp. 840–842, 2008.

[2] S. H. Woolf, "The meaning of translational research and why it matters," *Journal of the American Medical Association*, vol. 299, no. 2, pp. 211–213, 2008.

[3] D. C. Angus, W. T. Linde-Zwirble, J. Lidicker, G. Clermont, J. Carcillo, and M. R. Pinsky, "Epidemiology of severe sepsis in the United States: analysis of incidence, outcome, and associated costs of care," *Critical Care Medicine*, vol. 29, no. 7, pp. 1303–1310, 2001.

[4] J. L. Vincent, Y. Sakr, C. L. Sprung et al., "Sepsis in European intensive care units: results of the SOAP study," *Critical Care Medicine*, vol. 34, no. 2, pp. 344–353, 2006.

[5] J. A. Russell, "Management of sepsis," *The New England Journal of Medicine*, vol. 355, no. 16, pp. 1699–1713, 2006.

[6] J. Carlet, "Prescribing indications based on successful clinical trials in sepsis: a difficult exercise," *Critical Care Medicine*, vol. 34, no. 2, pp. 525–529, 2006.

[7] M. P. Glauser, "Pathophysiologic basis of sepsis: considerations for future strategies of intervention," *Critical Care Medicine*, vol. 28, no. 9, pp. S4–S8, 2000.

[8] L. Liaudet, J. G. Mabley, F. G. Soriano et al., "Inosine reduces systemic inflammation and improves survival in septic shock induced by cecal ligation and puncture," *American Journal of Respiratory and Critical Care Medicine*, vol. 164, no. 7, pp. 1213–1220, 2001.

[9] M. W. N. Nijsten, C. E. Hack, M. Helle, H. J. ten Duis, H. J. Klasen, and L. A. Aarden, "Interleukin-6 and its relation to the humoral immune response and clinical parameters in burned patients," *Surgery*, vol. 109, no. 6, pp. 761–767, 1991.

[10] O. Murch, M. Abdelrahman, M. Collino et al., "Sphingosylphosphorylcholine reduces the organ injury/dysfunction and inflammation caused by endotoxemia in the rat," *Critical Care Medicine*, vol. 36, no. 2, pp. 550–559, 2008.

[11] G. van den Berghe, P. Wouters, F. Weekers et al., "Intensive insulin therapy in critically ill patients," *The New England Journal of Medicine*, vol. 345, no. 19, pp. 1359–1367, 2001.

[12] F. L. Yeh, H. D. Shen, and R. H. Fang, "Deficient transforming growth factor β and interleukin-10 responses contribute to the

septic death of burned patients," *Burns*, vol. 28, no. 7, pp. 631–637, 2002.

[13] R. C. Bone, "Sir Isaac Newton, sepsis, SIRS, and CARS," *Critical Care Medicine*, vol. 24, no. 7, pp. 1125–1128, 1996.

[14] R. C. Bone, C. J. Grodzin, and R. A. Balk, "Sepsis: a new hypothesis for pathogenesis of the disease process," *Chest*, vol. 112, no. 1, pp. 235–243, 1997.

[15] J. A. Kellum, L. Kong, M. P. Fink et al., "Understanding the inflammatory cytokine response in pneumonia and sepsis: results of the Genetic and Inflammatory Markers of Sepsis (GenIMS) Study," *Archives of Internal Medicine*, vol. 167, no. 15, pp. 1655–1663, 2007.

[16] X. C. Xu, *Pharmacology of Traditional Chinese Medical Formulae*, Higher Educational Press, Beijing, China, 1994.

[17] C. Y. Liu, A. Tseng, and Y. Sue, *Chinese Herbal Medicine: Modern Applications of Traditional Formulas*, CRC Press, New York, NY, USA, 2005.

[18] G. Maciocia, *The Foundations of Chinese Medicine: A Comprehensive Text for Acupuncturists and Herbalists*, Elsevier Churchill Livingstone, Edinburgh, UK, 2005.

[19] C. H. Wang, M. J. Gee, C. Yang, and Y. C. Su, "A new model for outcome prediction in intra-abdominal sepsis by the linear discriminant function analysis of IL-6 and IL-10 at different heart rates," *Journal of Surgical Research*, vol. 132, no. 1, pp. 46–51, 2006.

[20] K. A. Wichterman, A. E. Baue, and I. H. Chaudry, "Sepsis and septic shock: a review of laboratory models and a proposal," *Journal of Surgical Research*, vol. 29, no. 2, pp. 189–201, 1980.

[21] R. P. Dellinger, M. M. Levy, J. M. Carlet et al., "Surviving Sepsis Campaign: international guidelines for management of severe sepsis and septic shock: 2008," *Critical Care Medicine*, vol. 36, no. 1, pp. 296–327, 2008.

[22] D. Vyas, P. Javadi, P. J. Dipasco, T. G. Buchman, R. S. Hotchkiss, and C. M. Coopersmith, "Early antibiotic administration but not antibody therapy directed against IL-6 improves survival in septic mice predicted to die on basis of high IL-6 levels," *American Journal of Physiology*, vol. 289, no. 4, pp. R1048–R1053, 2005.

[23] K. P. Rim, K. Kim, Y. H. Jo et al., "Effect of therapeutic hypothermia according to severity of sepsis in a septic rat model," *Cytokine*, vol. 60, no. 3, pp. 755–761, 2012.

[24] J. L. D. Souza Neto, I. Araújo Filho, A. C. M. Do Rego et al., "Effects of simvastatin in abdominal sepsis in rats," *Acta Cirurgica Brasileira*, vol. 21, supplement 4, pp. 8–12, 2006.

[25] J. Carlet, J. Cohen, T. Calandra, S. M. Opal, and H. Masur, "Sepsis: time to reconsider the concept," *Critical Care Medicine*, vol. 36, no. 3, pp. 964–966, 2008.

[26] C. C. Finnerty, D. N. Herndon, D. L. Chinkes, and M. G. Jeschke, "Serum cytokine differences in severely burned children with and without sepsis," *Shock*, vol. 27, no. 1, pp. 4–9, 2007.

[27] Z. Y. Peng, M. J. Carter, and J. A. Kellum, "Effects of hemoadsorption on cytokine removal and short-term survival in septic rats," *Critical Care Medicine*, vol. 36, no. 5, pp. 1573–1577, 2008.

[28] B. Echtenacher, W. Falk, D. N. Mannel, and P. H. Krammer, "Requirement of endogenous tumor necrosis factor/cachectin for recovery from experimental peritonitis," *Journal of Immunology*, vol. 145, no. 11, pp. 3762–3766, 1990.

[29] M. K. Eskandari, G. Bolgos, C. Miller, D. T. Nguyen, L. E. DeForge, and D. G. Remick, "Anti-tumor necrosis factor antibody therapy fails to prevent lethality after cecal ligation and puncture or endotoxemia," *Journal of Immunology*, vol. 148, no. 9, pp. 2724–2730, 1992.

[30] C. S. Deutschman, M. Cereda, E. A. Ochroch, and N. R. Raj, "Sepsis-induced cholestasis, steatosis, hepatocellular injury, and impaired hepatocellular regeneration are enhanced in interleukin-6 -/- mice," *Critical Care Medicine*, vol. 34, no. 10, pp. 2613–2620, 2006.

[31] A. Oberholzer, C. Oberholzer, and L. L. Moldawer, "Interleukin-10: a complex role in the pathogenesis of sepsis syndromes and its potential as an anti-inflammatory drug," *Critical Care Medicine*, vol. 30, supplement 1, pp. S58–S63, 2002.

[32] D. G. Remick, G. R. Bolgos, J. Siddiqui, J. Shin, and J. A. Nemzek, "Six at six: interleukin-6 measured 6 h after the initiation of sepsis predicts mortality over 3 days," *Shock*, vol. 17, no. 6, pp. 463–467, 2002.

Hindawi Publishing Corporation
Evidence-Based Complementary and Alternative Medicine
Volume 2013, Article ID 275390, 10 pages
http://dx.doi.org/10.1155/2013/275390

Research Article

The Application of SILAC Mouse in Human Body Fluid Proteomics Analysis Reveals Protein Patterns Associated with IgA Nephropathy

Shilin Zhao,[1] Rongxia Li,[1] Xiaofan Cai,[2] Wanjia Chen,[2] Qingrun Li,[1] Tao Xing,[1] Wenjie Zhu,[1] Y. Eugene Chen,[3] Rong Zeng,[1] and Yueyi Deng[2]

[1] *Key Laboratory of Systems Biology, Institute of Biochemistry and Cell Biology, Shanghai Institutes for Biological Science, Chinese Academy of Sciences, Shanghai 200031, China*
[2] *Department of Nephrology, Longhua Hospital, Shanghai University of Traditional Chinese Medicine, 725 Wanping Road, Shanghai 200032, China*
[3] *Cardiovascular Centre, Department of Internal Medicine, University of Michigan Medical Centre, Ann Arbor, MI 48109, USA*

Correspondence should be addressed to Rong Zeng; zr@sibs.ac.cn and Yueyi Deng; dengyueyi@medmail.com.cn

Received 31 December 2012; Accepted 18 April 2013

Academic Editor: Aiping Lu

Body fluid proteome is the most informative proteome from a medical viewpoint. But the lack of accurate quantitation method for complicated body fluid limited its application in disease research and biomarker discovery. To address this problem, we introduced a novel strategy, in which SILAC-labeled mouse serum was used as internal standard for human serum and urine proteome analysis. The SILAC-labeled mouse serum was mixed with human serum and urine, and multidimensional separation coupled with tandem mass spectrometry (IEF-LC-MS/MS) analysis was performed. The shared peptides between two species were quantified by their SILAC pairs, and the human-only peptides were quantified by mouse peptides with coelution. The comparison for the results from two replicate experiments indicated the high repeatability of our strategy. Then the urine from Immunoglobulin A nephropathy patients treated and untreated was compared by this quantitation strategy. Fifty-three peptides were found to be significantly changed between two groups, including both known diagnostic markers for IgAN and novel candidates, such as Complement C3, Albumin, VDBP, ApoA,1 and IGFBP7. In conclusion, we have developed a practical and accurate quantitation strategy for comparison of complicated human body fluid proteome. The results from such strategy could provide potential disease-related biomarkers for evaluation of treatment.

1. Introduction

Body fluid proteome generally is the most informative proteome from a medical viewpoint. Almost all tissues in the body communicate with body fluid and release their contents into it, especially upon damage or death [1]. This complicated matrix is believed to reflect the function changes within the body. Therefore, it is promising to identify novel, highly sensitive, and specific disease biomarkers from body fluid proteomics research [2]. With the significant advances in proteomic methods and instrumentation, current methods are sufficient to allow the identification of proteins directly in body fluid across no less than 7 orders of magnitude of protein abundance [3]. However, because of the high complexity and high dynamic range of protein concentrations in such samples, discovery of disease biomarkers from body fluid proteome remains extremely challenging [4, 5].

Multiple analytical approaches have been developed based on separation of proteins in-gel (2DE, DIGE) or gel-free platform utilizing various methods including labeling (ICAT, ^{18}O-labeling, iTRAQ) and label-free strategy. Both of these methods were widely used in quantitative proteomics analysis but also had some limitations. Label-free quantification was quite simple and straightforward, but the precision and accuracy were limited [6]. ^{18}O-labeling leaded to variability in peptide spacing, and the mass offset of 2 Da was not sufficient to optimally separate the isotopic envelopes

for differential quantification. iTRAQ technology provided an extensive quantification method that could be used in almost all kinds of samples with great utility. But because of the additional multiple steps of iTRAQ method, such as sample preparation and efficiency of chemical tagging, there was also some variability in this method. Besides, the reporter ions in MS/MS spectrum would influence the peptide identification [7].

Stable-isotope labeling by amino acids in cell culture (SILAC) method provided a comprehensive, robust, and accurate solution for quantitative proteomics analysis. But it is thought to be unsuitable for analyzing tissue and body fluid samples. Hence, a lot of other metabolic labeling methods were introduced in an alternative way such as protein standard absolute quantification (PSAQ), stable isotope-labeled proteome (SILAP), and secretome-derived isotopic tag (SDIT) strategies. However, PSAQ uses full-length isotope-labeled proteins as isotope-dilution standards for MS-based quantification of target proteins in complex matrices. It was difficult for the accurate quantitation of large numbers of serum proteins. In addition, it seems more appropriate for the combination of PSAQ and SRM (PSAQ-SRM) to allow highly accurate biomarker quantitation in serum samples. Serum mixed with SILAC-labeled secretome of culture cells (SILAP and SDIT) was easy to manipulate and quantify large numbers of serum proteins. However, serum contains all tissue proteomes as subsets. It was not adequate to use one or several kinds SILAC labeled secretome of cultured cells as standards in quantitative serum proteomic studies.

In this paper, we have proved that the serum from SILAC mouse could also be used as internal standards to quantify human serum and urine. With this novel strategy, we performed the quantitative proteomics analysis by extensive multidimensional separation coupled with tandem mass spectrometry (IEF-LC-MS/MS) for the urine from Immunoglobulin A nephropathy (IgAN) patients treated and untreated. As the quantification standards display the same biochemical features as urinary samples, they can be spiked into the samples at early stages of the analytical process, which can avoid differences that yielded in digestion and nonspecific losses suffered during extensive sample processing between internal standard SILAC mouse and human samples. In conclusion, our research provided a comprehensive and accurate solution for human body fluid analysis.

2. Materials and Methods

2.1. Materials. Urea, tris, sodium dodecyl sulfate (SDS), dithiothreitol (DTT), ammonium bicarbonate (NH_4HCO_3), and iodoacetamide (IAA) were purchased from Bio-Bad (Hercules, CA). The Lys-C enzyme was purchased from Wako (Osaka, Japan). Acetonitrile (HPLC grade) was obtained from Merck (Darmstadt, Germany). Formic acid was obtained from Aldrich (Milwaukee, WI, USA). All the water used in the experiments was prepared using a Milli-Q system (Millipore, Bedford, MA, USA). The $^{13}C_6$-lysine labeled mouse serum (MT-LYSC6-MSE) was purchased from Cambridge Isotope Laboratories, Inc.

2.2. Sample Collection and Preparation. Immediately after collection, fasting blood samples of healthy subjects were allowed to clot at room temperature for four hours, and the serum was collected and centrifugated at 3000 rpm/min for 15 min. Informed consent was obtained from each person in written format and approved by Longhua Hospital, Shanghai University of Traditional Chinese Medicine Review Committee.

The 24 h urine samples were collected from six healthy subjects. Informed consent was obtained from each person in written format and approved by Longhua Hospital, Shanghai University of Traditional Chinese Medicine Review Committee. Volume of 200 ml urine from each person was concentrated by the acetone precipitation approach [8] with some modification. All centrifugation work was performed at 4°C. First, the samples were centrifuged at 3000 g for 10 min to pellet exfoliated cells and residues. The supernatants were centrifuged at 16,000 g for 30 min to remove cell debris and residues. Then, the urine samples were precipitated by adding chilled acetone to 20% w/v and incubating the samples for 10 min at 4°C. Precipitates were sedimented at 16,000 g for 30 min at 4°C, and pellets were washed twice with neat acetone at 4°C with residual acetone removed by air drying. Dried pellets were resuspended in 3 ml of 50 mM NH_4HCO_3 buffer. The protein concentration of urine samples was determined by Bradford assay on a Microplate Reader (Bio-Rad, Model 680). Six normal urine samples were pooled together. The concentrate was frozen at −80°C until use.

The urine from IgAN patients with and without glucocorticosteroid treatment was collected and prepared as mentioned earlier for urine from healthy persons [9]. The patients of glucocorticosteroid treatment group were given one pack Bid (twice per day) only for 24 weeks (Bushen tongluo Decoction or Zibu ganshen Decoction). The dosage of glucocorticosteroid is 0.5–1 mg/kg.d. The glucocorticosteroid drugs were reduced regularly.

2.3. In-Solution Lys-C Digestion and OFFGEL Fractionation. The sample digestion was processed by FASP procedure as described previously [10]. Briefly, 150 μg human sample was mixed with 150 μg SILAC-labeled mouse serum sample and then transferred to a 10K filter and centrifuged at 10,000 g for 20 min at 20°C. so, 200 μL UA buffer (8 mol/L urea and 0.1 mol/L Tris-HCl, pH = 8.5) was added, and the sample was centrifuged at 10,000 g for 20 min again. This step was repeated once. The concentration was then mixed with 100 μL of 50 mmol/L IAA in UA buffer and incubated for an additional 40 min at room temperature in the dark. Next, the IAA was removed by centrifugation at 10,000 g for 20 min. Following two rounds of dilution in 200 μL of UA buffer and centrifugation, 200 μL of 50 mmol/L NH_4HCO_3 was added to the sample, which was then centrifuged at 10,000 g for 20 min. This step was repeated twice. Finally, 100 μL of 50 mmol/L NH_4HCO_3 and Lys-C (1 : 25, enzyme to protein) was added, and the mixture was incubated at 37°C for 20 h. The digested peptide mixtures were collected for further analysis.

The p*I*-based peptide OFFGEL separation was performed as previously reported [10]. The 3100 OFFGEL Fractionator and the OFFGEL Kit pH 3–10 (both Agilent Technologies)

with a 12-well setup were used according to the protocol of the supplier. The lyophilized samples were dissolved in focusing buffer to a final volume of 1.8 mL, and 150 μL of sample was loaded in each well. Electrofocusing of the peptides was performed at 20°C and 50 μA until the 100 kVh level was reached. After focusing, the rinses in each well were pooled with their corresponding peptide fraction. All fractions were evaporated by centrifugation under vacuum and maintained at −20°C. Prior to MS analysis, the samples were desalted onto an Empore C18 47-mm Disk. Immediately prior to nano-LC, the fractions were suspended in 20 μL of H_2O containing 0.1% (v/v) TFA.

2.4. 1D Nano-LC-MS/MS Analysis. A Surveyor liquid chromatography system (Thermo Finnigan, San Jose, CA, USA), consisting of degasser, MS Pump, and auto sampler, equipped with an analytical C18 column (RP, 75 μm × 150 mm, Column Technology Inc., CA, USA) was used. The HPLC solvents used were 0.1% formic acid (v/v) aqueous (A) and 0.1% formic acid (v/v) acetonitrile (B). The reversed-phase gradient was from 2% to 40% mobile phase B in 180 min at 120 μL/min flow rate before the split and 250 nL/min after the split. A linear ion trap/Orbitrap (LTQ-Orbitrap) hybrid mass spectrometer (ThermoFinnigan, San Jose, CA, USA) equipped with an NSI nanospray source was used to for MS/MS experiment with ion transfer capillary of 200°C and NSI voltage of 1.80 kv. Normalized collision energy was 35.0. The mass spectrometer was set that one full MS scan (m/z 400–1800) was acquired in the Orbitrap parallel ten MS/MS scans in the linear ion trap on the ten most intense ions from the full MS spectrum with the following Dynamic Exclusion settings: repeat count 2, repeat duration 30 seconds, and exclusion duration 90 seconds. The resolving power of the Orbitrap mass analyzer was set at 60,000 for the precursor ion scans (m/Δm 50% at m/z 400). The m/z (445.120025) was used as an internal lock mass and calibrant ions in the full MS scan.

2.5. Data Processing and Quantification. All raw mass spectrometric data were analyzed with the MaxQuant software (version 1.3.0.5 [11]. A false discovery rate (FDR) of 0.01 for proteins and peptides and a minimum peptide length of 7 amino acids are required. MS/MS spectra were searched by the Andromeda search engine incorporated in the MaxQuant software [12] against a combined IPI database (IPI HUMAN version 3.87, containing 91,491 entries and IPI MOUSE version 3.87, containing 59,546 entries) and concatenated with the reversed versions of all sequences. Lys-C digestion (Lys-C/P) was chosen as enzyme specificity. Cysteine carbamidomethylation was selected as a fixed modification, while protein N-terminal acetylation and methionine oxidation were selected as variable modifications. Maximally one missed cleavage was allowed. Initial mass deviation for the precursor ion was up to 7 ppm, and maximum allowed mass deviation for fragment ions was 0.5 Da.

In quantification, Lys6 in MaxQuant software was selected as heavy internal standard to get the intensity for heavy and light peptide and the SILAC ratio. The peptides shared between human and mouse were quantified by their SILAC pairs, and the human-only peptides were quantified by mouse peptides with nearest retention time.

2.6. Bioinformatics Analysis. All statistical analyses were conducted in the R environment (http://www.r-project.org/). The quantile normalization [13] was performed to normalize the quantitation results. The seqKNN method [14] was used for imputation of the missing values. The linear models in R package limma were applied to find significant differently expressed proteins [15].

3. Results and Discussion

3.1. The Experiment Design. SILAC method provided a comprehensive, robust, and accurate solution for quantitative proteomics analysis. And the development of SILAC mouse expanded its application into tissue and body fluid samples [16, 17]. The high similarity between samples and internal standard made SILAC mouse a valuable tool and facilitated proteomics research in many aspects. But currently quantitative researches for human body fluid proteome were still using label-free or iTRAQ methods. SILAC mouse has never been considered to be used in human subjects.

The major obstacle for the application of SILAC mouse in human samples was the different protein sequence between the two species. But as a necessary step of protein digestion in bottom-up proteomics, the compared results were in fact not protein sequences but digested peptide sequences, which increased the possibility for human sequence to find corresponding SILAC pair in labeled mouse internal standard. Even the proteins with different sequence between human and mouse may have consistent digested peptides and could be quantified. Hence, we proposed a novel workflow, in which the SILAC-labeled mouse serum was used as internal standard to quantify human body fluid (Figure 1(a)).

As the serum of SILAC mouse was labeled by lysine, the lysine-containing peptides from human samples and mouse internal standard could be distinguished in MS analysis, and the peptides without lysine were undistinguishable and helpless for quantitative analysis. To find the enzyme with better performance for such kind of experiment design, trypsin and Lys-C theoretic digestions for human IPI proteome database were performed and compared. As a result, Lys-C digestion produced more lysine-containing peptides in almost every molecular weight section (Figure 1(b)). In consideration of undistinguishable arginine-containing peptides produced by trypsin, Lys-C was more suitable for this experiment. We have also compared the Lys-C digestion peptides for human and mouse IPI proteome database. The peptides from two species showed about 30% overlap with each other, which proved the feasibility of our strategy (Figure 1(c)).

3.2. Preliminary Experiment Proved the Feasibility of the Design. Based on the results from theoretic digestions, there were still many human-only peptides. To make better use of these peptides, we divided the quantified peptides into three parts (Figure 2). The shared peptides between human and mouse were quantified by traditional SILAC method. The isotopic-labeled mouse peptides with same sequences

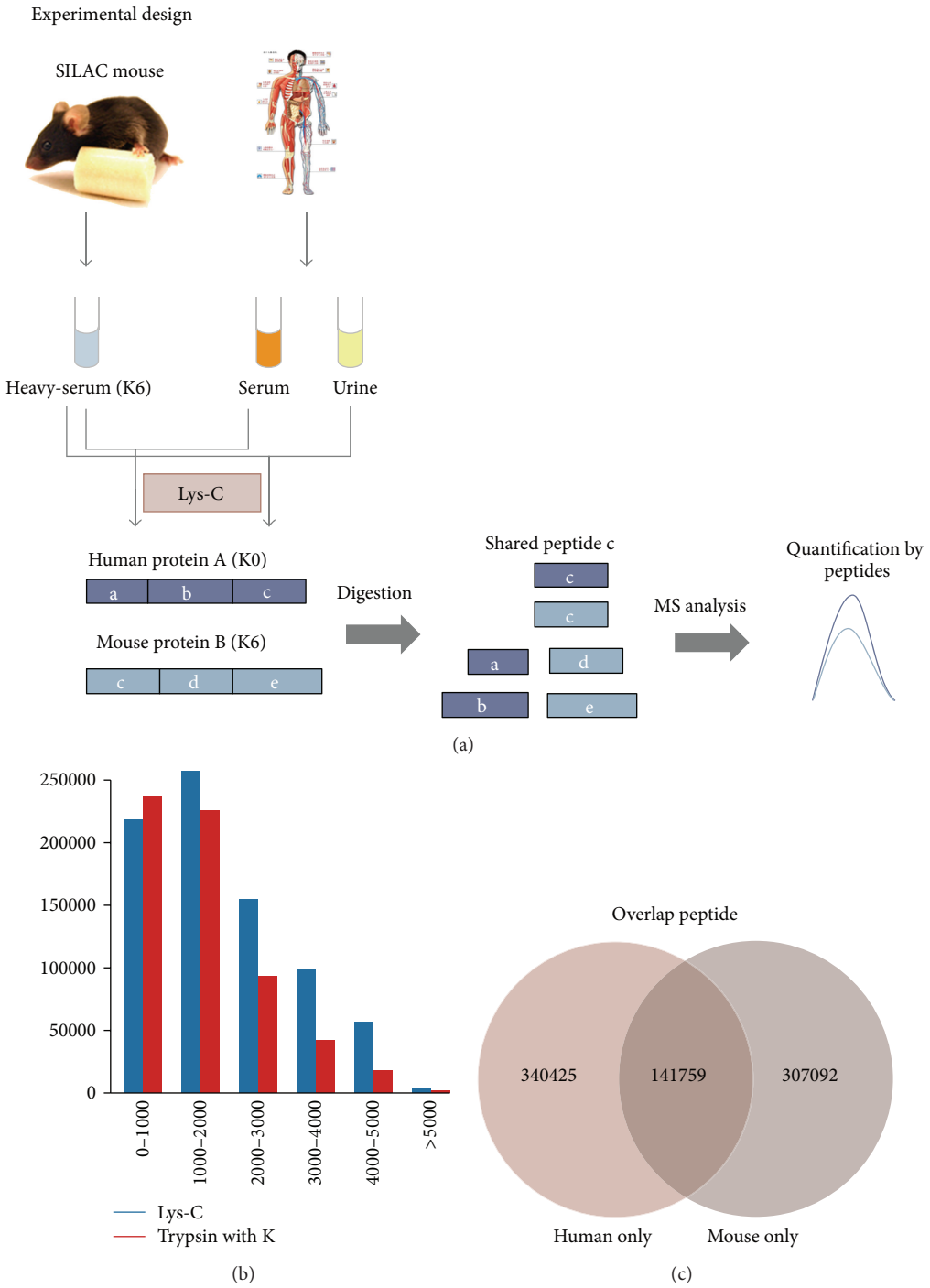

FIGURE 1: The experiment design and theoretic digestion result. (a) The serum of SILAC mouse was mixed with serum and urine from human, and then enzyme digestion was performed. The shared digested peptides between human and mouse could be selected as SILAC pair and quantified. (b) The comparison of molecular weight distribution for the theoretic digestion peptides of trypsin and Lys-C. (c) The comparison of Lys-C theoretic digestion peptides in human and mouse database.

were used as internal standards. The mouse-only peptides were screened, and only the peptides found in all of the experiments were kept as references. And then the human-only peptides could be quantified by isotopic-labeled mouse reference peptides with the nearest retention time [18].

To ensure the feasibility of our quantitation strategy, preliminary experiment with human serum and urine samples were performed. Initially, the serum and urine from healthy human subjects were collected and mixed with isotopic-labeled mouse serum, respectively. And two technical replications for each sample were performed. Then,

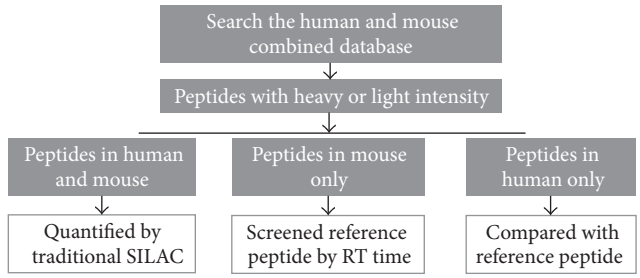

Figure 2: The demonstration for peptide quantification. The peptides were divided into 3 groups. The shared peptides between two species were quantified by traditional SILAC. The mouse-only peptides were taken as reference. And the human-only peptides were compared with co-elution reference peptides to get the quantification results.

peptide quantification was done as illustrated in Figure 2. The shared peptides were quantified by their own SILAC pair. And the human-only peptides were compared with the mouse only peptides found in all of the 4 experiments. At last, the quantification results from two parts were presented (Figure 3).

For the shared peptides, the ratios distributions (Figure 3(a)) for serum and urine peptides were different. The log transformed serum ratios were around zero, indicating the high consistency between human serum and mouse serum, while the log transformed urine ratios were composed by two peaks above or below zero, indicating that the concentration of shared peptides in human urine was different with mouse serum. These results were reasonable as the mouse serum should be similar with human serum, but different with human urine. We then analyzed the correlation coefficients between 4 experiments (Figure 3(b)). Both the scatter plots at lower side and the correlation coefficients at upper side indicated the high reproducibility between replication experiments, and the disperse points between serum and urine proved the reliability of the results at the other side. The comparison between the results in two replication experiments was also performed (Figure 3(c)). The narrow distribution for the ratios between replication experiments demonstrated that the strategy was applicative in both serum and urine.

The analysis for human-only peptides also showed advantageous result. In ratios distributions, there was a little shift for serum ratios and no obvious peak for urine ratios (Figure 3(d)). The correlation coefficients were a little lower than shared peptides (Figure 3(e)), and the ratios between replication experiments were a little wider but still within twofold changes (Figure 3(f)). These slight changes resulted from the variations introduced by reference peptides with different sequence, which indicated that the quantification for human-only peptides was also reliable.

3.3. Application in IgA Nephropathy Samples. IgA nephropathy is the most frequent type of glomerulonephritis and characterized at biopsy by a wide variability of features. Baseline proteinuria is one of the main predictors of IgAN progression. But few studies have evaluated whether some other components of proteinuria could improve the prediction of IgAN and evaluate the effect of therapeutic approaches.

Here the novel strategy was applied in the urine samples from IgAN patients treated and untreated. There were totally 3 patients, and two technical replications for each sample were performed (Figure 4).

The quantification results were also from shared peptides and human-only peptides, and the mouse-only peptides found in all samples were used as quantification reference (Figure 5). Firstly, the quantitation ratios between replication experiments for each sample were demonstrated (Figures 5(a) and 5(d)). Most of the ratio changes for replication experiments in each sample were within 2 folds.

Then, the limma package in R environment was used to find significant changed peptides between two groups. As a result, 9 and 44 peptides were selected, respectively, in shared peptides and human-only peptides with P value less than 0.05. Hierarchical cluster analysis (HCA) and principal component analysis (PCA) were then performed for the concentrations of these significant peptides, respectively (Figures 5(b)-5(c), and 5(e)-5(f)). In the HCA results, the replicate experiments were first grouped together, and then the samples treated and untreated were separated. In the PCA result, the replicate experiments located together, and the samples treated and untreated were separated by principal component 1. All of the previous results emphasized the high quality of our quantitation data.

3.4. Proteins Influenced by the Treatment of IgA Nephropathy. To further analyze the proteins influenced by the treatment and reveal their association with IgA nephropathy, a detailed literature search was performed. And the significant proteins associated with nephropathy were listed in Table 1.

Complement C3 is the most significant decreased protein after treatment in our result. IgA nephropathy is characterized by IgA deposition, and it is frequently accompanied by complement C3. The serum IgA/C3 ratio is taken as a diagnostic marker for the progression of IgAN [29]. And serum C3 was also proved to correlate with prognosis of IgAN [19, 30]. Because of the good correlation between urinary C3 concentrations and the deposition of C3 in glomerular capillary walls, the urinary level of complement C3 was also taken as an accurate indicator of continuing activity of glomerulonephritis [31]. The decrease of complement C3 in our results indicted the curative effect of the treatment.

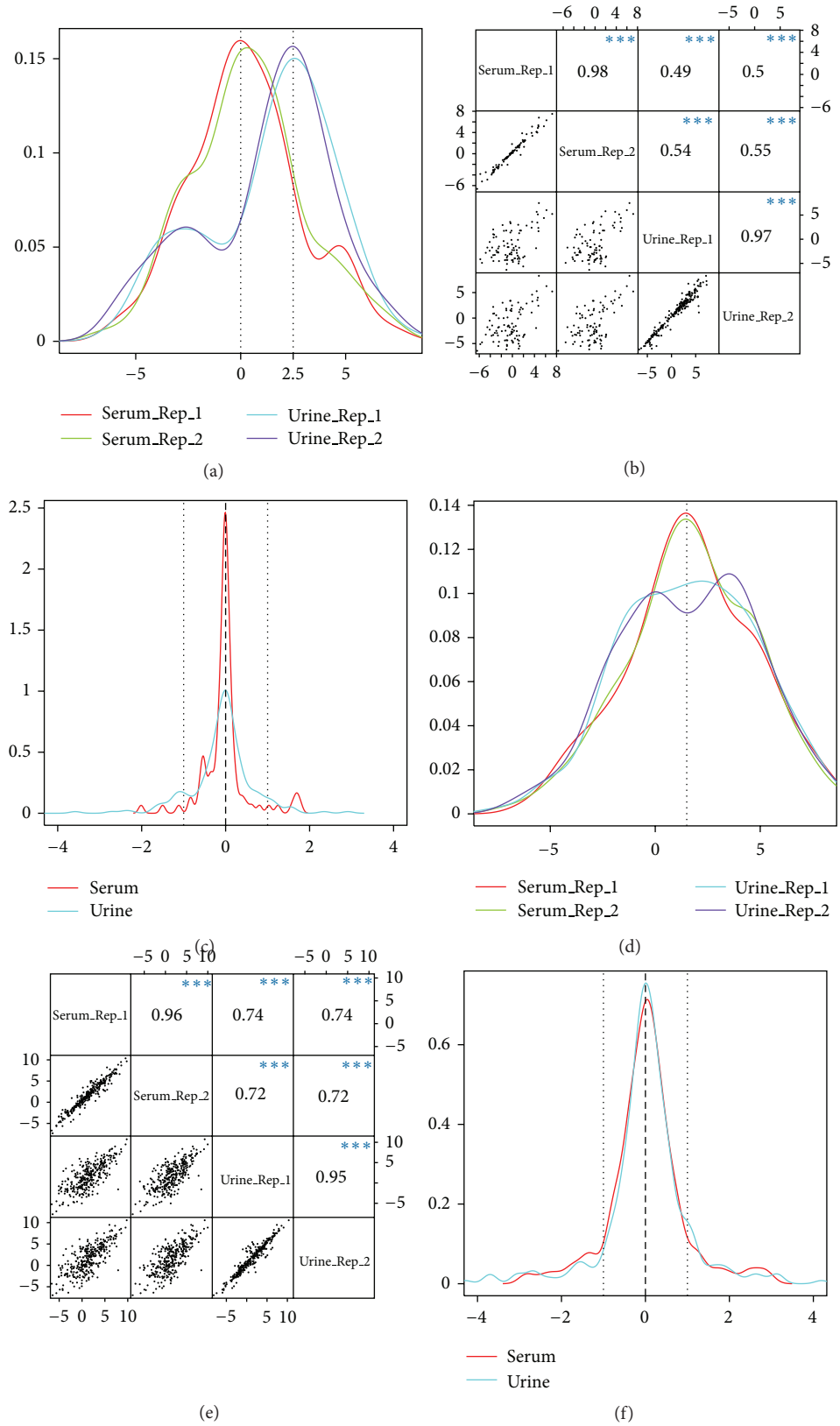

Figure 3: The quantitation results in preliminary experiment. (a) The ratio distribution of shared peptides. (b) The scatter plot and correlation coefficient for quantitation results of shared peptides. (c) The ratio distribution of shared peptides in comparison of replication experiments. (d) The ratio distribution of human-only peptides. (e) The scatter plot and correlation coefficient for quantitation results of human-only peptides. (f) The ratio distribution of human-only peptides in comparison of replication experiments.

Table 1: The significant proteins associated with nephropathy.

Peptide sequence	Protein name	Fold changes treated : untreated	Relevance with nephropathy	Reference
ACEPGVDYVYK	Complement C3	−3.3	Reported as a potentially novel predictor of progressive IgA nephropathy	[19]
HEVTGWVLVSPLSK	Insulin-like growth factor-binding protein 7	−3.2	The urinary levels of other IGFBPs correlated with the development of renal disease	[20]
VHTECCHGDLLECADDRADLAK	Albumin	−2.3	Most famous indicator for nephropathy	[21, 22]
YICENQDSISSKLK		−2.0		
AEFAEVSK		−1.9		
AAFTECCQAADKAACLLPK		−1.6		
HQPQEFPTYVEPTNDEICEAFRK	Vitamin D-binding protein isoform 3	−2.1	Enhanced excretion in urine during diabetic nephropathy	[23]
DSGRDYVSQFEGSALGK	Apolipoprotein A-I	−2.1	Increased in the plasma of diabetic nephropathy patients	[24]
HYYIGIIETTWDYASDHGEK	Ceruloplasmin	−1.7	Enhanced excretion in urine during diabetic nephropathy	[25, 26]
SSFVAPLEK	Pigment epithelium-derived factor	−1.6	A urinary marker for diabetic nephropathy	[27]
DSAHGFLK	Transferrin	−1.6	Enhanced excretion in urine during diabetic nephropathy	[22, 28]

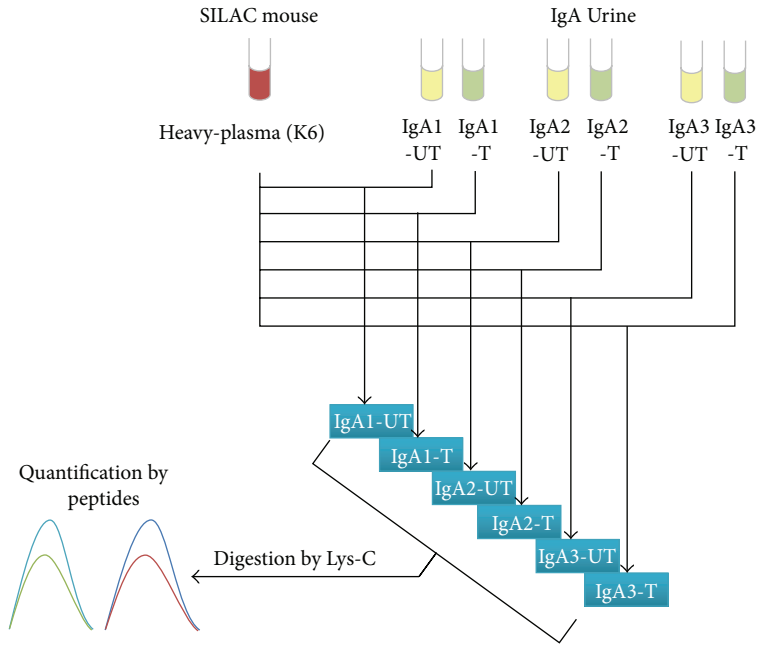

Figure 4: The experiment design for comparison of IgA patients' urine untreated and treated. The UT in the end of sample name indicated that the sample was untreated, and T in the end of sample name indicated that the sample was treated.

Albumin is the most famous indicator for renal disease [21, 32, 33]. It is the most abundant protein in disease urine and was clinically used to estimate the progression of renal disease [34]. There were four peptides belonging to albumin that showed significant difference between two groups, which indicated the treatment had effectively influenced the urine proteome.

Besides, we have also found four proteins, which are vitamin D binding protein [23, 35], ceruloplasmin [25], pigment epithelium-derived factor [27], and transferrin [28].

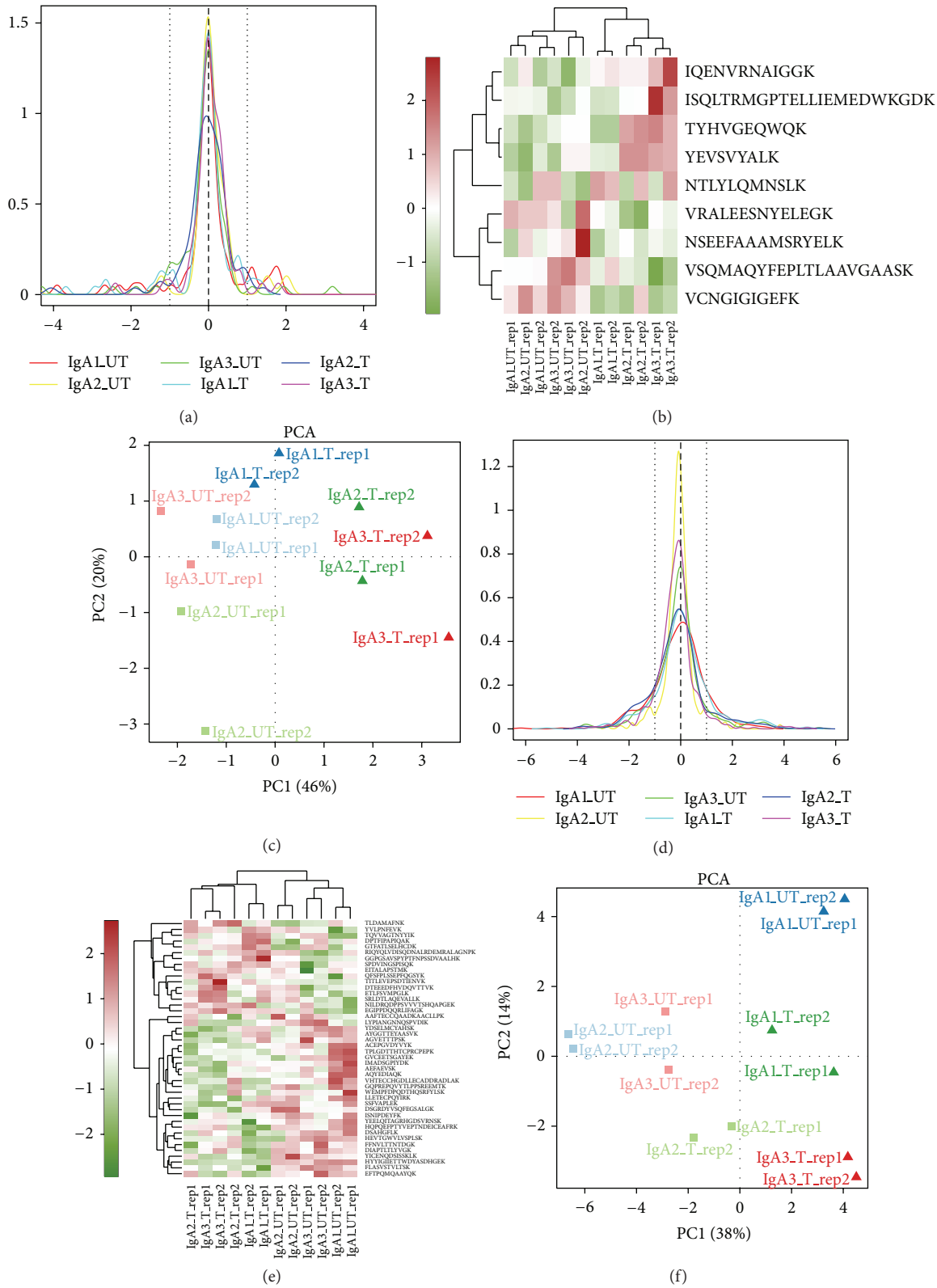

FIGURE 5: The quantitation results in analysis of IgA patients' urine. (a) The ratio distribution of shared peptides in comparison with replication experiments. (b) The hierarchical cluster analysis result of shared peptides. (c) The principal component analysis result of shared peptides. (d) The ratio distribution of human-only peptides in comparison with replication experiments. (e) The hierarchical cluster analysis result of human-only peptides. (f) The principal component analysis result of human-only peptides.

The urinary levels of them were reported to correlate with the development of renal disease. Vitamin D binding protein (VDBP) is responsible for binding to vitamin D and its metabolism products in plasma and then transports them to target tissues. As early as 1977, VDBP was found to be of underexcretion in the plasma of nephropathy patients, but of overexcretion in their urine [36]. The loss of plasma VDBP from urine was taken as the primary reason for vitamin D deficient in nephropathy patients. And the decrease of VDBP after treatment implied its loss was inhibited. Ceruloplasmin (CP) is the major copper-carrying protein in the blood and in addition plays a role in iron metabolism. The urinary copper concentrations were found to significantly increase in macroalbuminuric patients, which might be due to the excretion of CP and damaged renal tubules [25]. And the urinary changes of CP in IgA patients were confirmed by western blot [26]. Besides, the concentration of transferrin in the urine of IgA patients was validated by ELISA experiment [22]. We have also found some other proteins that had not been directly associated with nephropathy, such as insulin-like growth factor-binding protein 7 (IGFBP7) and Apolipoprotein A-I (ApoA1). Some other members of IGFBP family were reported to increase in urine from diabetic nephropathy patients [37], and ApoA1 was found to increase in the plasma of diabetic nephropathy patients [24]. All of these previous reports indicated their potential roles as indicator for nephropathy progression.

On the other side, there were some proteins of overexcretion in the urine of treatment group, including Annexin A1, Cystatin-A, Angiotensinogen, Gamma actin-like protein, and Zinc-alpha-2-glycoprotein. Most of these proteins had never been reported as nephropathy biomarkers or only found to be significant in large-scale expression analysis [38, 39]. As the treatment globally influenced the urinary proteome and the overall protein excretion was reduced in treatment group, the resource and function of overexcretion proteins need more investigation.

4. Conclusions

In this work, we proved that SILAC-labeled mouse serum could be used as internal standard for human body fluid proteome analysis. It provided comprehensive and reliable quantitative results and could specifically address the obstacles in this field. With the application of this strategy in patient samples, we can obtain valuable findings in biomarkers discovery for monitoring disease progression and evaluating therapeutic efficacies.

Authors' Contribution

S. Zhao, R. Li, and X. Cai contributed equally to this work.

Acknowledgments

The study is supported by the Foundation (no. SHDC12010114) of Joint Research Project of Shanghai Municipal Level Hospital and Technology Special Projects Major New Drug Development (2011ZX09302-006-04) as well as the Shanghai Government Foundation (10DZ1951202). The Authors gratefully acknowledge the support of SA-SIBS Scholarship Program.

References

[1] N. L. Anderson, M. Polanski, R. Pieper et al., "The human plasma proteome: a nonredundant list developed by combination of four separate sources," *Molecular & Cellular Proteomics*, vol. 3, no. 4, pp. 311–326, 2004.

[2] T. Z. Kristiansen, J. Bunkenborg, M. Gronborg et al., "A proteomic analysis of human bile," *Molecular & Cellular Proteomics*, vol. 3, no. 7, pp. 715–728, 2004.

[3] A. Taguchi and S. M. Hanash, "Unleashing the power of proteomics to develop blood-based cancer markers," *Clinical Chemistry*, vol. 59, no. 1, pp. 119–126, 2012.

[4] B. A. Lollo, S. Harvey, J. Liao et al., "Improved two-dimensional gel electrophoresis representation of serum proteins by using ProtoClear," *Electrophoresis*, vol. 20, no. 4-5, pp. 854–859, 1999.

[5] J. N. Adkins, S. M. Varnum, K. J. Auberry et al., "Toward a human blood serum proteome: analysis by multidimensional separation coupled with mass spectrometry," *Molecular & Cellular Proteomics*, vol. 1, no. 12, pp. 947–955, 2002.

[6] K. A. Neilson, N. A. Ali, S. Muralidharan et al., "Less label, more free: approaches in label-free quantitative mass spectrometry," *Proteomics*, vol. 11, no. 4, pp. 535–553, 2011.

[7] G. Pottiez, J. Wiederin, H. S. Fox, and P. Ciborowski, "Comparison of 4-plex to 8-plex iTRAQ quantitative measurements of proteins in human plasma samples," *Journal of Proteome Research*, vol. 11, no. 7, pp. 3774–3781, 2012.

[8] W. Sun, F. Li, S. Wu et al., "Human urine proteome analysis by three separation approaches," *Proteomics*, vol. 5, no. 18, pp. 4994–5001, 2005.

[9] C. Wanjia et al., "Jianpi bushen tongluo Decoction on Spleen Kidney Yang Deficiency and Blood Stasis Type, Progression of IgA Nephropathy," *Chinese Journal of Integrated Traditional and Western Nephrology*, vol. 13, no. 10, pp. 876–878, 2012.

[10] R. Li, W. Xu, Z. Wang, B. Liang, J. R. Wu, and R.. Zeng, "Proteomic characteristics of the liver and skeletal muscle in the Chinese tree shrew (Tupaia belangeri chinensis)," *Protein Cell*, vol. 3, no. 9, pp. 691–700, 2012.

[11] J. Cox and M. Mann, "MaxQuant enables high peptide identification rates, individualized p.p.b.-range mass accuracies and proteome-wide protein quantification," *Nature Biotechnology*, vol. 26, no. 12, pp. 1367–1372, 2008.

[12] J. Cox, N. Neuhauser, A. Michalski, R. A. Scheltema, J. V. Olsen, and M. Mann, "Andromeda: a peptide search engine integrated into the MaxQuant environment," *Journal of Proteome Research*, vol. 10, no. 4, pp. 1794–1805, 2011.

[13] B. M. Bolstad, R. A. Irizarry, M. Åstrand, and T. P. Speed, "A comparison of normalization methods for high density oligonucleotide array data based on variance and bias," *Bioinformatics*, vol. 19, no. 2, pp. 185–193, 2003.

[14] K. Y. Kim, B. J. Kim, and G. S. Yi, "Reuse of imputed data in microarray analysis increases imputation efficiency," *BMC Bioinformatics*, vol. 5, article 160, 2004.

[15] G. K. Smyth, "Limma: linear models for microarray data," in *Bioinformatics and Computational Biology Solutions using R and Bioconductor*, R. Gentleman, V. Carey, W. Huber et al., Eds., pp. 397–420, Springer, New York, NY, USA, 2005.

[16] M. Krüger, M. Moser, S. Ussar et al., "SILAC mouse for quantitative proteomics uncovers kindlin-3 as an essential factor for red blood cell function," *Cell*, vol. 134, no. 2, pp. 353–364, 2008.

[17] S. Zanivan, M. Krueger, and M. Mann, "In vivo quantitative proteomics: the SILAC mouse," *Methods in Molecular Biology*, vol. 757, pp. 435–450, 2012.

[18] Y. Ishihama, T. Sato, T. Tabata et al., "Quantitative mouse brain proteomics using culture-derived isotope tags as internal standards," *Nature Biotechnology*, vol. 23, no. 5, pp. 617–621, 2005.

[19] J. Zwirner, M. Burg, M. Schulze et al., "Activated complement C3: a potentially novel predictor of progressive IgA nephropathy," *Kidney International*, vol. 51, no. 4, pp. 1257–1264, 1997.

[20] K. Worthmann, I. Peters, P. Kmpers et al., "Urinary excretion of IGFBP-1 and -3 correlates with disease activity and differentiates focal segmental glomerulosclerosis and minimal change disease," *Growth Factors*, vol. 28, no. 2, pp. 129–138, 2010.

[21] M. L. Caramori, P. Fioretto, and M. Mauer, "Enhancing the predictive value of urinary albumin for diabetic nephropathy," *Journal of the American Society of Nephrology*, vol. 17, no. 2, pp. 339–352, 2006.

[22] H. Yokota, M. Hiramoto, H. Okada et al., "Absence of increased α1-microglobulin in IgA nephropathy proteinuria," *Molecular and Cellular Proteomics*, vol. 6, no. 4, pp. 738–744, 2007.

[23] K. M. Thrailkill, C. H. Jo, G. E. Cockrell, C. S. Moreau, and J. L. Fowlkes, "Enhanced excretion of vitamin D binding protein in type 1 diabetes: a role in vitamin D deficiency?" *Journal of Clinical Endocrinology and Metabolism*, vol. 96, no. 1, pp. 142–149, 2011.

[24] T. Nagai, T. Tomizawa, K. Nakajima, Y. Uehara, and M. Mori, "Effect of nephropathy on the composition of apolipoprotein-containing particles in NIDDM," *Journal of Atherosclerosis and Thrombosis*, vol. 5, no. 2, pp. 54–59, 1998.

[25] S. Ito, H. Fujita, T. Narita et al., "Urinary copper excretion in type 2 diabetic patients with nephropathy," *Nephron*, vol. 88, no. 4, pp. 307–312, 2001.

[26] P. G. Moon, J. E. Lee, S. You et al., "Proteomic analysis of urinary exosomes from patients of early IgA nephropathy and thin basement membrane nephropathy," *Proteomics*, vol. 11, no. 12, pp. 2459–2475, 2011.

[27] H. Chen, Z. Zheng, R. Li et al., "Urinary pigment epithelium-derived factor as a marker of diabetic nephropathy," *American Journal of Nephrology*, vol. 32, no. 1, pp. 47–56, 2010.

[28] M. Kanauchi, H. Nishioka, T. Hashimoto, and K. Dohi, "Diagnostic significance of urinary transferrin in diabetic nephropathy," *Nippon Jinzo Gakkai Shi*, vol. 37, no. 11, pp. 649–654, 1995.

[29] H. Komatsu, S. Fujimoto, S. Hara, Y. Sato, K. Yamada, and T. Eto, "Relationship between serum IgA/C3 ratio and progression of IgA nephropathy," *Internal Medicine*, vol. 43, no. 11, pp. 1023–1028, 2004.

[30] U. Janssen, F. Bahlmann, J. Köhl, J. Zwirner, M. Haubitz, and J. Floege, "Activation of the acute phase response and complement C3 in patients with IgA nephropathy," *American Journal of Kidney Diseases*, vol. 35, no. 1, pp. 21–28, 2000.

[31] A. D. Cumming, D. Thomson, A. M. Davison, and J. S. Robson, "Significance of urinary C3 excretion in glomerulonephritis," *Journal of Clinical Pathology*, vol. 29, no. 7, pp. 601–607, 1976.

[32] K. S. Eardley, M. A. S. Ferreira, A. J. Howie, P. Gosling, and G. W. Lipkin, "Urinary albumin excretion: a predictor of glomerular findings in adults with microscopic haematuria," *Monthly Journal of the Association of Physicians*, vol. 97, no. 5, pp. 297–301, 2004.

[33] A. Nakayama, J. Odake, A. Kanke, M. Sakatsume, T. Kasama, and K. Shiba, "Redox state of urinary albumin in patients with IgA nephropathy," *Rinsho Byori*, vol. 59, no. 11, pp. 1013–1018, 2011.

[34] J. Floege and J. Feehally, "Treatment of IgA nephropathy and Henoch-Schonlein nephritis," *Nature Reviews Nephrology*, 2013.

[35] R. Agarwal, "Vitamin D, proteinuria, diabetic nephropathy, and progression of CKD," *Clinical Journal of the American Society of Nephrology*, vol. 4, no. 9, pp. 1523–1528, 2009.

[36] J. M. Barragry, M. W. France, and N. D. Carter, "Vitamin-D metabolism in nephrotic syndrome," *The Lancet*, vol. 2, no. 8039, pp. 629–632, 1977.

[37] M. Shinada, A. Akdeniz, S. Panagiotopoulos, G. Jerums, and L. A. Bach, "Proteolysis of insulin-like growth factor-binding protein-3 is increased in urine from patients with diabetic nephropathy," *Journal of Clinical Endocrinology and Metabolism*, vol. 85, no. 3, pp. 1163–1169, 2000.

[38] S. N. Cox, F. Sallustio, G. Serino et al., "Altered modulation of WNT-B-catenin and PI3K/Akt pathways in IgA nephropathy," *Kidney International*, vol. 78, no. 4, pp. 396–407, 2010.

[39] S. C. Lim, D. Q. Liying, W. C. Toy et al., "Adipocytokine zinc alpha2 glycoprotein (ZAG) as a novel urinary biomarker for normo-albuminuric diabetic nephropathy," *Diabetic Medicine*, vol. 29, no. 7, pp. 945–949, 2012.

Hindawi Publishing Corporation
Evidence-Based Complementary and Alternative Medicine
Volume 2013, Article ID 259381, 7 pages
http://dx.doi.org/10.1155/2013/259381

Research Article

α-Synuclein Modification in an ALS Animal Model

Eun Jin Yang and Sun-Mi Choi

Department of Medical Research, Korea Institute of Oriental Medicine, 483 Expo-ro, Yuseong-gu, Daejeon 305-811, Republic of Korea

Correspondence should be addressed to Eun Jin Yang; yej4823@hanmail.net

Received 2 October 2012; Revised 11 February 2013; Accepted 28 February 2013

Academic Editor: Martin Kohlmeier

Amyotrophic lateral sclerosis (ALS) is a progressively paralytic neurodegenerative disease that can be caused by mutations in Cu/Zn-superoxide dismutase 1 (SOD1). Transgenic mice that overexpress mutant SOD1 develop paralysis and accumulate aggregates of mutant protein in the brainstem and spinal cord. Bee venom (BV), which is also known as apitoxin, is extracted from honeybees and is commonly used in oriental medicine for the treatment of chronic rheumatoid arthritis and osteoarthritis. The purpose of the present study was to determine whether BV affects misfolded protein aggregates such as alpha-synuclein, which is a known pathological marker in Parkinson disease, and ubiquitin-proteasomal activity in hSOD1^{G93A} mutant mice. BV was bilaterally administered into a 98-day-old hSOD1^{G93A} animal model. We found that BV-treated hSOD1^{G93A} transgenic mice showed reduced detergent-insoluble polymerization and phosphorylation of α-synuclein. Furthermore, phosphorylated or nitrated α-synuclein was significantly reduced in the spinal cords and brainstems of BV-treated hSOD1^{G93A} mice and reduced proteasomal activity was revealed in the brainstems of BV-treated symptomatic hSOD1^{G93A}. From these findings, we suggest that BV treatment attenuates the dysfunction of the ubiquitin-proteasomal system in a symptomatic hSOD1^{G93A} ALS model and may help to slow motor neuron loss caused by misfolded protein aggregates in ALS models.

1. Introduction

The neuropathological hallmarks of ALS are significant motor neuron loss, Bunina bodies, and the abnormal accumulation of insoluble ubiquitinated cytoplasmic inclusions in lower motor neurons. The neurodegenerative processes in motor neurons are complex. Although several genetic mutations are involved in motor neuron injury in familial ALS, less is known about the genetic and environmental factors that contribute to sporadic ALS. The etiology of ALS is a complex interplay between multiple pathogenic processes, which include misfolded protein aggregates, TDP-43 abnormalities, increased oxidative stress, mitochondrial dysfunction, ribosomal dysfunction, disturbance of intracellular trafficking, dysfunction of the ubiquitin-proteasomal and autophagic systems, increased glutamate excitotoxicity, and impaired axonal transport [1–6].

Parkinson's disease (PD), one of neurodegenerative movement disorders, is caused by selective degeneration of nigrostriatal dopamine neurons in the substantia nigra pars compacta (SNc). The physiological function of alpha-synuclein (α-synuclein), which is abundantly expressed in the central nervous system, is not fully understood. Its enrichment in presynaptic terminals and association with vesicles suggest a role for α-synuclein in synaptic dynamics. Synuclein has been extensively studied in the pathogenesis of Parkinson's disease (PD). Aggregation of α-synuclein in intracytoplasmic Lewy bodies is a key pathological feature of both sporadic and familial PD. In addition, duplication, triplication, or mutations in the α-synuclein gene cause some forms of familial PD [7]. Chung et al. have shown α-synuclein immunoreactivity in the brain and spinal cord of hSOD1^{G93A} mice [8].

Bee venom (BV) is an oriental medicine that has been used for the treatment of inflammatory diseases such as rheumatoid arthritis and for the relief of pain [9]. BV consists of many biologically active enzymes, peptides, and biogenic amines, such as melittin (the major active ingredient of bee venom), apamin, adolapin, and mast cell-degranulating peptide [10]. BV has been reported to cause growth arrest or cytotoxic effects in hepatocellular carcinoma cells [11]. In addition, the proliferation of melanoma cells, activity of

apoptotic enzymes (bcl-2 and caspase-3) in leukemic cells, and activation of the ERK and Akt signaling pathways in renal cancer cells have all been shown to be regulated and/or suppressed by BV [12]. Furthermore, we demonstrated that BV treatment reduced antineuroinflammatory events and increased the survival of hSOD1^{G93A} mice, an ALS animal model used in previous studies [13]. Moreover, we found an increase of modified α-synuclein (phosphorylation or nitration) in the spinal cord and brainstem of symptomatic hSOD1^{G93A} transgenic mice [14].

On the basis of these findings, we investigated BV effects on α-synuclein modification in the brainstem and spinal cord of symptomatic hSOD1^{G93A} mice. We found that BV treatment reduced the expression of α-synuclein modifications such as nitration and phosphorylation. In addition, BV treatment diminished ubiquitinated α-synuclein and recovered proteasomal activity in the spinal cord of hSOD1^{G93A} mice.

Taken together, we suggest that BV treatment could be a useful therapy to reduce cell loss or death caused by protein misfolding in a neurodegenerative disease model.

2. Materials and Methods

2.1. Animals. All of the mice were handled in accordance with the protocols approved by the Institutional Animal Care and Use Committees of the Korea Institute of Oriental Medicine. Hemizygous hSOD1^{G93A} transgenic B6SJL mice were originally obtained from Jackson Laboratories (Bar Harbor, ME). Transgenic mice were identified by PCR as described previously [15]. All of the mice were maintained in standard housing with free access to water and standard rodent chow purchased from Orient Bio (Orient, Gyeonggi-do, Korea).

2.2. Bee Venom Treatment. Bee venom (BV) was purchased from Sigma (St. Louis, MO) and diluted in saline. At a dose of 0.1 μg/g, BV was bilaterally injected (subcutaneously) twice a week into 14-week-old male hSOD1^{G93A} transgenic mice at the Zusanli (ST36) acupoint, as determined by the human acupoint landmark and a mouse anatomical reference [16], which is known to mediate anti-inflammatory effects in an ALS animal [13]. Control animals (hSOD1^{G93A}) were bilaterally injected (subcutaneously) with an equal volume of saline at the ST36 acupoint.

2.3. Immunoprecipitation and Western Blotting Analysis. After the mice were sacrificed, the brainstem and spinal cord were immediately homogenized in ice-cold RIPA buffer containing 50 mM Tris-HCl pH 7.4, 1% NP-40, 0.1% SDS, and 150 mM NaCl and then centrifuged at 14,000 rpm for 30 min at 4°C. The protein concentration in the supernatant was measured using a BCA kit according to the manufacturer's instructions. For immunoprecipitation (IP), 300 μg of protein lysates were immunoprecipitated using an anti-ubiquitin antibody and 10 μL of protein A agarose beads (Santa Cruz, CA, USA). Immunocomplexes were washed three times with RIPA buffer. Proteins were eluted from the beads by boiling in SDS sample buffer, and samples were analyzed by Western blotting with an α-synuclein antibody. For Western blotting analysis, proteins were loaded in a SDS-polyacrylamide gel and then transferred onto nitrocellulose membranes (Whatman, MO, USA). The membranes were blocked with 5% nonfat milk dissolved in TBS buffer (50 mM Tris-HCl, pH 7.6, 150 mM NaCl) for 1 h at 37°C. After blocking, the membranes were incubated with the following primary antibodies overnight at 4°C: α-synuclein (1 : 1000), phospho-α-synuclein (1 : 2000), nitrated-α-synuclein (1 : 1000), and ubiquitin (1 : 2000). After washing with TBST buffer (50 mM Tris-HCl, pH 7.6, 150 mM NaCl, and 0.2% Tween-20), the membranes were incubated with an anti-mouse or anti-rabbit IgG conjugated to horseradish peroxidase for 2 h at 4°C. The blots were then washed with TBST buffer and subsequently visualized using an enhanced chemiluminescence (ECL) method. The protein bands were quantitatively analyzed by Kodak Digital Science 1D software (Kodak Company, CT, USA).

2.4. Preparation of a Sequential Extraction of the Mouse Brain and Spinal Cord. Mouse brainstems and spinal cords were isolated and homogenized in ice-cold high salt buffer (50 mM Tris, pH 7.4, 750 mM NaCl, 10 mM NaF, 5 mM EDTA) with a proteinase inhibitor cocktail solution (Calbiochem, CA, USA). The homogenates were centrifuged at 14,000 rpm for 20 min at 4°C. The resulting supernatants were transferred into a new tube (high salt fraction), while the pellets were resuspended in RIPA buffer (50 mM Tris-HCl pH 7.4, 1% NP-40, 0.1% SDS, and 150 mM NaCl) and centrifuged at 14,000 rpm for 20 min at 4°C. The supernatants from this centrifugation were then transferred into a new tube (RIPA fraction), while the pellets were boiled with 0.5% SDS in PBS and centrifuged at 14,000 rpm for 20 min (0.5% SDS fraction).

2.5. Proteasomal Activity Assay. Twenty days after saline or BV injection, the male hSOD1^{G93A} transgenic mice were sacrificed. The brainstem and spinal cord from each mouse were removed and homogenized with RIPA lysis buffer and centrifuged at 14,000 rpm at 4°C for 20 min. Then, the supernatant fraction was collected into a new tube, and the protein concentration was determined using a BCA protein kit (Interchim, Paris, France). The proteasomal activity was measured according to the manufacturer's instructions for the 20S Proteasome Activity Assay kit (Chemicon Inc., CA, USA). The fluorescence of the samples was evaluated with a spectrofluorometer at excitation and emission wavelengths of 370 nm and 430 nm, respectively. Proteasomal activity was determined as an increase in the fluorescence of the reaction products.

2.6. Immunofluorescence. In this study, 16-week-old hSOD1^{G93A} mice were sacrificed after anesthetizing with pentobarbital and perfusion with phosphate-buffered saline (PBS). The spinal cord tissue of the hSOD1^{G93A} mice was fixed with 4% paraformaldehyde in PBS at 4°C overnight. The lumbar spinal cord was dissected, transferred into 30% sucrose, and then frozen. The lumbar spinal cord was

embedded in OCT compound, a freezing solution, and cut along the transverse plane on a Leica Microtome (Leica, Germany). Free-floating sections were washed three times with PBST and then incubated overnight at 4°C with primary antibodies (α-synuclein, 1 : 1000, and ubiquitin, 1 : 2000). The sections were washed three times in PBST and then incubated with Alexa Fluor 488 or 568 conjugated secondary antibodies (Molecular Probes, NY, USA). The ventral horns of the spinal cord sections were then imaged using an Olympus fluorescent microscope (Olympus, Tokyo, Japan) under identical exposure settings.

3. Results

3.1. BV Treatment Reduces Modified α-Synuclein Expression in the Brainstem and Spinal Cord of hSOD1^{G93A} Mice. To assess whether BV treatment affects the expression and modification of α-synuclein, the total proteins were extracted in RIPA buffer and loaded onto a 15% SDS-PAGE. Consistent with previous studies, high molecular α-synuclein proteins were detected in the saline-treated brainstem and spinal cord (Figure 1(a)). However, phosphorylated or nitrated α-synuclein was reduced by BV treatment in the brainstem and lumbar spinal cord of hSOD1^{G93A} mice (Figures 1(b) and 1(c)). Our data suggested that BV treatment attenuates α-synuclein modifications caused by motor neuron death in hSOD1^{G93A} mice.

To provide further evidence of increases in phosphorylated α-synuclein in symptomatic hSOD1^{G93A} mice, we examined the expression level of phospho-GSK3β with RIPA-extracted spinal cord and brainstem tissue in hSOD1^{G93A} mice. As shown in Figure 1(d), the expression of phosphorylated GSK3β at Ser 9 was increased in the brainstem and spinal cord of hSOD1^{G93A} mice. Interestingly, BV treatment reduced the phosphorylated levels of GSK3β in the brainstem and spinal cord of symptomatic hSOD1^{G93A} transgenic mice compared to age-matched hSOD1^{G93A} mice. This finding suggests that GSK3β activation may enhance α-synuclein phosphorylation at Ser 129 and contribute to motor neuron loss in symptomatic hSOD1^{G93A} mice.

3.2. Modified α-Synuclein Is a Soluble Protein in hSOD1^{G93A} Mice. To determine the solubility of modified α-synuclein in the brainstem and spinal cord of hSOD1^{G93A} mice, we examined the solubility of α-synuclein with sequentially different buffers (high salt, RIPA buffer and 0.5% SDS buffer as an insoluble buffer). As shown in Figure 2(a), monomeric or modified α-synuclein was extracted in high salt buffer as a soluble protein, and BV treatment reduced the expression of modified α-synuclein in the brainstem of hSOD1^{G93A} mice. Oligomeric (higher molecular weight) and modified (~26 kDa) α-synuclein of the spinal cord in symptomatic hSOD1^{G93A} mice were detected in high salt buffer as a soluble fraction, and modified α-synuclein was decreased by BV treatment (Figure 2(b)). However, insoluble α-synuclein was not detected in the brainstem or spinal cord of hSOD1^{G93A} mice (Figures 2(a), and 2(b)).

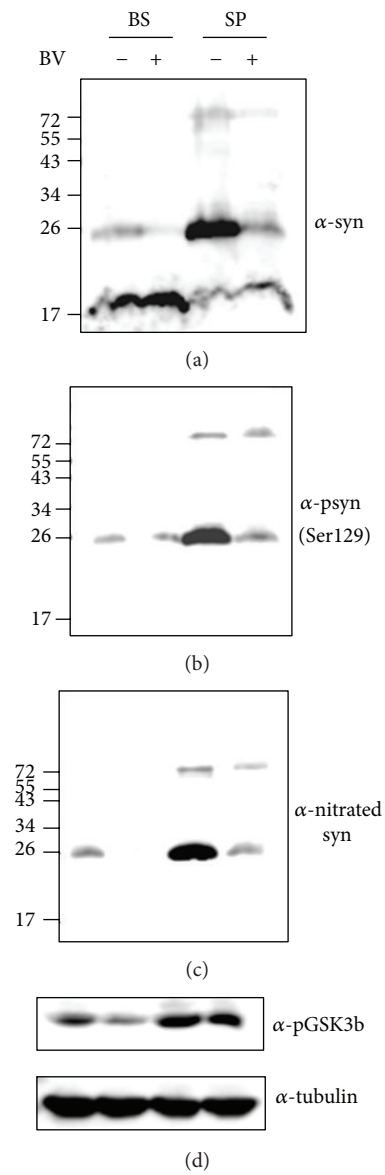

Figure 1: Western blotting analysis of α-synuclein expression levels in the spinal cord and brainstem of saline- ($n = 3$) or BV-treated hSOD1^{G93A} mice ($n = 3$). The blot shown is representative of three independent experiments. The total tissue homogenate was immunoblotted with an anti-α-synuclein antibody (a), anti-phospho-α-synuclein (Ser 129), and anti-nitrated α-synuclein. Tubulin served a loading control. BV: bee venom, BS: brainstem, SP: spinal cord.

3.3. BV Treatment Decreases Ubiquitinated α-Synuclein and Rescues the Reduced Proteasomal Activity in Symptomatic hSOD1^{G93A} Mice. However, it has been controversial whether it induces neuronal toxicity. To investigate the effects of BV on ubiquitinated α-synuclein, we examined the expression level of ubiquitinated α-synuclein in the brainstem and spinal cord of hSOD1^{G93A} mice.

As shown in Figure 3(a), ubiquitinated α-synuclein was reduced by BV treatment in the spinal cord of symptomatic

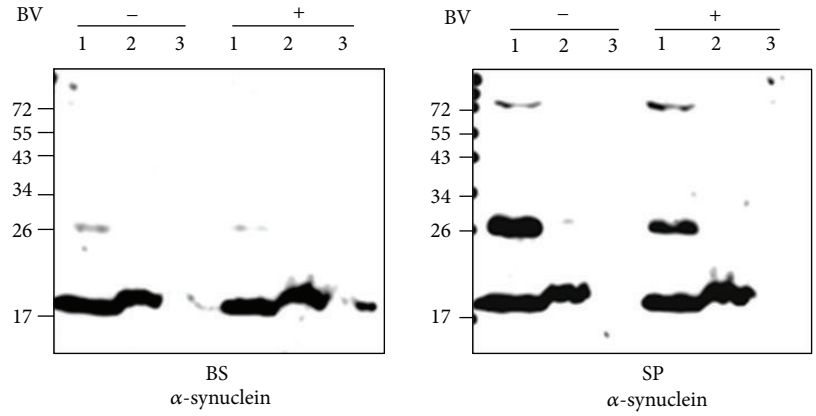

Figure 2: The soluble and insoluble protein fractions were collected from the brainstem (a) or spinal cord (b) of saline- ($n = 3$) or BV-treated hSOD1^{G93A} mice ($n = 3$). Equal amounts of total protein were subjected to a denaturing PAGE as previously described under Section 2, followed by Western blotting analysis with an anti-α-synuclein antibody. The blot shown is representative of three independent experiments. 1: high salt buffer, 2: RIPA buffer, 3: 0.5% SDS buffer, BV–: saline-treated hSOD1^{G93A} mice, BV+: BV-treated hSOD1^{G93A} mice.

hSOD1^{G93A} mice. In addition, we confirmed that ubiquitinated α-synuclein was localized in the motor neurons of hSOD1^{G93A} mouse spinal cords (Figure 3(b)).

Next, to investigate whether modified α-synuclein expression affects the protein degradation system, we examined the proteasomal activity in the brainstem and spinal cord of BV-treated or age-matched control hSOD1^{G93A} mice. BV treatment rescued 1.2-fold proteasomal activity in the spinal cord compared to that of age-matched symptomatic hSOD1^{G93A} mice ($P < 0.05$, Figure 3(c)).

4. Discussion

In this study, we demonstrated that two subcutaneous injections of 0.1 μg/mL BV resulted in the reduced expression of α-synuclein and modified α-synuclein (phosphorylation, nitration, or ubiquitination) in the brainstem and spinal cord of symptomatic SOD1^{G93A} transgenic mice. Furthermore, we observed that BV treatment diminished ubiquitinated α-synuclein and rescued proteasomal activity in the spinal cords of hSOD1^{G93A} transgenic mice.

Neuroinflammatory responses are induced as a consequence of oxidative and excitotoxic neuronal damage, mitochondrial dysfunction, and protein aggregation [17, 18]. In addition, neuroinflammation may be a direct response to protein aggregation in neurodegenerative diseases [19]. Neuroinflammation and accumulated protein aggregates are related to oxidative stress and mitochondrial dysfunction; accumulated protein aggregates trigger microglial activation and neuroimmune responses [20]. In the case of ALS, abnormal protein aggregation, ubiquitination, and deposition in the CNS are salient features of ALS [21, 22].

The role of neuroinflammation in the disease progression of neurodegenerative diseases, including PD and AD [23] in animal models, has been highlighted in recent studies. For example, in the presence of a preexisting PD-relevant insult, such as 6-OHDA, the loss of parkin or α-synuclein overexpression and induction of neuroinflammation synergistically worsen the disease process [24]. Chung et al. have demonstrated that changes in proteins relevant to synaptic transmission and axonal transport, coupled with neuroinflammation, precede α-synuclein-mediated neuronal death [25].

Recently, several studies have shown that α-synuclein is expressed in symptomatic hSOD1^{G93A} mice [8, 14]. In addition, our previous study demonstrated that α-synuclein modification increased in the brainstem and spinal cord of hSOD1^{G93A} transgenic mice compared to age-matched controls [14]. Furthermore, we have shown that treatment with melittin, one of the components of BV, reduced α-synuclein modification and increased the activity of proteasomes in the spinal cord of mutant (G93A) hSOD1-expressing mice [14]. This study showed that BV treatment also decreased the expression level of soluble modified α-synuclein (phosphorylation or nitration) in the spinal cords of symptomatic hSOD1^{G93A} transgenic mice (Figures 1 and 2). These findings suggest that anti-inflammation by BV treatment may be involved in the restoration of reduced proteasomal activity in symptomatic hSOD1^{G93A} transgenic mice.

Inclusions formed mainly by monoubiquitinated α-synuclein are toxic to cells [26]. Baba et al. have shown that the oligomeric or protofibrillar forms are more toxic than the fibrillar forms of α-synuclein in disease [27]. In addition, soluble aggregated α-synuclein mediates dopaminergic neurotoxicity in *Drosophila* [28]. In an ALS animal model, we found that the level of modified soluble α-synuclein (~ 26 kDa) was increased in the brainstem and spinal cord, and BV treatment reduced the modification of α-synuclein (Figure 2). Furthermore, we showed that the expression level of ubiquitinated α-synuclein was decreased in the spinal cord of symptomatic hSOD1^{G93A} transgenic mice compared to age-matched control mice (Figures 3(a), and 3(b)). This result suggests that BV treatment may attenuate the impairment

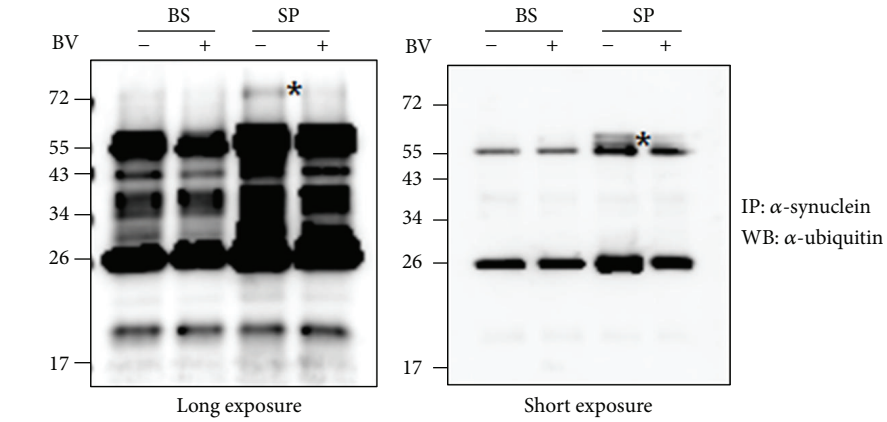

(a)

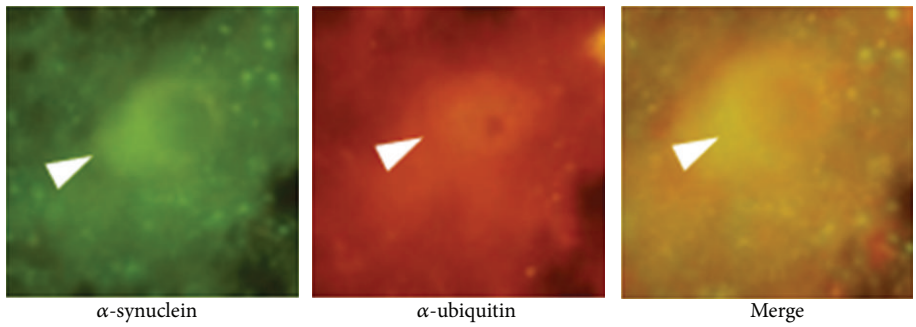

(b)

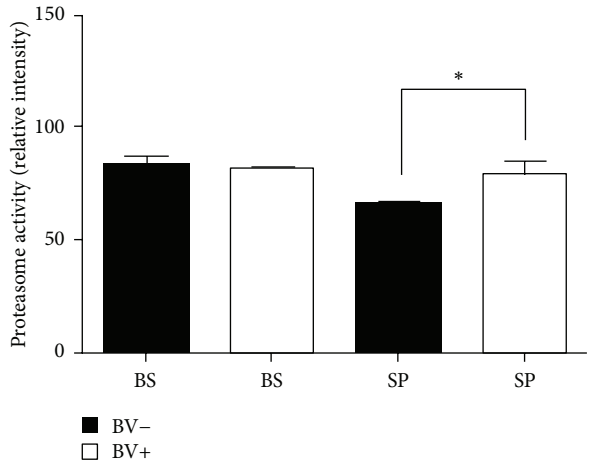

(c)

Figure 3: BV treatment attenuates ubiquitinated α-synuclein and recovered proteasomal activity in the spinal cord of symptomatic hSOD1^{G93A} mice. The total homogenate was immunoprecipitated with an anti-α-synuclein antibody and then immunoblotted with an anti-ubiquitin antibody (a). Ubiquitinated α-synuclein of high molecular weight (*) was detected in the spinal cords of saline-treated hSOD1^{G93A} mice, but not in BV-treated mice. Left upper panel is a long-exposure blot and the lower panel is a short-exposure blot. α-synuclein and ubiquitin were colocalized in the lumbar spinal motor neurons of symptomatic hSOD1^{G93A} mice (b). This image is representative of three independent experiments. Proteasomal activity was determined using a fluorescence enzymatic assay (c). BV treatment increased the proteasomal activity 1.5-fold in the spinal cords of symptomatic hSOD1^{G93A} mice ($n = 4$) compared to age-matched controls ($n = 4$). Proteasomal activity was reported in arbitrary fluorescence units (mean ± SEM of three independent experiments). Values that were significantly different from relative controls are indicated with an asterisk when $P < 0.01$. A.F.U.= arbitrary fluorescence units (mean ± SEM).

of proteasomal activity by the expression or accumulation of modified proteins involved in neurodegenerative events. However, further study of whether fibrillar or oligomeric forms α-synuclein are more toxic than soluble α-synuclein in ALS animal or cell models is needed.

The ubiquitin-proteasome system is a major proteinase system that plays important roles in a vast array of cellular processes, including protein trafficking, antigen presentation, and protein degradation under physiological conditions [29].

Ubiquitinated proteins accumulate to produce protein aggregates in AD, PD, and ALS [30–32]. In the case of ALS, these aggregates are thought to be composed of ubiquitin, SOD-1, some subunits of the proteasome, and neurofilaments [31, 33]. Accumulation of nitrated proteins is also found in the brains of patients with AD, PD, and ALS or in mutant Cu/Zn-superoxide dismutase (SOD-1) or mutant α-synuclein transgenic animals [31]. However, there is still no consensus regarding the pathway responsible for α-synuclein degradation. It is unclear whether α-synuclein degradation depends on the proteasome, chaperone-mediated autophagy, or macroautophagy [34, 35].

Autophagy inhibition promotes the accumulation and subsequent aggregation of monoubiquitinated forms of the α-synuclein protein [26]. Recent evidence suggests that autophagy may play a compensatory role when the UPS function is damaged, and vice versa [36]. Inhibition of the UPS has been shown to activate autophagy-mediated protein degradation [37], and suppression of autophagy leads to the accumulation of ubiquitinated proteins in the cytosol [38]. In ALS models, several studies have shown that autophagy dysfunction contributes towards motor neuron loss [39–42]. Thus, further studies are needed to demonstrate whether an increase of α-synuclein modification in an ALS animal model is caused by autophagy misregulation.

5. Conclusion

This paper demonstrated that BV-treated hSOD1^{G93A} transgenic mice showed reduced detergent-insoluble polymerization and phosphorylation of α-synuclein. Furthermore, phosphorylated or nitrated α-synuclein was significantly reduced in the spinal cords and brainstems of BV-treated hSOD1^{G93A} mice and reduced proteasomal activity was revealed in the brainstems of BV-treated symptomatic hSOD1^{G93A}. From these findings, we suggest that BV treatment attenuates the dysfunction of the ubiquitin-proteasomal system in a symptomatic hSOD1^{G93A} ALS model and may help to slow motor neuron loss caused by misfolded protein aggregates in ALS models.

Conflict of Interests

The authors declare no conflict of interests.

Acknowledgment

This work was supported by grants (K11010, K12010) from the Korea Institute of Oriental Medicine (KIOM).

References

[1] P. J. Shaw, "Molecular and cellular pathways of neurodegeneration in motor neurone disease," *Journal of Neurology, Neurosurgery and Psychiatry*, vol. 76, no. 8, pp. 1046–1057, 2005.

[2] E. Kabashi, P. N. Valdmanis, P. Dion, and G. A. Rouleau, "Oxidized/misfolded superoxide dismutase-1: the cause of all amyotrophic lateral sclerosis?" *Annals of Neurology*, vol. 62, no. 6, pp. 553–559, 2007.

[3] A.-L. Ström, J. Gal, P. Shi, L. J. Hayward, and H. Zhu, "Retrograde axonal transport and motor neuron disease," *Journal of Neurochemistry*, vol. 106, no. 2, pp. 495–505, 2008.

[4] J. D. Rothstein, "Current hypotheses for the underlying biology of amyotrophic lateral sclerosis," *Annals of Neurology*, vol. 65, supplement 1, pp. S3–S9, 2009.

[5] C. Lagier-Tourenne and D. W. Cleveland, "Rethinking ALS: the FUS about TDP-43," *Cell*, vol. 136, no. 6, pp. 1001–1004, 2009.

[6] K. Kanekura, H. Suzuki, S. Aiso, and M. Matsuoka, "ER stress and unfolded protein response in amyotrophic lateral sclerosis," *Molecular Neurobiology*, vol. 39, no. 2, pp. 81–89, 2009.

[7] A. B. Singleton, M. Farrer, J. Johnson et al., "alpha-Synuclein locus triplication causes Parkinson's disease," *Science*, vol. 302, no. 5646, p. 841, 2003.

[8] Y. H. Chung, K. M. Joo, M. J. Kim, and C. I. Cha, "Immunohistochemical study on the distribution of alpha-synuclein in the central nervous system of transgenic mice expressing a human Cu/Zn superoxide dismutase mutation," *Neuroscience Letters*, vol. 342, no. 3, pp. 151–154, 2003.

[9] Y. B. Kwon, J. D. Lee, H. J. Lee et al., "Bee venom injection into an acupuncture point reduces arthritis associated edema and nociceptive responses," *Pain*, vol. 90, no. 3, pp. 271–280, 2001.

[10] W. C. Tu, C. C. Wu, H. L. Hsieh, C. Y. Chen, and S. L. Hsu, "Honeybee venom induces calcium-dependent but caspase-independent apoptotic cell death in human melanoma A2058 cells," *Toxicon*, vol. 52, no. 2, pp. 318–329, 2008.

[11] B. Li, W. Gu, C. Zhang, X. Q. Huang, K. Q. Han, and C. Q. Ling, "Growth arrest and apoptosis of the human hepatocellular carcinoma cell line Bel-7402 induced by melittin," *Onkologie*, vol. 29, no. 8-9, pp. 367–371, 2006.

[12] D. O. Moon, S. Y. Park, M. S. Heo et al., "Key regulators in bee venom-induced apoptosis are Bcl-2 and caspase-3 in human leukemic U937 cells through downregulation of ERK and Akt," *International Immunopharmacology*, vol. 6, no. 12, pp. 1796–1807, 2006.

[13] E. J. Yang, J. H. Jiang, S. M. Lee et al., "Bee venom attenuates neuroinflammatory events and extends survival in amyotrophic lateral sclerosis models," *Journal of Neuroinflammation*, vol. 7, article 69, 2010.

[14] E. J. Yang, S. H. Kim, S. C. Yang, S. M. Lee, and S. M. Choi, "Melittin restores proteasome function in an animal model of ALS," *Journal of Neuroinflammation*, vol. 8, article 69, 2011.

[15] D. R. Rosen, T. Siddique, D. Patterson et al., "Mutations in Cu/Zn superoxide dismutase gene are associated with familial amyotrophic lateral sclerosis," *Nature*, vol. 362, pp. 59–62, 1993.

[16] C. S. Yin, H. S. Jeong, H. J. Park et al., "A proposed transpositional acupoint system in a mouse and rat model," *Research in Veterinary Science*, vol. 84, no. 2, pp. 159–165, 2008.

[17] E. J. Benner, R. Banerjee, A. D. Reynolds et al., "Nitrated α-synuclein immunity accelerates degeneration of nigral dopaminergic neurons," *PLoS ONE*, vol. 3, no. 1, Article ID e1376, 2008.

[18] D. K. Stone, A. D. Reynolds, R. L. Mosley, and H. E. Gendelman, "Innate and adaptive immunity for the pathobiology of Parkinson's disease," *Antioxidants and Redox Signaling*, vol. 11, no. 9, pp. 2151–2166, 2009.

[19] T. C. Frank-Cannon, L. T. Alto, F. E. McAlpine, and M. G. Tansey, "Does neuroinflammation fan the flame in neurodegenerative diseases?" *Molecular Neurodegeneration*, vol. 4, no. 1, article 47, 2009.

[20] K. Hensley, M. Mhatre, S. Mou et al., "On the relation of oxidative stress to neuroinflammation: lessons learned from the G93A-SOD1 mouse model of amyotrophic lateral sclerosis," *Antioxidants and Redox Signaling*, vol. 8, no. 11-12, pp. 2075–2087, 2006.

[21] M. Prudencio, P. J. Hart, D. R. Borchelt, and P. M. Andersen, "Variation in aggregation propensities among ALS-associated variants of SOD1: correlation to human disease," *Human Molecular Genetics*, vol. 18, no. 17, pp. 3217–3226, 2009.

[22] M. Chattopadhyay and J. S. Valentine, "Aggregation of copper-zinc superoxide dismutase in familial and sporadic ALS," *Antioxidants and Redox Signaling*, vol. 11, no. 7, pp. 1603–1614, 2009.

[23] H. Chen, E. Jacobs, M. A. Schwarzschild et al., "Nonsteroidal antiinflammatory drug use and the risk for Parkinson's disease," *Annals of Neurology*, vol. 58, pp. 963–967, 2005.

[24] J. B. Koprich, C. Reske-Nielsen, P. Mithal, and O. Isacson, "Neuroinflammation mediated by IL-1β increases susceptibility of dopamine neurons to degeneration in an animal model of Parkinson's disease," *Journal of Neuroinflammation*, vol. 5, article 8, 2008.

[25] C. Y. Chung, J. B. Koprich, H. Siddiqi, and O. Isacson, "Dynamic changes in presynaptic and axonal transport proteins combined with striatal neuroinflammation precede dopaminergic neuronal loss in a rat model of AAV α-synucleinopathy," *Journal of Neuroscience*, vol. 29, no. 11, pp. 3365–3373, 2009.

[26] R. Rott, R. Szargel, J. Haskin et al., "Monoubiquitylation of α-Synuclein by seven in absentia homolog (SIAH) promotes its aggregation in dopaminergic cells," *Journal of Biological Chemistry*, vol. 283, no. 6, pp. 3316–3328, 2008.

[27] M. Baba, S. Nakajo, P. H. Tu et al., "Aggregation of α-synuclein in Lewy bodies of sporadic Parkinson's disease and dementia with Lewy bodies," *American Journal of Pathology*, vol. 152, no. 4, pp. 879–884, 1998.

[28] M. Periquet, T. Fulga, L. Myllykangas, M. G. Schlossmacher, and M. B. Feany, "Aggregated α-synuclein mediates dopaminergic neurotoxicity in vivo," *Journal of Neuroscience*, vol. 27, no. 12, pp. 3338–3346, 2007.

[29] D. P. Hanger, J. P. Brion, J. M. Gallo, N. J. Cairns, P. J. Luthert, and B. H. Anderton, "Tau in Alzheimer's disease and Down's syndrome is insoluble and abnormally phosphorylated," *Biochemical Journal*, vol. 275, no. 1, pp. 99–104, 1991.

[30] E. Mezey, A. Dehejia, G. Harta, M. I. Papp, M. H. Polymeropoulos, and M. J. Brownstein, "Alpha synuclein in neurodegenerative disorders: murderer or accomplice?" *Nature Medicine*, vol. 4, no. 7, pp. 755–757, 1998.

[31] W. G. Johnson, "Late-onset neurodegenerative diseases—the role of protein insolubility," *Journal of Anatomy*, vol. 196, no. 4, pp. 609–616, 2000.

[32] N. F. Bence, R. M. Sampat, and R. R. Kopito, "Impairment of the ubiquitin-proteasome system by protein aggregation," *Science*, vol. 292, no. 5521, pp. 1552–1555, 2001.

[33] A. Alves-Rodrigues, L. Gregori, and M. E. Figueiredo-Pereira, "Ubiquitin, cellular inclusions and their role in neurodegeneration," *Trends in Neurosciences*, vol. 21, no. 12, pp. 516–520, 1998.

[34] M. C. Bennett, J. F. Bishop, Y. Leng, P. B. Chock, T. N. Chase, and M. M. Mouradian, "Degradation of α-synuclein by proteasome," *Journal of Biological Chemistry*, vol. 274, no. 48, pp. 33855–33858, 1999.

[35] J. L. Webb, B. Ravikumar, J. Atkins, J. N. Skepper, and D. C. Rubinsztein, "α-Synuclein is degraded by both autophagy and the proteasome," *Journal of Biological Chemistry*, vol. 278, no. 27, pp. 25009–25013, 2003.

[36] Q. Zheng, J. Li, and X. Wang, "Interplay between the ubiquitin-proteasome system and autophagy in proteinopathies," *International Journal of Physiology, Pathophysiology and Pharmacology*, vol. 1, no. 2, pp. 127–142, 2009.

[37] V. Crippa, D. Sau, P. Rusmini et al., "The small heat shock protein B8 (HspB8) promotes autophagic removal of misfolded proteins involved in amyotrophic lateral sclerosis (ALS)," *Human Molecular Genetics*, vol. 19, no. 17, Article ID ddq257, pp. 3440–3456, 2010.

[38] T. Hara, K. Nakamura, M. Matsui et al., "Suppression of basal autophagy in neural cells causes neurodegenerative disease in mice," *Nature*, vol. 441, no. 7095, pp. 885–889, 2006.

[39] S. Chen, X. Zhang, L. Song, and W. Le, "Autophagy dysregulation in amyotrophic lateral sclerosis," *Brain Pathology*, vol. 22, no. 1, pp. 110–116, 2012.

[40] S. Sasaki, "Autophagy in spinal cord motor neurons in sporadic amyotrophic lateral sclerosis," *Journal of Neuropathology and Experimental Neurology*, vol. 70, no. 5, pp. 349–359, 2011.

[41] N. Morimoto, M. Nagai, Y. Ohta et al., "Increased autophagy in transgenic mice with a G93A mutant SOD1 gene," *Brain Research*, vol. 1167, no. 1, pp. 112–117, 2007.

[42] S. Hadano, A. Otomo, R. Kunita et al., "Loss of ALS2/Alsin exacerbates motor dysfunction in a SOD1-expressing mouse ALS model by disturbing endolysosomal trafficking," *PloS One*, vol. 5, no. 3, Article ID e9805, 2010.

Hindawi Publishing Corporation
Evidence-Based Complementary and Alternative Medicine
Volume 2013, Article ID 240702, 7 pages
http://dx.doi.org/10.1155/2013/240702

Research Article

A Promise in the Treatment of Endometriosis: An Observational Cohort Study on Ovarian Endometrioma Reduction by N-Acetylcysteine

Maria Grazia Porpora,[1] Roberto Brunelli,[1] Graziella Costa,[2] Ludovica Imperiale,[1] Ewa K. Krasnowska,[2] Thomas Lundeberg,[3] Italo Nofroni,[4] Maria Grazia Piccioni,[1] Eugenia Pittaluga,[2] Adele Ticino,[1] and Tiziana Parasassi[2]

[1] *Dipartimento di Scienze Ginecologico-Ostetriche e Scienze Urologiche, Università di Roma Sapienza, Viale del Policlinico 155, 00161 Roma, Italy*
[2] *Istituto di Farmacologia Traslazionale, CNR, Via del Fosso del Cavaliere 100, 00133 Roma, Italy*
[3] *Foundation for Acupuncture and Alternative Biological Treatment Methods, Sabbatsbergs Hospital, Olivecronas väg 1, 113 24 Stockholm, Sweden*
[4] *Dipartimento di Sanità Pubblica e Malattie Infettive, Università di Roma Sapienza, Viale del Policlinico 155, 00161 Roma, Italy*

Correspondence should be addressed to Tiziana Parasassi; tiziana.parasassi@cnr.it

Received 15 January 2013; Revised 9 April 2013; Accepted 9 April 2013

Academic Editor: Martin Kohlmeier

Urged by the unmet medical needs in endometriosis treatment, often with undesirable side effects, and encouraged by N-acetylcysteine (NAC) efficacy in an animal model of endometriosis and by the virtual absence of toxicity of this natural compound, we performed an observational cohort study on ovarian endometriosis. NAC treatment or no treatment was offered to 92 consecutive Italian women referred to our university hospital with ultrasound confirmed diagnosis of ovarian endometriosis and scheduled to undergo laparoscopy 3 months later. According to patients acceptance or refusal, NAC-treated and untreated groups finally comprised 73 and 72 endometriomas, respectively. After 3 months, within NAC-treated patients cyst mean diameter was slightly reduced (−1.5 mm) versus a significant increase (+6.6 mm) in untreated patients ($P = 0.001$). Particularly, during NAC treatment, more cysts reduced and fewer cysts increased their size. Our results are better than those reported after hormonal treatments. Twenty-four NAC-treated patients—versus 1 within controls—cancelled scheduled laparoscopy due to cysts decrease/disappearance and/or relevant pain reduction (21 cases) or pregnancy (1 case). Eight pregnancies occurred in NAC-treated patients and 6 in untreated patients. We can conclude that NAC actually represents a simple effective treatment for endometriosis, without side effects, and a suitable approach for women desiring a pregnancy.

1. Introduction

Endometriosis is one of the most frequent benign gynecological diseases, characterized by the implant and growth of viable endometrial tissue outside the uterine cavity, producing a general inflammatory response. The reported endometriosis prevalence in women of reproductive age ranges up to 10% [1]. In infertile women, the prevalence may rise to 50% [2]. Nevertheless, these numbers are likely to be underestimated.

The most common clinical symptoms include chronic lower abdominal and pelvic pain, dysmenorrhea, dyspareunia, abnormal uterine bleeding, and infertility.

Surgical removal of ectopic lesions represents the first-line intervention but is hampered by a relevant percentage of recurrences [3, 4]. In addition, a variety of medical hormonal therapies, all aimed to reduce the levels of circulating estrogens, are currently available [5]. However, these treatments are often unsatisfactory and cannot be used over long periods

of time, due to the occurrence of severe adverse effects. Therefore, new and improved therapeutic solutions that can efficiently reduce lesions with limited side effects and no interference with the patient's fertility are definitely desirable.

We recently demonstrated that the well-known drug N-acetylcysteine (NAC), the acetylated form of the aminoacid cysteine naturally present in some substances like garlic [6], exerts a marked antiproliferative action *in vitro* on cancer cells of epithelial origin—the same origin of endometrial cells [7]. NAC action does not involve the induction of cell death nor is due to an unspecific toxic effect; rather, it is due to the establishment of a complex differentiation pathway, including the activation of several molecular mechanisms all converging into a proliferation-to-differentiation switch that implies a decreased cell proliferation and a decrease in cell locomotory behavior, particularly relevant in endometriosis. In addition, NAC also downregulates inflammatory protein activity and gene expression [8, 9]. Overall, NAC emerges as a thiol-containing compound active in the complex framework of redox signaling, with effects that are far beyond a generic antioxidant capability [10].

Translating *in vitro* findings into a murine model of endometriosis [11], we reported that NAC treatment induces a relevant reduction in endometriomas size, associated with decreased tissue inflammation and cell invasiveness. A similar effect of NAC in decreasing the production of hydrogen peroxide and in reducing cell proliferation was evidenced by using cellular and animal models of endometriosis and attributed to the regulation of the extracellular regulated kinase ERK1/2 [12].

Prompted by this background and with reference to both the unmet medical needs of endometriosis treatment and to the attractiveness of using NAC, virtually free of undesirable side effects and toxicity, we hereby report the successful treatment of ovarian endometriosis by using NAC.

2. Methods

Our observational cohort study was aimed at comparing the evolution of ovarian endometriomas in terms of mean diameter and volume, as evaluated by ultrasound, in NAC-treated and untreated control patients. The study protocol was approved by the Institutional Review Board of the University of Rome Sapienza (n.1451/11.09.08) and written informed consent was obtained from all patients.

Patients were enrolled in the study according to the following inclusion criteria: (1) presence of an assigned ultrasound diagnosis of ovarian endometrioma; (2) no steroid treatment in the previous 2 months; (3) scheduled laparoscopy due to the presence of at least one of the following conditions: large ovarian endometrioma(s) with a mean diameter ≥30 mm, pain, and infertility. Diagnosis of ovarian endometriosis was issued with reference to an accurate medical history, pelvic examination (PV), and the combined use of transvaginal pelvic ultrasound (TVUS) and color Doppler evaluation [13, 14], performed in the early follicular phase of three consecutive menstrual cycles preceding enrollment [15]. Overall, this diagnostic procedure should grant almost a 100% diagnostic accuracy [16]. Ultrasound diagnosis of ovarian endometriomas was assigned when in the presence of the following established criteria: (1) a unilocular mass with ground glass echogenicity and a color score between 1 and 3; or (2) a unilocular mass with ground glass echogenicity with a papillary projection, a color score of 1 or 2 and no flow inside the papillary projection [13]. In some patients (6 in the treated group and 4 in the control group) with deep infiltrating lesions possibly involving the bowel or the bladder, MRI was also performed [17]. At enrollment, patients were allocated to the control or to the NAC-treated group according to their refusal or acceptance of the proposed treatment with NAC; routine laboratory tests were normal in all patients of the two groups. The observation period was of 3 months, corresponding to the mean duration of the waiting list for scheduled laparoscopy. At enrollment, routine laboratory tests were normal in all patients of the two groups.

At enrollment and at the end of the 3-month period of observation, endometriomas were evaluated by a trained physician with 20 years of experience in pelvic ultrasound (MGPi), blind to treatment but aware that the purpose of the examination was a precise monitoring of endometriomas dimension. All measurements were performed during the early follicular phase, that is, within the 8th day of the menstrual cycle, using a Siemens Sonoline Elegra scanner (Siemens, Issaquah, WA, USA), equipped with transabdominal (3.5 MHz) and transvaginal (5 MHz) probes; blood flow of the cysts was analyzed by the Color Doppler imaging. Pain symptoms (dysmenorrhea, dyspareunia, and chronic pelvic pain) were assessed by means of a 10-point visual analogue scale (VAS) both at enrollment and at the end of observation. Laparoscopy was performed under general anesthesia by the same surgeon with more than 20 years of experience (MGPo). Endometriosis was staged according to the revised classification of the American Society of Reproductive Medicine (rASRM) [18]. Histological examination was performed in all cases that ultimately underwent laparoscopy.

NAC (Angenerico S.p.A., Ancona, Italy) was administered to patients *per os* for 3 months according to the following schedule: 600 mg three times a day, three consecutive days a week (Nactivia procedure, PMVENIRE, Stockholm, Sweden). The adoption of this procedure was based on the following considerations: (1) the daily total NAC dose of 1.8 g is virtually free of side effects and was already considered for other clinical indications [19]; (2) splitting the total dose in 3 is simple for patients and, with reference to the known NAC pharmacokinetics [20], grants a nearly constant plasma level of the drug; (3) the four-day medication-free interval provides a washout period useful to limit the reported decrease of NAC plasma level observed during prolonged treatments [20].

Immunohistochemical observation was performed on tissue samples obtained at laparoscopy from 2 NAC-treated and 2 untreated patients. Endometrioma tissue was processed using the method reported in [11]. Briefly, samples were fixed in 10% formalin, then paraffin-embedded, and 5 μm-thick sections stained using haematoxylin-eosin. For antigen retrieval, sections were microwaved for 6 min in 0.1 M citrate buffer (pH 6.0) and endogenous peroxidase activity

Table 1: Characteristics of patients.

	Controls ($n = 45$)	Treated ($n = 47$)	P
Age (years)	32.9 ± 6.5	32.5 ± 7.3	ns
Weight (kg)	57.8 ± 7.2	60.2 ± 13.3	ns
Height (cm)	164.3 ± 5.8	163.8 ± 6.8	ns
BMI	21.4 ± 2.5	22.5 ± 4.9	ns
Past hormonal therapy (n)	22	28	ns
Pregnancy desire (n)	14	15	ns
Parity (n)			
0	29	35	ns
1	11	10	ns
≥2	5	2	ns
Pregnancies post (n)[a]	6	8	ns
Infertility	10	13	ns
Previous surgery for endometriosis	17	12	ns
Deep infiltrating lesions	4	2	ns
Dysmenorrhea (1–10 VAS)	7.18 ± 2.58 ($n = 42$)	6.43 ± 3.39 ($n = 38$)	ns
Dyspareunia (1–10 VAS)	2.76 ± 3.27 ($n = 20$)	2.83 ± 3.19 ($n = 23$)	ns
Chronic pelvic pain (1–10 VAS)	2.07 ± 3.57 ($n = 12$)	2.47 ± 3.82 ($n = 15$)	ns
Patients with more than 1 cyst	21[b]	20[c]	ns
	($n = 72$)	($n = 73$)	
Cyst size			
Average diameter (mm)	31.6 ± 18.4	26.9 ± 14.9	ns
Average volume (mL)	35.1 ± 62.6	20.4 ± 31.3	ns

[a]Only 1 pregnancy in the treated group was reported during the 3 months. All other pregnancies occurred after the observation period and were reported by the patients. [b]$n = 17$: 2 cysts; $n = 3$: 3 cysts; $n = 1$: 5 cysts. [c]$n = 15$: 2 cysts; $n = 4$: 3 cysts; $n = 1$: 4 cysts.

was blocked by 20 min incubation in 3% H_2O_2/methanol. Sections were rinsed in PBS/Triton X-100, immersed for 15 min in PBS-bovine serum albumin, and then incubated with the selected primary antibody. For immunodetection, Cox-2 rabbit polyclonal antibody was from NeoMarkers, Lab Vision Corporation (Thermo Fisher Scientific, Fremont, CA); E-cadherin and β-catenin were from BD Biosciences (Milan, Italy). DAKO Cytomation LSAB2 System-HRP (Dako Italia, Milan, Italy) was used to reveal antigens. After counterstaining with haematoxylin, sections were observed with a Zeiss Axioplan microscope.

2.1. Statistical Methods. In a pilot study performed on a limited number of patients comprising a total of 32 ovarian endometriomas, we observed an average increase in the cyst volume of 5.9 mL in the NAC-treated group and of 30.1 mL in the untreated group, respectively, with a standard deviation SD = 69.4 in both groups. Given a first-type error $\alpha = 0.05$ and a test power of 90%, the needed sample size in each group resulted in 67 cysts; evaluating an average of 7% of drop-out patients, we established a final requested sample size of 72 cysts in each group. The evaluation of the significance for average variations in cyst dimension within each group was performed using the Student's t-test for paired data. In order to evaluate whether these mean variations were different between the two compared groups, the Student's t-test was used for independent samples after a preliminary evaluation of the homogeneity of variance using the Levene's test. Given the heterogeneous variation in cyst dimensions that, within each of the two groups, could alternatively increase, decrease, or remain unchanged, we also compared NAC-treated and untreated cysts by using the Pearson's chi-square test. Significance was defined as $P \leq 0.05$. Statistics were performed using SPSS software for Windows (release 13, 2004).

3. Results and Discussion

Between October 2008 and April 2011, 108 Italian women eligible for the study were consecutively enrolled; 7 patients in the NAC-treated group were not compliant to the scheduled therapy, and 9 patients in the control group dropped out. Therefore, a total of 92 patients, 47 in the NAC-treated group and 45 in the untreated group, were ultimately included in the study. Due to the contemporary presence of more than one cyst in several patients, we examined a total of 73 and 72 ovarian endometriomas in the NAC-treated and untreated group, respectively.

Patients in the two groups were comparable in terms of demographic characteristics, reproductive history, previous surgery for endometriosis, presence and severity of pain symptoms, and endometriomas size (Table 1).

For both groups, raw values of the variation in cyst mean diameter (a) and volume (b) are shown in Figure 1;

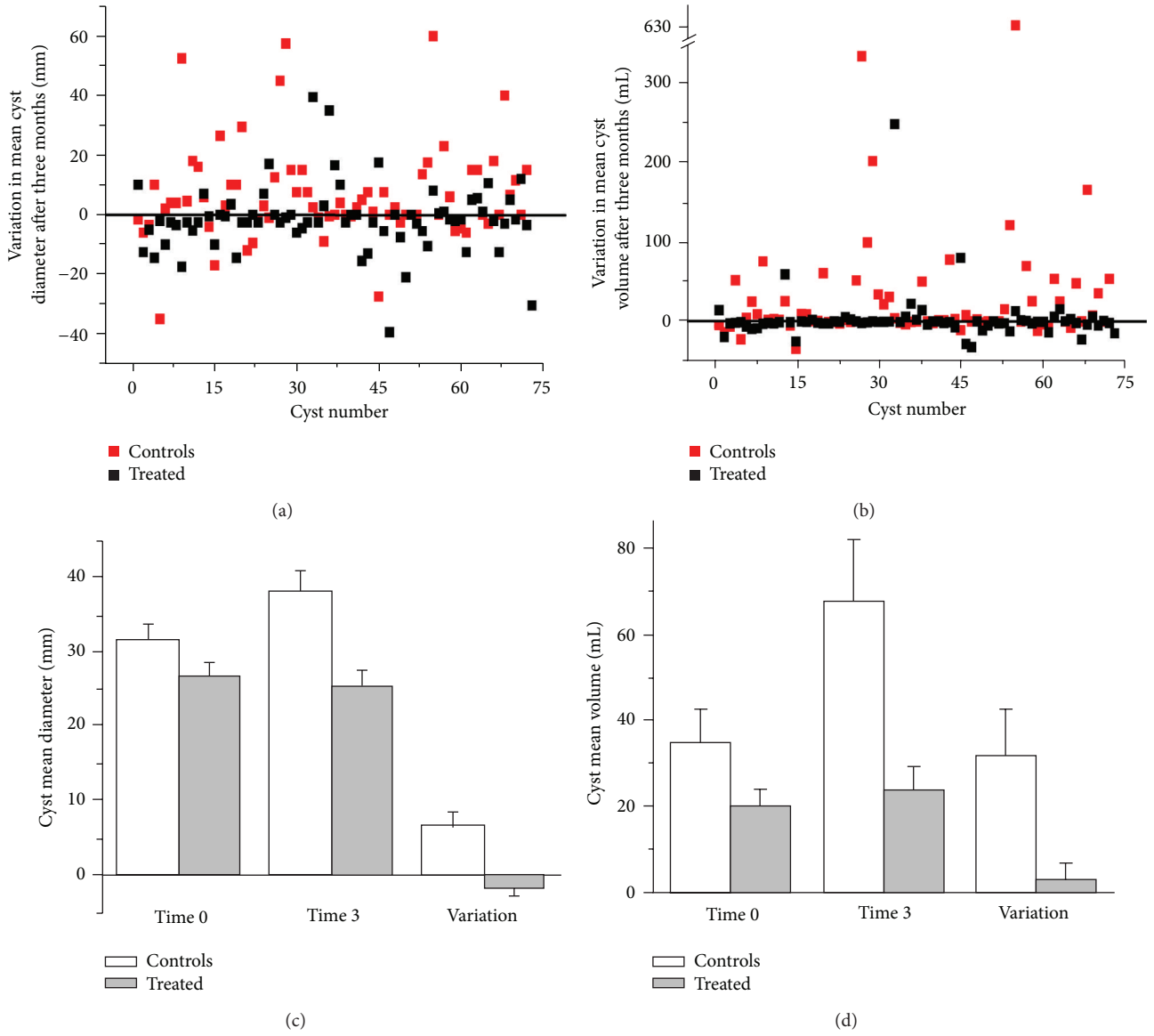

FIGURE 1: Variations in ovary cyst size after 3 months. Difference between the final and the initial mean diameters (a) and volumes (b) of all cysts in NAC-treated (black) and control (red) patients. Histogram of the averaged variations in mean diameter (c) and volume (d) in NAC-treated (gray) and control (white) patients. Statistical parameters are reported in detail in Table 2.

histograms of mean initial and final diameter (c) and volume (d), together with their respective variations, are also presented. Complete numeric values and statistical evaluations are detailed in Table 2. Notably, the significant increase in cysts size found in the control group was prevented by NAC.

As further outlined in Table 2, both in the NAC-treated and control group endometriomas alternatively decreased, increased, or remained unchanged; however, after NAC treatment more cysts underwent a size reduction and less cysts enlarged ($P < 0.001$). The number of reduced endometriomas also included disappeared cysts, 8 and 4 in NAC-treated and untreated patients, respectively; similarly, increased cysts included newly formed cysts, 4 and 7 in NAC-treated and untreated patients, respectively.

The initial ovarian endometrioma dimension did not influence the response to treatment ($P > 0.05$).

NAC was well tolerated by all patients and no adverse reactions were reported.

In the NAC-treated group, 24 patients cancelled the scheduled laparoscopy due to decreased (14 patients) or disappeared cysts (4 patients), pain reduction (21 patients), or pregnancy (1 patient). In the control group only 1 patient cancelled surgery. The rASRM stage, the disease score, and the pathology evaluation of all patients who ultimately underwent laparoscopy did not differ between the two groups (Table 3).

The hypothesis tested in our study was to verify whether the evolution of ovarian endometriomas size could be positively influenced by NAC treatment during a relatively short interval of 3 months. Indeed, when compared to untreated controls, NAC treatment led to an increased number of cysts

Table 2: Endometriomas size at enrollment and at the end of observation.

	Controls ($n = 72$)	Treated ($n = 73$)	P
Average diameter (mm)			
Initial	31.6 ± 18.4	26.9 ± 14.9	ns
Final	38.3 ± 23.2	25.4 ± 17.8	<0.001
Difference	6.62 ± 16.14	−1.53 ± 11.43	0.001
Average volume (mL)			
Initial	35.1 ± 62.6	20.4 ± 31.3	ns
Final	67.3 ± 123.2	23.6 ± 48.6	0.006
Difference	32.1 ± 89.9	3.20 ± 32.7	0.012
Number of cysts			
Increased	42 (58%) (7 newly formed)	20 (27%) (4 newly formed)	<0.001*
Decreased	20 (28%) (4 disappeared)	45 (62%) (8 disappeared)	
Unchanged	10 (14%)	8 (11%)	

*At the Pearson's chi-square test.

Table 3: Patients disease stage and score at laparoscopy.

	Controls ($n = 44$)	Treated ($n = 23$)	P
rARMS score	39.6 ± 27.5	49.7 ± 32.6	ns
rARMS stage			
II	4 (9%)	2 (9%)	ns
III	28 (64%)	15 (65%)	ns
IV	12 (27%)	6 (26%)	ns

that either shrank or disappeared, as well as in a smaller number of enlarged and newly formed cysts.

This effect is particularly remarkable because it favorably compares to the results reported in a randomized placebo controlled study performed on 100 patients treated for four months by using oral contraceptives (OC) [21]. Indeed, in this latter study, a reduction in cyst dimension was recorded not only in the OC-treated group but also in the placebo group. The overall reduction gain with OC (2.4 mL in volume and of 1.6 mm in average diameter) is far less impressive than that granted by NAC (28.9 mL in volume and of 8.2 mm in average diameter). A further comparison between OC and NAC treatments in terms of endometriomas stabilization, regression, or progression is made impossible by lack of disaggregated data in the OC study [21].

In NAC-treated and control patients we registered 6 and 8 pregnancies, respectively (Table 1); therefore, in striking contrast to all other available hormonal treatments of endometriosis (e.g., danazol, gonadotropin-releasing hormone analogues, progestins, and oral contraceptives) [22], NAC does not affect patient fertility and represents a suitable approach to treat endometriosis in women desiring pregnancy. Of the 8 pregnancies in the NAC-treated group, 1 occurred during treatment and 7 occurred within 2–12 months after completion of therapy (mean: 6 months).

Although the pathogenesis of endometriosis is still debated [23], several evidences highlight that both the onset and progression of this disease are supported by a derangement of invasive, proliferative, adhesive, and locomotory properties of endometrial cells, along with an increased production of inflammatory molecules [24]. In this regard, our rationale for testing NAC effectiveness in the clinical management of endometriosis was granted by our previous evidences showing that NAC, through its action on thiol redox signaling [10], positively modulates several pathways relevant in the pathogenesis of endometriosis [7–9, 11]. Indeed, *in vitro*, NAC decreases abnormal cell proliferation, cell locomotory characteristics, expression/activity of some inflammation-related genes, and stimulates terminal cell differentiation, that is, a finite cell lifespan [7–9]. Consistently, in an animal model, NAC treatment results in a reduction in size of experimentally induced endometriomas through a direct action on the endometrial tissue that displays (1) a differentiated morphology; (2) a decrease in cell invasive behavior, evidenced by an increase in cell-cell junctions and a decreased expression of metalloproteinases; and (3) a relevant decrease in the cyclooxygenase-2 (COX-2) gene and protein expression [11].

In agreement with these evidences, preliminary immunohistochemical examinations of cyst tissue obtained at laparoscopy anticipate that similar molecular mechanisms are at play also in the human and substantiate the present clinical findings. Indeed, in tissue from NAC-treated patients we observed (Figure 2) (1) a more differentiated morphology of the epithelial layer; (2) an increase in proteins of cell-cell junction complex such as E-cadherin and β-catenin, indicating a decrease in cell invasive behavior; and (3) a decrease in the inflammatory COX-2. This latter evidence suggests a possible explanation of the observed reduction in cysts dimensions. Indeed, a decrease in COX-2 ultimately reduces estrogens availability in the ectopic endometrium through a decreased production of prostaglandin E2—the most powerful stimulator of aromatase [25]. Of note, we foresee that NAC action on cell signaling and protein activity, with the overall effect of reverting a deranged proliferation to a physiological behavior, can help in preventing recurrences. However, both a complete elucidation of the mechanisms activated by NAC and its possible role in the prevention of recurrences deserve future wider studies.

Due to the bias represented by the absence of a placebo group, the observed variations in pain incidence and severity cannot be validated; however, while dysmenorrhea, dyspareunia, and chronic pelvic pain were similar in the two groups at enrollment, they were all significantly reduced in the NAC-treated group at the end of observation, with a decrease of 55% in dysmenorrhea ($P = 0.001$), of 50% in dyspareunia ($P = 0.027$) and of 59% in chronic pelvic pain ($P = 0.015$) (Table 4). These data definitely deserve a validation in placebo-controlled future studies; of note, pain amelioration represented the main reason for surgery cancellation in the NAC-treated group (21/47).

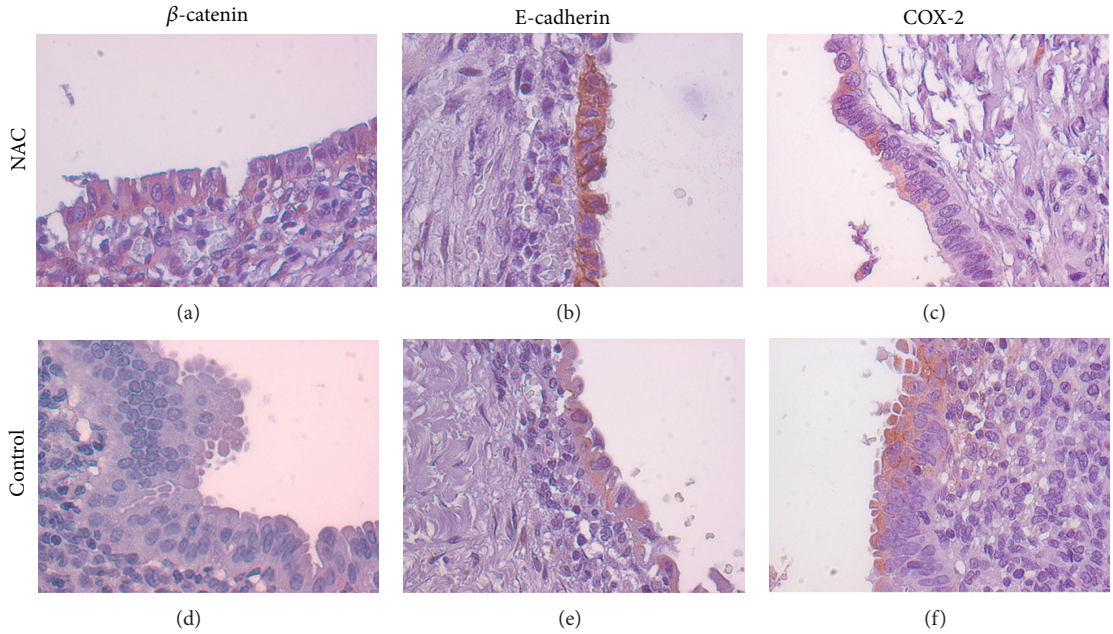

Figure 2: Immunohistochemical comparison of NAC-treated and untreated endometrioma tissue obtained at laparoscopy. Representative examples of NAC-treated (a, b, and c) and untreated (d, e, and f) tissue samples showing an increased labeling for proteins belonging to the cell-cell adhesion complexes, β-catenin (a) versus (d) and E-cadherin (b) versus (e) and a decrease in inflammatory COX-2 (c) versus (f). Original magnification 40x.

Table 4: Pain evaluation at enrollment and at the end of observation (1–10 VAS scale).

	Controls	Treated	P
Dysmenorrhea			
Initial	7.18 ± 2.58 (n = 42)	6.43 ± 3.39 (n = 38)	ns
Final	7.00 ± 2.79 (n = 41)	3.11 ± 3.33 (n = 24)	0.001
Dyspareunia			
Initial	2.76 ± 3.27 (n = 20)	2.83 ± 3.19 (n = 23)	ns
Final	2.78 ± 3.31 (n = 20)	1.38 ± 2.62 (n = 12)	0.027
Chronic pelvic pain			
Initial	2.07 ± 3.57 (n = 12)	2.47 ± 3.82 (n = 15)	ns
Final	1.87 ± 3.42 (n = 11)	0.77 ± 2.09 (n = 6)	0.015

4. Conclusions

In conclusion, with reference to the unmet medical needs of endometriosis, our results clearly show that, by targeting various molecular and biochemical pathways involved in the initiation and maintenance of this disease, NAC effectively treats ovarian endometriosis. In terms of reduction in cysts size, our data are even more favorable than those granted by the currently adopted hormonal treatments, with the further advantages of fertility preservation and of the virtual absence of undesired side effects. The low cost of this natural drug can also be of interest for public health institutions.

Acknowledgments

The authors thank Leopoldo Silvestroni for his valuable suggestions in the organization of the study. They also acknowledge Eliana Fuggetta, Serena Resta, and Deliar Yazdanian for their worthy contribution to the data collection. This work was supported by a research grant from the Iasomai AB, Stockholm, Sweden, to IFT (G. Costa, E. K. Krasnowska, E. Pittaluga, T. Parasassi). The funders had no role in study design, data collection and analysis, decision to publish, or preparation of the paper.

References

[1] B. Eskenazi and M. L. Warner, "Epidemiology of endometriosis," *Obstetrics and Gynecology Clinics of North America*, vol. 24, no. 2, pp. 235–258, 1997.

[2] D. W. Cramer and S. A. Missmer, "The epidemiology of endometriosis," *Annals of the New York Academy of Sciences*, vol. 955, pp. 11–22, 2002.

[3] P. Vercellini, E. Somigliana, P. Vigan, S. de Matteis, G. Barbara, and L. Fedele, "The effect of second-line surgery on reproductive performance of women with recurrent endometriosis: a systematic review," *Acta Obstetricia et Gynecologica Scandinavica*, vol. 88, no. 10, pp. 1074–1082, 2009.

[4] M. G. Porpora, D. Pallante, A. Ferro, B. Crisafi, F. Bellati, and P. Benedetti Panici, "Pain and ovarian endometrioma recurrence after laparoscopic treatment of endometriosis: a long-term prospective study," *Fertility and Sterility*, vol. 93, no. 3, pp. 716–721, 2010.

[5] V. M. Rice, "Conventional medical therapies for endometriosis," *Annals of the New York Academy of Sciences*, vol. 955, pp. 343–352, 2002.

[6] M. Nishikawa-Ogawa, H. Wanibuchi, K. Morimura et al., "N-acetylcysteine and S-methylcysteine inhibit MeIQx rat hepatocarcinogenesis in the post-initiation stage," *Carcinogenesis*, vol. 27, no. 5, pp. 982–988, 2006.

[7] T. Parasassi, R. Brunelli, L. Bracci-Laudiero et al., "Differentiation of normal and cancer cells induced by sulfhydryl reduction: biochemical and molecular mechanisms," *Cell Death and Differentiation*, vol. 12, no. 10, pp. 1285–1296, 2005.

[8] A. C. Gustafsson, I. Kupershmidt, E. Edlundh-Rose et al., "Global gene expression analysis in time series following N-acetyl L-cysteine induced epithelial differentiation of human normal and cancer cells in vitro," *BMC Cancer*, vol. 5, article 75, 2005.

[9] E. Edlundh-Rose, I. Kupershmidt, A. C. Gustafsson et al., "Gene expression analysis of human epidermal keratinocytes after N-acetyl L-cysteine treatment demonstrates cell cycle arrest and increased differentiation," *Pathobiology*, vol. 72, no. 4, pp. 203–212, 2005.

[10] T. Parasassi, R. Brunelli, G. Costa et al., "Thiol redox transitions in cell signaling: a lesson from N-acetylcysteine," *The Scientific World Journal*, vol. 10, pp. 1192–1202, 2010.

[11] E. Pittaluga, G. Costa, E. Krasnowska et al., "More than antioxidant: N-acetyl-L-cysteine in a murine model of endometriosis," *Fertility and Sterility*, vol. 94, no. 7, pp. 2905–2908, 2010.

[12] C. Ngô, C. Chéreau, C. Nicco, B. Weill, C. Chapron, and F. Batteux, "Reactive oxygen species controls endometriosis progression," *American Journal of Pathology*, vol. 175, no. 1, pp. 225–234, 2009.

[13] S. Guerriero, S. Ajossa, V. Mais, A. Risalvato, M. P. Lai, and G. B. Melis, "The diagnosis of endometriomas using colour Doppler energy imaging," *Human Reproduction*, vol. 13, no. 6, pp. 1691–1695, 1998.

[14] M. A. Pascual, F. Tresserra, L. López-Marín, A. Ubeda, P. J. Grases, and S. Dexeus, "Role of color doppler ultrasonography in the diagnosis of endometriotic cyst," *Journal of Ultrasound in Medicine*, vol. 19, no. 10, pp. 695–699, 2000.

[15] Y. Nemoto, K. Ishihara, T. Sekiya, H. Konishi, and T. Araki, "Ultrasonographic and clinical appearance of hemorrhagic ovarian cyst diagnosed by transvaginal scan," *Journal of Nippon Medical School*, vol. 70, no. 3, pp. 243–249, 2003.

[16] G. Hudelist, K. H. Oberwinkler, C. F. Singer et al., "Combination of transvaginal sonography and clinical examination for preoperative diagnosis of pelvic endometriosis," *Human Reproduction*, vol. 24, no. 5, pp. 1018–1024, 2009.

[17] L. Manganaro, F. Fierro, A. Tomei et al., "Feasibility of 3.0 T pelvic MR imaging in the evaluation of endometriosis," *European Journal of Radiology*, vol. 81, pp. 1381–1387, 2012.

[18] American Society for Reproductive Medicine, "Revised American Society for Reproductive Medicine classification of endometriosis: 1996," *Fertility and Sterility*, vol. 67, no. 5, pp. 817–821, 1997.

[19] K. R. Atkuri, J. J. Mantovani, L. A. Herzenberg, and L. A. Herzenberg, "N-acetylcysteine-a safe antidote for cysteine/glutathione deficiency," *Current Opinion in Pharmacology*, vol. 7, no. 4, pp. 355–359, 2007.

[20] L. Pendyala and P. J. Creaven, "Pharmacokinetic and pharmacodynamic studies of N-acetylcysteine, a potential chemopreventive agent during a phase I trial," *Cancer Epidemiology Biomarkers and Prevention*, vol. 4, no. 3, pp. 245–251, 1995.

[21] T. Harada, M. Momoeda, Y. Taketani, H. Hoshiai, and N. Terakawa, "Low-dose oral contraceptive pill for dysmenorrhea associated with endometriosis: a placebo-controlled, double-blind, randomized trial," *Fertility and Sterility*, vol. 90, no. 5, pp. 1583–1588, 2008.

[22] L. Muzii, F. Maneschi, R. Marana et al., "Oral estroprogestins after laparoscopic surgery to excise endometriomas: continuous or cyclic administration? Results of a multicenter randomized study," *Journal of Minimally Invasive Gynecology*, vol. 18, no. 2, pp. 173–178, 2011.

[23] L. C. Giudice, "Clinical practice. Endometriosis," *The New England Journal of Medicine*, vol. 362, no. 25, pp. 2389–2398, 2010.

[24] J. A. Maybin, H. O. D. Critchley, and H. N. Jabbour, "Inflammatory pathways in endometrial disorders," *Molecular and Cellular Endocrinology*, vol. 335, no. 1, pp. 42–51, 2011.

[25] F. M. Howard, "Endometriosis and mechanisms of pelvic pain," *Journal of Minimally Invasive Gynecology*, vol. 16, no. 5, pp. 540–550, 2009.

Hindawi Publishing Corporation
Evidence-Based Complementary and Alternative Medicine
Volume 2013, Article ID 356381, 9 pages
http://dx.doi.org/10.1155/2013/356381

Research Article

Assessing the Metabolic Effects of Aromatherapy in Human Volunteers

Yinan Zhang,[1] Yani Wu,[2] Tianlu Chen,[1] Lei Yao,[2] Jiajian Liu,[1] Xiaolan Pan,[2] Yixue Hu,[2] Aihua Zhao,[1] Guoxiang Xie,[1,3] and Wei Jia[1,3]

[1] *Center for Translational Medicine and Shanghai Key Laboratory of Diabetes Mellitus, Department of Endocrinology and Metabolism, Shanghai Jiao Tong University Affiliated Sixth People's Hospital, Shanghai 200233, China*
[2] *School of Agriculture and Biology, Shanghai Jiao Tong University, Shanghai 200240, China*
[3] *Center for Translational Biomedical Research, University of North Carolina at Greensboro, Kannapolis, NC 28081, USA*

Correspondence should be addressed to Yani Wu; ynwu@sjtu.edu.cn and Guoxiang Xie; g_xie@uncg.edu

Received 4 January 2013; Revised 12 April 2013; Accepted 14 April 2013

Academic Editor: Aiping Lu

Aromatherapy, a form of complementary and alternative medicine (CAM) that uses essential oils through inhalation, is believed to enhance physical and spiritual conditions. Although clinical studies suggest that the use of essential oils may have therapeutic potential, evidence for the efficacy of aromatherapy in treating medical conditions remains poor, with a particular lack of studies employing rigorous analytical methods that capture its identifiable impact on human biology. Here, we report a comprehensive metabolomics study that reveals metabolic changes in people after exposed to aroma inhalation for 10 continuous days. In this study, the metabolic alterations in urine of 31 females with mild anxiety symptoms exposed to aerial diffusion of aromas were measured by GC-TOF-MS and UPLC-Q-TOF-MS analyses. A significant alteration of metabolic profile in subjects responsive to essential oil was found, which is characterized by the increased levels of arginine, homocysteine, and betaine, as well as decreased levels of alcohols, carbohydrates, and organic acids in urine. Notably, the metabolites from tricarboxylic acid (TCA) cycle and gut microbial metabolism were significantly altered. This study demonstrates that the metabolomics approach can capture the subtle metabolic changes resulting from exposure to essential oils, which may lead to an improved mechanistic understanding of aromatherapy.

1. Introduction

Aromatherapy, the practice of using aromatic plant-derived essential oils for a variety of applications including mood enhancement, pain relief, and improved cognitive function, is increasingly being used in complementary and alternative medicine (CAM) units as well as primary care settings [1]. One of the methods used in aromatherapy is release of odor to a particular environment. The proposed mechanism of action of the respiratory administration of aromatherapy begins with the absorption of volatile odor molecules through the nasal mucosa. Odor molecules are then transformed into chemical signals, which travel to the olfactory bulb and then other parts of the limbic system of the brain and the cerebral cortex and the olfactory sensory center at the base of the brain, interacting with the neuropsychological framework to produce characteristic physiological and psychological effects on target tissues [2]. One study investigated the effects of various plant-derived or synthetic odors on task performance, reaction time, and autonomic parameters or evaluated the direct effects of odors on the brain via electroencephalogram patterns and functional imaging studies [3]. A lot of studies have demonstrated the antianxiety effect by essential oils from rose, lavender, lemon, and peppermint [4, 5]. These studies have consistently shown that odors can produce specific effects on human neuropsychological and autonomic function, suggesting that aromatherapy has beneficial effects in the context of stressful and adverse psychological conditions.

In recent years, researchers have studied the components of essential oil that have antianxiety effect and possible molecular principles. Umezu et al. [6] from Japan analyzed the antianxiety components of essential oil from lavender using GC-MS and identified linalool as the main antianxiety

pharmacological substance. Komiya et al. [7] studied the antianxiety effect of essential oil from rose, lavender, and lemon. They also researched the linkage of essential oil from lemon with benzodiazepine, 5-hydroxy tryptamine, dopamine, and adrenergic receptor and found essential oil from lemon increasing the nerve-energy of 5-hydroxy tryptamine from the suppression the activity of dopamine. Umezu [8] studied that dopamine might be involved in the mouse ambulation promoted by peppermint oil and its constituents. Wu et al. [9] have done a thorough metabolomic study on rats' brain tissue and urinary responses to aromatherapy. These metabolic changes include the increased carbohydrates and lowered levels of neurotransmitters (tryptophan, serine, glycine, aspartate, histamine, tyrosine, cysteine, phenylalanine, hypotaurine, histidine, and asparagine), amino acids, and fatty acids in brain. Elevated aspartate, carbohydrates (sucrose, maltose, fructose, and glucose), nucleosides (adenine and uridine), and organic acids such as lactate and pyruvate were also observed in urine.

Despite of the numerous results demonstrating beneficial effects on mood and relaxation observed in behavioral and emotional studies, evidence for the efficacy and mechanistic understanding of aromatherapy in treating medical conditions remains poor, with a particular lack of studies employing rigorous methodology [10, 11].

Here, we report a metabolomic study designed to evaluate the effect of an essential oil preparation in university female students. Urine samples were collected and analyzed by both gas chromatography time-of-flight mass spectrometry (GC-TOFMS) and ultraperformance liquid chromatography-quadrupole time-of-flight mass spectrometry (UPLC-QTOFMS) in conjunction with multivariate statistical analysis, including principal component analysis (PCA), partial least squares discriminant analysis (PLS-DA), and orthogonal partial least squares-discriminant analysis (OPLS-DA), to obtain significant endogenous metabolite markers of aromas-exposure.

2. Methods

2.1. Chemicals and Materials. The essential oil used in the study is the same as used in our previous report [9], prepared from 4 aromatic plants, *Lavandula angustifolia and Salvia sclarea L.* from China, *Santalum album* from India, and *Citrus sinensis* from the United States. The constituents of the essential oil were assayed by gas chromatography (GC) and GC-mass spectrometry (GC-MS) and were mainly limonene, linalool, linalyl acetate, polysantol, and other 30 chemicals (the detailed chemical composition of the essential oil was shown in our previous paper [9]). Acetonitrile and methanol of HPLC grade were obtained from Merck Chemicals (Darmstadt, Germany). Analytical-grade methanol was obtained from the Shanghai Lin Feng Chemical Reagent Co, Ltd. (China). All aqueous solutions were prepared with ultrapure water produced by a Milli-Q system (18.2 MΩ, Millipore, Bedford, MA). Chloroform was analytical grade and purchased from China National Pharmaceutical Group Corporation (Shanghai, China). L-2-Chlorophenylalanine was purchased from Intechem Tech. Co. Ltd. (Shanghai, China). BSTFA (1% TMCS), heptadecanoic acid, and methoxyamine were purchased from Sigma-Aldrich (St. Louis, MO).

2.2. Human Sample Treatment. Fifty-two female volunteers who were not allergic to essential oil with an average age of 20.29 ± 1.51 years from Shanghai Jiao Tong University were recruited in this study. They were allowed to do a double blind Symptom Check List-90 (SCL90) test. The checklist consists of nine subscales including somatization (SOM), obsessive-compulsive (O-C), interpersonal sensitivity (I-S), depression (DEP), anxiety (ANX), hostility (HOS), phobic anxiety (PHOB), paranoid ideation (PAR), and psychoticism (PSY). Thirty-one volunteers who have at least one subscale with a score over 2.0 were subject to the further study. We have arranged a quiet classroom (100 m^2, room temperature = 24 ± 1°C, and room humidity = 45 ± 15%) for the experiment. The doors and windows of the room were closed 15 minutes before the examination and in which the environment was fragranced by incenses of the essential oil. The examination was performed in the atmosphere of the aroma, and the doors and windows of the classroom were kept close until the end of the examination. The duration of the examination was 45 minutes a day for 10 continuously days. All the volunteers were required to eat only blander food in the 10 days and stay quietly (reading and writing) in the room. Urine samples were collected on day 0 (before exposed to essential oil inhalation, BE) and day 10 (after exposed to essential oil inhalation, AE). The protocol was approved by the Shanghai Jiao Tong University Review Board, and all participants gave informed consent before they were involved in the study.

2.3. Urine Sample Preparation for GC-TOFMS Analysis. Urine metabolites were chemically derivatized prior to mass spectrometry analysis following our previously published procedure with minor modifications [12]. An aliquot of 100 μL urine sample was spiked with two internal standard solutions (10 μL of L-2-chlorophenylalanine in water, 0.3 mg/mL; 10 μL of heptadecanoic acid in methanol, 1 mg/mL) and vortexed for 10 s. The mixed solution was extracted with 300 μL of methanol/chloroform (3 : 1) and vortexed for 30 s. After storing for 10 min at −20°C, the samples were centrifuged at 12 000 rpm for 10 min. An aliquot of the 300 μL supernatant was transferred to a glass sampling vial to vacuum-dry at room temperature. The residue was derivatized using a two-step procedure. First, 80 μL of methoxyamine (15 mg/mL in pyridine) was added to the vial and kept at 30°C for 90 min, followed by 80 μL of BSTFA (1% TMCS) at 70°C for 60 min.

2.4. GC-TOFMS Analysis. A 1 μL aliquot of the derivatized solution was injected in splitless mode into an Agilent 6890 N gas chromatograph coupled with a Pegasus HT time-of-flight mass spectrometer (Leco Corporation, St. Joseph, MI). Separation was achieved on a DB-5ms capillary column (30 m × 250 μm i.d., 0.25 μm film thickness; (5%-phenyl)-methylpolysiloxane bonded and cross-linked; Agilent J&W Scientific, Folsom, CA), with helium as the carrier gas at

a constant flow rate of 1.0 mL/min. The temperature of injection, transfer interface, and ion source was set to 270, 260, and 200°C, respectively. The GC temperature programming was set to 2 min isothermal heating at 80°C, followed by 10°C/min oven temperature ramps to 180°C, 5°C/min to 240°C, and 25°C/min to 290°C, and a final 9 min maintenance at 290°C. Electron impact ionization (70 eV) at full scan mode (m/z 30–600) was used, with an acquisition rate of 20 spectra/s in the TOFMS setting.

2.5. Urine Sample Preparation for UPLC-QTOFMS Analysis. Urine samples were preliminarily treated following our previously published procedure with minor modifications [12]. The collected urine samples were centrifuged at 13,000 rpm for 10 min at 4°C, and the resulting supernatants were immediately stored at −80°C pending UPLC-QTOFMS analysis. Also, 600 μL of ultrapure water (containing 5 μg/mL L-2-chlorophenylalanine as the internal standard) was added to urine (300 μL) and vortexed for 1 min and then filtered through a syringe filter (0.22 μm) and placed into the sampling vial pending UPLC-QTOFMS analysis.

2.6. UPLC-QTOFMS Analysis. Urine metabolite profiling was performed using a Waters ACQUITY UPLC system equipped with abinary solvent delivery manager and a sample manager (Waters Corporation, Milford, MA), coupled to a Micromass Q-TOF Premiermass spectrometer equipped with an electrospray interface (Waters Corporation, Milford, MA). Chromatographic separations were performed on a 2.1 × 100 mm 1.7 μm ACQUITY BEH C_{18} chromatography column. The column was maintained at 45°C and eluted with a 1%–99% acetonitrile (0.1% (v/v) formic acid)-aqueous formic acid (0.1% (v/v) formic acid) gradient over 10 min at a flow rate of 0.40 mL/min. A 5 μL aliquot sample was injected onto the column. The mass accuracy analysis and detailed MS parameters were optimized according to our previous work [12]. During metabolite profiling experiments, centroid data were acquired for each sample from 50 to 1000 Da with a 0.10 s scan time and a 0.01 s interscan delay over a 10 min analysis time.

2.7. Data Analysis. The acquired MS files from GC-TOFMS analysis were exported in NetCDF format by ChromaTOF software (v3.30, Leco Co., CA). CDF files were extracted using custom scripts (revised Matlab toolbox hierarchical multivariate curve resolution (H-MCR), developed by Par Jonsson et al. [13, 14] in the MATLAB 7.0 (The MathWorks, Inc.) for data pretreatment procedures such as baseline correction, denoising, smoothing, alignment, time-window splitting, and multivariate curve resolution (based on multivariate curve resolution algorithm)) [14]. The resulting three-dimensional data set included sample information, peak retention time, and peak intensities. Internal standards and any known artificial peaks, such as peaks caused by noise, column bleed, and BSTFA derivatization procedure, were removed from the data set. Additionally, compound identification was performed by comparing the mass fragments with NIST 05 standard mass spectral databases in NIST MS search 2.0 (NIST, Gaithersburg, MD) software with a similarity of more than 70% and finally verified by available reference compounds.

The UPLC-QTOFMS raw data were analyzed by the MarkerLynx Applications Manager version 4.1 (Waters, Manchester, UK) using parameters reported in our previous work [15]. A list of the ion intensities of each peak detected was generated, using retention time (RT) and the m/z data pairs as the identifier for each ion. The resulting three-dimensional matrix contained arbitrarily assigned peak indexes (retention time-m/z pairs), sample names (observations), and ion intensity information (variables). To obtain consistent differential variables, the resulting matrix was further reduced by removing any peaks with missing value (ion intensity) in more than 40% of the samples from both groups. The ion peaks generated by the internal standard were also removed. The data was then normalized by the sum of all peak intensities within the sample.

Then, the GC-TOFMS and UPLC-QTOFMS were put together and unit variance scaled during chemometric data analysis in the SIMCA-P + 13.0 Software package (Umetrics, Umeå, Sweden). Partial least squares-discriminant analysis (PLS-DA) was carried out to discriminate between different groups. On the basis of a variable importance in the projection (VIP) threshold of 1 from the PLS-DA model, a number of metabolites responsible for the difference in the metabolic profiles between two groups could be obtained. In parallel, the metabolites identified by the PLS-DA model were validated at a univariate level using the Student's t-test with the critical P value set to 0.05. The resultant P values for all metabolites were subsequently adjusted to account for multiple testing. The corresponding fold change shows how these selected differential metabolites varied between groups.

3. Results and Discussion

3.1. SCL-90 Test. The 31 volunteers were given the test before being exposed to essential oil inhalation and after being exposed to essential oil inhalation for 10 days, and the result was shown in Table 1. The values of normal Chinese University students were also included [16]. The BE values of the 31 volunteers are a little bit higher than the normal values which indicated that they were under slight anxiety. The AE values are lower or similar to the normal value which indicated they relieved their stress after inhaling the essential oil for 10 days.

3.2. Metabolic Profile of GC-TOFMS and UPLC-QTOFMS Analysis. A wide range of carbohydrates, amino acids, organic acids, and alcohols were detected using GC-TOFMS and UPLC-QTOFMS analyses of urine. Among a total of 388 chromatographic features obtained from the GC-TOFMS spectra of urine samples, 134 metabolites were identified with NIST 05 standard mass spectral databases with a similarity >70%, and 83 were further verified by available reference standards, respectively. Altogether, 5690 peaks were detected with our optimized UPLC-QTOFMS analysis protocol. And we were able to confirm 111 from reference standards and HMDB. These two datasets were normalized and put

Table 1: SCL-90 test checklist for volunteers before being exposed to essential oil inhalation and after being exposed to essential oil inhalation for 10 days.

Subscales	BE	AE	P	Norm of China (2008) (n = 9941)
SOM	1.59 ± 0.40	1.37 ± 0.36	0.03*	1.45 ± 0.49
O-C	2.40 ± 0.63	1.93 ± 0.66	0.01*	1.98 ± 0.63
I-S	2.80 ± 0.61	1.75 ± 0.63	0.04*	1.88 ± 0.63
DEP	1.97 ± 0.61	1.68 ± 0.54	0.05	1.74 ± 0.62
ANX	2.03 ± 0.73	1.65 ± 0.65	0.03*	1.61 ± 0.55
HOS	1.83 ± 0.66	1.49 ± 0.45	0.02*	1.61 ± 0.62
PHOB	1.55 ± 0.55	1.29 ± 0.39	0.03*	1.38 ± 0.49
PAR	1.74 ± 0.58	1.58 ± 0.48	0.22	1.72 ± 0.62
PSY	1.86 ± 0.60	1.57 ± 0.45	0.04*	1.59 ± 0.54
OTHER	1.98 ± 0.70	1.66 ± 0.59	0.06	—

Compared with BE; * $P < 0.05$.

together, and at last 215 metabolites were identified after combination. Figure 1(a) illustrates the scores plots of PLS-DA model of the subjects from BE and AE group. It is showed that 11 people are vulnerable to essential oil (Vulnerable group before being exposed to essential oil inhalation, VBE, and Vulnerable group after being exposed to essential oil inhalation, VAE), while the other 20 are invulnerable to essential oil (Invulnerable group before being exposed to essential oil inhalation, IBE, and Invulnerable group after being exposed to essential oil inhalation, IAE) (Figure 1(b)).

The trend of separation can be seen from the PCA scores plot between VBE and VAE groups using only identified metabolites as shown in Figure 2(a) (R2X = 0.306). We selected the differentially expressed urine metabolites in the VBE group relative to VAE group based on the VIP values (VIP > 1) by OPLS models with 1 predictive component and 2 orthogonal components (R2X = 0.333, R2Y = 0.979, and Q^2(cum) = 0.484) (Figure 2(b)) constructed with the identified metabolites. Univariate statistical analysis, Student's t-test, was performed on these metabolites to evaluate their significance. Differentially expressed metabolites in urine were obtained with a P value less than 0.05 (Table 2). All these metabolites remained statistically significant after multiple testing. On the other hand, there is no separation trend between IBE and IAE groups from the PCA scores plot, and the Q^2(cum) of the OPLS model is below zero; these illustrated that there is no significant difference between IBE and IAE groups on the level of metabolites.

3.3. Daily Exposure to Aromas Induces Significant Metabolic Changes. We detected 29 differentially expressed metabolites induced by aromas inhalation in human urine (Figure 3 and Table 2), which include a number of carbohydrates, alcohols, organic acids, and amino acids. As compared to themselves before being exposed to essential oil inhalation, people after being exposed to essential oil inhalation were characterized by higher levels of arginine, homocysteine, and betaine, lower levels of alcohols (threitol, sorbitol, and histidinol), carbohydrate (inositol, sucrose, and xylose), pyrimidine (uracil), and organic acids (hippurate, benzoate, methylmalonate, gluconate, ferulate, pipecolinic acid, homovanillate, 4-hydroxybenzoate, 4-hydroxyphenylacetic acid, threonic acid, glycerate, phenol, cis-aconite acid, and succinate).

Aromatherapy, a form of inexpensive and noninvasive CAM, uses of essential oils, the scented, volatile liquid substances extracted from plants using steam or pressure, which dates back centuries for the purpose of altering a person's mind, mood, cognitive function, or health [17]. Although there were already some findings on the pharmacological effect and mechanism of essential oil, most of them were in the field of behavioral and emotional science [18–20]. The effects of essential oil were evaluated from senses and experiences; thus, it is hard to scientifically assess and explain aromatherapy. This paper, however, is focused on using recent developed metabolomics technology to evaluate this CAM intervention by understanding metabolic variations.

From our previous publication [11], we found that alkenes, esters, and alcohols are the main constituents of the essential oil. None of them has been detected in our profiling data in human urine, which means that all the changes that we found were due to endogenous change and not due to breathe in extrinsic substances.

The result of SCL90 (Table 1) demonstrated that ANX and PHOB from 31 people after being exposed to essential oil inhalation were significantly different from themselves before being exposed to essential oil inhalation. Also, O-C and DEP were significantly different as well. This indicated that the essential oil used in this study not only relaxes anxious moods, but also has some effect on other psychological health. It does have some effect on mood adjustment, and it is in agreement with previous publications [4, 19, 20].

However, from our metabolomics results (Figure 1), it is found that some people's metabolic profiles were not changed much after aromatherapy while others were significantly altered. This is because individual experience of an odour may also affect response. The marked association of odours with emotional response is due to the prominence of afferent links from the olfactory bulb to the amygdala, where emotional significance is attached to incoming stimuli [21]. Consequently, study participants for whom a particular odour has strong negative (or positive) associations may be

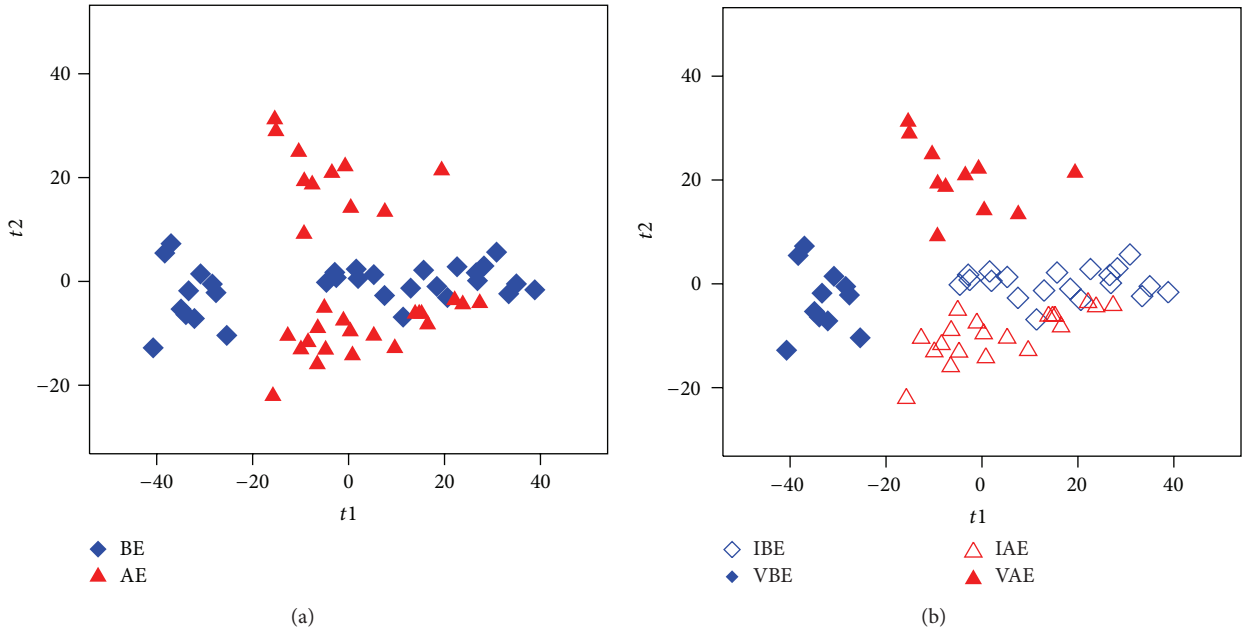

Figure 1: Metabolic profiles depicted by PLS-DA scores plot of GC-TOFMS and UPLC-QTOFMS spectral data from human urine of (a) BE group and AE group; (b) IBE group, VBE group, IAE group, and VAE group.

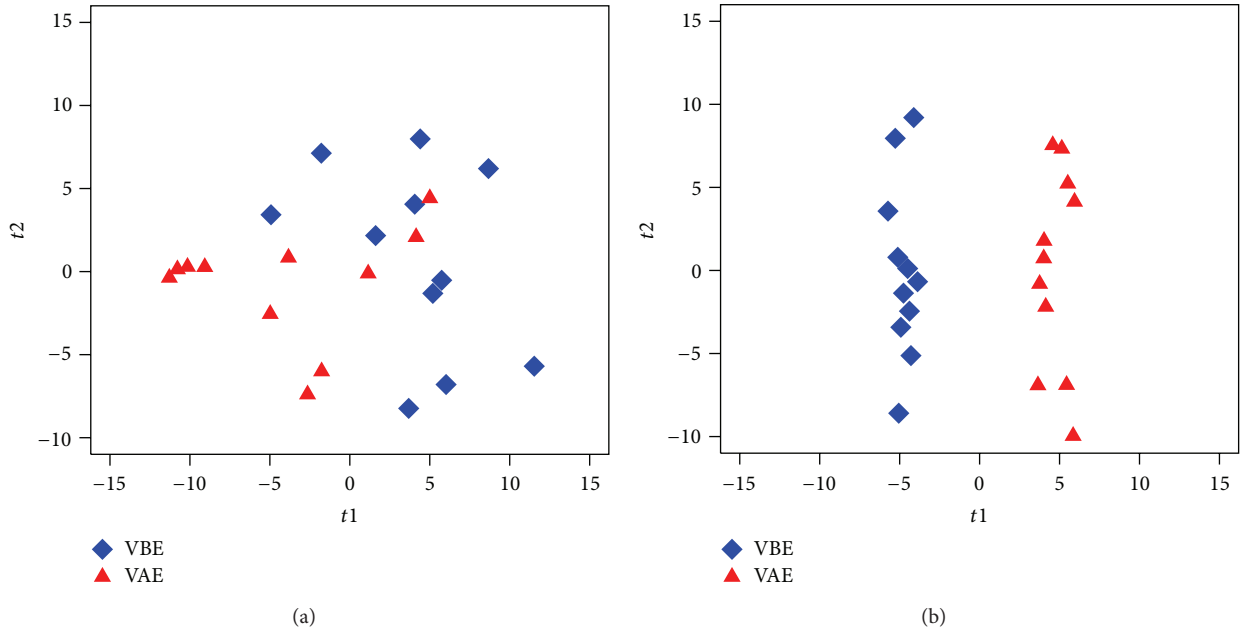

Figure 2: Metabolic profiles depicted by PCA scores plot (a) and OPLS scores plot (b) from the VBE group and VAE group with only identified metabolites.

expected to introduce further interindividual variability in outcome measures [22]. Hence, only eleven people out of 31 were susceptible to aromatherapy of this specific essential oil (Figure 1(b)).

An interesting finding of our analysis suggests the decreased carbohydrates in urine that are critically involved in the metabolic perturbation are derived from inhalation of aromas. Carbohydrates have been shown in several reports that have anxiolytic effects [23], and the significantly decreased levels of carbohydrates in urine may be due to the therapeutic effects of aromatherapy on anxiety. VAE group has a much lower level of Inositol than the VBE group. Myoinositol has been shown to have antidepressant and anxiolytic activities in both humans and animals [24, 25]. Also of interest is the finding that several energy metabolism related metabolites, including cis-aconitic acid, succinate,

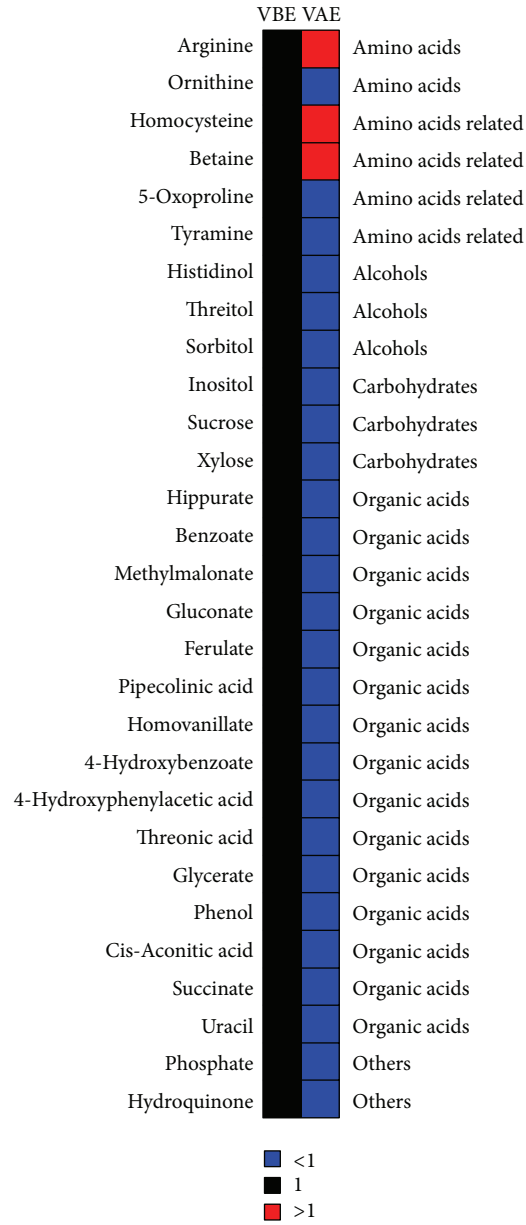

Figure 3: Heat map showing changes in metabolites in urine after being exposed to essential oil inhalation for 10 days (VAE group) to themselves before being exposed to essential oil inhalation (VBE group). Shades of red and blue represent fold increase and fold decrease of a metabolite, respectively, in VAE group relative to VBE group (see color scale).

and hydroquinone, were found at different levels between the VAE and VBE groups. It was found that oxidative stress was involved in the pathogenesis of neurological diseases, such as psychiatric disorders [26, 27] and anxiety [28, 29]. Oxidative stress is caused by altered mitochondrial energy pathways leading to abundant reactive oxidative stress compounds. It is therefore not surprising that metabolites and carbohydrates involved in TCA cycle were found to be significantly different between the VAE and VBE groups.

It is believed that there was a strong relationship between gastrointestinal symptoms and anxiety [30]. Changes of gastrointestinal functional ecology are directly linked to gut microbial populations and activities [31]. Urine of mammals contains many polar metabolites resulting from gut microbial-mammalian cometabolism [31, 32]. Therefore, metabolic variations of urinary excretion of many aromatic compounds (e.g., phenolics, indoles, and benzoyl derivatives) provide indirect information on the gut microbial metabolic activities [33]. Hippurate, 4-hydroxybenzoate, 4-hydroxyphenylacetic acid, benzoate, tyramine, and phenol were all significantly decreased in VAE group, reflecting an altered gut microbial metabolism associated with aromatherapy. Metabolite profiling of urine in this study revealed an entire lower level of gut microbe related metabolites after being exposed to essential oil inhalation for 10 days.

The aim of this study was to obtain metabolite markers in urine of human exposed to essential oil to gain mechanistic insights into the metabolic impact of aromatherapy. However,

Table 2: List of differential metabolites in urine after being exposed to essential oil inhalation for 10 days (VAE group) to themselves before being exposed to essential oil inhalation (VBE group).

Classes	Metabolites	VIP[1]	FC[2]	P[3]
Amino acids	Arginine	1.80	3.76	$2.44E-02$
	Ornithine	1.78	0.50	$2.66E-02$
Amino acids related	Homocysteine	1.98	2.05	$1.21E-02$
	Betaine	2.21	1.79	$4.21E-03$
	5-Oxoproline	2.03	0.61	$9.76E-03$
	Tyramine	2.58	0.47	$4.49E-04$
Alcohols	Histidinol	1.66	0.34	$4.02E-02$
	Threitol	2.77	0.48	$9.66E-05$
	Sorbitol	1.98	0.16	$1.19E-02$
Carbohydrates	Inositol	2.48	0.53	$8.67E-04$
	Sucrose	1.97	0.27	$1.29E-02$
	Xylose	1.90	0.61	$1.68E-02$
Organic acids	Hippurate	1.99	0.17	$1.14E-02$
	Benzoate	2.28	0.34	$2.90E-03$
	Methylmalonate	1.94	0.62	$1.42E-02$
	Gluconate	1.76	0.70	$2.86E-02$
	Ferulate	1.65	0.37	$4.20E-02$
	Pipecolinic acid	1.62	0.74	$4.60E-02$
	Homovanillate	2.34	0.40	$2.11E-03$
	4-Hydroxybenzoate	1.75	0.48	$2.93E-02$
	4-Hydroxyphenylacetic acid	1.99	0.44	$1.14E-02$
	Threonic acid	2.52	0.57	$6.78E-04$
	Glycerate	2.41	0.56	$1.38E-03$
	Phenol	1.80	0.49	$2.42E-02$
	Cis-Aconitic acid	1.91	0.53	$1.65E-02$
	Succinate	2.16	0.52	$5.23E-03$
Pyrimidine	Uracil	1.99	0.54	$1.16E-02$
Others	Phosphate	2.24	0.69	$3.48E-03$
	Hydroquinone	1.74	0.55	$3.08E-02$

[1]Variable importance in the projection (VIP) was obtained from PLS-DA model with a threshold of 1.0;
[2]fold change (FC) was obtained by comparing those metabolites in VAE group to VBE group;
[3]P values were calculated from Student's t-test;
FC with a value >1 indicates a relatively higher concentration present in VAE group, while a value <1 means a relatively lower concentration as compared to VBE.

there are limitations in the current metabolomic study. First, the sample size was a little bit small especially for people vulnerable to this essential oil. More people and longer essential oil inhale time may be tested in future study. Second, only urine was used in the experiments, and because of the blood-brain barrier, the metabolism of the brain is independent of peripheral circulation, and, hence, the metabolic variances induced by aromas inhalation were different between urine and brain. Additional mechanistic information and metabolite markers may be identified with brain tissue.

In conclusion, we identified the global metabolic responses to aromatherapy characterized by unique metabolic signatures in human urine involving carbohydrates, organic acids, amino acids, and pyrimidine. The metabolites involved in TCA cycle and gut microbe metabolism were significantly decreased after being exposed to essential oil inhalation for 10 days. These distinctions collectively constitute a metabolic window into essential oil effect, providing metabolic endpoints that complement the interpretation of behavioral research. The results of this study also highlight the potential of this sufficiently robust and noninvasive profiling approach for research on the CAM of aromatherapy.

Abbreviations

GC-TOF-MS: Gas chromatography time-of-flight mass spectrometry
UPLC-Q-TOFMS: Ultraperformance liquid chromatography-quadrupole time-of-flight mass spectrometry
CAM: Complementary and alternative medicine
PLS-DA: Partial least squares discriminant analysis
PCA: Principal component analysis

OPLS-DA: Orthogonal partial least squares-discriminant analysis
BE: Before exposed to essential oil inhalation
AE: After exposed to essential oil inhalation
VBE: Vulnerable group before exposed to essential oil inhalation
VAE: Vulnerable group after exposed to essential oil inhalation
IBE: Invulnerable group before exposed to essential oil inhalation
IAE: Invulnerable group after exposed to essential oil inhalation.

Acknowledgments

This work was financially supported by Drug Innovation Program of National Science and Technology Project (2011ZX09307-001-02), Shanghai Science and Technology funds (12DZ2295004).

References

[1] M. S. Lee, J. Choi, P. Posadzki, and E. Ernst, "Aromatherapy for health care: an overview of systematic reviews," *Maturitas*, vol. 71, no. 3, pp. 257–260, 2012.

[2] M. Lis-Balchin, "Essential oils and "aromatherapy": their modern role in healing," *Journal of the Royal Society of Health*, vol. 117, no. 5, pp. 324–329, 1997.

[3] G. Buchbauer, L. Jirovetz, W. Jager, C. Plank, and H. Dietrich, "Fragrance compounds and essential oils with sedative effects upon inhalation," *Journal of Pharmaceutical Sciences*, vol. 82, no. 6, pp. 660–664, 1993.

[4] J. Lehrner, G. Marwinski, S. Lehr, P. Johren, and L. Deecke, "Ambient odors of orange and lavender reduce anxiety and improve mood in a dental office," *Physiology and Behavior*, vol. 86, no. 1-2, pp. 92–95, 2005.

[5] B. F. Bradley, N. J. Starkey, S. L. Brown, and R. W. Lea, "The effects of prolonged rose odor inhalation in two animal models of anxiety," *Physiology and Behavior*, vol. 92, no. 5, pp. 931–938, 2007.

[6] T. Umezu, K. Nagano, H. Ito, K. Kosakai, M. Sakaniwa, and M. Morita, "Anticonflict effects of lavender oil and identification of its active constituents," *Pharmacology Biochemistry and Behavior*, vol. 85, no. 4, pp. 713–721, 2006.

[7] M. Komiya, T. Takeuchi, and E. Harada, "Lemon oil vapor causes an anti-stress effect via modulating the 5-HT and DA activities in mice," *Behavioural Brain Research*, vol. 172, no. 2, pp. 240–249, 2006.

[8] T. Umezu, "Evidence for dopamine involvement in ambulation promoted by pulegone in mice," *Pharmacology Biochemistry and Behavior*, vol. 94, no. 4, pp. 497–502, 2010.

[9] Y. N. Wu, Y. N. Zhang, G. X. Xie et al., "The metabolic responses to aerial diffusion of essential oils," *PLOS One*, vol. 7, no. 9, Article ID e44830, 2012.

[10] G. van der Watt and A. Janca, "Aromatherapy in nursing and mental health care," *Contemporary Nurse*, vol. 30, no. 1, pp. 69–75, 2008.

[11] A. E. Edris, "Pharmaceutical and therapeutic potentials of essential oils and their individual volatile constituents: a review," *Phytotherapy Research*, vol. 21, no. 4, pp. 308–323, 2007.

[12] Y. Ni, M. Su, Y. Qiu et al., "Metabolic profiling using combined GC-MS and LC-MS provides a systems understanding of aristolochic acid-induced nephrotoxicity in rat," *FEBS Letters*, vol. 581, no. 4, pp. 707–711, 2007.

[13] P. Jonsson, J. Gullberg, A. Nordström et al., "A strategy for identifying differences in large series of metabolomic samples analyzed by GC/MS," *Analytical Chemistry*, vol. 76, no. 6, pp. 1738–1745, 2004.

[14] P. Jonsson, A. I. Johansson, J. Gullberg et al., "High-throughput data analysis for detecting and identifying differences between samples in GC/MS-based metabolomic analyses," *Analytical Chemistry*, vol. 77, no. 17, pp. 5635–5642, 2005.

[15] G. Xie, R. Plumb, M. Su et al., "Ultra-performance LC/TOF MS analysis of medicinal Panax herbs for metabolomic research," *Journal of Separation Science*, vol. 31, no. 6-7, pp. 1015–1026, 2008.

[16] W. S. Zhong and L. Li, "Research on the new SCL-90 model on Chinese university students," *Chinese Journal of School Doctor*, vol. 23, no. 3, pp. 251–256, 2009.

[17] National Cancer Institute, U. S. N. I. o. H. Aromatherapy and essential oils (PDQs), http://www.cancer.gov/cancertopics/pdq/cam/aromatherapy/HealthProfessional.

[18] B. F. Bradley, N. J. Starkey, S. L. Brown, and R. W. Lea, "Anxiolytic effects of Lavandula angustifolia odour on the Mongolian gerbil elevated plus maze," *Journal of Ethnopharmacology*, vol. 111, no. 3, pp. 517–525, 2007.

[19] D. Shaw, J. M. Annett, B. Doherty, and J. C. Leslie, "Anxiolytic effects of lavender oil inhalation on open-field behaviour in rats," *Phytomedicine*, vol. 14, no. 9, pp. 613–620, 2007.

[20] M. M. Blanco, C. A. R. A. Costa, A. O. Freire, J. G. Santos, and M. Costa, "Neurobehavioral effect of essential oil of Cymbopogon citratus in mice," *Phytomedicine*, vol. 16, no. 2-3, pp. 265–270, 2009.

[21] D. L. Clark and N. N. Boutros, *The Brain and Behaviour: An Introduction to Behavioural Neuroanatomy*, Blackwell Science, Oxford, UK, 1999.

[22] C. Holmes and C. Ballard, "Aromatherapy in dementia," *Advances in Psychiatric Treatment*, vol. 10, no. 4, pp. 296–300, 2004.

[23] L. M. Chepulis, N. J. Starkey, J. R. Waas, and P. C. Molan, "The effects of long-term honey, sucrose or sugar-free diets on memory and anxiety in rats," *Physiology and Behavior*, vol. 97, no. 3-4, pp. 359–368, 2009.

[24] J. Benjamin, J. Levine, M. Fux, A. Aviv, D. Levy, and R. H. Belmaker, "Double-blind, placebo-controlled, crossover trial of inositol treatment for panic disorder," *American Journal of Psychiatry*, vol. 152, no. 7, pp. 1084–1086, 1995.

[25] H. Einat and R. H. Belmaker, "The effects of inositol treatment in animal models of psychiatric disorders," *Journal of Affective Disorders*, vol. 62, no. 1-2, pp. 113–121, 2001.

[26] J. Bouayed, H. Rammal, and R. Soulimani, "Oxidative stress and anxiety Relationship and cellular pathways," *Oxidative Medicine and Cellular Longevity*, vol. 2, no. 2, pp. 63–67, 2009.

[27] F. Ng, M. Berk, O. Dean, and A. I. Bush, "Oxidative stress in psychiatric disorders: evidence base and therapeutic implications," *International Journal of Neuropsychopharmacology*, vol. 11, no. 6, pp. 851–876, 2008.

[28] M. Kuloglu, M. Atmaca, E. Tezcan, B. Ustundag, and S. Bulut, "Antioxidant enzyme and malondialdehyde levels in patients with panic disorder," *Neuropsychobiology*, vol. 46, no. 4, pp. 186–189, 2002.

[29] S. Ersan, S. Bakir, E. Erdal Ersan, and O. Dogan, "Examination of free radical metabolism and antioxidant defence system elements in patients with obsessive-compulsive disorder," *Progress in Neuro-Psychopharmacology and Biological Psychiatry*, vol. 30, no. 6, pp. 1039–1042, 2006.

[30] T. T. Haug, A. Mykletun, and A. A. Dahl, "Are anxiety and depression related to gastrointestinal symptoms in the general population?" *Scandinavian Journal of Gastroenterology*, vol. 37, no. 3, pp. 294–298, 2002.

[31] G. W. Tannock, "New perceptions of the gut microbiota: implications for future research," *Gastroenterology Clinics of North America*, vol. 34, no. 3, pp. 361–382, 2005.

[32] I. K. S. Yap, J. V. Li, J. Saric et al., "Metabonomic and microbiological analysis of the dynamic effect of vancomycin-lnduced gut microbiota modification in the mouse," *Journal of Proteome Research*, vol. 7, no. 9, pp. 3718–3728, 2008.

[33] X. Zheng, G. Xie, A. Zhao et al., "The footprints of gut microbial-mammalian co-metabolism," *Journal of Proteomic Research*, vol. 10, no. 12, pp. 5512–5522, 2011.

Hindawi Publishing Corporation
Evidence-Based Complementary and Alternative Medicine
Volume 2013, Article ID 718305, 10 pages
http://dx.doi.org/10.1155/2013/718305

Research Article

Metabonomic Strategy to the Evaluation of Chinese Medicine Compound Danshen Dripping Pills Interfering Myocardial Ischemia in Rats

Xue Xin,[1] Haimiao Zou,[1] Ningning Zheng,[2] Xinchun Xu,[3] Yinmin Liu,[1] Xiaoxian Wang,[1] Hongbing Wu,[1] Lina Lu,[1] Jing Su,[1] Mingfeng Qiu,[1] and Xiaoyan Wang[4]

[1] *School of Pharmacy, Shanghai Jiao Tong University, Shanghai 200240, China*
[2] *Research Center for Traditional Chinese Medicine and Systems Biology, Shanghai University of Traditional Chinese Medicine, Shanghai 201203, China*
[3] *Xuhui District Central Hospital of Traditional Chinese Medicine, Shanghai 200031, China*
[4] *Ministry of Education, Key Laboratory of Systems Biomedicine, Shanghai Center for Systems Biomedicine, Shanghai Jiao Tong University, Shanghai 200240, China*

Correspondence should be addressed to Mingfeng Qiu; mfqiu@sjtu.edu.cn and Xiaoyan Wang; cathywxy@126.com

Received 4 January 2013; Revised 17 March 2013; Accepted 29 March 2013

Academic Editor: Rong Zeng

Coronary heart disease (CHD) is one of the highest mortality diseases in the world. Traditional Chinese medicine compound Danshen dripping pills (CDDPs) have currently made a great achievement in treating CHD. However, the therapeutic mechanism of CDDP is often poorly interpreted. In this study, a GC-MS-based metabonomic study was conducted to assess the holistic efficacy of CDDP for myocardial infarction in male Sprague-Dawley rats, which were divided into the control group, the sham group, the model group, the control + CDDP group, and the model + CDDP, with CDDP at a dose of 107 mg/kg·d (equal to 1.8 mL/kg·d). The metabonomic findings demonstrated great differences of metabolic pattern among sham, model, and the model + CDDP in the orthogonal partial least squares discriminant analysis (OPLS-DA) models, which coordinated well with the assessment of plasma biochemistry and histopathological assay. Differentially expressed metabolites suggested that energy metabolism, glycolysis, and lipid metabolism might be disrupted by myocardial infarction. Both the potential metabolic biomarkers and the biochemical histopathological indices were regulated effectively by CDDP.

1. Introduction

Coronary heart disease (CHD) is caused by atherosclerotic coronary artery stenosis, leading to insufficient blood supply of coronary, myocardial ischemia (MI), and heart attack. CHD, including its most serious complication MI, is the most common cause of death in industrialized countries, and the morbidity is increasing dramatically in developing countries [1]. The effectiveness of current antiischemic medicines, for example, β-blockers or calcium channel blockers, nitroglycerin, and angiotensin inhibitors, is limited by their side effects, such as hypotension and bradycardia [2]. With little side effect, significant effect, and a unique medical theory, especially by hitting multiple targets with the combination and compatibility of multicomponents drugs, traditional Chinese medicine (TCM) is getting more recognition in current researches.

Compound Danshen dripping pills (CDDPs, *Fufang Danshen Diwan* in Chinese) are developed on the basis of TCM theory and modern preparation technologies, consisting of *Radix salvia miltiorrhizae, Radix notoginseng*, and *Borneolum* [3]. With its multi-components, multieffects, and multitargets characters, CDDPs are generally applied in the prevention and treatment of coronary arteriosclerosis, angina pectoris, and hyperlipaemia in China [4], which leads to phase II clinical research in the USA in 2010 [5]. However, the widely employment of CDDPs is still facing a bottleneck in the United States of America and some European countries, not

only because of the complex compounds, but also because of lack of an overall systemic evaluation and a standard to refer.

The emergency of metabolomics/metabolomics technology, which applies multivariate statistical techniques to analyze the highly complex data sets generated by advanced analytic instruments, such as nuclear magnetic resonance (NMR) and mass spectrometry (MS), has provided an opportunity for the resolution of this issue [6]. Metabonomics reflects the function of organisms from the end products of the metabolic network and the metabolic changes of a complete system caused by interventions in a holistic context [7]. This property accords with the holistic thinking of TCM, suggesting that metabonomics has a potential impact on our understanding of the theory behind the evidence-based TCM [8]. Consequently, metabonomics has been successfully utilized in understanding many aspects of TCM, such as the analysis of Chinese herbs [9], Chinese medicine syndromes [10], the mechanisms of Chinese medicine [11], and safety assessment [12].

Up to date, global metabolic profiling of biofluids (e.g., urine and sera) has been used meaningfully in understanding and biomarker detection of CHD [13], especially in the early diagnosis [14] and classification of Chinese syndromes of CHD [15, 16]. In the present study, combined with conventional pharmacological approaches, the metabonomic method is sought to be applied to investigate the change of endogenous metabolites in MI rats based on coronary artery ligation.

The finding of biopathways and potential biomarkers will be helpful in clarifying the mechanism of CDDP in treating MI.

2. Materials and Methods

2.1. Chemicals and Animals. HPLC grade methanol was purchased from Merck; HPLC grade chloroform and pyridine were purchased from Tedia. The following compounds were obtained from Sigma-Aldrich (St. Louis, MO, USA): O-methoxamine-HCL, bis (trimethylsilyl)-trifluoroacetamide (BSTFA, with 1% trimethylchlorosilane, TMCS), heptadecanoic acid, L-2-chlorophenylglycine, myristic acid, and urease. The assay kits for creatine kinases (CK), superoxide dismutase (SOD), and malondialdehyde (MDA) were purchased from Nanjing Jiancheng Bioengineering Institute (Nanjing, China). CDDP was purchased from Tasly Pharmaceutical Co., Ltd. (Tianjin, China). Ultrapure water (18.2 MΩ) was purified with a Milli-Q system (Millipore, MA, USA). All other chemicals used were of analytical grade.

Male Sprague-Dawley rats, 6 to 7 weeks of age with body weights of 180 ± 8 g, were purchased from Sino British Sippr/BK Lab. Animal Co., Ltd. All animals were kept in an animal room with free access to food and water under standard conditions of temperature (23 ± 2°C), humidity (60 ± 5%), and light (12 h dark/light cycle). The experiment animals were housed under the above conditions for a 2-week acclimation period. All animal studies complied with current ethical considerations with the approval (SYXK-2007-0025) of Shanghai Jiao Tong University.

2.2. Myocardial Infarction Study and Drug Administration. The myocardial infarction (MI) of rats was induced by ligation of the left ventricular coronary artery [17]. 90 rats were randomly selected to undergo MI or sham surgery. First, animals were anesthetized with chloral hydrate (30 mg/kg, i.p.), fixed on the operating table while their backs were placed and intubated with a 16-gauge plastic catheter, which was connected with an animal breathing machine (rate: 85/min, respiratory ratio: 1 : 1, and volume: 18 mL), and electrocardiograms (ECG) was monitored by MPA 2000 biosignal analysis system (Alcott Biotech Co., Ltd., Shanghai, China) through electrocardioelectrode (lead II). Then, by separating subcutaneous tissue and muscle, thoracotomy was placed in the fourth left intercostal space. The heart was held gently outside the chest, while a silk suture was threaded beneath the left coronary artery 2-3 mm below the origin. After the heart had been returned to its normal position, the suture was ligated. The thorax was closed layer by layer under negative pressure, and a dose of penicillin (10,000 u/250 g, s.c.) was given one hour after surgery. Sham-operated rats were treated by using the similar manner except that coronary artery ligation was not done on them.

During the 24 h after operation, 44 of the 75 MI rats died because of acute pumps failure or lethal arrhythmias; 31 animals survived and were randomly divided into model group and mod. + CDDP group. 4 out of 15 sham surgery animals died throughout the experiment. 20 rats without undergoing experiment were randomly divided to control group and con. + CDDP (10 each group). The CDDP was dissolved in a certain amount of water to a certain concentration of per milliliter of drug solution. The con. + CDDP group and mol. + CDDP group were treated with drug solution at a dose of 107 mg/kg·d (equal to 1.8 mL/kg·d). Meanwhile, control group, sham group, and model group were treated with the same volume of 0.9% saline solution. The five animal groups were consecutively administrated as above for 28 days. During the administrated period, one rat in model group died.

2.3. Sample Collection and Preparation. On the day before operation (day-1) and days 3, 14, and 28, blood samples were collected from the vena ophthalmica, added, respectively, into 2.5 mL heparin-coated tubes, and then centrifuged at 3500 rpm for 10 min at 4°C. The supernatant obtained was frozen immediately, stored at −80°C, and thawed before analysis. On the 29th day after operation, all rats were anesthetized and subjected to autopsy. Their hearts were taken out immediately; 3 hearts of each group were fixed in 10% formalin, and the others were stored at −80°C.

2.4. Cardiac Enzymology and Histopathology. Plasma concentrations of CK were measured by ultraviolet spectrophotometer at 660 nm. The hearts were ground and diluted for 10 times in 0.9% saline solution at 0°C and then centrifuged at 3500 rpm for 10 min; the supernatant concentrations of superoxide dimutse (SOD) and malondialdehyde (MDA) were measured at 550 nm and 532 nm, respectively. Heart samples fixed in formalin were fixed and embedded in

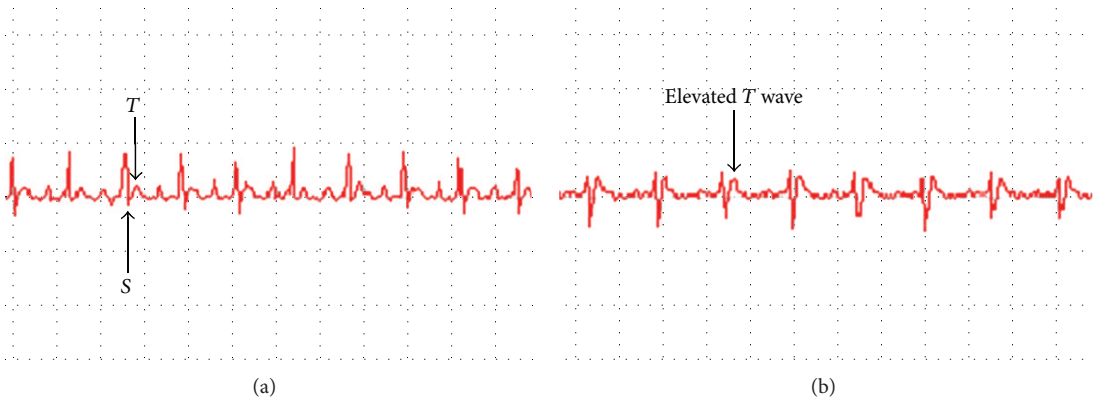

Figure 1: Electrocardiogram before (a) and after (b) coronary artery ligation.

paraffin wax; 4-5 μm of histologic sections of tissues was stained with hematoxylin-eosin. The sections were examined under microscope, and photomicrographs were taken.

2.5. GC-MS Spectral Acquisition of Plasma Samples and Data Pretreatment. Plasma metabolites were subjected to trimethylsilyl derivatization and analyzed by gas chromatograph-mass spectrometer (GC-MS) [18]. Two internal standard solutions (10 μL of L-2-chlorophenylalanine in water, 0.3 mg/mL; 10 μL of heptadecanoic acid in methanol, 1 mg/mL) were spiked into a 100 μL thawed aliquot of plasma sample. A mixture of methanol/chloroform (3 : 1) (300 μL) was used to extract the metabolites from the plasma. After a vortexing period of 30 s and storage for 10 min at −20°C, the samples were centrifuged at 12000 rpm for 10 min. An aliquot of the 300 μL supernatant was vacuum-dried at room temperature in a glass vial. The residue was derived with 80 μL of methoxyamine (15 mg/mL in pyridine) at 30°C for 90 min and followed by 80 μL of BSTFA (1%TMCS) at 70°C for 60 min.

Each 1 μL of solution of derivatives was injected into an Agilent 6890 GC-MS at 260°C in splitless mode. Metabolite separation was achieved on a DB-5 ms capillary column (30 m × 250 μm i.d., 0.25 μm film thickness; Agilent J&W Scientific, Folsom, CA, USA) with helium as the carrier gas at a constant flow rate of 1.0 mL/min. The GC oven temperature programming was started at 80°C and maintained for 2 min, followed by 10°C/min ramps to 180°C, 5°C/min to 240°C, and 25°C/min to 290°C and a final 9 min maintenance at 290°C. The temperature of transfer interface and ion source was set to 280 and 230°C, respectively. Electron impact ionization (70 eV) was used. Mass data was collected after a 5 min solvent delay at full scan mode (m/z 30–550) with an acquisition ate of 20 spectrum/second.

All GC/MS files were converted to CDF format via Agilent MSD software. CDF files were processed with XCMS in R 2.7.2 (Free Software Foundation, Inc.) for data pretreatment procedures, such as baseline correction, smoothing and alignment, time-window splitting, and peak feature extraction. Three-dimensional output data results were obtained with arbitrary peak index information (retention time m/z pairs), sample names (observations), and peak intensity (variables).

2.6. Data Processing. The resulting three-dimensional data sets from GC-MS analysis were introduced into SIMCA-P 11.5 software (Umetrics, Umeå, Sweden) for multivariate statistics [19]. Prior to multivariate statistics, the data was mean-centered and pareto-scaled. The unsupervised principal component analysis (PCA) was first used in all samples to see the general separation and find the outliers. Then, supervised partial least squares (PLS) and orthogonal partial least squares discriminant analyses (OPLS-DA) were performed. Plasma differential variables associated with MI and the effect of CDDP were selected based on a threshold of variable importance in the projection (VIP) value (VIP > 1) from a typical 7-fold cross-validated OPLS-DA model. In parallel, these differential metabolites from the OPLS-DA model were validated at a univariate level using Student's t-test. The critical P value of the test was set to 0.05 in this study. The corresponding fold change showed how the metabolites varied from MI compared with sham group. Compound identification was performed in NIST library 2005, with a similarity threshold of 70%. The analysis of the metabolites pathway was based on Kyoto Encyclopedia of Genes and Genomes (KEGG).

3. Result

3.1. Plasma Enzymes and Histological Assay

3.1.1. Electrocardiograms and Cardiac Enzymology. The changes of T wave and S-T segment of ECG are generally considered as a main index to evaluate animal model of MI [20]. As shown in Figure 1, we found that T waves of ECG in MI model rats were inversed after ligation. Enzymes and biochemical materials in plasma or tissue, such as CK, SOD, and MDA, are cited as important parameters in the assessment of MI [21–24]. On day 3, the level of CK in plasma revealed a significant elevation in the model group compared to the controls and the sham surgery group (Table 1), suggesting the success of the MI model after

Table 1: CK, SOD, and MDA content of rats (mean ± sd, $n = 6$).

Group	CK (U/mL)	SOD (U/mL)	MDA (nmol/mg prot)
Control	0.756 ± 0.18^{a}	330.5 ± 78.8^{a}	0.728 ± 0.122^{a}
Con. + CDDP	0.837 ± 0.13^{a}	330.4 ± 20.6^{a}	0.832 ± 0.131^{a}
Sham	0.748 ± 0.24^{a}	323.5 ± 46.3^{a}	0.833 ± 0.174^{a}
Model	1.144 ± 0.44^{b}	279.4 ± 102.9^{b}	1.430 ± 0.468^{b}
Mod. + CDDP	0.851 ± 0.35^{a}	334.0 ± 29.0^{a}	0.884 ± 0.094^{a}

CK: creatine kinases; SOD: superoxide dismutase; MDA: malondialdehyde. compared with the model group, $^{a}P < 0.05$; Compared with the control group, $^{b}P < 0.05$.

Table 2: The weight of rats, heart, and heart-body ratio (mean ± sd, $n = 6$).

Group	Body weight (g)	Heart weight (g) (nmol/mg prot)	Heart-body ratio (mg/g) (U/mg prot)
Control	336.300 ± 33.853	1.015 ± 0.092^{a}	3.029 ± 0.243^{a}
Con. + CDDP	333.900 ± 40.932	1.005 ± 0.119^{a}	3.020 ± 0.207^{a}
Sham	349.636 ± 36.825	$1.199 \pm 0.179^{b,a}$	$3.438 \pm 0.420^{b,a}$
Model	339.000 ± 37.165	$1.298 \pm 0.102^{b,c}$	$3.866 \pm 0.461^{b,c}$
Mod. + CDDP	349.133 ± 41.461	$1.204 \pm 0.146^{b,a}$	$3.470 \pm 0.410^{b,a}$

Compared with the model group, $^{a}P < 0.05$; compared with the control group, $^{b}P < 0.01$; compared with the sham group, $^{c}P < 0.05$.

coronary artery ligation. There was no statistical significance ($P > 0.05$) in the comparison between the control group and con. + CDDP, demonstrating that CDDP had little effect upon health rats. And a statistically significant restoration in CK level was observed in mod. + CDDP group compared with model group ($P < 0.05$), indicating that the effect of CDDP in recovering the plasma enzymes emerged within 3 days. On day 28, when compared with the control group, the concentrations of MDA ($P < 0.05$) in model group were significantly increased, while the levels of SOD ($P < 0.05$) were remarkably decreased. Restoration of the concentrations of SOD and MDA was observed in mod. + CDDP group, demonstrating the good performance of CDDP in treating MI after coronary artery ligation.

3.1.2. Effects of MI on Cardiac Tissue. After treatment, weight measurement of rats' hearts revealed statistical significance in the comparison among all groups (Table 2), demonstrating that the model group had little recovery after MI and CDDP had little effect upon health rats but exerted beneficial effects on MI rats greatly for rehabilitation. As shown in Figure 2, histopathological examination of myocardial tissue of control (Figure 2(a)) and con. + CDDP (Figure 2(b)) groups showed clear the orderly structure of heart without abnormality. In the sham group (Figure 2(c)), integrity of myocardial cell membrane was observed except a few myocardial cell necrosis and granulation tissue hyperplasia. However, in the model group (Figure 2(d)), there was serious necrobiosis with fibroblastic proliferation and presence of chronic inflammatory cells and lymphocytic infiltration. Moreover, edema and vacuolar, appeared along with absorption of myocardial cells near myocardial infarction areas, were clearly visible in the model group, whereas in the mod. + CDDP (Figure 2(e)), a reduction in inflammatory cells and less serious area of subendocardial damage was observed when compared with the model group. The above observations suggested that CDDP could decrease myocardial damage in MI rats but showed little influence on health rats.

3.2. Metabolomic Study of Plasma Samples

3.2.1. PCA Processing of GC-MS Data. Though the typical GC-MS total ion chromatograms (TIC) of plasma samples derived from each group, excluding internal standards, a total of 128 individual metabolites were consistently detected in nearly 90% of the plasma samples, including amino acids, organic acids, and amines. PCA approaches are frequently used to distinguish between classes expected to show metabolic differences. In this work, we performed PCA models of the plasma metabonomic data to exhibit classification of each group (as shown in Figure 3). In the PCA map, each spot represented a sample and each assembly of samples indicated a particular metabolic pattern of different groups. As shown in Figure 3(a), the metabolic state of each spot on day-1 mixed disorderly, which indicated that endogenous substances showed little difference in each group prior to MI surgery. On day 3 (Figure 3(b)), the metabolic state of model and mod. + CDDP groups was far away from the control, con. + CDDP, and sham position, and mod. + CDDP group could be classified with the model group, which suggested that MI altered the metabolic fingerprints of plasma compared to the normal state, and CDDP disturbed the endogenous substances compared with the model. On day 14 (Figure 3(c)) and day 28 (Figure 3(d)), the trajectory of mod. + CDDP group gradually gathered with the sham group, but the model group was still far away from them, revealing that CDDP had promoted the recovery of the disturbed metabolism state compared with the sham but still did not return to the normal state. The operation placed on rats also had influence on endogenous substances.

3.2.2. Identification of MI-Related Metabolites. OPLS-DA, which is a common supervised pattern recognition to handle metabolomic data, picks out discriminating ions that are contributing to the classification of samples and remove noncorrelated variations contained within spectra. When the supervised pattern recognition was employed, the integrity of the mathematical model was evaluated first before being used for further interpretation. Commonly, R^2Y provides an estimate of how well the model fits the Y data, whereas Q^2Y is an estimate of how well the model predicts the Y. Both the Q^2Y and R^2Y close to 1 indicate an excellent model.

Thus, we used OPLS-DA models with satisfactory modeling and predictive abilities to compare between the sham and the model samples to find out biomarkers of MI in our study (Figure 4). Metabolites that significantly contributed to the clustering and discrimination were generated and identified

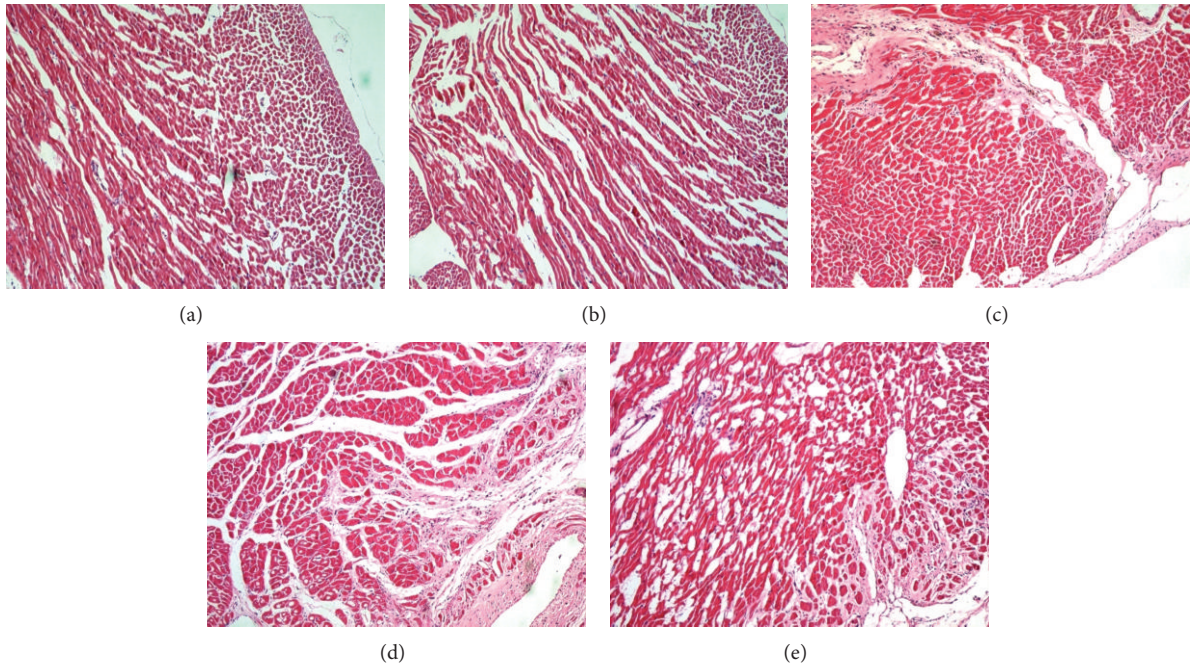

Figure 2: Myocardial tissue in light microscope (×100). (a) Control, (b) con. + CDDP, (c) sham, (d) model, and (e) mod. + CDDP.

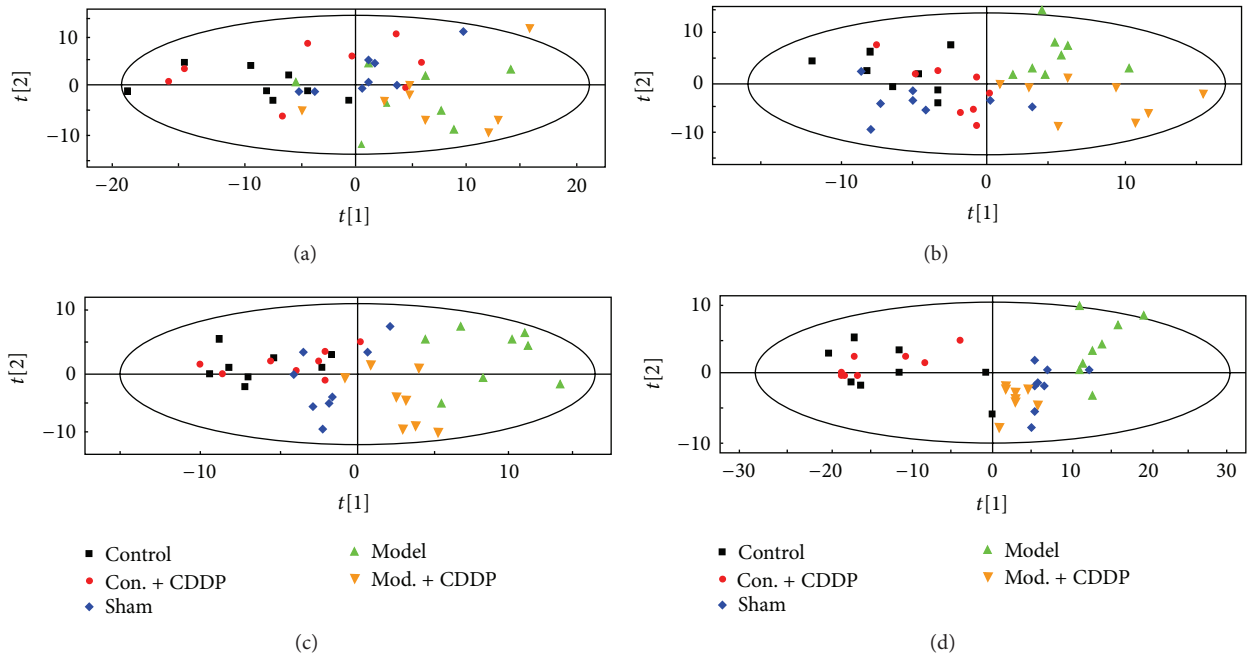

Figure 3: PCA scores plots of comparison of control, con. + CDDP, sham, model, and mod. + CDDP groups of rat plasma data on day-1 (a), day 3 (b), day 14 (c), and day 28.

according to 2.7. 20 significantly differential endogenous metabolites were selected for further study, and the results were listed in Table 3. The alterations of peak intensity of the 20 potential biomarkers of five groups were summarized in Table 4. Among the 20 metabolites, the levels of 11 compounds were observed significantly increased, and other 9 compounds were decreased in the model group. At the same time, 9 of the 20 metabolites, such as succinic acid, 2-butenedioic acid, creatinine, citric acid, D-glucose, urea, lactic acid, L-aspartic acid, and L-threonine, were observed significantly altered in the mod. + CDDP group compared to the model group. Therefore, these significantly differential endogenous metabolites in each group were assumed as potential biomarkers, which may be related to the diagnosis of

Table 3: List of identified differential metabolites between the sham and model group on day 3.

tR (min)	Metabolites	VIP[a]	P[b]	Fold change[c] (model/sham)	Metabolic pathways
6.34	Glycine	1.6	0.0029	−1.1	Amino acid metabolism
7.14	Urea	1.4	0.0221	1.4	Nucleic acid metabolism
7.64	L-alanine	1.4	0.0134	1.3	Amino acid metabolism
8.72	L-isoleucine	2.5	0.0000	−1.1	Amino acid metabolism
8.9	Cadaverine	1.6	0.0058	2.1	Not known
9.01	Succinic acid	1.2	0.0532	−1.3	Energy metabolism
9.52	2-Butenedioic acid	1.9	0.0003	−3.4	Energy metabolism
9.96	L-threonine	2.0	0.0002	−1.1	Amino acid metabolism
11.06	Aminomalonic acid	1.3	0.0236	−1.2	Amino acid metabolism
11.69	L-aspartic acid	2.3	0.0000	1.1	Amino acid metabolism
11.72	L-proline	2.0	0.0002	−2.3	Amino acid metabolism
12.14	Creatinine	1.7	0.0010	1.2	Amino acid metabolism
13.04	L-phenylalanine	1.3	0.0192	1.4	Energy metabolism
16.18	Citric acid	1.3	0.0407	−1.1	Energy metabolism
16.86	D-xylose	1.2	0.0328	1.2	Nucleic acid metabolism
16.89	D-glucose	1.7	0.0017	1.7	Energy metabolism
17.19	Lactic acid	1.8	0.0010	1.6	Energy metabolism
17.58	L-tyrosine	1.7	0.0016	1.2	Amino acid metabolism
19.84	Propanoic acid	1.3	0.0138	−1.1	Energy metabolism
21.95	L-tryptophan	1.7	0.0012	1.1	Amino acid metabolism

[a] Variable importance in the projection (VIP) was obtained from OPLS-DA with a threshold of 1.0. [b] P values were calculated from Student's t-test. [c] Fold change was calculated from the arithmetic mean values of each group. Fold change with a positive value indicates a relatively higher concentration present in model group while a negative value means a relatively lower concentration as compared to the sham group.

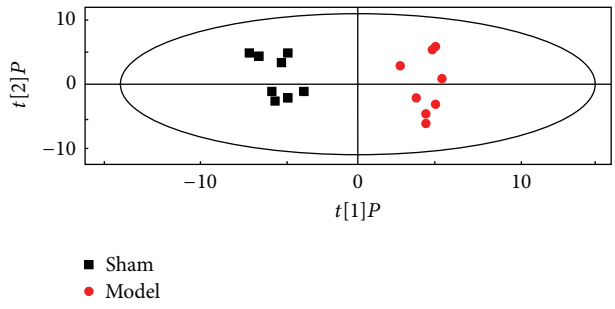

Figure 4: OPLS-DA score plot of GC-MS data from sham and model groups on day 3 ($R^2Y = 0.862$, $R^2X = 0.264$, and $Q^2Y = 0.569$).

MI and may be used as a potential efficacy indicator for drug effect. Figure 5 was the alteration of peak intensity of each potential biomarker of five groups on each day. It was obvious that 7 listed biomarkers in mod. + CDDP group revealed recovery after the therapeutic intervention.

4. Discussion

The chemical analysis of CDDP reported previously shows that the main ingredients are salvianolic acids and sennosides [25, 26]. Salvianolic acids have been reported to improve cardiac function through improving antioxidant activity [27] and preventing cardiomyocyte apoptosis [28]. Senosides (including ginsenosides and notoginsenoside) could protect against myocardial damage and decrease lipid peroxidation [29]. By hitting multiple targets from a combination of multiple components, CDDP exerts the synergistic therapeutic efficacies of the prevention and treatment of cardiovascular diseases, including lowering blood fat, reducing blood viscosity, and resisting arteriosclerosis and antiplatelet aggregation [30].

The changes in the levels of CK, SOD, and MDA have been considered as important markers in the assessment of MI [21, 31]. Generation of oxygen-free radicals and subsequent formation of reactive oxygen species, which may cause lipid peroxidation and oxidative stress, has been implicated as a major causative factor for myocardial injury [22]. SOD is one of the antioxidants that can protect the heart from peroxidation, whoseconsequence damages the tissues by inactivating the oxygen-free radicals. MDA is a poisonous end-product of lipid peroxidation, whose level can represent the rate and extent of lipid peroxidation directly and show the capability of eliminating free radicals indirectly [32]. In this study, the significant alternation in the levels of CK, SOD, and MDA was observed in the comparison between the model and the sham group, as well as the mod. + CDDP and the model group. These findings were in conformity with previous reports and demonstrated that myocardial ischemia was established in rats, and that CDDP had virtual significance in treating MI [1].

Combined with conventional assessment of drug effects, our GC-MS-based metabonomic approach was employed to capture the differentially expressed endogenous metabolites

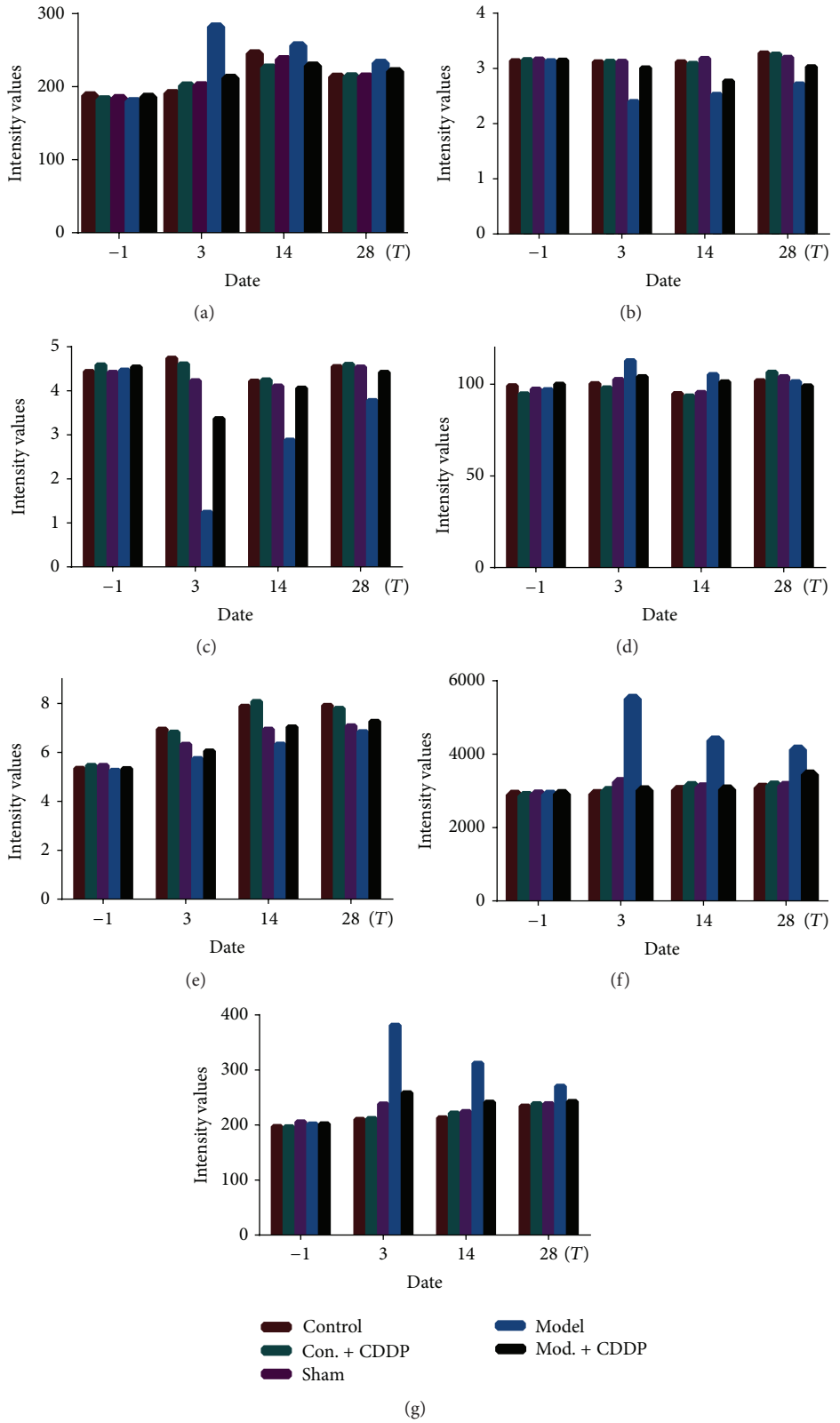

Figure 5: Summary of intensity values of urea (a), succinic acid (b), 2-butenedioic acid (c), L-aspartic acid (d), citric acid (e), D-glucose (f), and Lactic acid (g) in each group on each day.

Table 4: Summary of intensity values of potential biomarkers in each group on day 3.

Biomarkers	Peak intensity (mean ± sd, $n = 6$)				
	Control	Con. + CDDP	Sham	Model	Mod. + CDDP
Glycine	$5.86 \pm 0.6^{b,c}$	5.51 ± 0.96^{b}	4.85 ± 0.94^{a}	4.41 ± 1.65^{a}	$5.94 \pm 1.8^{b,c}$
Urea	190.9 ± 112.08^{b}	201.44 ± 108.76^{b}	201.59 ± 55.12^{b}	$282.23 \pm 72.75^{a,c}$	211.97 ± 48.32^{b}
L-alanine	444.97 ± 64.71^{b}	432.48 ± 74.21^{b}	450.96 ± 56.85^{b}	$586.25 \pm 64.89^{a,c}$	443.53 ± 98.11^{b}
L-isoleucine	$260.88 \pm 34.02^{b,c}$	254.42 ± 39.69^{b}	$211.84 \pm 34.61^{a,b}$	$192.58 \pm 33.25^{a,c}$	205.51 ± 54.06^{a}
Cadaverine	22.75 ± 11.3^{b}	23.12 ± 4.15^{b}	21.68 ± 11.31^{b}	$45.53 \pm 11.1^{a,c}$	36.9 ± 14.92^{b}
Succinic acid	3.12 ± 2.16^{b}	3.13 ± 0.94^{b}	3.13 ± 1.63^{b}	2.40 ± 1.01^{a}	3.01 ± 2.07^{b}
2-Butenedioic acid	4.74 ± 1.61^{b}	4.61 ± 3.24^{b}	4.23 ± 3.98^{b}	$1.24 \pm 3.92^{a,c}$	$3.37 \pm 3.98^{a,b}$
L-threonine	$209.33 \pm 25.38^{b,c}$	208.3 ± 27.54^{b}	$181.25 \pm 22.81^{a,b}$	$164.77 \pm 35.78^{a,c}$	189.33 ± 44.05^{b}
Aminomalonic acid	46.73 ± 29.21^{b}	46.21 ± 18.02^{b}	43.69 ± 44.56^{b}	$36.41 \pm 28.42^{a,c}$	39.85 ± 25.14^{a}
L-aspartic acid	100.32 ± 11.51^{b}	97.98 ± 13.89^{b}	102.57 ± 7^{b}	$112.83 \pm 13.89^{a,c}$	104.12 ± 21.12^{b}
L-proline	$280.57 \pm 22.74^{b,c}$	289.33 ± 56.22^{b}	$218.72 \pm 31.35^{a,b}$	$95.1 \pm 15.54^{a,c}$	248.84 ± 64.37^{b}
Creatinine	$6.39 \pm 1.59^{b,c}$	6.27 ± 3.44^{b}	$7.25 \pm 3.23^{a,b}$	$8.7 \pm 3.73^{a,c}$	$7.71 \pm 3.24^{a,b}$
L-phenylalanine	$110.09 \pm 10.46^{b,c}$	106.57 ± 14.11^{b}	$126.76 \pm 8.24^{a,b}$	$177.46 \pm 12.68^{a,c}$	$148.95 \pm 24.79^{a,b}$
Citric acid	6.95 ± 5.52^{b}	6.83 ± 4.4^{b}	6.33 ± 4.45^{b}	$5.75 \pm 2.64^{a,c}$	$6.06 \pm 3.71^{a,b}$
D-xylose	$7.01 \pm 1.96^{b,c}$	7.08 ± 1.06^{b}	$8.13 \pm 1.07^{a,b}$	$9.76 \pm 1.77^{a,c}$	8.07 ± 1.15^{b}
D-glucose	2912.13 ± 190.45^{b}	2993.74 ± 210.95^{b}	3239.06 ± 255.96^{b}	$5506.4 \pm 255.01^{a,c}$	3012.34 ± 209.33^{b}
Lactic acid	210.17 ± 15.22^{b}	211.91 ± 22.87^{b}	238.35 ± 16.13^{b}	$381.36 \pm 24.33^{a,c}$	258.68 ± 16.45^{b}
L-tyrosine	$44.57 \pm 5.36^{b,c}$	43.47 ± 7.74^{b}	$56.62 \pm 5.38^{a,b}$	$67.94 \pm 9.93^{a,c}$	62.72 ± 9.05^{a}
Propanoic acid	$21.98 \pm 6.65^{b,c}$	22.5 ± 10.64^{b}	11.98 ± 6.28^{a}	10.89 ± 9.27^{a}	$14.96 \pm 10.47^{a,b}$
L-tryptophan	421.7 ± 67.69^{b}	417.94 ± 69.49^{b}	434.8 ± 82.32^{b}	$478.28 \pm 118.65^{a,c}$	$451.78 \pm 101.75^{a,b}$

Compared with the control group, $^{a}P < 0.05$; compared with the model group, $^{b}P < 0.05$; compared with the sham group, $^{c}P < 0.05$.

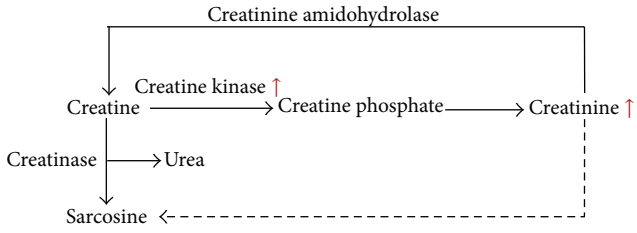

Figure 6: Creatinine and creatine in arginine and proline metabolism.

associated with MI. 20 differential metabolites in the plasma samples were identified. Table 3 showed that most of the metabolites bounded up with MI were involved in metabolic processes related to myocardial energy metabolism, especially the TCA cycle (citric acid, succinic acid, and 2-butenedioic acid) and glycolysis (lactic acid and glucose). After MI surgery, myocardial blood flow of rats became inadequate in oxygen supply, and myocardial ischemia was developed. MI led to reducing formation of adenosine triphosphate (ATP) via aerobic mechanisms and accelerated anaerobic ATP production by glycolysis [11]. Meanwhile, creatine supplied the shortage of ATP and transformed into creatine by creatine kinase (as shown in Figure 6). Fatty acids are the main fuel for the healthy heart, with a lesser contribution coming from the oxidation of glucose and lactate. Myocardial ischemia dramatically alters fuel metabolism, causing an accelerated rate of glucose conversion to lactate and a switch from lactic acid uptake by the heart to lactate production. This causes a dramatic disruption in cell homeostasis (e.g., lactate accumulation and a decrease in pH and ATP) [33]; the lactate acid represents the end product of anaerobic or nonoxidative glycolysis and has been used as a marker of ischemia [34]. As shown in Figure 7, under the condition of MI, the levels of citric acid, succinic acid, and 2-butenedioic acid in tricarboxylic acid (TCA) cycle were decreased, whereas the lactic acid via glycolysis was increased. Meanwhile, the TCA cycle was not only the pathway of sugar decomposition but also the pathway of fuel molecules oxidation, such as fatty acids and amino acids. Therefore, the reduction of TCA cycle intermediates led to the alteration of fatty acid and amino acid metabolites, including L-alanine, phenylalanine, L-aspartic acid, L-isoleucine, and creatinine. After the administration of CDDP, the levels of these MI-related metabolites, citric acid, lactic acid, succinic acid, 2-butenedioic acid, and L-aspartic acid, in the mod. + CDDP group, were restored to the normal status (not significant with the sham group), suggesting that CDDP had exerted its therapeutic efficacies by regulating metabolites disrupted by MI.

5. Conclusion

In this work, GC-MS-based metabonomic strategy was used to investigate therapeutic effects of CDDP in treating MI. Combined with serum biochemistry and histopathological

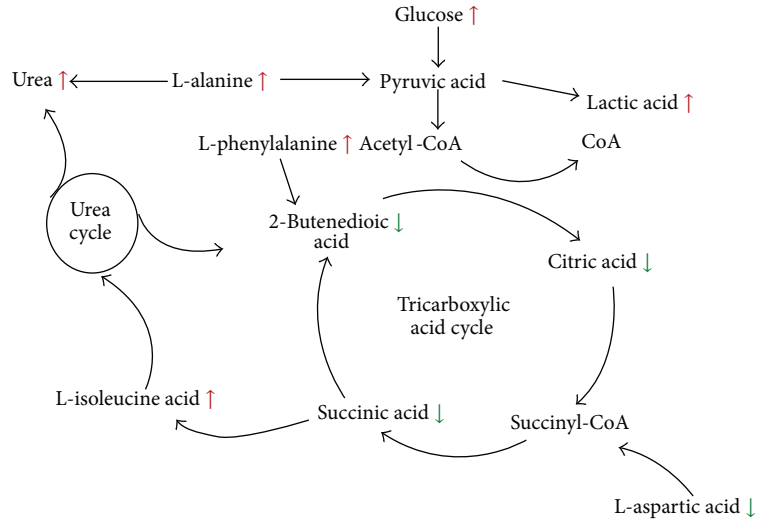

Figure 7: Metabolomic network in plasma of rats with myocardial ischemia.

assessment such as assay, our metabonomic findings suggested that CDDP exerted its therapeutic efficacies by regulating energy metabolism, glycolysis, and lipid metabolism disrupted by MI.

Abbreviations

CHD: Coronary atherosclerotic heart disease
MI: Myocardial ischemia
TCM: Traditional Chinese medicine
CDDP: Compound Danshen dripping pills
GC/MS: Gas chromatography/mass spectrometry
CK: Creatine kinases
SOD: Superoxide dismutase
MDA: Malondialdehyde
VIP: Variable importance in the project
PCA: Principal component analysis
PLS-DA: Partial least square-discriminant analysis
OPLS: Optimized potentials for liquid simulations
KEGG: Kyoto Encyclopedia of Genes and genomes
TIC: Total ion chromatograms
TCA: Tricarboxylic acid cycle.

Authors' Contribution

Xue Xin, Haimiao Zou, Ningning Zheng, and Xinchun Xu have contributed equally to this work and should be considered co-first authors.

Acknowledgment

This work was financially supported by the National Natural Science and Technology Foundation project (30772789).

References

[1] A. Kibos and A. Guerchicoff, "Susceptibility genes for coronary heart disease and myocardial infarction," *Acute Cardiac Care*, vol. 13, no. 3, pp. 136–142, 2011.

[2] P. Parang, B. Singh, and R. Arora, "Metabolic modulators for chronic cardiac ischemia," *Journal of Cardiovascular Pharmacology and Therapeutics*, vol. 10, no. 4, pp. 217–223, 2005.

[3] *Chinese Pharmacopeia(I)*, 2010.

[4] Y. Chu, L. Zhang, X. Y. Wang, J. H. Guo, Z. X. Guo, and X. H. Ma, "The effect of Compound Danshen Dripping Pills, a Chinese herb medicine, on the pharmacokinetics and pharmacodynamics of warfarin in rats," *Journal of Ethnopharmacology*, vol. 137, no. 3, pp. 1457–1461, 2011.

[5] "Anonymous compound danshen dripping pills passed Phase II clinical trials by FDA," *China Journal of Pharmaceutical Economics*, vol. 4, p. 94, 2010.

[6] D. G. Robertson, M. D. Reily, and J. D. Baker, "Metabonomics in pharmaceutical discovery and development," *Journal of Proteome Research*, vol. 6, no. 2, pp. 526–539, 2007.

[7] A. Zhang, H. Sun, Z. Wang, W. Sun, P. Wang, and X. Wang, "Metabolomics: towards understanding traditional Chinese medicine," *Planta Medica*, vol. 76, no. 17, pp. 2026–2035, 2010.

[8] X. Wang, H. Sun, A. Zhang, W. Sun, P. Wang, and Z. Wang, "Potential role of metabolomics apporoaches in the area of traditional Chinese medicine: as pillars of the bridge between Chinese and Western medicine," *Journal of Pharmaceutical and Biomedical Analysis*, vol. 55, no. 5, pp. 859–868, 2011.

[9] L. Dong, C. Deng, J. Wang, and X. Shen, "Fast determination of paeonol in plasma by headspace solid-phase microextraction followed by gas chromatography-mass spectrometry," *Analytica Chimica Acta*, vol. 585, no. 1, pp. 76–80, 2007.

[10] Y. H. Lu, H. P. Hao, and G. J. Wang, "Metabolomics approach to the biochemical differentiation of Traditional Chinese Medicine syndrome types of hypertension," *Chinese Journal of Clinical Pharmacology and Therapeutics*, vol. 12, no. 10, pp. 1144–1150, 2007.

[11] X. Liang, X. Chen, Q. Liang et al., "Metabonomic study of Chinese Medicine Shuanglong Formula as an effective treatment for myocardial infarction in rats," *Journal of Proteome Research*, vol. 10, no. 2, pp. 790–799, 2011.

[12] Y. M. Lao, J. G. Jiang, and L. Yan, "Application of metabonomic analytical techniques in the modernization and toxicology research of traditional chinese medicine," *British Journal of Pharmacology*, vol. 157, no. 7, pp. 1128–1141, 2009.

[13] S. H. Shah, J. R. Bain, M. J. Muehlbauer et al., "Association of a peripheral blood metabolic profile with coronary artery disease and risk of subsequent cardiovascular events," *Circulation*, vol. 3, no. 2, pp. 207–214, 2010.

[14] G. D. Lewis, R. Wei, E. Liu et al., "Metabolite profiling of blood from individuals undergoing planned myocardial infarction reveals early markers of myocardial injury," *Journal of Clinical Investigation*, vol. 118, no. 10, pp. 3503–3512, 2008.

[15] H. S. Zhang, Y. H. Jia, H. Y. Hua et al., "Study on phlegm syndrome and blood stasis syndrome in coronary artery disease with angina pectoris based on metabolomics of urine," *Chinese Journal of Basic Medicine in Traditional Chinese Medicine*, vol. 16, no. 2, pp. 126–128, 2010.

[16] J. Weixiong, Y. Zhaokai, H. Xianping et al., "Analysis on urine metabolomics of coronary heart disease patients with the heart blood stasis syndrome," *Journal of Traditional Chinese Medicine*, vol. 51, no. 8, pp. 729–732, 2010.

[17] J. Wang, X. Liu, B. Ren, H. Rupp, N. Takeda, and N. S. Dhalla, "Modification of myosin gene expression by imidapril in failing heart due to myocardial infarction," *Journal of Molecular and Cellular Cardiology*, vol. 34, no. 7, pp. 847–857, 2002.

[18] Z. Zhang, Y. Qiu, Y. Hua et al., "Serum and urinary metabonomic study of human osteosarcoma," *Journal of Proteome Research*, vol. 9, no. 9, pp. 4861–4868, 2010.

[19] Q. Zhang, G. Wang, Y. Du, and L. Zhu, "GC/MS analysis of the rat urine for metabonomic research," *Journal of Chromatography B*, vol. 854, no. 1-2, pp. 20–25, 2007.

[20] H. Li, Y. Ni, M. Su et al., "Pharmacometabonomic phenotyping reveals different responses to xenobiotic intervention in rats," *Journal of Proteome Research*, vol. 6, no. 4, pp. 1364–1370, 2007.

[21] V. A. Khazanov, A. A. Kiseliova, K. Y. Vasiliev, and G. A. Chernyschova, "Cardioprotective effects of trimetazidine and a combination of succinic and malic acids in acute myocardial ischemia," *Bulletin of Experimental Biology and Medicine*, vol. 146, no. 2, pp. 218–222, 2008.

[22] T. Hayashi, A. Tabata, Y. Kaneda, and T. Tanaka, "Myocardial LDH- and CK-isoenzymes and their clinical significances," *The Japanese Journal of Clinical Pathology*, vol. 30, no. 8, pp. 861–868, 1982.

[23] K. Kodama, A. Hirayama, and K. Komamura, "Human plasma superoxide dismutase (SOD) activity on reperfusion injury with successful thrombolysis in acute myocardial infarction," *Japanese Journal of Medicine*, vol. 28, no. 2, pp. 202–206, 1989.

[24] S. Zhang, B. He, J. Ge, C. Zhai, X. Liu, and P. Liu, "Characterization of chemical composition of Agaricus brasiliensis polysaccharides and its effect on myocardial SOD activity, MDA and caspase-3 level in ischemia-reperfusion rats," *International Journal of Biological Macromolecules*, vol. 46, no. 3, pp. 363–366, 2010.

[25] Z. Xiaohui, Z. Xinfeng, Z. Xin, W. Shixiang, W. Yinmao, and Z. Jianbin, "Determination of the main bioactive metabolites of Radix Salvia miltiorrhizae in Compound Danshen Dripping Pills and the tissue distribution of Danshensu in rabbit by SPE-HPLC-MSn," *Journal of Separation Science*, vol. 30, no. 6, pp. 851–857, 2007.

[26] Y. Li, S. Hou, Y. Bi et al., "Novel two-step release system for the traditional Chinese medicine compound Danshen," *Yakugaku Zasshi*, vol. 127, no. 9, pp. 1473–1484, 2007.

[27] S. B. Wang, S. Tian, F. Yang, H. G. Yang, X. Y. Yang, and G. H. Du, "Cardioprotective effect of salvianolic acid A on isoproterenol-induced myocardial infarction in rats," *European Journal of Pharmacology*, vol. 615, no. 1–3, pp. 125–132, 2009.

[28] M. Li, M. Q. Zhao, S. S. Kumar Durairajan et al., "Protective effect of tetramethylpyrazine and salvianolic acid B on apoptosis of rat cerebral microvascular endothelial cell under high shear stress," *Clinical Hemorheology and Microcirculation*, vol. 38, no. 3, pp. 177–187, 2008.

[29] J. Q. Ruan, W. I. Leong, R. Yan, and Y. T. Wang, "Characterization of metabolism and in vitro permeability study of notoginsenoside R1 from radix notoginseng," *Journal of Agricultural and Food Chemistry*, vol. 58, no. 9, pp. 5770–5776, 2010.

[30] R. Y. Yuan and G. P. Li, "Multi-target effects of compound Danshen dripping pills in prevention and treatment of cardiovascular diseases," *Chinese Journal of New Drugs*, vol. 18, no. 5, pp. 377–380, 2009.

[31] X. Su, Y. Ma, R. Huang, X. Wang, and Y. Wang, "Effects of Shenmai Injection on blood SOD activity and MDA level in senile patients in coronary heart disease," *Journal of Traditional Chinese Medicine*, vol. 25, no. 1, pp. 50–53, 2005.

[32] V. Schettler, H. Methe, D. Staschinsky, P. Schuff-Werner, G. A. Muller, and E. Wieland, "Review: the oxidant/antioxidant balance during regular low density lipoprotein apheresis," *Therapeutic Apheresis*, vol. 3, no. 3, pp. 219–226, 1999.

[33] A. A. Wolff, H. H. Rotmensch, W. C. Stanley, and R. Ferrari, "Metabolic approaches to the treatment of ischemic heart disease: the clinicians' perspective," *Heart Failure Reviews*, vol. 7, no. 2, pp. 187–203, 2002.

[34] J. R. Dyck, J. F. Cheng, W. C. Stanley et al., "Malonyl coenzyme a decarboxylase inhibition protects the ischemic heart by inhibiting fatty acid oxidation and stimulating glucose oxidation," *Circulation Research*, vol. 94, no. 9, pp. e78–84, 2004.

Hindawi Publishing Corporation
Evidence-Based Complementary and Alternative Medicine
Volume 2013, Article ID 706762, 9 pages
http://dx.doi.org/10.1155/2013/706762

Research Article

Exploration of Macro-Micro Biomarkers for Dampness-Heat Syndrome Differentiation in Different Diseases

Jianye Dai,[1] Shujun Sun,[1] Jinghua Peng,[2] Huijuan Cao,[1] Ningning Zheng,[1] Junwei Fang,[1] Qianhua Li,[1] Jian Jiang,[2] Yongyu Zhang,[1] and Yiyang Hu[2]

[1] *Center for Traditional Chinese Medicine and Systems Biology, Shanghai University of Traditional Chinese Medicine, Shanghai 201203, China*
[2] *Institute of Liver Diseases, Shuguang Hospital, Key Laboratory of Liver and Kidney Diseases of Ministry of Education, Shanghai University of Traditional Chinese Medicine, Shanghai 201203, China*

Correspondence should be addressed to Yongyu Zhang; dryyz@sina.com and Yiyang Hu; yyhuliver@163.com

Received 3 January 2013; Revised 6 February 2013; Accepted 17 February 2013

Academic Editor: Wei Jia

Increased attention is being paid to traditional Chinese medicine (TCM) as a complementary and alternative medicine to provide an effective approach for personalized diagnosis and clinical treatment. TMC performs treatment based on differentiation of TCM syndrome (ZHENG), which may identify special phenotypes by symptoms and signs of patients even if they are in different diseases. There has, however, been skepticism and criticism because syndrome classification only depends on observation, knowledge, and clinical experience of TCM practitioners, which lacks objectivity and repeatability. In order to transform syndrome classification into mainstream medicine, we introduce a macro-micro approach that combines symptoms, clinical indicators, and metabolites. The present paper explores the macro-micro biomarkers of dampness-heat syndrome in chronic hepatitis B and nonalcoholic fatty liver patients, which could provide the basis for developing a possible population-screening tool for selecting target individuals and creating an evaluation index for personalized treatment.

1. Introduction

Chronic hepatitis B (CHB) and nonalcoholic fatty liver disease (NFL) are two common diseases occurring throughout the world that have continuously increasing morbidity [1]. It is worth noting that 12.1% [2] and 37.1% [3] of patients with CHB and NFL, respectively, exhibit the same symptoms (e.g., yellow and slimy fur), which are characteristics of dampness-heat syndrome (DH) in traditional Chinese medicine (TCM). Although CHB and NFL have different etiologies in Mainstream Medicine, TCM practitioners may perform the same treatment for these patients.

Actually, different diseases may be treated similarly in TCM particularly when the same syndrome appears in these diseases [4]. In this respect, syndrome differentiation and treatment (bian zheng lun zhi) may provide some new revelations to modern personalized medicine [5–7]. Syndrome differentiation is still debated, because it depends on clinical observation and TCM practitioners' experiences, which are thought to be subjective and unrepeatable. The success of personalized medicine relies on having accurate diagnostic tests that identify those patients who can benefit from targeted therapies [8]; thus, the ability to achieve objectivity and repeatability in TCM diagnosis would provide a greatly needed breakthrough.

Recently, researchers and scientists of TCM have explored incorporating several potentially beneficial methods, including, for example, physiology and biochemistry [9], molecular biology [10], and tongue image digitization [11, 12]. However, the classifications have been less than satisfactory. The main reason might be that these methods only focus on one or several indicators and thus cannot generalize the entire state of the syndrome. We therefore conceived the possibility of a macro-micro approach that includes a combination of metabolites, symptoms, and clinical indicators. Clinical manifestations are the macroeconomic performance, and metabolic molecules and indicators are microscopic. To serve in TCM diagnosis and treatment, here we report our findings

from a case study that allowed us to preliminarily explore the macro-micro biomarkers of DH in CHB and NFL patients.

2. Experimental

2.1. Subjects and Experiment Design. Twenty healthy volunteers and 115 patients (60 patients for training and another 55 patients for testing) of dampness-heat syndrome chronic hepatitis B (DHHB), nondampness-heat syndrome chronic hepatitis B (NDHHB), and dampness-heat syndrome nonalcoholic fatty liver (DHFL) were enrolled in the study. The clinical study was approved by the local ethics committee and was performed in accordance with the principals contained in the Declaration of Helsinki. All individuals provided informed consent before inclusion into the study. Diagnostic standard of HB and FL patients was referred to "the guideline of prevention and treatment for chronic hepatitis B" [13] and "guidelines for management of nonalcoholic fatty liver disease: an updated and revised edition" [14]. Cases meeting the diagnostic criteria for chronic hepatitis B and nonalcoholic fatty liver, respectively, at 18–65 (39.9 mean ± 13.5 std. dev.) years of age who signed the informed consent form were included in the study. Individuals were excluded from the study if they met any of the following criteria. (1) Cases complicated with other hepatotropic virus hepatitis and alcoholic fatty liver. (2) Chronic severe hepatitis. (3) HB and FL patients associated with serious primary disease of heart, kidney, lung, endocrine, blood, metabolic and gastrointestinal, or psychotic patients. (4) Pregnant or lactating women. A junior medical physician made the initial diagnosis and recorded the information of four traditional examinations accurately and completely. Three more senior physician (either chief or deputy physicians) subsequently confirmed the initial diagnosis by the records and gave the hierarchical results of typical degree. Only those cases that were identified as classical DH patients by both the junior and the senior physicians were included in the study to guarantee the correctness of ZHENG differentiation.

2.2. Chemicals and Drugs. N,O-bis (trimethylsilyl) trifluoroacetamide (BSTFA with 1% TMCS) and urease were purchased from Sigma-Aldrich Co. LLC (USA). Methoxyamine hydrochloride, methanol, ethanol, myristic acid, chloroform and pyridine were purchased from China National Pharmaceutical Group Corporation (Shanghai, China).

2.3. Sample Collection and Preparation. A complete physical examination was given, and the health condition was recorded on a scale including the information obtained through four traditional examinations: looking, listening and smelling, asking, and touching when the patient entered the study. Seventy-one clinical indicators and 115 contents from the four methods of examinations were acquired for the basic information.

Urine samples were collected from all subjects and were stored at −80°C until GC-MS assay. All urine samples were thawed in an ice water bath and vortex-mixed before analysis. Each 1 mL aliquot of standard mixture or urine sample was placed into a screw top tube, samples were centrifuged for 10 min at (12,000 rpm), and 150 μL supernatants were then transferred into clean screw top tubes. After adding 70 μL of urease (4 mg/mL) and vortex-mixing for 30 s, samples were conditioned at 37°C for 15 min to remove the urea. After the addition of 800 μL methanol and 10 μL of myristic acid in methanol (1 mg/mL) and mixing for 1 min, the solution was centrifuged at 13,000 rpm for 10 min. A 200 μL aliquot of supernatant was then transferred into a GC vial and evaporated to dryness under N_2 at 30°C. Fifty μL of methoxyamine in pyridine (15 mg/mL) was added to the GC vial, and vortex-mixed for 1 min, and the methoximation reaction was carried out for 90 min rocking in a shaker at 30°C, then 50 μL of BSTFA plus 1% TMCS was added to the samples for trimethylsilylation for another 1 h at 70°C. In the final step, 30 μL of heptane was added to the GC vial, and the solution was analyzed utilizing GC-MS after vortex for 30 s.

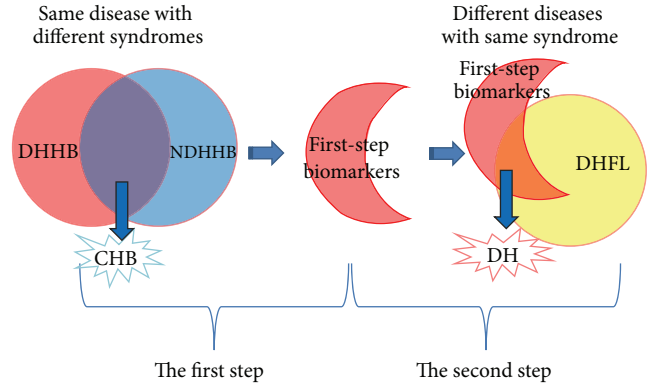

Figure 1: Schematic diagram of research approach for selection of DH.

2.4. Data Acquisition. All GC-MS analyses were performed by a mass spectrometer 5975B (Agilent technologies, USA) coupled to an Agilent 6890 (Agilent technologies, USA) gas chromatography instrument. In the gas chromatographic system, a catabletary column (Agilent J&W DB-5 ms Ultra Inert 30 m × 0.25 mm, film thickness 0.25 μm) was used. Helium carrier gas was used at a constant flow rate of 1.0 mL $*$ min^{-1}. One μL of derivatized samples was injected into the GC/MS instrument, and splitless injection mode was used. A programmed column temperature was optimized to acquire a well separation. The temperatures of the injection port, the interface, and source temperature were set at 280°C, 260°C and 230°C, respectively. The measurements were made with electron impact ionization (70 eV) in the full scan mode (m/z 30–550). The solvent post time was set to 5 min. The GC-MS operating condition was the same as the previous experiment [15] except the column temperature program.

2.5. Data Analysis. Due to experimental variation and column aging, shifts in retention time between fingerprints may occur. When the total ion current chromatograms (TICs) were obtained, peak-alignment or warping techniques are commonly applied to compensate for minor shifts in retention times. Thus, in the subsequent data processing, the same variable manifested synchronous information in every

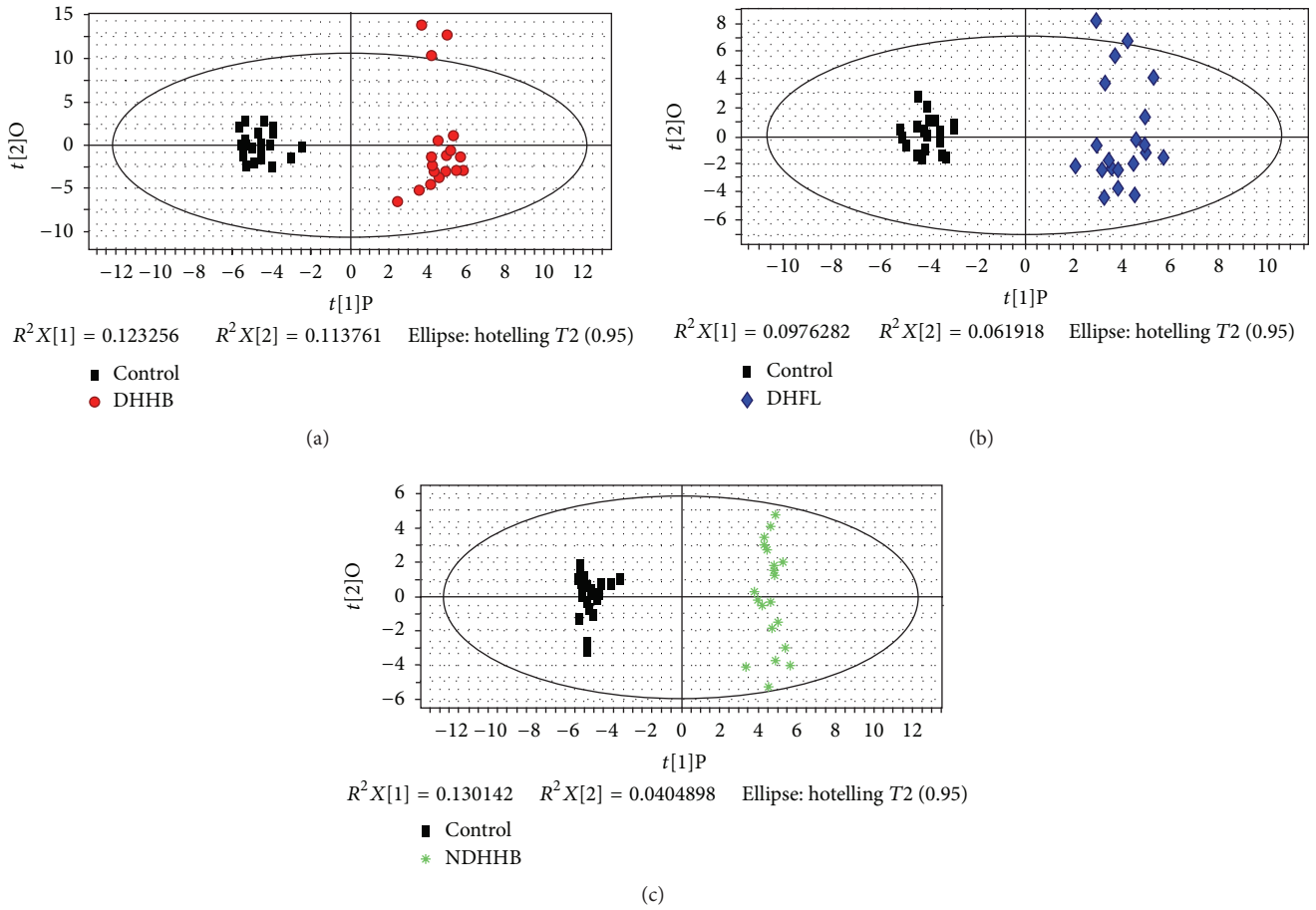

Figure 2: OPLS score plot of three syndromes compared to a healthy control group by symptoms and clinical indicators. (a) OPLS score plot of control and DHHB. (b) OPLS score plot of control and DHFL. (c) OPLS score plot of control and NDHHB.

profile. Therefore, all GC-MS raw files were converted to CDF format via the Agilent MSD Workstation software, and were subsequently processed by the XCMS toolbox (http://metlin.scripps.edu/download/) using XCMS's default settings with the following exceptions: xcmsSet (full width at half-maximum: fwhm = 5; S/N cutoff value: snthresh = 10, max = 25), group (bw = 5). The resulting table (CSV file) was exported into Microsoft Excel (Microsoft Inc., USA) where normalization was performed prior to multivariate analyses. The resulting three-dimensional matrix involving peak index (RT-m/z pair), sample names (observations), and normalized peak area percent was introduced into Simca-P 11.5 Umetrics software (Umea, Sweden) that was used for analysis of principal component analysis (PCA), partial least squares discriminant analysis (PLS-DA), and orthogonal partial least squares (OPLSs). Differential variables with VIP values [16] exceeding 1.5 between two different groups were generated from OPLS loadings plot. Subsequently, those variables were further analyzed by Mann-Whitney U-test to confirm the changes in metabolites by SPSS 17.0 (SPSS, Chicago, IL, USA) with the threshold P value set at 0.1. Firstly, the variables were identified by searching in NIST 2005 database. Then, standard compounds were used to confirm some of the identified metabolites.

Figure 1 shows a schematic diagram of the steps followed to determine the final list of potential biomarkers. The first step was to remove the differential information of CHB from the DHHB by removing the intersection of NDHHB and DHHB's differential information based on the ideas of the "same disease with different syndrome." The reduced set of first-step biomarkers were further filtered by taking advantage of the "different diseases with same syndrome." The final biomarkers were obtained from the intersection of the first-step DH biomarkers and biomarkers of DHFL.

3. Results

3.1. Establishment of the Potential Biomarkers of Clinical Symptoms and Indicators. All symptoms and clinical indicators were analyzed and utilized to distinguish the three syndrome groups (DHHB, NDHHB, and DHFL) and the healthy control group (control). Orthogonal partial least squares (OPLSs) was used to effectively extract variables responsible for the separation by removing variables unrelated to pathological status. Figures 2(a), 2(b), and 2(c) depict the OPLS score plots, which show that DHHB, NDHHB, and DHFL groups were clearly separated from the control group. The most meaningful characteristics were screened by OPLS loading

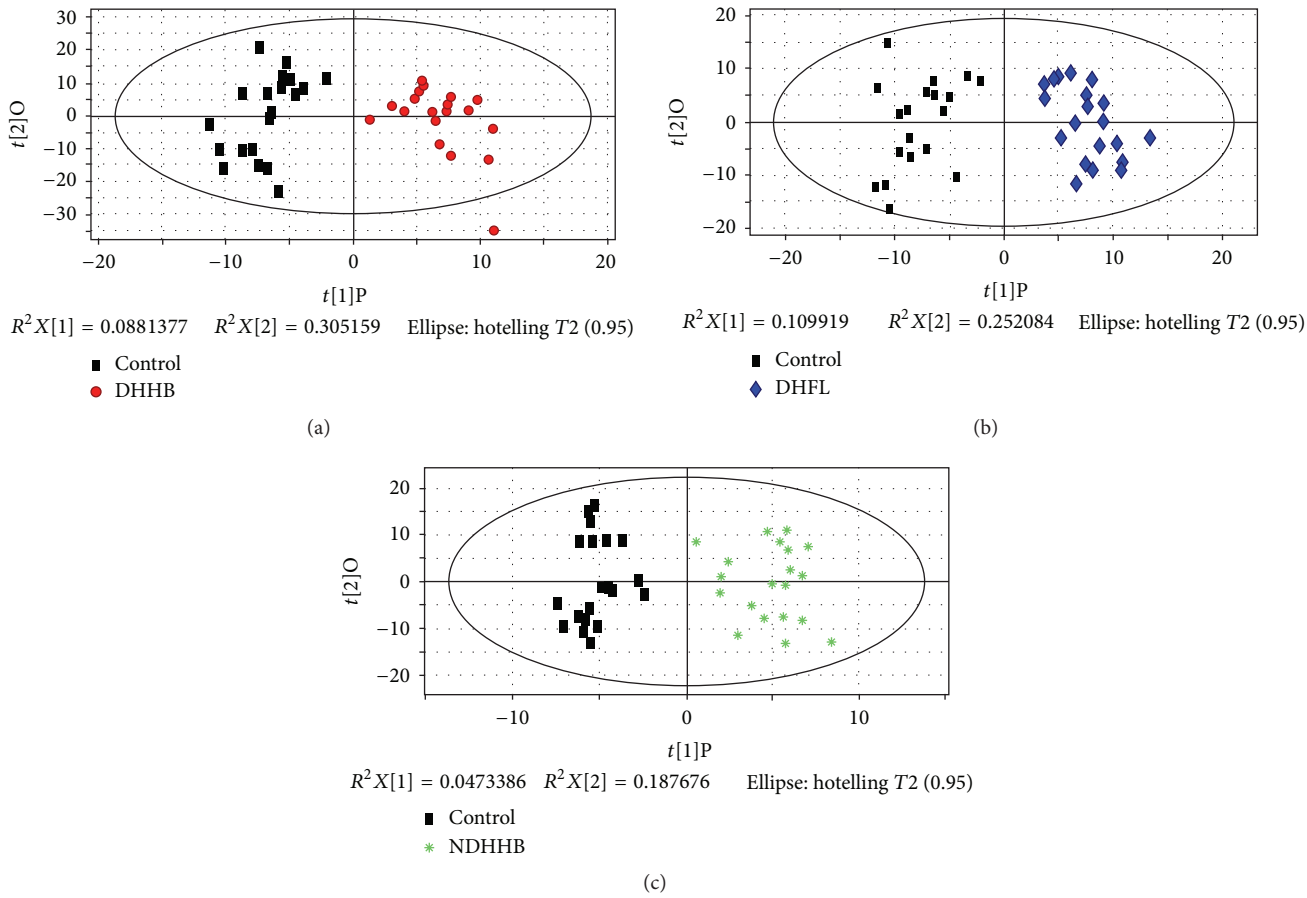

Figure 3: OPLS score plot of three syndromes compared to healthy control group by metabolites. (a) OPLS score plot of control and DHHB. (b) OPLS score plot of control and DHFL. (c) OPLS score plot of control and NDHHB.

plot analysis and are listed in Table 1. The quality of the model was characterized by two performance statistics, R^2Y (cum) and Q^2Y (cum), indicating the total explanation and predictability of the model [17]. The information of models is summarized in Table 4.

3.2. Establishment of the Potential Biomarkers of Urinary Metabolic Profiles. Urine profiles obtained from GC-MS were analyzed for distinctions among the three syndromes and the control group by OPLS. Figures 3(a), 3(b) and 3(c) indicate the OPLS score plot, which show a clear separation for DHHB, NDHHB, and DHFL groups from the control group. The most important variables for the discriminative models were screened by loading plot analysis. The potential metabolic biomarkers of each syndrome differentiated from control group were identified by the NIST database and are summarized in Table 2. Model information is summarized in Table 4.

3.3. Establishment of Potential Biomarkers of DH in CHB and FL. Because groups of selected markers may contain information of syndrome and disease, the biomarkers of DH were further filtered. Thus the final set of potential biomarkers considered were those that remained after the intersection of DHHB and NDHHB was removed from DHHB, and were intersected with DHFL. Figure 1 shows a schematic diagram of the steps. As to the former works, the potential macro-micro biomarkers were obtained from the integration of differential metabolites, hierarchical corresponding symptoms and clinical indicators. The potential biomarkers are listed in Table 3.

3.4. Preliminary Verification of Identified Biomarkers. The potential biomarkers were verified in 55 blind test cases of CHB with two Syndromes (Dampness-Heat Syndrome (DH) and Non-Dampness-Heat Syndrome (NDH)) for Syndrome classification. Using only the potential biomarkers or only the clinical symptoms and indicators did not differentiate the two syndromes satisfactorily (Figures 4(a) and 4(b)); however, by including metabolites, symptoms, and clinical indicators in the analysis, resulted in a stronger differentiation (Figure 4(c)). It is worth mentioning that former classifications (in Sections 3.1 and 3.2) were performed by supervised OPLS, owing to the complexity of clinical samples. However, the DH could be classified from NDH by unsupervised PCA in this verification with the selected biomarkers, which revealed the strong ability of DH differentiation, though they need further verification in clinical.

Table 1: Significantly different symptoms and clinical indicators identified in the three syndromes compared to a healthy control group.

Indicators and symptoms	Group	VIP[a]	P(M-W)[b]	FN[c]
Alkaline phosphatase	DHHB	1.69	0.00	+2.03
Apolipoprotein A-1	DHHB	1.74	0.00	+1.91
Aspartate aminotransferase	DHHB	1.62	0.00	+2.77
Glutamyltransferase	DHHB	1.65	0.00	+2.06
Immunoglobulin G	DHHB	2.01	0.00	+2.06
Prealbumin	DHHB	2.8	0.00	−2.56
β-globin	DHHB	2.52	0.00	+2.67
Thick fur	DHHB	1.81	0.00	+1.73
Bitter taste	DHHB	1.79	0.00	+1.89
Slimy and curdy fur	DHHB	1.75	0.00	−1.73
Mean corpuscular hemoglobin concentration	DHHB	1.84	0.00	+2.15
Tongue color	DHHB	2.15	0.00	+1.96
Basophil	DHHB	2.07	0.00	+2.56
Fur color	DHHB	2.68	0.00	+2.58
String-like pulse	DHHB	1.81	0.00	+1.73
Alanine aminotransferase	DHFL	2.08	0.00	+2.16
Aspartate aminotransferase	DHFL	1.78	0.00	+1.82
Total cholesterol	DHFL	2.10	0.00	+1.87
Triglyceride	DHFL	2.44	0.00	+2.60
β-globin	DHFL	2.54	0.00	+2.31
Thick fur	DHFL	1.92	0.00	+1.64
Lack of strength	DHFL	2.11	0.00	+1.64
Dysphoria	DHFL	1.98	0.00	+1.67
Slimy and curdy fur	DHFL	2.58	0.00	−2.03
Uric acid	DHFL	2.45	0.00	+2.31
Glucose	DHFL	1.95	0.00	+1.92
Tongue color	DHFL	2.03	0.00	+1.68
Systolic pressure	DHFL	1.89	0.00	+2.02
Diastolic pressure	DHFL	2.29	0.00	+2.37
Fur color	DHFL	3.08	0.00	+2.58
Weight	DHFL	2.79	0.00	+2.44
String-like pulse	DHFL	1.92	0.00	+1.64
Alkaline phosphatase	NDHHB	1.61	0.00	+1.87
Apolipoprotein A-1	NDHHB	2.07	0.00	+2.39
Activated partial thromboplastin time	NDHHB	1.60	0.00	+1.68
Hepatitis B core antibody	NDHHB	2.85	0.00	+2.90
Hepatitis B core antibody-immunoglobulin M	NDHHB	1.76	0.00	+2.90
Hepatitis B surface antigen	NDHHB	3.04	0.00	+2.90
Immunoglobulin G	NDHHB	1.60	0.00	+1.97
Prealbumin	NDHHB	2.38	0.00	−2.28
Triglyceride	NDHHB	1.77	0.00	+1.85
Total protein	NDHHB	1.85	0.00	+2.01
β-globin	NDHHB	2.54	0.00	+2.79
Teeth-marked tongue	NDHHB	2.11	0.00	+1.92
Gallbladder	NDHHB	2.04	0.00	+1.92
Relaxed pulse	NDHHB	1.69	0.00	+1.56
Lack of strength	NDHHB	1.93	0.00	+1.73
Mean corpuscular hemoglobin concentration	NDHHB	1.79	0.00	+2.11
Pre-S1 antibodies	NDHHB	3.14	0.00	+2.90
Pre-S1 antigen	NDHHB	3.14	0.00	+2.90

Table 1: Continued.

Indicators and symptoms	Group	VIP[a]	P(M-W)[b]	FN[c]
Luxuriant or withered tongue	NDHHB	1.73	0.00	+1.73
Soggy pulse	NDHHB	1.93	0.00	+1.73
Basophil	NDHHB	2.34	0.00	+2.41
Diastolic pressure	NDHHB	1.56	0.00	+1.72
Mean platelet volume	NDHHB	2.30	0.00	+2.58

[a]VIP: variable importance in the project.
[b]P(M-W) value was obtained from Mann-Whitney test (syndromes compared to healthy control).
[c]FN is fold change of mean ranks calculated by the Mann-Whitney test (syndromes compared to healthy control). "+" means upregulated and "−" means downregulated.

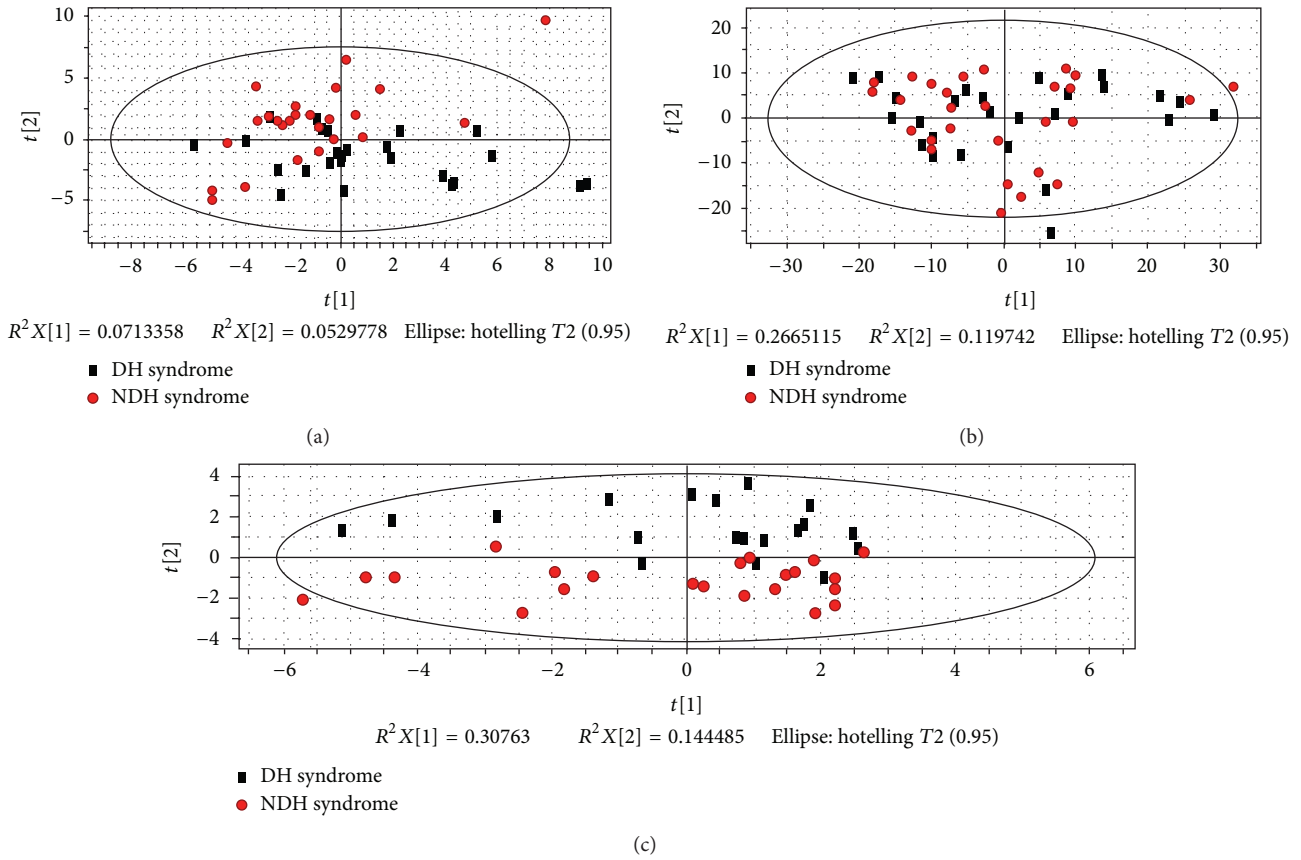

Figure 4: PCA score plot of DH versus NDH with potential biomarkers. (a) PCA score plot of DH and NDH only by symptoms and clinical indicators. (b) PCA score plot of DH and NDH only by metabolites. (c) PCA score plot of DH and NDH by macro-micro biomarkers from the integration of differential metabolites, hierarchical corresponding symptoms and clinical indicators.

4. Discussion

In this study, we attempted to explore the macro-micro biomarkers of DH, which could provide the feasibility and robustness for syndrome differentiation. The selected metabolites of DH were considered to be related with the pathogenesis. By analysis of KEGG (http://www.genome.jp/ kegg/), the 11 metabolic markers are related to biosynthesis of secondary metabolism, microbial metabolism in diverse environments, carbon fixation pathway in prokaryote, proteins digestion and absorption, and carbohydrate digestion and absorption, which could be classified in microbial metabolism and digestive capacity. These may correspond with "the disorder in transportation and transformation of the essence from food and drink" in TCM, which was regarded as one important reason for Dampness-Heat Syndrome [18, 19].

Aspartate transaminase (AST) is the only clinical indicator in our biomarkers. It may suggest that the clinical indicators are limited to classify the syndromes. But AST has been reported to be connected to DH, with odds ratio (OR) value equal to 5.49 [20]. There is thus strong evidence that DH reflects inflammation of the liver damage.

Table 2: Significantly different metabolites identified in the three syndromes compared to a healthy control group.

Compound	Group	VIP[a]	P(M-W)[b]	FN[c]
Acetic acid*	DHHB	1.87	0.00	−2.07
Succinic acid*	DHHB	1.85	0.01	−1.61
D-Xylose*	DHHB	2.22	0.00	−1.96
Maltose	DHHB	1.92	0.00	+1.89
Butyrate*	DHHB	1.87	0.00	−1.72
Aminolevulinic acid*	DHHB	1.67	0.00	−1.75
Ribitol	DHHB	2.22	0.00	−1.93
Creatinine*	DHHB	1.77	0.01	−1.63
Benzene*	DHHB	1.88	0.01	−1.56
2-Butenoic acid*	DHHB	1.81	0.02	−1.53
(R)-Mandelic acid*	DHHB	1.68	0.01	−1.59
Glutaconic acid*	DHHB	1.68	0.02	−1.54
Tartronic acid	DHHB	2.28	0.00	−2.10
Benzophenone	DHHB	1.58	0.02	−1.53
Pteridine	DHHB	1.75	0.00	−1.71
3-Amino-1,2,4-triazole	DHHB	1.74	0.02	−1.51
3-Indole butanoic acid*	DHHB	1.61	0.02	−1.50
1-Cyclohexene carboxylic acid	DHHB	1.93	0.01	−1.66
3-Indole acetic acid*	DHHB	1.58	0.00	−1.73
Pyrazinoic acid*	DHHB	1.62	0.00	−2.00
Acetic acid*	DHFL	1.52	0.00	−1.70
Succinic acid*	DHFL	1.90	0.00	−1.81
D-Fructose	DHFL	1.58	0.00	−1.75
D-Galactose	DHFL	1.69	0.00	−1.99
Benzoic acid	DHFL	1.51	0.01	−1.59
Butyrate*	DHFL	1.54	0.01	−1.65
D-Gluconic acid	DHFL	1.51	0.00	−1.70
Amino levulinic acid*	DHFL	1.54	0.00	−1.82
Glutarate	DHFL	1.57	0.01	−1.61
Creatinine*	DHFL	1.65	0.00	−1.69
Gulonic acid	DHFL	1.65	0.00	−1.72
Glucaric acid	DHFL	1.63	0.00	−2.02
3-Indole acetic acid*	DHFL	1.72	0.00	−2.09
(R)-Mandelic acid*	DHFL	1.76	0.00	−1.75
3-Indole butanoic acid*	DHFL	1.68	0.00	−1.68
1-Cyclohexenecarboxylic acid	DHFL	1.86	0.00	−1.81
Pseudouridine	DHFL	1.79	0.00	−2.10
Glutaconic acid*	DHFL	1.77	0.00	−1.71
Tetradecanoic acid	DHFL	1.68	0.00	−1.74
Ethylene	DHFL	1.51	0.01	−1.57
Pteridine	DHFL	1.57	0.00	−1.73
Pyrazinoic acid*	DHFL	1.53	0.00	−2.19
1-(1-Benzyl-1H-indol-3-yl)-2,2,2-trifluoroethanone	DHFL	1.63	0.00	−1.83
Glycine*	NDHHB	2.11	0.01	+1.62
D-Xylose*	NDHHB	2.15	0.01	−1.57
D-Gluconic acid	NDHHB	1.87	0.00	+1.85
Ribitol	NDHHB	2.19	0.01	−1.57
2,3-Butanedione	NDHHB	1.89	0.02	+1.56
Tartronic acid	NDHHB	2.21	0.00	−1.66
Vanillylmandelic acid	NDHHB	1.94	0.05	+1.42
3-Amino-1,2,4-triazole	NDHHB	2.31	0.03	−1.48

[a]VIP: variable importance in the project.

[b]P(M-W) value was obtained from Mann-Whitney test (syndromes compared to healthy control).

[c]FN is fold change of mean ranks calculated by the Mann-Whitney test (syndromes compared to healthy control). "+" means upregulated and "−" means downregulated.

*These metabolites were identified by NIST library and standards; others were only identified by NIST library.

Table 3: List of the macro-micro biomarkers of DH in CHB and NFL.

Biomarkers	Category
(R)-mandelic acid	Metabolites
1-Cyclohexenecarboxylic acid	Metabolites
3-Indole acetic acid	Metabolites
3-Indole butanoic acid	Metabolites
Acetic acid	Metabolites
Amino levulinic acid	Metabolites
Butyrate	Metabolites
Creatinine	Metabolites
Glutaconic acid	Metabolites
Pteridine	Metabolites
Pyrazinoic acid	Metabolites
Succinic acid	Metabolites
Aspartate aminotransferase	Indicators
Thick fur	Symptoms
Slimy and curdy fur	Symptoms
Tongue color	Symptoms
Fur color	Symptoms
String-like pulse	Symptoms

Table 4: Summary of the modeling quality of OPLS analysis.

Name	No[a]	R^2X_{cum} [b]	R^2Y_{cum} [c]	Q^2Y_{cum} [d]
1A	1P + 1O[e]	0.24	0.97	0.91
1B	1P + 1O	0.16	0.96	0.78
1C	1P + 1O	0.17	0.98	0.93
2A	1P + 2O	0.50	0.89	0.70
2B	1P + 3O	0.56	0.90	0.48
2C	1P + 3O	0.49	0.91	0.57

[a]No represents the number of components.
[b,c]R^2X_{cum} and R^2Y_{cum} represent the cumulative sum of squares (SSs) of all the X's and Y's explained by all extracted components.
[d]Q^2Y_{cum} is an estimate of how well the model predicts the Y's.
[e]1P + 1O: one predictive component and one orthogonal component for establishing the OPLS model.

Tongue diagnosis is of great importance for syndrome differentiation in TCM, determining the treating principle, prescribing a formula, and predicting the prognosis [21]. Except string-like pulse, other differential symptoms are the characterization of tongue, which is one of the direct objective bases for TCM clinical diagnosis and treatment. In our opinion, pulse diagnosis is as important as tongue diagnosis, so ultimately a more comprehensive analysis for the combination of them is needed.

Although only metabonomics was utilized in this study, we suggest that it would be valuable to expand beyond Metabonomics to system biology owing to the similarity between the various omics. Including a full System Biology approach to the determination of informative biomarkers will provide a more comprehensive and accurate syndrome differentiation. We thus suggest that genes, proteins, metabolites, and clinical information should all be integrated in future analyses.

5. Conclusion

This study is the first time that biomarkers of DH were obtained by a macro-micro approach with the integration of omic and clinical information to provide an effective and objective and repeatable approach for Chinese personalized medicine. Moreover, the preliminary verification indicated the feasibility and robustness of the approach for dampness-heat syndrome differentiation. Thus, these DH biomarkers could be used to provide a foundation on which we can to develop a possible population-screening tool for selecting target individuals and for creating an evaluation index for personalized treatment based on syndrome differentiation.

Authors' Contribution

Jianye Dai, Shujun Sun, and Jinghua Peng contributed equally to this work and should be considered cofirst authors.

Acknowledgments

This work was supported by the National Science and Technology Major Project (2012ZX10005001-004 and 2012ZX09303009-001), Shanghai Interdisciplinary Cultivation Platform of Outstanding and Innovative Postgraduates, and Shanghai "085" Science, and Technology Innovation Supporting Project for Top-grade Discipline Construction.

References

[1] Y. F. Liaw, N. Leung, J. H. Kao et al., "Asian-Pacific consensus statement on the management of chronic hepatitis B: a 2008 update," *Hepatology International*, vol. 2, no. 3, pp. 263–283, 2008.

[2] H. Y. Wang, H. M. Li, B. Yang, and J. J. Xu, "The relationship between distribution characteristics of TCM constitution and Syndromes in 141 patients with fatty liver," *Journal of Beijing University of TCM*, vol. 33, no. 7, pp. 500–502, 2010.

[3] J. Chang, X. F. Pan, W. W. Qiu, G. Y. Yang, and L. Q. Wang, "Objectivized study on syndrome differentiation for chronic hepatitis B," *Jiangsu Journal of TCM*, vol. 27, no. 5, pp. 26–27, 2006.

[4] J. L. Tang, B. Y. Liu, and K. W. Ma, "Traditional Chinese medicine," *The Lancet*, vol. 372, no. 9654, pp. 1938–1940, 2008.

[5] W. Zhang, T. Leonard, F. Bath-Hextall et al., "Chinese herbal medicine for atopic eczema," *Cochrane Database of Systematic Reviews*, no. 2, Article ID CD002291, 2005.

[6] J. M. Ezzo, M. A. Richardson, A. Vickers et al., "Acupuncture-point stimulation for chemotherapy-induced nausea or vomiting," *Cochrane Database of Systematic Reviews*, no. 2, Article ID CD002285, 2006.

[7] M. H. Pittler and E. Ernst, "Artemether for severe malaria: a meta-analysis of randomized clinical trials," *Clinical Infectious Diseases*, vol. 28, no. 3, pp. 597–601, 1999.

[8] M. A. Hamburg and F. S. Collins, "The path to personalized medicine," *The New England Journal of Medicine*, vol. 363, no. 4, pp. 301–304, 2010.

[9] J. L. Yuan, H. Zhang, L. Wang et al., "Biochemical characteristics of traditional Chinese medicine syndromes and their elements

in patients with hepatitis B cirrhosis," *Journal of Chinese Integrative Medicine*, vol. 9, no. 4, pp. 374–381, 2011.

[10] L. H. Zhao, C. Xiao, X. P. Yan et al., "Correlation between heat or cold syndrome and cytokine, and laboratory index in women with early rheumatoid arthritis," *Acta Universitatis Traditionis Medicalis Sinensis Pharmacologiaeque Shanghai*, vol. 20, no. 1, pp. 21–24, 2006.

[11] X. Q. Yue and Q. Liu, "Analysis of studies on pattern recognition of tongue image in traditional Chinese medicine by computer technology," *Journal of Chinese Integrative Medicine*, vol. 2, no. 5, pp. 326–329, 2004.

[12] B. Pang, D. Zhang, N. Li, and K. Wang, "Computerized tongue diagnosis based on Bayesian networks," *IEEE Transactions on Biomedical Engineering*, vol. 51, no. 10, pp. 1803–1810, 2004.

[13] Chinese Society of Hepatology and Chinese Society of Infectious Diseases, Chinese Medical Association, "The guideline of prevention and treatment for chronic hepatitis B, (2010 version)," *Chinese Journal of Hepatology*, vol. 19, no. 1, pp. 13–24, 2011.

[14] F. Jian-gao and Chinese Liver Disease Association, "Guidelines for management of nonalcoholic fatty liver disease: an updated and revised edition," *Chinese Journal of Hepatology*, vol. 18, no. 3, pp. 163–166, 2010.

[15] S. J. Sun, J. Y. Dai, W. Y. Wang et al., "Metabonomic evaluation of ZHENG differentiation and treatment by fuzhenghuayu tablet in hepatitis-B-caused cirrhosis," *Evidence-Based Complementary and Alternative Medicine*, vol. 2012, Article ID 453503, 8 pages, 2012.

[16] L. Eriksson, E. Johansson, and N. Kettaneh-Wold, *Multiand Megavariate Data Analysis, Part 1: Basic Principles and Applications*, Umetrics AB, Umeå, Sweden, 2nd edition, 2001.

[17] P. Yin, D. Wan, C. Zhao et al., "A metabonomic study of hepatitis B-induced liver cirrhosis and hepatocellular carcinoma by using RP-LC and HILIC coupled with mass spectrometry," *Molecular BioSystems*, vol. 5, no. 8, pp. 868–876, 2009.

[18] J. B. Zhang, "Complete Works of Jingyue (jing yue quan shu)," 1640.

[19] T. S. Ye, "Treatise on Worm Heat Disease (wen bing lun)," 1746.

[20] N. J. Li, J. Wang, and S. K. Yao, "Relationship between Dampness-Heat Syndrome and liver inflammation indicators," *Chinese Journal of Basic Medicine in Traditional Chinese Medicine*, vol. 17, no. 3, pp. 294–295, 2011.

[21] T. F. Wang, *Diagnostics of Traditional Chinese Medicine*, People's Medical Publishing House, Beijing, China, 2nd edition, 2007.

Hindawi Publishing Corporation
Evidence-Based Complementary and Alternative Medicine
Volume 2013, Article ID 672873, 12 pages
http://dx.doi.org/10.1155/2013/672873

Review Article

Hyperthermia versus Oncothermia: Cellular Effects in Complementary Cancer Therapy

Gabriella Hegyi,[1] Gyula P. Szigeti,[2] and András Szász[3]

[1] *Department of Complementary and Alternative Medicine, University of Pécs, Hungary*
[2] *Department of Physiology, University of Debrecen, and Institute of Human Physiology and Clinical Experimental Research, Semmelweis University, Hungary*
[3] *Department of Biotechnics, St. Istvan University, Gödöllő, Hungary*

Correspondence should be addressed to Gabriella Hegyi; drhegyi@hu.inter.net

Received 7 October 2012; Accepted 1 January 2013

Academic Editor: Wei Jia

Hyperthermia means overheating of the living object completely or partly. Hyperthermia, the procedure of raising the temperature of a part of or the whole body above normal for a defined period of time, is applied alone or as an adjunctive with various established cancer treatment modalities such as radiotherapy and chemotherapy. However, hyperthermia is not generally accepted as conventional therapy. The problem is its controversial performance. The controversy is originated from the complications of the deep heating and the focusing of the heat effect. The idea of oncothermia solves the selective deep action on nearly cellular resolution. We would like to demonstrate the force and perspectives of oncothermia, as a highly specialized hyperthermia in clinical oncology. Our aim is to prove the ability of oncothermia to be a candidate to become a widely accepted modality of the standard cancer care. We would like to show the proofs and the challenges of the hyperthermia and oncothermia applications to provide the presently available data and summarize the knowledge in the topic. Like many early stage therapies, oncothermia lacks adequate treatment experience and long-range, comprehensive statistics that can help us optimize its use for all indications.

1. Introduction

In oncology, the term "hyperthermia" refers to the treatment of malignant diseases by administering heat in various ways. Hyperthermia is usually applied as an adjunct to an already established treatment modality (radiotherapy and chemotherapy), where tumor temperatures in the range of 40–46°C are aspired. Interstitial hyperthermia, hyperthermic chemoperfusion, and whole-body hyperthermia are still under clinical investigation, and a few positive comparative trials have already been completed. In parallel to clinical research, several aspects of heat action have been examined in numerous preclinical studies.

The traditional *hyperthermia* is controlled the only single thermodynamic intensive parameter, with the temperature. *Oncothermia*, which is a "spin-off" form of the hyperthermia, is based on the paradigm of the energy-dose control, replacing the single temperature concept [1]. With this approach, oncothermia returned to the gold standards of the dose concepts in medicine; instead of the parameter, which cannot be regarded as dose (the temperature does not depend on the volume or mass), oncothermia uses the energy (kJ/kg [=Gy]) like the radiation oncology uses the same (Gy) to characterize the dosing of the treatment.

This paper deals with discussions concerning the direct and indirect cytotoxic effect of heat and energy; heat-and energy-induced alterations of the tumor microenvironment; synergism of heat in conjunction with radiation and drugs; the presumed cellular effects of hyperthermia and oncothermia including the expression of heat-shock proteins (HSPs), induction and regulation of apoptosis, signal transduction, and modulation of drug resistance by hyperthermia or oncothermia.

2. Biophysical and Metabolic Differences between Healthy and Cancerous Cells

The clue to find the mechanisms, which could create the requested optimization, selection and control of the energy

intake based on the clear biophysical differences between healthy and cancerous cells, finding the biophysical property to focus the energy on the desired cellular membranes. The main difference could be found in the metabolic processes of malignant cells and their healthy counterparts. In consequence of the physical differences, the malignant cell are distinguishable by their biophysical parameters. The electric properties of the cancerous cells differ from normal, and the main differences are.

(i) The efficacy of the ATP production in cancerous cell is low. The large ATP demand for the proliferative energy consumption allows less ATP for active membrane stabilization by K^+ and Na^+ transport; so the membrane potentiating weakens.

(ii) The cellular membrane of cancerous cells is anyway electrochemically also different from the normal, as well as its charge distribution also deviates.

(iii) The membrane of the cancerous cell differs in its lipid and sterol content form their healthy counterpart.

(iv) The membrane permeability is changed by the previous differences. In consequences of these, the efflux of the K^+, Mg^{2+}, and Ca^{2+} ions, while the efflux of Na^+ decreases together with the water transport from the cell. Consequently the cell swallows, its membrane potential decreases further. (The efflux of K^+ regulates the pH of the cell and takes the protons out form the cytosol.) The concentration of Na^+ increases in the cytosol, and parallel of this, the negative ion-concentration also grows on the glycocalix shell, decreasing the membrane potential and the tumor will be negatively polarized in average. This fact was well used for direct current treatment (electrochemical cancer therapy (ECT)) by Nordenstrom and others.

(v) The conductivity and the dielectric constant of the tumor tissue will be higher than normal.

The healthy cells work collectively, and their energy-consumption as well as their life-cycles and the availability of resources are controlled on collective way by the various form of the self-organizing. The healthy cells are organized in this way, and their standard cycles, reactions, and structures are complexly regulated in both internal and external areas.

The malignant cells behave in completely different way. This process is the "ancient" chemical reaction, which was characteristic at the beginning of the evolution of the life, when the oxygen, the general electron acceptor, was available only in a small amount in the atmosphere. It is the fermentative way to utilize the energy of glucose converts it into lactic acid ($CH_3CHOHCOOH$), producing 2 ATPs in one cycle, while the healthy cycle (Krebs cycle) produces 36 ATPs [2].

The enormously large demand of malignant cells for nutrients, not only the ionic density in the surrounding, makes the malignant cells distinguishable, but their structure is also very different. Their demand for the huge energy production pushes them for the permanent competition for the sufficient amount of nutrition. The cells became independent competitors instead of the normal cooperation, and the harmony had been replaced by autonomy. The intercellular contacts in healthy network are broken in cancer, the order of the tissue had been lost, and the "social signal" between the cells vanished. The malignant cells become disordered, nonconnected, and isolated. The malignancy has definitely different structure that its healthy counterpart, and its dielectric constant and optical refractive index deviates from normal. The lost intercellular contacts block the natural control over the structural changes, and the disordered structure changes the optical properties also [2].

3. Hyperthermia

Hyperthermia is the process of raising the body temperature, either locally or globally, for medicinal purposes. Historically, hyperthermia has been recognized for its curative power in treating tumors [3, 4]. The first application of hyperthermia for regional cancer control dates to 1898 when the Swedish gynecologist Westermark [5] treated cervical cancer by running hot water through an intracavitary spiral tube. He noted excellent clinical response in the seven patients treated. More recent clinical studies have shown that the success of a hyperthermia cancer treatment is related to the minimum temperature rise occurring in the tumour tissue [6, 7]. Unfortunately, prolonged exposure of normal, healthy tissue to elevated temperatures has a detrimental effect [8].

3.1. The Basic Concept. To reach temperatures clearly above the systemic temperature of 37.5°C in a defined target volume is a technical challenge. The effectiveness of hyperthermia treatment is related to the temperature achieved during the treatment, as well as the length of treatment and cell and tissue characteristics. To ensure that the desired temperature is reached, but not exceeded, the temperature of the tumour and surrounding tissues is monitored throughout the hyperthermia procedure. Another important challenge was to minimize damage to healthy tissue and other adverse effects, and physicians carefully monitor the temperature of the affected area. The goal is to keep local temperatures under 44°C to avoid damage to surrounding tissues, and the whole body temperatures under 42°C, which is the upper limit compatible with life.

Most clinical hyperthermia systems operate by causing a target volume of tissue to be exposed to electromagnetic or ultrasound radiation. A structure is needed that is capable of transferring energy into biological tissue and getting the best approximation of the area to be treated by 3D distribution of SARs. The majority of the hyperthermia treatments are applied using external devices (applicators), employing energy transfer to the tissue [9, 10]. For a heating system to be effective, it must be able to produce final time and temperature histories that include a set of tumor temperatures that can be maintained for long enough times to result in clinically effective thermal doses without also producing unacceptable normal tissue temperatures [11].

A great deal of current research focuses on precisely positioning heat-delivery devices (catheters, microwave and

ultrasound applicators, etc.) using ultrasound or magnetic resonance imaging, as well as developing new types of nanoparticles that make them particularly efficient absorbers while offering little or no concerns about toxicity to other tissues. Applicators are positioned around or near the appropriate region, and energy is focused on the tumor to raise its temperature. To describe the different applicators and hyperthermia methods is not our aim in this paper; however, the summary of the effects of regional especially the locoregional hyperthermia on cell and tissue level is in the next chapters. Regional hyperthermia heats a larger part of the body, such as an entire organ. Usually, the goal is to weaken cancer cells so that they are more likely to be killed by radiation and chemotherapeutic medications.

3.2. Mechanisms of Hyperthermia. The cellular effect of hyperthermia is more complicated. Briefly, hyperthermia may kill or weaken tumor cells, and is controlled to limit effects on healthy cells. Tumor cells, with a disorganized and compact vascular structure, have difficulty dissipating heat. Hyperthermia may therefore cause cancerous cells to undergo apoptosis in direct response to applied heat, while healthy tissues can more easily maintain a normal temperature. Even if the cancerous cells do not die outright, they may become more susceptible to ionizing radiation therapy or to certain chemotherapy drugs, which may allow such therapy to be given in smaller doses. Intense heating will cause denaturation and coagulation of cellular proteins, rapidly killing cells within the targeted tissue. A mild heat treatment combined with other stresses (excitation of the appropriate signal pathways) can cause cell death by apoptosis. There are many biochemical consequences to the heat shock response within the cell, including slowed cell division and increased sensitivity to ionizing radiation therapy. Hyperthermia can kill cells directly, increasing blood flow to the warmed area, perhaps doubling perfusion in tumors, while increasing perfusion in normal tissue by ten times or even more [12]. This enhances the delivery of medications. Hyperthermia also increases oxygen delivery to the area, which may make radiation more likely to damage and kill cells, as well as preventing cells from repairing the damage induced during the radiation session.

While it is acknowledged that at the tissue, organ, and whole body level there are numerous effects that can contribute to the clinical uses of hyperthermia, this review focuses mainly on effects at the cellular level. The goal of hyperthermia research is to find the molecular mechanisms by which heat kills tumour cells or any cells and the mechanisms by which hyperthermia radiosensitizes cells to radiation or chemotherapeutic agents. A major problem is that hyperthermia causes a large number of macromolecular changes and affects functions in all cellular compartments at temperatures above 43°C.

The potential importance of the hyperthermia for cancer treatment has been highlighted by Coffey et al. [13, 14]. Specifically, the review addresses four topics: (1) hyperthermia induced cell killing, (2) vascular, (3) cellular and intracellular mechanisms of thermal effects in the hyperthermia temperature range, and (4) effects on proteins that contribute to resistance to other stresses, for example, DNA damage.

3.3. Vascular Changes of Thermal Effects in the Hyperthermia. Mild heat temperatures cause an increase in blood flow. At the same time, there is a corresponding increase in the oxyhaemoglobin saturation of the individual red blood cells within tumour microvessels. These changes will lead to an overall increase in oxygen availability and improve tumour oxygenation status [15, 16]. At higher temperatures one may see a very transient increase in blood flow during the heating period, but vascular damage soon begins to occur and this will rapidly lead to a decrease in tumour blood flow [17–19]. With higher heat temperatures, there is also a corresponding decrease in oxyhaemoglobin saturation, and these changes will result in a decrease in overall oxygen availability. This lack of oxygen will also give rise to a decrease in tumour pH and ultimately lead to ischemia and cell death [17]. The degree of vascular shutdown at the higher temperatures appears to be dependent on the time and temperature of heating and the tumour type. Normal tissues typically show a very different vascular response to heat, with flow essentially increasing as the temperature increases, even at temperatures that produce substantial vascular occlusion in tumours [20, 21].

3.4. Thermal Cell Killing and Other Cellular Effects of Hyperthermia. In the hyperthermia, the main effects at the cellular level that are of relevance to cancer therapy are cell killing. It has been long recognized that hyperthermia in the 40–47°C temperature range kills cells in a reproducible time and temperature dependent manner. In the hyperthermic region there are three particularly significant and important cellular responses for thermal therapy: cytotoxicity, radiosensitization, and thermotolerance [22, 23]. Survival curves for temperatures in the 43–47°C range typically show a shoulder with an exponential reduction in clonogenic survival as a function of time at a given temperature [14]. The "shoulder" of the survival curve reflects a two-step process of cell killing. This is marked by a linear growth arrest in the beginning of heat exposure (reflecting a reversible, nonlethal heat damage), that is followed by exponential cell death. One fundamental observation is that the capability to induce cell death in vitro at lower temperatures <42–43°C is markedly lower than above 43°C [14].

The changes induced by hyperthermia at the cellular level must be due to temperature-induced alterations in molecular pathways, which usually involve inhibition of DNA, RNA, and protein synthesis [23]. However, while protein synthesis is inhibited during heating at higher temperatures, at milder temperatures and after return to normal growth temperature the induction of heat shock proteins occurs [24], which is an inducing event and closely associated with the induction of thermotolerance. Thus, heat shock can lead to both inactivating and activating responses. A fundamental question is the identity of the molecular events leading to the cellular sensing of altered temperature with subsequent alterations in cellular function. The principal conclusion from these studies is that

for hyperthermia, thermal dose is a combination of time and temperature.

The intensity of cell death in hyperthermia is showed cell cycle dependence. In general, high heat sensitivity can be observed during the S and M phases. Microscopic examinations of M-phase cells subjected to hyperthermia show damage of their mitotic apparatus leading to inefficient mitosis and consecutive polyploidy. S-phase cells are also sensitive to hyperthermia, where chromosomal damage is observed. Both S- and M-phase cells undergo a "slow mode of cell death" after hyperthermia, whereas those exposed to heat during G1-phase are relatively heat resistant and do not show any microscopic damage. Cells during G1-phase may follow a "rapid mode of death" immediately after hyperthermia. These variations existing between the different cell cycle phases indicate the possible diversity of molecular mechanisms of cell death following hyperthermia [24–26].

The thermal reactions promote numerous other effects than simple cell-killing. The most important for this complementary therapy are those effects that alter the resistance of cells to radiation and/or chemotherapeutic agents. The challenge is to determine which molecular changes are critical for the relevant endpoint such as tumour cell killing and sensitization to chemo- and radiation therapy [3, 27].

To answer the question, there is an unfolding story of tumour pH and its consequences have become clearer over the last two decades [2]. Using new intracellular methods the intra- and/or extracellular pH is measurable in tissues. Under many conditions it has now been confirmed that the intracellular pH in tumour cells is neutral to alkaline as long as tumours are not oxygen and energy deprived [28]. Tumour cells have mechanisms for exporting protons into the extracellular space. It means that a strong pH gradient exists across the cell membrane in tumours ($pH_i > pH_e$). Interestingly, this gradient is the reverse of that found in normal tissues where pH_i is lower than pH_e [9, 29, 30]. Under anaerobic condition cancer cells intensively split glucose to lactic acid, and other relevant pathogenetic mechanisms yielding an intensified tissue acidosis are based on substantial ATP hydrolysis, glutaminolysis, ketogenesis, and CO_2/carbonic acid production. Acidosis can sensitise tumour tissue to single heat treatments and to fractionated hyperthermia. Summarising the relevant data, it can be stated that tumour temperatures >42.5°C, and appropriate heating can reduce both intracellular and extracellular pH, which may further sensitise tumour cells to hyperthermia in the sense of a positive feedback mechanism [28]. Relevant pathogenetic mechanisms leading to an intensified acidosis upon heat treatment (which is reversible after hyperthermia) are

(1) an increased glycolytic rate with accumulation of lactic acid,

(2) an intensified ATP-hydrolysis,

(3) an increased ketogenesis with accumulation of acetoacetic acid and β-hydroxybutyric acid,

(4) an increase in CO_2 partial pressures,

(5) changes in chemical equilibria of the intra- and extracellular buffer systems (DpH/DT = −0.016 pH units/C),

(6) an inhibition of the Na^+/H^+ antiporter in the cell membrane [3, 31].

The ATP decline observed upon heat treatment is mostly due to

(1) an increased ATP turnover rate (i.e., intensified ATP hydrolysis), and as a result of an increased ATP degradation, an accumulation of purine catabolites has to be expected together with a formation of H^+ ions and reactive oxygen species at several stages during degradation to the final product uric acid,

(2) a poorer ATP yield as a consequence of a shift from oxidative glucose breakdown to glycolysis [28].

The significance of the baseline pH_e and pH_i values and changes occurring during hyperthermia in clinical studies still remains unclear, since—in contrast to in vitro and in vivo data derived from experimental tumours treated with hyperthermia alone—the results are equivocal so far. Further clarification of these effects is urgently needed.

Thermal sensitivity has been shown to greatly depend on the efficacy of tumour blood flow and parameters defining the metabolic microenvironment such as hypoxia, acidosis, substrate deprivation, accumulation of metabolic waste products, and energy depletion. If recent experimental data are critically evaluated, there is some evidence that besides microcirculatory function, intracellular pH and the bioenergetic status may be decisive factors ultimately modulating the thermosensitivity of cancer cells.

Israël and Schwartz [2] in 2011 summarized the metabolism of cancer cells. Briefly, in tumour cells the glycolysis is elevated, but a pyruvate kinase (PK) "bottleneck" interrupts phosphoenol pyruvate (PEP) to pyruvate conversion. Thus, alanine following muscle proteolysis transaminates to pyruvate, feeding lactate dehydrogenase, converting pyruvate to lactate (Warburg effect) and NAD^+ required for glycolysis. Cytosolic malate dehydrogenase also provides NAD^+ (in OAA to MAL direction). Malate moves through the shuttle giving back OAA in the mitochondria. Below the PK-bottleneck, pyruvate dehydrogenase (PDH) is phosphorylated (second bottleneck). However, citrate condensation increases; acetyl-CoA will thus come from fatty acids b-oxydation and lipolysis, while OAA sources are via PEP carboxy kinase and malate dehydrogenase (pyruvate carboxylase is inactive). Citrate quits the mitochondria, (note interrupted Krebs cycle). In the cytosol, ATP citrate lyase cleaves citrate into acetyl CoA and OAA. Acetyl CoA will make fatty acids triglycerides. Above all, OAA pushes transaminases in a direction usually associated to gluconeogenesis! This consumes protein stores, providing alanine (ALA); like glutamine, it is essential for tumors. The transaminases output is aspartate (ASP) it joins with ASP from the shuttle and feeds ASP transcarbamylase, starting pyrimidine synthesis. ASP in not processed by argininosuccinate synthetase, which is blocked, interrupting

the urea cycle. Arginine gives ornithine via arginase, and ornithine is decarboxylated into putrescine by ornithine decarboxylase. Putrescine and SAM form polyamines (spermine spermidine) via SAM decarboxylase. The other product 5-methylthioadenosine provides adenine. Arginine deprivation should affect tumors. The SAM destruction impairs methylations, particularly of PP2A, removing the "signaling kinase brake," PP2A also fails to dephosphorylate PK and PDH, forming the "bottlenecks." (Black arrows = interrupted pathways.).

Israël and Schwartz [2] suggested some new cancer treatments based on the previously described metabolic advantage of tumour cells.

(1) Inhibit alanine transaminase, glutaminase, ornithine decarboxylase, and arginase and decrease alanine, glutamine, arginine, and supplies.

(2) Open PK and PDH bottlenecks (enzyme kinase inhibition and PP2A phosphatase activation by methylation helpers).

(3) Close citrate synthase, ATP citrate lyase, and increase the NADH mitochondrial potential.

(4) Decrease GH/IGF and "tyrosine kinase receptor" signals.

(5) Cancel epigenetic changes using HDAC inhibitors and then HAT inhibition

(6) Boost immune NK protection.

So important is the steps 1–4 showing strong ATP dependence. The hyperthermia treatment as we described before reduces the intracellular ATP concentration. The major consequence of the low ATP is the inhibition the ATP dependent enzyme activity.

3.5. Effects on Heat Shock Proteins and the Consequent Immunomodulation. Protein damage is the main molecular event underlying the biological effects of hyperthermia in the clinically relevant temperature range (39–45°C). The activation energies for protein denaturation and heat-induced cell death are within the same range [32]. Despite the fact that it is known that protein damage plays a central role in the biological effects of hyperthermia, little is known about what finally kills the cells [33]. Temperature elevations transiently upregulate heat shock genes that encode a class of heat shock proteins (HSPs). The mechanism responsible for the heat shock response is an autoregulatory loop; HSPs normally keep the responsible transcription factor (HSF-1) inactive but upon heating HSP bind with higher affinity to unfolded proteins, triggering the release of HSF-1 from HSP which initiates HSP gene transcription. Once the protein damage/aggregation is restored after the heat shock by the HSP, substrate-free HSP themselves seem involved in attenuating the response by rebinding HSF-1 [34]. As a result, HSP levels transiently rise after heating but also gradually decline again upon prolonged stress free periods. The upregulation of HSP is closely associated with a transient resistant state of cells towards a subsequent second heat shock. It is thought that the elevated HSP levels, by their chaperone activity, protect cells against protein damage induced by the 2nd heating.

HSPs were originally described with respect to their roles as chaperones induced by temperature shock as well as various other types of stress [12]. HSP are usually divided into small HSP (molecular mass less than 40 kDa) and the HSP 60, HSP 70, HSP 90, and HSP 100 proteins families. Today, at least HSP 27 and HSP 70 are supposed to represent "general survival proteins" that are able to defend cells against a variety of potentially lethal (proapoptotic) stimuli [12]. In hyperthermia, HSPs are thought to be involved in the protection of cells against heat damage. Intracellular HSP synthesis increases when cultured cells are exposed to moderate heat application. At higher temperatures, inhibition of HSP synthesis occurs above a distinct threshold temperature. In general, the temperature, respectively, thermal dose, at which HSP synthesis is inhibited in a given experimental system varies between different cell types, but the respective threshold can be lowered when further (proapoptotic) stimuli are added. As lack of HSP synthesis is associated with exponential cell death, and it is generally accepted that HSPs prevent cells from lethal thermal damage [12, 35–37].

Recently, an additional role has been ascribed to HSPs which should be importance in hyperthermia as activators of the immune system. The importance of the HSP family, including HSP70 and HSP90 in immune reactions has been demonstrated, and several researchers have reported that heat-treated tumor cells can play a vaccine-like role and elicit antitumor immunity [12, 35–37]. HSP have been found to play important roles in eliciting potent anticancer immune responses mediated by T-cells, antigen-presenting cells (APCs), and natural-killer (NK) cells. In order to explain the paradoxical situation of how highly conserved HSP mediate cancer immunity, Srivastava et al. [38] proposed the following four paradigms:

(a) due to short nonconserved immunogenic regions,

(b) because a tissue specific expression pattern HSP can act as classical foreign antigens,

(c) HSP could mimic classical T-cell epitopes,

(d) act as carrier molecules for immunogenic peptides.

Presently, experimental evidence exists for possibilities (a) and (c). Tumour-derived HSP (HSP 70, Hsc70) and gp96 have been shown to chaperone immunogenic peptides to MHC molecules that elicit T-cell responses against primary tumours and metastases. Antigen-presenting cells have been found to be key for mediating this specific immune response. The membrane-bound HSP 70 provides a target recognition structure for transiently plastic adherent NK cells. A correlation of the cytolytic activity of NK cells with the amount of plasma membrane-bound HSP 70 has been determined. Although an HSP 70-NK cell interaction could be demonstrated in binding studies (unpublished data), the mechanism of how NK cells lyse Hsp70 positive tumour target cells remains to be elucidated. HSP 70 expressing tumour cells are more sensitive to lysis mediated by IL-2 stimulated, transiently plastic adherent NK cells, as compared to HSP 70 membrane negative tumour cell. Selectively transiently

plastic adherent NK cells, but not T-cells, exhibit an increased cytolytic activity against Hsp70 membrane positive tumour target cells [12, 35–37].

In summary, the data provide evidence that membrane-bound HSP 70 or the extracellular exposed HSP 70 peptide TKD might provide a tumour-selective target recognition structure for CD94 positive NK cells. The elucidation of potential coreceptors or partner molecules of CD94 that mediate triggering signals following contact with HSP 70 protein or HSP 70 peptides is currently under investigation.

4. Problem with the Hyperthermia

The requested job is to kill the malignant cells, for what a definite energy dose is necessary [39]. The historical energy-dose-like control (temperature multiplied by its application time) is physically incorrect and operates with an overall energy average in the area, instead of a directed and well-measurable energy dose (measured in kJ). The high energy application could cause controversies the high temperature burns the malignant cells but because it is missing selectivity and it damages the healthy cells and starts unwanted physiological reactions as well as enlarged dissemination possibility. These conditions make the hyperthermia effect not controlled, irrespective that the temperature could be kept on a certain level in the tumor or not. In reality the selectivity which would be necessary for the actions is missing, and the heating attacks all the cells in the target and also unselectively provokes the psychological control and regulation. The original idea of the hyperthermia was the "fire by fire" concept; set a controlled contrafire depleting the possible firesupply, blocking the coming large bush-fire endangering a house. The heated tumor is forced to higher metabolism; high metabolic rate of the cancer lesion is gained by elevated temperature. However, when the surrounding is intact, it delivers the same amount of nutrients than before and does not deliver more glucose for the forced metabolism. The tumor very quickly deflates from nutrients, empties all its energies, suffers, and burns away. However, by the large heating energy heats up the healthy surrounding us well, the blood flow will be enhanced, the nutrients supply will be higher, we make opposite than our aim was to do. The situation became even worst by continuing the high-energy heating: the high blood flow helps the dissemination and could gain the metastases. With this we can definitely worsen the survival and the quality of life of the patient. The blood flow is an important thermodynamic modification factor, which makes the dominant addition to the temperature development in the tumor. According to the fits of measurements, actually the blood flow for tumor and the healthy tissues are both definitely temperature dependent, and in general there is a threshold when the blood flow of the tumor became lower than the blood flow of the healthy surroundings. Below this threshold the efficacy of radiotherapy (which is propositional with the oxygenation of the tissue) and the chemotherapy, which is proportional with the drug-concentration in the tissue) is growing by the increasing of the temperature, because both of these properties are delivered by the increasing blood-flow. However, the complementary therapies over the threshold are suppressed by the decreasing of the blood-flow in the tumor.

5. Change of Paradigm: The Oncothermia

Oncothermia technology heats nonequally; concentrating the absorbed energy to the intercellular electrolytes [40]. This method creates inhomogeneous heating, microscopic temperature differences far from thermal equilibrium. The definitely large temperature gradient between the intra- and extracellular liquids changes the membrane processes and ignites signal pathways for natural programmed cell-death, avoiding the toxic effects of the simple necrosis. The synergy of electric field with the thermal effects potently and selectively makes the job [41].

5.1. How the Oncothermia Works, Generally. Advantage of oncothermia, that while the classical artificially focused hyperthermia has to heat up in case of the multiple lesions overlapping all the volume, which contains these lesions; contrary, oncothermia automatically focuses on the lesions in their multiple places, without treating the healthy tissue between. Oncothermia has a simple technical setup. The modulated radiofrequency current (RF) flows through the lesion. The RF current which flows through the cancerous lesion automatically focused by its lower impedance will flow mainly in the extracellular electrolyte, because the cells are electronically isolated by their membrane by more than one-million V/m field strength. The membrane disruption is one of the targeted aims, and many research groups are dealing with the electric field action on the cellular divisions. The main advantage of the electric field application is the missing control of the organism, physiology control over this effect; no physiology feedback is directly limiting the electric field and only its consequences could be regulated. The process made by oncothermia has its main energy delivery into the extracellular liquid, heating it up, and creating a little (1/1000°C) difference between the inner and outer temperature of the cell. This looks only a small difference, but regarding of the very tiny membrane layer (5 nm), the small difference in standard conditions is pretty high: ~200,000°C/m! This starts a prompt heat flow from outside to the cell through the membrane and permanently acts till the temperature difference exists. Despite of the quick heat-flow through this tiny membrane, the heat current is long-lasting, till the full cellular interior is not heated up to the same temperature than outside [42–44].

Oncothermia does not require high temperature for the treatment, the energy used for distortion of the selected malignant cells is that of thermodynamic effects (heat-flows are applied instead of the general average isotherms). Oncothermia is based on the modulated electric field effect, which works in synergy of the classical temperature-based hyperthermia concept. In preclinical conditions (in vivo and in vitro) many measurements were done in animals and there are many interested users who tried up till now the temperature development by the method, which is a complex, invasive measurement approach. A well-controlled clinical

temperature measurement by the CT-guided fluoroptic sensor showed the temperature increase facility of oncothermia also [44].

However, the main advantage of oncothermia is that the nonequilibrium heating creates a heat-flow through the membrane into the cytosol, which is active till the equilibrium is reached. This gains the efficacy and the reliability of the treatment. The membrane effect by electric field was expected having a thermal limit. It was questioned, and later it was rigorously shown that the effect of oncothermia is not limited in this issue. To enhance the selection for membrane distortion, and enhance the collective (apoptotic) control on the cell-death, a special modulation is built in the oncothermia process [45].

The not so high radiofrequency (13.56 MHz) is absorbed in all the electrolytes, but the main energy absorption is in the membrane and the extracellular electrolyte. This creates an extreme SAR between the cells, which makes temperature gradient through the membrane. The treated tissue will be inhomogenicly heated, and heat flows from extracellular to cytosol through the membrane, accompanying with definite other thermodynamical and chemical changes. These definite thermal currents will be continued till the extra- and intracellular temperature reaches equilibrium; so the intracellular electrolyte had been heated up to the equal level.

5.2. Oncothermia Is Microscopic Heating of Nanoscopic Targets. The general idea of microscopic heating is simple; the heating energy is not liberated in a sudden single step, but regulated and multiple small, microscopic energy liberation makes the same job. In our case the forwarded energy targets the most influential areas selectively. Instead of the high, general energy pumping into the lesion, the energy is liberated at the membranes of the malignant cells, in a nanometer range. Anyway, the microscopic effect, instead of the large energy liberation, is one of the most update thinking in energy source developments. In the modern technologies, the relatively low efficacy combusting engines are intended to replace by the fuel-cell energy sources and electric motors, which are based on the membrane regulated microscopic reactions of gases. In our case the microenergy liberation at the nanoscopic cellular membrane hits the most sensitive part of the tumor cells.

The efficacy of the energy depletion intended to pump into the tumor is limited by the energy loss outside of the malignant target. The main factors of the useless energy absorptions are

(i) the absorbed energy by the tissues transfers the effect to the deep-seated tumor;

(ii) the heat exchange by the blood flow;

(iii) the heat exchange by the heat conduction from the tumor to the surroundings;

(iv) these heat sinks are modifying the overall performance of the treatment and make uncontrolled the full heating process for the malignancy. The real effect which used for the intended treatment is to be less than the losses, and the efficacy is usually less than 25%, which is very low. The problem of this is not only that the large part of energy is wasted, but also the useless energy part could be dangerous by overheating the healthy tissues as well as increasing the metabolic rate and also making physiology answer on this effect which tries to break the homeostasis. The massively heated tumor volume intensifies the control of physiology and weakens the expected effect.

The adequate corrective actions for these challenges would be the more precise targeting, decreasing the losses in the surrounding and avoid the physiological corrections to suppress the desired effect. Construction the solution some new effects have been used increasing the efficacy.

(i) Apply the electric field as carrier of the energy, and that field cannot be compensated by homeostatic control.

(ii) Apply a correct microscopic targeting, using the energy absorption cell-by-cell efficiently.

(iii) Apply such mechanisms, which initializes natural effects kill the malignant cells.

(iv) Apply mechanism, which carries information for disseminated cells to be blocked.

According to the calculations a relatively small amount of energy can heat up the average-sized tumors to the appropriate temperature, if it targets the tumor accurately enough. The relatively low bioimpedance of malignant lesions makes possible the automatic focusing; the applied RF-current will choose the "easiest" way to flow, automatically loading the tumor with highest current density [46].

The approach using electric impedance for quality assurance is partly comparable with the ion concentration concept of ionizing radiation characterization: the old unit measured the ion pair production, 1 R (roentgen) = $2.58 * 10^{-4}$ C/kg. Note, interestingly, that an electric field application without an increase in temperature (using less than 5W power) has also been found effective against cancer, by using galvanic (DC) current applications, producing ion-pair effects in extracellular electrolyte. This electric tumor treatment measures and controls the tissue resistance and the quality parameter is the applied charge load (in Coulombs, C), with results reported in several peer-reviewed journals and conferences organized on the subject. Yet few studies discuss the biological mechanisms involved in electromagnetic field induced hyperthermia. However, the effect of electric field remains to be a hot topic in science [40].

Oncothermia works with much less forwarded energy, by focusing energy directly on the malignant tissue using its impedance selectivity even by cellular resolution. This effect is based on the low impedance of the tumor, due to its metabolism, which is higher than that of its healthy counterpart's. This special focusing in fact makes the treatment safer and really nontoxic. The high and fermentative glucose → 2ATP process [3, 47] produces higher ionic concentration in the more active cellular environments and different physiological conditions and allows even spatial resolution by this effect. The real focusing could be measured by RF-current

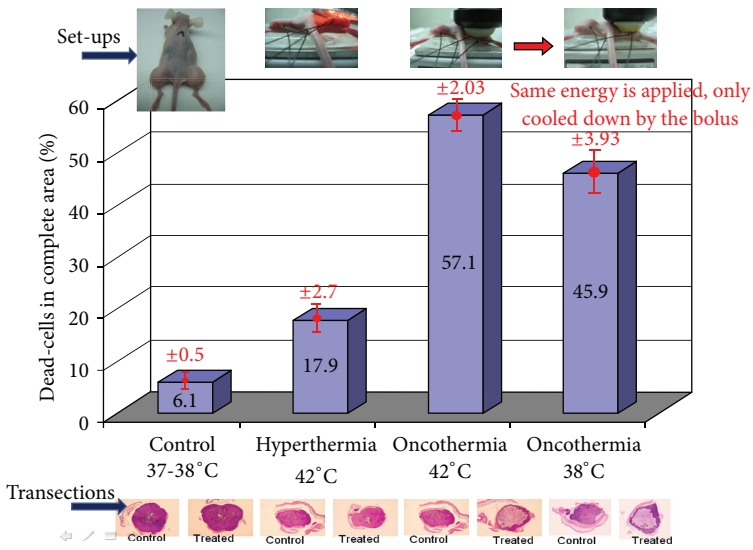

FIGURE 1: The cell-destruction ability of oncothermia is three times higher than of conventional hyperthermia at the same 42°C temperature (single shot treatment, 30 min). Pumping the same energy as for temperature 42°C, but cooling the lesion by outside water-bolus (to 38°C temperature), the efficacy of the cell-destruction remained much higher in oncothermia than in hyperthermia at 42°C temperature.

density image, which spectacularly shows the focusing of the current in the tumor. The focusing effect in this meaning is very similar to the PET picture, which shows the enhanced metabolic activity of the tumor.

Model of oncothermia method producing higher efficacy could be demonstrated with a simple parallelism with the solutions of modern energy sources. The conventional engines in vehicles use the energy of explosion of different chemicals (e.g., petrol, diesel, and kerosene). The explosion by a spark or heating over their activation energy liberates large energy in a short time, and only a small fraction of this could be applied beneficially, while most of the energy is radiated, conducted, or lost in various other ways. One of the largest loss is the heat exchange by the high temperature, which somehow has to be used again (e.g., intercooler and turbo). The most modern solution, however, is the set of microscopic explosions, promoting the chemical reactions individually by a membrane control (i.e., fuel cell solution) and using the energy step-by-step as a sum of the microreactions. This model is anyway learned from the living organisms, when the energy is liberated gradually in a "ladder" of multistep processes, and also moderated by surface reactions.

In this case, the lost energy is minimal; the efficacy of the energy utilization and its control is maximal. The energy is concentrated in this case directly to the chemical reactions and does not involve the previously listed losses. The energy liberated by the microreactions are used for the desired job in full, while the explosion-like, huge energy-supply in short time cannot be optimally used, because the intensity of the immediate offer for the available energy is too much for prompt use. This causes a large demand of waste and a low efficacy of the desired effect. The problem of the heating however shows a false, specious effect of applications in biology. When the liberated energy is not used as active biochemical or biophysical driving-force than the waste appears as a simple growth of the temperature in the target. This deceptive illusion looks as higher efficacy. This process is of course a better heating, wasting the energy and not used for the actually necessary processes, distributing the excess energy in the neighborhood, and gaining the average energy of all the particles in the target.

This is a typical loose of aims by illusions: the temperature makes only conditions that are implements and not the aim. The question "Tool or goal?" became relevant to study the temperature alone. By a simple example of mixing the tool and the goal in our everyday life, the graduation is a tool for our professional life, however, when somebody makes regards the certificate of studies as a goal, its application, the aim of the study looses. Mixing the tool with the action creates false goal in hyperthermia application, increasing the temperature alone. This "auto-suggestion" creates such situation that magnetic resonance imaging (MRI) is applied to control the temperature during the treatment, instead of using this capable imaginary method to see what is happening in the tumor indeed.

The non-temperature-dependent cell destruction is studied by ultrasound and widely by electric fields, which is a hot topic in science [40, 47]. Anther line of the development of energy absorption in depth for killing the malignant cells was parallel: the electromagnetic treatments to cure cancer. The first famous name was D'Arsonval. His method had fantastic popularity at the turn of the 19th-20th centuries. Numerous devices were developed and applied widely, but the expected breakthrough result was missing. The first conference in this field was organized in 1992 in Beijing. In the beginning the galvanic electric current was used to treat cancer. This method had delivered remarkable results; the biological mechanisms involved in electromagnetic field are intensively investigated and the effect of electric field is studied on various side of its complex behavior. Some

special treatments are established to direct electric treatment of the tumor (mainly with DC-current), controlling the tissue resistance, and the quality parameter is the applied charge load. Several good surprising results reported and conferences organized on the subject. Yet few studies discuss the biological mechanisms involved in electromagnetic field induced hyperthermia.

Based on microscopic effects, there not only the heating makes the effect, but the electric field itself has a strong synergy with this (see Figure 1), having significantly larger cell killing in malignancy at 38°C, than the conventional hyperthermia has on 42°C. The process is selective [48]. The RF current is choosing the "easiest" path to flow, and due to the high ionic concentration of the near-neighborhood of malignant cells, the current will be densest at the tumor cells. The experimental results well support this idea. In the case of healthy cells, the load is equal for all the cells, with no difference between the treated and control samples. When we gain the metabolism (immortalized cells) but not yet malignant acceleration, the effect is selectively higher but not significant. However, when the malignancy is present, the cellular growth is aggressive, the selection became effective, and it kills the tumor cells without affecting the healthy ones in the coculture.

This electric field effect well demonstrates, that the average kinetic energy (temperature) has not decisional effect. The main action is the targeted energy-delivery, which could be done on such low average energy as the standard healthy body temperature.

The cell killing needs energy, and afterwards the overall energy of the system would be decreased from a well ordered (bounded) state (which was in the case of the living cell) to a disordered chemical state with some broken chemical bonds. The transition from the ordered (chemically higher energy) state to the disordered (chemically lower state) arrangement the well-known gap energy must be pumped. This gap-energy has different components. For hyperthermia the heat energy gives the full energy consumption however, in oncothermia a significant field effect takes part in the distortion mechanism. This simple allows easier cell-destruction by oncothermia (see Figure 2); similar to the well known catalytic reactions.

The large extracellular SAR makes not only thermal but also electric inhomogenity in the tissue; the extracellular matrix has higher current density than the other electrolytes. The current density gradient is accompanied with the gradient of the electric field, which could reorient the high-dielectric constant proteins in the extracellular liquid. The orientation of these protein molecules would be constrained perpendicular on the membrane surface. By this effect the lost adherent connections could be rebuilt in between the malignant cells, which were indeed shown experimentally. This effect helps to suppress the metastatic dissemination as well as promotes the intercellular signals to activate the natural cell-killing mechanisms.

5.3. Oncothermia Promotes the Programmed Cell-Deaths of Tumor. The selection and the tumor destruction of oncothermia became trivial hours later of the treatment. The time

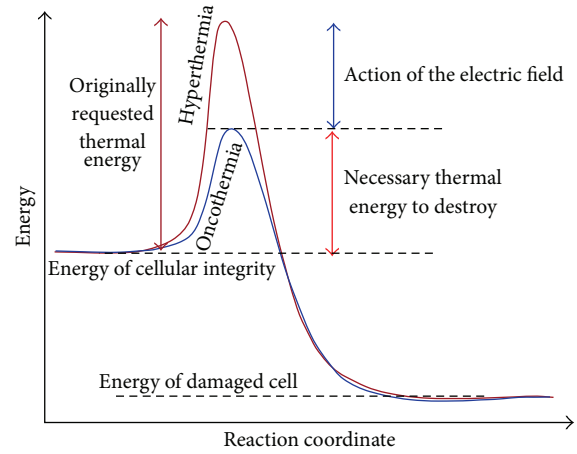

Figure 2: Oncothermia needs less thermal energy to make the same distortion than the classical hyperthermia does. Part of the thermal energy is replaced by the electric field.

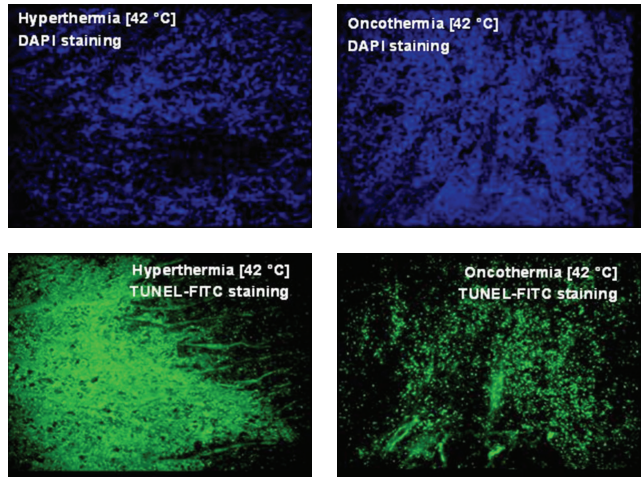

Figure 3: Upper panel: DAPI staining (stains the double strains of DNA only); lower panel: TUNEL-FITC staining (enzymatic label of the strain-break of the DNA). TUNEL is typical for necrosis (diffuse staining) in hyperthermia and for apoptosis (staining of nuclei locations) in oncothermia treatments.

delay indicates the long-duration processes, which were identified as programmed cell-death (apoptosis) [49]. Detecting the double strains of DNA (DAPI staining; see Figure 3 upper panel) and measuring the enzymatic labeled strain-breaks of DNA (TUNEL-FICT; see Figure 3 lower panel), the apoptosis is highly likely in oncothermia, while at identical temperature in classical hyperthermia the necrosis is preferred. Consequently, the main effect in oncothermia is the apoptosis contrary to the conventional hyperthermia, which operates mainly by necrosis. Investigating the apoptosis by various methods (morphology, beta-catenin relocation, p53 expression, Connexin 43, Tunel, DNA-laddering, etc.), the effects are indicating the same apoptotic process. This process is non-toxic (no inflammatory reactions afterwards) and promotes the immune reactions (parallel work with these) and not makes processes against those.

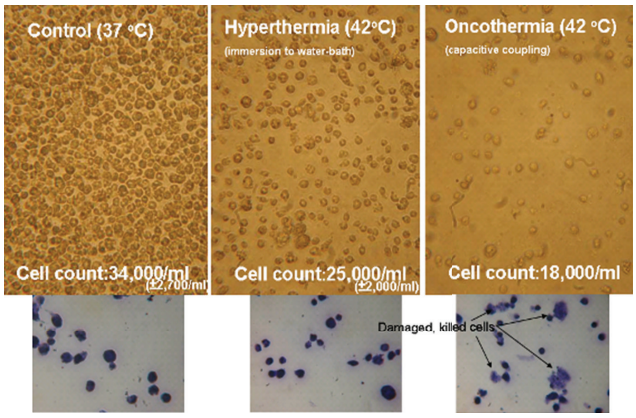

FIGURE 4: Lethality comparison with traditional hyperthermia in vitro experiments (fixed suspension sample): HL-60 leukemia cell line.

5.4. Oncothermia Limits the Dissemination of Malignant Cell. Dissemination is blocked by the sticking of the cells to each other. The adherent connections and the junctions between the malignant cells are reestablished, the cells are connected again, their autonomy is limited, and the possibility of the dissemination decreases. The immune system (with presently not clear mechanism) acts against the metastatic lesions (abscopal, bystander effect), and the local treatment of the primary tumor decreases the distant metastases as well. These effects are the most important for the survival and quality of life.

The main threat of life by tumorous diseases is the distortion of the organs which are essential for the life of the organism. When the tumor grows somewhere without endanger the important systems like the respiratory system, central nervous system, cardiovascular system, and so forth, it has no life-threatening efect. These tumors are local (benign or early malignant), and effect their elimination is possible. The real life-threatening is the malignancy, when the cells are disseminated from the tumor-lesion by the various transport systems (lymph and blood), or their effect become systemic by one of the general mechanisms of the organism. The problem of the classical hyperthermia is that sometimes it promotes the dissemination of the malignant cells.

Oncothermia is different from this point of view as well. It blocks the dissemination, avoiding their motility due to the lazy connections to the tumor. Oncothermia makes it by reestablishing the cellular connections, which is also great success to save the life. The built up connections could force not only the sticking together, but makes bridges between the cells for information exchange to limit the individuality, the competitive behavior of the malignant cells.

Comparison of hyperthermia and oncothermia combined both methods with mitomycin-c (MMC) single dose chemotherapy in vivo at tissue and cellular level using histological examinations is shown. HT29 human colorectal carcinoma cell line derived xenograft tumor model in nude mouse: 2 animals for hyperthermia (42°C) + 3 mg/kg MMC ip. (30 min before the treatment) and 2 animals for oncothermia (42°C) + 3 mg/kg MMC ip. (30 min before the treatment). The constrained thermodynamic transport effects destabilizes the cell membrane, increases its permeability and could make its bobbling and distortion. These are high efficacy factors favoring oncothermia over its temperature-equivalent hyperthermia counterpart; see Figure 4. It also produces higher concentration of HSPs in the outer membrane and in the extracellular matrix. The higher HSP concentration in the vicinity of the malignant cells together with the changes of the adherent connections between the cells induces apoptosis.

The setup made possible a fine temperature control, which allowed to keep the heating, keeping and cooling dynamist also identical. This makes identical heat-shock protein induction by the temperature changes. The temperature-dependent equality was controlled by luciferase transient transfected HEK293 cell lines. Despite the equal temperature curves, oncothermia produces higher concentration of HSPs in the outer membrane and in the extracellular matrix. The higher HSP concentration, in the vicinity of the malignant cells, is one of the factors to induce apoptosis.

Changes of adherent connections (E-cadherin and β-catenin) are also indicators of the gain of the social signals promoting the apoptosis. Remarkable change could be observed on beta-catenin dynamic development by time after the treatment. on HepG2 human hepatocellular carcinoma cell line. This considerable change after 24 hours of the treatment is sharply different from hyperthermia on the same temperature and supports the other observations of the non-temperature-dependent processes. The sudden regrouping the beta-catenin and its enrichment at the cell-nuclei could be an indicator of apoptosis [50, 51].

Many in vitro and in vivo preclinical studies as well as twenty years of entirely positive practice and huge number of retrospective clinical studies are behind of oncothermia [52–57].

Disclosure

According to European Medical Device Directive (MDD) oncothermia is certified by TUV, Munich, by medical CE certificate; both safety and efficacy are certified. All the devices are manufactured according to the ISO 9001 and ISO 13458. The devices work over 25 countries actively, and the oncothermia is twenty years on the market. No serious toxicity or side effects were reported. Minor adipose burns happen in about 3% of all the large number of treatments. As anecdotal benefit, patients report less side effects from the conventional treatment if oncothermia is complementary applied. They report furthermore better quality of life and improved well-being.

Acknowledgment

Authors acknowledge the experimental work and fruitful discussions of Dr. Nora Meggyeshazi and Dr. Gabor Andocs.

References

[1] A. Szasz, "Physical background and technical realization of hyperthermia," in *Locoregional Radiofrequency-Perfusional- and Wholebody-Hyperthermia in Cancer Treatment: New Clinical Aspects*, G. F. Baronzio and E. D. Hager, Eds., pp. 27–59, Springer Science and Eurekah.com, 2006.

[2] M. Israël and L. Schwartz, "The metabolic advantage of tumor cells," *Molecular Cancer*, vol. 10, article 70, 2011.

[3] A. Szentgyorgyi, *Electronic Biology and Cancer*, Marcel Dekker, New York, NY, USA, 1998.

[4] B. B. Singh, "Hyperthermia—a new dimension in cancer treatment," *Indian Journal of Biochemistry and Biophysics*, vol. 27, no. 4, pp. 195–201, 1990.

[5] F. Westermark, "Uber die Behandlung des ulcerirenden Cervix carcinoma mittels Knonstanter Warme," *Zentralblatt für Gynäkologie*, pp. 1335–1339, 1898.

[6] H. R. Moyer and K. A. Delman, "The role of hyperthermia in optimizing tumor response to regional therapy," *International Journal of Hyperthermia*, vol. 24, no. 3, pp. 251–261, 2008.

[7] C. T. Lee, T. Mace, and E. A. Repasky, "Hypoxia-driven immunosuppression: a new reason to use thermal therapy in the treatment of cancer?" *International Journal of Hyperthermia*, vol. 26, no. 3, pp. 232–246, 2010.

[8] E. Jones, D. Thrall, M. W. Dewhirst, and Z. Vujaskovic, "Prospective thermal dosimetry: the key to hyperthermia's future," *International Journal of Hyperthermia*, vol. 22, no. 3, pp. 247–253, 2006.

[9] E. R. Lee, "Electromagnetic superficial heating technology," in *Thermoradiotherapy and Thermochemotherapy*, M. H. Seegenschmiedt, P. Fessenden, and C. C. Vernon, Eds., pp. 193–217, Springer, Berlin, Germany, 1995.

[10] P. Wust, M. Seebass, J. Nadobny, and R. Felix, "Electromagnetic deep heating technology," in *Thermoradiotherapy and Thermochemotherapy*, M. H. Seegenschmiedt, P. Fessenden, and C. C. Vernon, Eds., pp. 219–251, Springer, Berlin, Germany, 1995.

[11] R. B. Roemer, "Engineering aspects of hyperthermia therapy," *Annual Review of Biomedical Engineering*, vol. 1, pp. 347–376, 1999.

[12] B. Hildebrandt, P. Wust, O. Ahlers et al., "The cellular and molecular basis of hyperthermia," *Critical Reviews in Oncology/Hematology*, vol. 43, no. 1, pp. 33–56, 2002.

[13] D. S. Coffey, R. H. Getzenberg, and T. L. Deweese, "Hyperthermic biology and cancer therapies: a hypothesis for the "Lance Armstrong effect"," *Journal of the American Medical Association*, vol. 296, no. 4, pp. 445–448, 2006.

[14] J. L. Roti, "Cellular responses to hyperthermia (40–46°C): cell killing and molecular events," *International Journal of Hyperthermia*, vol. 24, no. 1, pp. 3–15, 2008.

[15] K. Iwata, A. Shakil, W. J. Hur, C. M. Makepeace, R. J. Griffin, and C. W. Song, "Tumour pO2 can be increased markedly by mild hyperthermia," *British Journal of Cancer*, vol. 74, supplement, pp. S217–S221, 1996.

[16] C. A. Vidair and W. C. Dewey, "Two distinct modes of hyperthermic cell death," *Radiation Research*, vol. 116, no. 1, pp. 157–171, 1988.

[17] B. Gyldenhof, M. R. Horsman, and J. Overgaard, "Hyperthermia-induced changes in the vascularity and histopathology of a murine tumour and its surrounding normal tissue," in *Hyperthermic Oncology*, C. Franconi, G. Arcangeli, and R. Cavaliere, Eds., vol. 2, pp. 780–782, Tor Vergata, Rome, Italy, 1996.

[18] M. R. Horsman and J. Overgaard, "Can mild hyperthermia improve tumour oxygenation?" *International Journal of Hyperthermia*, vol. 13, no. 2, pp. 141–147, 1997.

[19] C. W. Song, M. S. Patten, L. M. Chelstrom, J. G. Rhee, and S. H. Levitt, "Effect of multiple heatings on the blood flow in RIF-1 tumours, skin and muscle of C3H mice," *International Journal of Hyperthermia*, vol. 3, no. 6, pp. 535–545, 1987.

[20] P. Vaupel, F. Kallinowski, and P. Okunieff, "Blood flow, oxygen and nutrient supply, and metabolic microenvironment of human tumors: a review," *Cancer Research*, vol. 49, no. 23, pp. 6449–6465, 1989.

[21] P. W. Vaupel, "Effects of physiological parameters on tissue response to hyperthermia: new experimental facts and their relevance to clinical problems," in *Hyperthermia Oncology*, E. W. Gerner and T. C. Cetas, Eds., pp. 17–23, Tucson Arizona Board of Regents, Tucson, Ariz, USA, 19921993.

[22] H. H. Kampinga, J. R. Dynlacht, and E. Dikomey, "Mechanism of radiosensitization by hyperthermia (43°C) as derived from studies with DNA repair defective mutant cell lines," *International Journal of Hyperthermia*, vol. 20, no. 2, pp. 131–139, 2004.

[23] A. Laszlo, "The effects of hyperthermia on mammalian cell structure and function," *Cell Proliferation*, vol. 25, no. 2, pp. 59–87, 1992.

[24] K. C. Kregel, "Invited review: heat shock proteins: modifying factors in physiological stress responses and acquired thermotolerance," *Journal of Applied Physiology*, vol. 92, no. 5, pp. 2177–2186, 2002.

[25] R. A. Coss, W. C. Dewey, and J. R. Bamburg, "Effects of hyperthermia on dividing Chinese hamster ovary cells and on microtubules in vitro," *Cancer Research*, vol. 42, no. 3, pp. 1059–1071, 1982.

[26] A. Westra and W. C. Dewey, "Variation in sensitivity to heat shock during the cell-cycle of Chinese hamster cells in vitro," *International Journal of Radiation Biology & Related Studies in Physics, Chemistry & Medicine*, vol. 19, pp. 467–477, 1971.

[27] D. Stehelin, H. E. Varmus, J. M. Bishop, and P. K. Vogt, "DNA related to the transforming gene(s) of avian sarcoma viruses is present in normal avian DNA," *Nature*, vol. 260, no. 5547, pp. 170–173, 1976.

[28] P. W. Vaupel and D. K. Kelleher, "Pathophysiological and vascular characteristics of tumours and their importance for hyperthermia: heterogeneity is the key issue," *International Journal of Hyperthermia*, vol. 26, no. 3, pp. 211–223, 2010.

[29] K. Newell and I. Tannock, "Regulation of intracellular pH and viability of tumor cells," *Funktionsanalyse Biolog Systeme*, vol. 13, pp. 219–234, 1991.

[30] M. Stubbs, P. M. J. McSheehy, J. R. Griffiths, and C. L. Bashford, "Causes and consequences of tumour acidity and implications for treatment," *Molecular Medicine Today*, vol. 6, no. 1, pp. 15–19, 2000.

[31] P. Vaupel and D. K. Kelleher, "Metabolic status and reaction to heat of normal and tumor tissue," in *Thermoradiotherapy and Thermochemotherapy*, M. H. Seegenschmiedt, P. Fessenden, and C. C. Vernon, Eds., vol. 1, pp. 157–176, Springer, New York, NY, USA, 1995.

[32] W. C. Dewey, "Arrhenius relationships from the molecule and cell to the clinic," *International Journal of Hyperthermia*, vol. 10, no. 4, pp. 457–483, 1994.

[33] J. R. Lepock, H. E. Frey, and K. P. Ritchie, "Protein denaturation in intact hepatocytes and isolated cellular organelles during heat shock," *Journal of Cell Biology*, vol. 122, no. 6, pp. 1267–1276, 1993.

[34] R. I. Morimoto, "Regulation of the heat shock transcriptional response: cross talk between a family of heat shock factors, molecular chaperones, and negative regulators," *Genes and Development*, vol. 12, no. 24, pp. 3788–3796, 1998.

[35] H. Kai, M. Ann Suico, S. Morino et al., "A novel combination of mild electrical stimulation and hyperthermia: general concepts and applications," *International Journal of Hyperthermia*, vol. 25, no. 8, pp. 655–660, 2009.

[36] S. Lindquist, "The heat-shock response," *Annual Review of Biochemistry*, vol. 55, pp. 1151–1191, 1986.

[37] T. Torigoe, Y. Tamura, and N. Sato, "Heat shock proteins and immunity: application of hyperthermia for immunomodulation," *International Journal of Hyperthermia*, vol. 25, no. 8, pp. 610–616, 2009.

[38] P. K. Srivastava, A. B. DeLeo, and L. J. Old, "Tumor rejection antigens of chemically induced sarcomas of inbred mice," *Proceedings of the National Academy of Sciences of the United States of America*, vol. 83, no. 10, pp. 3407–3411, 1986.

[39] A. Szasz, N. Szasz, and O. Szasz, *Oncothermia—Principles and Practices*, Springer, 2010.

[40] G. Andocs, H. Renner, L. Balogh, L. Fonyad, C. Jakab, and A. Szasz, "Strong synergy of heat and modulated electromagnetic field in tumor cell killing," *Radiology and Oncology*, vol. 185, no. 2, pp. 120–126, 2009.

[41] S. Camazine, J. L. Deneubourg, N. R. Franks et al., *Self-Organization in Biological Systems. Princeton Studies in Complexity*, Princeton University Press, Princeton, NJ, USA, 2003.

[42] E. D. Kirson, Z. Gurvich, R. Schneiderman et al., "Disruption of cancer cell replication by alternating electric fields," *Cancer Research*, vol. 64, no. 9, pp. 3288–3295, 2004.

[43] A. Szasz, G. Vincze, O. Szasz, and N. Szasz, "An energy analysis of extracellular hyperthermia," *Electromagnetic Biology and Medicine*, vol. 22, no. 2-3, pp. 103–115, 2003.

[44] G. Vincze, N. Szasz, and A. Szasz, "On the thermal noise limit of cellular membranes," *Bioelectromagnetics*, vol. 26, no. 1, pp. 28–35, 2005.

[45] C. D. McCaig, A. M. Rajnicek, B. Song, and M. Zhao, "Controlling cell behavior electrically: current views and future potential," *Physiological Reviews*, vol. 85, no. 3, pp. 943–978, 2005.

[46] L. D. Johns, "Nonthermal effects of therapeutic ultrasound: the frequency resonance hypothesis," *Journal of Athletic Training*, vol. 37, no. 3, pp. 293–299, 2002.

[47] O. Warburg, *Oxygen, The Creator of Differentiation, Biochemical Energetics*, Academic Press, New York, NY, USA, 1966, O. Warburg. The Prime Cause and Prevention of Cancer, Revised lecture at the meeting of the Nobel-Laureates on June 30, 1966 at Lindau, Lake Constance, Germany.

[48] R. M. Bremnes, R. Veve, F. R. Hirsch, and W. A. Franklin, "The E-cadherin cell-cell adhesion complex and lung cancer invasion, metastasis, and prognosis," *Lung Cancer*, vol. 36, no. 2, pp. 115–124, 2002.

[49] M. E. Van Gijn, F. Snel, J. P. M. Cleutjens, J. F. M. Smits, and W. M. Blankesteijn, "Overexpression of components of the Frizzled-Dishevelled cascade results in apoptotic cell death, mediated by β-catenin," *Experimental Cell Research*, vol. 265, no. 1, pp. 46–53, 2001.

[50] EUROCARE-3, "European Cancer Database," http://www.eurocare.org/.

[51] "Surveillance, Epidemiology, and End Results (SEER)," National Cancer Institute, http://www.seer.cancer.gov/.

[52] J. Bogovič, F. Douwes, G. Muravjov, and J. Istomin, "Post-treatment histology and microcirculation status of osteogenic sarcoma after a neoadjuvant chemo- and radiotherapy in combination with local electromagnetic hyperthermia," *Onkologie*, vol. 24, no. 1, pp. 55–58, 2001.

[53] A. Dani, A. Varkonyi, T. Magyar, and A. Szasz, "Clinical study for advanced pancreas cancer treated by oncothermia," *Forum Hyperthermia, Forum Medizine*, vol. 2, pp. 13–19, 2008.

[54] V. D. Ferrari, S. De Ponti, F. Valcamonico et al., "Deep electrohyperthermia (EHY) with or without thermo-active agents in patients with advanced hepatic cell carcinoma: phase II study," *Journal of Clinical Oncology*, vol. 25, 18S, Article ID 15168, 2007.

[55] G. Fiorentini, P. Giovanis, S. Rossi et al., "A phase II clinical study on relapsed malignant gliomas treated with electrohyperthermia," *In Vivo*, vol. 20, no. 6 A, pp. 721–724, 2006.

[56] E. D. Hager, H. Dziambor, D. Höhmann, D. Gallenbeck, M. Stephan, and C. Popa, "Deep hyperthermia with radiofrequencies in patients with liver metastases from colorectal cancer," *Anticancer Research*, vol. 19, no. 4, pp. 3403–3408, 1999.

[57] H. Sahinbas, D. H. W. Grönemeyer, E. Böcher, and A. Szasz, "Retrospective clinical study of adjuvant electro-hyperthermia treatment for advanced brain-gliomas," *Deutsche Zeitschrift für Onkologie*, vol. 39, no. 4, pp. 154–160, 2007.

Hindawi Publishing Corporation
Evidence-Based Complementary and Alternative Medicine
Volume 2013, Article ID 616737, 7 pages
http://dx.doi.org/10.1155/2013/616737

Research Article

Carica papaya Leaves Juice Significantly Accelerates the Rate of Increase in Platelet Count among Patients with Dengue Fever and Dengue Haemorrhagic Fever

Soobitha Subenthiran,[1] Tan Chwee Choon,[2] Kee Chee Cheong,[3] Ravindran Thayan,[4] Mok Boon Teck,[1] Prem Kumar Muniandy,[1] Adlin Afzan,[1] Noor Rain Abdullah,[1] and Zakiah Ismail[1]

[1] *Bioassay Unit, Herbal Medicine Research Center, Institute for Medical Research, Jalan Pahang, 50588 Kuala Lumpur, Malaysia*
[2] *Department of Internal Medicine, Tengku Ampuan Rahimah Hospital, Jalan Langat, 41200 Klang, Malaysia*
[3] *Epidemiology and Biostatistics Unit, Institute for Medical Research, Jalan Pahang, 50588 Kuala Lumpur, Malaysia*
[4] *Virology Unit, Infectious Disease Research Center, Institute for Medical Research, Jalan Pahang, 50588 Kuala Lumpur, Malaysia*

Correspondence should be addressed to Soobitha Subenthiran; drsoobi@hotmail.com

Received 7 January 2013; Revised 21 March 2013; Accepted 21 March 2013

Academic Editor: Martin Kohlmeier

The study was conducted to investigate the platelet increasing property of *Carica papaya* leaves juice (CPLJ) in patients with dengue fever (DF). An open labeled randomized controlled trial was carried out on 228 patients with DF and dengue haemorrhagic fever (DHF). Approximately half the patients received the juice, for 3 consecutive days while the others remained as controls and received the standard management. Their full blood count was monitored 8 hours for 48 hours. Gene expression studies were conducted on the ALOX 12 and PTAFR genes. The mean increase in platelet counts were compared in both groups using repeated measure ANCOVA. There was a significant increase in mean platelet count observed in the intervention group ($P < 0.001$) but not in the control group 40 hours since the first dose of CPLJ. Comparison of mean platelet count between intervention and control group showed that mean platelet count in intervention group was significantly higher than control group after 40 and 48 hours of admission ($P < 0.01$). The ALOX 12 (FC = 15.00) and PTAFR (FC = 13.42) genes were highly expressed among those on the juice. It was concluded that CPLJ does significantly increase the platelet count in patients with DF and DHF.

1. Introduction

Malaysia is blessed with 12000 species of flowering plants of which 1300 have medicinal properties [1]. There is a rapidly growing response to the use of medicinal plants by the Malaysian population. WHO estimates that in many countries 80% of the rural patients seek alternative treatment using medicinal plants.

Carica papaya is a member of the Caricaceae and is a dicotyledonous, polygamous, and diploid species [2]. It originated from Southern Mexico, Central America, and the northern part of South America. It is now cultivated in many tropical countries such as Bangladesh, India, Indonesia, Sri Lanka, the Philippines, and the West Indies including Malaysia. Malaysia is known to be one of the top 5 papaya exporting countries [3]. The papaya fruit is globally consumed either in its fresh form or the form of juices, jams, and crystallized dry fruit [4]. The ripe fruit is said to be a rich source of vitamin A, C, and calcium [5]. There are many commercial products derived from the different parts of the *C. papaya* plant, the most prominent being papain and chymopapain, which is produced from the latex of the young fruit, stem, and the leaves. *C. papaya* leaves have been used in folk medicine for centuries. Recent studies have shown its beneficial effect as an anti-inflammatory agent [6], for its wound healing properties [7], antitumour as well as immunemodulatory effects [8] and as an antioxidant [9]. A toxicity study (acute, subacute, and chronic toxicity) conducted on

Sprague Dawley rats administered with *Carica papaya* leaves juice (CPLJ) of the sekaki variant revealed that it was safe for oral consumption [10].

Dengue is an arthropod-borne viral disease carried by *Aedes aegypti* as the vector, caused by 4 possible viral serotypes, namely, serotype 1, 2, 3, and 4 of the Flaviviridae family. In Malaysia, dengue cases have been on the rise since 2002. Total of 18,371 cases of dengue fever (DF) and dengue haemorrhagic fever (DHF) were reported last year and had claimed 33 lives in the same year [11]. There is no specific antiviral drug available for the treatment of dengue infection. Infected patients receive supportive management with fluids, blood and blood, products complying to the Ministry of Health Clinical Practice Guidelines (CPGs) on Management of Dengue, 2010. Each episode of infection is known to induce a life-long protective immunity to the homologous serotype but confers only partial and transient protection against subsequent infection by the other serotypes. Secondary infection is a major risk factor for DHF possibly due to antibody-dependent enhancement. A patient with dengue fever presents typically with fever, headache, and rash known as the dengue triad. There are many other nonspecific signs and symptoms associated with DF and patient can progress to DHF and typically manifests as abdominal pain, bleeding, and even circulatory collapse. The clinical course of dengue has an abrupt onset followed by three phases, namely, the febrile phase, the critical phase and the recovery phase. It is during the critical phase that thrombocytopaenia, characterized by a decrease in platelet count below 100 000 per mm^3 from the baseline and haemoconcentration, characterized by an increase of haematocrit by 20% or more, is detectable before the subsidence of fever and the onset of shock [12].

Certain genes have been shown to influence platelet production and platelet aggregation, namely, the Arachidonate 12-lipoxygenase (ALOX 12) also known as the Platelet-type Lipoxygenase as well as the Platelet-Activating Factor Receptor (PTAFR). An increase in activity of these genes is required for platelet production and activation. The ALOX 12 gene is strongly expressed in megakaryocytes and has been known to be responsible for the 12-Hydroxyeicosatetraenoic acid (12-HETE) production of platelets [13]. The PTAFR gene was been found to be expressed in megakaryocytes indicating that it could be a precursor for platelet production in addition to its well known role in platelet aggregation [14].

Safety studies based on OECD guidelines for acute, subacute, and chronic toxicity were conducted on *C. papaya* extract and showed that it was found to be safe for human consumption [10]. The present study was conducted to determine and investigate the traditional claim that CPLJ increases the platelet count in patients with DF and DHF.

2. Materials and Method

2.1. Plant Material and Sample Preparation. *C. papaya* leaves of the the sekaki variant were chosen for the study based on fingerprinting and safety analysis which also contained allowable limit of heavy metals and microbial content. For the purpose of the study, a private plantation certified by the Ministry of Agriculture in Semenyih, Selangor was identified to provide the leaves for the entire duration of the study to ensure similar source of authenticated raw material used. The trees in this plantation were kept free of herbicides, pesticides, and insecticides. Juice was prepared fresh from the leaves that were washed thoroughly with an organic vegetable cleaning agent and reverse osmosis water few times. Juice was extracted from 50 grams of fresh leaves using a juice extractor without any addition of water, under sterile conditions. The fresh juice was aliquoted at a volume of approximately 30 mLs in sterile glass vials and transported daily in an icebox and kept at a temperature of below 4°C to the study site at the male and female dengue wards of Hospital Tengku Ampuan Rahimah, Klang, Selangor.

The juice was characterized and standardized using a High Performance Liquid Chromatography Diode Array Detector according to three markers: manghaslin, clitorin, and rutin. The chemical fingerprinting of the leaves was consistent throughout the study.

2.2. Subjects. An open labeled randomized controlled trial was conducted to provide clinical data in support of the proposed claims. The number of patients involved was determined based on the following calculation.

With plan to have a continuous response variable from independent control and experimental subjects with 1 control(s) per experimental subject, expecting the platelet count to increase by 20,000 after administration of CPLJ for three consecutive days, setting the standard deviation for platelet count at 40,000 in a normal population [15], type I error (alpha) = 0.01 and power of study of 90%, the sample size calculated by using PS software [16] was 242 with each arm of 121 intervention group and control group. Anticipating dropout rate to be 20%, the final sample size was 290 (145 each for intervention and control group).

All the patients meeting the inclusion criteria were recruited from the Dengue Ward of Hospital Tengku Ampuan Rahimah, Klang, Selangor Malaysia. Subjects were randomly assigned to either intervention or control group using the block of 10 method. This method was used to ensure that an equal number of participants were allocated to interventional and control groups. Therefore, with the block size of ten, of every ten consecutively enrolled participants, five will be allocated to one interventional group and five to the control group. For the randomization, 10 identical opaque envelopes with five envelopes each contained a card labelled as "interventional group" and other 5 envelopes each contained a card labelled as "control group." These envelopes were given to the field investigator during the patient enrolment. The field investigator then blindly selected an envelope for each patient thus assigning the patient to interventional or control groups. This procedure was repeated until the targeted sample size was achieved.

The inclusion and exclusion criteria were used to select patients who volunteered to be enrolled into the study. Inclusion criteria were (a) male and female patients above 18 years and below 60 years old, (b) all patients who could

understand or read Bahasa Malaysia or English irrespective of race, (c) patients who were confirmed to have DF or DHF grade I and II, (d) patients with a platelet count of less than or equal to 100,000/μL, (e) patients with a baseline alanine transaminase (ALT) level of not more than 3 times of the upper limit of the normal range (not more than 165 U/L), and (f) patients with a creatinine kinase (CK) value of less than 500 U/L.

The exclusion criteria were (a) dengue hemorrhagic fever grade III and IV, (b) pregnant or lactating women, (c) patients who have received blood or blood products transfusion during the current hospital stay, (d) patients with underlying comorbids, (e) patients who developed Hepatitis with a serum ALT level 3 times higher than the upper limit of the normal range (>165 U/L), and (f) patients with a creatinine kinase (CK) value of more than 500 U/L.

The study was conducted in accordance with the ethical principles as outlined in the declaration of Helsinki, October 2008, following approval from the Medical Review and Ethical Committee (MREC), Ministry of Health, Malaysia and was consistent with Good Clinical Practice (GCP) and applicable regulatory requirements. The National Medical Research Registry number is NMRR-09-883-4768. Written informed consent was obtained from every volunteer prior to clinical trial participation.

2.3. Diagnosis of DF or DHF and Dengue Serotyping. A clinical diagnosis of DF and DHF was made by the clinician based on patients' presentation and blood investigations. In addition a rapid dengue bedside test (SD Dengue Duo NS1 Ag + Ab Combo, Standard Diagnostics, Korea) was used to determine dengue status before the subjects were given the *Carica papaya* leave juice. This test is able to detect the presence of NS1 antigen or dengue IgM or IgG antibodies. However, for ease of interpretation of dengue status only patients who had either NS1 or IgM or both detected were included in the study. The detection of the NS1 antigen or IgM antibodies within the first five to 7 days of onset of symptoms usually indicates a current dengue infection. Subsequently, all the samples were subjected to multiplex real time RT-PCR for determination of dengue serotypes.

2.4. Treatment of the Subjects. Once a current dengue infection was confirmed, a thorough screening of the patient was conducted. Baseline investigations included full blood count, bleeding profile, renal as well as liver function test, and cardiac enzymes. Patients in the intervention group received fresh juice from 50 grams of *C. papaya* leaves, once daily, 15 minutes after breakfast for 3 consecutive days while receiving the standard management as per the National Clinical Practice Guidelines for the Management of Dengue. The controls received the standard management.

2.5. Study Parameters. Full blood count was monitored 8 hours for the first 48 hours during the study, to determine the changes in platelet count and haematocrit levels while bleeding profile, renal profile, and liver function test were monitored daily to ensure the safety of the juice. The haematological and biochemical tests were conducted by the Pathology Department at Hospital Tengku Ampuan Rahimah, Klang and the validated results were later traced and recorded. Mean and standard deviation of the baseline haematological and biochemical parameters were then calculated as shown in Table 1.

Blood for RNA extraction was taken on day 3 after the last dose of the juice to conduct expression studies on the PTAFR and the ALOX 12 genes. RNA Later by Ambion (United States of America) was added to the whole blood in an EDTA tube to prevent degradation of RNA.

The RNA extraction was carried out at the Institute for Medical research using an RNA extraction kit by Ambion. The RNA concentration and purity were determined using the Nanodrop 2000 Spectrophotometer by Thermo Scientific. The RNA was then converted to cDNA using the High Capacity RNA to cDNA kit by Applied Biosystems. The cDNA concentration was then determined using the Nanodrop 2000 Spectrophotometer by Thermo Scientific.

Gene expression was determined using gene expression assays by Applied Biosystems on the ABI 7500 Fast System on 12 RNA samples from the experimental group and 12 RNA samples from the control group. Specific predesigned MGB probes were used for ALOX 12 and the PTAFR gene. The 18S Ribosome was used as an endogenous control. A 10 μL reaction volume was used using the TaqMan Fast Universal PCR Mastermix (2X). The probe product ID and sequence used were ALOX 12 (Hs 00167524_M1, NM_000697.2, 5′-FAM-ATTGCCATCCAGCTCAACAAATCC-MGB-3′) and PTAFR (Hs 00265399_S1, NM_001164723.1, 5′-FAM-GCCCGTAATTTATCGCGCTTACTAT_MGB-2′).

2.6. Statistical Analysis. Repeated measure ANCOVA was used to determine the effect of CPLJ on the mean platelet count over 48 hours (time effect). Multiple comparisons of mean platelet count 8 hours after admission with mean platelet count at the 16, 24, 32, 40, and 48 hours after admission for interventional and control group were performed. Multiple paired t-test was conducted to demonstrate if there is any significant different in mean platelet count for each comparison. Hence, Bonferroni correction was applied to reduce the possibility of rejecting a true null hypotheses (commit a type 1 error). Therefore, Bonferroni correction was used to adjust the level of significance to $P < 0.01$ (0.05/number of comparison = 0.05/5 = 0.01). The efficacy of treatment of CPLJ (treatment effect) and treatment over time (time-treatment interaction) in increasing the mean platelet count was analysed by comparing mean difference in platelet count between interventional and control group. All the statistical analyses were done using PASW 18.0 (SPSS Inc., Chicago, USA). The comparative C_T method was used to determine the relative quantification of the genes expressed.

3. Results

A total of 145 patients were recruited into the interventional group while 145 patients were recruited into the control

Table 1: Demographic characteristics and baseline biochemistry investigation of respondents by treatment.

Demographic characteristics	Interventional group n (%)	Control group n (%)	χ^2 (df)*	P value
Gender				
Men	91 (46.9)	103 (53.1)	1.644 (1)	0.200
Women	20 (58.8)	14 (41.2)		
Ethnicity				
Malay	77 (48.1)	83 (51.9)		
Chinese	4 (57.1)	3 (42.9)		
Indian	11 (50.0)	11 (50.0)		
Others	19 (48.7)	20 (51.3)		
Age (mean/SD)	30.4 (10.3)†	26.4 (7.3)†	−3.370††	0.001
Type of dengue fever				
Classical dengue fever	42 (53.2)	37 (46.8)	0.971 (1)	0.324
Dengue haemorrhagic fever	69 (46.3)	80 (53.7)		
Baseline Haematology investigation				
Platelet count ($\times 10^3/\mu$L)	66.4 (22.8)†	69.0 (22.6)†	0.847††	0.398
Total white blood cell ($\times 10^3/\mu$L)	3.4 (1.7)†	3.3 (1.6)	−0.297††	0.766
Haemoglobin (g/%)	13.9 (1.5)†	14.2 (1.4)†	1.595††	0.112
Haematocrit (%)	41.5 (4.2)†	42.9 (6.0)†	1.878††	0.062
Lymphocytes (%)	41.8 (14.2)†	40.9 (14.8)†	−0.459††	0.646
Neutrophils (%)	42.1 (17.7)†	42.1 (19.4)†	0.017††	0.987

*Pearson Chi-Square. Df (degree of freedom), †mean and standard deviation, ††t-value for independent samples T-test.

Table 2: Comparison of platelet count in each group based on time.

Type of laboratory investigation	Interventional group (n = 111)			Control group (n = 117)		
Platelet count	Mean difference (95% CI)	t	P value	Mean difference (95% CI)	t	P value
8–16 hours	0.993 (−1.660, 3.645)	0.740	0.460	−1.411 (−3.961, 1.140)	−1.094	0.276
8–24 hours	−0.432 (−4.422, 3.558)	−0.214	0.831	2.213 (−0.523, 4.948)	1.600	0.112
8–32 hours	−2.716 (−7.540, 2.107)	−1.114	0.267	2.775 (−0.796, 6.347)	1.537	0.127
8–40 hours	−7.890 (−14.472, −1.310)	−2.374	0.019	0.867 (−3.472, 5.207)	0.395	0.693
8–48 hours	−16.764 (−24.566, −8.964)	−4.256	<0.001	−7.703 (−14.055, 1.351)	−2.399	0.018

Repeated measure ANCOVA within group analysis was applied followed by multiple paired t-tests.
*Bonferroni correction was applied by correcting the level of significance (0.05/5 = 0.01). Potential covariate (age) was controlled by using repeated measures ANCOVA (ANCOVA controlled for age).

group. At the end of the study, 111 patients from the interventional group and 117 controls were included in the statistical analysis. Sixty-two patients were excluded from the analysis as 38 patients were lost to followup and 24 patients had incomplete data (missing results due to sample rejection).

Table 1 shows demographic characteristics and baseline biochemistry investigation of respondents by treatment. In terms of dengue status, all patients recruited had either dengue NS1 or IgM or both detected, while the percentage distribution of the dengue serotypes among them was DEN1 (30.4%), DEN2 (28.4%), DEN 3 (20.6%), and DEN 4 (20.6%). Hence, all serotypes were well represented in the study.

Table 2 presents the multiple comparisons of mean platelet count 8 hours after admission with mean platelet count at 16, 24, 32, 40, and 48 hours after admission for interventional and control group Multiple paired t-test was conducted to demonstrate if there was any significant difference in mean platelet count for each comparison. Hence, Bonferroni correction was applied to reduce the possibility of rejecting a true null hypothesis (committing a type 1 error). Based on the number of patients recruited with complete data (111 patients from the intervention group and 117 control), the power of study was 87.0% (standard deviation of platelet count of 40,000, type I error probability of 0.01, and the true difference in mean platelet count of 20,000 between the intervention and control group). Overall, there was a significant increase in mean platelet count over 40 hours in both groups (Wilk's Lambda = 0.939, P = 0.015, effect size

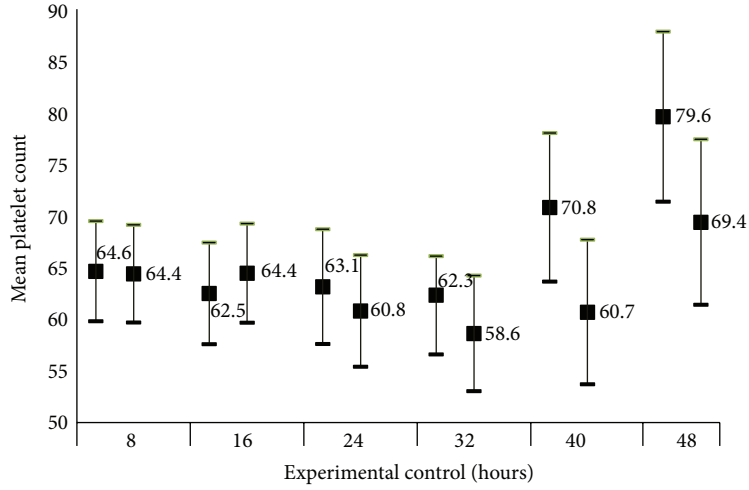

Figure 1: Comparison of mean platelet count between intervention and control group based on time (time-treatment effect).

Table 3: Comparison of platelets count between experiment and control group (treatment effect regardless of time).

Type of lab. Investigation	Mean difference (95% CI)	*P* value
Platelet count	2.349 (−5.151, 9.850)	0.538

Repeated measure ANCOVA between group analyses was applied. Level of significance was set at 0.05 (two-tailed).

= 0.06, and power = 84.0%) after adjusting for age. Further analysis by using multiple paired *t*-test on each of the groups showed that there was a significant increase in mean platelet count at 40 hours compared to 8 hours after intervention in the intervention group ($t = -4.256$, $P \leq 0.001$) but not in the control group ($t = -2.399$, $P = 0.018$) after adjustment of Bonferroni correction ($P = 0.05/5 = 0.01$).

Table 3 presents the overall efficacy of CPLJ supplementation by comparing the mean platelet count of interventional and control group regardless the time period. Study on the treatment effect of CPLJ on platelet count regardless of time did not show any significant difference in mean platelet count between intervention and control group ($F = 1.128$, $P = 0.289$). However, analysis of the effect of CPLJ over the study period (time and treatment effect) showed that there was a significant interaction between treatment groups and time (Wilk's Lambda = 0.934, effect size = 0.06, and power = 87.0%).

Figure 1 shows the time-treatment effect of CPLJ. The intervention group had a significantly higher mean platelet count than control group at 40 hours and 48 hours of intervention.

Data from the gene expression study were analyzed using the "PCR Array Data Analysis versus 3.3" software, recommended by Applied Biosystems and showed that ALOX12 (ΔCT mean = 16.02, FC = 15.00) and PTAFR genes (ΔCT mean = 14.87, FC = 13.42) were found to be highly expressed in the intervention group when compared to the control group.

4. Discussion

The study conducted shows that there is a rationale behind the use of CPLJ in the treatment of some of DF and DHF. It is definitely worth investigating this plant for its potential medicinal benefits. With rapid urbanization and global travel leading to drastic demographic changes, dengue is a threat to almost 40% of the world's population. There is still no specific treatment for dengue. Previous attempts to identify a potential antiviral for the treatment of dengue has been faced with several challenges such as the presence of four distinct viral serotypes which frequently undergo mutations, finding an appropriate model for infection and protective action of a given drug as well as yield interesting therapeutic avenues for tailored response modifier drugs. The current available mouse model (AG129) available has its limitations such as low viral load and a short period of viraemia. The journey to drug discovery through the study of immune-modulatory effects against dengue infection lies on the research of generic compounds and natural products [17].

Research groups around Asia have attempted to study the efficacy of CPLJ in rapidly increasing platelet counts in DF as well as DHF induced thrombocytopenia but there has been no conclusive evidence drawn from those studies. Dengue is generally a self-limiting disease and the disease induced thrombocytopenia usually reverses itself after taking a slight dip during the phase of defervescence. However, a significant number of patients succumb to the disease during the thrombocytopenic period. Many mechanisms come into play during the critical phase of the disease to help reverse the disease state at this point. Animal studies in elucidating safety data have been conducted on normal *Sprague Dawley* rats using freeze dried CPLJ; however, no significant increase in platelet count was observed among the rats given the juice and the rats kept as control [10]. This was probably due to the fact that the juice was freeze dried and certain essential compounds could have been lost during the process of freeze drying or perhaps the right disease model was not

used for the study. Haematocrit level, which is an important parameter which is usually monitored to determine the rate of improvement in haemoconcentration, was found to be significantly reduced in both groups of people. White Blood cell count which is found to be reduced in viral infections was also found to increase in both groups.

The RNA was extracted from the blood of the patients recruited and gene expression of two genes, namely, the ALOX 12 and the PTAFR which were conducted so far. There was a 15-fold increase in the ALOX 12 gene activity among the patients in the experimental group as compared to those in the control group at the end of the 3 days. ALOX 12 is known to be associated with increased megakaryocyte production as well as its conversion to platelets through 12-HETE mediated pathway which in turn leads to increased platelet production. A study was conducted at the Royal College of Surgeons, Ireland, to determine the platelet specific genes. The Alox 12 gene was highly expressed in platelets and found to be a platelet specific gene by McRedmond et al. [18]. A study conducted in Temple University School of Medicine, Philadelphia provided evidence that ALOX12 is a direct target of transcription factor RUNX1 in megakaryocytes and platelets. RUNX1 is a transcription factor that regulates the expression of haemopoietic-specific genes. When there is RUNX1 haplodeficiency, it affects overall haemopoiesis and hence, ALOX 12 expression in platelets is decreased. There was also an agonist-induced decreased 12-HETE production in platelets with the decrease in ALOX 12 expression. This provides further evidence that platelet production is associated with ALOX 12 expression [13].

This finding supports the claim that the juice consumption during the course of dengue infection has the potential to induce the rapid production of platelets. This was clearly demonstrated by the significant increase in the mean platelet count after 40 hours and 48 hours of juice consumption. The PTAFR gene which is known to be responsible for increased platelet production and aggregation was expressed 13.42-folds among the patients who consumed the juice as compared to the control group indicating that the juice had played an important role in addressing the arresting of bleeding tendencies among these patients. A study conducted in Brazil showed that injection of Platelet Activating Factor (PAF/PTAFR) in mice induced an increase in platelet count. However, after a certain level, further administration of PAF failed to induce platelet production indicating autosensitization. These findings show that PAF/PTAFR can induce the release of platelets which may be relevant to thrombocytosis [19]. We are currently investigating many other genes to determine other roles of the CPLJ other than its role in platelet production and activation.

As all plants *C. papaya* leaves are rich in compounds of different properties. Further studies need to be conducted before determining the inflammatory pathways affected by the juice, unopposed. However, it can be concluded that the administration of CPLJ in DF and DHF is safe and does induce the rapid increase in platelet count. It may play a valuable role in the management of DF in the near future.

Conflict of Interests

The research was conducted in the absence of any commercial or financial relationships that could be construed as a potential conflict of interests.

Acknowledgments

The authors would like to thank the Director General of Health, Ministry of Health, Malaysia and the Director of the Institute for Medical Research for giving them the permission to publish this paper. This research was funded by the Ministry of Health, Malaysia (project code: JPP-IMR 09-003). They would like to thank Dr. Nor Asiah, biostatistician of IMR for reviewing their statistical analysis, the Director of Hospital Tengku Ampuan Rahimah for allowing them to use the hospital facilities and the staff of The Department of Medicine and the Department of Pathology for their guidance, support, and cooperation during the study.

References

[1] I. H. Burkill, *A Dictionary of the Economic Products of the Malay Peninsula*, vol. 1, The Crown Agents for the Colonies, London, UK, 1935.

[2] K. Arumuganathan and E. D. Earle, "Nuclear DNA content of some important plant species," *Plant Molecular Biology Reporter*, vol. 9, no. 3, pp. 208–218, 1991.

[3] FAOSTAT:Papaya marketing-general information. GFruit Web site, 2012, http://www.itfnet.org/gfruit/Templates%20English/papaya.market.info.htm.

[4] V. N. Villegas, "*Carica papaya* L," in *Plant Resources of South-East Asia 2: Edible Fruits and Nuts*, E. M. W. Verheij and R. E. Coronel, Eds., vol. 2, pp. 223–225, PROSEA, Wageningen, The Netherlands, 1997.

[5] H. Y. Nakasone and R. E. Paull, *Tropical Fruits*, CAB International, Walllingford, NY, USA, 1998.

[6] B. V. Owoyele, O. M. Adebukola, A. A. Funmilayo, and A. O. Soladoye, "Anti-inflammatory activities of ethanolic extract of *Carica papaya* leaves," *Inflammopharmacology*, vol. 16, no. 4, pp. 168–173, 2008.

[7] S. Gurung and N. Škalko-Basnet, "Wound healing properties of *Carica papaya* latex: *in vivo* evaluation in mice burn model," *Journal of Ethnopharmacology*, vol. 121, no. 2, pp. 338–341, 2009.

[8] N. Otsuki, N. H. Dang, E. Kumagai, A. Kondo, S. Iwata, and C. Morimoto, "Aqueous extract of *Carica papaya* leaves exhibits anti-tumor activity and immunomodulatory effects," *Journal of Ethnopharmacology*, vol. 127, no. 3, pp. 760–767, 2010.

[9] N. A. Imaga, G. O. Gbenle, V. I. Okochi et al., "Phytochemical and antioxidant nutrient constituents of *Carica papaya* and parquetina nigrescens extracts," *Scientific Research and Essays*, vol. 5, no. 16, pp. 2201–2205, 2010.

[10] S. Z. Halim, N. R. Abdullah, Z. Afzan, B. A. Abdul Rashid, I. Jantan, and Z. Ismail, "Acute toxicity of *Carica papaya* leaf extract in Sprague Dawley rats," *Journal of Medicinal Plants Research*, vol. 5, no. 10, pp. 1867–1872, 2011.

[11] Ministry of Health of Malaysia. Vector borne disease control unit report, 2010.

[12] World Health Organization. Clinical diagnosis, 16, 2011.

[13] G. Kaur, G. Jalagadugula, G. Mao, and A. K. Rao, "RUNX1/core binding factor A2 regulates platelet 12-lipoxygenase gene (*ALOX12*): studies in human RUNX1 haplodeficiency," *Blood*, vol. 115, no. 15, pp. 3128–3135, 2010.

[14] I. C. Macaulay, M. R. Tijssen, D. C. Thijssen-Timmer et al., "Comparative gene expression profiling of in vitro differentiated megakaryocytes and erythroblasts identifies novel activatory and inhibitory platelet membrane proteins," *Blood*, vol. 109, no. 8, pp. 3260–3269, 2007.

[15] A. M. Butkiewicz, H. Kemona, V. Dymicka-Piekarska, J. Matowicka-Karma, P. Radziwon, and A. Lipska, "Platelet count, mean platelet volume and thrombocytopoietic indices in healthy women and men," *Thrombosis Research*, vol. 118, no. 2, pp. 199–204, 2006.

[16] W. D. Dupont and W. D. Plummer, "Power and sample size calculations: a review and computer program," *Controlled Clinical Trials*, vol. 11, no. 2, pp. 116–128, 1990.

[17] B. Selisko, H. Dutartre, J. C. Guillemot et al., "Comparative mechanistic studies of de novo RNA synthesis by flavivirus RNA-dependent RNA polymerases," *Virology*, vol. 351, no. 1, pp. 145–158, 2006.

[18] J. P. McRedmond, S. D. Park, D. F. Reilly et al., "Integration of proteomics and genomics in platelets: a profile of platelet proteins and platelet-specific genes," *Molecular & Cellular Proteomics*, vol. 3, no. 2, pp. 133–144, 2004.

[19] M. A. Martins, P. M. Martins, H. C. Faria Neto et al., "Intravenous injections of PAF-acether induce platelet aggregation in rats," *European Journal of Pharmacology*, vol. 149, no. 1-2, pp. 89–96, 1988.

Hindawi Publishing Corporation
Evidence-Based Complementary and Alternative Medicine
Volume 2013, Article ID 425707, 8 pages
http://dx.doi.org/10.1155/2013/425707

Research Article

Platelet Aggregation Pathway Network-Based Approach for Evaluating Compounds Efficacy

Jiangyong Gu,[1] Qian Li,[1,2] Lirong Chen,[1] Youyong Li,[3] Tingjun Hou,[3] Gu Yuan,[1] and Xiaojie Xu[1]

[1] *Beijing National Laboratory for Molecular Sciences (BNLMS), State Key Laboratory of Rare Earth Materials Chemistry and Applications, College of Chemistry and Molecular Engineering, Peking University, Beijing 100871, China*
[2] *Beijing National Laboratory for Molecular Sciences (BNLMS), Center for Molecular Sciences, State Key Laboratory for Structural Chemistry of Unstable and Stable Species, Institute of Chemistry, Chinese Academy of Sciences, Beijing 100190, China*
[3] *Institute of Functional Nano, Soft Materials, Soochow University, Soochow Jiangsu 215123, China*

Correspondence should be addressed to Lirong Chen; lirongchen@pku.edu.cn and Xiaojie Xu; xiaojxu@pku.edu.cn

Received 2 January 2013; Accepted 5 March 2013

Academic Editor: Rong Zeng

Traditional Chinese medicines (TCMs) contain a large quantity of compounds with multiple biological activities. By using multitargets docking and network analysis in the context of pathway network of platelet aggregation, we proposed network efficiency and network flux model to screen molecules which can be used as drugs for antiplatelet aggregation. Compared with traditional single-target screening methods, network efficiency and network flux take into account the influences which compounds exert on the whole pathway network. The activities of antiplatelet aggregation of 19 active ingredients separated from TCM and 14 nonglycoside compounds predicated from network efficiency and network flux model show good agreement with experimental results (correlation coefficient = 0.73 and 0.90, resp.). This model can be used to evaluate the potential bioactive compounds and thus bridges the gap between computation and clinical indicator.

1. Introduction

Translational research moves basic biological discoveries from the basic bench into the clinic applications, and it uses the clinic observations to indicate future directions for basic research. The biomarkers which are the molecular, biological, or physical characteristics of a specific physiologic state have an immense impact on the prevention and treatment of diseases. For example, the use of blood pressure and cholesterol as biomarkers for diagnostics and therapies has contributed to a 50 percent decrease in cardiovascular mortality in the USA over the past 30 years [1]. Most biomarkers of a specific physiologic state are related to biological pathways. Therefore, the studies on related pathways could help to find the links between the molecules, pathways, cellular entities, and clinic biomarkers.

Biological pathways are a defined group of biological entities that are organized in a specified order and can perform specified biological functions. Networks based on pathways will play an important role in the development of novel polypharmacological strategies to evaluate compounds which will alter the entire pathway rather than inhibit/activate the single target protein. Since many compounds and enzymes whose biological functions are not explored completely in biological pathways, it is time-consuming and expensive to determine biological functions through biological experiments for each. Therefore, it is highly desired if a computational approach can be developed to address this problem [2, 3].

Along with the progress of system biology, many complex diseases such as cancer, cardiovascular disease, and mental disorders are much more complex than initially anticipated because they are often caused by system-wide multifactors rather than being the result of a single defect [4–8]. System biology provides a platform for integrating multiple components and interactions in health and disease

state, while conventional approaches focused on a single event. The biological networks are becoming increasingly important for chemical biology and drug discovery. Analysis of biological networks offers an opportunity for integration of biological complexities and multilevel relationships and provides a new framework to understand the molecular basis of physiological or pathophysiological states. The network-based chemical biology and drug discovery aim to harness this knowledge to investigate and understand the impact of interventions of small molecules in the context of biological networks [9, 10].

Several traditional computational approaches such as pharmacophore, quantitative structure activity relationship, molecular similarity, and molecular docking have been used frequently. However, these methods cannot handle the problems in systems level. In recent years, computational polypharmacology approaches have been developed [11–13]. Encouraged by the successes of using computational approaches to tackle various problems in different biological systems, we have developed a novel and valuable computational approach to evaluate the efficacy of ligands by calculating the influence on pathway network [14].

Platelet aggregation plays an important role in myocardial infarction, thrombosis, stroke, and many other related disorders. Normal platelet aggregation is an essential part of hemostatic process which could protect mammalian from injuries of blood vessels. However, improper hemostatic stimuli in the blood could lead to a series of serious disorders and even death. Therefore, antiplatelet aggregation agents may be useful for regulating the platelet aggregation and treating the relative disorders. In this work, we developed a computational approach based on network efficiency and network flux to evaluate the antiplatelet aggregation activities of active ingredients separated from TCM.

2. Materials and Methods

2.1. Network Construction and Analysis. The network was constructed by using the information retrieved from five published literatures [15–19], Reactome [20], and KEGG [21]. The enzymes which participated in the pathway were proposed as nodes, and arrows between nodes represented the connections. The direction of the arrow meant that the node in the end of the arrow was in the downstream of the node in the front. First, Xiang et al. and Broos et al. have constructed the main framework [15, 16]. The information of GPCRs and synthesis of thromboxane was supplemented from other references. Finally, the pathway network of platelet aggregation (Figure 1) contains 64 nodes and 91 edges (arrows).

2.2. Multitarget Docking. Nineteen proteins (Table 1) in the pathway network were chosen as targets for docking. The protein-ligand complex structures (crystal or NMR) of each protein were downloaded from RCSB Protein Data Bank (http://www.rcsb.org/pdb/home/home.do). The structures of targets PAR1 and PAR4 were prepared by homology modeling based on crystal structure of bovine rhodopsin (PDB entry: 1U19). The AutoDock4.01 program in DOVIS 2.0 [22] was used for the virtual screening because of the better performance of its scoring function [23]. First, polar hydrogen atoms were added, and nonpolar hydrogen atoms were merged by the hydrogen module in AutoDock Tools (ADTs) for nineteen targets after water molecule was removed. Then, Kollman united atom partial charges were assigned. The grid map of the docking simulation was established by a $40 \times 40 \times 40$ cube centered on the target active site, with a spacing of 0.375 Å between the grid points. When every ligand was docked to a target, the Lamarckian genetic algorithm was used to optimize the conformation of ligands in the binding pocket. The set of parameters was listed as follows: the size of the population was 150. The number of energy evaluations was set to 2.5×10^7 as the run terminates. For clustering the conformations, the root mean square deviation tolerance was 2.0. Twenty independent docking runs were carried out for every ligand. Other parameters were set to default. The original ligands in the complex structures or known inhibitors (Table 1) were used as reference compounds to determine the affinity of compounds to corresponding targets. The compound database used for multitarget docking contained 413 natural products from Chinese herbs which were preserved in our laboratory. Each compound was docked to each target.

2.3. Calculation of Network Efficiency and Network Flux. The damage induced by the attacks on the network is characterized by the network efficiency (NE), which is defined as the sum of the reciprocals of the shortest path lengths between all pairs of nodes [24]. Due to a global topological property of a network which could be applied to measure the integrity of the network, the network efficiency was assumed to be used as a measure for drug efficiency [13, 14, 25]. The NE of a graph G is measured by the shortest paths between pairs of nodes with the following

$$\mathrm{NE} = \sum_{i \neq j \in G} \frac{1}{d_{ij}}, \tag{1}$$

where d_{ij} is the length of the shortest path between nodes i and j and the sum is over all $N(N-1)/2$ pairs of nodes with a total number N of nodes in the graph G. If the network is weighted, d_{ij} is the path with the minimum weight. The initial edge values of every edge were arbitrarily set to 10. To give a relative network efficiency, this quantity NE is divided by the initial network efficiency. Thus, we considered the network efficiency of the initial network as 100% and measured the relative network efficiency after each attack.

The compounds' effects on the network rely on the docking scores. We supposed that the compounds could inhibit the target well while the docking scores were relatively high. For a ligand, we transformed its docking scores with a target to edge values (EVs) of all direct downstream edges of the target in the network and then calculated the network efficiency. In other words, the edge values of all edges, which point to the other nodes from this target, were reassigned based on the docking score between the compound and the target. The edge values threshold was set to 10, so any edge

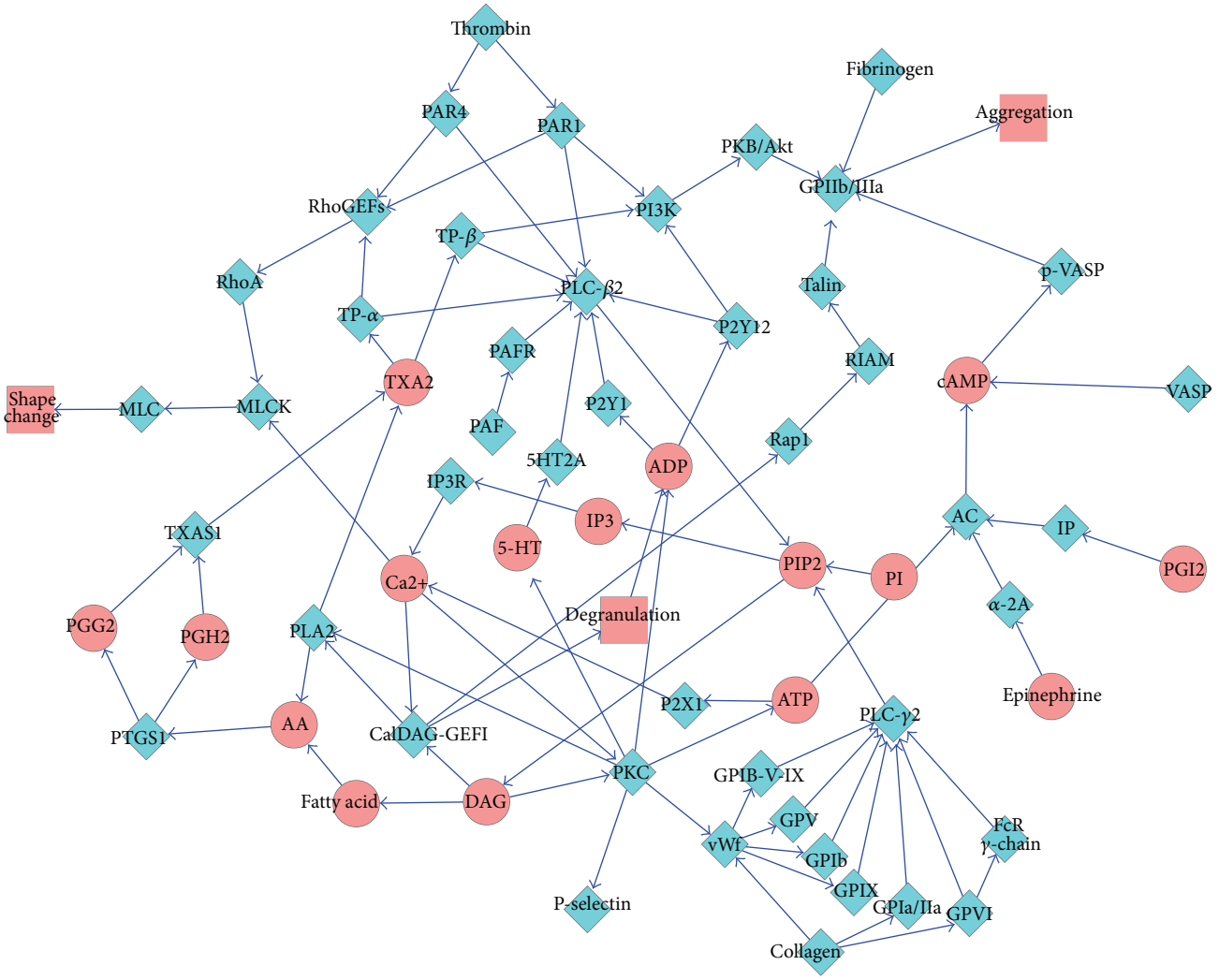

Figure 1: Pathway network of platelet aggregation. Blue diamond and red ellipse represent proteins and small molecules, respectively.

values which were less than 10 were fixed to 10. We defined that the reference ligand would knock the target by 99.95%. Therefore, the reference ligand could make the value of the edges that come out of the target enzyme as 200. The edge values of the edges which did not come out of the target enzyme were defined as 10. The edge values of the edges in the network were calculated with the follwing

$$\mathrm{EV} = 10^{(\mathrm{score}_{\mathrm{ligand}}/\mathrm{score}_{\mathrm{reference}})\times 2.30}, \quad (2)$$

where $\mathrm{score}_{\mathrm{reference}}$ represents the docking score of the reference ligand, $\mathrm{score}_{\mathrm{ligand}}$ represents the docking score of other compounds, and EV that are the edge values of the edges, come out of the target in the network. Therefore, different ligands would show different effects on each target. For each ligand, the network efficiency was then calculated using the redefined edge values. The network efficiency of each ligand was ranked by the decrease of the network efficiency. The more the network efficiency decreases, the more potent the ligand would be. The program of network efficiency calculation was written in C++ language using the Dijkstra algorithm.

Network efficiency was a global parameter of a network. However, it could not reflect the different importance of each node in the pathway network. Typically, further down the stream the node is located in a pathway network, the more important it would be. Therefore, we proposed network flux (NF) as a new indicator to evaluate the extent to which compounds influence the pathway network. NF was defined as follows:

$$\mathrm{NF} = \sum_{i \neq j \in G, j = \mathrm{exit}} \frac{1}{d_{ij}}. \quad (3)$$

Network flux was reduced from network efficiency, and NF includes only those shortest paths from upstream node to the exit of the pathway network. The decrease of NE and NF for each compound was listed in Table 2.

Table 1: Nineteen target proteins in pathway network of platelet aggregation.

Protein name	Uniprot	PDB	Ligand[b]	Score[c]
Adenylate cyclase	O60266	1AB8	1AB8	6.38
Glycoprotein IIb/IIIa complex	P05106	2VDM	2VDM	5.29
Inositol 1,4,5-trisphosphate receptor	Q14643	1N4K	1N4K	9.14
P2X purinoceptor 1	P51575	4DW1	4DW1	5.20
P2Y purinoceptor 1	P47900	1Y36	AMP	5.38
P2Y purinoceptor 12	Q9H244	1T78	AMP	3.84
Proteinase-activated receptor 1	P25116	Model[a]	F16357	5.38
Proteinase-activated receptor 4	Q96RI0	Model[a]	YD3	4.28
phosphatidylinositol 3-kinase	P48736	4FUL	4FUL	6.78
RAC-alpha serine/threonine-protein kinase	P31751	3D0E	3D0E	5.39
Protein kinase C	P17252	3IW4	3IW4	6.89
Phospholipase A2	P14555	1J1A	1J1A	5.22
Phosphoinositide phospholipase C beta-2	Q00722	2ZKM	U73122	5.62
Phosphoinositide phospholipase C gamma-2	P16885	2W2W	U73122	5.00
Prostaglandin G/H synthase 1	P23219	3N8X	3N8X	5.05
Ras-related protein	Q9H0U4	3NKV	3NKV	5.30
Thrombin	P00734	3DUX	3DUX	5.02
Thromboxane A2 receptor alpha	P21731	1LBN	SQ29548	7.90
Thromboxane A2 receptor beta	P21731	1LBN	SQ29548	7.90

[a] The structures of targets PAR1 and PAR4 were prepared by homology modeling based on crystal structure of bovine rhodopsin (PDB entry: 1U19).
[b] If the ligand was equal to the PDB entry, the structure was a ligand-protein complex; otherwise the reference ligand was a known inhibitor.
[c] Docking score of reference ligand for each target protein.

2.4. Experimental Validation. The inhibition of platelet aggregation induced by ADP was determined by Chronolog Model 700 Whole Blood/Optical Lumi-Aggregometer (Chrono-Log, Havertown, USA) in Experimental Research Center, China Academy of Chinese Medical Science. First, the blood (4~6 mL per rat) was collected from abdominal aorta, and 10% of (v/v) heparin sodium solution (0.1% dissolved in saline) was added to prevent clotting. Second, the blood was diluted 1-fold with saline for storage. Third, 1 mL of blood was added to the aggregometer and incubated with 10 μL of compound solution (10 mM in DMF) in 37.5°C for 120 seconds. Finally, 10 μL of ADP saline solution (20 μM) was added to the blood, and the inhibition effect was determined by turbidimetric method according to standard protocol. The inhibition effect of each compound was listed in Table 2.

3. Results and Discussion

3.1. Pathway Network Characteristics. The nodes in the pathway network (Figure 1) covered most of the important enzymes that participated in the process of platelet aggregation, such as GPIIb/IIIa, PAR1, PAR4, PLA2, P2Y1, P2Y12, and PI3K. The network mainly reflected the process of platelet aggregation and was suitable for multitarget virtual screening. Furthermore, the average degree of each node and the average shortest path length were 2.84 and 5.69, respectively. The pathway network showed apparent scale-free property, which meant that this network had strong robustness.

3.2. Active Compounds Prediction. The network efficiency could reflect the multitarget interaction of drugs [26]. In order to know the influence by knocking out the 19 docking targets, we measured the network efficiency in fully connected (all edge values were set to 10) or fully blocked (all edge values were set to 99999) state. When there was not any inhibition on the platelet aggregation network, the network efficiency of the whole system was 48.496. To the contrary, the knockout of all the edges that came out from the 19 targets made the efficiency decrease to 8.849.

For each screening compound, we have calculated the network efficiency in which the target proteins were inhibited by this compound. Then, we sorted the 413 screening compounds by the decrease of network efficiency and took out the first 40 compounds for antiplatelet aggregation tests. Experimental results of the whole blood antiplatelet aggregation tests showed that there were 19 compounds with antiplatelet aggregation activities among the 40 compounds, and the percentage of hits was 47.5%. Among the 19 active ingredients, silybin and papaverine were the most two potent molecules that were even comparing favorably with tirofiban which was an effective drug used in treatment of acute myocardial infarction. The papaverine, silybin, and tirofiban could completely inhibit the rat's whole blood platelet aggregation at the concentration of 100 μM. Decrease of the dosage to 34 μM slightly reduced the inhibitory effect, and the inhibitory rates for papaverine, silybin, and tirofiban were 67%, 64%, and 73%, respectively. Furthermore, to examine the quantitative predicting abilities of the model, we also

Table 2: Decrease of network efficiency and network flux, experimental results of each compound.

Compounds	Inhibition[a]	NE decrease %	NF decrease %	Combination of NE and NF[d]
Papaverine	0.67	45.5	79.8	61.8
Tirofiban[b]	0.64	39.9	61.5	49.6
Deoxycholic acid	0.66	60.8	83.4	61.9
Scutellarin[c]	0.51	52.1	77.9	57.8
Rhaponticin[c]	0.65	42.8	65.6	47.3
Dipyridamole[b]	0.60	41.8	74.1	55.6
Chrysin	0.68	47.9	75.5	65.6
Wogonin	0.67	55.6	68.7	58.8
Rhein	0.67	68.8	63.4	59.8
Silybin	0.73	56.6	96.6	71.6
Danshensu	0.57	32.2	43.4	38.3
Quercetin	0.67	47.9	89.7	76.7
Chlorogenic acid	0.54	34.6	37.9	38.6
Icariin[c]	0.65	53.4	62.0	55.6
Quercitrin[c]	0.57	41.8	60.0	50.1
Baicalin[c]	0.61	55.3	62.2	54.9
Liquiritin[c]	0.66	52.7	80.3	65.0
Salvianolic acid C	0.55	33.2	50.9	41.1
Kaempferol	0.63	50.4	71.9	60.3
Salvianolic acid B	0.53	25.0	22.8	23.9
Picroside II[c]	0.51	24.7	68.8	44.6

[a] The inhibition effect determined in the final concentration of tested compounds was 34 μM.
[b] Tirofiban and dipyridamole are two approved drugs.
[c] These seven molecules are glycoside compounds.
[d] Combination of NE decrease and NF decrease: the square root of the product of the percentage of NE decrease and the percentage of NF decrease.

compared the predicted potent value and the experimental results. Numerical analysis showed that the linear correlation coefficient of the decrease of network efficiency and whole blood antiplatelet aggregation experimental results was 0.67 (Figure 2(a)).

The linear correlation coefficient was not very high. This may be because the more important effect the downstream nodes may exert had not been taken into account in the calculation of network efficiency. However, network flux can complement network efficiency. After the addition of NF, the linear correlation coefficient increased to 0.73 (Figure 2(c)).

Given that docking program could not treat glycoside with great accuracy because there were many flexible groups, we only considered 14 nonglycoside compounds. In this case, the linear correlation coefficients for the least square fitting of NE, NF, and the combination of NE and NF with experimental results were 0.80, 0.87, and 0.90, respectively (Figure 3). It showed that the combination model could not only qualitatively classify the active and the nonactive compounds but also quantitatively predict the efficacy of the compounds to a certain extent.

Traditional Chinese medicine has been used for thousands of years. TCM presents much diversity in structure and bioactivity, and less toxicity and is an attractive source of new active compounds in drug discovery. The conventional approach to find active compounds in TCM involves selecting a potential plant and isolating compounds following bioassay guidance. This approach has been playing an important part in drug development. However, it was often time-consuming and can contain false positives. We have reported a reverse approach (from finding bioactive molecules to related plant) [27]. Papaverine was isolated mainly from *Papaver somniferum* L. and often used to cause dilation of the blood vessels. Silybin was a flavonolignan isolated from *Silybum marianum* G. with antioxidative and antiinflammatory activities. Therefore, these two herbs would deserve some attention for antiplatelet aggregation activity.

3.3. Comparison with Single Target Screening. To reveal the importance of the biological network system in this approach, we compared the predictions generated by single target docking scores with those of network efficiencies and network flux based on the multitarget docking.

The docking results showed that most of the compounds could interact with many targets rather than a single target. When calculated by applying the single target docking scores, the correlation coefficients of the docking score and the experimental data for GPIIb/IIIa, PLA2, P2Y1, and P2Y12, which were approved targets by FDA and supposed as very important targets in platelet aggregation process, were 0.57, 0.20, 0.07, and 0.23, respectively. However, the correlation coefficient between the predictions based on network efficiencies, network flux, and the experimental data

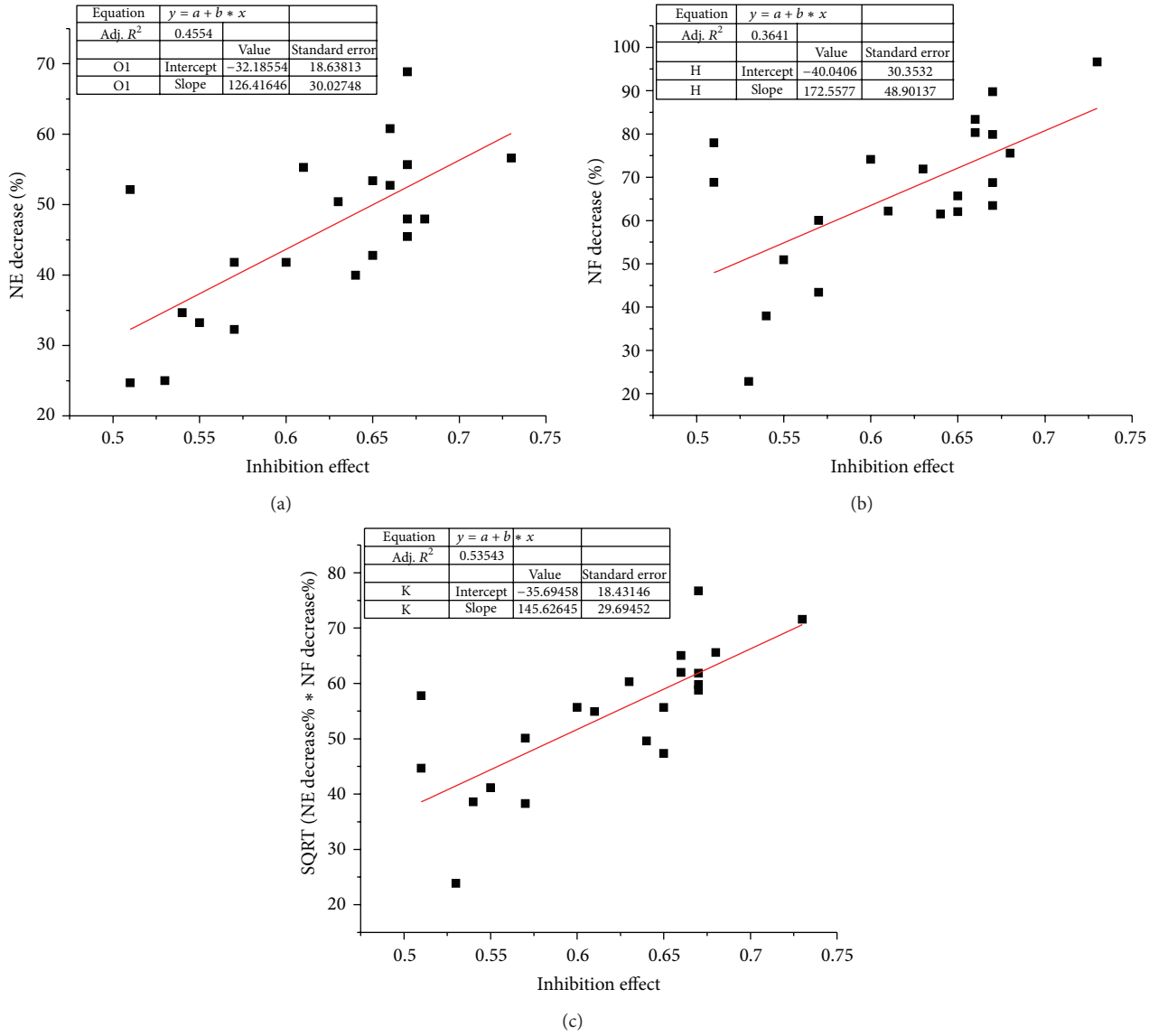

FIGURE 2: Linear regression between predicated activities of 19 natural products and two drugs and experimental inhibition effects. (a) network efficiency; (b) network flux; (c) combination of network efficiency and network flux.

was improved by applying the multitarget strategy ($r = 0.90$, Figure 3). It suggested that overall consideration of the contribution of the biological network might be better than only consideration of the contribution of single target for the accurate predictions of the biological activities. The single target docking cannot capture the biological effects of the ligands comprehensively, and the multitarget screening was really necessary to characterize the complicated binding properties of ligands with multiple targets involved in biological network.

Like all virtual screening methods, our approach had many advantages as well as some limitations. One of the obvious advantages of the method was that it specifically considered the role of every target in the whole platelet aggregation process and assigned the weightiness on every target by biological network analysis. The other advantage was that the affinity evaluation in the method was not limited to molecular docking and scoring, as used in this study. Other binding energy prediction methods could also be used, such as pharmacophore, quantitative structure-activity relationship, or comparative molecular field analysis. It was also assumed that the consideration of flexibility of the targets in molecular docking might improve the accuracy of the network efficiency and network flux. On the other hand, one clear disadvantage of this technique was that its accuracy relies heavily on the reliability of network construction and the accuracy of binding affinity assessment.

4. Conclusions

In summary, we developed a novel computational approach that combines multitarget docking, network efficiency, and

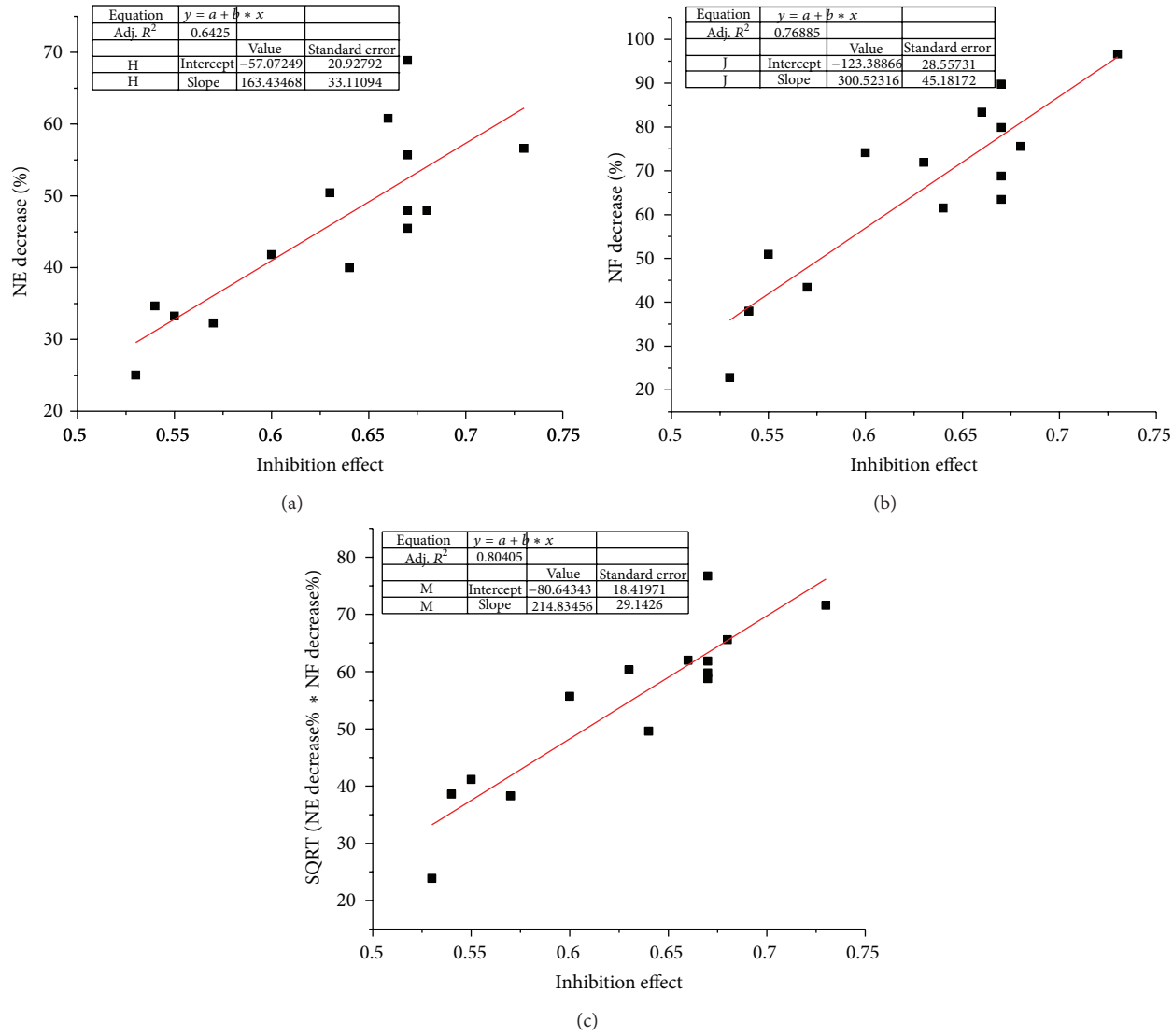

Figure 3: Linear regression between predicated activities of 14 nonglycoside natural products and experimental inhibition effects. (a) Network efficiency; (b) network flux; (c) combination of network efficiency and network flux.

network flux for the predictions of active ingredients separated from TCM with reasonable accuracy. The method integrated the scores generated by the multitarget docking and network analysis in the context of biological pathway. This approach can evaluate the ligands' efficacy more comprehensively than traditional single target docking with much better prediction accuracy and would be very useful for chemical biology and drug discovery. Meanwhile, top two potent compounds (silybin and papaverine) and their source herbs could be promising drugs for antiplatelet aggregation. It remains to be determined what extent and complexity the pathway network takes effect to the biological activity, and the relevant work is underway.

Conflict of Interests

The authors declare that they have no conflict of interests.

Acknowledgments

This work was financially supported by National Key Special Project of Science and Technology for Innovation Drugs (Grant nos. 2008ZX09401-006, 2009ZX09502-015, and 2012ZX09501001-004) and the country support National Science and Technology Project (no. 2008BAI51BOO).

References

[1] E. A. Zerhouni, "Translational research: moving discovery to practice," *Clinical Pharmacology and Therapeutics*, vol. 81, no. 1, pp. 126–128, 2007.

[2] K. X. Zhang and B. F. Ouellette, "Pandora, a pathway and network discovery approach based on common biological evidence," *Bioinformatics*, vol. 26, no. 4, pp. 529–535, 2010.

[3] R. A. Pache, A. Zanzoni, J. Naval, J. M. Mas, and P. Aloy, "Towards a molecular characterisation of pathological pathways," *FEBS Letters*, vol. 582, no. 8, pp. 1259–1265, 2008.

[4] H. Kitano, "Computational systems biology," *Nature*, vol. 420, no. 6912, pp. 206–210, 2002.

[5] C. T. Keith, A. A. Borisy, and B. R. Stockwell, "Multicomponent therapeutics for networked systems," *Nature Reviews Drug Discovery*, vol. 4, no. 1, pp. 71–78, 2005.

[6] E. C. Butcher, E. L. Berg, and E. J. Kunkel, "Systems biology in drug discovery," *Nature Biotechnology*, vol. 22, no. 10, pp. 1253–1259, 2004.

[7] P. Kohl, E. J. Crampin, T. A. Quinn, and D. Noble, "Systems biology: an approach," *Clinical Pharmacology and Therapeutics*, vol. 88, no. 1, pp. 25–33, 2010.

[8] A. M. Henney, "Who will take up the gauntlet?: challenges and opportunities for systems biology and drug discovery," *EMBO Reports*, vol. 10, no. 1, pp. S9–S13, 2009.

[9] D. K. Arrell and A. Terzic, "Network systems biology for drug discovery," *Clinical Pharmacology and Therapeutics*, vol. 88, no. 1, pp. 120–125, 2010.

[10] S. C. Janga and A. Tzakos, "Structure and organization of drug-target networks: insights from genomic approaches for drug discovery," *Molecular BioSystems*, vol. 5, no. 12, pp. 1536–1548, 2009.

[11] A. L. Hopkins, "Network pharmacology: the next paradigm in drug discovery," *Nature Chemical Biology*, vol. 4, no. 11, pp. 682–690, 2008.

[12] E. E. Schadt, S. H. Friend, and D. A. Shaywitz, "A network view of disease and compound screening," *Nature Reviews Drug Discovery*, vol. 8, no. 4, pp. 286–295, 2009.

[13] V. Agoston, P. Csermely, and S. Pongor, "Multiple weak hits confuse complex systems: a transcriptional regulatory network as an example," *Physical Review E*, vol. 71, no. 5, Article ID 051909, pp. 1–7, 2005.

[14] Q. Li, X. Li, C. Li et al., "A network-based multi-target computational estimation scheme for anticoagulant activities of compounds," *PLoS ONE*, vol. 6, no. 3, Article ID e14774, 2011.

[15] Y. Z. Xiang, L. Y. Kang, X. M. Gao, H. C. Shang, J. H. Zhang, and B. L. Zhang, "Strategies for antiplatelet targets and agents," *Thrombosis Research*, vol. 123, no. 1, pp. 35–49, 2008.

[16] K. Broos, S. F. De Meyer, H. B. Feys et al., "Blood platelet biochemistry," *Thrombosis Research*, vol. 129, no. 3, pp. 245–249, 2012.

[17] S. P. Jackson and S. M. Schoenwaelder, "Antiplatelet therapy: in search of the 'magic bullet'," *Nature Reviews Drug Discovery*, vol. 2, no. 10, pp. 775–789, 2003.

[18] Y. Z. Xiang, Y. Xia, X. M. Gao, H. C. Shang, L. Y. Kang, and B. L. Zhang, "Platelet activation, and antiplatelet targets and agents: current and novel strategies," *Drugs*, vol. 68, no. 12, pp. 1647–1664, 2008.

[19] K. Sangkuhl, A. R. Shuldiner, T. E. Klein, and R. B. Altman, "Platelet aggregation pathway," *Pharmacogenetics and Genomics*, vol. 21, no. 8, pp. 516–521, 2011.

[20] G. Joshi-Tope, M. Gillespie, I. Vastrik et al., "Reactome: a knowledgebase of biological pathways," *Nucleic Acids Research*, vol. 33, pp. D428–D432, 2005.

[21] M. Kanehisa, S. Goto, M. Furumichi, M. Tanabe, and M. Hirakawa, "KEGG for representation and analysis of molecular networks involving diseases and drugs," *Nucleic Acids Research*, vol. 38, no. 1, Article ID gkp896, pp. D355–D360, 2009.

[22] X. Jiang, K. Kumar, X. Hu, A. Wallqvist, and J. Reifman, "DOVIS 2.0: an efficient and easy to use parallel virtual screening tool based on AutoDock 4.0," *Chemistry Central Journal*, vol. 2, no. 1, article 18, 2008.

[23] H. Park, J. Lee, and S. Lee, "Critical assessment of the automated AutoDock as a new docking tool for virtual screening," *Proteins: Structure, Function and Genetics*, vol. 65, no. 3, pp. 549–554, 2006.

[24] V. Latora and M. Marchiori, "Efficient behavior of small-world networks," *Physical Review Letters*, vol. 87, no. 19, Article ID 198701, pp. 1–4, 2001.

[25] P. Csermely, V. Ágoston, and S. Pongor, "The efficiency of multi-target drugs: the network approach might help drug design," *Trends in Pharmacological Sciences*, vol. 26, no. 4, pp. 178–182, 2005.

[26] Z. Spiro, I. A. Kovacs, and P. Csermely, "Drug-therapy networks and the prediction of novel drug targets," *Journal of Biology*, vol. 7, no. 6, article 20, 2008.

[27] X. Xu, "New concepts and approaches for drug discovery based on traditional Chinese medicine," *Drug Discovery Today*, vol. 3, no. 3, pp. 247–253, 2006.

Hindawi Publishing Corporation
Evidence-Based Complementary and Alternative Medicine
Volume 2013, Article ID 510146, 8 pages
http://dx.doi.org/10.1155/2013/510146

Research Article

Expert Consensus on the Treatment of Hypertension with Chinese Patent Medicines

Li Ying Wang,[1] Kam Wa Chan,[2] Ya Yuwen,[1] Nan Nan Shi,[1] Xue Jie Han,[1] and Aiping Lu[1,3]

[1] *Institute of Basic Research in Clinical Medicine, China Academy of Chinese Medical Sciences, Beijing 100700, China*
[2] *Tung Wah Group of Hospitals, Hong Kong Special Administrative Region, Hong Kong*
[3] *School of Chinese Medicine, Hong Kong Baptist University, Hong Kong Special Administrative Region, Hong Kong*

Correspondence should be addressed to Xue Jie Han; xuejiehan@126.com and Aiping Lu; lap64067611@126.com

Received 17 January 2013; Accepted 27 February 2013

Academic Editor: Wei Jia

Objectives. This study was aimed to determine the therapeutic principle and identify Chinese Patent Medicine (CPM) with corresponding indications for hypertension treatment. *Methods*. Three rounds of Delphi survey were mailed among 40 cardiovascular integrative medicine specialists. Items with agreement of more than 80% respondents were included in the consensus. *Results*. According to majority of the panelists, CPM is suitable for most hypertensive patients and should be used according to traditional Chinese medicine pattern classification. CPM could be used alone for grade 1 hypertension and could be used in combination with Western biomedicine (WM) for both grade 2 and grade 3 hypertension. It is recommended that less than two CPMs are used simultaneously. For the treatment of grade 2 and 3 hypertension, CPM and WM should be taken separately. Recommended CPMs included Tianma Gouteng granule, Qiju Dihuang capsule, Jinkui Shenqi pill, Yinxingye tablet, Niuhuang Jiangya pill and Banxia Tianma pill. The indications of 4 CPMs were specified with symptoms related to TCM pattern classification by the experts. *Conclusions*. An expert consensus on CMP application was formed for the treatment of hypertension in the form of integrative medicine. A flow of IM hypertension management was proposed based on the results of the survey.

1. Introduction

Hypertension is an alarming global health issue with increasing longevity and prevalent contributing factors, such as obesity, physical inactivity, and an unhealthy diet [1–3]. It is of highest morbidity rate of chronic diseases in China [4]. The current prevalence in many developing countries is reaching that of developed countries [5, 6].

TCM has been used widely in treating hypertension in China [7], and recently more Chinese patent medicines (CPMs) were developed for convenient application and better quality control [8–13]. Currently, there are 86 CPMs available for the treatment of hypertension as listed in the Chinese pharmacopoeia (2010 edition) [14]. These CPMs were used not only by TCM doctors but also by WM doctors. Since most of the WM doctors have inadequate training in TCM, the misuse of CPMs is a practical concern.

Different CPMs should be used to treat diseases with different TCM patterns according to TCM pattern differentiation theory. In China, there are no mandatory guidelines for the application of CPMs as a treatment for hypertension. We aimed to develop a guideline for best practice of using CPM to treat hypertension through a Delphi survey among a cohort of cardiovascular experts in IM.

Delphi surveys are commonly used to reach agreement of clinical protocols [15]. A Delphi survey involves a group of experts with equal opportunity to contribute to decision making in an anonymous, iterative, regulated, and statistically assisted manner [16]. This process prevents negative effects of group interactions including dominance of vocal group members and imposes few geographical constraints [17]. To ensure easy understanding and application among doctors without TCM training, we presented the indications of CPM with common symptoms.

2. Methods

2.1. Participating Experts. A clinical expert consensus management group was formed. 40 IM cardiovascular experts were selected with three criteria: (1) with more than ten years clinical experience in the treatment of hypertension with CPMs; (2) have published at least 4 peer reviewed papers related to the treatment of hypertension with IM; (3) recommended by the Cardiovascular Disease Division of China Association of Chinese Medicine.

2.2. Questionnaire. For the first round of survey, a questionnaire focused on the general therapeutic principle was deliberated among and set by the management group. A list of top 20 commonly used CPMs was generated from a systematic literature search in PubMed and Chinese CNKI. All these included 33 items covering the following areas: the general principle of using CPMs, the commonly used CPMs and the corresponding indications.

Experts were invited to add any comments that they perceived to be necessary and the CPMs that they used frequently in their clinical practice.

2.3. Delphi Process. Three rounds of consultation were carried out in this study. The questionnaire was mailed to the panelists. A month after the deadline of response, a reminder was sent to experts who did not respond.

In the first round, the experts were invited to finish the questionnaire and add the general principles of CPMs application and CPMs they commonly used in treatment of hypertension. The results were collected and submitted to the management group.

After analysis and discussion, a revised questionnaire for the second round consultation was generated and subsequently disseminated to the experts who responded in the first round. Items were accepted as consensus directly when 80% of respondents reached agreement. Items receiving less than 20% support were removed. Items receiving between 20% and 80% were recirculated to the next round consultation. A list of top 20 commonly used CPMs together with the CPMs suggested by the experts were included. The third round of questionnaire was composed of the same questions which did not achieve consensus in previous consultation. All respondents had access of second round scores of the whole group to provide information for consensus items from the second round and achieve the final consensus. As it is well understood that the application of CPMs varies among different CM doctors and different pattern of disease, we included CPMs with consensus over 70% so as to provide more options on treatment. Corresponding confidence intervals were shown as reference.

3. Results

3.1. Participants. The questionnaire was mailed to the 40 experts satisfying the inclusion criteria. All of them completed the first round of consultation, 37 experts completed the second round, and 33 experts finished the third round.

Table 1: Demographics of panelists.

General information	Number (percentage)[*1]
Age (years old)	
<40	1 (2.5%)
40~50	11 (27.5%)
50~60	24 (60.0%)
>60	4 (10.0%)
Ranking	
Professor	31 (77.5%)
Associate professor	9 (22.5%)
Clinical experience (years)	
10~20	9 (22.5%)
20~30	18 (45.0%)
≥30	13 (32.5%)

[*1]The total number of panelists at round 1 is 40.

The panelists aged from 37 to 70 and were all ranked of professor or associate professor. Table 1 shows the demographics of the panelists.

3.2. Items Endorsed in the Consensus. After three rounds of consultation, the items with consensus included 12 general therapeutic principles of CPMs application, six CPMs with indications and precautions. Figure 1 shows the management flow of hypertension with CPMs based on the results in the survey.

In the first round of consultation, 21 items on general therapeutic principle and 20 CPMs for the treatment of hypertension were collected from literature review and constituted the questionnaire for the first round of consultation. The questionnaires were mailed to the panelists. Four items which reached consensus from more than 80% experts were accepted directly (Table 2), including "CPMs and WMs should be used according to hypertension grades in WM diagnosis," "CPMs could reduce the side effect of western medicines in hypertension treatment," "CPMs and WMs could be used in combination with other types of TCM non-drug therapy," and "Physical activity is suitable for hypertension treatment".

In the second round of consultation, 7 items on general therapeutic principle reached consensus from more than 80% experts (Table 2), including "CPMs could be used alone in grade 1 hypertension treatment," "CPMs should be used according to TCM pattern classification," "Less than two kinds of CPMs were recommended to be used simultaneously," "Doctors should monitor the symptom changes to avoid side effect of CPMs," "CPMs should be used with WMs together in grade 2 and grade 3 hypertension treatment," "CPMs and WMs should be taken separately when used together" (Table 2).

In the third round of consultation, 1 more item of the general therapeutic principle for CPM application was selected by more than 80% experts, and 6 kinds of CPMs were selected by 70% or more experts (Table 2). Selected CPMs included Tianma Gouteng (TMGT) granule (90.00%), Qiju Dihuang (QJDH) capsule (87.50%), Jinkui Shenqi (JKSQ)

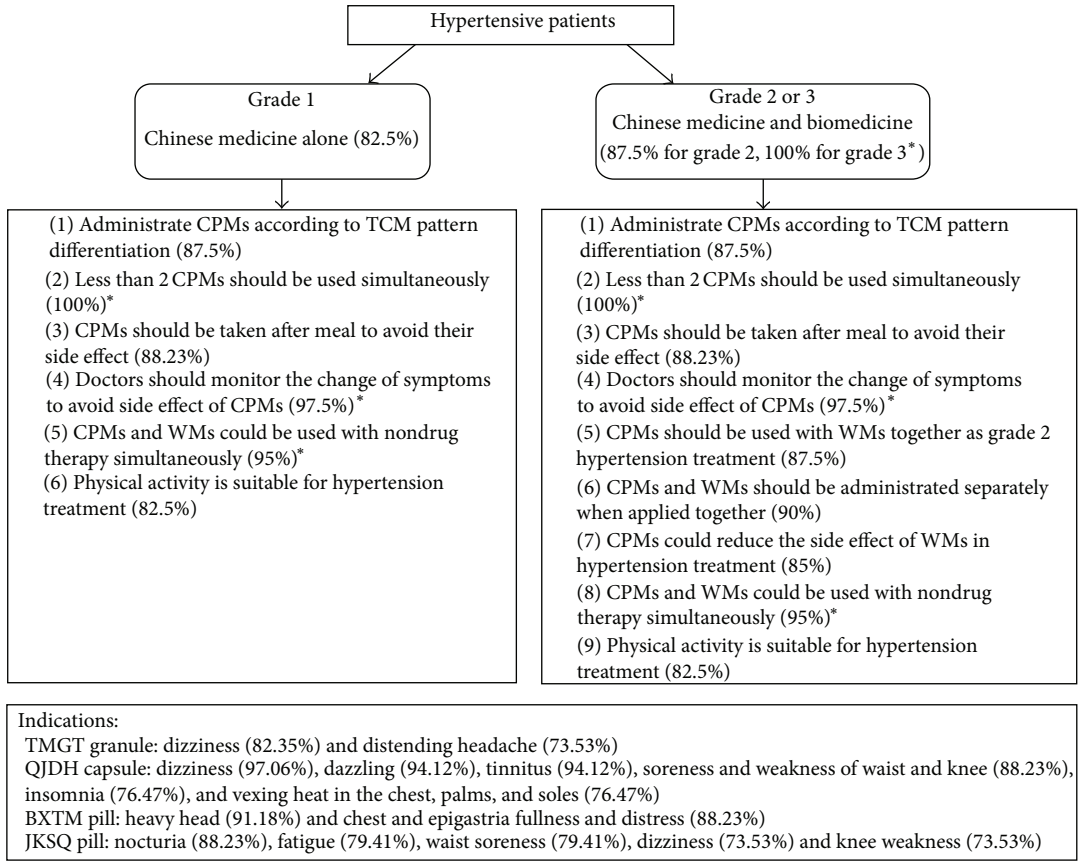

*$P < 0.05$.

Figure 1: Proposed flow of hypertension management in the integrative medicine perspective.

pill (80.00%), Yinxingye (YXY) tablet (80.00%), Niuhuang Jiangya (NHJY) pill (76.47%), and Banxia Tianma (BXTM) Pill (70.59%). Detailed information about the 6 selected CPMs were shown in Table 3. In addition, the specific indication based on TCM symptoms of 4 selected CPMs was identified by more than 70% experts and shown in Table 4.

4. Discussion

We aimed to reach an expert consensus on CPMs treatment for hypertension for WM doctors who intend to use CPMs in hypertension management. We used the Delphi method which enabled us to utilize both the research and clinical experience of the experts who participated with no geographical limitations. All panelists of the consultation were IM cardiologist. They were all recommended by the Cardiovascular Disease Division of China Association of Chinese Medicine. Compared with the TCM doctors who use herbal decoctions more frequently than CPMs, IM doctors treat hypertension with both CPMs and WMs simultaneously more often. We selected IM doctors as they had both WM and CM education background as well as clinical experience on the use of both CPMs and WMs. We believe that they are more capable to explain with TCM terms and have richer experience on clinical use of related CPMs and WMs.

The consensus included twelve general therapeutic principles of CPMs and six CPMs with corresponding indications. Majority agreed that CPMs could be used for most patients with hypertension and the application varies among different stages of hypertension. CPM could be used alone in grade 1 hypertension and should be used along with WM for grade 2 and grade 3 hypertension. The results are coherent with the clinical practice in China currently. Previous studies showed that CPMs have similar effect in treating grade 1 hypertension as WMs [18]. Furthermore, the clinical effectiveness is enhanced with the concurrent use of WMs in grade 2 and grade 3 hypertension management [19, 20]. Therefore, CPMs should be used with WMs together when treating grade 2 and grade 3 hypertensive patients.

CPMs are developed based on TCM theory as a result, they should be used according to TCM pattern classification in the treatment of hypertension. Hypertensive patients usually presented with headache and dizziness, and sometimes tinnitus, soreness and weakness of waist and knee, and fear of cold and cold limbs. All these could be classified into different patterns. Studies have shown the correlation between hypertension and different TCM patterns [21, 22] with typical symptoms. In this study, we listed a wide range of symptoms for pattern classification in the consultation in order to yield symptom-based indications of recommended CPMs.

Table 2: General principles for hypertension treatment achieving consensus.

No.	Consensus	Round for consensus	Percentage of consensus (95% confidence interval)
1	CPMs and WMs could be used with nondrug therapy simultaneously	1	95.00% (82.6% to 100%)*
2	CPMs could reduce the side effect of WMs in hypertension treatment	1	85.00% (72.6% to 97.4%)
3	CPMs and WMs should be used according to WM diagnostic system	1	82.50 (70.1% to 94.9%)
4	Physical activity is suitable for hypertension treatment	1	82.50 (70.1% to 94.9%)
5	Less than two CPMs should be used simultaneously	2	100.00 (87.1% to 100%)*
6	CPMs should be used with WMs together as grade 3 hypertension treatment	2	100.00 (87.1% to 100%)*
7	Doctors should monitor the change of symptoms to avoid side effect of CPMs	2	97.50 (84.6% to 100%)*
8	CPMs and WMs should be administrated separately when applied together	2	90.00 (77.1% to 100%)
9	CPMs should be used with WMs together as grade 2 hypertension treatment	2	87.50 (74.6% to 100%)
10	CPMs should be used according to TCM pattern differentiation theory	2	87.50 (74.6% to 100%)
11	CPMs could be used alone as grade 1 hypertension treatment	2	82.50 (69.6% to 95.4%)
12	CPMs should be taken after meal to avoid their side effect	3	88.23 (74.6% to 100%)

*$P < 0.05$.

Hypertension is associated with multiple cardiovascular risk factors, and the concurrent use of multiple CPMs for hypertension treatment is a common practice. According to most of the IM or TCM experts, simultaneous application of CPMs may have an additive effect. However, in recent years, there have been an increasing number of reports on the side effect of concurrent use of CPMs [23]. To avoid the side effects, experts recommended that less than two CPMs should be used simultaneously. In addition, CPMs should be taken after meal, and the practitioners should monitor the change of symptoms to avoid the side effects.

The concurrent use of TCM and WM has been popular in China which leads to a new medical model known as integrated traditional and western medicine or integrative medicine. With regard to hypertension treatment, this approach is being used clinically, involving CPMs and different categories of WMs such as diuretics, Beta-blockers, CCBs, and ACEIs [24]. It is shown in many studies that combined treatments are more effective in disease control and symptoms modification when compared with single treatment [25].

In this survey, 87.5% of experts agreed that CPMs and WMs should be administered separately in the treatment of grade 2 and grade 3 hypertension. It is sensible to take CPMs and WMs apart in clinical practice, as CPMs are complex and there may be interaction between the medicines. Some studies showed that CPMs and Chinese herbal medicines (CHM) have the effect of reducing side effects of WMs in hypertension treatment [26], and 85% of the panelists agreed with that.

A range of lifestyle modifications have been shown in clinical trials with the effect of lowering blood pressure and reducing the incidence of hypertension, similar to majority (82.5%) of the panelists' viewpoint. Physical activity is one of the most important among them [27, 28].

In this study, more than 70% of the experts selected six CPMs for hypertension treatment including TMGT, QJDH JKSQ, YXY, NHJY, and BXTM. TMGT, QJDH, YXY, NHJY and BXTM were recorded in the Chinese pharmacopoeia (2010 edition). TMGT granule, with highest consensus and the only CPM selected by more than 90% of panelists, is a recommended treatment in the clinical practice guideline for hypertension in TCM [9]. TMGT granule is composed of the herbs Gastrodiae Rhizoma (Tian Ma), Uncariae Ramulus Cum Uncis (Gou Teng), Haliotidis Concha (Shi Jue Ming), Gardeniae Fructus (Zhi Zi), Astragali Radix (Huang Qi), Achyranthis Bidentatae Radix (Niu Xi), Eucommiae Cortex (Yan Du Zhong), Leonuri Herba (Yi Mu Cao), Taxilli Herba (Sang Ji Sheng), Polygoni Multiflori Caulis (Shou Wu Teng), and Poria (Fu Ling). The indication of TMGT granule includes headache, dizziness, tinnitus, dazzle, tremor, and insomnia, which can be categorized as liver-yang hyperactivity according to TCM pattern differentiation [14]. It has been proven that TMGT granule is effective in lowering blood pressure and modifying symptoms when used alone [29] and that is even enhanced when used with WM concurrently [30]. Pharmacological researches demonstrated that TMGT granule can attenuate myocardial and aorta hypertrophy induced by renovascular hypertension and suppress the rise of tissue Ang II significantly [31].

QJDH capsule consists of eight herbal medicines including Lycii Fructus (Gou Qi Zi), Mume Flos (Ju Hua), Rehmanniae Radix Praeparata (Shu Di Huang), Corni Fructus (Shan Zhu Yu), Moutan Cortex (Mu Dan Pi), Dioscoreae Rhizoma (Shan Yao), Poria (Fu Ling), and Aliamria Rhizoma (Yan Ze Xie). The indication of QJDH capsule includes vertigo, tinnitus, photophobia, and epiphora with wind and blurred vision, which can be categorized as liver-kidney yin deficiency [14]. It is shown that QJDH capsule is effective in regulating immunologic function and improving clinical symptoms [32]. The effect of controlling blood pressure is enhanced when QJDH capsule was used with verapamil simultaneously [33].

NHJY pill is composed of fourteen herbal medicines including Saigae Tataricae Cornu (Ling Yang Jiao), Margaritifera Concha (Zhen Zhu Mu), Bubali Cornu (Shui Niu Jiao), Bovis Calculus (Ren Gong Niu Huang), Borneolum

Table 3: General information on the CPMs achieving consensus.

Name	Source of information	Composition	Specification	Recommended dosage
Tianma Gouteng (TMGT) granule	Chinese pharmacopoeia (2010 edition)	Gastrodiae Rhizoma (Tian Ma), Uncariae Ramulus Cum Uncis (Gou Teng), Haliotidis Concha (Shi Jue Ming), Gardeniae Fructus (Zhi Zi), Astragali Radix (Huang Qi), Achyranthis Bidentatae Radix (Niu Xi), Eucommiae Cortex (Yan Du Zhong), Leonuri Herba (Yi Mu Cao), Taxilli Herba (Sang Ji Sheng), Polygoni Multiflori Caulis (Shou Wu Teng), and Poria (Fu Ling)	10 g/bag	10 g/t; t.i.d.
Qiju Dihuang (QJDH) capsule	Chinese pharmacopoeia (2010 edition)	Lycii Fructus (Gou Qi Zi), Mume Flos (Ju Hua), Rehmanniae Radix Praeparata (Shu Di Huang), Corni Fructus (Shan Zhu Yu), Moutan Cortex (Mu Dan Pi), Dioscoreae Rhizoma (Shan Yao), Poria (Fu Ling), and Aliamria Rhizoma (Yan Ze Xie).	0.3 g/granule	5-6 granules/t; t.i.d.
Niuhuang Jiangya (NHJY) pill	Chinese pharmacopoeia (2010 edition)	Saigae Tataricae Cornu (Ling Yang Jiao), Margaritifera Concha (Zhen Zhu Mu), Bubali Cornu (Shui Niu Jiao), Bovis Calculus (Ren Gong Niu Huang), Borneolum Syntheticum (Bing Pian), Paeoniae Radix Alba (Bai Shao), Salviae Miltiorrhizae Radix Et Rhizoma (Dang Shen), Astragali Radix (Huang Qi), Cassiae Semen (Jue Ming Zi), Chuanxiong Rhizoma (Chuan Xiong), Scutellariae Radix (Huang Qin Ti Qu Wu), Nardostachyos Radix Et Rhizoma (Gan Song), Menthae Haplocalycis Herba (Bo He), and Curcumae Radix (Yu Jin)	20 pills/1.3 g 1 pill/g	1.3 g–2.6 g/t; q.d. 1.6 g–3.2 g/t; q.d.
Banxia Tianma (BXTM) pill	Chinese pharmacopoeia (2010 edition)	Pinelliae Rhizoma Praeparatum (Fa Ban Xia), Gastrodiae Rhizoma (Tian Ma), Astragali Radix Praeparata Cum Melle (Zhi Huang Qi), Ginseng Radix Et Rhizoma (Ren Shen), Atractylodis Rhizoma (Cang Zhu), Atractylodis Macrocephalae Rhizoma (Chao Bai Zhu), Poria (Fu Ling), Citri Reticulatae Pericarpium (Chen Pi), Aliamria Rhizoma (Ze Xie), Massa Medicata Fermentata (Liu Shen Qu), Hordei Fructus Germinatus (Chao Mai Ya), and Phellodendri Chinensis Cortex (Huang Bai)	100 pills/6 g	6 g/t; b.i.d./t.i.d.
Yinxingye (YXY) tablet	Chinese pharmacopoeia (2010 edition)	Ginkgo Folium	12 mg/tablet; 24 mg/tablet;	24 mg/t; t.i.d.
Jinkui Shenqi (JKSQ) pill	State Drug Approval Document No: Z11020054	Aconiti Lateralis Rddix Praeparata (Fu Zi), Cinnamomi Ramulus (Gui Zhi), Achyranthis Bidentatae Radix (Niu Xi), Rehmanniae Radix (Di Huang), Corni Fructus (Shan Zhu Yu), Dioscoreae Rhizoma, Poria (Fu Ling), Aliamria Rhizoma (Ze Xie), Plantaginis Semen (Che Qian Zi), and Moutan Cortex (Mu Dan Pi)	6 mg/granule	b.i.d.

Syntheticum (Bing Pian), Paeoniae Radix Alba (Bai Shao), Salviae Miltiorrhizae Radix Et Rhizoma (Dang Shen), Astragali Radix (Huang Qi), Cassiae Semen (Jue Ming Zi), Chuanxiong Rhizoma (Chuan Xiong), Scutellariae Radix (Huang Qin Ti Qu Wu), Nardostachyos Radix Et Rhizoma (Gan Song), Menthae Haplocalycis Herba (Bo He), and Curcumae Radix (Yu Jin). The indication of NHJY pill includes light headedness, headache, insomnia, and dysphoria which can be categorized as heat in heart and liver and phlegm heat obstruct [14]. Clinical studies demonstrated that NHJY pill is suitable for grade 1 and grade 2 hypertension treatments [34]. It can relieve headache, irritability, anxiety and depress sympathetic nervous activity [35]. NHJY pill includes many metallic elements such as sodium, calcium, magnesium, potassium, iron, chromium, manganese, nickel, cadmium, copper, and zinc [36]. The side effect of NHJY pill includes minor gastric discomfort which can be relieved after symptomatic treatment [37].

YXY tablet was mainly composed of flavonol glycosides, an extract of Chinese herbal medicine ginkgo leaf. The indications of YXY tablet are cardialgia, stroke, and hemiplegia, which can be categorized in TCM pattern as obstruction of collaterals by blood stasis [14]. Clinical studies showed that YXY tablet has good effect on lowering blood pressure and improving the quality of life for hypertensive patient when used alone or combined with WMs [38, 39]. Pharmacological research showed that it can inhibit hypertension ventricle remodeling by downregulating the serum TGF-p1 [40]. The side effect of YXY tablet includes urticaria, which would disappear after cessation of medication [41].

Table 4: Clinical indications of the CPMs achieving consensus.

CPMs	TCM symptom-based indications	Percentage of consensus (%)
TMGT granule	Dizziness	82.35
	Distending headache	73.53
QJDH capsule	Dizziness	97.06*
	Dazzling	94.12*
	Tinnitus	94.12*
	Soreness and weakness of waist and knee	88.23
	Insomnia	76.47
	Vexing heat in the chest, palms, and soles	76.47
BXTM pill	Heavy head	91.18
	Chest and epigastric fullness and distress	88.23
JKSQ pill	Nocturia	88.23
	Fatigue	79.41
	Waist soreness	79.41
	Dizziness	73.53
	Knee weakness	73.53

* $P < 0.05$.

BXTM pill consists of Pinelliae Rhizoma Praeparatum (Fa Ban Xia), Gastrodiae Rhizoma (Tian Ma), Astragali Radix Praeparata Cum Melle (Zhi Huang Qi),Ginseng Radix Et Rhizoma (Ren Shen), Atractylodis Rhizoma (Cang Zhu), Atractylodis Macrocephalae Rhizoma (Chao Bai Zhu), Poria (Fu Ling), Citri Reticulatae Pericarpium (Chen Pi), Aliamria Rhizoma (Ze Xie), Massa Medicata Fermentata (Liu Shen Qu), Hordei Fructus Germinatus (Chao Mai Ya), and Phellodendri Chinensis Cortex (Huang Bai). Indication includes dizziness, headache, and chest and epigastric fullness and distress which can be categorized as damp abundance due to splenic asthenia and stagnation of endogenous retention of phlegm [14].

JKSQ pill is listed in the national essential medicine list and consists of Aconiti Lateralis Rddix Praeparata (Fu Zi), Cinnamomi Ramulus (Gui Zhi), Achyranthis Bidentatae Radix (Niu Xi), Rehmanniae Radix (Di Huang), Corni Fructus (Shan Zhu Yu), Dioscoreae Rhizoma, Poria (Fu Ling), Aliamria Rhizoma (Ze Xie), Plantaginis Semen (Che Qian Zi), and Moutan Cortex (Mu Dan Pi). The indication includes edema, soreness and weakness of waist and knees, dysuria, and extreme chilliness which can be categorized as deficiency of the kidney [14]. Clinical studies showed JKSQ pill has a high effective rate (91.25%) in hypertension treatment [42]. It also demonstrates promising effect on decreasing microalbuminuria when administered with WMs [43]. Side effect of JKSQ pill includes skin eruption, nausea, and abdominal pain [44].

There are several limitations in this study. First, it is difficult to achieve perfect consensus on CPMs for the treatment of hypertension, as there were many different CPMs available with different TCM pattern based indications. Also, they were in lack of evidence from quality trials. To provide maximum information for WM doctors, we accepted items that agreed by more than 70% of panelists in this study.

Secondly, we did not use TCM pattern as the primary form of indication for CPMs. The aim of this study is to help WM doctors to apply CPMs for the treatment of hypertension accurately; therefore, we used clinical symptoms instead of TCM pattern as the form of indication. In TCM, pattern differentiation is based primarily on symptoms and signs including tongue appearance and pulse feelings. It would be hard for WM doctors to understand the context if the indications were illustrated with TCM patterns, as all these were derived from specialized TCM concepts. Lastly, because of inadequate related studies, we did not have consensus on the indication and possible side effect of YXY tablet and NHJY pill when used as the treatment of hypertension.

In conclusion, we formed a consensus on the application of CPMs in the treatment of hypertension for WM doctors through three rounds of consultations. We believe it would help WM doctors to use CPMs more accurately in clinical hypertension management. We presented the indications in the form of typical symptoms instead of classical pattern differentiation in common TCM consensus or clinical practice guidelines (CPGs) as to assist the WM doctors or other doctors without TCM background to understand and apply CPMs easily. In addition to general therapeutic principles and specific CPM with indications, we also consulted the side effect of different CPMs so as to enhance the safety in clinical practice. This expert consensus could serve as the foundation of CPGs for treatment of hypertension in the future when more evidence on the treatment is established.

Acknowledgments

The authors appreciate all experts who participated in this consultation. This study was financially supported by State Administration of Traditional Chinese Medicine (no. ZYYS-2008) and China Academy of Chinese Medical Sciences (no. Z02114).

References

[1] R. B. Singh, I. L. Suh, V. P. Singh et al., "Hypertension and stroke in Asia: prevalence, control and strategies in developing countries for prevention," *Journal of Human Hypertension*, vol. 14, no. 10-11, pp. 749–763, 2000.

[2] World Health Organization, *World Health Statistics*, 2012.

[3] S. Yusuf, S. Reddy, S. Ôunpuu, and S. Anand, "Global burden of cardiovascular diseases. Part I: general considerations, the epidemiologic transition, risk factors, and impact of urbanization," *Circulation*, vol. 104, no. 22, pp. 2746–2753, 2001.

[4] S. S. Hu, L. Z. Kong, R. L. Gao et al., "Outline of the report on cardiovascular disease in China, 2010," *Biomedical and Environmental Science*, vol. 25, no. 3, pp. 251–256, 2012.

[5] G. L. Khor, "Cardiovascular epidemiology in the Asia-Pacific region," *Asia Pacific Journal of Clinical Nutrition*, vol. 10, no. 2, pp. 76–80, 2001.

[6] H. H. Vorster, "The emergence of cardiovascular disease during urbanisation of Africans," *Public Health Nutrition*, vol. 5, no. 1, pp. 239–243, 2002.

[7] D. F. Gu, K. Reynolds, X. Wu et al., "Prevalence, awareness, treatment, and control of hypertension in China," *Hypertension*, vol. 40, no. 6, pp. 920–927, 2002.

[8] J. A. Whitworth, "2003 World Health Organization (WHO)/International Society of Hypertension (ISH) statement on management of hypertension," *Journal of Hypertension*, vol. 21, no. 11, pp. 1983–1992, 2003.

[9] H. X. Cao and Y. Y. Wang, "Evidence-based guidelines of clinical practice in Chinese medicine internal medicine (internal medicine)," *China Press of Traditional Chinese Medicine*, pp. 227—249, 2011.

[10] L. Dai and Y. J. Wang, "Clinical study on the effect of niuhuang jiangya pill in treating hypertension with anxiety," *China Journal of Chinese Materia Medica*, vol. 31, pp. 1743–1744, 2006.

[11] Y. S. Tan, S. M. Deng et al., "Study on clinical effectiveness and mechanism of compound qishao jiangya tablet in treating hypertension," *Chinese Traditional Patent Medicine*, vol. 26, pp. 71–73, 2004.

[12] S. X. Liu, M. Sun, and Y. F. Luo, "Clinical study on the effect of niuhuang Jiangya capsule in treating primary hypertension," *Chinese Journal of Integrative Medicine*, vol. 24, no. 6, pp. 554–556, 2004.

[13] Z. Z. Tang and Z. T. Wang, "Effect of radix salviae injection on hemorheology and blood lipid in primary hypertension," *Journal of Third Military Medical University*, vol. 26, pp. 1123–1124, 2004.

[14] *Chinese Pharmacopoeia Commission. Chinese Pharmacopoeia*, China Press of Medical Technology, Beijing, China, 2010.

[15] J. Green and N. Thorogood, *Qualitative Methods for Health Research*, SAGE, 2009.

[16] G. Rowe and G. Wright, "The Delphi technique as a forecasting tool: issues and analysis," *International Journal of Forecasting*, vol. 15, no. 4, pp. 353–375, 1999.

[17] U. G. Gupta and R. E. Clarke, "Theory and applications of the Delphi technique: a bibliography (1975–1994)," *Technological Forecasting and Social Change*, vol. 53, no. 2, pp. 185–211, 1996.

[18] J. Z. Lin and Y. Y. Liu, "Clinical study on the effect of tianma gouteng yin in treating grade 1 hypertension with young and middle aged people," *Journal of Cardiovascular Disease*, vol. 8, p. 649, 2010.

[19] J. F. Xiao and J. Z. Cai, "Clinical study on the effect of integrative medicine in improving life quality of aged patients with grade 2 hypertension," *Fujian Journal of Traditional Chinese Medicine*, vol. 33, pp. 10–11, 2002.

[20] H. B. Chen and T. H. Shan, "Clinical study on the effect of integrative medicine in treating aged patients with grade 3 hypertension of 72cases," *Henan Traditional Chinese Medicine*, vol. 23, pp. 60–61, 2003.

[21] T. S. Zhang, L. Han, and L. Wang, "Relation of syndrome types to hypertension grades and risk stratification in patients with primary hypertension," *Chinese Journal of Clinical Rehabilitation*, vol. 9, no. 27, pp. 232–233, 2005.

[22] C. J. Bai, Y. Zhou, L. Wang, D. L. Zhang, and Y. Yang, "Delamination of cardiovascular risk factor, staging and grading of hypertension and the changing characteristics of blood lipids and hemorheological indexes in hypertensive patients with different syndromes of traditional Chinese medicine," *Chinese Journal of Clinical Rehabilitation*, vol. 9, no. 23, pp. 145–147, 2005.

[23] L. Xie, "Description of the incompatibility between Chinese patent medicines commonly used in clinical practice," *Beijing Journal of Traditional Chinese Medicine*, vol. 29, pp. 130–131, 2010.

[24] K. J. Chen, "Study on the treatment of hypertension with integrated traditional and western medicine," *Chinese Journal of Integrative Medicine*, pp. 30–45, 2010.

[25] X. M. Fang, F. Li et al., "Clinical study on the effect of tianma gouteng yin combining with captopril in improving life quality of hypertensive patients," *Chinese Journal of Integrative Medicine on Cardiovascular Disease*, vol. 6, pp. 3–4, 2008.

[26] X. G. Deng, "The thinking and methods on clinical diagnosis and treatment of hypertension with integrated traditional and western medicine," *Journal of Traditional Chinese Medicine*, vol. 41, pp. 113–115, 2000.

[27] S. Ebrahim and G. Davey Smith, "Lowering blood pressure: a systematic review of sustained effects of non-pharmacological interventions," *Journal of Public Health Medicine*, vol. 20, no. 4, pp. 441–448, 1998.

[28] V. J. Stevens, E. Obarzanek, N. R. Cook et al., "Long-term weight loss and changes in blood pressure: results of the trials of hypertension prevention, phase II," *Annals of Internal Medicine*, vol. 134, no. 1, pp. 1–11, 2001.

[29] D. Z. Zhang and Y. F. Wang, "Clinical study on the effect of tianma gouteng granule in treating hypertension with 318 cases," *Heilongjiang Medical Journal*, vol. 26, p. 704, 2002.

[30] Q. M. Jia and S. Y. Liu, "Clinical study on the effect of tianma gouteng granule combining with levamlodipine besylate tablets in treating hypertension with 34 cases," *Chinese Community Doctors*, vol. 6, pp. 52–54, 2004.

[31] D. Q. Wang, W. Wang, X. F. Sun, D. Z. Zhao, and G. Y. Du, "Effect of Tianma Gouteng recipe on interfering LV and aortic hypertrophy in renovascular hypertension rats," *China Journal of Chinese Materia Medica*, vol. 30, no. 8, pp. 606–609, 2005.

[32] Z. Q. Zhang, "Clinical study on the effect of qiju dihuang capsule in treating hypertension with yin deficiency and yang excess pattern," *New Journal of Traditional Chinese Medicine*, vol. 31, pp. 12–14, 1999.

[33] Y. P. Ouyang, "Treatment and observation of 34 cases of elderly hypertension with verapamjl and qiju dihuang pills," *Hunan Guiding Journal of Traditional Chinese Medicine*, vol. 8, pp. 15–16, 2002.

[34] S. X. Liu, M. Sun et al., "Clinical study on the effect of niuhuang jiangya capsule in treating primary hypertension," *Chinese Journal of Integrative Medicine*, vol. 24, pp. 553–555, 2004.

[35] S. Y. Yu, "Clinical study on the effect of niuhuang jiangya pill in lowering blood pressure and influencing sympathetic activity," *China Journal of Chinese Materia Medica*, vol. 32, pp. 172–175, 2007.

[36] S. X. Liu, M. Sun, and Y. F. Luo, "Clinical study on treatment of primary hypertension by niuhuang jiangya pill," *Chinese Journal of Integrative Medicine*, vol. 24, no. 6, pp. 553–555, 2004.

[37] S. Dong, Z. Zhu, Y. Zhang, Z. Xu, and J. Cheng, "Determination of 11 metal elements in niuhuang jiangya wan by atomic absorption spectrophotometer," *Spectroscopy and Spectral Analysis*, vol. 19, no. 3, pp. 417–418, 1999.

[38] J. C. Zhou, Y. P. Li et al., "Effect of ginkgo leaf tablet on quality of life of hypertensive patients," *Journal of China Pharmacy*, vol. 18, pp. 213–215, 2007.

[39] C. G. Li and R. H. Zhang, "Clinical study on the effect of ginkgo leaf tablet combining with felodipine in treating hypertension

with 96-case," *Clinical Medicine of China*, vol. 23, no. 1, p. 88, 2007.

[40] Q. S. Liu, "Study on influence of ginkgo leaf tablet in ventricular remodeling of hypertension basing on regulating transforming growth factor-β1," *Chinese Journal of Cardiovascular Rehabilitation*, vol. 17, no. 1, pp. 78–80, 2008.

[41] W. Li, "Ginkgo leaf tablet caused one case of acute urticarial," *Chinese Journal of Misdiagnostics*, vol. 5, no. 9, p. 1774, 2005.

[42] B. T. Li, J. Y. Zhang, and X. M. Zhang, "Clinical study on the effect of jinkui shenqi pill in treating hypertension with 68 cases," *Journal of Traditional Chinese Medicine*, vol. 44, p. 757, 2003.

[43] Y. L. Liu, "Clinical study on the effect of jinkui shenqi pill for influencing microalbuminuria in hypertension patient," *New Journal of Traditional Chinese Medicine*, vol. 40, pp. 37–38, 2008.

[44] Y. Li, "Problems in the application of jinkui shenqi pill in clinical practice," *Lishizhen Medicine and Materia Medica Research*, vol. 15, pp. 792–793, 2004.

Hindawi Publishing Corporation
Evidence-Based Complementary and Alternative Medicine
Volume 2013, Article ID 819147, 12 pages
http://dx.doi.org/10.1155/2013/819147

Review Article

Towards Polypharmacokinetics: Pharmacokinetics of Multicomponent Drugs and Herbal Medicines Using a Metabolomics Approach

Ke Lan,[1] Guoxiang Xie,[2] and Wei Jia[2]

[1] *Key laboratory of Drug Targeting and Drug Delivery System of the Education Ministry, West China School of Pharmacy, Sichuan University, Chengdu 610041, China*
[2] *Center for Translational Biomedical Research, University of North Carolina at Greensboro, North Carolina Research Campus, Kannapolis, NC 28081, USA*

Correspondence should be addressed to Wei Jia; w_jia@uncg.edu

Received 27 December 2012; Accepted 29 January 2013

Academic Editor: Aiping Lu

Determination of pharmacokinetics (PKs) of multicomponent pharmaceuticals and/or nutraceuticals (polypharmacokinetics, poly-PKs) is difficult due to the vast number of compounds present in natural products, their various concentrations across a wide range, complexity of their interactions, as well as their complex degradation dynamics *in vivo*. Metabolomics coupled with multivariate statistical tools that focus on the comprehensive analysis of small molecules in biofluids is a viable approach to address the challenges of poly-PK. This paper discusses recent advances in the characterization of poly-PK and the metabolism of multicomponent xenobiotic agents, such as compound drugs, dietary supplements, and herbal medicines, using metabolomics strategy. We propose a research framework that integrates the dynamic concentration profile of bioavailable xenobiotic molecules that result from *in vivo* absorption and hepatic and gut bacterial metabolism, as well as the human metabolic response profile. This framework will address the bottleneck problem in the pharmacological evaluation of multicomponent pharmaceuticals and nutraceuticals, leading to the direct elucidation of the pharmacological and molecular mechanisms of these compounds.

1. Introduction

Multicomponent herbal medicines have gained popularity as complementary interventions against a number of conditions, including metabolic diseases and cancer [1, 2]. Distinct from the pharmacology of chemical drugs (single compounds), the pharmacology of multi-component agents, including botanical-based nutraceuticals, entails a "network" approach, in which multiple compounds interact *in vivo* with multiple targets with interdependent activities to achieve an optimal effect [3, 4]. The vast number of metabolites present in natural products and their wide dynamic range are inextricable obstacles for pharmacological evaluation and nutraceutical/drug development. Furthermore, the coexistence of multiple compounds may lead to metabolic and pharmacokinetic interactions. Due to the complexity of both botanicals and biological samples (e.g., blood, urine, tissues), the analytical approaches to quantitatively measure the time-dependent concentration profiles of bioavailable plant molecules (i.e., poly-PK) are beyond the scope of traditional research. In fact, herbal medicine PK that simultaneously monitors multiple metabolites (i.e., poly-PK) has only been reported in a handful of studies [5, 6]. As a result, poly-PK has been a long-standing bottleneck in botanical-based medical and nutritional research.

The traditional approach to understand the pharmacology of a multi-component agent is to study the effects of single components on single biological reactions, enzymes, genes, and so forth, and gradually assemble the findings into a whole picture. However, assembling the results obtained from such a reductionist approach to achieve a system understanding of a concerted pharmacological intervention

has proven impractical [7]. In fact, the results of such attempts failed to accurately capture the complex pharmacokinetic behavior of herbal medicines. Additionally, the PK of a given compound in a multi-component assay may be significantly different from that in a single-compound assay due to drug-drug interactions. With such a complex network involving a large number of variables, it is technically challenging to identify each metabolite that changes significantly in the global metabolite pool, and to assess the human (endogenous) biochemical responses to exposure to these exogenous (xenobiotic) compounds.

The complicated metabolic fate of chemicals in the human body is primarily determined by the chemical's structure and greatly varies according to dose, routes of exposure, inter- and intraindividual genetic differences, gut microbiota, diet, life style, and environment, as well as other xenobiotics intentionally or unintentionally present. In order to simplify these intricate factors, a knowledge-based engine that sequentially manipulates each factor *in silico* for prediction, coupled with *in vitro* screening and identification, and *in vivo* validation is deployed for xenobiotic metabolism studies [8]. However, because cross-platform extrapolations are not always the reliable or robust [9], the *in vivo* xenobiotic metabolite studies require special attention; these compounds are often intermixed against the background of endogenous metabolites in biological samples. Recent advances in liquid, and gas chromatography (LC and GC) and capillary electrophoresis (CE) coupled with mass spectrometry (LC-MS, GC-MS, and CE-MS) and nuclear magnetic resonance (NMR) have made it possible to simultaneously detect various small-molecule metabolites [10].

Metabolomics is the study of the metabolome, the complete set of endogenous metabolites in a biological sample. In context of systems biology [11, 12], metabolomics is favored not only for decoding how a biological system responds to a stimulus by identifying the most significantly affected endogenous metabolites and their metabolic pathways, but also resolving the relationships between endogenous and xenobiotic metabolic processes [13]. Metabolomics techniques have offered xenobiotic studies a novel way to differentiate the exogenous from the endogenous by untangling the interactive metabolic pathways for both. Capable of simultaneously analyzing hundreds and thousands of variables, metabolomics is uniquely suited to develop a new generation of PK platforms that can measure multiple nutraceutical components *in vivo*, as well as identify characteristic metabolic alterations in humans exposed to nutraceuticals [14, 15]. Along these lines, utilizing metabolomics to study herbal medicine efficacy and toxicity has been a key focus of recent herbal and pharmaceutical research [16–20]. Recently, we proposed an integrated metabolomic profiling strategy for PK and PD studies of multi-component drugs using tandem mass spectrometry (MS/MS) [21] and conducted a proof-of-concept poly-PK study of Pu-erh tea intervention in humans based on metabolomics [6].

Metabolomics might assume the new mission to model the variations of both exogenous and endogenous metabolites through a given biological system, which has vital implications in both systems biology and multi-component herbal medicine. The aim of this review is to discuss recent progress in the characterization of poly-PK and metabolism of multi-component xenobiotic agents such as compound drugs, dietary supplements, and herbal medicines using metabolomics. We also propose a research framework that integrates the dynamic concentration profile of bioavailable xenobiotic molecules that result from *in vivo* absorption, and hepatic and gut bacterial metabolism, as well as the human metabolic response profile.

2. Metabolomics in Xenobiotic Intervention Study

Metabolomics enables the profiling of a vast number of small-molecule metabolites in an organism or a biological system as a whole, and helps understand how these metabolites respond to a stimulus, highlighting the most relevant potential biomarkers. When the stimulus is a xenobiotic intervention, metabolomics techniques are employed to profile the metabolite pool with and without the xenobiotic and highlight the differential variables to identify the xenobiotic metabolites. A comparison of a typical protocol for xenobiotic intervention studies using LC-MS-based metabolomics and the classical LC-MS-based workflow is illustrated in Figure 1. The major difference between the two methods is the data processing procedure to differentiate exogenous metabolites against the endogenous metabolite background. The metabolomics strategy employs multivariate data pretreatment methods [22] (e.g., deconvolution, alignment, integration) coupled with multivariate analyses [15, 23] (e.g., principle component analysis (PCA), partial least squares discriminant analysis (PLS-DA)). In contrast, the classical strategy utilizes arbitrary endogenous background subtraction and/or knowledge-based mass defect filtering, which takes advantage of known mass changes between the parent ion and metabolite ions [24].

Such a metabolomics-based protocol was first proposed in 2003 by Plumb and colleagues in an attempt to find the *in vivo* metabolites of GSK-X, the structure of which was unknown to the investigators [29]. Shortly after, another metabolomics-based protocol identified several new metabolites of citalopram [30]. Consequently, Dr. Gonzalez from National Cancer Institute at the National Institute of Health expanded LC-MS-based metabolomics for xenobiotic metabolism studies by developing various strategies, including (1) identification of metabolites by metabolomic analysis with or without xenobiotic intervention (Figure 1, and [31]), (2) validation of metabolites through metabolomic comparison between xenobiotic treatments with or without stable isotope label in order to highlight the xenobiotic metabolites in contrast to the endogenous ones altered by xenobiotic intervention, (3) identification of metabolic pathways through metabolomic comparison of wild-type and genetically-modified mice, and (4) identification of polymorphisms of genes encoding human xenobiotic metabolism enzymes (XMEs) that may be responsible for adverse drug reactions [31]. Two recent reviews address the technical issues and progress in this field [32, 33].

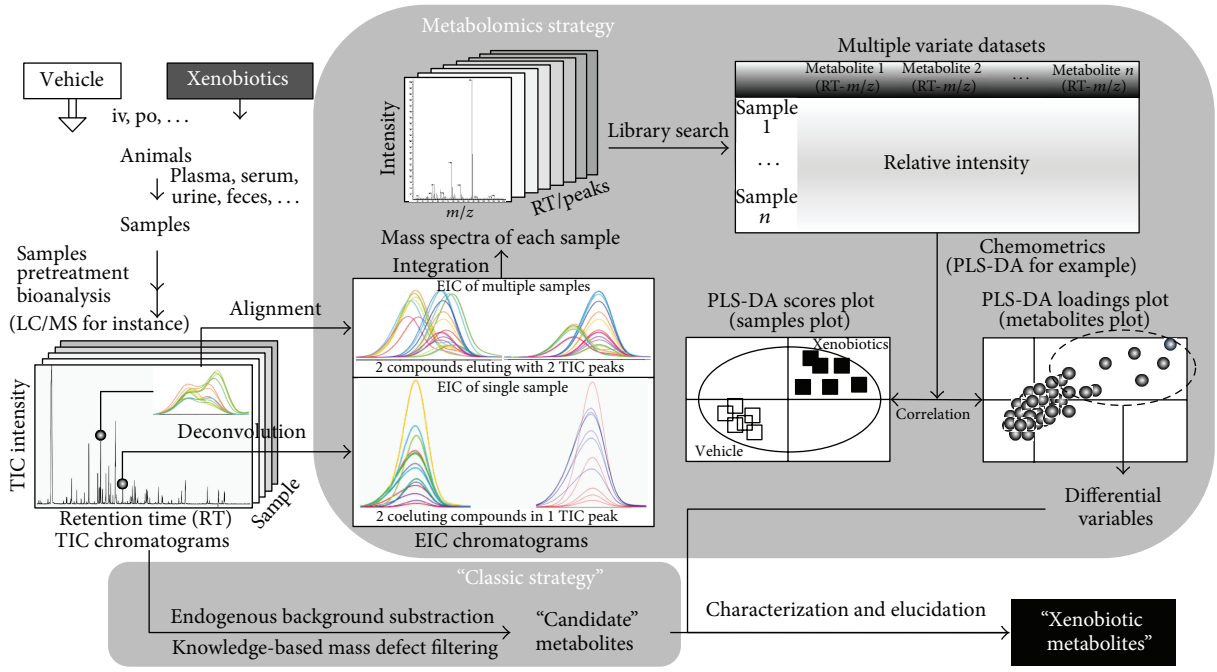

FIGURE 1: LC-MS protocol for xenobiotic intervention studies with and without the incorporation of metabolomics. Iv: intravenous; po: oral; EIC: extracted ion chromatogram; PLS-DA: partial least squares-discriminant analysis; TIC: total ion chromatogram.

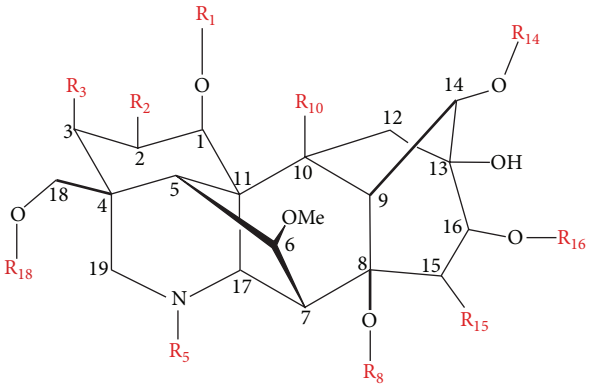

Major aconitum alkaloids in aconite roots

	R_1	R_2	R_3	R_5	R_8	R_{10}	R_{14}	R_{15}	R_{16}	R_{18}
Aconitine	Me	H	OH	Et	Ac	H	Bz	OH	Me	Me
Mesaconitine	Me	H	OH	Me	Ac	H	Bz	OH	Me	Me
Hypaconitine	Me	H	H	Me	Ac	H	Bz	OH	Me	Me
Jesaconitine	Me	H	OH	Et	Ac	H	As	OH	Me	Me
Yunaconitine	Me	H	OH	Et	Ac	H	As	H	Me	Me

In vitro metabolites of aconitine

	R_1	R_2	R_3	R_5	R_8	R_{10}	R_{14}	R_{15}	R_{16}	R_{18}
Aconitine	Me	H	OH	Et	Ac	H	Bz	OH	Me	Me
In vitro rat CYP450 (Wang et al. [25])										
M1	Me	H	OH	Et	Ac	H	Bz	OH	H	Me
M2	Me	H	OH	Et	Ac	H	Bz	OH	Me	H
M3	Me	H	OH	Et	Ac	H	Bz	OH	H	H
M4	Me	H	OH	Et	H	H	Bz	OH	Me	Me
M5	Me	H	=O	Et	Ac	H	Bz	OH	Me	Me
M6	Me	H	OH	H	Ac	H	Bz	OH	Me	Me
In vitro human intestinal bacteria (Zhao et al. [26])										
M1, M4										
M7	Me	H	H	Et	Ac	H	Bz	OH	Me	Me
M8	Me	H	H	Et	Ac	H	Bz	OH	H	Me
M9	Me	H	OH	Et	R	H	Bz	OH	Me	Me
R for M9: more than 20 kinds of esterification products with fat acids.										
In vitro rat intestinal bacteria (Wang et al. [28])										
M4, M7, M9										
M10	Me	H	OH	Et	Ac	H	Bz	H	Me	Me
M11	Me	H	OH	Et	H	H	Bz	H	Me	Me
M12	Me	H	OH	Et	Ac	OH	Bz	OH	Me	Me
R for M9: octenoyl, hexenoyl, propionyl, butyryl, and 3-hydroxy-butyryl.										
In vitro human CYP450 (Tang et al. [27])										
M1, M5, M6.										
M13	Me	OH	OH	Et	Ac	H	Bz	OH	Me	Me
M14	H	H	OH	Et	Ac	H	Bz	OH	Me	Me
M15	H	H	OH	Et	Ac	H	Bz	OH	H	Me

FIGURE 2: Major aconitum alkaloids in aconite roots and *in vitro* metabolites of aconitine [25–28]. Me: methyl group; Et: ethyl group; Ac: acetyl group; Bz: benzoyl group; As: anisoyl group.

Compared to the classical methods in xenobiotic intervention studies, metabolomics strategies have clear advantages, firstly, in the capacity of handling a great number of variables—which allows a shift in purpose from targeting xenobiotic metabolites to profiling the complete set of metabolites in biological samples—and secondly, in the unbiased selection of variables that are significantly altered—which facilitates the discrimination of xenobiotic metabolites from endogenous ones. Due to these advantages of metabolomic strategies, a novel, evidence-based methodology that starts with mapping *in vivo* metabolites and leads to further *in vitro* characterization has been established, which is in stark contrast to the classic, knowledge-based methodology that starts with *in vitro* identification to *in vivo* characterization, and is frequently muddled by inconsistent results. Such a methodological shift obviates potential false-negative results that usually result from traditional empirical strategies, and significantly deepens our insight into the *in*

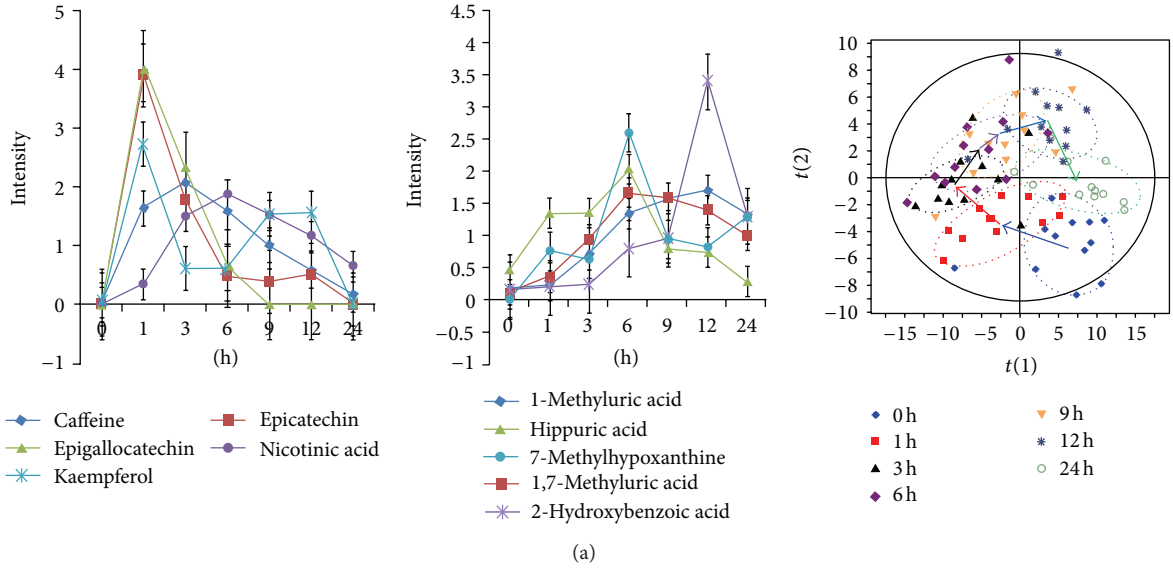

(a)

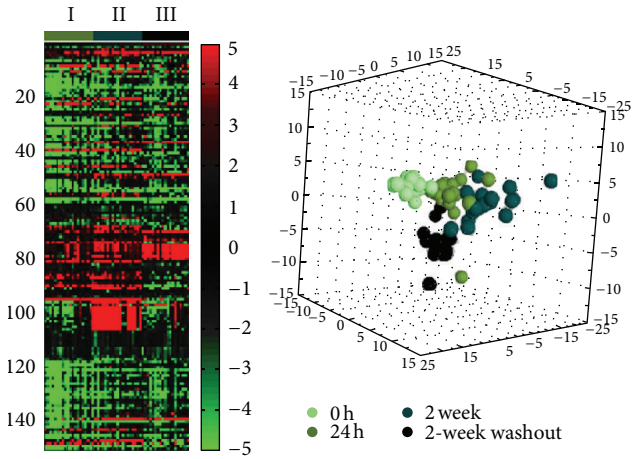

(b)

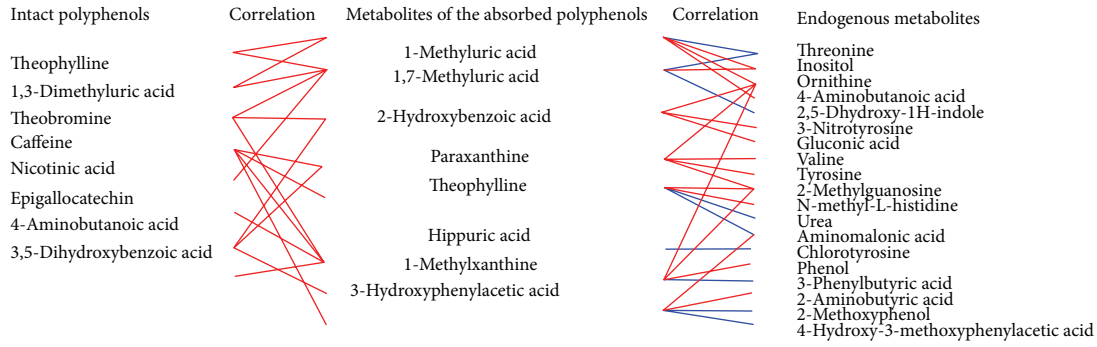

(c)

Figure 3: Dynamic concentration profile of bioavailable Pu-erh tea polyphenols due to *in vivo* absorption, and hepatic and gut bacterial metabolism, as well as the human metabolic response profile. (a) Urine concentration-time course of some representative substances, intact polyphenols, metabolites of the absorbed polyphenols, and altered endogenous metabolites, after Pu-erh tea intake; (b) effect of Pu-erh tea intake on human urine metabolite endpoints. (left panel) Heatmap showing differences in altered endogenous metabolites detected from the metabolome after Pu-erh tea intake (postdose) as compared to predose metabolome. (I) metabolomic changes at 24 h postdose relative to predose; (II) 2-week postdose versus predose; (III) 2-week washout versus predose. Each cell in the heat map represents the fold change between the two time points (e.g., postdose versus the predose) for a particular metabolite. (right panel) 3D PCA scores plot of urinary metabolic profiles at predose, 24 h postdose, 2 week postdose, and 2 week washout postdose; (c) correlation of intact polyphenols, metabolites of the absorbed polyphenols, and altered endogenous metabolites in response to Pu-erh tea exposure. The relationships among the three groups of compounds were visualized in the form of correlation maps, which are displayed by red (positive) or blue (negative) lines.

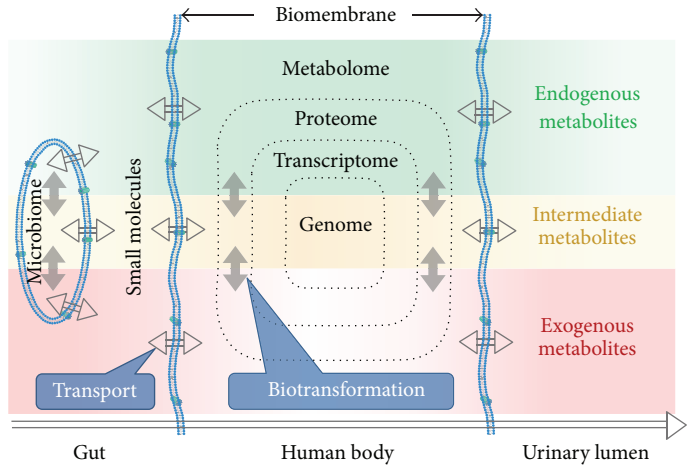

Figure 4: Research framework to integrate the dynamic concentration profile of bioavailable xenobiotic molecules due to *in vivo* absorption and the hepatic and gut bacterial metabolism, as well as the human metabolic response profile.

vivo metabolic map of xenobiotics in at least two ways. First, metabolomics captures *in vivo* xenobiotic metabolites that are otherwise easily overwhelmed by the endogenous background. Examples of such metabolites are those with unexpected skeleton biotransformation or those at extremely trace levels with potential clinical significance and wide usage in the general population. Second, the consideration of genetic and environmental factors affecting the metabolism of xenobiotics in metabolomics studies facilitates the *in vivo* identification of metabolic pathways and factors affecting them.

3. Current Status of Single Xenobiotic Intervention Studies with Metabolomics Strategy

To date, metabolomics techniques have been employed in metabolism studies of dozens of single xenobiotics with diverse chemical structures (Table 1), including GSK-X [29], citalopram [30], aminoflavone [34], arecoline/arecaidine [35], PhIP [36], arecoline 1-oxide [37], ferulic and sinapic acids [38], acetaminophen [39–42], dextromethorphan [43], melatonin [44, 45], vitamin E [46], fenofibrate [47, 48], tolcapone [49], cyclophosphamide/ifosfamide [50], tipranavir [51], nefazodone [52], valproic acid [53], ritonavir [54], pulegone/clozapine [42], thioTEPA [55], isoliquiritigenin [56], ethanol [57], and procainamide [58]. Remarkably, majority of these studies were carried out *in vivo*. It has been proposed that such metabolomics strategies can be used to study any organic molecule in any animal model, provided that the protocol is carefully designed, controlled, and executed [32]. In our opinion, a metabolomics approach is especially useful for studying xenobiotics with known toxicities and multiple metabolite endpoints predicted by their chemical structures. As a result, the insights from metabolomics extend our knowledge of how a xenobiotic affects human body from a list of its major metabolites to the complete *in vivo* metabolite map. The detailed information about multiple bioactive metabolites may significantly advance our understanding of various and rare adverse drug reactions in the general population.

4. Progress and Challenges of Herbal Exposure Studies

Multicomponent drugs and herbal medicines have an extremely complicated and highly variable chemical composition and introduce multiple xenobiotics into the human body. The metabolism of these xenobiotics may provide insights as to why and how they work by revealing changes *in vivo* due to herbal exposure. However, the unclear metabolic fate of herbal medicines causes significant limitations in understanding the efficacy and toxicity of these substances. Compared to single xenobiotics, of which there are significant advances in terms of metabolic fate, multi-component herbal medicines present a challenge due to their complex nature.

For the development of *in vivo* xenobiotic metabolism protocols for multi-component drugs and herbal medicines, there are several major obstacles: (1) the difficulty to determine and standardize the chemical composition of multi-component drugs and herbal medicines, (2) the overlap between the chemical composition of herbal medicines with that of daily diets, (3) the extensive microbial-mammalian co-metabolism in the gut of herbal components [67] that vary by species (e.g., see the *in vitro* metabolites of aconitine, illustrated in Figure 2 [25–28]), (4) the difficulty of differentiating exogenous metabolites from the endogenous background 1–3, and (5) the difficulty of resolving the intercrossed metabolic pathways of different herbal components that share similar chemical skeletons (for an example, see aconitum alkaloids in aconite roots, illustrated in Figure 2). Therefore, current research to elucidate the xenobiotic metabolism of herbal exposures is still in its infancy, exploring and developing solutions to these challenges.

Table 1: Summary of PK studies of single chemicals and multicomponent drugs or herbal medicines using metabolomics.

Substance	Type of biological sample	Bioanalysis technique	Multivariate analysis method	Reference
GSK-X	Rat urine	LC-TOFMS	PCA, Ward's HCA	[29]
Citalopram	Rat urine	LC-MS	PCA, PLS, PARAFAC, N-PLS	[30]
Ferulic acid and sinapic acid	Rat urine	HPLC-QTOFMS	PLS-DA	[38]
Fenofibrate	Rat urine	UPLC-QTOFMS	PLS-DA	[47]
Isoliquiritigenin	Rat urine	UPLC-QTOFMS	PCA, PLS-DA	[56]
Tolcapone	Rat urine	UPLC-QTOFMS	PCA	[49]
Acetaminophen	Rat urine	UPLC/MS, NMR	PCA, PLS-DA	[41]
Valproic acid	Mouse urine	LC-MS	PCA	[53]
ThioTEPA	Mouse urine	UPLC-QTOFMS	OPLS	[55]
NSC686288 (aminoflavone)	Mouse urine	UPLC-QTOFMS	PCA	[31, 34]
Ethanol	Mouse urine	UPLC-QTOFMS	PLS-DA, OPLS	[57]
Arecoline and arecaidine	Mouse urine	UPLC-QTOFMS	PCA, PLS-DA	[35]
(±)-Arecoline 1-oxide	Mouse urine	UPLC-QTOFMS	PCA	[37]
PhIP*	Mouse urine	UPLC-QTOFMS	PCA	[36]
Acetaminophen	Mouse urine	UPLC-QTOFMS	PCA	[39]
Cyclophosphamide/ifosfamide	Mouse urine	UPLC-QTOFMS	OPLS	[50]
Vitamin E	Mouse urine	UPLC-TOFMS	PCA, PLS-DA	[46]
Melatonin	Mouse urine	IPLC-TOFMS, LC-MS/MS	PCA, OPLS	[44]
Tipranavir	Mouse urine, feces, tissue	UPLC-TOFMS	PCA, OPLS-DA	[51]
Ritonavir	Mouse urine and feces	UPLC-TOFMS	OPLS-DA	[54]
Procainamide	Mouse and human urine	UPLC-QTOFMS	PCA, PLS-DA	[58]
Fenofibrate	Monkey urine	UPLC-QTOFMS	PLS-DA	[48]
Pulegone/clozapine	Mouse liver	UPLC-TOFMS	PCA, OPLS-DA	[42]
Dextromethorphan	Human urine	LC-MS/MS	PCA, OPLS-DA	[43]
3,4-Dehydro-debrisoquine	Human urine	UPLC-QTOFMS	OPLS	[31, 59]
Cocoa powder	Human urine	HPLC-QTOFMS	PLS-DA, two-way HCA	[60]
Almond skin extract	Human urine	LC-QTOFMS	PCA, OPLS-DA	[61]
Pu-erh tea	Human urine	UPLC-QTOFMS, GC-TOFMS	PCA, OPLS-DA	[6, 62]
A mix of wine extract and grape juice extract	Human urine	^{1}H NMR	ANOVA-PCA/PLS	[63]
Dried black tea extract and red grape extract	Human urine	^{1}H NMR	ANOVA-PCA/PLS	[64]
Chamomile tea	Human urine	^{1}H NMR	PCA, PLS, OSC	[14]
Dark chocolate	Human urine, plasma	^{1}H NMR, LC-MS, LC-MS/MS	PCA, OPLS-DA	[65]
Nefazodone	NADPH-supplemented human liver microsomal incubation samples	LC-MS	PCA	[52]
Rifampicin, phenobarbital, and CITCO**	Human hepatocytes	UPLC-TOFMS	PCA, OPLS, SUS plot	[66]

*2-Amino-1-methyl-6-phenylimidazo[4,5-b]pyridine.
**6-(4-Chlorophenyl)imidazo[2,1-b][1,3]thiazole-5-carbaldehydeO-3,4-dichlorobenzyl) oxime.
LC-MS: liquid chromatography-mass spectrometry; UPLC-QTOFMS: ultraperformance liquid chromatography-quadrupole time of flight mass spectrometry; NMR: nuclear magnetic resonance; GC-TOFMS: gas chromatography-time of flight mass spectrometry; PCA: principle component analysis; PLS: partial least squares; OPLS-DA: orthogonal partial least squares-discriminant analysis; DAPARAFAC: parallel factor analysis; N-PLS: multilinear partial least squares; OSC: orthogonal signal correction.

4.1. Classic Strategy. The strategies and techniques for *in vitro* and *in vivo* herbal exposure studies following classic, knowledge-based methodologies have recently been discussed [68, 69]. With the advances in bioanalytical methods, many metabolites of herbal interventions were successfully captured. For example, a recent study of the herbal supplement Danggui Buxue Tang detected and identified 142 metabolites from bile and plasma samples [70]. However, from the efforts to map the metabolites of single xenobiotics, it has become clear that the predictive and provisional approaches used in classic strategies can be inaccurate and lack reproducibility.

Nevertheless, two strategies have accomplished noteworthy advances in metabolite mapping of xenobiotics. One of these strategies was developed from the identification of individual metabolites of licorice [71]. In fact, more than 60 metabolites were identified and PK profiles of 55 were obtained [72]. This strategy was robust and managed to reveal intraherb metabolic interactions; however, it requires prior knowledge of herbal components and is time consuming. The other strategy was based on matching the "chemicalome" (referring to LC-MS data of the tested herbal medicine) to the "metabolome" (referring to LC-MS data including tentative herbal metabolites acquired by endogenous background subtraction) upon the injection of the herbal medicine Mailuoning [73]. Matching was performed by mass defect filtering, which incorporated accurate mass changes of 62 types of metabolic reactions. Using this approach, 143 metabolites were identified in urine. This strategy exhibited clear superiority in labor-saving predictions; however, the endogenous background subtraction was arbitrary, introducing false positives and excluding false negative results.

4.2. Metabolomics-Based Strategy. The Recent advances in metabolomics encouraged researchers to start exploring the effects of multi-component drugs/herbal medicines using metabolomics strategies. To the best of our knowledge, the first attempt of this kind was the NMR-based metabolomics study on human nutritional intervention of grape/wine extract reported by van Velzen and colleagues in 2008 [63]. This study aimed to distinguish between-subject and within-subject variations in metabolomic data matrices using multivariate paired data analyses corresponding to a crossover design. Since its major results concerned metabolites of polyphenols, the integration of PK modeling into metabolomics was developed in a later study by the same group [64]. The proposed multivariate paired data analysis [74] and dynamic metabolomic data analysis [75], in combination with study designs that tackle the challenges arising from dietary metabolite background and microbial-human cometabolism in the gut [76], have collectively coined the term "nutrikinetics," a new discipline that combines cutting-edge technologies and new methodologies to get a complete picture of what happens to the consumed metabolites and supplements in the human body [77]. Nutritkinetics relies heavily on metabolomics biostatistical analyses. To date, there have been a number of studies on dietary exposure incorporating metabolomics, which were summarized in a recent review on nutrimetabolomic strategies [78].

The metabolomics-based strategies using LC-MS have clear advantages, as they can handle a great number of variables and large datasets, enable graphic representation of metabolism-related sample classification, and identify drug compounds and significant drug metabolites. In fact, several publications reported the use of metabolomics to capture both drug-derived and drug-induced metabolites [66] and the alterations of metabolites in urine after cocoa powder consumption [60] (Table 1). Despite the fact that metabolomics can be employed in PK studies of herbal medicines, it is almost impossible to detect the complete pool of metabolites in a biological sample the existing analytical platforms [79]. Indeed, categorizing the origins of altered metabolites as a result of herbal intervention still present with significant challenges [21], including the categorization of: (1) intact herbal components absorbed into circulation, (2) xenobiotic metabolites processed by hepatic enzymes and gut microbes, and (3) endogenous metabolites that are significantly altered in response to the intake of plant-derived compounds.

We believe that categorization of these metabolites in herbal intervention studies will benefit more from developments in multivariate analyses than in advances in analytical techniques. To this end, we have proposed a multivariate similarity analysis to categorize the altered metabolites as a result of herbal intervention [21]. Recently, we used this strategy to analyze the metabolic fates of Pu-erh tea polyphenols in humans [6]. Urine samples were collected at baseline and at different time periods for 6 weeks. Volunteers ingested Pu-erh tea daily, followed by a wash-out phase during these 6 weeks. The urine samples were analyzed using ultraperformance liquid chromatography-quadrupole time of flight mass spectrometry (UPLC-QTOFMS) and gas chromatography-time of flight mass spectrometry (GC-TOFMS). The resulting dataset composed of 6,028 detected features was subjected to univariate statistical analysis, yielding 2,476 and 176 altered variables from UPLC-QTOFMS and GC-TOFMS were highlighted, respectively ($P < 0.05$). Using multivariate similarity analysis to compare the altered variables to the plant metabolome or the predose human metabonome, 19, 26, and 118 metabolites were categorized as intact tea polyphenols, metabolites of the absorbed polyphenols, and endogenous metabolites altered due to tea intake, respectively. The subsequent dynamic correlation analysis produced, for the first time, a correlation between the herbal metabolic network and endogenous metabolism (Figure 3).

As discussed above, despite great challenges, a strategy based on metabolomics has great potential capabilities to discover not only the components in herbal exposure and their *in vivo* metabolites, but also the endogenous metabolites altered by herbal interventions. In this regard, the metabolic shells covering the interactions between multiple xenobiotics and human biological system will be shucked in future metabolomics incorporating xenobiotic metabolism.

5. Proposed Research Framework

The essence of balances in traditional Chinese medicine and herbal medicines align very closely with the core concepts

of systems biology [80], which aims to theoretically and experimentally describe homeostasis of a biological system and its allostasis with an "-omics" approach [81, 82]. Metabolomics, as a "top-down" -omics technology, evaluating small-molecule metabolites as the ultimate downstream products of genomic, transcriptomic, and/or proteomic perturbations, is encouraging herbal medicine researchers to tackle existing issues in the field from chemistry to biology. However, besides its phytochemical applications, which focus on the quality assessments of botanic products [83–85], metabolomics in herbal medicine mostly addresses biomedical implications for the endogenous metabolism [86–90], while paying little attention to the metabolism of the xenobiotics, which is tightly linked to and has important implications for human metabolic networks.

Based on the above and guidance from related studies, we propose a research framework to integrate the dynamic concentration profile of bioavailable xenobiotic molecules due to *in vivo* absorption and the hepatic and gut bacterial metabolism,as well as the human metabolic response profile in Figure 4. Our framework highlights the flux of small-molecule metabolites through the human body with gut as the major entrance and urinary lumen as the major exit points. Recent multicompartmental (plasma, urine, and caecal contents) metabolomic work depicted this framework in a smaller scale [91]. In our proposed model, the human body has evolved as a superorganism encompassing the genome, transcriptome, proteome, metabolome, and symbiotic gut microbiome, that latter coexisting with the host depending on genetic and environmental factors [92–96]. It is of special importance for the gut microbiome and the host to maintain ceaseless substance exchange, in which the small-molecule metabolites can permeate the biomembrane barrier. These metabolites can be divided into endogenous and exogenous metabolites according to their predicted sources; however, the distinction between endogenous and exogenous is not so clear due to the gut microbiome. As a result, metabolites with unclear origins can be classified in an intermediate group. For example, endogenous ethanol is not a metabolite of human metabolism, but a byproduct of gut microbes [97, 98], which is associated with nonalcoholic fatty liver disease [99]. In all, biotransformation (metabolism) and transportation are essential to the metabolic network of host and microbial interactions to dispose of endogenous and exogenous metabolites.

The host-gut microbial metabolic networks for endogenous and exogenous metabolites are highly interactive but with subtle differences in metabolic fates. It is beyond doubt that the superorganism's metabolism has to strike a balance between the uptake of essential nutrients and the elimination of superfluous metabolites to maintain homeostasis, yielding a relatively stable internal environment of endogenous metabolites. The involvement of gut microbiota in endogenous metabolic pathways [100–104], as a matter of fact, has given rise to interactive host-microbiota metabolic, signaling, and immuneinflammatory axes that physiologically connect the gut, liver, muscle, and brain [105]. On the other hand, the superorganism cannot be too lenient with regard to exogenous metabolites, maintaining allostasis to achieve a stable internal environment by eliminating exogenous metabolites. Gut microbiota supplements the human metabolic system with xenobiotics [106] by directly taking part in their metabolism, especially in the metabolism of natural products such as flavonoids, saponins [67], polyphenols [76], and alkaloids [26, 28], as well as the metabolism of exogenous metabolites, such as the competitive sulfation of acetaminophen and p-cresol [107], and the regulation of XMEs [108, 109]. Based on the distinction between the metabolic fates of exogenous and endogenous metabolites, trend analysis was proposed as an alternative to metabolite discovery [110].

Therefore, the superorganism has evolved a highly delicate and interactive host-gut microbiota metabolic network to keep its homeostasis and trigger allostasis. Following our framework, in combination with advances in genomics, transcriptomics, proteomics, and metagenomics, future metabolomics strategies will contribute to our understanding of how the balance emphasized in comprehensive herbal medicine is correlated with the homeostasis and allostasis addressed in systems biology.

6. Conclusion

In conclusion, recent studies suggest that metabolomics coupled with multivariate statistical tools can offer an alternative to address the challenges of the determination of PK of multi-component pharmaceuticals and/or nutraceuticals. We believe that the use of a metabolomics strategy in pharmacological studies has important advantages over conventional approaches for multi-component therapeutics. The integration of metabolomics to study the metabolism of xenobiotics will unravel the complicated variations in multiple metabolites of endogenous and exogenous origin within the host-gut microbial symbiotic network, and tease out the underlying mechanisms of homeostasis and allostasis in terms of systems biology. Progress in this field will definitely help the poly-PK studies of multi-component herbal medicines to assess their efficacy. Acquisition of a complete and dynamic panel of pharmacokinetic parameters for multi-component dosage regimens to achieve desired therapeutic efficacies is essential to minimize toxicity, reduce overdosing and drug complications, keep healthcare costs at a minimum, and ultimately, increase patient compliance and quality of life.

References

[1] R. L. Blaylock, "New developments in phytoprevention and treatment of cancer," *The Journal of the American Nutraceutical Association*, vol. 2, pp. 19–29, 1999.

[2] J. M. Hollander and J. I. Mechanick, "Complementary and alternative medicine and the management of the metabolic syndrome," *Journal of the American Dietetic Association*, vol. 108, no. 3, pp. 495–509, 2008.

[3] K. Chan, "Progress in traditional Chinese medicine," *Trends in Pharmacological Sciences*, vol. 16, no. 6, pp. 182–187, 1995.

[4] G. W. Plumb, M. T. Garcia-Conesa, P. A. Kroon, M. Rhodes, S. Ridley, and G. Williamson, "Metabolism of chlorogenic acid by

human plasma, liver, intestine and gut microflora," *Journal of the Science of Food and Agriculture*, vol. 79, no. 3, pp. 390–392, 1999.

[5] S. M. He, E. Chan, and S. F. Zhou, "ADME properties of herbal medicines in humans: evidence, challenges andstrategies," *Current Pharmaceutical Design*, vol. 17, no. 4, pp. 357–407, 2011.

[6] G. Xie, A. Zhao, L. Zhao et al., "Metabolic fate of tea polyphenols in humans," *Journal of Proteome Research*, vol. 11, no. 6, pp. 3449–3457, 2012.

[7] T. Xue and R. Roy, "Studying traditional Chinese medicine," *Science*, vol. 300, no. 5620, pp. 740–741, 2003.

[8] A. E. F. Nassar and R. E. Talaat, "Strategies for dealing with metabolite elucidation in drug discovery and development," *Drug Discovery Today*, vol. 9, no. 7, pp. 317–327, 2004.

[9] O. Pelkonen, A. Tolonen, T. Korjamo, M. Turpeinen, and H. Raunio, "From known knowns to known unknowns: predicting in vivo drug metabolites," *Bioanalysis*, vol. 1, no. 2, pp. 393–414, 2009.

[10] A. Tolonen, M. Turpeinen, and O. Pelkonen, "Liquid chromatography-mass spectrometry in in vitro drug metabolite screening," *Drug Discovery Today*, vol. 14, no. 3-4, pp. 120–133, 2009.

[11] J. C. Lindon, E. Holmes, and J. K. Nicholson, "Metabonomics: systems biology in pharmaceutical research and development," *Current Opinion in Molecular Therapeutics*, vol. 6, no. 3, pp. 265–272, 2004.

[12] J. K. Nicholson and J. C. Lindon, "Systems biology: metabonomics," *Nature*, vol. 455, no. 7216, pp. 1054–1056, 2008.

[13] J. K. Nicholson and I. D. Wilson, "Understanding "global" systems biology: metabonomics and the continuum of metabolism," *Nature Reviews Drug Discovery*, vol. 2, no. 8, pp. 668–676, 2003.

[14] Y. Wang, H. Tang, J. K. Nicholson, P. J. Hylands, J. Sampson, and E. Holmes, "A metabonomic strategy for the detection of the metabolic effects of chamomile (*Matricaria recutita* L.) ingestion," *Journal of Agricultural and Food Chemistry*, vol. 53, no. 2, pp. 191–196, 2005.

[15] L. W. Sumner, E. Urbanczyk-Wochniak, and C. D. Broeckling, "Metabolomics data analysis, visualization, and integration," *Methods in Molecular Biology*, vol. 406, pp. 409–436, 2007.

[16] G. Xie, R. Plumb, M. Su et al., "Ultra-performance LC/TOF MS analysis of medicinal Panax herbs for metabolomic research," *Journal of Separation Science*, vol. 31, no. 6-7, pp. 1015–1026, 2008.

[17] S. C. Wu, G. C. Yen, B. S. Wang et al., "Antimutagenic and antimicrobial activities of pu-erh tea," *LWT—Food Science and Technology*, vol. 40, no. 3, pp. 506–512, 2007.

[18] B. S. Wang, H. M. Yu, L. W. Chang, W. J. Yen, and P. D. Duh, "Protective effects of pu-erh tea on LDL oxidation and nitric oxide generation in macrophage cells," *LWT—Food Science and Technology*, vol. 41, no. 6, pp. 1122–1132, 2008.

[19] Y. Ni, M. Su, J. Lin et al., "Metabolic profiling reveals disorder of amino acid metabolism in four brain regions from a rat model of chronic unpredictable mild stress," *FEBS Letters*, vol. 582, no. 17, pp. 2627–2636, 2008.

[20] X. Q. Chen, Y. Ye, H. Cheng, J. F. Yin, and C. Sun, "Comparative analysis of theanine, caffein and polyphenolic constituents in green tea, black tea and puer tea," *Food Research and Development*, vol. 28, no. 12, pp. 141–144, 2007.

[21] K. Lan and W. Jia, "An Integrated metabolomics and pharmacokinetics strategy for multi-component drugs evaluation," *Current Drug Metabolism*, vol. 11, no. 1, pp. 105–114, 2010.

[22] X. Wei, X. Shi, S. Kim et al., "Data preprocessing method for liquid chromatography-mass spectrometry based metabolomics," *Analytical Chemistry*, vol. 84, no. 18, pp. 7963–7971, 2012.

[23] J. Trygg, E. Holmes, and T. Lundstedt, "Chemometrics in metabonomics," *Journal of Proteome Research*, vol. 6, no. 2, pp. 469–479, 2007.

[24] S. Ma and S. K. Chowdhury, "Analytical strategies for assessment of human metabolites in preclinical safety testing," *Analytical Chemistry*, vol. 83, no. 13, pp. 5028–5036, 2011.

[25] Y. Wang, S. Wang, Y. Liu, L. Yan, G. Dou, and Y. Gao, "Characterization of metabolites and cytochrome P450 isoforms involved in the microsomal metabolism of aconitine," *Journal of Chromatography B*, vol. 844, no. 2, pp. 292–300, 2006.

[26] Y. F. Zhao, F. R. Song, X. H. Guo, and S. Y. Liu, "Studies on the biotransformation of aconitine in human intestinal bacteria using soft-ionization mass spectrometry," *Chemical Journal of Chinese Universities*, vol. 29, no. 1, pp. 55–59, 2008.

[27] L. Tang, L. Ye, C. Lv, Z. Zheng, Y. Gong, and Z. Liu, "Involvement of CYP3A4/5 and CYP2D6 in the metabolism of aconitine using human liver microsomes and recombinant CYP450 enzymes," *Toxicology Letters*, vol. 202, no. 1, pp. 47–54, 2011.

[28] X. Wang, Z. Pi, W. Liu, Y. Zhao, and S. Liu, "Effect of pH on the metabolism of aconitine under rat intestinal bacteria and analysis of metabolites using HPLC/MS-MSn technique," *Chinese Journal of Chemistry*, vol. 28, no. 12, pp. 2494–2500, 2010.

[29] R. S. Plumb, C. L. Stumpf, J. H. Granger, J. Castro-Perez, J. N. Haselden, and G. J. Dear, "Use of liquid chromatography/time-of-flight mass spectrometry and multivariate statistical analysis shows promise for the detection of drug metabolites in biological fluids," *Rapid Communications in Mass Spectrometry*, vol. 17, no. 23, pp. 2632–2638, 2003.

[30] H. Idborg, P. O. Edlund, and S. P. Jacobsson, "Multivariate approaches for efficient detection of potential metabolites from liquid chromatography/mass spectrometry data," *Rapid Communications in Mass Spectrometry*, vol. 18, no. 9, pp. 944–954, 2004.

[31] C. Chen, F. J. Gonzalez, and J. R. Idle, "LC-MS-based metabolomics in drug metabolism," *Drug Metabolism Reviews*, vol. 39, no. 2-3, pp. 581–597, 2007.

[32] A. D. Patterson, F. J. Gonzalez, and J. R. Idle, "Xenobiotic metabolism: a view through the metabolometer," *Chemical Research in Toxicology*, vol. 23, no. 5, pp. 851–860, 2010.

[33] C. H. Johnson, A. D. Patterson, J. R. Idle, and F. J. Gonzalez, "Xenobiotic metabolomics: major impact on the metabolome," *Annual Review of Pharmacology and Toxicology*, vol. 52, pp. 37–56, 2012.

[34] C. Chen, L. Meng, X. Ma et al., "Urinary metabolite profiling reveals CYP1A2-mediated metabolism of NSC686288 (aminoflavone)," *Journal of Pharmacology and Experimental Therapeutics*, vol. 318, no. 3, pp. 1330–1342, 2006.

[35] S. Giri, J. R. Idle, C. Chen, T. M. Zabriskie, K. W. Krausz, and F. J. Gonzalez, "A metabolomic approach to the metabolism of the areca nut alkaloids arecoline and arecaidine in the mouse," *Chemical Research in Toxicology*, vol. 19, no. 6, pp. 818–827, 2006.

[36] C. Chen, X. Ma, M. A. Malfatti et al., "A comprehensive investigation of 2-amino-1-methyl-6-phenylimidazo [4,5-b] pyridine (PhIP) metabolism in the mouse using a multivariate data analysis approach," *Chemical Research in Toxicology*, vol. 20, no. 3, pp. 531–542, 2007.

[37] S. Giri, K. W. Krausz, J. R. Idle, and F. J. Gonzalez, "The metabolomics of (±)-arecoline 1-oxide in the mouse and its formation by human flavin-containing monooxygenases," *Biochemical Pharmacology*, vol. 73, no. 4, pp. 561–573, 2007.

[38] A. Fardet, R. Llorach, A. Orsoni et al., "Metabolomics provide new insight on the metabolism of dietary phytochemicals in rats," *Journal of Nutrition*, vol. 138, no. 7, pp. 1282–1287, 2008.

[39] C. Chen, K. W. Krausz, J. R. Idle, and F. J. Gonzalez, "Identification of novel toxicity-associated metabolites by metabolomics and mass isotopomer analysis of acetaminophen metabolism in wild-type and Cyp2e1-null mice," *Journal of Biological Chemistry*, vol. 283, no. 8, pp. 4543–4559, 2008.

[40] J. Cheng, X. Ma, K. W. Krausz, J. R. Idle, and F. J. Gonzalez, "Rifampicin-activated human pregnane X receptor and CYP3A4 induction enhance acetaminophen-induced toxicity," *Drug Metabolism and Disposition*, vol. 37, no. 8, pp. 1611–1621, 2009.

[41] J. Sun, L. K. Schnackenberg, and R. D. Beger, "Studies of acetaminophen and metabolites in urine and their correlations with toxicity using metabolomics," *Drug Metabolism Letters*, vol. 3, no. 3, pp. 130–136, 2009.

[42] F. Li, J. Lu, and X. Ma, "Profiling the reactive metabolites of xenobiotics using metabolomic technologies," *Chemical Research in Toxicology*, vol. 24, no. 5, pp. 744–751, 2011.

[43] U. Lutz, N. Bittner, R. W. Lutz, and W. K. Lutz, "Metabolite profiling in human urine by LC-MS/MS: method optimization and application for glucuronides from dextromethorphan metabolism," *Journal of Chromatography B*, vol. 871, no. 2, pp. 349–356, 2008.

[44] X. Ma, C. Chen, K. W. Krausz, J. R. Idle, and F. J. Gonzalez, "A metabolomic perspective of melatonin metabolism in the mouse," *Endocrinology*, vol. 149, no. 4, pp. 1869–1879, 2008.

[45] S. Niu, F. Li, D. X. Tan et al., "Analysis of N^1-acetyl-N^2-formyl-5-methoxykynuramine/N^1-acetyl-5-methoxy-kynuramine formation from melatonin in mice," *Journal of Pineal Research*, vol. 49, no. 2, pp. 106–114, 2010.

[46] J. Y. Cho, D. W. Kang, X. Ma et al., "Metabolomics reveals a novel vitamin E metabolite and attenuated vitamin E metabolism upon PXR activation," *Journal of Lipid Research*, vol. 50, no. 5, pp. 924–937, 2009.

[47] A. Liu, Y. Chen, Z. Yang et al., "New metabolites of fenofibrate in SpragueDawley rats by UPLC-ESI-QTOF-MS-based metabolomics coupled with LC-MS/MS," *Xenobiotica*, vol. 39, no. 4, pp. 345–354, 2009.

[48] A. Liu, A. D. Patterson, Z. Yang et al., "Fenofibrate metabolism in the cynomolgus monkey using ultraperformance liquid chromatography-quadrupole time-of-flight mass spectrometry-based metabolomics," *Drug Metabolism and Disposition*, vol. 37, no. 6, pp. 1157–1163, 2009.

[49] J. Sun, L. S. Von Tungeln, W. Hines, and R. D. Beger, "Identification of metabolite profiles of the catechol-O-methyl transferase inhibitor tolcapone in rat urine using LC/MS-based metabonomics analysis," *Journal of Chromatography B*, vol. 877, no. 24, pp. 2557–2565, 2009.

[50] F. Li, A. D. Patterson, C. C. Höfer, K. W. Krausz, F. J. Gonzalez, and J. R. Idle, "Comparative metabolism of cyclophosphamide and ifosfamide in the mouse using UPLC-ESI-QTOFMS-based metabolomics," *Biochemical Pharmacology*, vol. 80, no. 7, pp. 1063–1074, 2010.

[51] F. Li, L. Wang, G. L. Guo, and X. Ma, "Metabolism-mediated drug interactions associated with ritonavir-boosted tipranavir in mice," *Drug Metabolism and Disposition*, vol. 38, no. 5, pp. 871–878, 2010.

[52] R. P. Schneider, H. Zhang, L. Mu, A. S. Kalgutkar, and R. Bonner, "Utility of multivariate analysis in support of in vitro metabolite identification studies: retrospective analysis using the antidepressant drug nefazodone," *Xenobiotica*, vol. 40, no. 4, pp. 262–274, 2010.

[53] J. Sun, L. K. Schnackenberg, D. K. Hansen, and R. D. Beger, "Study of valproic acid-induced endogenous and exogenous metabolite alterations using LC-MS-based metabolomics," *Bioanalysis*, vol. 2, no. 2, pp. 207–216, 2010.

[54] F. Li and X. Ma, "Metabolomic screening and identification of the bioactivation pathways of ritonavir," *Chemical Research in Toxicology*, vol. 24, no. 12, pp. 2109–2114, 2011.

[55] F. Li, A. D. Patterson, C. C. Höfer, K. W. Krausz, F. J. Gonzalez, and J. R. Idle, "A comprehensive understanding of thioTEPA metabolism in the mouse using UPLC-ESI-QTOFMS-based metabolomics," *Biochemical Pharmacology*, vol. 81, no. 8, pp. 1043–1053, 2011.

[56] G. Tan, Z. Lou, X. Dong, W. Li, and Y. Chai, "Urinary metabolites of isoliquiritigenin in wistar rats using UHPLC–TOF–MS-based xenometabolomics," *Chromatographia*, vol. 74, no. 3-4, pp. 341–348, 2011.

[57] X. Shi, D. Yao, and C. Chen, "Identification of N-acetyltaurine as a novel metabolite of ethanol through metabolomics-guided biochemical analysis," *Journal of Biological Chemistry*, vol. 287, no. 9, pp. 6336–6349, 2012.

[58] F. Li, A. D. Patterson, K. W. Krausz et al., "Metabolomics reveals the metabolic map of procainamide in humans and mice," *Biochemical Pharmacology*, vol. 83, no. 10, pp. 1435–1444, 2012.

[59] Y. Zhen, O. Slanař, K. W. Krausz et al., "3,4-Dehydrodebrisoquine, a novel debrisoquine metabolite formed from 4-hydroxydebrisoquine that affects the CYP2D6 metabolic ratio," *Drug Metabolism and Disposition*, vol. 34, no. 9, pp. 1563–1574, 2006.

[60] R. Llorach-Asunción, O. Jauregui, M. Urpi-Sarda, and C. Andres-Lacueva, "Methodological aspects for metabolome visualization and characterization. A metabolomic evaluation of the 24 h evolution of human urine after cocoa powder consumption," *Journal of Pharmaceutical and Biomedical Analysis*, vol. 51, no. 2, pp. 373–381, 2010.

[61] R. Llorach, I. Garrido, M. Monagas et al., "Metabolomics study of human urinary metabolome modifications after intake of almond (Prunus dulcis (Mill.) D.A. Webb) skin polyphenols," *Journal of Proteome Research*, vol. 9, no. 11, pp. 5859–5867, 2010.

[62] G. Xie, M. Ye, Y. Wang et al., "Characterization of pu-erh tea using chemical and metabolic profiling approaches," *Journal of Agricultural and Food Chemistry*, vol. 57, no. 8, pp. 3046–3054, 2009.

[63] E. J. J. van Velzen, J. A. Westerhuis, J. P. M. van Duynhoven et al., "Multilevel data analysis of a crossover designed human nutritional intervention study," *Journal of Proteome Research*, vol. 7, no. 10, pp. 4483–4491, 2008.

[64] E. J. J. van Velzen, J. A. Westerhuis, J. P. M. van Duynhoven et al., "Phenotyping tea consumers by nutrikinetic analysis of polyphenolic end-metabolites," *Journal of Proteome Research*, vol. 8, no. 7, pp. 3317–3330, 2009.

[65] F. P. J. Martin, S. Rezzi, E. Peré-Trepat et al., "Metabolic effects of dark chocolate consumption on energy, gut microbiota, and stress-related metabolism in free-living subjects," *Journal of Proteome Research*, vol. 8, no. 12, pp. 5568–5579, 2009.

[66] V. Croixmarie, T. Umbdenstock, O. Cloarec et al., "Integrated comparison of drug-related and drug-induced ultra performance liquid chromatography/mass spectrometry metabonomic profiles using human hepatocyte cultures," *Analytical Chemistry*, vol. 81, no. 15, pp. 6061–6069, 2009.

[67] H. Li, M. Zhou, A. Zhao, and W. Jia, "Traditional Chinese medicine: balancing the gut ecosystem," *Phytotherapy Research*, vol. 23, no. 9, pp. 1332–1335, 2009.

[68] P. Li, E.-H. Liu, and X.-D. Wen, "Analysis of Chinese herbal medicines with holistic approaches and integrated evaluation models," *TrAC—Trends in Analytical Chemistry*, vol. 27, no. 1, pp. 66–77, 2008.

[69] G.-Z. Xin, L.-W. Qi, Z.-Q. Shi, G.-J. Wang, and J. Shang, "Strategies for integral metabolism profile of multiple compounds in herbal medicines: pharmacokinetics, metabolites characterization and metabolic interactions," *Current Drug Metabolism*, vol. 12, no. 9, pp. 809–817, 2011.

[70] C. Y. Li, L. W. Qi, and P. Li, "Correlative analysis of metabolite profiling of Danggui Buxue Tang in rat biological fluids by rapid resolution LC-TOF/MS," *Journal of Pharmaceutical and Biomedical Analysis*, vol. 55, no. 1, pp. 146–160, 2011.

[71] C. Xiang, X. Qiao, Q. Wang, D. Guo, and M. Ye, "From single compounds to herbal extract: a strategy to systematically characterize the metabolites of licorice in rats," *Drug Metabolism and Disposition*, vol. 39, no. 9, pp. 1597–1608, 2011.

[72] X. Qiao, M. Ye, C. Xiang, Q. Wang, W.-J. Miao, and D.-A. Guo, "Analytical strategy to reveal the in vivo process of multi-component herbal medicine: a pharmacokinetic study of licorice using liquid chromatography coupled with triple quadrupole mass spectrometry," *Journal of Chromatography A*, vol. 1258, pp. 84–93, 2012.

[73] P. Gong, N. Cui, L. Wu et al., "Chemicalome and metabolome matching approach to elucidating biological metabolic networks of complex mixtures," *Analytical Chemistry*, vol. 84, no. 6, pp. 2995–3002, 2012.

[74] A. K. Smilde, J. A. Westerhuis, H. C. J. Hoefsloot et al., "Dynamic metabolomic data analysis: a tutorial review," *Metabolomics*, vol. 6, no. 1, pp. 3–17, 2010.

[75] J. A. Westerhuis, E. J. J. van Velzen, H. C. J. Hoefsloot, and A. K. Smilde, "Multivariate paired data analysis: multilevel PLSDA versus OPLSDA," *Metabolomics*, vol. 6, no. 1, pp. 119–128, 2010.

[76] J. van Duynhoven, E. E. Vaughan, D. M. Jacob et al., "Metabolic fate of polyphenols in the human superorganism," *Proceedings of the National Academy of Sciences of the United States of America*, vol. 108, supplement 1, pp. 4531–4538, 2011.

[77] J. P. M. van Duynhoven, E. J. J. van Velzena, and J. A. Westerhuis, "Nutrikinetics: concept, technologies, applications, perspectives," *Trends in Food Science and Technology*, vol. 26, no. 1, pp. 4–13, 2012.

[78] R. Llorach, M. Garcia-Aloy, S. Tulipani, and C. Andres-Lacueva, "Nutrimetabolomic strategies to develop new biomarkers of intake and health effects," *Journal of Agricultural and Food Chemistry*, vol. 60, no. 36, pp. 8797–8808, 2012.

[79] E. M. Lenz and I. D. Wilson, "Analytical strategies in metabonomics," *Journal of Proteome Research*, vol. 6, no. 2, pp. 443–458, 2007.

[80] J. van der Greef, "Perspective: all systems go," *Nature*, vol. 480, no. 7378, p. S87, 2011.

[81] T. Ideker, T. Galitski, and L. Hood, "A new approach to decoding life: systems biology," *Annual Review of Genomics and Human Genetics*, vol. 2, pp. 343–372, 2001.

[82] H. Kitano, "Systems biology: a brief overview," *Science*, vol. 295, no. 5560, pp. 1662–1664, 2002.

[83] K. Lan, Y. Zhang, J. Yang, and L. Xu, "Simple quality assessment approach for herbal extracts using high performance liquid chromatography-UV based metabolomics platform," *Journal of Chromatography A*, vol. 1217, no. 8, pp. 1414–1418, 2010.

[84] Z. Wang, H. Hu, F. Chen et al., "Metabolic profiling assisted quality assessment of Rhodiola rosea extracts by high-performance liquid chromatography," *Planta Medica*, vol. 78, no. 7, pp. 740–746, 2012.

[85] L.-X. Duan, M. Li, M. Chen et al., "Use of the metabolomics approach to characterize chinese medicinal material Huangqi," *Molecular Plant*, vol. 5, no. 2, pp. 376–386, 2012.

[86] M. Wang, R. J. A. N. Lamers, H. A. A. J. Korthout et al., "Metabolomics in the context of systems biology: Bridging Traditional Chinese Medicine and molecular pharmacology," *Phytotherapy Research*, vol. 19, no. 3, pp. 173–182, 2005.

[87] A. Zhang, H. Sun, Z. Wang, W. Sun, P. Wang, and X. Wang, "Metabolomics: towards understanding traditional Chinese medicine," *Planta Medica*, vol. 76, no. 17, pp. 2026–2035, 2010.

[88] X. Wang, H. Sun, A. Zhang, W. Sun, P. Wang, and Z. Wang, "Potential role of metabolomics apporoaches in the area of traditional Chinese medicine: as pillars of the bridge between Chinese and Western medicine," *Journal of Pharmaceutical and Biomedical Analysis*, vol. 55, no. 5, pp. 859–868, 2011.

[89] P. Liu, S. Liu, D. Tian, and P. Wang, "The applications and obstacles of metabonomics in traditional Chinese medicine," *Evidence-Based Complementary and Alternative Medicine*, vol. 2012, Article ID 945824, 4 pages, 2012.

[90] T. Wu, M. Yang, H.-F. Wei, S.-H. He, S.-C. Wang, and G. Ji, "Application of metabolomics in traditional chinese medicine differentiation of deficiency and excess syndromes in patients with diabetes mellitus," *Evidence-Based Complementary and Alternative Medicine*, vol. 2012, Article ID 968083, 11 pages, 2012.

[91] M. Jové, J. C. E. Serrano, N. Ortega et al., "Multicompartmental LC-Q-TOF-based metabonomics as an exploratory tool to identify novel pathways affected by polyphenol-rich diets in mice," *Journal of Proteome Research*, vol. 10, no. 8, pp. 3501–3512, 2011.

[92] P. J. Turnbaugh, R. E. Ley, M. Hamady, C. M. Fraser-Liggett, R. Knight, and J. I. Gordon, "The Human Microbiome Project," *Nature*, vol. 449, no. 7164, pp. 804–810, 2007.

[93] J. Qin, R. Li, J. Raes et al., "A human gut microbial gene catalogue established by metagenomic sequencing," *Nature*, vol. 464, no. 7285, pp. 59–65, 2010.

[94] M. Arumugam, J. Raes, E. Pelletier et al., "Enterotypes of the human gut microbiome," *Nature*, vol. 473, no. 7346, pp. 174–180, 2011.

[95] T. H. M. P. Consortium, "A framework for human microbiome research," *Nature*, vol. 486, no. 7402, pp. 215–221, 2012.

[96] T. H. M. P. Consortium, "Structure, function and diversity of the healthy human microbiome," *Nature*, vol. 486, no. 7402, pp. 207–214, 2012.

[97] I. Rosabelle McManus, A. O. Contag, and R. E. Olson, "Characterization of endogenous ethanol in the mammal," *Science*, vol. 131, no. 3393, pp. 102–103, 1960.

[98] G. Spinucci, M. Guidetti, E. Lanzoni, and L. Pironi, "Endogenous ethanol production in a patient with chronic intestinal pseudo-obstruction and small intestinal bacterial overgrowth," *European Journal of Gastroenterology and Hepatology*, vol. 18, no. 7, pp. 799–802, 2006.

[99] D. Compare, P. Coccoli, A. Rocco, O. M. Nardone, S. De Maria, and G. Nardone, "Gut-liver axis: the impact of gut microbiota on non alcoholic fatty liver disease," *Nutrition, Metabolism and Cardiovascular Diseases*, vol. 22, no. 6, pp. 471–476, 2012.

[100] F. P. J. Martin, M. E. Dumas, Y. Wang et al., "A top-down systems biology view of microbiome-mammalian metabolic interactions in a mouse model," *Molecular Systems Biology*, vol. 3, article 112, 2007.

[101] F. P. J. Martin, Y. Wang, N. Sprenger et al., "Probiotic modulation of symbiotic gut microbial-host metabolic interactions in a humanized microbiome mouse model," *Molecular Systems Biology*, vol. 4, article 157, 2008.

[102] F. P. J. Martin, N. Sprenger, I. K. S. Yap et al., "Panorganismal gut microbiome-host metabolic crosstalk," *Journal of Proteome Research*, vol. 8, no. 4, pp. 2090–2105, 2009.

[103] F. P. J. Martin, Y. Wang, I. K. S. Yap et al., "Topographical variation in murine intestinal metabolic profiles in relation to microbiome speciation and functional ecological activity," *Journal of Proteome Research*, vol. 8, no. 7, pp. 3464–3474, 2009.

[104] X. Zheng, G. Xie, A. Zhao et al., "The footprints of gut microbial-mammalian co-metabolism," *Journal of Proteome Research*, vol. 10, no. 12, pp. 5512–5522, 2011.

[105] J. K. Nicholson, E. Holmes, R. Burcelin, and S. Pettersson, "Host-gut microbiota metabolic interactions," *Science*, vol. 336, no. 6086, pp. 1262–1267, 2012.

[106] I. D. Wilson and J. K. Nicholson, "The role of gut microbiota in drug response," *Current Pharmaceutical Design*, vol. 15, no. 13, pp. 1519–1523, 2009.

[107] T. A. Clayton, D. Baker, J. C. Lindon, J. R. Everett, and J. K. Nicholson, "Pharmacometabonomic identification of a significant host-microbiome metabolic interaction affecting human drug metabolism," *Proceedings of the National Academy of Sciences of the United States of America*, vol. 106, no. 34, pp. 14728–14733, 2009.

[108] W. Meinl, S. Sczesny, R. Brigelius-Flohé, M. Blaut, and H. Glatt, "Impact of gut microbiota on intestinal and hepatic levels of phase 2 xenobiotic-metabolizing enzymes in the rat," *Drug Metabolism and Disposition*, vol. 37, no. 6, pp. 1179–1186, 2009.

[109] B. Björkholm, C. M. Bok, A. Lundin, J. Rafter, M. L. Hibberd, and S. Pettersson, "Intestinal microbiota regulate xenobiotic metabolism in the liver," *PLoS ONE*, vol. 4, no. 9, Article ID e6958, 2009.

[110] S. Peters, H. G. Janssen, and G. Vivó-Truyols, "Trend analysis of time-series data: a novel method for untargeted metabolite discovery," *Analytica Chimica Acta*, vol. 663, no. 1, pp. 98–104, 2010.

Hindawi Publishing Corporation
Evidence-Based Complementary and Alternative Medicine
Volume 2013, Article ID 760804, 8 pages
http://dx.doi.org/10.1155/2013/760804

Research Article

Beneficial Effects of an 8-Week, Very Low Carbohydrate Diet Intervention on Obese Subjects

Yunjuan Gu,[1,2,3,4,5] Haoyong Yu,[1,2,3,4] Yuehua Li,[4] Xiaojing Ma,[1,2,3,4] Junxi Lu,[1,2,3,4] Weihui Yu,[1,2,3,4] Yunfeng Xiao,[4] Yuqian Bao,[1,2,3,4] and Weiping Jia[1,2,3,4]

[1] *Department of Endocrinology and Metabolism, Shanghai Jiao Tong University Affiliated Sixth People's Hospital, Shanghai Diabetes Institute, Shanghai Clinical Centre of Diabetes, Shanghai 200233, China*
[2] *Shanghai Key Laboratory of Diabetes Mellitus, Shanghai 200233, China*
[3] *Department of Endocrinology and Metabolism, Affiliated Hospital of Nantong University, Nantong 226001, Jiangsu Province, China*
[4] *Department of Radiology, Shanghai Jiao Tong University Affiliated Sixth People's Hospital, Shanghai 200233, China*
[5] *Department of Endocrinology and Metabolism, Affiliated Hospital of Nantong University, Nantong, Jiangsu Province, China*

Correspondence should be addressed to Weiping Jia; wpjia@sjtu.edu.cn

Received 31 December 2012; Revised 18 February 2013; Accepted 18 February 2013

Academic Editor: Wei Jia

Aim. To investigate the effects of weight loss during an 8-week very low carbohydrate diet (VLCD) on improvement of metabolic parameters, adipose distribution and body composition, and insulin resistance and sensitivity in Chinese obese subjects. *Methods*. Fifty-three healthy obese volunteers were given an 8-week VLCD. The outcomes were changes in anthropometry, body composition, metabolic profile, abdominal fat distribution, liver fat percent (LFP), and insulin resistance and sensitivity. *Results*. A total of 46 (86.8%) obese subjects completed the study. The VLCD caused a weight loss of -8.7 ± 0.6 kg (mean ± standard error (SE), $P < 0.0001$) combined with a significant improvement of metabolic profile. In both male and female, nonesterified fatty acid (NEFA) significantly decreased (-166.2 ± 47.6 μmol/L, $P = 0.001$) and β-hydroxybutyric acid (BHA) increased (0.15 ± 0.06 mmol/L, $P = 0.004$) after eight weeks of VLCD intervention. The significant reductions in subcutaneous fat area (SFA), visceral fat area (VFA), and LFP were -66.5 ± 7.9 cm^2, -35.3 ± 3.9 cm^2, and -16.4 ± 2.4%, respectively (all P values $P < 0.0001$). HOMA IR and HOMA β significantly decreased while whole body insulin sensitivity index (WBISI) increased (all P values $P < 0.001$). *Conclusion*. Eight weeks of VLCD was an effective intervention in obese subjects. These beneficial effects may be associated with enhanced hepatic and whole-body lipolysis and oxidation.

1. Introduction

In the past decades, the prevalence of overweight and obesity has increased rapidly worldwide. Obesity is a major risk factor for several chronic diseases such as type 2 diabetes mellitus, cardiovascular disease, and some kinds of cancer [1]. Because of the severe comorbidities of obesity, people attempt to lose weight through several alternative diets. Recently, there has been a resurgence of interest in VLCD as a means of weight loss and metabolic improvements. Evidence from clinical studies and meta-analyses suggested that VLCD can decrease body weight, improve metabolic parameters, insulin resistance/sensitivity, and nonalcoholic fatty liver disease (NAFLD) [2]. However, the effect of VLCD on β cell function and insulin sensitivity is still controversial. Svendsen et al. reported that when ten obese women lost 11% of their baseline weight after an 8-week VLCD diet, their subcutaneous and intra-abdominal fatty tissue significantly decreased, but HOMA IR increased and peripheral insulin sensitivity was unaltered [3]. Malandrucco et al. observed that the metabolic profile of 14 severely obese patients with type 2 diabetes with a 7-day VLCD intervention were improved markedly primarily due to the amelioration of β cell function (disposition index increased), but with no change in insulin sensitivity [4]. Viljanen et al. found that after 16 obese subjects underwent a 6-week VLCD, visceral adipose and abdominal subcutaneous fat decreased while whole body insulin sensitivity increased, but adipose tissue regional glucose uptake

remained unchanged [5]. Therefore, it is necessary to further assess the beneficial effect of VLCD, especially its impact on β cell function and insulin sensitivity.

It has been reported that the amount of carbohydrate intake affects blood glucose and insulin levels and even metabolic consequences [6]. However, in traditional Chinese dietary, carbohydrate contributes more than half of the total daily energy consumption. The method of VLCD to lose weight is less popular in Chinese comparing with that in westerns. Therefore, this is the first time to investigate the beneficial effects of VLCD on weight loss, improvements of body composition, insulin sensitivity and resistant, and plasma metabolic parameters in Chinese obese subjects.

2. Methods

2.1. Participants. We recruited 53 obese healthy volunteers (31 men, 22 women, aged 18–52 years, BMI $\geq$ 28 kg/m^2) from the outpatient clinic of endocrinology and metabolism department of Shanghai Jiao Tong University Affiliated Sixth People's Hospital. All the subjects underwent a general health examination before entering the study. Exclusion criteria were as follows: pregnant or plan for pregnant; lactation or postmenopausal women; use of any prescription medication in previous 2 months; had any weight loss diet or pill during the past 6 months; consuming >20 g/day of alcohol; tobacco use within 6 month; cardiovascular or endocrine disease history; hypertension history or current elevated blood pressure (systolic blood pressure (SBP): ≥150 mm Hg; diastolic blood pressure (DBP) ≥90 mm Hg; current treatment for hypertension); diabetes mellitus; acute or chronic infections; hepatopathy, kidney disease, gastrointestinal disease or any other acute or chronic diseases requiring treatment.

This study was approved by the institutional review board of Shanghai Jiao Tong University Affiliated Sixth People's Hospital in accordance with the principles of the Helsinki Declaration II. Written informed consent was obtained from each participant. There were no monetary incentives for participation.

2.2. Experimental Protocol. One week before initiation of the study, all subjects were asked to maintain their habitual energy intake. At baseline and after the 8-week VLCD treatment, standard 75-g oral glucose tolerance tests (OGTT) were performed. At weeks 0, 4, and 8, anthropometric parameters, bioimpedance assessments, biochemical indices, insulin resistance and sensitivity, LFP, SFA, and VFA were measured.

2.3. Dietary Intervention. All subjects were given individual instructions on how to follow the VLCD. Energy intake was restricted to less than 800 kcal/day (carbohydrate intake < 20 g/d). All daily meals were replaced as follows: a cup of soybean milk (200 mL) and a boiled egg at breakfast; a diet nutrition bar (106 Kcal: 2.8 g carbohydrate, 11.2 g protein and 5.6 g fat; Nutriease Health Technology Co., Ltd., Hangzhou, China), nonstarchy vegetables (<200 kcal), and 50 g protein from meat (i.e., beef, lean pork, skinned chicken, fish) at lunch and dinner. Supplementation of multivitamins and minerals was provided per day. Subjects were also encouraged to drink at least 1.8 litres of water per day, and asked to maintain their habitual level of physical activity. Regular telephone contact to individual by nutritionists was provided for nutrient support. After the 8-week dietary intervention, there was a 1-week recovery period when the eucaloric intake was allowed to overcome the catabolic state. Then participants restarted normal eating and were provided with information about portion size and healthy eating.

2.4. Measurements

2.4.1. Bioimpedance Assessments. Before and after the VLCD, whole body skeletal muscle mass and fat mass were measured by a multifrequency impedance plethysmograph body composition analyzer (InBody 720, Biospace, Korea). Before analyzing, participants stand on the electrodes embedded in the scale platform of the respective analyzers and wipe the bottom of their feet with a proprietary electrolyte tissue. Then they were asked to stand upright grasping the handles of the analyzer in order to contact with 4 pairs of electrodes (octapolar technology). Resistance was measured at five specific frequencies (1 kHz, 50 kHz, 250 kHz, 500 kHz, and 1 MHz) and reactance at three specific frequencies (5 kHz, 50 kHz, and 250 kHz). Total body water (TBW) was estimated from area, volume, length, impedance, and a constant proportion (specific resistivity). Fat-free mass was estimated by dividing TBW by 0.73. After the participant's identification number, sex, age, and height were typed into the analyzer; the fat mass percentage (FMP) and skeletal muscle mass percentage of whole body weight (SMMP) were calculated by the computer software automatically [7].

2.4.2. 1H Magnetic Resonance Spectroscopy (1H MRS) Measurement of Liver Fat Percent. Liver magnetic resonance imaging and in vivo single-voxel MRS were performed using Philips Achieva 3.0T MRI system (Philips Medical Systems, Eindhoven, The Netherlands) equipped with an 8-channel phase coil. Anatomical T1-weighted spin-echo MR images were obtained using the following parameters: repetition time (TR) = 550 ms; echo time (TE) = 10 ms; flip angle = 60; field of view (FOV) = 21 cm; slice thickness = 3 mm; slice spacing = 0.1 mm. ^{1}H-MRS was performed for quantification analysis of metabolite concentrations in liver. Firstly, 2D-spin-echo images in the coronal and sagittal regions were obtained for image-guided localization of voxels of interest (VOI) for spectroscopic data acquisition. Secondary, single-voxel MRS was performed by a stimulated echo acquisition mode (STEAM) sequence by using the following parameters: TE = 20 ms; TR = 1,500 ms; VOX = 15 × 15 × 15 mm; total number of points = 128; total number of average = 64. Finally, eight-step phase cycling was used to suppress unwanted signals or artifacts. Signal intensities of the water peak at 4.7 p.p.m. (Sw) and the fat peak at 1.2 p.p.m. (Sf) were measured and liver fat

percentage (LFP) was calculated as follows: LFP = 100 × Sf/(Sf + Sw) [8]. A LFP of 5.56% by 1H MRS is used as cutoff value for diagnosing NAFLD [9].

2.4.3. Magnetic Resonance Imaging (MRI) Measurement of Abdominal Fat Areas. SFA and VFA were assessed by Philips Achieva 3.0T MRI system (Philips Medical Systems, Eindhoven, The Netherlands) using standard array coils with the subject supine. Breath-hold FISP images were centered on the L4-L5 intervertebral disc using standard localizer images with the following parameters: TR = 4 ms, TE = 2 ms, number of slices = 12, slice thickness = 8 mm, image matrix 256 × 256, and field-of-view = 500 × 500 mm. The 4 slices that were best aligned with the L4-L5 disc were analyzed by SliceOmatic 5.0 software package (Escape Medical Viewer V3.2) to define VFA and SFA [10]. VFA and SFA were measured by fitting a spline curve to points on the border of the subcutaneous and visceral regions. Nonfat regions within the visceral region were also outlined with a spline fit and subtracted from the total visceral region [11].

2.4.4. Laboratory Evaluation. At baseline and week 8, all participants underwent a 75-g OGTT in the morning after 10 h overnight fasting. Their venous blood samples were drawn at 0 (fating state), 30, 60, and 120 minutes. Plasma glucose concentration was measured using a glucose oxidase method. Serum insulin levels were tested by a radioimmunoassay using the insulin detection kit, according to the manufacturer's instructions (Beijing North Institute of Biological Technology, Beijing, China). The following indices were measured by standard commercial methods on a parallel, multichannel analyzer (Hitachi 7600-020, Tokyo, Japan): liver function panel including aspartate aminotransferase (AST), alanine aminotransferase (ALT), γ-glutamyl transferase (γ-GT); renal function panel including serum creatinine, uric creatinine, and uric acid; lipid panel including total cholesterol (TC), triacylglycerol (TG), high density lipoprotein (HDL), and low-density lipoprotein cholesterol (LDL); NEFA and BHA. Urinary albumin were tested using the first-morning void urine samples by immunonephelometry on the BN II analyzer (Siemens Diagnostics) and its concentration was then corrected by urine creatinine.

2.5. Calculations. β cell function and insulin resistance were evaluated using the following formulas: (1) HOMA β (mIU/mmol/L) = 20 × fasting insulin (mIU/L)/(fasting glucose (mmol/L) − 3.5) [12]; (2) HOMA IR (mIU·mmol/L^2) = fasting insulin (mIU/L) × fasting glucose (mmol/L)/22.5 [13]; (3) Whole Body Insulin Sensitivity Index (WBISI, L^2/mmol^2) = 10000/square root of [fasting glucose (mmol/L) × fasting insulin (mIU/L) × mean insulin (mIU/L) × mean glucose (mmol/L)]; mean glucose = [fasting glucose (mmol/L) + 2 h postprandial glucose (mmol/L)]/2; mean insulin = [fasting insulin (mIU/L)+ 2 h postprandial insulin (mIU/L)]/2 [14].

2.6. Statistical Analysis. All continuous variables were tested for normal distribution by the Kolmogorov–Smirnov normality test. Log-transformations were used to normalize skewed variables. Data were presented as mean ± SE. Chi-square test was used for categorical variables, repeated-measures ANOVA for comparison among different time points, and paired t-test for comparison of variables before and after the study. P values <0.05 (2-tailed tests) were considered to be statistically significant. Statistical analysis was performed using SPSS 17.0 (SPSS, Chicago, IL, USA).

3. Results

Of 53 obese subjects, 46 (86.8%) completed the study. Among the 7 participants who withdrew, one was diagnosed of type 2 diabetes, one had urine microalbumin/creatinine ≥30 ug/mg at baseline, two dropped out for stomachache, and three for noncompliance.

3.1. Body Weight, Waist, and Blood Pressure. As shown in Table 1, after the 8-week VLCD intervention, from baseline, mean weight loss was −8.7 ± 0.6 kg (−9.0 ± 0.5%, $P < 0.0001$), representing a mean reduction in BMI of −3.0 ± 0.2 kg/m^2 (−9.0 ± 0.5%, $P < 0.0001$). Mean waist circumference change was −5.9 ± 1.2 cm (from 104.5 ± 1.7 cm to 98.6 ± 1.4 cm, $P < 0.0001$), mean reductions in SBP and DBP were −13.1 ± 2.8 mmHg and −8.2 ± 1.6 mmHg respectively (all P values < 0.0001).

3.2. Body Composition and Liver Fat Percent. As shown in Table 2, significant decrement in mean SFA (−66.5 ± 7.9 cm^2, $P < 0.0001$) and VFA (−35.3 ± 3.9 cm^2, $P < 0.0001$) was observed after the 8-week VLCD diet. FMP significantly decreased (−3.0 ± 0.4%, $P < 0.0001$) while SMMP significantly increased (1.7 ± 0.2%, $P < 0.0001$). Moreover, with LFP significantly decreasing (−16.4±2.4%, $P < 0.0001$), about half of the subjects who were NAFLD at baseline experienced a reversal at the end of the study (from 87.0% to 43.5%, $P = 0.021$). Furthermore, all the improvements of body composition and liver fat percent were significantly presented in both male and female subjects (Figure 1).

3.3. Plasma Metabolic Parameters and Hepatic Enzymes Concentrations. Together with weight loss from baseline to the end of the study, liver enzymes of ALT, AST, γ-GT were all significantly improved (Table 1). Concentrations of TC (from 5.12 ± 0.12 mmol/L to 4.79 ± 0.14 mmol/L, $P < 0.0001$) and TG (from 1.98 ± 0.23 mmol/L to 1.08 ± 0.09 mmol/L, $P < 0.0001$) significantly decreased and HDL significantly increased (from 1.15 ± 0.04 mmol/L to 1.19 ± 0.04, $P = 0.01$). However, the LDL level did not significantly change after the dietary intervention. The level of NEFA did not change at week 4 but decreased significantly at week 8 (baseline: 729.8 ± 34.9 μmmol/L *versus* week 4: 729.3 ± 43.2 μmmol/L *versus* week 8: 574.7 ± 37.0 μmmol/, $P = 0.001$). Although the concentration of BHA significantly increased at week 4 (baseline: 0.06 ± 0.01 mmol/L *versus* week 4: 0.56 ± 0.13 mmol/L, $P < 0.0001$), it subsequently decreased at the end of study, with its concentration remaining significantly higher than that at baseline (baseline: 0.06 ± 0.01 mmol/L *versus* week 8: 0.24 ± 0.07 mmol/L, $P = 0.004$). As concerned with renal

Table 1: Effects of anthropometric and biochemical parameters in obese subjects after a VLCD intervention.

	Baseline	Week 4	Week 8	Change from baseline to Week 8	P
Weight, Kg	96.1 ± 2.7	90.1 ± 2.6*	87.4 ± 2.5*	−8.7 ± 0.6	<0.0001
BMI, Kg/m^2	32.6 ± 0.6	30.6 ± 0.6*	29.7 ± 0.6*	−3.0 ± 0.2	<0.0001
Waist, cm	104.5 ± 1.7	100.7 ± 1.5*	98.6 ± 1.4*	−5.9 ± 1.2	<0.0001
SBP, mmHg	135.2 ± 2.8	124.1 ± 2.0*	121.7 ± 2.0*	−13.1 ± 2.8	<0.0001
DBP, mmHg	82.7 ± 1.7	76.7 ± 1.5*	73.9 ± 1.6*	−8.2 ± 1.6	<0.0001
ALT, U/L	42.9 ± 5.1	31.6 ± 3.5*	22.3 ± 1.6*	−20.6 ± 5.2	0.002
AST, U/L	26.2 ± 1.9	23.0 ± 1.5**	20.3 ± 1.5*	−6.0 ± 1.7	0.001
γ-GT, U/L	55.1 ± 6.5	27.2 ± 2.4*	27.8 ± 3.5*	−30.4 ± 6.3	<0.0001
Serum uric acid, μmol/L	395.1 ± 13.5	382.5 ± 14.2	369.2 ± 17.0**	−26.1 ± 10.0	0.035
UACR, μg/mg	8.7 ± 1.0	7.5 ± 0.9	7.1 ± 0.7	−1.9 ± 0.9	0.059
TC, mmol/L	5.12 ± 0.12	4.60 ± 0.13*	4.79 ± 0.14*	−0.37 ± 0.14	<0.0001
TG, mmol/L	1.98 ± 0.23	1.11 ± 0.10*	1.08 ± 0.09*	−0.98 ± 0.23	<0.0001
HDL, mmol/L	1.15 ± 0.04	1.09 ± 0.03**	1.19 ± 0.04	0.02 ± 0.03	0.01
LDL, mmol/L	3.09 ± 0.12	3.01 ± 0.12	3.13 ± 0.13	0.05 ± 0.10	0.407
NEFA, μmmol/L	729.8 ± 34.9	729.3 ± 43.2	574.7 ± 37.0*	−166.2 ± 47.6	0.001
BHA, mmol/L	0.06 ± 0.01	0.56 ± 0.13*	0.24 ± 0.07*	0.15 ± 0.06	0.004

Data are presented as mean ± standard error (SE). BMI: body mass index; SBP: systolic blood pressure; DBP: systolic bold pressure; TC: total cholesterol; TG: triacylglycerol; HDL: high density lipoprotein; LDL: low density lipoprotein; NEFA: non-esterified fatty acid; BHA: β-hydroxybutyric acid; ALT: alanine aminotransferase; AST: aspartate aminotransferase; γ-GT: γ-glutamyl transferase; UACR: urine microalbumin creatinine ratio. P: changes of sequential data within experiments from baseline to week 8. Significant difference observed versus baseline: $^*P < 0.001$; $^{**}P < 0.05$.

Table 2: Effects of fat distribution, glucose homeostasis, and insulin sensitivity in obese subjects after a VLCD intervention.

	Baseline	Week 4	Week 8	Change from baseline to week 8	P
SFA, cm^2	348.0 ± 16.7	299.4 ± 16.2	264.0 ± 16.4	−66.5 ± 7.9	<0.0001
VFA, cm^2	113.9 ± 5.8	96.6 ± 4.9	79.8 ± 3.7	−35.3 ± 3.9	<0.0001
Liver fat, %	22.3 ± 2.7	13.5 ± 3.2	6.5 ± 1.4	−16.4 ± 2.4	<0.0001
SMMP, %	33.7 ± 0.9	34.1 ± 1.3	36.7 ± 0.8	1.7 ± 0.2	<0.0001
FMP, %	37.2 ± 1.4	38.9 ± 2.0	34.3 ± 1.3	−3.0 ± 0.4	<0.0001
FPG, mmol/L	5.3 ± 0.1	5.0 ± 0.1	5.2 ± 0.1	−0.07 ± 0.15	0.001
2h PG, mmol/L	7.5 ± 0.3	—	6.9 ± 0.3	−0.59 ± 0.31	0.061
FINS, μU/mL	22.5 ± 4.0	10.2 ± 0.8	11.8 ± 1.4	−11.5 ± 4.3	0.003
2h INS, μU/mL	134.2 ± 11.3	—	71.1 ± 8.2	−57.2 ± 11.3	<0.0001
HOMA IR	6.1 ± 1.5	2.3 ± 0.2	2.8 ± 0.4	−3.6 ± 1.7	0.006
HOMA β	235.7 ± 21.6	140.3 ± 11.4	136.2 ± 12.1	−104.8 ± 18.3	<0.0001
WBISI	67.0 ± 6.9	—	123.7 ± 12.8	54.2 ± 13.9	<0.0001

Data are presented as mean ± standard error (SE). SFA: subcutaneous fat area; VFA: visceral fat area; SMMP: skeletal muscle mass percentage of whole body weight; FMP: fat mass percentage of whole body weight;. FPG: fasting plasma glucose; 2hPG: 2h postprandial glucose; FINS: fasting insulin; WBISI: whole body insulin sensitivity index. P: changes of sequential data within experiments from baseline to week 8. Significant difference observed versus baseline: $^*P < 0.001$; $^{**}P < 0.05$.

function, we observed the serum uric acid level significantly reduced (baseline: 395.1 ± 13.5 μmol/L *versus* week 8: 369.2 ± 17.0 μmol/L, $P = 0.035$), but urine microalbumin creatinine ratio (UACR) did not significantly decrease (baseline: 8.7 ± 1.0 μg/mg *versus* week 8: 7.1 ± 0.7 μg/mg, $P = 0.059$).

3.4. Glucose Homeostasis and Insulin Sensitivity. As shown in Table 2, significant reductions in fasting plasma glucose (FPG), fasting insulin (FINS), and 2 h postprandial insulin (2hINS) were observed (all P values < 0.01). However, the change of 2 h postprandial plasma glucose (2hPG) was not statisticaly significant at the end of the study ($P = 0.061$). HOMA IR and HOMA β significantly improved with the reduction of −3.6 ± 1.7 and −104.8 ± 18.3 (all P values < 0.0001), respectively. WBISI significantly increased from 67.0 ± 6.9 to 123.7 ± 12.8 ($P < 0.0001$). Moreover, as shown in Figure 2, FINS, 2hINS, HOMA IR, HOMA β, and WBISI

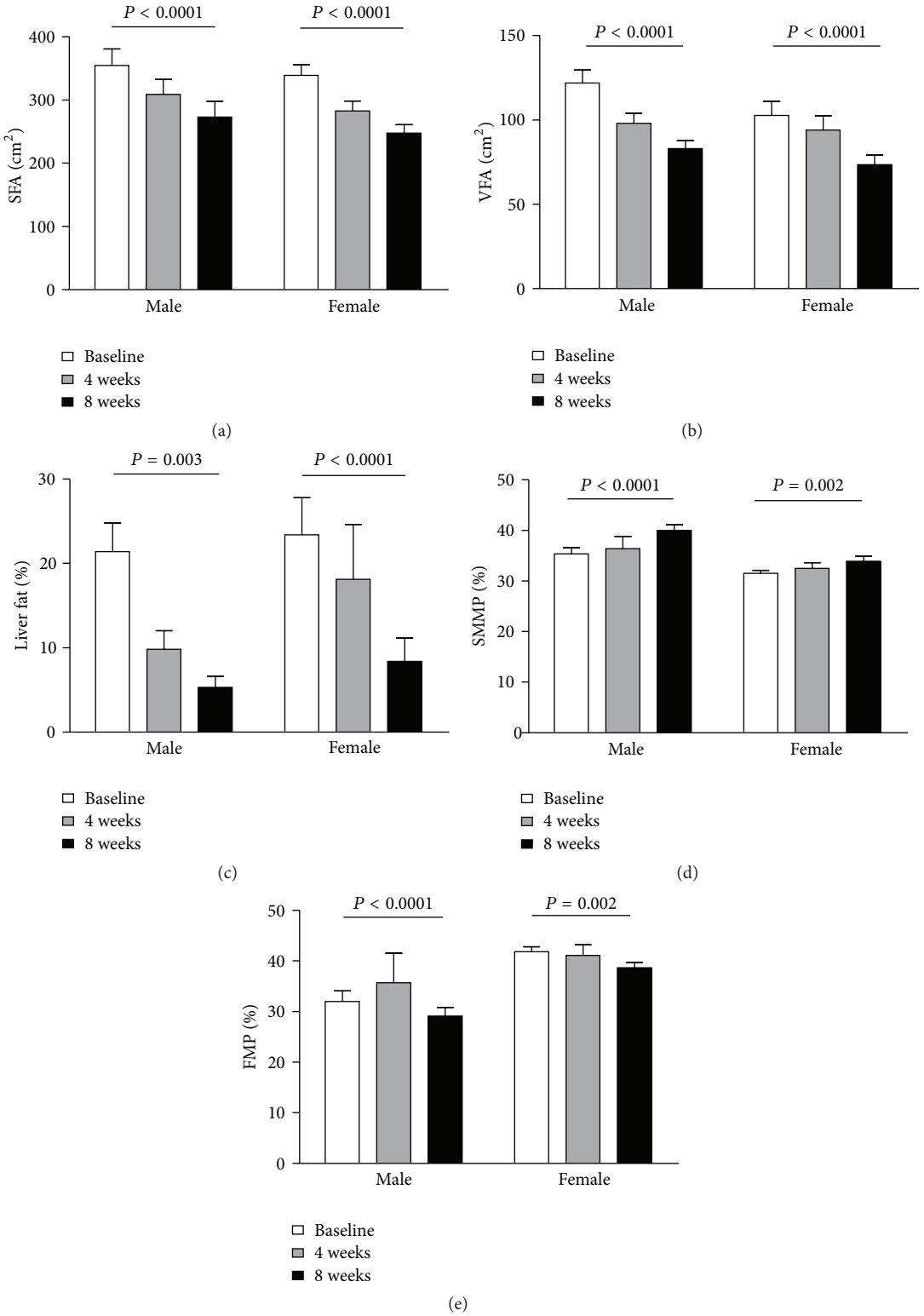

Figure 1: Improvement of body fat composition after an 8-week VLCD intervention. SFA: subcutaneous fat area; VFA: visceral fat area; SMMP: skeletal muscle mass percentage of whole body weight; VMP: fat mass percentage of whole body weight.

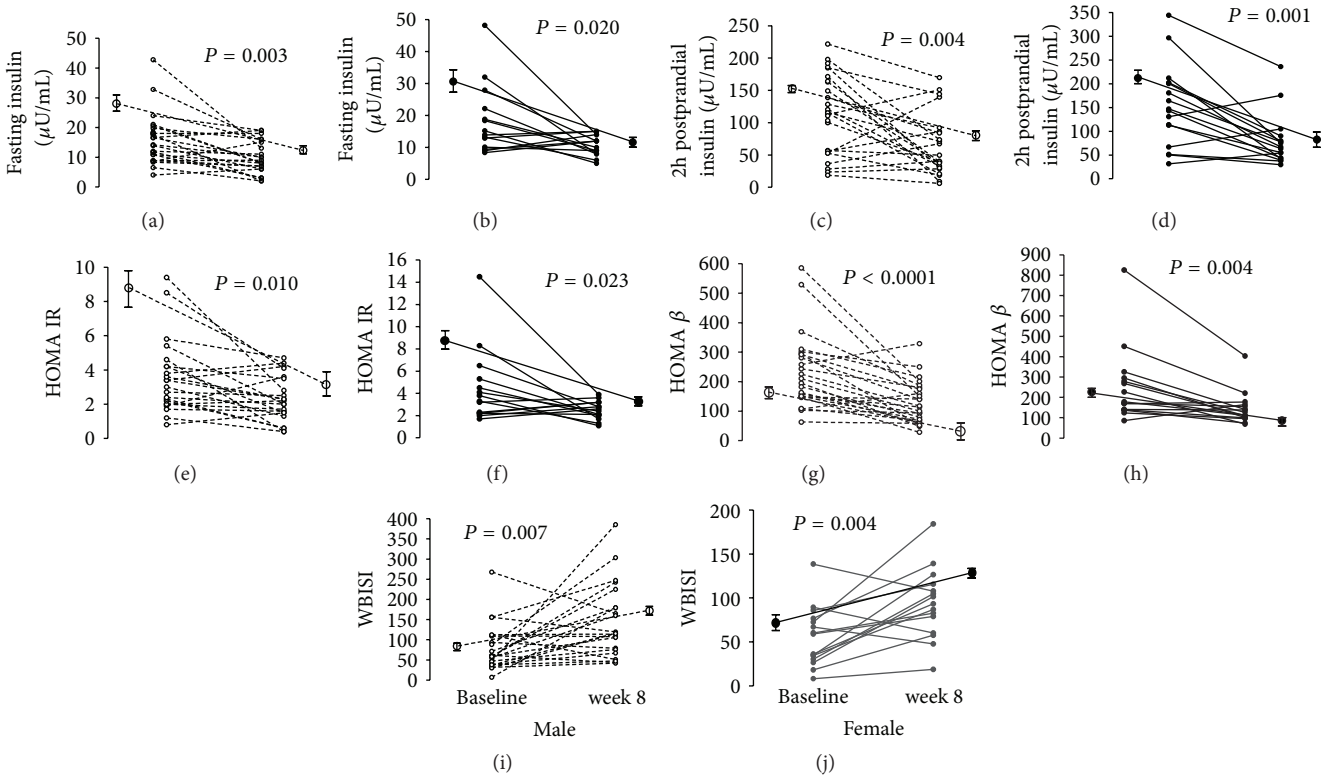

Figure 2: Changes of insulin resistance and sensitivity in male and female after 8 weeks of VLCD intervention. Solid lines represent the changes in male and dashed lines represent the changes in female.

were all improved in both male and female subjects (all P values < 0.05).

4. Discussion

The major finding in the present study was that an 8-week VLCD intervention induced a significant weight loss with reduction of abdominal subcutaneous and visceral fat mass. This hypocarbohydrate dietary also had significant effects on liver fat content reduction and improvements of metabolic parameters and insulin responsiveness. These observations suggested that a VLCD diet intake resulted in a lower insulin/glucagon ratio, which enhanced adipose tissue lipolysis and oxidation with a subsequent promotion of liver ketone bodies production for energy needs [15].

In our study, we only observed a significant reduction of NEFA at week 8. As a product of fat lipolysis and oxidation, BHA was in its peak level in week 4 and subsequently decreased in week 8, with its concentration remaining significantly higher than that at baseline. Recently, a study reports that NEFA significantly increased in the first 7 days but decreased in week 8 in diabetic patients who participated in an 8-week VLCD intervention [16]. Therefore, we tentatively suppose that in our study, there might also exist a similar peak of NEFA caused by lipolysis at week 1 which we did not observe. Considering the changes of NEFA and BHA together, the two level curves might reflect the process of fat burning during the 8-week period.

It has long been presumed that weight loss after VLCD was associated with water loss [17] until Volek et al. applied dual-energy X-ray absorptiometry to examine the change of body composition in subjects who switched from their habitual diet (48% carbohydrate, 32% fat) to a VLCD (8% carbohydrate, 61% fat) for 6 weeks [18]. They surprisingly found that fat mass significantly decreased and lean body mass significantly increased, despite no change in physical activity. Our results were similar to their findings that SMMP significantly increased and FMP significantly decreased at the end of the dietary intervention. It was suggested that water may account for some of the initial rapid weight loss, but fat loss subsequently accelerated and lean tissue was preserved over a longer period, which may be the main cause of weight loss [19].

After the 8-week dietary intervention, with the LFP significantly decreasing, half of the obese subjects with NAFLD had a reversal. Meanwhile, significant improvements of ALT, AST, and γ-GT were observed. Additionally, significant reduction of TC and TG and increment of HDL may have beneficial effects on the prevention of cardiovascular disease.

Several intervention studies and meta-analyses, varying in length from days to months have explored the impacts of VLCD diet on β cell function and insulin sensitivity [2, 4, 20, 21]. Most of the studies found that insulin sensitivity improved together with weight loss. In the present study, we found the similarities that HOMA IR, HOMA β, and WBISI were all significantly improved. There were several

mechanisms involved in the amelioration of β cell function and insulin sensitivity. One of the major hypothesis was that the reduction of triacylglycerol stores in pancreas and liver contributed to the normalization of β cell function [16]. Furthermore, decreasing of triacylglycerol in skeletal muscle may be another cause of hepatic resistance alleviation [22]. However, the results from several studies demonstrated that insulin sensitivity did not alter after a short-term VLCD intervention for 5–7 days [4, 23]. It might be a too short intervention period to detect the changes in insulin sensitivity [23].

In order to observe whether the effects of a VLCD were similar in different gender, we further analysed the body composition and insulin sensitivity in male and female, respectively. The results presented a similar beneficial effects in both genders.

The present study has some limitations. Firstly, we did not measure the metabolic parameters at the first week which may contribute to interpret the acute effect of VLCD. Secondly, for the lacking measurement of intramuscular triacylglycerol content, the relation between the change of it and improvement of insulin sensitivity was unclear. Finally, being a short-term designed study, the evidence of the longer effects of VLCD was unclear. So longer-term and further studies are needed to be designed to investigate the effects and to reveal the underlying mechanisms of VLCD in the future.

In conclusion, in both male and female, rapid weight reduction induced by an 8-week VLCD intervention effectively decreased total abdominal subcutaneous and visceral adipose tissue compartments, and liver fat content, increased skeletal muscle percentage of whole body weight, improved metabolic profile, and insulin resistance and sensitivity. All these beneficial effects might have been due to enhanced hepatic and whole-body lipolysis and oxidation.

Authors' Contribution

Y. Gu and H. Yu contributed equally to this paper.

Acknowledgments

This study was supported by grants from national 973 program (2011CB504001), specific research fund from Ministry of Health (201002002), and national science and technology major project: significant creation of new drugs (2011zx09307-001-02). This study was funded in part by Nutriease Health Technology Co., Ltd.

References

[1] World Health Organization, "Diet, nutrition and the prevention of chronic diseases," Joint WHO/FAO Expert Consultation, WHO Technical Report Series no 916, WHO, Geneva, Switzerland, 2003.

[2] M. E. Frigolet, V. E. R. Barragan, and M. T. Gonzalez, "Low-carbohydrate diets: a matter of love or hate," *Annals of Nutrition and Metabolism*, vol. 58, no. 4, pp. 320–334, 2011.

[3] P. F. Svendsen, F. K. Jensen, J. J. Holst, S. B. Haugaard, L. Nilas, and S. Madsbad, "The effect of a very low calorie diet on insulin sensitivity, beta cell function, insulin clearance, incretin hormone secretion, androgen levels and body composition in obese young women," *Scandinavian Journal of Clinical and Laboratory Investigation*, vol. 72, no. 5, pp. 410–419, 2012.

[4] I. Malandrucco, P. Pasqualetti, I. Giordani et al., "Very-low-calorie diet: a quick therapeutic tool to improve beta cell function in morbidly obese patients with type 2 diabetes," *The American Journal of Clinical Nutrition*, vol. 95, no. 3, pp. 609–613, 2012.

[5] A. P. M. Viljanen, R. Lautamäki, M. Järvisalo et al., "Effects of weight loss on visceral and abdominal subcutaneous adipose tissue blood-flow and insulin-mediated glucose uptake in healthy obese subjects," *Annals of Medicine*, vol. 41, no. 2, pp. 152–160, 2009.

[6] Y. Ahn, S. J. Park, H. K. Kwack, M. K. Kim, K. P. Ko, and S. S. Kim, "Rice-eating pattern and the risk of metabolic syndrome especially waist circumference in Korean genome and epidemiology study (KoGES)," *BMC Public Health*, vol. 13, no. 1, article 61, 2013.

[7] E. Völgyi, F. A. Tylavsky, A. Lyytikäinen, H. Suominen, M. Alén, and S. Cheng, "Assessing body composition with DXA and bioimpedance: effects of obesity, physical activity, and age," *Obesity*, vol. 16, no. 3, pp. 700–705, 2008.

[8] M. F. Xia, H. M. Yan, H. D. Lin et al., "Elevation of liver enzymes within the normal limits and metabolic syndrome," *Clinical and Experimental Pharmacology and Physiology*, vol. 38, no. 6, pp. 373–379, 2011.

[9] L. S. Szczepaniak, P. Nurenberg, D. Leonard et al., "Magnetic resonance spectroscopy to measure hepatic triglyceride content: prevalence of hepatic steatosis in the general population," *The American Journal of Physiology*, vol. 288, no. 2, pp. E462–E468, 2005.

[10] B. Chowdhury, L. Sjostrom, M. Alpsten, J. Kostanty, H. Kvist, and R. Lofgren, "A multicompartment body composition technique based on computerized tomography," *International Journal of Obesity*, vol. 18, no. 4, pp. 219–234, 1994.

[11] M. R. Hoenig, G. Cowin, R. Buckley, C. McHenery, and A. Coulthard, "Liver fat percent is associated with metabolic risk factors and the metabolic syndrome in a high-risk vascular cohort," *Nutrition and Metabolism*, vol. 7, article 50, 2010.

[12] D. R. Matthews, J. P. Hosker, and A. S. Rudenski, "Homeostasis model assessment: insulin resistance and β-cell function from fasting plasma glucose and insulin concentrations in man," *Diabetologia*, vol. 28, no. 7, pp. 412–419, 1985.

[13] M. Fukushima, A. Taniguchi, M. Sakai et al., "Homeostasis model assessment as a clinical index of insulin resistance: comparison with the minimal model analysis," *Diabetes Care*, vol. 22, no. 11, pp. 1911–1912, 1999.

[14] M. Matsuda, Y. Liu, S. Mahankali et al., "Altered hypothalamic function in response to glucose ingestion in obese humans," *Diabetes*, vol. 48, no. 9, pp. 1801–1806, 1999.

[15] A. Adam-Perrot, P. Clifton, and F. Brouns, "Low-carbohydrate diets: nutritional and physiological aspects," *Obesity Reviews*, vol. 7, no. 1, pp. 49–58, 2006.

[16] E. L. Lim, K. G. Hollingsworth, B. S. Aribisala, M. J. Chen, J. C. Mathers, and R. Taylor, "Reversal of type 2 diabetes: normalisation of beta cell function in association with decreased pancreas and liver triacylglycerol," *Diabetologia*, vol. 54, no. 10, pp. 2506–2514, 2011.

[17] G. L. Blackburn, J. C. C. Phillips, and S. Morreale, "Physician's guide to popular low-carbohydrate weight-loss diets," *Cleveland Clinic Journal of Medicine*, vol. 68, no. 9, pp. 761–774, 2001.

[18] J. S. Volek, M. J. Sharman, D. M. Love et al., "Body composition and hormonal responses to a carbohydrate-restricted diet," *Metabolism*, vol. 51, no. 7, pp. 864–870, 2002.

[19] J. S. Volek and E. C. Westman, "Very-low-carbohydrate weight-loss diets revisited," *Cleveland Clinic Journal of Medicine*, vol. 69, no. 11, pp. 849–858, 2002.

[20] G. D. Foster, H. R. Wyatt, J. O. Hill et al., "A randomized trial of a low-carbohydrate diet for obesity," *The New England Journal of Medicine*, vol. 348, no. 21, pp. 2082–2090, 2003.

[21] I. Shai, D. Schwarzfuchs, Y. Henkin et al., "Weight loss with a low-carbohydrate, Mediterranean, or low-fat diet," *The New England Journal of Medicine*, vol. 359, no. 3, pp. 229–241, 2008.

[22] L. G. Grunnet, E. Laurila, O. Hansson et al., "The triglyceride content in skeletal muscle is associated with hepatic but not peripheral insulin resistance in elderly twins," *Journal of Clinical Endocrinology and Metabolism*, vol. 97, no. 12, pp. 4571–4577, 2012.

[23] C. C. Wang, R. L. Adochio, J. W. Leitner, I. M. Abeyta, B. Draznin, and M. A. Cornier, "Acute effects of different diet compositions on skeletal muscle insulin signalling in obese individuals during caloric restriction," *Metabolism*, 2012.

Hindawi Publishing Corporation
Evidence-Based Complementary and Alternative Medicine
Volume 2013, Article ID 647452, 10 pages
http://dx.doi.org/10.1155/2013/647452

Research Article

A Metabolomics Profiling Study in Hand-Foot-and-Mouth Disease and Modulated Pathways of Clinical Intervention Using Liquid Chromatography/Quadrupole Time-of-Flight Mass Spectrometry

Cheng Lu,[1] Xinru Liu,[2] Xiaorong Ding,[1] Xiao Chen,[3] Haiwei Fan,[3] Yunqiang Liu,[3] Ning Xie,[3] Yong Tan,[1] Joshua Ko,[4] Weidong Zhang,[2] and Aiping Lu[1,4]

[1] *Institute of Basic Research in Clinical Medicine, China Academy of Chinese Medical Science, Beijing 100700, China*
[2] *Department of Medicinal Chemistry of Nature Product, School of Pharmacy, Second Military Medical University, Shanghai 200433, China*
[3] *Jiangxi Qingfeng Pharmaceutical Inc., Ganzhou 341000, China*
[4] *School of Chinese Medicine, Hong Kong Baptist University, Kowloon Tong, Hong Kong*

Correspondence should be addressed to Weidong Zhang; wdzhangy@hotmail.com and Aiping Lu; lap64067611@126.com

Received 12 November 2012; Revised 23 December 2012; Accepted 28 December 2012

Academic Editor: Wei Jia

Hand-foot-and-mouth disease (HFMD), with poorly understood pathogenesis, has become a major public health threat across Asia Pacific. In order to characterize the metabolic changes of HFMD and to unravel the regulatory role of clinical intervention, we have performed a metabolomics approach in a clinical trial. In this study, metabolites profiling was performed by liquid chromatography/quadrupole time-of-flight mass spectrometry (LC-Q-TOF-MS) platform from the HFMD clinical patient samples. The outcome of this study suggested that 31 endogenous metabolites were mainly involved and showed marked perturbation in HFMD patients. In addition, combination therapy intervention showed normalized tendency in HFMD patients in differential pathway. Taken together, these results indicate that metabolomics approach can be used as a complementary tool for the detection and the study of the etiology of HFMD.

1. Introduction

Hand-foot-and-mouth disease (HFMD), being caused by a group of enteric viruses including enterovirus 71 (EV71), coxsackievirus A16 (CVA16), and coxsackievirus A10 (CVA10), is currently a serious epidemic in China [1]. HFMD is a common, mild, and self-limiting rash-associated illness in children under the age of 6 but could lead to mortality in large-scale outbreaks. Since first being described in California in 1969, there have been many reports on large EV71 outbreaks all over the world. Generally, severe cases of HFMD were associated with severe neurologic disorders like acute flaccid paralysis, pulmonary edema, myocarditis, and fatal encephalitis [2]. HFMD has already been emerged as an imperative global hazard, not only threatening the health of the children, but also causing tremendous loss and burden to both families and society.

Despite substantial progress that has been made in understanding many aspects of the biology and pathogenesis of HFMD, continuous search for new and more effective agents against HFMD has never been relented as the appropriate vaccines and antiviral drugs remain unavailable [3]. At the present moment, there is still no effective treatment that can work against the disease clinically [4]. Hence, Traditional Chinese Medicine (TCM) that has been proven as excellent alternative remedy against viral infection [5] could be a potential HFMD treatment option. More researches have shown that TCM plays a crucial role in improving the disease progression of HFMD over the past few decades [6]. In addition, extracts of Chinese medicines such as kappa

carrageenan [3], geraniin [4], and Kalanchoe gracilis [7] have exerted strong and effective anti-EV71 and anti-CVA16 activities both *in vitro* and *in vivo*. However, since the exact pathogenesis of HFMD and the complex components of effective TCM remain unclear, it is hard to fully understand the mechanism of TCM action in the human body. Thus, the establishment of a more efficient and reliable method to evaluate the remedial effects of TCM on HFMD intervention will be of imminent importance.

The metabolomic approach has focused on studying the endogenous metabolites with low molecular weight in the biological samples. According to our knowledge, the small molecular-sized endogenous metabolites play an important role in the physiological system and represent attractive candidates for better understanding of biological phenotypes [8]. Metabolomics is a newly emerging field in analytical biochemistry other than genomics and proteomics and can be regarded as the endpoint of the "omics" cascade [9]. It aims to characterize and quantify all small metabolites that are related to drug toxicity, disease progression, environmental stimuli, and genetic variations by using nuclear magnetic resonance (NMR) spectroscopy or mass spectrometry (MS) [10]. Several studies have described the metabolomics-based research on TCM, for instance, in our laboratory when investigating pattern differentiation [11, 12] and pharmacological mechanisms [13] and in other laboratories performing quality control of Chinese herbs [14]. As metabolomics can readily detect subtle changes in the metabolic network, it is uniquely poised to increase our understanding of HFMD and the related intervention methods.

In the present study based on the liquid chromatography/quadrupole time-of-flight mass spectrometry (LC-Q-TOF-MS) platform, we investigated the serum metabolic characteristics of HFMD to gain more insight of the metabolic perturbations associated with the disease for the first time. Besides, the potential therapeutic effects and the underlying mechanisms were also explored.

2. Materials and Methods

2.1. Chemicals. LC-MS grade acetonitrile and methanol was purchased from Honeywell Burdick and Jackson (Muskegon, USA). Mass Spectroscopic grade formic acid was purchased from Fluka (Buchs, Switzerland). Distilled water was purified "in-house" using a Milli-Q20 system (Millipore; MA, USA). All metabolites standards were obtained from Sigma-Aldrich (MO, USA).

2.2. Sample Collection and Preparation. Eighteen severe patients with clinical symptoms of HFMD were recruited if they met the Guideline for the Diagnosis and Treatment of HFMD in China (Ministry of Health, 2010) [15] from Beijing YouAn Hospital (China) during September and October, 2010. Additional inclusion criteria were ages 1–13 years and no more than 24 hours after the occurrence of central nervous system symptoms, with any of the following: lethargy and weakness, agitation or irritability, headache, vomiting, limb weakness or acute flaccid paralysis, myoclonic jerks, ataxia, nystagmus, or oculomotor palsies. Patients who have been suffering from neurogenic pulmonary edema or heart or respiratory failure were excluded. All patients were identified as EV71-positive by a diagnostic kit (RT-PCR double Fluorescence Taqman probes, Da An Gene Company Limited, China). The patients were then assigned to combination therapy (with combination of conventional Western medicine and Chinese medicine treatments). Conventional Western medicine treatments included mannitol (0.5–1.0 g/kg) administered IV over a period of 30–40 min for every 4–8 h; glucocorticoid methylprednisolone (1-2 mg/kg/24 h); hydrocortisone (3–5 mg/kg/24 h); dexamethasone (0.2–0.5 mg/kg/24 h); intravenous immunoglobulin (IVIG; 2 g/kg) for 2–5 days. Herb derived compound Andrographolide Sulfonate (called Xiyanping injection), approved for clinical use by State Food and Drug Administration (China), is recommended for the treatment of HFMD. Xiyanping injection was administered as intravenous infusion (5–10 mg/kg/day; in 5% dextrose). The Xiyanping injection used in our study appeared as light yellow to orange clear liquid, which is composed of total andrographolide sulfonate, and manufactured by Jiangxi Qingfeng Pharmaceutical Inc. (GMP certificated). The criteria for the quality of injection procedures were in accordance with the Chinese pharmacopoeia (2010) [16]. The Xiyanping injection treatment was given in combination with conventional Western medicine cocktail for 7–10 days. The average hospital stay of these children was 7.6 days. Venous blood samples were collected in the morning preprandially from HFMD patients (before and 7 days after drug treatment) and age-matched healthy control subjects ($n = 18$). Between HFMD patient and health control group, the difference of age was not significant ($P = 0.628$, t test, Table 1). An Institutional Review Board had approved the previous research protocols on human subjects based on ethical and safety considerations prior to the commencement of the study and all participants had provided their informed consent in writing. One hundred μL of the collected serum sample was added to 300 μL methanol, and the mixture was vortexed vigorously for 30 s. After centrifugation at 9562.5 ×g for 10 min at 4°C, the supernatant was stored at −80°C until analysis [17].

Table 1: Basic feature of HFMD group and healthy control group.

Group	Number (n)	Gender (n)		Age (month)[a]
		Male	Female	
Healthy control	18	13	5	27.1 ± 10.9
HFMD	18	11	7	28.9 ± 11.6

[a] Data are expressed as mean ± SD.

2.3. LC-Q-TOF-MS Analysis. The LC-Q-TOF-MS analysis was performed by using an Agilent-1200 LC system, which was coupled with an electrospray ionization (ESI) source (Agilent Technologies, Palo Alto, CA, USA) and an Agilent-6520 Q-TOF mass spectrometry. The separation of all samples was performed on an Eclipse plus C18 column (1.8 μm, 2.1 mm × 100 mm, Agilent) with a column temperature being set at 45°C. The flow rate was 400 μL/min, and the mobile

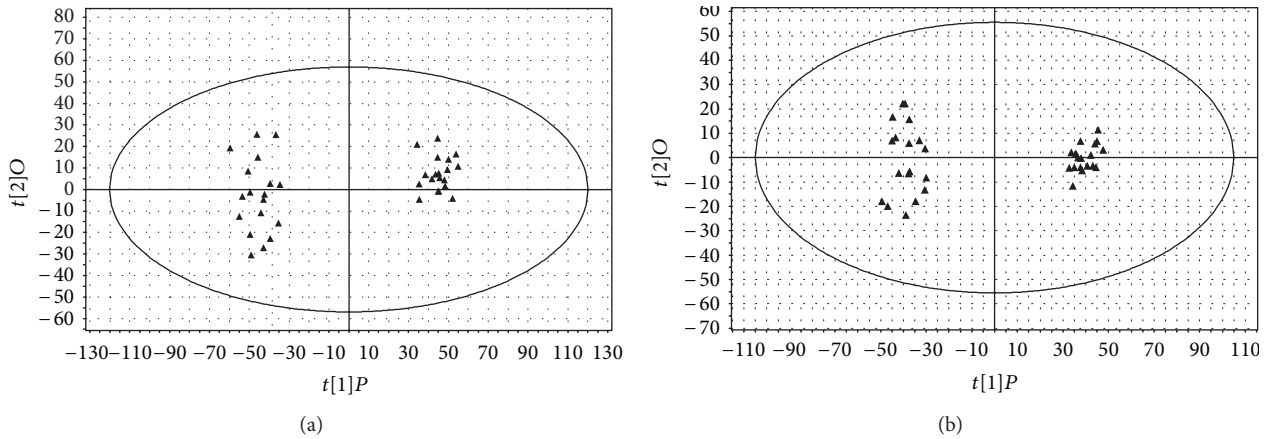

Figure 1: OPLS score of healthy control group and HFMD group. The score plot showed that levels of markers in serum of healthy control and HFMD patients were different. (a) Positive ion mode ($k = 11001$, $n = 36$, $R^2Y = 0.985$, $R^2X = 0.321$, $Q^2 = 0.947$, $A = 1 + 1$). (b) Negative ion mode ($k = 11700$, $n = 36$, $R^2Y = 0.986$, $R^2X = 0.263$, $Q^2 = 0.931$, $A = 1 + 1$). Each point represents an individual sample. (Left side, ▲) Samples from HFMD patients. (Right side, ▲) Samples from healthy controls.

phase consisted of ultrapure water with 0.1% formic acid (A) and acetonitrile (B). The following gradient program was used: 0-1 min, 2% B; 1–3 min, 2–20% B; 3–6 min, 20–30% B; 6–11 min, 30–85% B; 11–18 min, washed with 100% B and followed by a reequilibration step of 6 min. The sample injection volume was 2 μL. Mass detection was operated in both positive and negative ion modes with the following setting: drying gas (N_2) flow rate, 8 L/min; gas temperature, 330°C; pressure of nebulizer gas, 35 psig; Vcap, 4100 V (positive mode) and 3900 V (negative mode); fragmentor, 130 V; skimmer, 65 V; scan range, m/z 80–1000. MS/MS analysis was acquired under targeted MS/MS mode with collision energy from 10 to 40 V.

2.4. Sequence of Analysis. The pooled QC sample was analyzed at the beginning, the end, and randomly through the analytical run to monitor the stability of sequence analysis. The typical batch sequence of serum samples consisted of the consecutive analysis of 1 QC serum sample (at the beginning of the study), followed by 6 unknown serum samples, 1 QC serum sample, before running another 6 unknown serum samples, and so forth. Meanwhile, samples were analyzed in a random order for a normal good practice. An identical sequence was repeated to complete the total set of injections ($n = 64$, including QCs) analyzed in less than 1 day per mode [18].

2.5. Data Analysis. The LC-MS raw data were exported and analyzed by the Agilent Mass Hunter Qualitative Analysis Software (Agilent Technologies, Palo Alto, CA, USA). Before undergoing multivariate analysis, each data was normalized by the total area to correct for the MS response shift due to the long duration between first and last injections. After this modulation, the sum of the ion peak areas within each sample was set to 10,000. Partial least squares discriminant analysis (PLS-DA) and orthogonal partial least square (OPLS) were used for analysis of metabolite profiles. Multivariate analysis was performed by the SIMCA-P software (11th version; Umetrics AB, Umeå, Sweden). Variable importance projection (VIP) was used to select differential metabolites responsible for the intergroup discrimination of each model. Statistical significance was determined by the one-way analysis of variance (ANOVA) using SPSS 13.0 for Windows (SPSS Inc., Chicago, IL, USA), followed by Duncan post hoc tests. P values less than 0.05 were considered significant. We obtained information about prediction of candidate metabolites corresponding with these significant m/z values by searching the biofluid metabolites database. Then, the differential RT-m/z pairs were identified between two groups by matching with tandem MS fragmentation patterns with reference standards. Relationships between differentially expressed metabolites were investigated in pathway analysis using the Ingenuity Pathway Analysis (IPA) software (Ingenuity, Redwood City, CA).

3. Results

3.1. Sample Repeatability. Extracts from six aliquots of a random blood sample were continuously injected to evaluate the repeatability. Five common extracted ion chromatograms (EICs) shared by these injections were selected according to their different chemical polarities and m/z values. The relative standard derivations (RSDs) of these peaks were 3.29%–14.54% for peak areas and 0.03%–0.96% for retention times.

3.2. System Stability. The LC-MS system stability for the large-scale sample analysis was demonstrated by the test of pooled QC samples. The principal components analysis (PCA) result shows that QC samples are tight clustered. Moreover, peak areas, retention times, and mass accuracies of five selected EICs in five QC samples also showed good system stability. RSDs of the five peaks were 4.74%–14.18% for peak areas, 0.02%–0.98% for retention times, and $0.10E{-}04\%$–$0.79E{-}04\%$ for mass accuracies. The result

Table 2: Identified markers between healthy control and HFMD.

Mode	R.T (min)	Exact mass	Formula	Compound (Resource)	Significance/fold change		
					G2 versus G1	G3 versus G2	G3 versus G1
ESI (+)	1.8	145.1103	$C_7H_{15}NO_2$	Acetylcholine (HMDB)	**/ 1.48	**/ 0.65	**/ 0.77
	2.5	202.1205	$C_{10}H_{18}O_4$	Sebacic acid (HMDB)	**/ 1.58	**/ 0.67	N.S
	2.6	90.0317	$C_3H_6O_3$	Lactic acid (HMDB)	**/ 13.4	N.S	**/ 13.4
	3.6	258.0141	$C_6H_{11}O_9P$	2-Keto-3-deoxy-6-phosphogluconic acid (HMDB)	**/ 5.55	**/ 0.12	N.S
	3.7	247.0246	$C_8H_{10}NO_6P$	Pyridoxal phosphate (HMDB)	**/ 5.23	**/ 0.31	N.S
	6.0	219.1107	$C_9H_{17}NO_5$	D-Pantothenic acid (HMDB)	**/ 0.47	**/ 2.28	N.S
	6.2	138.0429	$C_6H_6N_2O_2$	Urocanic acid (HMDB)	**/ ∞	N.S	**/ ∞
	10.1	180.0634	$C_6H_{12}O_6$	beta-D-Glucose (HMDB)	**/ 0.38	N.S	**/ 0.37
	13.7	519.3325	$C_{26}H_{50}NO_7P$	1-18:2(9Z,12Z) Lysophosphatidylcholine (HMDB)	**/ 0.49	**/ 1.84	N.S
	12.71	169.0504	$C_4H_{12}NO_4P$	Phosphorylcholine (HMDB)	**/ 0.13	**/ 5.98	N.S
	12.72	250.1205	$C_{14}H_{18}O_4$	Ubiquinone (HMDB)	**/ 0.27	**/ 0.22	**/ 0.06
	14.1	671.489	$C_{37}H_{70}NO_7P$	Phosphatidylethanolamine (KEGG)	**/ 0	N.S	**/ 0
	14.3	714.5223	$C_{47}H_{70}O_5$	Diacylglycerol (HMDB)	**/ 0	N.S	**/ 0
	14.7	571.3638	$C_{30}H_{54}NO_7P$	1-Acyl-sn-glycerol-3-phosphocholine (HMDB)	**/ 2.02	*/ 0.88	*/ 1.78
	16.4	103.0997	$C_5H_{13}NO$	Choline (HMDB)	**/ 1.69	**/ 0.69	*/ 1.17
	17.8	522.3604	$C_{28}H_{50}N_4O_3S$	Oleic acid (HMDB)	**/ 0	N.S	**/ 0
ESI (−)	1.5	146.1055	$C_6H_{14}N_2O_2$	L-Lysine (HMDB)	**/ 1.56	**/ 1.48	**/ 2.02
	1.6	336.0484	$C_{11}H_{15}NO_9P$	Nicotinate D-ribonucleotide (HMDB)	**/ 2.58	N.S	**/ 2.73
	1.8	131.0695	$C_4H_9N_3O_2$	Creatine (HMDB)	**/ 0.43	**/ 2.08	N.S
	2.1	119.0582	$C_4H_9NO_3$	L-Threonine (HMDB)	**/ 0.46	**/ 2.07	N.S
	4.28	366.0577	$C_{10}H_{15}N_4O_9P$	FAICAR (ChemSpider)	**/ 16.24	**/ 0.04	N.S
	4.29	104.0473	$C_4H_8O_3$	(S)-3-Hydroxy-2-methylpropanoic acid (HMDB)	**/ 1.77	**/ 0.54	N.S
	5.4	165.0426	$C_8H_7NO_3$	2-(Formylamino)-benzoic acid (HMDB)	*/ 2.08	**/ 0.35	N.S
	5.6	180.0786	$C_{10}H_{12}O_3$	Coniferyl alcohol (HMDB)	**/ ∞	**/ 0	N.S
	6.5	258.1106	$C_8H_{21}NO_6P$	sn-glycero-3-Phosphocholine (HMDB)	**/ 0.26	*/ 7.93	N.S
	8.0	248.1161	$C_{13}H_{16}N_2O_3$	6-Hydroxymelatonin (ChemSpider)	**/ 0.18	*/ 4.25	N.S
	10.0	276.1321	$C_{11}H_{20}N_2O_6$	Saccharopine (HMDB)	**/ ∞	**/ 0.24	**/ ∞
	10.8	324.0359	$C_9H_{13}N_2O_9P$	Pseudouridylic acid (ChemSpider)	**/ ∞	**/ 0	N.S
	12.8	308.041	$C_9H_{13}N_2O_8P$	dUMP (HMDB)	**/ 26.7	**/ 0.1	*/ 46.8
	15.0	364.2613	$C_{22}H_{36}O_4$	Prostaglandin E2 (HMDB)	**/ 2.10	N.S	**/ 1.83
	16.6	226.1933	$C_{14}H_{26}O_2$	9Z-Tetradecenoic acid (HMDB)	**/ 0.49	N.S	**/ 0.47

G1: healthy control group; G2: HFMD group; G3: combination therapy group; HMDB: Human Metabolome Database; KEGG: Kyoto Encyclopedia of Genes and Genomes. (∞: represented denominator is zero; $^{*}P < 0.05$; $^{**}P < 0.01$; N.S: no significance).

indicated that large-scale sample analysis had hardly any effect on the reliability of data.

3.3. Metabolic Comparison Based on OPLS between HFMD and Healthy Control. The difference between HFMD group (patients prior to drug treatment) and healthy control group is our initial focus in this study. To maximize the difference of their metabolic profiles, a sophisticated orthogonal partial least squares projection to latent analysis (OPLS) model was applied. OPLS is a supervised method to pick out discriminating ions [19] that are contributing to the classification of samples and would remove noncorrelated variations contained within spectra [18]. Thus, OPLS was carried out to identify candidate metabolites of HFMD in this study. The OPLS models were validated in the SIMCA-P software by a default 7-round cross-validation procedure with exclusion of 1/7th of the samples from the model in each round in order to avoid the modeling overfitting caused by supervised mathematical methods [20]. The first two components were used in the OPLS model. As shown in Figures 1(a) and 1(b), there was a distinguishable classification between the clustering of HFMD group and healthy

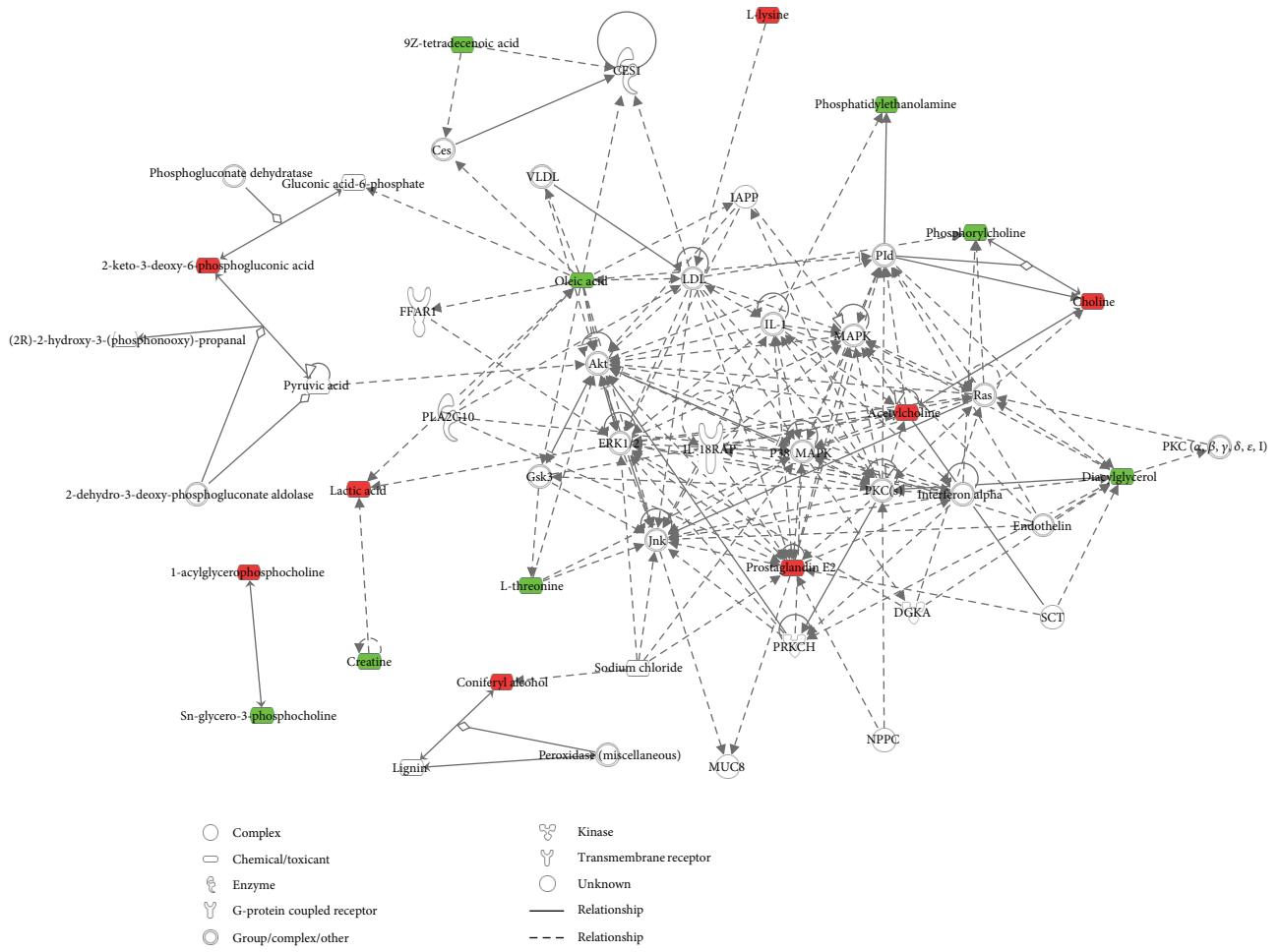

Figure 2: Top five significant molecular networks of HFMD related metabolites merged by IPA. Metabolites are represented as nodes, and the biological relationship between two nodes is represented as a line. Note that the colored symbols represent metabolites that occur in our data, while the transparent entries are molecules from the Ingenuity Knowledge Database. Red symbols represent upregulated metabolites in HFMD patients; green symbols represent downregulated metabolites in HFMD patients. Solid lines between molecules indicate direct physical relationship between molecules; dotted lines indicate indirect functional relationships.

control group. Q^2Y and R^2Y in the OPLS models indicated that the class prediction ability of all models was high, and there was a clear difference being observed between HFMD group and healthy control group. We searched for the presumed molecular formula in the Human Metabolome Database, ChemSpider, KEGG, and some other databases to confirm possible chemical composition. According to the results, a total of the top significant 200 variables (sum of variables detected in both positive mode and negative mode) contributed to the classification of the control, and HFMD groups were selected. Furthermore, among these perturbed variables, 31 endogenous metabolites (16 in positive and 15 in negative) had been identified (Table 2).

3.4. The Network of Identified Metabolites between HFMD Group and Healthy Control Group. Among the 31 identified metabolites, 13 were downregulated in the serum of HFMD patients, while the other 18 were upregulated (Table 2). In order to further understand the correlation between these candidate metabolites, bioinformatics analyses were performed using the IPA software, and these analyses led to the identification of biological association networks. As shown in Figure 2, it was found that most of the differential metabolites were tightly connected with each other. The established networking functions of HFMD include lipid metabolism, molecular transport, cell signaling, drug metabolism, and small molecule biochemistry, of which all play important roles in the development of HFMD. Meanwhile, the IPA software represented five top canonical pathways, including phospholipases, renin-angiotensin signaling, choline biosynthesis III, phosphatidylcholine biosynthesis I, and TREM1 signaling (Figure 2).

3.5. Metabolic Profiling Comparison Based on PLS among Healthy Control, HFMD, and Combination Therapy Groups. In order to determine whether the serum metabolome represented in this study could be used to discriminate among different groups, partial least squares discriminant analysis

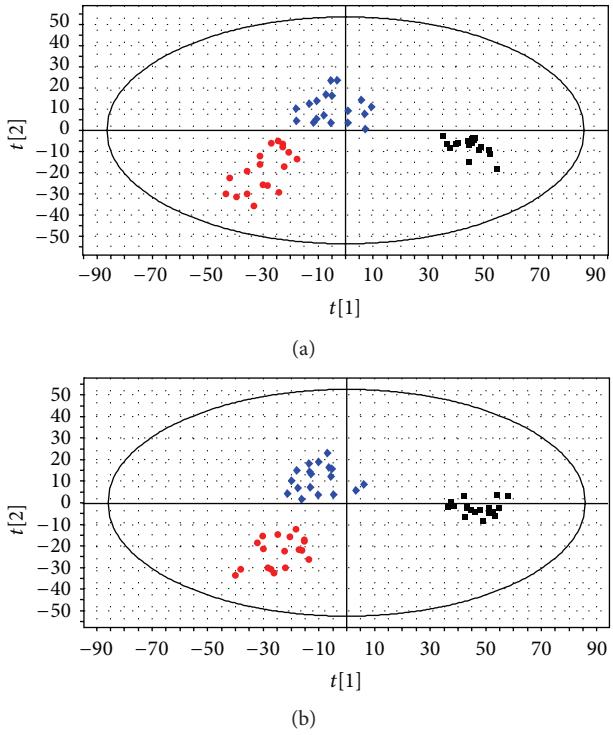

Figure 3: PLS-DA score plots based on the data from the healthy controls and the HFMD patients. (a) PLS-DA score plots under positive ESI ion mode. (b) PLS-DA score plots under negative ESI ion mode. The black square: healthy control group; the red circle: HFMD group; the blue diamond: combination therapy group.

(PLS-DA), a well-established supervised method that has been widely used in metabolomic study [21], was adopted so as to specify the metabolic variations associated with the disease and drug intervention. The first two components were used in the PLS-DA model. As shown in Figure 3, there was a distinguishable classification between the clustering of HFMD group, CT group (patients 7 days after combination therapy), and control group. Figures 3(a) and 3(b) displayed that separation of the groups could be achieved with the model parameters $R^2Y = 0.875$, $Q^2 = 0.710$ for positive ESI ion mode and $R^2Y = 0.908$, $Q^2 = 0.727$ for negative ESI ion mode. Q^2Y obtained from cross-validation procedure represents the predictive accuracy of the model, and R^2Y shows how well the model fits to the data. The previous parameters indicated that the two models had good ability to explain the data. Moreover, the results from permutation tests also showed that the two models were not over-fitting and were efficient and reliable (intercepts: $R^2 = 0.167$, $Q^2 = -0.172$ for positive ion mode data and $R^2 = 0.541$, $Q^2 = -0.209$ for negative ion mode data). We therefore conclude that HFMD had altered the serum metabolic profiles of patients when compared with healthy individuals, with the perturbations occurring in CT group.

3.6. The Evaluation of Combination Therapy. By using a similar method, we have identified the significant variables (sum of variables being detected in both positive mode and negative mode) based on the LC-Q-TOF-MS platform, which could contribute to the classification among the groups. As shown in Table 2, the metabolites with dashed area (15 metabolites) were modulated to the normal level in CT group, indicating the potential treatment targets of combination therapy. Associated network functions represented by IPA software include amino acid metabolism, molecular transport, and small molecule biochemistry. IPA also performed five top canonical pathways of these metabolites, including creatine-phosphate biosynthesis, sphingomyelin metabolism, glycine degradation, threonine degradation II, and choline biosynthesis III (Figure 4).

4. Discussion

Human EV71-associated HFMD has become a leading cause of childhood infection in China since 2008. Epidemic and molecular characteristics of HFMD have been examined in many areas of the country [2]. However, clinical and metabolomic characterization of HFMD remains scarce. Metabolomics approach can reveal the profile of endogenous metabolites of low molecular weight in biofluids that are related to disease progression, since it seeks to discover and capitalize on the metabolic derangements that occurred in the body as a result of the mutated genotype being manifested before actual gross phenotypic changes [22]. Many metabolomic efforts have been made to investigate the biomarkers and efficacy evaluation in viral diseases, such as infections by hepatitis C virus (HCV) [23], influenza A virus [24], and HIV-1 [25]. In the present study, the application of metabolomics is well suited for exploration of HFMD.

The compendium that we generated on the changes during the disease processes of HFMD has highlighted a wide variety of molecular and metabolic alterations. More detailed analyses of networks and pathways bring influenced were performed by IPA software. Our data have suggested lipid metabolism as the first important network function of perturbation in HFMD group. From the differentiating metabolites in HFMD, evident alteration in lipid metabolism was observed in HFMD patients following EV71 infection. This finding in fact echoes with another similar work at the proteomic level [26]. Lipid metabolism can be affected in a variety of ways during viral infection, whereas the major lipid changes involve triglycerides, free fatty acids, and ketone bodies, and so on [27]. Studies have demonstrated the relationship between HIV [28], HCV [29–31], and lipid metabolism, with evaluation of the role of interventions during dyslipidemia. Concomitantly, IPA had generated three related pathways, namely, phospholipases, choline biosynthesis III, and phosphatidylcholine biosynthesis I, which provides direct evidence in the perturbation of lipid metabolism in HFMD. These interrelated pathways implicate that lipid metabolism may be influenced by virus infection. Furthermore, we mainly focused on evaluating individual candidate metabolites during the analysis of lipid metabolism. We observed significantly lower levels of diacylglycerol (DAG) in HFMD patients when compared with those in the healthy control group. DAG is a versatile molecule that participates

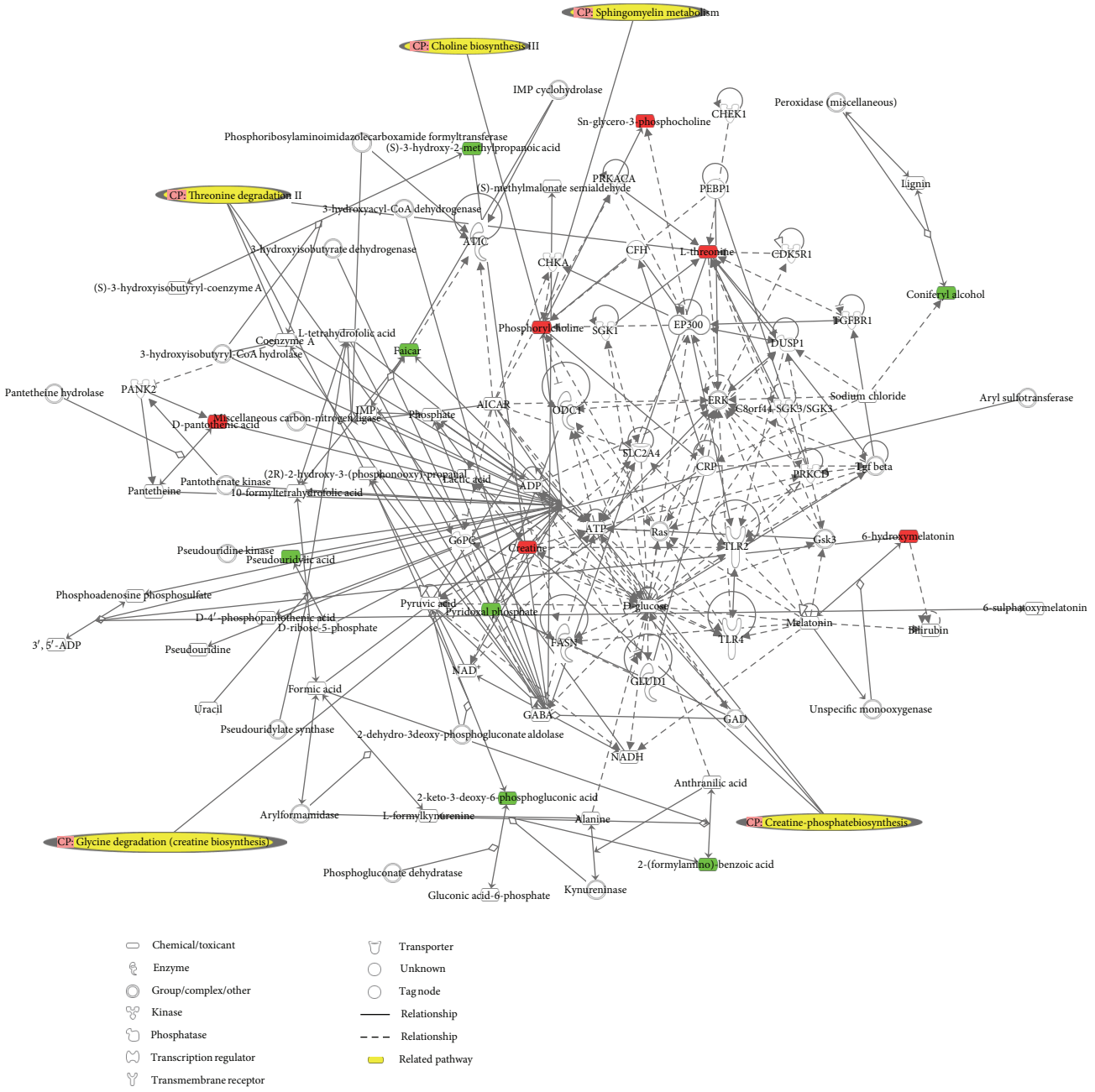

Figure 4: Significant molecular network of combination therapy related metabolites. Metabolites are represented as nodes, and the biological relationship between two nodes is represented as a line. Note that the colored symbols represent metabolites that occur in our data, while the transparent entries are molecules from the Ingenuity Knowledge Database. Red symbols represent up-regulated metabolites in HFMD patients after combination therapy; green symbols represent down-regulated metabolites in HFMD patients after combination therapy. Solid lines between molecules indicate direct physical relationship between molecules; dotted lines indicate indirect functional relationships. The yellow dashed area denotes the related pathway.

as substrate in the synthesis of structural and energetic lipids. DAG in lipid droplets from cytoplasm liver cells is associated with insulin resistance in nondiabetic obese human [32]. The termination of DAG signaling by DAG kinases can lead to inhibition of antiviral cytokine production. HIV-1 virus gene expression can be induced by DAG synthesized on a five-member ring platform [33]. This finding might well supplement the pathogenesis of HFMD. Nonetheless, phosphatidylethanolamine (PE) level was found to be decreased in HFMD patients. As a major component in the mammalian plasma membrane, PE is mainly present in the inner leaflet of the membrane bilayer in viable and typical mammalian cells. PE is likely to be a versatile chemical species that plays certain role in the regulation of defined biological and physiological

activities [34]. Choline, the basic constituent of lecithin that is found in many plants and animal organs, is up-regulated in HFMD patients. It is essential as a precursor of acetylcholine, as a methyl donor in various metabolic processes, and also in lipid metabolism [35]. Nevertheless, alterations of the cerebral choline can be observed in HCV-infection patients [36, 37]. Altogether, the altered lipid metabolite may be a sign of HFMD and reflect the abnormal lipid metabolism status in HFMD patients. Our results could provide a hint for further understanding of the role of lipid metabolism in the pathogenesis of HFMD.

From the signal transduction perspective, renin-angiotensin signaling is closely related. It is well known that renin-angiotensin proteins are key regulators of other signaling cascades, controlling many biological processes such as proliferation, differentiation, and apoptosis [38]. Renin-angiotensin signaling could be potential drug targets to determine the appropriate therapeutic intervention of HFMD. Nevertheless, additional prospective work is needed to investigate the precise mechanism.

It is of interest to note that inflammatory reactions were found to be dysregulated in HFMD patients. It has been considered that inflammation plays an important role during the HFMD process. The milder HFMD cases presented systemic inflammatory response syndrome status in clinical trials [39]. Moreover, patients with central nervous system diseases were found to have acute inflammation of the grey matter at the brain stem [40]. In a basic research, investigators had identified that human P-selectin glycoprotein ligand-1 (PSGL-1; CD162), a sialomucin membrane protein expressed on leukocytes, may play a major role in early stages of inflammation by interacting with selections and chemokines, as a functional receptor for EV71 [41]. Another report also indicated that massive induction of proinflammatory cytokines is responsible for the pathogenicity of EV71 [42]. Urocanic is a breakdown (deamination) product of histidine. In the liver, urocanic acid (UCA) is an intermediate in the conversion of histidine to glutamic acid, whereas in the epidermis, it accumulates and may be both a UV protectant and an immunoregulator [43]. *cis*-UCA can increase cytokine protein production including that of TNF-alpha, IL-6, and IL-8 in a dose-dependent manner [44]. Prostaglandin E_2 (PGE_2) is the most common and biologically active prostanoid among mammalian prostaglandins, which has been traditionally regarded as a mediator of immune inflammation [45]. It is interesting that PG-endoperoxide synthase-2 is dramatically induced by *cis*-UCA, resulting in an enhanced secretion of PGE_2. A relatively high level of UCA, together with PGE_2, was concurrently found in the HFMD group. These results suggest that the inflammation-related processes in HFMD may be largely perturbed.

HFMD has multiple alternative pathogenic pathways that lead to a particular pathophysiological state, with a wide range of resulting phenotypes. Thus, it provides a significant treatment venture in clinical practice. In this study, we performed combination therapy to determine metabolic changes in HFMD patients. Among 31 HFMD-related metabolites, 15 metabolites were reversed to the level of the health control group, suggesting that the combination therapy has a positive impact on repairing the abnormal metabolic profiles in HFMD. In CT group, the altered pathways include amino acid metabolism (threonine degradation II and glycine degradation) and lipid metabolism (creatine-phosphate biosynthesis, sphingomyelin metabolism, and choline biosynthesis III) (Figure 4). Amino acid metabolism, especially that of threonine degradation II, glycine degradation being addressed by IPA, is involved in the modulation process of combination therapy based on results from this study. In agreement with previous observation, the amino acid metabolism in patients with hepatitis B virus (HBV) infection is significantly changed [46]. Conserved glycine 33 residue in flexible domain I of HCV core protein is critical for its virulent activity [47]. A previous study has demonstrated that HBV E-antigen physically associates with receptor interaction serine/threonine protein kinase 2 [48]. As a result, our data are consistent with the phenomenon on the interference of glycine and threonine metabolism in viral diseases. We therefore believe that the primary regulatory targets of combination therapy involve modulation of amino acid metabolism. Interestingly, the related pathway of lipid metabolism again showed important role in the regulation of HFMD in CT group, consistent well with the before mentioned. Manipulation of these pathways could aim at the prime targets in successful HFMD therapy in CT group.

5. Conclusions

In summary, a metabolomic approach based on LC-Q-TOF-MS platform was employed to study the metabolic characteristics between HFMD patients and healthy individuals, as well as combination therapy interventions. A clear separation between HFMD patients and healthy subjects was achieved. As a result, 31 endogenous metabolites showed marked perturbation in HFMD patients. We also observed a number of important pathway perturbations in HFMD patients in association with lipid metabolism and inflammation reaction, and so forth. Combination therapy shows positive modulation in HFMD patients in different pathway. Metabolomic technique was deemed useful in the exploration of the complex metabolic states of HFMD, which can also provide a theoretical basis for the prevention and treatment of the disease.

Abbreviations

HFMD:	Hand-foot-and-mouth disease
EV71:	Enteric viruses including enterovirus 71
CVA16:	Coxsackievirus A16
CVA10:	Coxsackievirus A10
TCM:	Traditional Chinese Medicine
LC-Q-TOF-MS:	Liquid chromatography/quadrupole time-of-flight mass spectrometry
ESI:	Electrospray ionization.

Conflict of Interests

The authors declare no financial conflict of interests.

Authors' Contribution

C. Lu and X. Liu contributed equally to this work.

Acknowledgment

This research is supported in part by the National Specific Program on TCM (no. 200907001), National Science Foundation of China (no. 30825047 and 30902000) and National Post-doctorate Scientific Research (no. 20100470522). The authors would especially like to thank the clinical trial team, Dr Xiuhui Li from Beijing Youan Hospital.

References

[1] G. Chen, C. Lu, Q. Zha et al., "A network-based analysis of traditional Chinese medicine cold and hot patterns in rheumatoid arthritis," *Complementary Therapies in Medicine*, vol. 20, no. 1-2, pp. 23–30, 2012.

[2] X. Wang, C. Zhu, W. Bao et al., "Characterization of full-length enterovirus 71 strains from severe and mild disease patients in northeastern China," *PLoS ONE*, vol. 7, no. 3, Article ID e32405, 2012.

[3] Y.-H. Chiu, Y.-L. Chan, L.-W. Tsai, T.-L. Li, and C.-J. Wu, "Prevention of human enterovirus 71 infection by kappa carrageenan," *Antiviral Research*, vol. 95, no. 2, pp. 128–134, 2012.

[4] Y. Yang, L. Zhang, X. Fan, C. Qin, and J. Liu, "Antiviral effect of geraniin on human enterovirus 71 in vitro and in vivo," *Bioorganic and Medicinal Chemistry Letters*, vol. 22, no. 6, pp. 2209–2211, 2012.

[5] C. Wang, B. Cao, Q.-Q. Liu et al., "Oseltamivir compared with the Chinese traditional therapy maxingshigan-yinqiaosan in the treatment of H1N1 influenza: a randomized trial," *Annals of Internal Medicine*, vol. 155, no. 4, pp. 217–226, 2011.

[6] B. Xue, Z. Yao, and R. Yu, "Studies on anti-EV71 virus activity of traditional Chinese medicine and its clinical application in treatment of HFMD," *Zhongguo Zhongyao Zazhi*, vol. 36, no. 23, pp. 3366–3370, 2011.

[7] C.-Y. Wang, S.-C. Huang, Y. Zhang et al., "Antiviral ability of Kalanchoe gracilis leaf extract against Enterovirus 71 and coxsackievirus A16," *Evidence-based Complementary and Alternative Medicine*, vol. 2012, Article ID 503165, 13 pages, 2012.

[8] A. E. Allen, C. L. Dupont, M. Oborník et al., "Evolution and metabolic significance of the urea cycle in photosynthetic diatoms," *Nature*, vol. 473, no. 7346, pp. 203–207, 2011.

[9] K. Dettmer and B. D. Hammock, "Metabolomics—a new exciting field within the "omics" sciences," *Environmental Health Perspectives*, vol. 112, no. 7, pp. A396–A397, 2004.

[10] A. D. Maher, J. C. Lindon, and J. K. Nicholson, "H NMR-based metabonomics for investigating diabetes," *Future Medicinal Chemistry*, vol. 1, no. 4, pp. 737–747, 2009.

[11] H. Van Wietmarschen, K. Yuan, C. Lu et al., "Systems biology guided by Chinese medicine reveals new markers for sub-typing rheumatoid arthritis patients," *Journal of Clinical Rheumatology*, vol. 15, no. 7, pp. 330–337, 2009.

[12] Y. Gu, C. Lu, Q. Zha et al., "Plasma metabonomics study of rheumatoid arthritis and its Chinese medicine subtypes by using liquid chromatography and gas chromatography coupled with mass spectrometry," *Molecular BioSystems*, vol. 8, no. 5, pp. 1535–1543, 2012.

[13] H. Zhao, J. Li, X. He et al., "The protective effect of Yi Shen Juan Bi Pill in arthritic rats with castration-induced kidney deficiency," *Evidence-based Complementary and Alternative Medicine*, vol. 2012, Article ID 102641, 8 pages, 2012.

[14] H. Dong, A. Zhang, H. Sun et al., "Ingenuity pathways analysis of urine metabolomics phenotypes toxicity of Chuanwu in Wistar rats by UPLC-Q-TOF-HDMS coupled with pattern recognition methods," *Molecular BioSystems*, vol. 8, no. 4, pp. 1206–1221, 2012.

[15] *The Ministry of Health Guideline for the Diagnosis and Treatment of Hand Foot and Mouth Disease*, The Ministry of Health of the People's Republic of China, Beijing, China, 2010.

[16] *Pharmacopoeia Committee of People's Republic of China: Chinese Pharmacopoeia*, Beijing, China, 2010.

[17] W. B. Dunn, D. Broadhurst, P. Begley et al., "Procedures for large-scale metabolic profiling of serum and plasma using gas chromatography and liquid chromatography coupled to mass spectrometry," *Nature Protocols*, vol. 6, no. 7, pp. 1060–1083, 2011.

[18] Y. Lv, X. Liu, S. Yan et al., "Metabolomic study of myocardial ischemia and intervention effects of Compound Danshen Tablets in rats using ultra-performance liquid chromatography/quadrupole time-of-flight mass spectrometry," *Journal of Pharmaceutical and Biomedical Analysis*, vol. 52, no. 1, pp. 129–135, 2010.

[19] H. S. Tapp and E. K. Kemsley, "Notes on the practical utility of OPLS," *TrAC—Trends in Analytical Chemistry*, vol. 28, no. 11, pp. 1322–1327, 2009.

[20] P. Jiang, W. Dai, S. Yan et al., "Potential biomarkers in the urine of myocardial infarction rats: a metabolomic method and its application," *Molecular BioSystems*, vol. 7, no. 3, pp. 824–831, 2011.

[21] R. E. Williams, E. M. Lenz, J. A. Evans et al., "A combined 1H NMR and HPLC-MS-based metabonomic study of urine from obese (fa/fa) Zucker and normal Wistar-derived rats," *Journal of Pharmaceutical and Biomedical Analysis*, vol. 38, no. 3, pp. 465–471, 2005.

[22] S. L. Taylor, S. Ganti, N. O. Bukanov et al., "A metabolomics approach using juvenile cystic mice to identify urinary biomarkers and altered pathways in polycystic kidney disease," *American Journal of Physiology*, vol. 298, no. 4, pp. F909–F922, 2010.

[23] M. M. G. Godoy, E. P. A. Lopes, R. O. Silva et al., "Hepatitis C virus infection diagnosis using metabonomics," *Journal of Viral Hepatitis*, vol. 17, no. 12, pp. 854–858, 2010.

[24] S. Lin, N. Liu, Z. Yang et al., "GC/MS-based metabolomics reveals fatty acid biosynthesis and cholesterol metabolism in cell lines infected with influenza A virus," *Talanta*, vol. 83, no. 1, pp. 262–268, 2010.

[25] A. D. Maher, L. A. Cysique, B. J. Brew, and C. D. Rae, "Statistical integration of 1H NMR and MRS data from different biofluids and tissues enhances recovery of biological information from individuals with HIV-1 infection," *Journal of Proteome Research*, vol. 10, no. 4, pp. 1737–1745, 2011.

[26] L. Deng, H. L. Jia, C. W. Liu et al., "Analysis of differentially expressed proteins involved in hand, foot and mouth disease and normal sera," *Clinical Microbiology and Infection*, vol. 18, pp. E188–E196, 2012.

[27] G. L. Blackburn, "Lipid metabolism in infection," *American Journal of Clinical Nutrition*, vol. 30, no. 8, pp. 1321–1332, 1977.

[28] M. P. Dubé and J. J. Cadden, "Lipid metabolism in treated HIV infection," *Best Practice and Research: Clinical Endocrinology and Metabolism*, vol. 25, no. 3, pp. 429–442, 2011.

[29] K. Koike, T. Tsutsumi, H. Yotsuyanagi, and K. Moriya, "Lipid metabolism and liver disease in hepatitis C viral infection," *Oncology*, vol. 78, supplement 1, pp. 24–30, 2010.

[30] F. Negro, "Abnormalities of lipid metabolism in hepatitis C virus infection," *Gut*, vol. 59, no. 9, pp. 1279–1287, 2010.

[31] P. Targett-Adams, S. Boulant, M. W. Douglas, and J. McLauchlan, "Lipid metabolism and HCV infection," *Viruses*, vol. 2, no. 5, pp. 1195–1217, 2010.

[32] N. Kumashiro, D. M. Erion, D. Zhang et al., "Cellular mechanism of insulin resistance in nonalcoholic fatty liver disease," *Proceedings of the National Academy of Sciences of the United States of America*, vol. 108, no. 39, pp. 16381–16385, 2011.

[33] D. H. Hamer, S. Bocklandt, L. McHugh et al., "Rational design of drugs that induce human immunodeficiency virus replication," *Journal of Virology*, vol. 77, no. 19, pp. 10227–10236, 2003.

[34] M. Zhao, "Lantibiotics as probes for phosphatidylethanolamine," *Amino Acids*, vol. 41, no. 5, pp. 1071–1079, 2011.

[35] http://www.hmdb.ca/metabolites/HMDB00097.

[36] K. Weissenborn, A. B. Tryc, M. Heeren et al., "Hepatitis C virus infection and the brain," *Metabolic Brain Disease*, vol. 24, no. 1, pp. 197–210, 2009.

[37] D. M. Forton, J. M. Allsop, I. J. Cox et al., "A review of cognitive impairment and cerebral metabolite abnormalities in patients with hepatitis C infection," *AIDS*, vol. 19, supplement 3, pp. S53–S63, 2005.

[38] E. Castellano and J. Downward, "Role of RAS in the regulation of PI 3-kinase," *Current topics in Microbiology and Immunology*, vol. 346, pp. 143–169, 2010.

[39] D. Fu, C. R. Li, Y. X. He et al., "Changes of immune function in patients with enterovirus 71 infection," *Chinese Journal of Pediatrics*, vol. 47, no. 11, pp. 829–834, 2009.

[40] G. A. Koroleva, A. N. Lukashev, L. V. Khudyakova, A. N. Mustafina, and V. A. Lashkevich, "Encephalomyelitis caused by enterovirus type 71 in children," *Voprosy Virusologii*, vol. 55, no. 6, pp. 4–10, 2010.

[41] Y. Nishimura, M. Shimojima, Y. Tano, T. Miyamura, T. Wakita, and H. Shimizu, "Human P-selectin glycoprotein ligand-1 is a functional receptor for enterovirus 71," *Nature Medicine*, vol. 15, no. 7, pp. 794–797, 2009.

[42] W. X. Khong, D. G. W. Foo, S. L. Trasti, E. L. Tan, and S. Alonso, "Sustained high levels of interleukin-6 contribute to the pathogenesis of enterovirus 71 in a neonate mouse model," *Journal of Virology*, vol. 85, no. 7, pp. 3067–3076, 2011.

[43] http://www.hmdb.ca/metabolites/HMDB00301.

[44] K. Kaneko, U. Smetana-Just, M. Matsui et al., "Cis-urocanic acid initiates gene transcription in primary human keratinocytes," *Journal of Immunology*, vol. 181, no. 1, pp. 217–224, 2008.

[45] D. Sakata, C. Yao, and S. Narumiya, "Prostaglandin E2, an immunoactivator," *Journal of Pharmacological Sciences*, vol. 112, no. 1, pp. 1–5, 2010.

[46] K. M. Castorena, K. A. Stapleford, and D. J. Miller, "Complementary transcriptomic, lipidomic, and targeted functional genetic analyses in cultured *Drosophila* cells highlight the role of glycerophospholipid metabolism in Flock House virus RNA replication," *BMC Genomics*, vol. 11, no. 1, article 183, 2010.

[47] A. G. N. Angus, A. Loquet, S. J. Stack et al., "Conserved glycine 33 residue in flexible domain I of hepatitis C virus core protein is critical for virus infectivity," *Journal of Virology*, vol. 86, no. 2, pp. 679–690, 2012.

[48] S. Wu, T. Kanda, F. Imazeki et al., "Hepatitis B virus e antigen physically associates with receptor-interacting serine/threonine protein kinase 2 and regulates IL-6 gene expression," *Journal of Infectious Diseases*, vol. 206, no. 3, pp. 415–420, 2012.

Hindawi Publishing Corporation
Evidence-Based Complementary and Alternative Medicine
Volume 2013, Article ID 518421, 12 pages
http://dx.doi.org/10.1155/2013/518421

Research Article

The effect of PN-1, a Traditional Chinese Prescription, on the Learning and Memory in a Transgenic Mouse Model of Alzheimer's Disease

Zhi-Gang Yao, Ling Zhang, Liang Liang, Yu Liu, Ya-Jun Yang, Lan Huang, Hua Zhu, Chun-Mei Ma, and Chuan Qin

Comparative Medical Center, Institute of Laboratory Animal Science, Peking Union Medical College (PUMC), Chinese Academy of Medical Science (CAMS), Beijing 100021, China

Correspondence should be addressed to Chuan Qin; qinchuan@pumc.edu.cn

Received 14 October 2012; Revised 13 January 2013; Accepted 15 January 2013

Academic Editor: Wei Jia

Traditional Chinese Medicine (TCM) is a complete medical system that has been practiced for more than 3000 years. Prescription number 1 (PN-1) consists of several Chinese medicines and is designed according to TCM theories to treat patients with neuropsychiatric disorders. The evidence of clinical practice suggests the benefit effects of PN-1 on cognitive deficits of dementia patients. We try to prove and explain this by using contemporary methodology and transgenic animal models of Alzheimer's disease (AD). The behavioral studies were developed to evaluate the memory of transgenic animals after intragastric administration of PN-1 for 3 months. Amyloid beta-protein (Aβ) neuropathology was quantified using immunohistochemistry and ELISA. The western blotting was used to detect the levels of plasticity associated proteins. The safety of PN-1 on mice was also assessed through multiple parameters. Results showed that PN-1 could effectively relieve learning and memory impairment of transgenic animals. Possible mechanisms showed that PN-1 could significantly reduce plaque burden and Aβ levels and boost synaptic plasticity. Our observations showed that PN-1 could improve learning and memory ability through multiple mechanisms without detectable side effects on mice. We propose that PN-1 is a promising alternative treatment for AD in the future.

1. Introduction

Cognitive impairment or dementia in the elderly is associated with many disorders, such as Alzheimer's disease (AD) and vascular dementia (VaD) [1]. According to the traditional Chinese medicine (TCM), there is no distinction between AD and VaD. The term "senile dementia" refers to a clinical syndrome characterized by the progressive decline of memory and some related cognitive functions in the elderly [2]. In the ancient Chinese medicine literature, senile dementia falls into the category of "dementia," or "idiocysyndrome" resulting from deficiency of kidney essence and marrow, obstruction by phlegm and blood stasis, and so forth [3, 4]. According to these traditional viewpoints, prescriptions composed of a complex variety of many different herbs, minerals, or animal parts are used to treat dementia clinically, such as Six Flavors Rehmannia Pills (*Liu Wei Di Hang Wan*), Nourish the Heart Decoction (*Yang Xin Tang*) and Gastrodia and Uncaria Drink (*Tian Ma Gou Teng Yin*) [5]. Prescription number 1 (PN-1) is a compound Chinese medicine designed entirely based on TCM theories. From a western medical view, this prescription has a wide range of pharmacological activities in clinical application to treat cerebellar atrophy, dystaxia, and cerebral palsy with minor side effects. In addition, the clinical effectiveness on poor memory of the elderly suggests a potential role of PN-1 in dementia therapeutics. Indeed, the efficacy of PN-1 in senile dementia was demonstrated by a nonblinded, open-label design performed by the Beijing Xuanwu Hospital in China (unpublished data).

As the most common type of dementia in western medicine, AD is a neurodegenerative disorder characterized clinically by progressive memory loss and neuropathologically by extracellular amyloid plaques [6]. The plaques are primarily composed of aggregated β-amyloid (Aβ) peptides

derived from the β-amyloid precursor protein (APP) [7, 8]. Recent studies indicate that the increased Aβ production in the hippocampus and cortex leads to synaptic impairment, neuronal loss, and memory deficits [9–11]. Indeed, synaptic dysfunction was found in the association cortices and hippocampus of AD brain [12]. These findings suggest the excess production of Aβ peptides in the brain is a central event in AD pathology [13, 14]. In addition, synapse is the basis of learning and memory [15]. Hence, reactivating synaptic function is the key to improve learning and memory. In this study, we detected the effects of PN-1 on memory-associated behavior tests in transgenic mouse models of AD. Moreover, Aβ burden and synaptic function were investigated to understand the benefits of PN-1 to learning and memory deficits.

2. Material and Methods

2.1. Transgenic Mice. The APPswe/PS1dE9 (APP/PS1) transgenic mouse model of AD overexpresses the Swedish (K594M/N595L) mutation of APP together with presenilin 1 (PS1) deleted in exon 9 in a C57BL/6J genetic background. These mice show learning and memory deficits and increased senile plaques in behavioral and neuropathological analyses [16, 17]. The use of animals was in compliance with the National Institutes of Health Guide for Care and Use of Laboratory Animals. The study protocol was approved by the Institutional Animal Care and Use Committee of the Institute of Laboratory Animal Science (permit number: ILAS-PL-2010-004). The study and all procedures were conducted in accordance with institutional guidelines. All efforts were made to minimize suffering.

2.2. Preparation for PN-1. PN-1 is composed of more than 20 kinds of Chinese medicines, in which the main herbs used are Radix Astragali, Radix Codonopsis, Rhizoma Atractylodis Macrocephalae, and Cistanches Herba in a dry weight ratio of 8 : 2 : 3 : 2. All components were authenticated macroscopically and microscopically according to pharmacopoeias [18]. In details, macroscopic examinations included measurements of appearance, size, shape, color, texture, odor, taste, fracture, and other characteristics of a herb. Microscopic examinations determined characteristic elements of each herb in both tissue and powder forms. In powder analysis, each component was pulverized to 200 mesh in size, mounted on a microscope slide, cleared with chloral hydrate, lactochloral and/or sodium hypochlorite, and then examined for the presence, size, shape, and numbers of characteristic elements and inclusions such as vessels, calcium crystals, crystalline fibers, stone cells, and starch grains. The examination protocols followed the World Health Organization (WHO) Quality Control Methods for Medicinal Plant Materials [19], the Pharmacopoeia of the People's Republic of China (CP) [18]. A mixture of powdered materials (500 g) were extracted three times with total 20 L of distilled water in a hot-water bath for 3 h, and, after filtration, the filtrates were mixed together and adjusted to a final concentration of 0.1 mg/mL (equivalent to dry weight of raw materials).

2.3. Experimental Procedures. Concentrated PN-1 extract was dissolved or suspended in distilled water. Transgenic APP/PS1 mice at 5 months of age were randomized into the vehicle-treated group (vehicle) and three experimental groups, including PN-1 0.6 mg/kg (low dose), 1.2 mg/kg (middle dose), and 2.4 mg/kg (high dose) once a day. Mice in the vehicle-treated group were orally given distilled water. The doses of the PN-1 used in this study were converted into raw material weights and given orally to mice for 4 months. We also introduced a positive control group, which was given Aricept (generic name donepezil, 2 mg/kg once a day) orally. Aricept is approved by FDA for the clinical treatment of AD and is usually used as a positive control in experiments [20, 21]. In addition, the age-matched C57BL/6 wild-type (WT) mice were required as control. Twenty animals (10 males and 10 females) were used for each group. Body weight, food and water intakes were measured every two weeks until behavior tests. At 8 months of age, the novel object recognition (NOR) task was performed to detect recognition memory of mice. One week after NOR task, spatial learning and memory of animals were assessed by the Morris water maze (MWM) test. Thereafter, all mice were sacrificed by decapitation under intraperitoneal injection anesthesia using sodium pentobarbital (45 mg/kg).

2.4. Novel Object Recognition Task. The NOR task consisted of a habituation phase, a training phase, and a testing phase. During habituation, each mouse was habituated to the open-field apparatus (30 cm wide, 45 cm long, and 20 cm high) made of polyvinyl chloride plastic for 5 min daily on 2 consecutive days in the absence of objects. No data were collected during habituation. In the training trial, mice were placed in the experimental apparatus and allowed to freely explore the arena in the presence of two identical objects (blue wooden cubes of side 3 cm) for 5 min daily on 3 consecutive days. The test phase was performed 24 h later. Each mouse was placed in the arena with an object they explored during the training phase (familiar object) and a new (novel) object (a yellow wooden cylinder of diameter 3 cm and height 3 cm). The open-field arena and the objects were cleaned thoroughly between trials to ensure the absence of olfactory cues. A mouse was scored as exploring an object when its head was oriented toward the object within a distance of 1 cm or when the nose was touching the object. Sitting on or going around the objects was not considered exploratory behavior. The exploration time for the familiar (T_F) or the new object (T_N) during the test phase was videotaped and analyzed using the Noldus Ethovision XT software (Noldus Information Technology, Wageningen, The Netherlands). Memory was defined by the discrimination index (DI) for the novel object as the following formula: $\mathrm{DI} = (T_N - T_F)/(T_N + T_F) \times 100\%$ [22, 23].

2.5. Morris Water Maze Test. The Morris water maze (MWM) test was performed in a circular pool (100 cm in diameter) filled with water at a temperature of 22 ± 1°C. The water was colored opaque with powdered nonfat milk. An overhead video camera coupled to a computer and tracking software (Ethovision system, Noldus Information Technology,

Wageningen, The Netherlands) was used to track movements. The tank was placed in a dimly light, sound proof test room with various visual cues. The pool was divided into four quadrants of the equal area. A white platform (6 cm in diameter and 29 cm high) was centered in one of the pool quadrants. One day prior to hidden platform test, the mouse was allowed to swim for 60 sec in the pool with the visible platform projecting 1 cm above the water surface. The mouse was then given two trial sessions each day for five consecutive days, during which the platform was left in the same position and submerged 0.5 cm below the water surface. The time taken to reach the platform (escape latency) was measured, and the average of two trials was determined. 24 h after the last trial of the hidden platform test, the mouse was subjected to a probe trial in which the platform was removed from the pool, allowing the mouse to swim for 60 seconds in search of it. The frequency of target platform crossings was recorded. After the swim, the mouse was kept dry in a plastic holding cage on an electric heater.

2.6. Assessment of Alzheimer Pathology. Brains were fixed in formalin and embedded in paraffin. For each specimen, 30 serial sections of 5 μm thickness were coronally sliced for two to three such series, spaced 50 μm apart. Sections were deparaffinized in xylenes and rehydrated via an ethanol gradient. Antigen retrieval was performed using 88% formic acid treatment for 5 min and incubated for 30 min with 0.3% H_2O_2 thereafter. Sections were blocked with 10% goat serum and incubated with primary antibody overnight at 4°C. The immunoreaction was visualized using horseradish peroxidase (HRP) labeled IgG as secondary antibody incubated at 37°C for 30 min and followed by diaminobenzidine (ZSGB, Beijing, China) staining. For the quantification of plaque levels, microscopic images of Aβ monoclonal antibody, 6E10 (1 : 1,000, Covance/Signet Laboratories, Dedham, MA)-stained cortex, and hippocampus were captured. The potential subregional variations of cortex and hippocampus were systematically analyzed. For thioflavin-S staining, the dewaxed sections were immersed in 1% thioflavin-S solution for 5 min and decolorized with 2 washes of 50% ethanol followed by washing and dehydration in increasing ethanol concentrations from 70% to 100%. The quantification of plaque number and size after immunostaining were analyzed using Aperio's ImageScope Viewer software (Aperio. Technologies). Thioflavin-S stained sections were observed by an Olympus BX40 microscope (Olympus, Tokyo, Japan), and the signal intensity was analyzed using ImageJ software (1.43u, NIH, USA).

2.7. Quantitation of Aβ in Brain Extracts. The extraction of soluble and insoluble Aβ species (including Aβ40 and Aβ42) of the cortex and hippocampus homogenates was described in previous studies [24–26]. Briefly, The frozen mouse cortex and hippocampus were weighed and homogenized with ice-cold Trisbuffered saline (TBS) consisting of 20 mM Tris-HCl, 150 mM NaCl, and pH 7.4 to the frozen cortex at 4 : 1 (TBS volume/brain wet weight). The homogenate was centrifuged at 4°C for 30 min at 20,000 g. The supernatant containing soluble Aβ peptide fraction (called TBS extract) was aliquoted and then stored at −80°C, and the pellet containing insoluble Aβ was sonicated in an equal volume (v/v) of TBS plus 5 M guanidine HCl, pH 8.0, and incubated for 3-4 h at room temperature. The homogenate were centrifuged at 4°C for 30 min at 20,000 g. The supernatant was collected (called GuHCl extract) and regarded as the insoluble Aβ peptide fraction. Protein concentrations were estimated in both fractions using the NanoDrop 2000 spectrophotometer (Thermo Scientific, Wilmington, DE, USA). Aβ40 and Aβ42 levels were quantified by ELISA according to the manufacturer's recommendations (Invitrogen, CA, USA).

2.8. Western Blotting Analysis. Brains tissue samples were homogenized using RIPA lysis buffer (50 mM Tris-HCl pH 7.4, 150 mM NaCl, 1% Triton X-100, 1% sodium deoxycholate, and 0.1% SDS) containing 1 mM PMSF. Total proteins from brain samples were measured using the NanoDrop 2000 spectrophotometer (Thermo Scientific, Wilmington, DE, USA). Equal amounts of protein were loaded on a 10% SDS-PAGE run at 90 V for 1.5 h at room temperature and transferred onto polyvinylidene fluoride (PVDF) membranes (Millipore, Billerica, MA, USA) and then probed with the primary antibodies overnight at 4°C. The primary antibodies and secondary antibodies were selected from the antibodies listed in Supplemental Table S1, available online at http://dx.doi.org/10.1155/2013/518421 including their dilution and commercial supplier. Then, membranes were incubated with peroxidase-labeled secondary antibody at room temperature for 1 h. Bands were visualized using enhanced chemiluminescent (ECL) substrate (Pierce, Rockford, IL USA) and quantitated by densitometry using NIH ImageJ software (1.43u, NIH, USA). Glyceraldehyde-3-phosphate dehydrogenase (GAPDH) was used as a loading control. Specific bands were quantified densitometrically, and the ratio between intensity of phospho-CaMKIIα and CaMKIIα, CREB and phospho-CREB from the same homogenate were calculated.

2.9. Assessment of PN-1 Toxicity. Blood was collected after sacrifice by cardiopuncture. Serum was collected by clotting blood specimens for 10 min at room temperature followed by centrifugation at 2000 g for 10 min at 4°C. Serum was immediately subjected to total bilirubin (TB), alanine aminotransferase (ALT), aspartate aminotransferase (AST), creatinine (Cr), and blood urea nitrogen (BUN) analysis using commercial enzyme assays according to the manufacturer's instructions (Kang-Lan biotechnology Co. Ltd., Beijing). Tissues of liver, kidney, brain, and so forth, were collected after sacrifice. After fixation with 10% formaldehyde for 48 h, tissues were embedded in paraffin according to routine procedures. Five μm thick sections were cut and stained with hematoxylin-eosin (H&E) for histopathological evaluation. Two expert pathologists at the Institute of Laboratory Animals blindly analyzed the tissue slices.

2.10. Statistical Analysis. All data were presented as means ± SEM. The group differences of escape latencies in the MWM test were analyzed using two-way ANOVA with repeated measures. Treatments were compared using a one-way

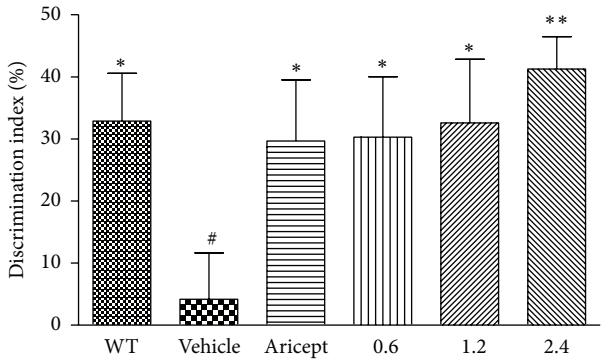

Figure 1: Effects of PN-1 treatment (mg/kg once a day) on the performance of the novel object recognition (NOR) task. Data represent means ± SEM ($n = 17$ mice/group). $^{*}P < 0.05$, $^{**}P < 0.01$ versus the vehicle-treated group; $^{\#}P < 0.05$ versus the wild-type group.

ANOVA followed by Dunnett's multiple-comparison post hoc test using the GraphPad Prism. Significant differences were determined at $P < 0.05$.

3. Results

3.1. PN-1 Treatment Improves Recognition Memory Deficits in APP/PS1 Mice. As shown in Figure 1, the discrimination index (DI) was significantly reduced by 87% for vehicle-treated group compared to the wild-type (WT) group ($P < 0.05$). When compared with the vehicle-treated group, DI was significantly increased in Aricept- and PN-1-treated groups by approximately 6–8 folds ($P < 0.05$ for the Aricept, low- and middle-dose group; $P < 0.01$ for the high-dose group).

3.2. PN-1 Treatment Improves Spatial Memory Deficits in APP/PS1 Mice. In the hidden platform test (Figure 2(a)), the vehicle-treated group showed significantly increased escape latencies from day 2 compared to the wild-type group ($P < 0.05$ for day 2; $P < 0.01$ for day 3–5). When compared with the vehicle-treated group, escape latencies were significantly decreased in PN-1-treated groups from day 4 ($P < 0.05$ for day 4-5). At day 5, the Aricept-treated mice also showed significantly decreased escape latency ($P < 0.05$). In the probe trial (Figure 2(b)), vehicle-treated group showed significantly decreased frequency of crossing within the platform quadrant compared to wild-type group ($P < 0.01$). When compared with the vehicle-treated group, the frequency was increased in Aricept- and PN-1-treated groups ($P < 0.05$ for the Aricept and low-dose group; $P < 0.01$ for the middle- and high-dose group). The typical behavioral traces from each group in the probe trial appear in Figure 2(c).

3.3. PN-1 Treatment Reduces Plaque Burden in the Brains of APP/PS1 Mice. Globally, results showed no Aβ deposition in wild-type brains (figure not shown). As shown in Figure 3(a), results showed significant reduction in the percentage of cortical and hippocampal area occupied by amyloid plaques in PN-1-treated groups compared to the vehicle-treated group ($P < 0.05$ for all PN-1-treated groups). In the cortex, the area of plaques was reduced by nearly 69% in PN-1-treated groups ($P < 0.01$ for all PN-1-treated groups). In hippocampus, PN-1 treatment also decreased the area of plaques by 57%–80% in PN-1-treated groups ($P < 0.05$ for the low- and high-dose group; $P < 0.01$ for the middle-dose group). Moreover, the staining distribution pattern of plaques was distinguishable between groups (Figure 3(b)). PN-1 treatment showed significant reduction of plaque number in the primary sensory cortex (S1C, $P < 0.01$ for the middle- and high-dose group) and entorhinal cortex (EC, $P < 0.05$ for the middle- and high-dose group) by approximately 60%–70%, as compared with the vehicle-treated group. In the hippocampus, the plaque number in the stratum oriens (Or, $P < 0.01$ for all PN-1-treated groups), stratum radiatum (Ra, $P < 0.01$ for the high-dose group), and stratum lacunosum-moleculare (LM, $P < 0.01$ for all PN-1-treated groups) of CA1 area and the molecular layer (Mo, $P < 0.01$ for all PN-1-treated groups) of dentate gyrus (DG) was also significantly decreased by nearly 70%, 70%, 60%, and 45%, respectively. However, there is no significant difference in the number of plaques in the motor cortex (MC) and hippocampal hilus (polymorphic layer of DG). In addition, PN-1 treatment showed the significant effectiveness on plaque density decline (by nearly 80%) by assessing the signal intensity of thioflavin-S positive plaques in the cortex ($P < 0.01$ for the middle- and high-dose group) and hippocampus ($P < 0.01$ for all PN-1-treated groups) as shown in Figure 3(c).

3.4. PN-1 Treatment Decreases Aβ Levels in the Brains of APP/PS1 Mice. To extract and characterize Aβ1–40 and Aβ1–42 peptides present in mouse brains, we prepared soluble Aβ peptide fraction (TBS extract) and insoluble Aβ peptide fraction (GuHCl extract) by the sequential centrifugation of cortical and hippocampal homogenates. In the wild-type mouse brain, we detected much less soluble and insoluble Aβ peptides (Figure 4). As shown in Figure 4(a), the results showed the significant increase in soluble Aβ1–40 level in the low-dose group ($P < 0.05$) as well as the significant decrease (by nearly 50%) in insoluble Aβ1–40 level in the middle- and high-dose group ($P < 0.05$), as compared with the vehicle-treated group. For total cortical soluble and insoluble Aβ1–42 levels (Figure 4(b)), the results revealed no significant PN-1 treatment effects ($P > 0.05$ for all PN-1-treated groups). PN-1 treatment significantly lowered hippocampal total soluble Aβ1–40 ($P < 0.05$ for all PN-1-treated groups, Figure 4(c)) and Aβ1–42 ($P < 0.01$ for all PN-1-treated groups, Figure 4(d)) levels by approximately 40% and 50%, respectively. However, there was no significant effect of PN-1 on the levels of hippocampal insoluble Aβ1–40 ($P > 0.05$ for all PN-1-treated groups, Figure 4(c)) and Aβ1–42 ($P > 0.05$ for all PN-1-treated groups, Figure 4(d)).

3.5. PN-1 Treatment Upregulates the Expressions of Plasticity-Related Proteins. To further investigate the potential mechanisms underlying the beneficial effects of PN-1 on memory impairment of transgenic animals, presynaptic and postsynaptic proteins in the brain were analyzed using western blotting. As compared with the wild-type group, the levels

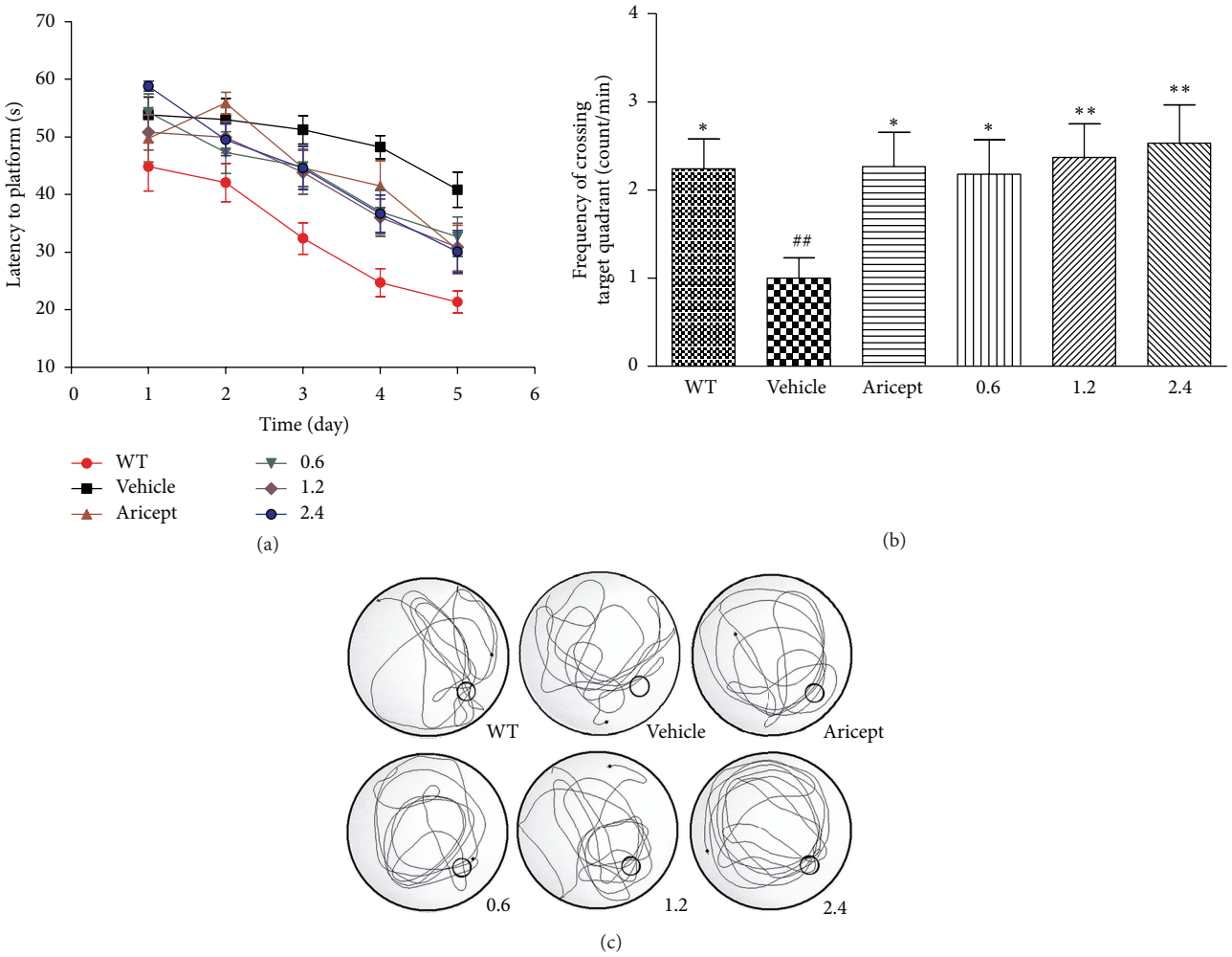

Figure 2: Effects of PN-1 treatment (mg/kg once a day) on the performance of the Morris water maze test. (a) The escape latency time in 5 days in the hidden platform test. Each point represents the mean latency of two trials per day for 5 consecutive days of testing. (b) The frequency of crossing within the platform quadrant detected in the probe trial. (c) An illustration of typical behavioral traces in the probe trial. Data represent means ± SEM ($n = 17$ mice/group). $^{*}P < 0.05$, $^{**}P < 0.01$ versus the vehicle-treated group; $^{\#\#}P < 0.01$ versus the wild-type group.

of Syt 1, CaM, and BDNF expressions in the vehicle-treated group were decreased by 0%, 45%, and 37%, respectively (Figure 5(a), $P > 0.05$ for Syt 1; $P < 0.05$ for CaM and BDNF). The levels of Syt 1 in the middle- and high-dose of PN-1 treatment group were significantly upregulated by approximately 1.5-fold, as compared with the vehicle-treated group ($P < 0.01$). CaM levels were significantly increased by 78%, 159%, and 151% in the low-, middle-, and high-dose of PN-1-treated groups, respectively ($P < 0.05$ for the low-dose group, $P < 0.01$ for the middle- and high-dose group). Compared to the vehicle-treated mice, BDNF levels nearly raised by 90% in all PN-1-treated groups ($P < 0.05$ for the low- and high-dose group, $P < 0.01$ for the middle-dose group).

Considering the crucial role of phosphorylated proteins in synaptic plasticity [27], we furtherly discussed the phosphorylation status of CaMKIIα and CREB (Figure 5(b)). The results showed no significant changes of CaMKIIα and CREB levels in each group after normalization using GAPDH (data not shown). As compared with the wild-type group, the ratios of p-CaMKIIα/CaMKIIα and p-CREB/CREB in the vehicle-treated group were significantly declined by 46% and 27%, respectively ($P < 0.01$ for p-CaMKIIα/CaMKIIα; $P < 0.05$ for p-CREB/CREB). In all PN-1-treated groups, the ratios of p-CaMKIIα/CaMKIIα significantly raised by 79%, 91%, and 117%, respectively ($P < 0.01$ for all PN-1-treated groups). In addition, the ratios of p-CREB/CREB in PN-1-treated groups significantly raised by approximately 40% ($P < 0.05$ for all PN-1-treated groups).

3.6. PN-1 Treatment Shows No Detectable Side Effects on Mice. During the long-term administration of PN-1, a battery of studies designed to detect possible side effects on animals. However, there was no detectable difference in body weight, food intake, or water intake between each group over the 3-month treatment period (Supplementary Figure S1). It suggested that PN-1 did not influence the

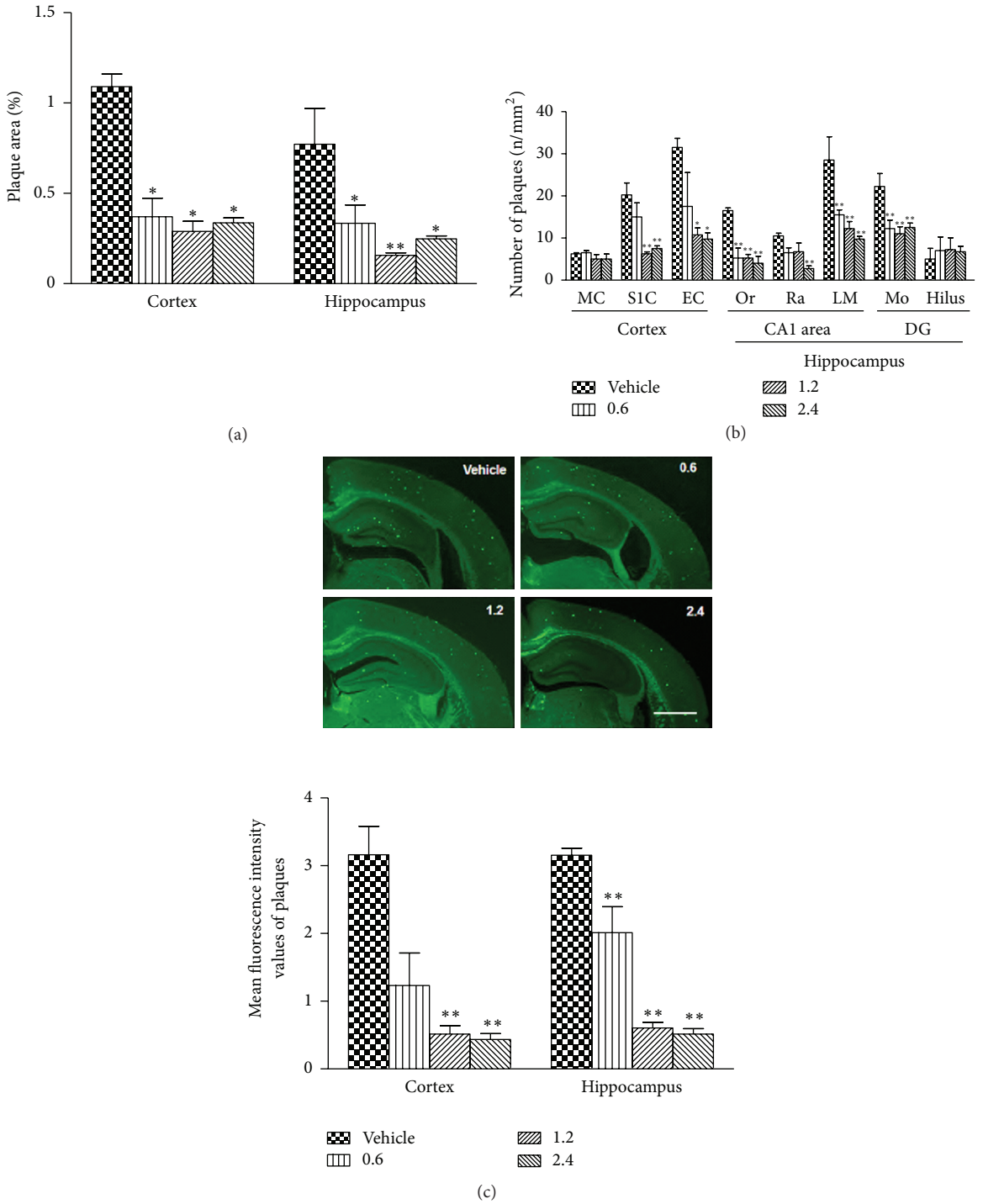

FIGURE 3: Effects of PN-1 treatment (mg/kg once a day) on plaque pathology. (a) The percentage area occupied by plaques in the cortex and hippocampus. (b) The average number of plaques per square millimeter in the cortical primary sensory cortex (S1C), entorhinal cortex (EC), and motor cortex (MC) and hippocampal stratum oriens (Or), stratum radiatum (Ra), stratum lacunosum-moleculare (LM), molecular layer (Mo), and dentate gyrus (DG) hilus. (c) The mean fluorescence intensity of thioflavin-S positive staining plaques in the cortex and hippocampus (scale bar, 1 cm). Data represent means ± SEM (n = 6 mice/group) from 2 and 3 independent experiments. $^{*}P < 0.05$, $^{**}P < 0.01$ versus the vehicle-treated group.

metabolic function of mice. Moreover, liver enzyme measurements and kidney function tests were also performed at the end of PN-1 administration. The results showed no significant effect on the liver or kidney function, as reflected by normal serum levels of total bilirubin (TB), alanine aminotransferase (ALT), aspartate aminotransferase (AST), creatinine (Cr), and blood urea nitrogen (BUN) (Supplementary Table 2). Microscopic examinations of the different tissues

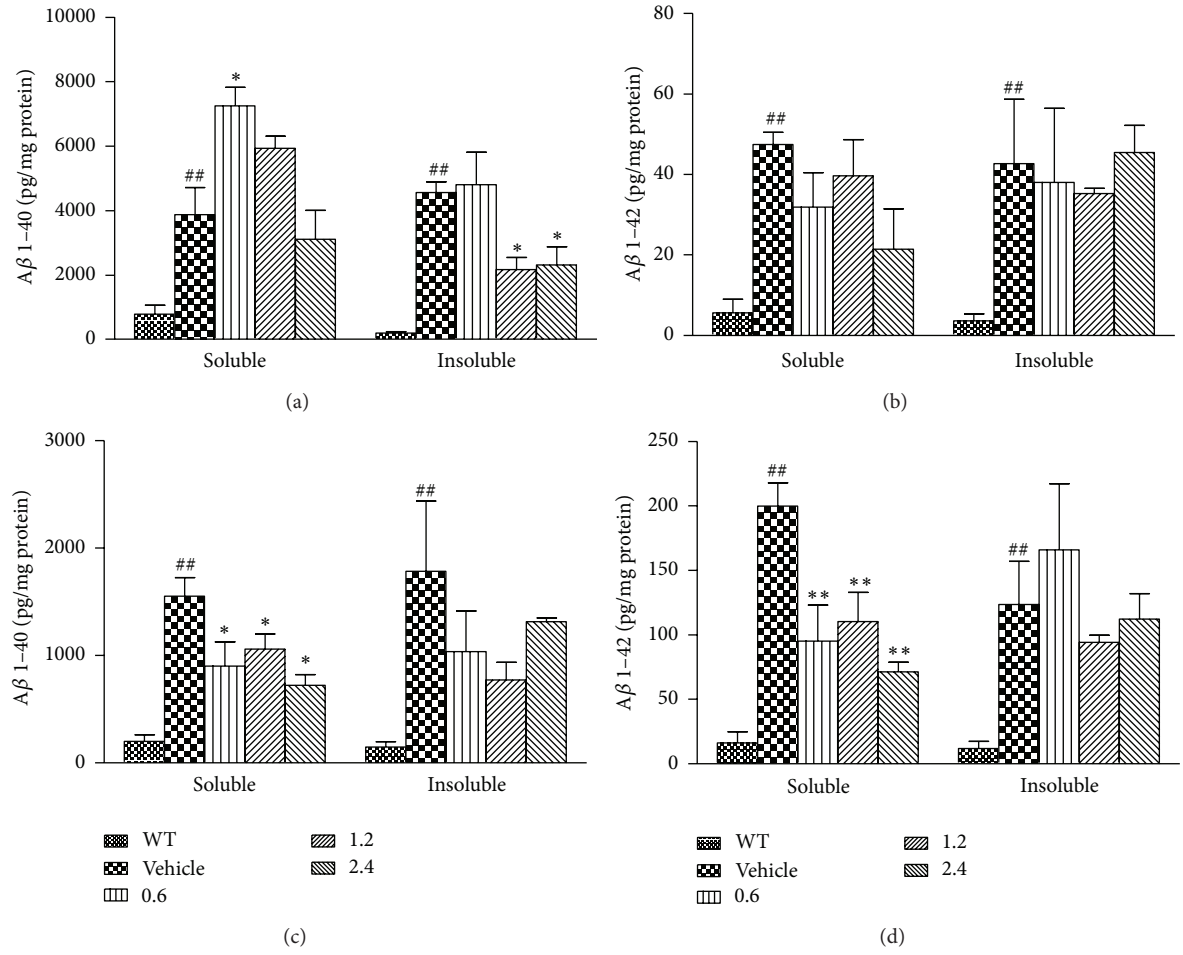

Figure 4: Effects of PN-1 treatment (mg/kg once a day) on Aβ levels. (a) The levels of cortical soluble and insoluble Aβ1–40. (b) The levels of cortical soluble and insoluble Aβ1–42. (c) The levels of hippocampal soluble and insoluble Aβ1–40. (d) The levels of hippocampal soluble and insoluble Aβ1–42. Data represent means ± SEM ($n = 4$ mice/group). $^{*}P < 0.05$, $^{**}P < 0.01$, versus the vehicle-treated group; $^{\#\#}P < 0.01$ versus the wild-type group.

(brain, liver, kidney, lung, heart, spleen, etc.) showed no abnormal tissue architecture and cell morphology between vehicle- and PN-1-treated animals (Supplementary Figure S2).

4. Discussion

Although more than one hundred years had passed since AD was first described by Alois Alzheimer in 1906, the treatment is limited to the use of acetyl-cholinesterase inhibitors and N-methyl D-aspartic acid (NMDA) receptor antagonists [28]. In recent decades, many oriental medicine prescriptions have documented the efficacy and effectiveness in AD therapeutics, such as Yokukansan (Yi Gan San) [29–32] and Chotosan (Gou Teng San) [33–35]. They all contain a large number of components. These prescriptions exert potential benefits to cognitive functions in clinical trials and animal model studies and may unveil new strategy for dementia treatment as new beneficial candidates to widen therapeutic options for AD.

In this study, we first assessed the effect of PN-1 on the recognition memory for the NOR task, which is widely-used to assess nonspatial working, declarative memory task [36]. In our study, vehicle-treated mice could no longer discriminate a novel from a familiar object. However, Aricept- and PN-1-treated mice spent more time exploring novel objects versus familiar ones. The findings may suggest that PN-1 contributes to recognition memory consolidation. The MWM test has been used to assess hippocampal-dependent long-term spatial learning and memory [37, 38]. Vehicle-treated mice exhibited significantly impaired spatial learning and memory performance both in the hidden platform test and probe trial. However, this impairment was ameliorated after PN-1 treatment, suggesting that PN-1 may improve hippocampal-dependent long-term spatial learning and memory. Besides, NOR and MWM data provide additional evidence that PN-1 may have clinical beneficial effects on behavioral disturbances of Alzheimer-type dementia, such as getting lost behavior or misidentification [39, 40].

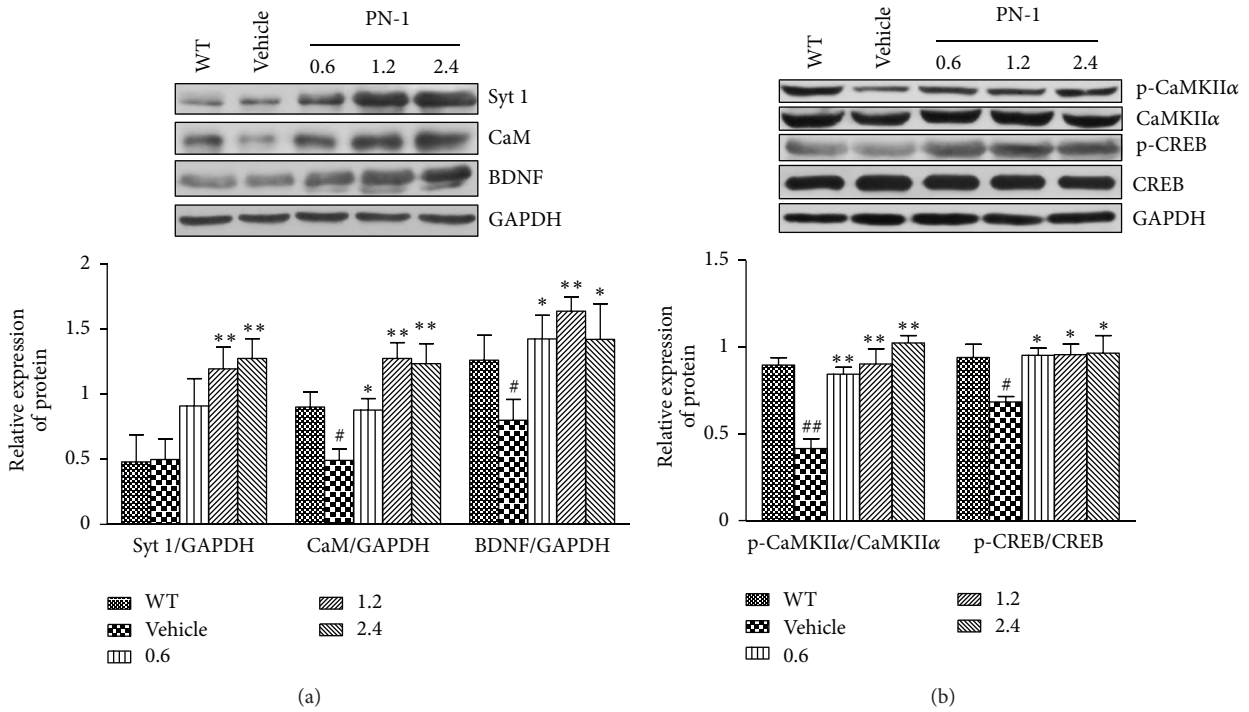

Figure 5: Effects of PN-1 treatment (mg/kg once a day) on the expressions of plasticity-related proteins. The top panels show a representative western blots, and the bottom panels show the quantitation of changes in protein levels by densitometry. (a) The levels of Syt 1, CaM, and BDNF expressions. (b) The phosphorylation status of CaMKIIα and CREB. Data represent means ± SEM ($n = 6$ mice/group) from 3 independent experiments. $^{*}P < 0.05$, $^{**}P < 0.01$ versus the vehicle-treated group. $^{\#}P < 0.05$, $^{\#\#}P < 0.01$ versus the wild-type group.

Since the accumulation of Aβ peptides in the brain is a central event of AD pathogenesis [13, 14] and strongly associates with cognitive decline [41], we next analyzed neuropathological changes after PN-1 treatment. The immunohistochemical results showed that PN-1 reduced plaque number and plaque size most effectively in the cortex and hippocampus of transgenic animals. Interestingly, the current data also demonstrated that PN-1 could reduce plaque number in subregions, such as cortical S1C and EC, hippocampal CA1 area, and DG molecular layer. In addition, we used thioflavin-S staining to detect dense-core plaques, which have more fibrillar Aβ42 with β sheet secondary structures associated with neuronal loss [42]. In our present study, the intensity of thioflavin-S positive staining decreased significantly following PN-1 treatment observed in the cortex and hippocampus. Furthermore, accumulating evidence has demonstrated that dense-core plaques associate with neuritic and inflammatory pathology in AD patients as well as in mouse models [43]. Therefore, our study also suggests the potential effects of PN-1 on neuroinflammation. Overall, neuropathological findings confirm that PN-1 can reduce amyloid plaque burden located in the brain of the transgenic mouse. We speculated that these changes are beneficial to learning and memory.

The fact that PN-1 affects the plaque burden suggests that it may influence Aβ metabolism in the brain. We observed suppressed soluble Aβ (including Aβ1–40 and Aβ1–42) levels in the hippocampus of PN-1-treated mouse. A recent study has shown that soluble Aβ is associated with AD [44]. Especially, the relative levels of Aβ42 are the key regulators of Aβ aggregation into amyloid plaques. Thus, Aβ42 has been implicated as the initiating molecule in the pathogenesis of AD [45, 46]. Additionally, Aβ40 associates with amyloid deposits in the cerebral vasculature (congophilic angiopathy, CAA) [47] and also causes age-dependent learning defects [48]. The decreased soluble Aβ level after PN-1 treatment may explain its ameliorating effects on hippocampus-dependent tasks of learning and memory tested by NOR and MWM. In contrast, neither hippocampal insoluble Aβ1–40 and Aβ1–42 levels nor cortical soluble Aβ1–40 and insoluble Aβ1–42 levels were changed by PN-1 treatments. We speculate the effects of PN-1 on Aβ levels are regional dependent, consistent with the immunohistochemical results in our study. Indeed, the inhomogeneous distribution of amyloid in the cerebral cortex was demonstrated in AD patients and animal models [49, 50]. Further studies are needed to investigate the possible mechanisms of PN-1 on Aβ metabolism, including Aβ production and clearance. In our study, endogenous Aβ40 and Aβ42 levels were also detected in the wild-type mouse brain, which coincides with previous reports [51].

Considering the toxic effects of soluble Aβ on synaptic functions [9–11], we next evaluated the actions of PN-1 on presynaptic and postsynaptic proteins. We first assessed the effect of PN-1 on CaMKII expression, which is a key mediator in regulating synaptic plasticity and long-memory formation [52]. The results showed there was no significant change

in CaMKIIα expression among wild-type, vehicle-, and PN-1-treated mice. However, PN-1 treatment could strikingly increase phosphorylated CaMKIIα (Tyr286), which keeps CaMKII at an active state [53]. Then, the raised CaM, which is one of the upstream molecules in the CaMKII pathway and critical for CaMKII activation [54], was also detected in PN-1-treated mice. Here, both findings suggest that PN-1 may benefit the impaired long-term memory of transgenic mice through ameliorated CaM/CaMKII/CREB signaling pathway [55, 56]. This hypothesis was confirmed by the increased phosphorylation of CREB at Ser133, resulting in the activation of gene transcription and long-term memory formation [57, 58]. Evidence suggests that phosphorylation of CREB at Ser133 occurs in response to the BDNF expression [59]. The raised BDNF following PN-1 administration in our study suggests that BDNF is also involved in the effects of PN-1 on the improvement of learning and memory deficits in transgenic mice by regulating CaMKII/CREB system [60]. Interestingly, the raised synaptotagmin 1 (Syt 1) in PN-1-treated groups implies that PN-1 also has the potential impact on synaptic vesicles at presynaptic terminals, in which Syt 1 acts as a synaptic vesicle-associated protein that triggers Ca^{2+}-sensitive, rapid neurotransmitter release [61, 62]. In this study, we also detected the expressions of N-Methyl-D-aspartate (NMDA) receptor 2B subunit (NR2B) and AMPA receptor GluR1 subunit. However, there was no significant difference of NR2B and GluR1 expressions among the six groups, suggesting that PN-1 may act on NMDA receptor and AMPA receptor through other mechanisms [63, 64]. Alternatively, the recruitment of NMDA receptor and AMPA receptor to postsynaptic membrane may also contribute to Ca^{2+} influx and subsequent activation of CaMKII to trigger synaptic plasticity observed in PN-1-treated mice abovementioned [65, 66], whereas the total amounts of NMDA receptor and AMPA receptor showed no significant change between each group. These data provide us with other research interests in the future.

We also examined the possible toxic side effects of PN-1 on the animals. Results showed no significant side effect of PN-1 on the metabolism, tissue structure, and function. In the main compositions of PN-1, Radix Astragali, as a traditional Chinese medicine, has been widely used for several thousand years with a lowtoxicity [67, 68]. Both Radix Codonopsis and Rhizoma Atractylodis Macrocephalae are usually used to protect neurons in brain ischemia [69, 70] and improve memory in dementia [71, 72] without significant side effect [72, 73]. Cistanches Herba could promote neuronal growth [74, 75] and enhance learning and memory of the mouse [74]. A new report, however, shows that Cistanches Herba induced cytotoxicity in the male reproductive systems of mice [76]. In our study, we found no evidence of toxicity to the male reproductive systems. According to the TCM theories, Chinese herbal prescriptions always contain numerous individual herbs, which work synergistically together to magnify their healing power and simultaneously counteract the potential side effects of other herbs involved [5]. Anyways, further studies are necessary to evaluate the long-term chronic toxicity of PN-1 in the future.

5. Conclusions

In summary, although the detailed chemical components and the exact targets of PN-1 are unknown now, the results of this study demonstrate that chronic treatment with PN-1 has a robust impact on memory deficits in transgenic mouse models of AD without detectable side effects. The potential mechanisms involved in the PN-1 actions include (1) reduction of amyloid burden in the cortex and hippocampus, (2) inhibition of hippocampal Aβ levels, and (3) reactivation of synaptic function-associated signal pathway. We think the present study has given us more insight into the actions of PN-1 in future research interests. Moreover, the development of such multicomponent herbal medicines targeting multiple sites could be useful for future drug discovery. Also, mechanism studies and identification of active compounds could lead to new discoveries in biological and biomedical sciences. These studies are underway.

References

[1] M. A. Henson, A. C. Roberts, K. Salimi et al., "Developmental regulation of the NMDA receptor subunits, NR3A and NR1, in human prefrontal cortex," *Cerebral Cortex*, vol. 18, no. 11, pp. 2560–2573, 2008.

[2] Y. S. Ho, K. F. So, and R. C. Chang, "Drug discovery from Chinese medicine against neurodegeneration in Alzheimer's and vascular dementia," *Chinese Medicine*, vol. 6, article 15, 2011.

[3] Z. Lin, J. Gu, J. Xiu, T. Mi, J. Dong, and J. K. Tiwari, "Traditional Chinese medicine for senile dementia," *Evidence-Based Complementary and Alternative Medicine*, vol. 2012, Article ID 692621, 13 pages, 2012.

[4] H. Yan, L. Li, and X. C. Tang, "Treating senile dementia with traditional Chinese medicine," *Clinical Interventions in Aging*, vol. 2, no. 2, pp. 201–208, 2007.

[5] B. Flaws and P. Sionneau, *The Treatment of Modern Western Medical Diseases with Chinese Medicine: A Textbook & Clinical Manual*, Blue Poppy Press, Boulder, Colo, USA, 2001.

[6] D. A. Evans, H. H. Funkenstein, M. S. Albert et al., "Prevalence of Alzheimer's disease in a community population of older persons. Higher than previously reported," *Journal of the American Medical Association*, vol. 262, no. 18, pp. 2551–2556, 1989.

[7] A. M. A. Brands, G. J. Biessels, E. H. F. De Haan, L. J. Kappelle, and R. P. C. Kessels, "The effects of type 1 diabetes on cognitive performance: a meta-analysis," *Diabetes Care*, vol. 28, no. 3, pp. 726–735, 2005.

[8] D. J. Selkoe, "Alzheimer's disease: genes, proteins, and therapy," *Physiological Reviews*, vol. 81, no. 2, pp. 741–766, 2001.

[9] L. F. Lue, Y. M. Kuo, A. E. Roher et al., "Soluble amyloid β peptide concentration as a predictor of synaptic change in Alzheimer's disease," *American Journal of Pathology*, vol. 155, no. 3, pp. 853–862, 1999.

[10] S. Li, M. Jin, T. Koeglsperger, N. E. Shepardson, G. M. Shankar, and D. J. Selkoe, "Soluble a β oligomers inhibit long-term potentiation through a mechanism involving excessive activation of extrasynaptic NR2B-containing NMDA receptors," *Journal of Neuroscience*, vol. 31, no. 18, pp. 6627–6638, 2011.

[11] F. Kamenetz, T. Tomita, H. Hsieh et al., "APP processing and synaptic function," *Neuron*, vol. 37, no. 6, pp. 925–937, 2003.

[12] G. M. Shankar and D. M. Walsh, "Alzheimer's disease: synaptic dysfunction and Aβ," *Molecular Neurodegeneration*, vol. 4, no. 1, article 48, 2009.

[13] B. J. Cummings and C. W. Cotman, "Image analysis of β-amyloid load in Alzheimer's disease and relation to dementia severity," *Lancet*, vol. 346, no. 8989, pp. 1524–1528, 1995.

[14] G. Blessed, B. E. Tomlinson, and M. Roth, "The association between quantitative measures of dementia and of senile change in the cerebral grey matter of elderly subjects," *British Journal of Psychiatry*, vol. 114, no. 512, pp. 797–811, 1968.

[15] H. Okano, T. Hirano, and E. Balaban, "Learning and memory," *Proceedings of the National Academy of Sciences of the United States of America*, vol. 97, no. 23, pp. 12403–12404, 2000.

[16] S. M. Yuan, K. Gao, D. M. Wang et al., "Evodiamine improves congnitive abilities in SAMP8 and APP swe/PS1ΔE9 transgenic mouse models of Alzheimer's disease," *Acta Pharmacologica Sinica*, vol. 32, no. 3, pp. 295–302, 2011.

[17] X. Wang, P. Liu, H. Zhu et al., "miR-34a, a microRNA up-regulated in a double transgenic mouse model of Alzheimer's disease, inhibits bcl2 translation," *Brain Research Bulletin*, vol. 80, no. 4-5, pp. 268–273, 2009.

[18] State Pharmacopoeia Commission of PRC, *Pharmacopoeia of the People's Republic of China*, Beijing, China, 2010.

[19] World Health Organization, *Quality Control Methods for Medicinal Plant Materials*, Geneva, Switzerland, 1998.

[20] Z. W. Tan, H. Y. Hu, and X. Chen, "Effect of qingxin kaiqiao recipe saponin on the expressions of Bax, Bcl-2, Abeta, and betaAPP in the cortex and hippocampus of Alzheimer's disease rats," *Zhongguo Zhong Xi Yi Jie He Za Zhi*, vol. 32, no. 9, pp. 1258–1263, 2012.

[21] L. Gao, Q. Tang, X. He, and M. Bi, "Effect of icariin on learning and memory abilities and activity of cholinergic system of senescence-accelerated mice SAMP10," *Zhongguo Zhong Yao Za Zhi*, vol. 37, no. 14, pp. 2117–2121, 2012.

[22] J. M. Maler, H. Esselmann, J. Wiltfang et al., "Memantine inhibits ethanol-induced NMDA receptor up-regulation in rat hippocampal neurons," *Brain Research*, vol. 1052, no. 2, pp. 156–162, 2005.

[23] G. Arqué, V. Fotaki, D. Fernández, M. M. de Lagrán, M. L. Arbonés, and M. Dierssen, "Impaired spatial learning strategies and novel object recognition in mice haploinsufficient for the dual specificity tyrosine-regulated kinase-1A (Dyrk1A)," *PLoS ONE*, vol. 3, no. 7, Article ID e2575, 2008.

[24] G. M. Shankar, S. Li, T. H. Mehta et al., "Amyloid-beta protein dimers isolated directly from Alzheimer's brains impair synaptic plasticity and memory," *Nature Medicine*, vol. 14, no. 8, pp. 837–842, 2008.

[25] S. P. Handattu, D. W. Garber, C. E. Monroe et al., "Oral apolipoprotein A-I mimetic peptide improves cognitive function and reduces amyloid burden in a mouse model of Alzheimer's disease," *Neurobiology of Disease*, vol. 34, no. 3, pp. 525–534, 2009.

[26] D. Paris, N. J. Ganey, V. Laporte et al., "Reduction of β-amyloid pathology by celastrol in a transgenic mouse model of Alzheimer's disease," *Journal of Neuroinflammation*, vol. 7, article 17, 2010.

[27] H. Schulman, "Protein phosphorylation in neuronal plasticity and gene expression," *Current Opinion in Neurobiology*, vol. 5, no. 3, pp. 375–381, 1995.

[28] F. Mangialasche, A. Solomon, B. Winblad, P. Mecocci, and M. Kivipelto, "Alzheimer's disease: clinical trials and drug development," *The Lancet Neurology*, vol. 9, no. 7, pp. 702–716, 2010.

[29] Y. Hayashi, Y. Ishida, T. Inoue et al., "Treatment of behavioral and psychological symptoms of Alzheimer-type dementia with Yokukansan in clinical practice," *Progress in Neuro-Psychopharmacology and Biological Psychiatry*, vol. 34, no. 3, pp. 541–545, 2010.

[30] K. Sekiguchi, T. Yamaguchi, M. Tabuchi, Y. Ikarashi, and Y. Kase, "Effects of yokukansan, a traditional Japanese medicine, on aggressiveness induced by intracerebroventricular injection of amyloid β protein into mice," *Phytotherapy Research*, vol. 23, no. 8, pp. 1175–1181, 2009.

[31] M. Tateno, W. Ukai, T. Ono, S. Saito, E. Hashimoto, and T. Saito, "Neuroprotective effects of Yi-Gan San against beta amyloid-induced cytotoxicity on rat cortical neurons," *Progress in Neuro-Psychopharmacology and Biological Psychiatry*, vol. 32, no. 7, pp. 1704–1707, 2008.

[32] H. Ai, W. Yang, M. Ye, W. Lu, L. Yao, and J. H. Luo, "Differential regulation of AMPA receptor GluA1 phosphorylation at serine 831 and 845 associated with activation of NMDA receptor subpopulations," *Neuroscience Letters*, vol. 497, no. 2, pp. 94–98, 2011.

[33] T. Suzuki, S. Futami, Y. Igari et al., "A Chinese herbal medicine, choto-san, improves cognitive function and activities of daily living of patients with dementia: a double-blind, randomized, placebo-controlled study," *Journal of the American Geriatrics Society*, vol. 53, no. 12, pp. 2238–2240, 2005.

[34] Q. Zhao, Y. Murakami, M. Tohda, R. Obi, Y. Shimada, and K. Matsumoto, "Chotosan, a Kampo formula, ameliorates chronic cerebral hypoperfusion-induced deficits in object recognition behaviors and central cholinergic systems in mice," *Journal of Pharmacological Sciences*, vol. 103, no. 4, pp. 360–373, 2007.

[35] Y. Mizushima, S. Kan, S. Yoshida, Y. Irie, and Y. Urata, "Effect of Choto-san, a Kampo medicine, on impairment of passive avoidance performance in senescence accelerated mouse (SAM)," *Phytotherapy Research*, vol. 17, no. 5, pp. 542–545, 2003.

[36] J. K. Wide, K. Hanratty, J. Ting, and L. A. M. Galea, "High level estradiol impairs and low level estradiol facilitates non-spatial working memory," *Behavioural Brain Research*, vol. 155, no. 1, pp. 45–53, 2004.

[37] S. C. Mueller, V. Temple, E. Oh et al., "Early androgen exposure modulates spatial cognition in congenital adrenal hyperplasia (CAH)," *Psychoneuroendocrinology*, vol. 33, no. 7, pp. 973–980, 2008.

[38] A. C. G. Souza, C. A. Brüning, M. R. Leite, G. Zeni, and C. W. Nogueira, "Diphenyl diselenide improves scopolamine-induced memory impairment in mice," *Behavioural Pharmacology*, vol. 21, no. 5-6, pp. 556–562, 2010.

[39] J. P. Hwang, C. H. Yang, S. J. Tsai, and K. M. Liu, "Behavioural disturbances in psychiatric inpatients with dementia of the Alzheimer's type in Taiwan," *International Journal of Geriatric Psychiatry*, vol. 12, no. 9, pp. 902–906, 1997.

[40] M. Harciarek and A. Kertesz, "The prevalence of misidentification syndromes in neurodegenerative diseases," *Alzheimer Disease and Associated Disorders*, vol. 22, no. 2, pp. 163–169, 2008.

[41] E. K. Perry, B. E. Tomlinson, and G. Blessed, "Correlation of cholinergic abnormalities with senile plaques and mental test scores in senile dementia," *British Medical Journal*, vol. 2, no. 6150, pp. 1457–1459, 1978.

[42] M. Rak, M. R. Del Bigio, S. Mai, D. Westaway, and K. M. Gough, "Dense-core and diffuse Aβ plaques in TgCRND8 mice studied with synchrotron FTIR microspectroscopy," *Biopolymers*, vol. 87, no. 4, pp. 207–217, 2007.

[43] T. Bussière, F. Bard, R. Barbour et al., "Morphological characterization of Thioflavin-S-positive amyloid plaques in transgenic Alzheimer mice and effect of passive Aβ immunotherapy on their clearance," *American Journal of Pathology*, vol. 165, no. 3, pp. 987–995, 2004.

[44] J. M. Mc Donald, G. M. Savva, C. Brayne et al., "The presence of sodium dodecyl sulphate-stable Aβ dimers is strongly associated with Alzheimer-type dementia," *Brain*, vol. 133, no. 5, pp. 1328–1341, 2010.

[45] T. E. Golde, "The pathogenesis of Alzheimer's disease and the role of Abeta42," *CNS Spectrums*, vol. 12, no. 1, supplement1, pp. 4–6, 2007.

[46] E. McGowan, F. Pickford, J. Kim et al., "Aβ42 is essential for parenchymal and vascular amyloid deposition in mice," *Neuron*, vol. 47, no. 2, pp. 191–199, 2005.

[47] S. A. Gravina, L. Ho, C. B. Eckman et al., "Amyloid β protein (Aβ) in Alzheimer's disease brain. Biochemical and immunocytochemical analysis with antibodies specific for forms ending at Aβ40 or Aβ42(43)," *Journal of Biological Chemistry*, vol. 270, no. 13, pp. 7013–7016, 1995.

[48] K. Iijima, H. P. Liu, A. S. Chiang, S. A. Hearn, M. Konsolaki, and Y. Zhong, "Dissecting the pathological effects of human Aβ40 and Aβ42 in *Drosophila*: a potential model for Alzheimer's disease," *Proceedings of the National Academy of Sciences of the United States of America*, vol. 101, no. 17, pp. 6623–6628, 2004.

[49] T. Bussière, P. D. Friend, N. Sadeghi et al., "Stereologic assessment of the total cortical volume occupied by amyloid deposits and its relationship with cognitive status in aging and Alzheimer's disease," *Neuroscience*, vol. 112, no. 1, pp. 75–91, 2002.

[50] A. W. Bero, P. Yan, J. H. Roh et al., "Neuronal activity regulates the regional vulnerability to amyloid-β 2 deposition," *Nature Neuroscience*, vol. 14, no. 6, pp. 750–756, 2011.

[51] Y. Sano, T. Nakaya, S. Pedrini et al., "Physiological mouse brain Aβ levels are not related to the phosphorylation state of threonine-668 of Alzheimer's APP," *PLoS ONE*, vol. 1, no. 1, article e51, 2006.

[52] G. A. Wayman, Y. S. Lee, H. Tokumitsu, A. Silva, and T. R. Soderling, "Calmodulin-kinases: modulators of neuronal development and plasticity," *Neuron*, vol. 59, no. 6, pp. 914–931, 2008.

[53] O. S. Rosenberg, S. Deindl, R. J. Sung, A. C. Nairn, and J. Kuriyan, "Structure of the autoinhibited kinase domain of CaMKII and SAXS analysis of the holoenzyme," *Cell*, vol. 123, no. 5, pp. 849–860, 2005.

[54] K. Fukunaga, D. Muller, and E. Miyamoto, "CaM kinase II in long-term potentiation," *Neurochemistry International*, vol. 28, no. 4, pp. 343–358, 1996.

[55] M. Sheng, M. A. Thompson, and M. E. Greenberg, "CREB: a Ca^{2+}-regulated transcription factor phosphorylated by calmodulin-dependent kinases," *Science*, vol. 252, no. 5011, pp. 1427–1430, 1991.

[56] A. J. Shaywitz and M. E. Greenberg, "CREB: a stimulus-induced transcription factor activated by a diverse array of extracellular signals," *Annual Review of Biochemistry*, vol. 68, pp. 821–861, 1999.

[57] M. R. Montminy, G. A. Gonzalez, and K. K. Yamamoto, "Regulation of cAMP-inducible genes by CREB," *Trends in Neurosciences*, vol. 13, no. 5, pp. 184–188, 1990.

[58] T. E. Meyer and J. F. Habener, "Cyclic adenosine 3′,5′-monophosphate response element binding protein (CREB) and related transcription-activating deoxyribonucleic acid-binding proteins," *Endocrine Reviews*, vol. 14, no. 3, pp. 269–290, 1993.

[59] D. D. Ginty, A. Bonni, and M. E. Greenberg, "Nerve growth factor activates a ras-dependent protein kinase that stimulates c-fos transcription via phosphorylation of CREB," *Cell*, vol. 77, no. 5, pp. 713–726, 1994.

[60] F. Gómez-Pinilla, J. R. Huie, Z. Ying et al., "BDNF and learning: evidence that instrumental training promotes learning within the spinal cord by up-regulating BDNF expression," *Neuroscience*, vol. 148, no. 4, pp. 893–906, 2007.

[61] J. Xu, Z. P. Pang, O. H. Shin, and T. C. Südhof, "Synaptotagmin-1 functions as a Ca^{2+} sensor for spontaneous release," *Nature Neuroscience*, vol. 12, no. 6, pp. 759–766, 2009.

[62] G. Van Den Bogaart, S. Thutupalli, J. H. Risselada et al., "Synaptotagmin-1 may be a distance regulator acting upstream of SNARE nucleation," *Nature Structural and Molecular Biology*, vol. 18, no. 7, pp. 805–812, 2011.

[63] T. Manabe, A. Aiba, A. Yamada et al., "Regulation of long-term potentiation by H-Ras through NMDA receptor phosphorylation," *Journal of Neuroscience*, vol. 20, no. 7, pp. 2504–2511, 2000.

[64] H. K. Lee, K. Takamiya, J. S. Han et al., "Phosphorylation of the AMPA receptor GluR1 subunit is required for synaptic plasticity and retention of spatial memory," *Cell*, vol. 112, no. 5, pp. 631–643, 2003.

[65] H. Lin, R. Huganir, and D. Liao, "Temporal dynamics of NMDA receptor-induced changes in spine morphology and AMPA receptor recruitment to spines," *Biochemical and Biophysical Research Communications*, vol. 316, no. 2, pp. 501–511, 2004.

[66] B. A. Clark and S. G. Cull-Candy, "Activity-dependent recruitment of extrasynaptic NMDA receptor activation at an AMPA receptor-only synapse," *Journal of Neuroscience*, vol. 22, no. 11, pp. 4428–4436, 2002.

[67] S. Y. Yu, H. T. OuYang, J. Y. Yang et al., "Subchronic toxicity studies of *Radix astragali* extract in rats and dogs," *Journal of Ethnopharmacology*, vol. 110, no. 2, pp. 352–355, 2007.

[68] Y. W. Lin and B. H. Chiang, "Anti-tumor activity of the fermentation broth of *Cordyceps militaris* cultured in the medium of *Radix astragali*," *Process Biochemistry*, vol. 43, no. 3, pp. 244–250, 2008.

[69] L. Zhong, Z. F. Wang, and B. J. Xiao, "Research on the antioxidant effect of Enshi banqiao radix codonopsis on brain ischemia/reperfusion (I/R)injury," *Zhongguo Ying Yong Sheng Li Xue Za Zhi*, vol. 28, no. 4, pp. 314–316, 2012.

[70] Q. Gao, Z. H. Ji, Y. Yang, R. Cheng, and X. Y. Yu, "Neuroprotective effect of Rhizoma Atractylodis macrocephalae against excitotoxicity-induced apoptosis in cultured cerebral cortical neurons," *Phytotherapy Research*, 2012.

[71] I. H. Jung, S. E. Jang, E. H. Joh, J. Chung, M. J. Han, and D. H. Kim, "Lancemaside A isolated from *Codonopsis lanceolata* and its metabolite echinocystic acid ameliorate scopolamine-induced memory and learning deficits in mice," *Phytomedicine*, vol. 20, no. 1, pp. 84–88, 2012.

[72] Z. Lin, Y. Yan, D. Zhu, B. Yu, and Q. Wang, "Protective effects of FBD—an experimental Chinese traditional medicinal formula on memory dysfunction in mice induced by cerebral ischemia-reperfusion," *Journal of Ethnopharmacology*, vol. 97, no. 3, pp. 477–483, 2005.

[73] Z. Li, L. Zhu, H. Zhang et al., "Protective effect of a polysaccharide from stem of *Codonopsis pilosula* against renal ischemia/reperfusion injury in rats," *Carbohydrate Polymers*, vol. 90, no. 4, pp. 1739–1743, 2012.

[74] J. G. Choi, M. Moon, H. U. Jeong, M. C. Kim, S. Y. Kim, and M. S. Oh, "Cistanches Herba enhances learning and memory

by inducing nerve growth factor," *Behavioural Brain Research*, vol. 216, no. 2, pp. 652–658, 2011.

[75] B. S. Koo, Y. K. Kim, K. S. Park, K. H. Chung, and C. H. Kim, "Attenuating effect of a traditional Korean formulation, Paeng-Jo-Yeon-Nyeon-Baek-Ja-In-Hwan (PJBH), on hydrogen peroxide-induced injury in PC12 cells," *Phytotherapy Research*, vol. 18, no. 6, pp. 488–493, 2004.

[76] S. W. Kim, S. H. Yoo, H. J. Lee et al., "Cistanches herba induces testis cytotoxicity in male mice," *Bulletin of Environmental Contamination and Toxicology*, vol. 88, no. 1, pp. 112–117, 2012.

Hindawi Publishing Corporation
Evidence-Based Complementary and Alternative Medicine
Volume 2013, Article ID 298183, 11 pages
http://dx.doi.org/10.1155/2013/298183

Research Article

Random Forest in Clinical Metabolomics for Phenotypic Discrimination and Biomarker Selection

Tianlu Chen, Yu Cao, Yinan Zhang, Jiajian Liu, Yuqian Bao, Congrong Wang, Weiping Jia, and Aihua Zhao

Center for Translational Medicine and Shanghai Key Laboratory of Diabetes Mellitus, Department of Endocrinology and Metabolism, Shanghai Jiao Tong University Affiliated Sixth People's Hospital, Shanghai 200233, China

Correspondence should be addressed to Aihua Zhao; zhah@sjtu.edu.cn

Received 10 November 2012; Accepted 11 December 2012

Academic Editor: Wei Jia

Metabolomic data analysis becomes increasingly challenging when dealing with clinical samples with diverse demographic and genetic backgrounds and various pathological conditions or treatments. Although many classification tools, such as projection to latent structures (PLS), support vector machine (SVM), linear discriminant analysis (LDA), and random forest (RF), have been successfully used in metabolomics, their performance including strengths and limitations in clinical data analysis has not been clear to researchers due to the lack of systematic evaluation of these tools. In this paper we comparatively evaluated the four classifiers, PLS, SVM, LDA, and RF, in the analysis of clinical metabolomic data derived from gas chromatography mass spectrometry platform of healthy subjects and patients diagnosed with colorectal cancer, where cross-validation, R^2/Q^2 plot, receiver operating characteristic curve, variable reduction, and Pearson correlation were performed. RF outperforms the other three classifiers in the given clinical data sets, highlighting its comparative advantages as a suitable classification and biomarker selection tool for clinical metabolomic data analysis.

1. Introduction

Metabolomics [1] or metabonomics [2, 3] is an emerging-omics approach using nuclear magnetic resonance (NMR) spectroscopy or gas chromatography/liquid chromatography-mass spectrometry (GC-MS or LC-MS) technologies. It constitutes a field of science that deals with the measurement of metabolite variations in a biological compartment for the study of the physiological processes in response to xenobiotic interventions that is complementary to organ-specific biochemical and histological findings. Through the analysis of one or several kinds of biofluids including serum, urine, saliva, and tissue samples, the global and dynamic alterations in metabolism can be deciphered [4]. Therefore, metabolomics has been increasingly used in many applications such as identifying metabolite markers for clinical diagnosis and prognosis [5], monitoring the chemical-induced toxicity [6], exploring the potential mechanism of diverse diseases [7], and assessing therapeutic effects of treatment modalities [8, 9]. Univariate and/or multivariate statistical methods are routinely used in metabolomics studies, aiming at successful classification of samples with metabolic phenotypic variations and identification of potential biomarkers while minimizing the technical variations.

To date, the most widely used classification methods in metabolomic data processing include principal component analysis (PCA), projection to latent structures (PLS) analysis, support vector machine (SVM), Linear discriminant analysis (LDA), and univariate statistical analysis such as Student's t-test and analysis of variance (ANOVA) test [10, 11]. We recently applied some of these methods in combination to identify metabolite-based biomarkers in hepatocellular carcinoma [5], gastric cardia cancer [12], knee osteoarthritis [13], oral cancer [14], and schizophrenia [7]. Nevertheless, more effective and robust bioinformatics tools are in critical need for metabolomic data analysis especially when dealing with clinical samples with large individual variability due to diverse demographic and genetic background of patients and various pathological conditions or treatments.

A machine learning method, random forest (RF), is reported as an excellent classifier with the following advantages: simple theory, fast speed, stable and insensitive to noise, little or no overfitting, and automatic compensation mechanism on biased sample numbers of groups [15]. RF has been widely used in microarray [16–18] and single nucleotide polymorphism (SNP) [19] data analysis achieving good performance. However, in the field of clinical metabolomic data analysis, it has not got enough attention and concern. In addition, no comprehensive performance evaluation about this classifier is reported.

In this research, RF was used in the analysis of a GC-MS derived clinical metabolomic dataset. Its classification and biomarker selection performances were compared with PLS, LDA, and SVM comprehensively. The score plot based on cross validation was used for classification accuracy evaluation. The cross-validation and ROC (receiver operating characteristic) curve were carried out to test their prediction ability and stability. The R^2/Q^2 plot was adopted for overfitting measurement. Variable number dependence of the 4 classifiers was explored by eliminating variables step by step. Besides these classification performances, the variable ranking and putative biomarker selection power of RF was examined as well by Pearson correlation.

2. Methods

2.1. Metabolomic Data Set. Colorectal cancer (CRC) is one of the common types of cancer and the leading causes of cancer death in the world [20]. Urinary samples of 67 CRC patients (67 preoperation samples and 63 matched postoperation ones) and 65 healthy volunteers were collected from the Cancer Hospital affiliated to Fudan University (Shanghai, China). Patients enrolled in this study were not on any medication before preoperative sample collection. The postoperative samples were collected on the 7 day after surgery. Sample collection protocol was approved by the Cancer Hospital Institutional Review Board and written consents were signed by all participants prior to the study. The healthy volunteers were selected by a routine physical examination, and any subjects with inflammatory conditions or gastrointestinal tract disorders were excluded. Other background information such as diet and alcohol consumption was considered during sample selection to minimize the diet-induced metabolic variations. All the samples were collected in the morning before breakfast, immediately centrifuged, and stored at −80°C until analysis. Clinical characteristics of all the samples in this study are provided in Table 1. All the samples were chemically derivatized and subsequently analyzed by GC-MS following our previously published procedures [21].

The acquired MS data were pretreated and processed according to our previously published protocols [5, 7]. A total of 187 variables (areas of peaks, denoting concentrations of metabolites), 35 metabolites were obtained from the spectral data analysis. Normalization (to the total intensity to compensate for the overall variability during sample extraction, injection, detection, and disparity of urine volume), mean centering, and unit variance scaling of the data sets were performed prior to statistical analysis. Finally, the data set contains 187 variables and 195 samples. Two cases: (a) Normal versus CRC patients (preoperative) and (b) Preoperative versus postoperative patients were involved for analysis.

2.2. Random Forest. Random forest (RF), developed by Breiman [22], is a combination of tree-structured predictors (decision trees). Each tree is constructed via a tree classification algorithm and casts a unit vote for the most popular class based on a bootstrap sampling (random sampling with replacement) of the data. The simplest random forest with random features is formed by selecting randomly, at each node, a small group of input variables to split on. The size of the group is fixed throughout the process of growing the forest. Each tree is grown by using the CART (classification and regression tree) methodology without pruning. The tree number of the forest in this study is set to be 200, the number of input variables tried for each node is the square root of the number of total variables, and the minimum size of the terminal nodes is set to be 2. The "score" of RF is the scaled sum of votes derived from the trained trees for out-of-bag samples.

RF includes two methods for measuring the importance of a variable or how much it contributes to predictive accuracy. The default method is the Gini score (the method of this study). For any variable, the measure is the increase in prediction error if the values of that variable are permuted across the out-of-bag observations. This measure is computed for every tree, then averaged over the entire ensemble, and divided by the standard deviation over the entire ensemble. Therefore, the larger the Gini score is (ranges from 1 to 100), the more important a variable is.

Please refer to the appendices for the introduction of other classifiers (PLS, SVM, and LDA).

2.3. Evaluation of Classification Performance. The classification performance of RF as well as PLS, LDA, and SVM can be evaluated and compared using several approaches: cross-validation, R^2/Q^2 plot, ROC, and reduction of variable number.

2.3.1. Cross-Validation: Prediction Ability and Stability. Two types of cross-validations: k-fold and x% hold out were employed to estimate the prediction ability with low bias and low variance. (1) In the k-fold cross-validation, the training set was first divided into k subsets (the folds) of approximately equal size. Sequentially each subset was tested using the classifier trained on the remaining k−1 subsets, where k was set to be 7 and 10 in this study. (2) Holdout cross-validation is similar to k-fold cross-validation except for the repeatedly (100 times) random selection of the two mutually exclusive training and testing (holdout) subsets in accordance with a given ratio. This method was used with an understanding that the more instances left for the holdout set, the higher the bias of the estimate would be. On the other hand, fewer holdout set instances mean that the confidence

Table 1: Sample information.

Data set	CRC		
Sample type	urine		
Group	Normal	CRC (preoperation)	postoperation
Number	65	67	63
Age (Mean (minimum, maximum))	55 (38, 74)	59 (40, 76)	60 (40, 77)
Gender (male : female)	23 : 40	35 : 28	36 : 24
Dimension (Sample × variable)	Case A (Normal versus CRC): 132 × 187 Case B (Pre versus Post): 130 × 187		

interval for the accuracy would be wider. Besides accuracy and prediction ability, the repeated holdout cross-validation was used to test the stability of a classifier. The holdout ratios were set as 10%, 15%, and 33%, respectively, on all the classifiers.

2.3.2. R^2/Q^2 Plot—Overfitting. Consider

$$R^2 = 1 - \frac{\sum_{i=1}^{n} (y_i - \widehat{y}_i)^2}{\sum_{i=1}^{n} (y_i - \overline{y}_i)^2},$$
$$Q^2 = 1 - \frac{\sum_{i=1}^{n} \left(y_i - \widehat{y}_{(i)}\right)^2}{\sum_{i=1}^{n} \left(y_i - \overline{y}_{(i)}\right)^2}. \quad (1)$$

In the equations, n represents total number of samples, y_i is the predicted class (0 or 1) of the ith sample when all the samples are used for model building, $\widehat{y}_i$ is the actual class, $\overline{y}_i$ is the average of the predicted class, and $y_{(i)}$ is the predicted class when all the samples except the ith sample are used for model building (leave one out cross-validation).

The criteria for classifier validity are as follows. (1) All the R^2 and Q^2 values on the permuted data set are lower than those on the actual data set. (2) The regression line of Q^2 (line joining the actual Q^2 point to the centroid of the cluster of permuted Q^2 values) has a negative intercept value on the vertical axis.

2.3.3. Receiver Operating Characteristic (ROC): Diagnosis Potential. ROC analysis is a classic method from signal detection theory and is now commonly used in clinical research [23]. ROC of a classifier shows its performance as a tradeoff between specificity and sensitivity. Sensitivity is defined as the proportion of subjects with disease whose tests is positive, and calculated by the formula, TruePositive/(TruePositive+FalseNegative). Specificity, on the other hand, is defined as the proportion of subjects without disease whose tests is negative, and calculated in the formula, TrueNegative/(TrueNegative+FalsePositive). Typically, 1-specificity is plotted on the x-axis and sensitivity is plotted on the vertical axis. All the predictive behavior of a classifier can be represented by the points in the ROC curve independent of class distributions or error cost [23]. The area under the ROC curve (AUC) is a statistic summary of its diagnostic potential.

2.3.4. Variable Number Dependence. Generally, too many irrelevant variables are liable to result in overfitting decisions, whereas differences between groups cannot be extracted and depicted completely if crucial variables are not concerned [24]. Variable number dependence is therefore a necessary factor for classifier performance evaluation.

To avoid bias, it is advisable to rank and eliminate variables one by one. Initially, the whole dataset is taken when a classifier is computed. Then, a list of variables in descending order relative to classification importance is established and the variable in the end is eliminated for subsequent analysis. This process is repeated until only one variable is left for classifier building. The last few variables are of great potential to be biomarkers for separating the groups.

2.4. Evaluation of Biomarker Selection Performance. Prediction ability and stability, overfitting, diagnosis potential, and variable number dependence are important aspects for a classifier. Variable ranking and biomarker selection is of the same importance in metabolomics study.

For RF, variables are ranked by Gini score, a measurement of average accuracy of all trees containing a particular variable [22]. For PLS, the conventional VIP (variable importance in projection) value is used for variable ranking. For LDA, the coefficients of variables in the discriminant function indicate their importance. As to SVM, the importance of variables is evaluated by the SVM recursive feature elimination (SVM-RFE) algorithm [25].

As each classifier possesses its own algorithm for variable importance ranking with its own strength and weakness, the Pearson correlation coefficient of every two ranks was used to evaluate their consistency and the rank of t-test (by ascending order of variable P values) was taken as an unbiased reference. The consistency comparison was conducted on two levels: ranks of all variables and ranks of identified metabolites.

All the metabolites were identified and verified by public libraries such as HMDB, KEGG, and/or reference standards available in our laboratory.

All the classifiers andevaluation methods were carried out using Matlab toolbox (Version 2009a, Mathworks).

3. Results and Discussion

3.1. Classification Performance. RF as well as PLS, LDA, and SVM were applied on the dataset for the two comparative

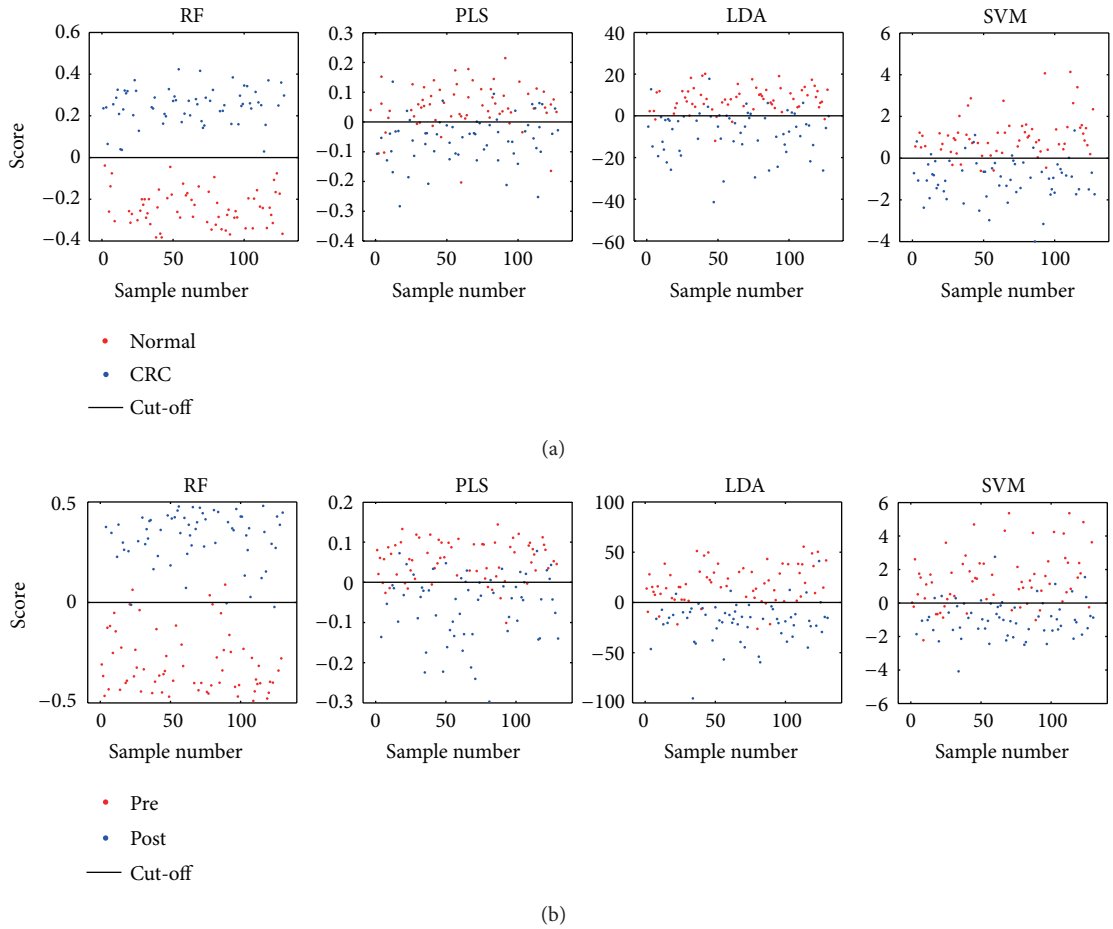

Figure 1: Classification score plots of RF, PLS, LDA, and SVM on cases (a) and (b) based on urinary metabolomic data derived from GC-MS. x-axis is the sample index and y-axis is the classification scores. (a) Normal versus CRC, (b) pre versus post.

cases (Figures 1(a) and 1(b)). In Figure 1(a), red and blue dots represent the normal and CRC patients, respectively. x-axis is the sample index and y-axis is the corresponding "score" of every classifier. RF achieved the best separation with no miss-classified samples (the accuracy is 100%). The performance of SVM, LDA, and PLS was good, with descending accuracy of 90.9%, 87.1%, and 82.6%, respectively. Similarly, Figure 1(b) shows the separation between CRC preoperative patients (red dots) and CRC postoperative patients (blue dots). RF yielded 95.4%, a higher classification accuracy than that of LDA, SVM, and PLS, which achieved 90.8%, 80.8%, and 80.8%, respectively.

3.2. Prediction Ability, Stability, Overfitting, and Diagnostic Ability Evaluation. The accuracy of classification is crucial for a classifier, while other classification behaviors such as prediction ability, stability, degree of overfitting and diagnostic ability are of equal significance as well.

The holdout cross-validation results (33% holdout samples, 100 times) of RF (purple), PLS (blue), LDA (red), and SVM (green) on the two cases are presented as box plots (Figure 2). The y-axis denotes the error rate (the smaller, the better). The purple box of RF is always the lowest and shortest in both cases. As to the other three classifiers, their performances are similar showing no significant difference. These results were validated further by more cross-validation results listed in Table 2. As expected, the average error rates and standard deviations (S.D.s) of (1) holdout cross-validations on 10% and 15% samples; and (2) 7-and 10-fold cross-validations by PLS, SVM, and LDA are at almost the same level and are all greater than that of RF. Therefore, RF is the one with highest prediction ability and best stability among all the classifiers.

Figures 3(a) and 3(b) display the correlation between the actual y-variable and the permuted y-variable (x-axis) versus the R^2/Q^2 values (y-axis) of RF (purple), PLS (blue), LDA (red), and SVM (green) on the two cases, respectively. A dot denotes R^2 and a circle represents Q^2. The straight line and dash dot line are the regression lines (lines linking the value from the actual data set and the 100 permuted ones) of R^2 and Q^2, respectively. Obviously, the R^2/Q^2 values of RF on the permuted data sets are all under zero and are well lower than those on the actual data set. Consequently, RF does not over fit the data and so will give out reliable result on new samples. As to SVM, its R^2 values on the permuted data sets are slightly

Table 2: Averaged error rates and their standard deviations of RF, PLS, LDA, and SVM on 2 cases by 7- and 10-fold cross-validation as well as 10% and 15% hold out cross-validation (100 times).

Case	Evaluation item	RF error rate mean (S.D.)		PLS error rate mean (S.D.)		SVM error rate mean (S.D.)		LDA error rate mean (S.D.)	
(A) Normal versus CRC	7-fold CV	0.071	$(8.364E-03)$	0.134	$(7.845E-02)$	0.148	$(7.998E-02)$	0.227	$(9.897E-02)$
	10-fold CV	0.069	$(7.482E-03)$	0.094	$(8.990E-02)$	0.126	$(6.673E-02)$	0.188	$(1.375E-01)$
	15% holdout CV	0.065	$(6.545E-03)$	0.132	$(7.009E-02)$	0.117	$(7.344E-02)$	0.189	$(8.206E-02)$
	10% holdout CV	0.065	$(5.445E-03)$	0.121	$(8.407E-02)$	0.113	$(8.572E-02)$	0.181	$(1.073E-01)$
(B) Pre versus post	7-fold CV	0.102	$(3.687E-03)$	0.130	$(7.321E-02)$	0.170	$(8.069E-02)$	0.108	$(5.517E-02)$
	10-fold CV	0.096	$(3.954E-03)$	0.169	$(1.242E-01)$	0.163	$(1.524E-01)$	0.096	$(1.069E-01)$
	15% holdout CV	0.088	$(3.592E-03)$	0.137	$(6.687E-02)$	0.186	$(8.412E-02)$	0.127	$(7.958E-02)$
	10% holdout CV	0.083	$(3.188E-03)$	0.145	$(9.883E-02)$	0.161	$(8.644E-02)$	0.114	$(9.375E-02)$

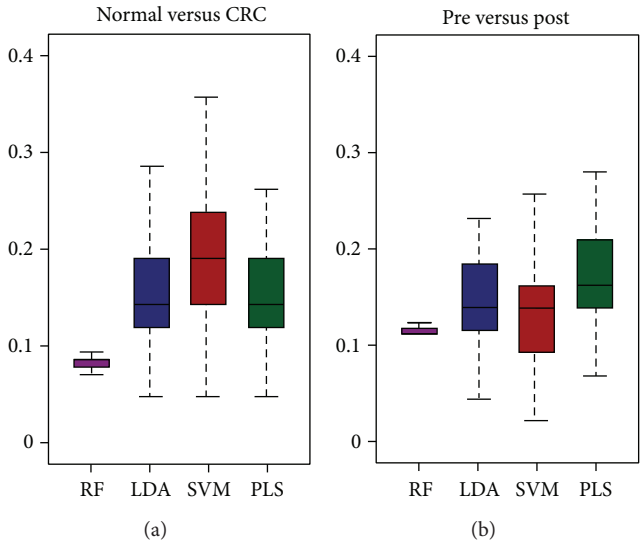

Figure 2: Box plots of holdout cross-validation error rates (y-axis) on randomly selected 33% samples (repeated 100 times) on (a) normal versus CRC, and (b) pre versus post. Purple: RF, blue: PLS, brown: LDA, and green: SVM.

lower than or close to that on actual data set, although most of its Q^2 values on the permuted data sets are under zero and lower than those on the actual data set. Hence, SVM is overfitted and false positive result is prone to appear. This probably caused by its dependence on kernel functions and support vectors.

The ROC curve coupled with its area under the curve (AUC) is a common method used to estimate the diagnosis potential of a classifier in clinical applications. A larger AUC indicates higher prediction ability. The ROC curves and AUC values of all the classifiers in the two cases are plotted in Figure 4. RF outperforms the others once more with the greatest AUC values (AUC > 0.97).

3.3. Variable Number Dependence. Figures 5(a) and 5(b) show the classification error rates (y-axis) against the number of variables (x-axis) involved in the two cases, respectively. It can be seen that with the decrease of variable number used for classifier building, all the curves keep stable initially, and then rise gradually. Further reduction of variables degrades the classifier performance heavily because of the shortage of useful information. The point (or short section) where the curve begins to rise correlates to the optimum number of variables for classifier building. Additionally, RF usually needs fewer variables to achieve the same error rate as the other three classifiers. In case (B), for example, when the error rate is restricted to be less than 0.18 (the red line), RF needs minimum 10 variables whereas PLS, LDA, and SVM require about 150, 45, and 125 ones at least.

3.4. Putative Biomarker Selection. Variable number dependence section is to evaluate whether and how much the performance of RF depends on the number of variables involved. This section is to evaluate its capability on important variable (putative biomarker) selection. The Pearson correlation matrixes of ranks from every two classifiers (including t-Test) based on all variables (A-B) and identified metabolites (C-D) in the two cases are listed in Table 3. On the whole, RF, PLS and t-Test have good consistency with each other (high Pearson correlation coefficients) regardless of whether all variables (Figure 6(a)) or identified metabolites (Figure 6(b)) are involved.

Interestingly, in Table 3, the highest and second highest correlation coefficients are 0.794 for PLS and t-Test (case A) and 0.756 for RF and PLS (case B) indicating the consistency and mutual complementarity of classifiers. All the important metabolites selected by both t-Test ($P < 0.05$) and PLS (VIP > 1) could be filtered by RF (Gini > 50) as well. Consistent with previous metabolomics study, dysregulated metabolic pathways, such as glycolysis, TCA cycle, urea cycle, pyrimidine metabolism, polyamine metabolism as well as gut microbial-host cometabolism were observed [26]. Additionally, more significant metabolites in the above pathways could be found by RF (case A) providing complementary information for CRC study. Figure 7 presents some box plots of intensity in corresponding groups.

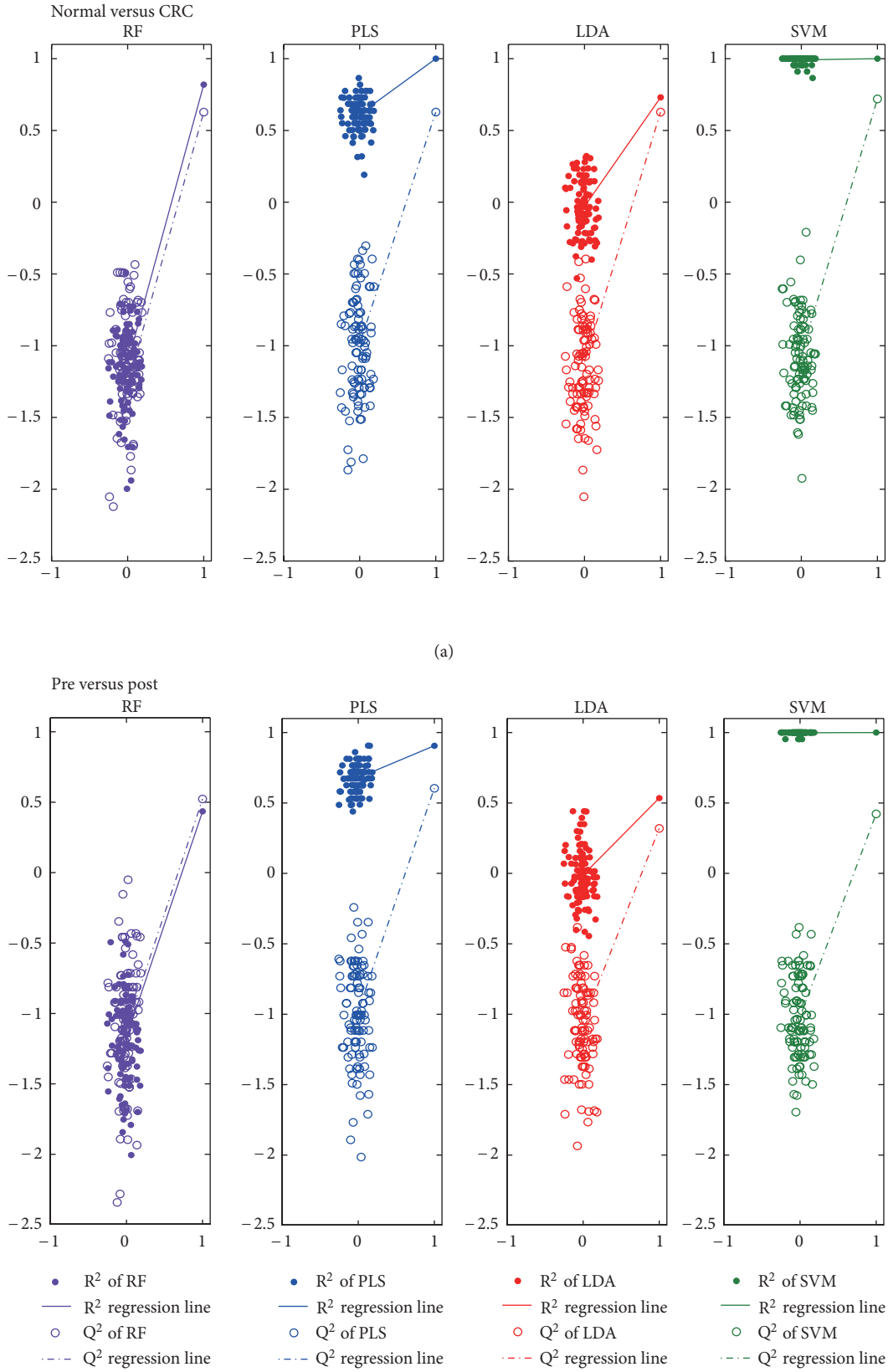

FIGURE 3: R^2/Q^2 plots of 4 classifiers on 2 cases. Correlation between the actual y-variable and the permuted y-variable (x-axis) versus the R^2 and Q^2 values (y-axis) on (a) Normal versus CRC, and (b) pre versus post. Dot: R^2, circle: Q^2, straight line: R^2 regression line, dash dot line: Q^2 regression line. Purple: RF, blue: PLS, brown: LDA, and green: SVM.

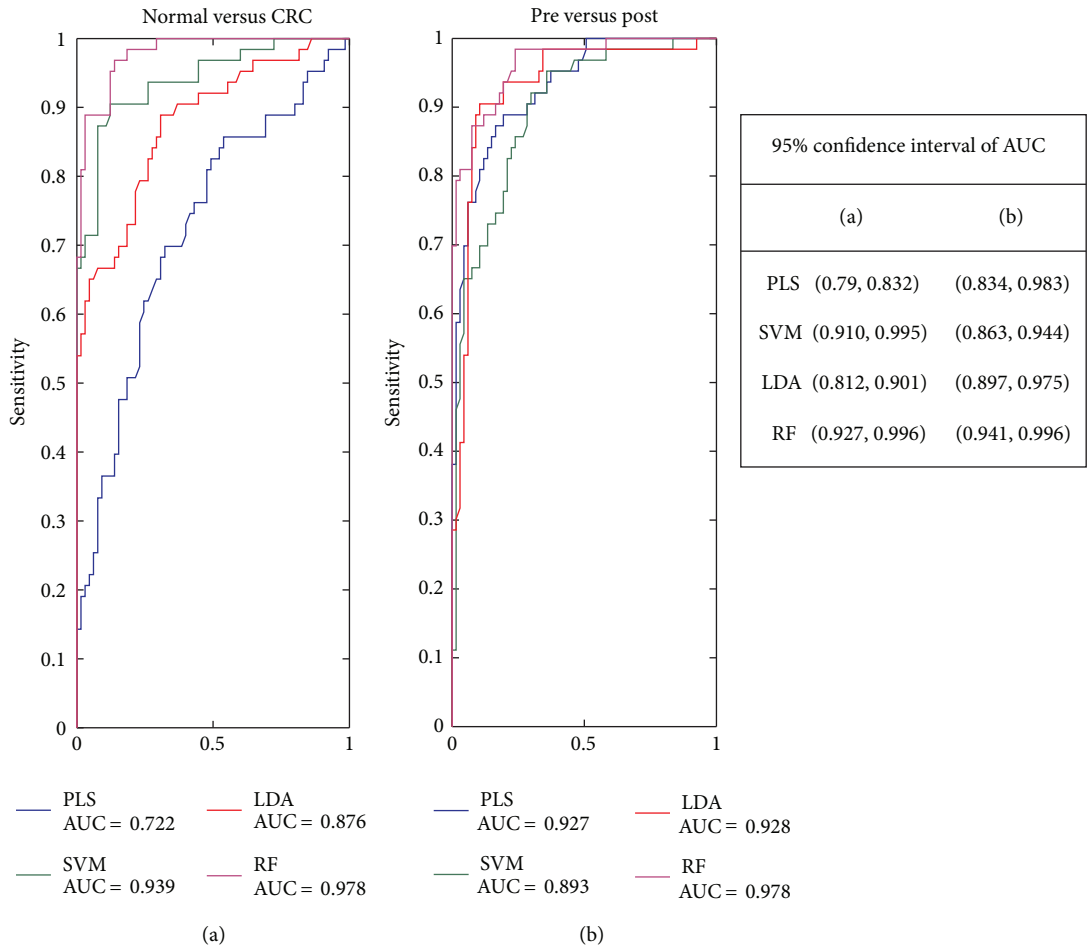

95% confidence interval of AUC		
	(a)	(b)
PLS	(0.79, 0.832)	(0.834, 0.983)
SVM	(0.910, 0.995)	(0.863, 0.944)
LDA	(0.812, 0.901)	(0.897, 0.975)
RF	(0.927, 0.996)	(0.941, 0.996)

Figure 4: Receiver operating characteristic curves of 4 classifiers on 2 cases. Receiver operating characteristic curve and area under curve (AUC) of PLS (blue), LDA (brown), SVM (green), and RF (Purple) on (a) Normal versus CRC and (b) pre versus post.

4. Conclusion

In this study, RF was applied successfully in metabolomic data analysis for clinical phenotype discrimination and biomarker selection. Its various performances were evaluated and compared with the other three classifiers PLS, SVM, and LDA by two types of cross-validations, R^2/Q^2 plot, ROC curve, variable elimination, and Pearson correlation. RF demonstrated the best overall performance including accuracy, prediction ability, overfitting, diagnosis potential, stability, and putative biomarker selection, highlighting its potential as an excellent classification and biomarker selection tool for clinical metabolomic data analysis. PLS outperforms the others in variable ranking and putative biomarker selection whereas its classification ability is not satisfactory enough. LDA demonstrates reasonably good performance in classification but its biomarker selection ability is open to question. SVM may be slightly overfitting regardless of its good classification accuracy and diagnosis potential.

The combinational usage of multiple methods, RF, t-Test, and PLS, for example, may provide more comprehensive information for a "global" understanding of the metabolomics or other "omics" data.

Appendices

A. Projection to Latent Structures (PLS)

The basic object of PLS is to find the linear (or polynomial) relationship between the superior variable Y (a vector indicating sample groups) and the dataset X (variables). The modeling consists of simultaneous projections of both the X and Y spaces on low dimensional hyper planes. The coordinates of the points (projection of X and Y) on these hyper planes constitute the elements of the matrix T (X scores), U (Y scores), P (loadings), and C (weights). The analysis has the following objectives.

(a) To well approximate the X and Y spaces,

(b) To maximize the correlation between X and Y. That is, to maximize the covariance between the sample positions (from different groups) on the hyper planes.

The PLS model accomplishing these objectives can be expressed as

$$X = TP^T + E,$$
$$Y = UC^T + F. \quad (A.1)$$

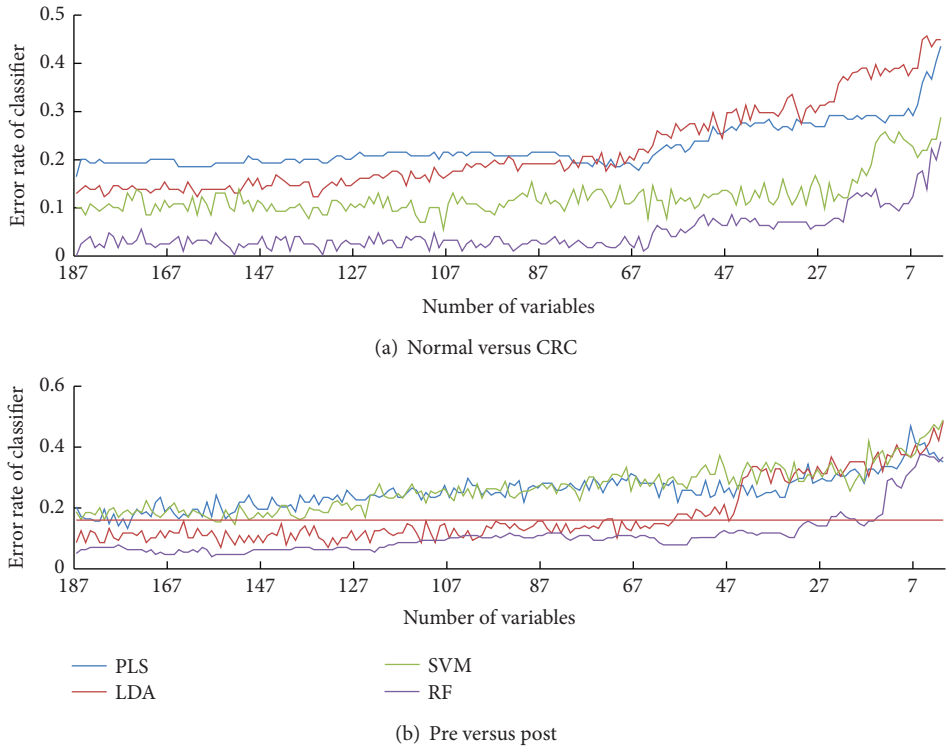

FIGURE 5: Variable dependence plots of 4 classifiers on 2 cases. Error rate (y-axis) of RF (Purple), PLS (blue), LDA (brown), and SVM (green) with decreasing variable number (x-axis) in (a) Normal versus CRC, and (b) pre versus post.

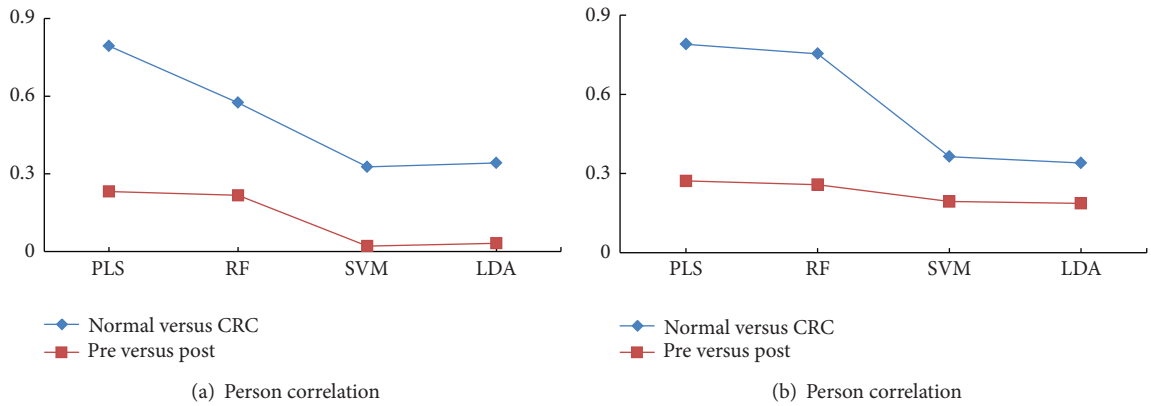

FIGURE 6: Pearson correlation values between ranks of t-test and each classifier in 2 cases by (a) all variables and (b) identified metabolites. x-axis is the classifiers and y-axis is the Pearson correlation coefficients of classifiers and t- test. Blue line: case (A) (Normal versus CRC) and brown line: case (B) (pre versus post).

The model will iteratively compute one component at a time, that is: one vector derived from X-scores T, Y-scores U, weights C (or w), and loadings P. The component extraction process will stop when the predictive accuracy obtained in 7-fold cross-validation (Q^2 value) begin to descend. All the components are calculated in descending order of importance. The "score" of PLS is the score of the first component which contains most information of X dataset.

The formula to calculate VIP (variable importance) can be expressed as

$$\mathrm{VIP}_{AK} = \sqrt{\sum_{a=1}^{A} \left(w_{ak}^2 * \left(SSY_{a-1} - SSY_a\right)\right) * \frac{K}{\left(SSY_a - SSY_A\right)}}, \tag{A.2}$$

where A is the number of components extracted and K is the number of variables in dataset X. w_{ak} is the correlation

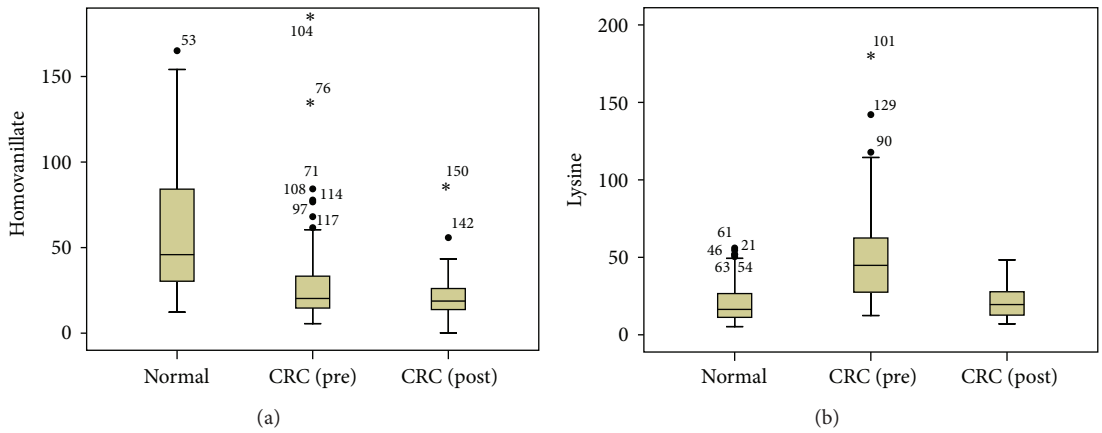

Figure 7: Box plots of significant metabolites selected by RF (case A) only. x-axis is the groups (normal, CRC (pre), and post) and y-axis is the intensity of metabolites ((a) for homovanillate and (b) for lysine).

Table 3: Pearson correlation coefficient matrixes of rank lists by t-test, PLS, SVM, and RF in 2 cases based on all variables (A-B) and identified metabolites (C-D).

Method	tRank[a]	PLSRank[b]	RFRank[c]	SVMRank[d]	LDARank[e]
Pearson correlation coefficient matrix based on all variables					
(A) Normal versus CRC					
tRank	1.000	0.794[f]	0.575	0.327	0.342
PLSRank	0.794	1.000	0.574	0.328	0.342
RFRank	0.575	0.574	1.000	0.210	0.256
SVMRank	0.327	0.328	0.210	1.000	0.167
LDARank	0.342	0.342	0.256	0.167	1.000
(B) Pre versus post					
tRank	1.000	0.232	0.217	0.021	0.032
PLSRank	0.232	1.000	0.652	0.066	0.066
RFRank	0.217	0.652	1.000	0.086	0.057
SVMRank	0.021	0.066	0.086	1.000	0.007
LDARank	0.032	0.066	0.057	0.007	1.000
Pearson correlation coefficient matrix based on identified metabolites					
(C) Normal versus CRC					
tRank	1.000	0.753	0.754	0.364	0.340
PLSRank	0.753	1.000	0.756	0.267	0.340
RFRank	0.754	0.756	1.000	0.495	0.308
SVMRank	0.364	0.267	0.495	1.000	0.190
LDARank	0.340	0.340	0.308	0.190	1.000
(D) Pre versus post					
tRank	1.000	0.272	0.258	0.194	0.187
PLSRank	0.272	1.000	0.733	0.048	0.044
RFRank	0.258	0.733	1.000	0.034	0.041
SVMRank	0.194	0.048	0.034	1.000	0.187
LDARank	0.187	0.044	0.041	0.187	1.000

[a]variable rank by the P value of t-test.
[b]variable rank by the VIP value of PLS.
[c]variable rank by the Gini value of RF.
[d]variable rank by the SVM-REF.
[e]variable rank by the LDA coefficient.
[f]Pearson correlation coefficient of PLS and t-test variable rank lists for differentiating Normal and CRC.

between X and $U(Y)$ expressed by component a. SSY_a is the explanation of Y by component a. SSY_A is the explanation of Y by all the components. The Sum of squares of all VIP*s* is equal to the number of variables in the model hence the average VIP is equal to 1.

The VIP*s* derived from the first component is used for variable ranking. Variables with larger VIP, larger than 1 in particular, are the most relevant for explaining Y (classification).

B. Support Vector Machine (SVM)

The key to the success of SVM is the kernel function which maps the data from the original space into a high dimensional (possibly infinite dimensional) feature space. By constructing a linear boundary in the feature space, the SVM produces nonlinear boundaries in the original space. Given a training sample, a maximum-margin hyper plane splits a given training sample in such a way that the distance from the closest cases (support vectors) to the hyper plane ($W^T X + b = 0$) is maximized where W is the weight matrix, X is the dataset, and b is a constant term. The "score" of SVM is computed by Score $= W^T X + b$.

SVM Recursive Feature elimination (SVM-RFE) is a wrapper approach which uses the norm of the weights W to rank the variables (the larger the norm of W is, the more important the corresponding variable is). Initially whole of the data is taken and a classifier is computed. The norm of W is computed for each of the features and the feature with the smallest norm is eliminated. This process is repeated till all the features are ranked.

Linear kernel was used for SVM classification and feature selection. This kernel was chosen to reduce the computational complexity and eliminate the need for retuning kernel parameters for every new subset of variables. Another important advantage of choosing a linear kernel is that the norm of the weight W can be directly used as a ranking criterion; however this is not possible in other kernels such as the radial basis function kernel or a sigmoid kernel.

C. LDA

LDA adopts a linear combination of variables ($F_{\text{LDA}} = WX + E$) as a predictor to characterize or separate two or more classes of objects or events.

Different with PLS which look for linear combinations of variables to best explain both the data set X and the superior variable Y, the criterion of LDA is to maximize the ratio (S) of the variance between the classes to the variance within the classes:

$$S = \frac{\sigma^2_{\text{between}}}{\sigma^2_{\text{within}}} = \frac{\left(W \cdot \mu_{y=1} - W \cdot \mu_{y=0}\right)^2}{W' \sum_{y=1} W + W' \sum_{y=0} W} = \frac{\left(W \cdot \left(\mu_{y=1} - \mu_{y=0}\right)\right)^2}{W' \left(\sum_{y=0} + \sum_{y=1}\right) W}, \quad \text{(C.1)}$$

where σ^2 is the variance between or within groups, μ is the mean of variables from corresponding group, and W is the coefficients of variables.

The "score" of LDA is the F value of testing samples and the coefficients W are used for variable ranking.

Abbreviations

GC-MS: Gas chromatography mass spectrometry
RF: Random forest
LDA: Linear discriminant analysis
SVM: Support vector machine
PCA: Principal component analysis
PLS: Projection to latent structures
ROC: Receiver operating characteristic
CRC: Colorectal cancer
NMR: Nuclear magnetic resonance
MS: Mass spectrometry.

Acknowledgment

This work was financially supported by the National Basic Research Program of China (2007CB914700), National Natural Science Foundation of China Program (81170760), and the Natural Science Foundation of Shanghai, China (10ZR1414800).

References

[1] O. Fiehn, "Metabolomics—the link between genotypes and phenotypes," *Plant Molecular Biology*, vol. 48, no. 1-2, pp. 155–171, 2002.

[2] J. K. Nicholson, J. Connelly, J. C. Lindon, and E. Holmes, "Metabonomics: a platform for studying drug toxicity and gene function," *Nature Reviews Drug Discovery*, vol. 1, no. 2, pp. 153–161, 2002.

[3] J. K. Nicholson, J. C. Lindon, and E. Holmes, "'Metabonomics': understanding the metabolic responses of living systems to pathophysiological stimuli via multivariate statistical analysis of biological NMR spectroscopic data," *Xenobiotica*, vol. 29, no. 11, pp. 1181–1189, 1999.

[4] J. Schnabel, "Targeting tumour metabolism," *Nature Reviews Drug Discovery*, vol. 9, pp. 503–504, 2010.

[5] T. L. Chen, G. X. Xie, X. Y. Wang et al., "Serum and urinemetabolite profiling reveals potential biomarkers of human hepatocellular carcinoma," *Molecular & Cellular Proteomics*, vol. 10, pp. 1–13, 2011.

[6] G. X. Xie, X. J. Zheng, X. Qi et al., "Metabonomic evaluation of melamine-induced acute renal toxicity in rats," *Journal of Proteome Research*, vol. 9, no. 1, pp. 125–133, 2010.

[7] J. Yang, T. Chen, L. Sun et al., "Potential metabolite markers of schizophrenia," *Molecular Psychiatry*, vol. 18, no. 1, pp. 67–78, 2013.

[8] Y. Q. Bao, T. Zhao, X. Y. Wang et al., "Metabonomic variations in the drug-treated type 2 diabetes mellitus patients and healthy volunteers," *Journal of Proteome Research*, vol. 8, no. 4, pp. 1623–1630, 2009.

[9] X. Wang, J. Lin, T. Chen, M. Zhou, M. Su, and W. Jia, "Metabolic profiling reveals the protective effect of diammonium glycyrrhizinate on acute hepatic injury induced by carbon tetrachloride," *Metabolomics*, vol. 7, no. 2, pp. 226–236, 2010.

[10] J. Trygg, E. Holmes, and T. Lundstedt, "Chemometrics in metabonomics," *Journal of Proteome Research*, vol. 6, no. 2, pp. 469–479, 2007.

[11] H. W. Cho, S. B. Kim, M. K. Jeong et al., "Discovery of metabolite features for the modelling and analysis of high-resolution NMR spectra," *International Journal of Data Mining and Bioinformatics*, vol. 2, no. 2, pp. 176–192, 2008.

[12] Z. Cai, J. Zhao, X. Wang et al., "A combined proteomics and metabolomics profiling of gastric cardia cancer reveals characteristic dysregulations in glucose metabolism," *Molecular & Cellular Proteomics*, vol. 9, pp. 2617–2628, 2010.

[13] X. Li, S. Yang, Y. Qiu et al., "Urinary metabolomics as a potentially novel diagnostic and stratification tool for knee osteoarthritis," *Metabolomics*, vol. 6, no. 1, pp. 109–118, 2010.

[14] J. Wei, G. X. Xie, Z. T. Zhou et al., "Salivary metabolite signatures of oral cancer and leukoplakia," *International Journal of Cancer*, vol. 129, no. 9, pp. 2207–2217, 2011.

[15] D. Amaratunga, J. Cabrera, and Y. S. Lee, "Enriched random forests," *Bioinformatics*, vol. 24, no. 18, pp. 2010–2014, 2008.

[16] A. Statnikov, L. Wang, and C. F. Aliferis, "A comprehensive comparison of random forests and support vector machines for microarray-based cancer classification," *BMC Bioinformatics*, vol. 9, pp. 319–328, 2008.

[17] X. Y. Wu, Z. Y. Wu, and K. Li, "Identification of differential gene expression for microarray data using recursive random forest," *Chinese Medical Journal*, vol. 121, no. 24, pp. 2492–2496, 2008.

[18] A. Acharjeea, B. Kloosterman, R. C. H. D. Vos et al., "Data integration and network reconstruction with ~omics data using Random Forest regression in potato," *Analytica Chimica Acta*, vol. 705, no. 1-2, pp. 56–63, 2011.

[19] R. Jiang, W. W. Tang, X. B. Wu, and W. H. Fu, "A random forest approach to the detection of epistatic interactions in case-control studies," *BMC Bioinformatics*, vol. 10, supplement 1, pp. 65–76, 2009.

[20] A. Jemal, R. Siegel, J. Xu, and E. Ward, "Cancer statistics, 2010," *CA Cancer Journal for Clinicians*, vol. 60, no. 5, pp. 277–300, 2010.

[21] Y. Qiu, M. Su, Y. Liu et al., "Application of ethyl chloroformate derivatization for gas chromatography-mass spectrometry based metabonomic profiling," *Analytica Chimica Acta*, vol. 583, no. 2, pp. 277–283, 2007.

[22] L. Breiman, "Random forests," *Machine Learning*, vol. 45, no. 1, pp. 5–32, 2001.

[23] A. P. Bradley, "The use of the area under the ROC curve in the evaluation of machine learning algorithms," *Pattern Recognition*, vol. 30, no. 7, pp. 1145–1159, 1997.

[24] K. Duan, S. S. Keerthi, and A. N. Poo, "Evaluation of simple performance measures for tuning SVM hyperparameters," *Neurocomputing*, vol. 51, pp. 41–59, 2003.

[25] I. Guyon, J. Weston, S. Barnhill, and V. Vapnik, "Gene selection for cancer classification using support vector machines," *Machine Learning*, vol. 46, no. 1–3, pp. 389–422, 2002.

[26] Y. P. Qiu, G. X. Cai, M. M. Su et al., "Serum metabolite profiling of human colorectal cancer using GC–TOFMS and UPLC–QTOFMS," *Journal of Proteome Research*, vol. 8, no. 10, pp. 4844–4850, 2009.

Hindawi Publishing Corporation
Evidence-Based Complementary and Alternative Medicine
Volume 2013, Article ID 190281, 8 pages
http://dx.doi.org/10.1155/2013/190281

Research Article

Suppressions of Migration and Invasion by Cantharidin in TSGH-8301 Human Bladder Carcinoma Cells through the Inhibitions of Matrix Metalloproteinase-2/-9 Signaling

Yi-Ping Huang,[1] Chien-Hang Ni,[2] Chi-Cheng Lu,[3] Jo-Hua Chiang,[3] Jai-Sing Yang,[4] Yang-Ching Ko,[5] Jing-Pin Lin,[6] Jehn-Hwa Kuo,[7,8] Shu-Jen Chang,[9] and Jing-Gung Chung[10,11,12]

[1] *Department of Physiology, China Medical University, Taichung 404, Taiwan*
[2] *Department of Chinese Medicine, E-DA Hospital/I-Shou University, Kaohsiung 824, Taiwan*
[3] *Department of Life Sciences, National Chung Hsing University, Taichung 402, Taiwan*
[4] *Department of Pharmacology, China Medical University, Taichung 404, Taiwan*
[5] *Division of Pulmonary and Critical Care Medicine, Department of Internal Medicine, St. Martin De Porres Hospital, Chiayi 600, Taiwan*
[6] *School of Chinese Medicine, China Medical University, Taichung 404, Taiwan*
[7] *Special Class of Healthcare, Industry Management, Central Taiwan University of Science and Technology, Taichung 406, Taiwan*
[8] *Department of Urology, Jen-Ai Hospital, Taichung 412, Taiwan*
[9] *School of Pharmacy, China Medical University, Taichung 404, Taiwan*
[10] *Department of Biological Science and Technology, China Medical University, Taichung 404, Taiwan*
[11] *Department of Microbiology, China Medical University, Taichung 404, Taiwan*
[12] *Department of Biotechnology, Asia University, Taichung 413, Taiwan*

Correspondence should be addressed to Shu-Jen Chang; sjchang@mail.cmu.edu.tw
and Jing-Gung Chung; jgchung@mail.cmu.edu.tw

Received 11 October 2012; Revised 10 December 2012; Accepted 11 December 2012

Academic Editor: Wei Jia

Cancer metastasis becomes an initial cause of cancer death in human population. In many cancers, it has been shown that the high levels of matrix metalloproteinase (MMP)-2 and/or MMP-9 are associated with the invasive phenotypes of cancer cells. In this study, we investigated the effects of cantharidin, a derivative of *blister beetles* which is one of the traditional Chinese medicines, on the adhesion, migration, and invasion of human bladder cancer TSGH-8301 cells. Cantharidin effectively suppressed TSGH-8301 cell adhesion, migration, and invasion in a concentration-dependent manner. Results from Western blotting, RT-PCR, and gelatin zymography assays indicated that cantharidin blocked the protein levels, gene expression (mRNA), and activities of MMP-2 and -9 in TSGH-8301 cells. Cantharidin also significantly suppressed the protein expressions of p-p38 and p-JNK1/2 in TSGH-8301 cells. Taken together, cantharidin was suggested to present antimetastatic potential *via* suppressing the levels of MMP-2 and MMP-9 expression that might be mediated by targeting the p38 and JNK1/2 MAPKs pathway in TSGH-8301 human bladder cancer cells.

1. Introduction

In genitourinary tumor, bladder cancer is a significant cause of morbidity and mortality [1]. In the United States, bladder cancer is the fourth most common malignancy, and new cases about 70,530 (52,760 men and 17,770 women) and deaths for the year 2010 were 14,680 (10,410 men and 4270 women) [2]. In Taiwan, about 2.3 individuals per 100,000 die annually from bladder cancer on the basis of the 2011 report from the Department of Health, Taiwan. In bladder cancer of patients, 75% present with superficial disease and 25% with invasive disease [3].

During the metastasis development, there are about 50% of patients with muscle invasive bladder cancer within 2 years of cystectomy [4, 5]. Muscle-invasive bladder cancer is an aggressive epithelial tumor; almost 50% of these patients develop metastases and ultimately succumb to their disease with poor long-term survival [6, 7]. Invasion and metastasis are predominant properties in cancer cells that led to hard-to-cure patients [8, 9]. It is well documented that the activities of matrix metalloproteinases (MMPs) play an important role in the cancer cell's metastasis process, including cell adhesion, migration, and invasion [10–12]. Therefore, blockage of the activities of MMPs may be a strategy to inhibit the cancer cell metastasis.

Cantharidin, a derivative of *Blister Beetles*, is protein phosphatase 1 (PP1) and protein phosphatase 2A (PP2A) inhibitors [13, 14] and has been used in traditional Chinese medicine [15]. Cantharidin induced cell cycle arrest [16, 17] and triggered apoptosis in various types of tumor cells, including hepatoma [18], myeloma [19], oral buccal carcinoma [20], leukemia cells [21, 22], and intestinal epithelial cells [23]. Recently, cantharidin was found in our laboratory to provoke apoptosis in human bladder carcinoma TSGH-8301 and colorectal cancer colo 205 cells [24, 25] but there is no report to show that cantharidin inhibited the migration and invasion of TSGH-8301 cells. Therefore, the current study investigated the effects of cantharidin on migration and invasion and explored its signaling molecules in *in vitro* study. Our results demonstrated that cantharidin potently inhibited the migration and invasion of TSGH-8301 human bladder carcinoma cells through inhibiting the p38 and JNK1/2-modulated MMP-2/-9 signaling *in vitro*.

2. Materials and Methods

2.1. Chemicals and Reagents. Cantharidin, dimethyl sulfoxide (DMSO), propidium iodide (PI) and anti-β-Actin were purchased from Sigma-Aldrich Corp. (St. Louis, MO, USA). Cantharidin was dissolved in DMSO at a stock concentration of 50 mM and followed to dilute in further experiments. RPMI-1640 medium, L-glutamine, fetal bovine serum (FBS), penicillin-streptomycin, and trypsin-EDTA were obtained from Gibco/Life Technologies (Grand Island, NY, USA). Anti-MMP-9 (Cat. AB19016) and Millicell Hanging Cell Culture Inserts (Cat. PIEP12R48) were brought from Merck Millipore Corp. (Billerica, MA, USA). The antibodies to p-p38, p-JNK1/2, p-ERK1/2, and MMP-2 and horseradish-peroxidase- (HRP-) conjugated secondary antibodies were purchased from Santa Cruz Biotechnology, Inc. (Santa Cruz, CA, USA).

2.2. Cell Culture. The human bladder carcinoma TSGH-8301 cell line was purchased from the Food Industry Research and Development Institute (Hsinchu, Taiwan). TSGH-8301 cells were maintained in RPMI-1640 medium supplemented with 10% FBS, 100 Units/mL penicillin, and 100 μg/mL streptomycin in 75 cm^2 tissue culture flasks and grown at 37°C under a humidified atmosphere with 5% CO_2 as previously described [24, 26].

2.3. Assessment for Cell Viability. TSGH-8301 cells were seeded at a density of 2×10^5 cells/well in 12-well plates and were incubated with 0, 0.25, 0.5, 1, 2, and 2.5 μM of cantharidin for 24 h. DMSO at the concentration of 0.5% served as a vehicle control. Cells were harvested and were stained with PI (5 μg/mL) and then were analyzed by flow cytometry (BD Biosciences, FACSCalibur, San Jose, CA, USA) for viability determinations as previously described [24, 27].

2.4. Adhesion Assay. TSGH-8301 cells at the density of 5×10^4 cells/well were preincubated with cantharidin (0, 1, and 2.5 μM) and 0.5% DMSO (vehicle control) for 24 or 48 h at 37°C in 96-well plates precoated with type I collagen (10 μg/mL) (EMD Millipore) for 60 min at 37°C. After a 3 h incubation, the unattached cells were removed, and attached cells were fixed in 1% glutaraldehyde in PBS for 20 min. Then cells were stained with 0.02% crystal violet solution for 5 min at room temperature. For quantification of the attached cells, 70% ethanol was used to dissolve the crystal violet, and O.D. was measured at 570 nm by using microplate reader and reference 405 nm. The percentage of adhesion was calculated based on the adhesion cells compared to control [28, 29].

2.5. Wound Healing Assay. TSGH-8301 cells at the density of 5×10^5 cells/well were maintained in 6-well plates and incubated at 37°C for 24 h. After cells were grown in confluent then cells were scratched with a 200-μL pipette tip, cells in the plate were washed with PBS, and then added the new complete medium then were treated with or without 1 and 2.5 μM of cantharidin for 24 h and 0.5% DMSO served as a vehicle control. At the end of incubation, the cells were examined and were photographed under a fluorescence microscope. The number of cells that migrated into the scratched area was calculated as described elsewhere [28, 30].

2.6. In Vitro Migration and Invasion Assays. TSGH-8301 cell migration or invasion was conducted using 24-well Transwell inserts (8 μm pore filters, Merck Millipore) individually coated with 30 μg type I collagen (Merck Millipore) (for migration) or Matrigel (BD Biosciences, Bedford, MA, USA) (for invasion) [28]. In brief, TSGH-8301 cells (2×10^4 cells/well) were cultured for 24 h in serum-free RPMI-1640 medium, and then cells were placed in the upper chamber of the Transwell insert and treated with 0.5% DMSO (as a control) or cantharidin (1 or 2.5 μM) for 24 h. In the lower chamber, the medium containing 10% FBS was placed. At the end of incubation, the nonmigrated cells were removed using a cotton swab; the invaded cells maintained in the upper chamber were fixed with 4% formaldehyde and stained with 2% crystal violet. In the lower surface of the filter, cells penetrated were counted and photographed under a phase-contract microscope at a 200x magnification. Three independent experiments were performed as described elsewhere [31, 32].

2.7. Western Blotting Analysis. For investigating the protein levels associated with migration and invasion, whether are

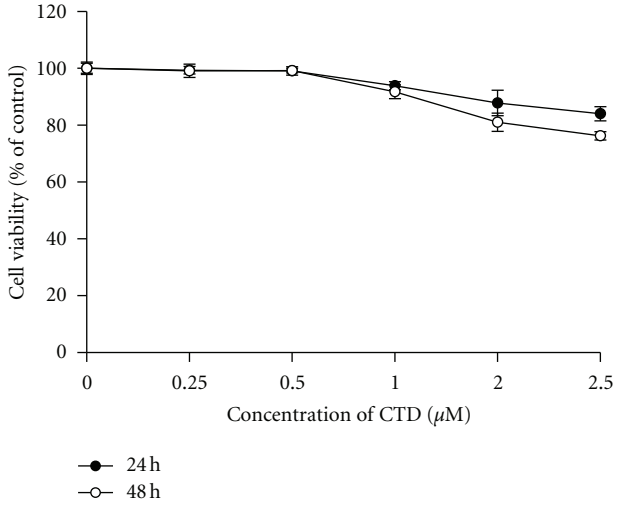

Figure 1: Cantharidin has no dramatic influence on the percentage of viable TSGH-8301 cells. Cells in 12-well plate were incubated with or without 0, 0.25, 0.5, 1, 2, and 2.5 μM of cantharidin for 24 h and 48 h and then harvested for determination of the percentage of viable cells by flow cytometry as described in Section 2. Data represents mean ± S.D. in triplicate.

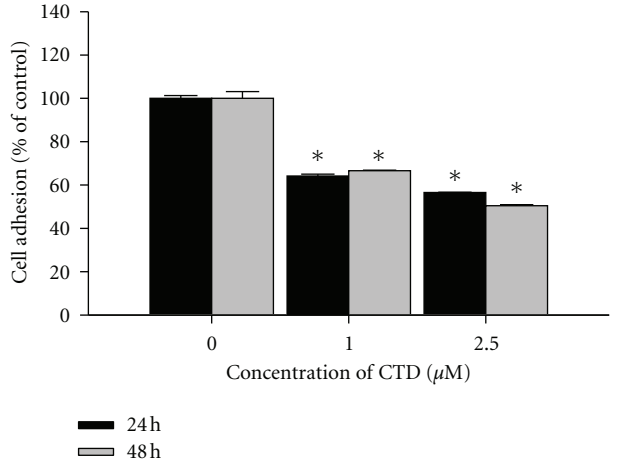

Figure 2: Cantharidin decreases cell adhesion of TSGH-8301 cells. Cells were incubated with or without 0, 1, and 2.5 μM of cantharidin for 24 h and 48 h; then cells were measured the percentage of cell adhesion as described in Section 2. Data represents mean ± SD in triplicate and $^*P < 0.05$, significant difference between cantharidin-treated groups and the control as analyzed by Dunnett's posttest.

affected or not by cantharidin, we determined related signaling molecules by Western blotting as described elsewhere [27, 33, 34]. Briefly, TSGH-8301 cells (1×10^6 cells/well) were placed in 6-well plates for 24 h and then were incubated with cantharidin (0, 1, or 2.5 μM) for 24 h. At the end of incubation, cells were harvested from each treatment and were individually lysed in lysis buffer (PRO-PREP protein extraction solution, iNtRON Biotechnology, Seongnam-si, Gyeonggi-do, Korea). The total protein amount was individually determined using a Bio-Rad protein assay kit (Bio-Rad Laboratories, Hercules, CA, USA). The protein abundance of p-p38, p-JNK1/2, p-ERK1/2, MMP-2, and MMP-9 was examined by sodium dodecyl sulfate-polyacrylamide gel electrophoresis (SDS-PAGE) and Western blotting as previously described [33, 34]. The relative abundance of each band which represents associated protein expression was quantified using the NIH ImageJ [35].

2.8. Gelatin Zymography Assay. TSGH-8301 cells at the density of 1×10^6 cells/well were plated in 12-well plates and then were incubated in serum-free RPMI-1640 medium in the presence of 0, 1, or 2.5 μM of cantharidin for 24 and 48 h. In the end of incubation, the conditioned medium was harvested, placed on 10% SDS-PAGE containing 0.2% gelatin (Sigma-Aldrich Corp.), and then separated by electrophoresis. The gels were soaked in 2.5% Triton X-100 in dH_2O twice for a total of 60 min at 25°C to remove SDS. Gels were incubated at 37°C with substrate buffer (50 mM Tris HCl, 5 mM $CaCl_2$, 0.02% NaN_3, and 1% triton X-100, pH 8.0) for 18 h. The gel was stained using 0.2% Coomassie blue for 1 h, was destained in water containing 10% acetic acid and 50% methanol, and bands corresponding to the activity of MMP-2 and -9 were quantified with the NIH ImageJ software as previously described [28, 36].

2.9. Real-Time PCR of MMP-2 and -9 mRNA Expressions. TSGH-8301 cells at the density 1×10^6 cells/well were placed in 6-well plates for 24 h and then were incubated with cantharidin (0, 1, or 2.5 μM) for 24 h. Cells from each treatment were harvested and total RNA was extracted as previously described [33]. RNA samples were reverse-transcribed at 42°C with High Capacity cDNA Reverse Transcription Kit for 30 min according to the protocol of the supplier (Applied Biosystems, Foster City, CA, USA). The primers were set as MMP-2F: CCCCAGACAGGTGATCTTGAC; MMP-2R: GCTTGCGAGGGAAGAAGTTG; MMP-7F: GGATGGTAGCAGTCTAGGGATTAACT; MMP-9F: CGCTGGGCTTAGATCATTCC; MMP-9R: AGGTTGGATACATCACTGCATTAGG; GAPDH-F: ACACCCACTCCTCCACCTTT; GAPDH-R: TAGCCAAATTCGTTGTCATACC. Each assay was performed in triplicate by using the Applied Biosystems 7300 Real-Time PCR system, and the expression fold changes were performed by using the comparative C_T (threshold cycle) method [31, 34].

2.10. Statistical Analysis. Statistical differences were determined using one-way analysis of variance (ANOVA) followed by Dunnett's posttest and considered significant at the $P < 0.05$ between experimental and control samples. All data are presented as means ± standard deviation (SD) in triplicate of at least three independent experiments.

3. Results

3.1. Cantharidin Has No Effect on Percentage of Viable TSGH-8301 Cells. It is well documented that cantharidin decreased the percentage of viable cells in many types of human cancer cell lines [18–20, 22, 23]. TSGH-8301 cells were treated with various concentrations of cantharidin in serum-containing medium for 24 and 48 h, and cell viability was determined by flow cytometric assay. Results are shown in Figure 1 and

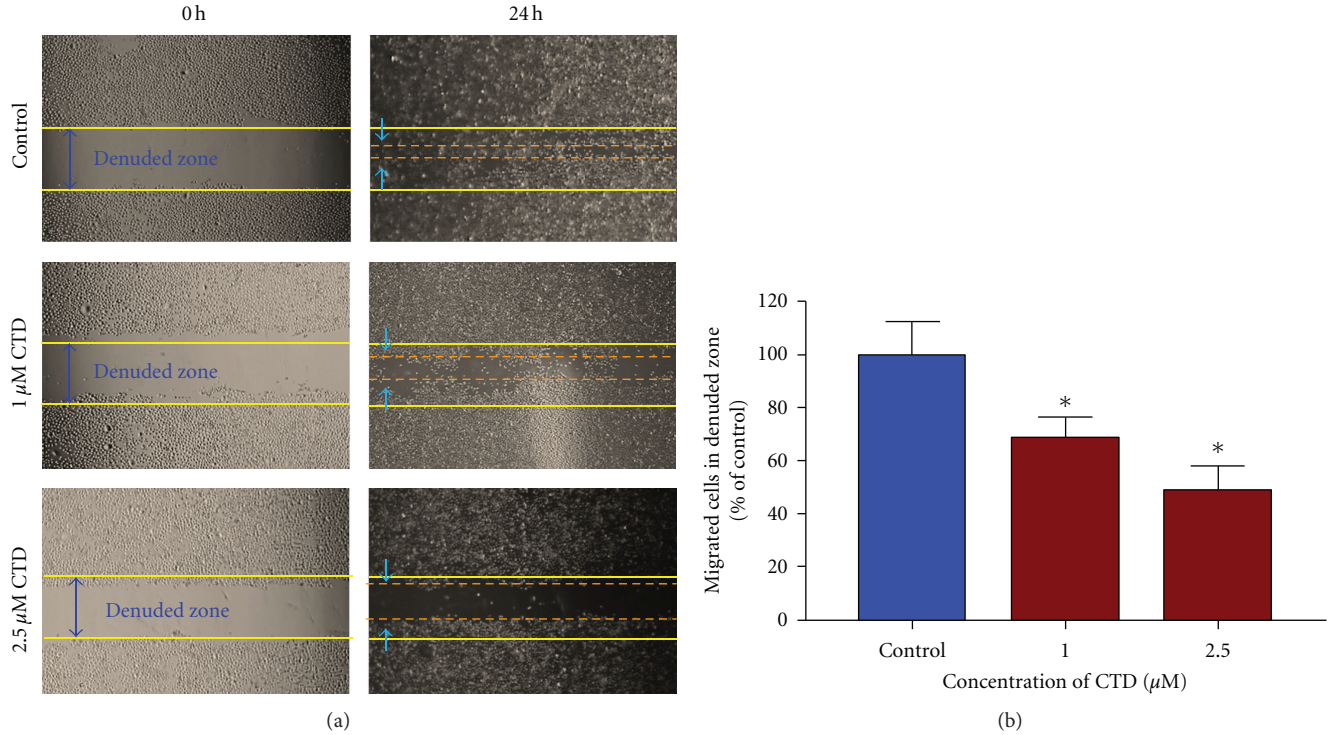

FIGURE 3: Wound healing assay for the effects of cantharidin on the migration of TSGH-8301 cells. Cells were placed for 24 h; then a wound was performed by scraping confluent cell layers with a pipette tip. Cantharidin was added to the cells at the final concentration were 0, 1 and 2.5 μM and then incubated for 24. (a) Some of the representative photographs of invading treated and untreated cells are presented. Three separate experiments with similar results were carried out. (b) The migrated cells in the five random fields after exposure for 24 h were counted to quantify, and data was expressed as mean ± S.D. on the basis of untreated cells (control) represented as 100%. $^{*}P < 0.05$, significant difference between cantharidin-treated groups and the control as analyzed by Dunnett's posttest.

indicated that cantharidin slightly decreased cell viability at the concentration of 1 μM but cantharidin at 2.5 μM decreased cell viability by approximately 17% and 30% at 24 and 48 h, respectively (Figure 1).

3.2. Cantharidin Decreases Cell Adhesion of TSGH-8301 Cells. To investigate the effects of cantharidin on the adhesion of TSGH-8301 cells, adhesive cells were quantified, and results are demonstrated in Figure 2. TSGH-8301 cells after incubation with cantharidin at the final concentrations (0, 1, and 2.5 μM) for 24 and 48 h indicated that cantharidin significantly inhibited cell adhesion in a concentration- and time-dependent manner. Approximately 52% and 58% reduction were seen within 2.5 μM treatment for 24 and 48 h, respectively.

3.3. Cantharidin Blocks TSGH-8301 Cell Migration by Wound Healing Examination. Since data in Figure 2 indicated that cantharidin inhibited the adhesion of TSGH-8301 cells, we used wound-healing assay to examine the inhibition of cell migration of TSGH-8301 *in vitro*. Figure 3 displays that the migration distance between the leading edge and the wound line was compared between cantharidin-treated and untreated cells (Figure 3(a)). The results demonstrated that cantharidin suppressed the migration of TSGH-8301 cells in a concentration-dependent manner (Figure 3(b)).

3.4. Cantharidin Inhibits the Migration and Invasion of TSGH-8301 Cells In Vitro. For further investigating if cantharidin inhibits the migration and invasion of TSGH-8301 cells, Boyden chamber assay was performed and results are shown in Figures 4(a), 4(b), 4(c), and 4(d). These results were obtained due to the effects of cantharidin on cell migration (Figures 4(a) and 4(b)) and invasion (Figures 4(c) and 4(d)) in TSGH-8301 cells that were treated with 0, 1, and 2.5 μM of cantharidin for 24 and 48 h (cell migration and invasion). Results indicated that cantharidin reduced the migration and invasion of TSGH-8301 cells substantially in a concentration-dependent manner.

3.5. Cantharidin Affects the Levels of Associated Protein and Gene Levels for Migration and Invasion of TSGH-8301 Cells. We further examined the effects of cantharidin on the inhibition of migration and invasion of TSGH-8301 cells, which are involved in the effects of associated protein levels of migration and invasion; those changes of associated protein were measured by SDS-PAGE and Western blotting. TSGH-8301 cells were treated with cantharidin (0, 1, and 2.5 μM) for 24 h and then subjected to Western blotting, and results are shown in Figure 5(a). Results from Western blotting showed that cantharidin could reduce the phosphorylation of p38 and JNK1/2 as well as MMP-2 and -9 in TSGH-8301 cells. However, the protein level of p-ERK1/2 was no significant alteration in comparison to untreated control. Figure 5(b)

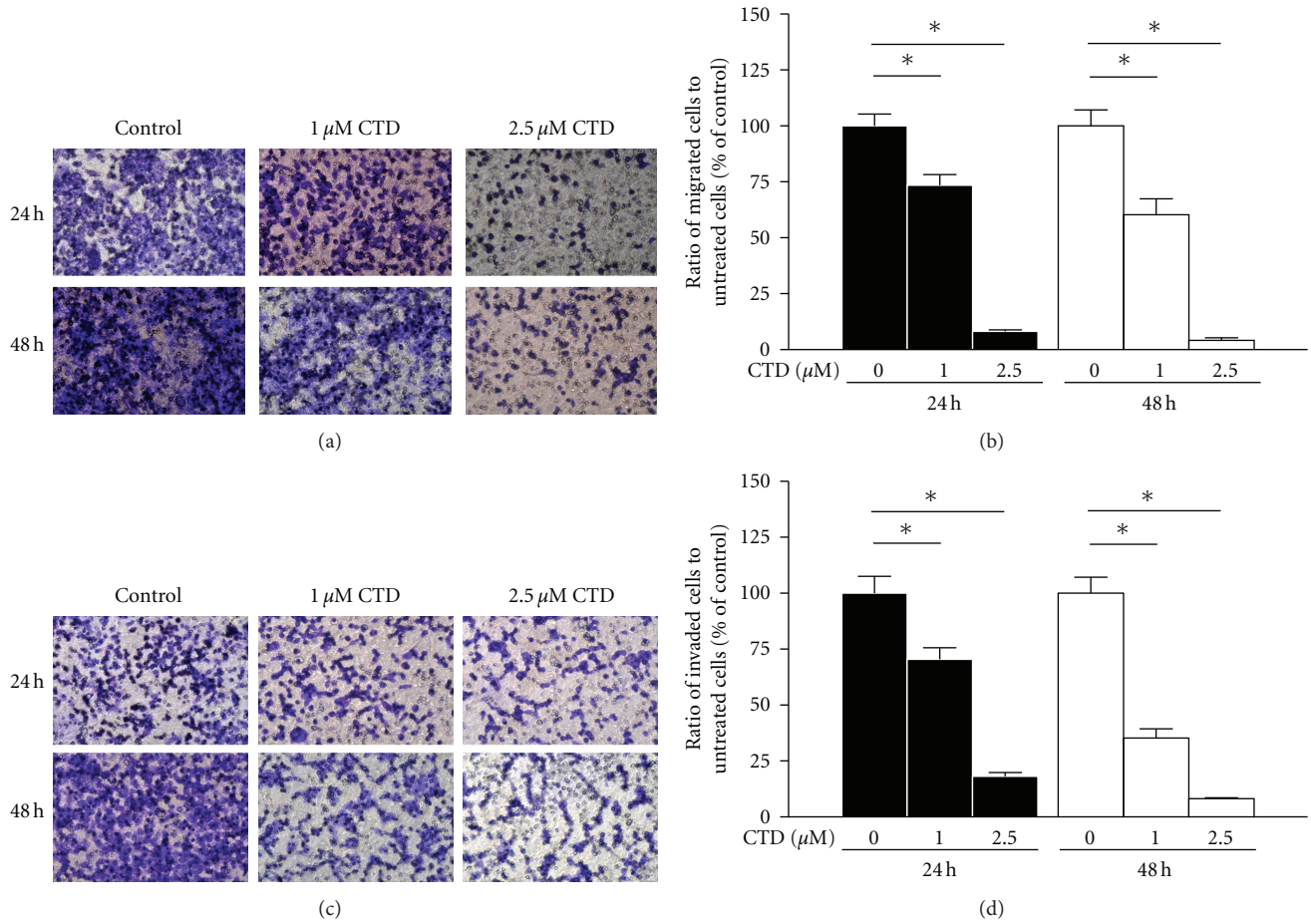

Figure 4: Cantharidin inhibits the migration and invasion of TSGH-8301 cells *in vitro*. Cells were placed in the well at the density of 5×10^4 cells/well and then were treated with 0, 1, and 2.5 μM cantharidin then that penetrated through with or without the Matrigel to the lower surface of the filter were examined. Cells were stained with crystal violet and then were examined and photographed under a light microscope at 200x (a and c). The quantification of cells from each treatment in the lower chambers was counted at 200x (b) and (d). Columns repeat the mean from three independent experiments. $^*P < 0.05$, significant difference between cantharidin-treated groups and the control as analyzed by Dunnett's posttest.

indicated that cantharidin suppressed the gene expression of MMP-2 and -9 in TSGH-8301 cells.

3.6. Cantharidin Suppresses the Activities of Matrix Metalloproteinases (MMPs) in TSGH-8301 Cells. Gelatin zymography was used for analysis of MMP-2 and -9 activities. As shown in Figure 6, cantharidin treatment may lead to reduced activity of MMP-2 and -9 in a dose-dependent manner. This also confirmed that cantharidin inhibited the gene expression (mRNA) of MMP-2 and -9 in TSGH-8301 cells (Figure 5(b)).

4. Discussion

Numerous reports have demonstrated that cantharidin processes antitumor properties [16–23] but there is no report to show the inhibition of migration and invasion of human bladder cancer cells. In this study, we investigated the inhibitory effects of cantharidin on the adhesion, invasion, and migration of TSGH-8301 cells. Results indicated that cantharidin inhibited the cell adhesion, invasion and migration on TSGH-8301 cells (Figures 2 and 3). Cantharidin decreased the protein expressions, gene expression (mRNA) and activities of MMP-2 and -9 in TSGH-8301 (Figures 5(a) and 5(b) and 6). In general, metastasis of cancer cells involves multiple processes, proteins function, and various physiological changes. Furthermore, the degradation or breakdown of the ECM through protease is a critical step in tumor invasion or migration [29, 30]. The involved proteases in migration and invasion, in particular, MMP-2 and MMP-9 were reported to play an important role in cancer invasion and metastasis [37, 38].

Mitogen-activated protein kinases (MAPKs) include p38, c-Jun-*N*-terminal kinase (JNK), and extracellular signal-regulated kinase (ERK) [35], and MAPKs activation is followed by phosphorylation of a variety of cytosolic substrates associated with cell proliferation, cell differentiation, cell invasion, cell migration, and cell death [39, 40]. It was reported that MAPK pathways were involved in the regulation of MMPs and uPA expression in tumor-cell invasion

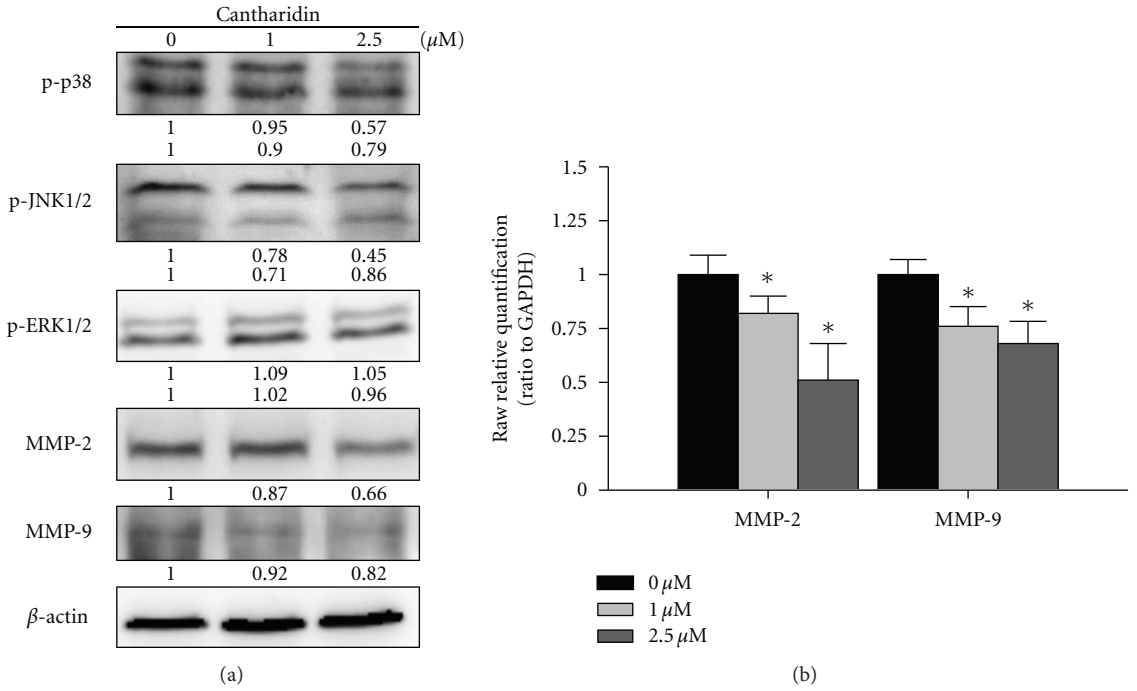

Figure 5: Cantharidin affects the levels of associated proteins and gene levels in migration and invasion of TSGH-8301 cells. Cells were treated with cantharidin (0, 1, and 2.5 μM) for 24 h, and then cells were collected. The total protein extract was quantified and determined as described in Section 2. The levels of p-p38, p-JNK1/2, p-ERK1/2, MMP-2, and MMP-9 protein expressions (a) were estimated by Western blotting as described in Section 2. (b) The total RNA was extracted from cantharidin-treated cells, and the RNA samples were reverse-transcribed to cDNA for real-time PCR as described in Section 2. The ratios between MMP-2, MMP-9, and GAPDH mRNA are used and data represents mean ± SD in duplicate of at least three independent experiments. $^{*}P < 0.05$ was considered significantly as analyzed by Dunnett's posttest.

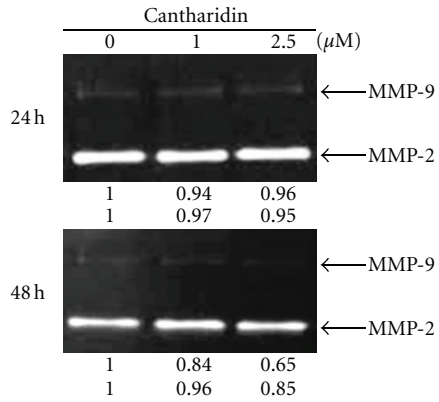

Figure 6: Cantharidin suppresses the activities of matrix metalloproteinases (MMPs) in TSGH-8301 cells. Gelatin zymography was used to evaluate the activities of MMP-2 and MMP-9 as described in Section 2. The different activity of MMP-2 and -9 was determined by densitometry analysis, and results are expressed as % of control. Similar results were obtained from three independent experiments.

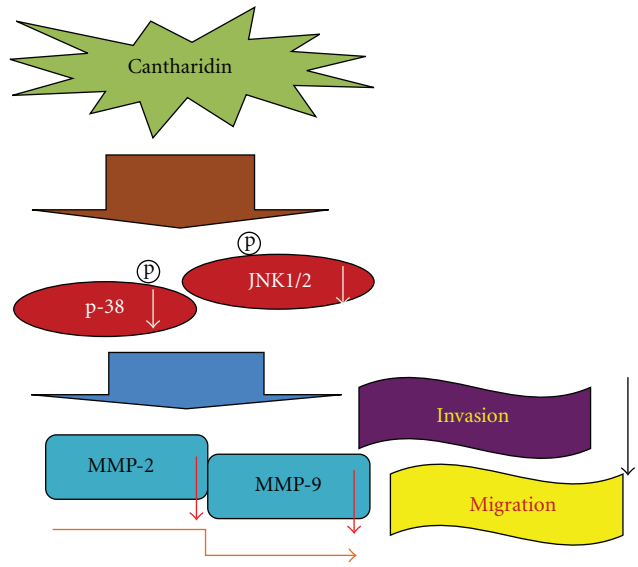

Figure 7: The possible working model and signaling transduction molecules for cantharidin-inhibited cell invasion and migration of TSGH-8301 human bladder cancer cells.

[41, 42]. Herein, we verified that cantharidin has an inhibitory effect on migration and invasion through the suppression of MMP-2 and -9 in TSGH-8301 cells. We further found that cantharidin inhibited the p-JNK1/2 and p-p38. Thus, our results suggested that cantharidin downregulated MMP-2 and MMP-9 protein expression and suppressed metastatic effect through JNK1/2 and p38 MAPKs signals but not ERK1/2 molecule on TSGH-8301 cells.

Taken together, the present study showed novel findings addressing that cantharidin exerts an inhibitory effect on

several essential steps of cancer cell metastasis, including cell adhesion, invasion, and migration *via* regulating the activities of metastasis-associated proteases such as MMP-2 and -9. Based on those observations, we suggest that cantharidin could be a powerful candidate for development of preventive agents against bladder cancer metastasis in the future. Overall, we showed that cantharidin effectively inhibits the expressions of p-p38 and p-JNK1/2, causing downregulation of MMP-2 and -9 in TSGH-8301 cells that can be seen in Figure 7. Thus, cantharidin could be tested further *in vivo* to justify its effectiveness in the prevention of bladder tumor cell invasion or migration during cancer treatment.

Authors' Contribution

S. J. Chang and J. G. Chung contributed equally to this work.

Acknowledgment

This work was supported by the research Grants CMU99-COL-40-1 and CMU99-COL-40-2 from China Medical University, Taichung, Taiwan.

References

[1] S. A. Hussain and N. D. James, "The systemic treatment of advanced and metastatic bladder cancer," *Lancet Oncology*, vol. 4, no. 8, pp. 489–497, 2003.

[2] B. Y. Hernandez, M. D. Green, K. D. Cassel, A. M. Pobutsky, V. Vu, and L. R. Wilkens, "Preview of Hawaii cancer facts and figures 2010," *Hawaii Medical Journal*, vol. 69, no. 9, pp. 223–224, 2010.

[3] E. M. Messing, T. B. Young, V. B. Hunt et al., "Comparison of bladder cancer outcome in men undergoing hematuria home screening versus those with standard clinical presentations," *Urology*, vol. 45, no. 3, pp. 387–397, 1995.

[4] W. F. Whitmore Jr., "Management of invasive bladder neoplasms," *Seminars in Urology*, vol. 1, no. 1, pp. 34–41, 1983.

[5] X. Zhang, X. Shi, J. Li et al., "A novel therapeutic vaccine of mouse GM-CSF surface modified MB49 cells against metastatic bladder cancer," *Journal of Urology*, vol. 187, no. 3, pp. 1071–1079, 2012.

[6] D. Raghavan, W. U. Shipley, M. B. Garnick, P. J. Russell, and J. P. Richie, "Biology and management of bladder cancer," *New England Journal of Medicine*, vol. 322, no. 16, pp. 1129–1138, 1990.

[7] J. P. Stein, G. Lieskovsky, R. Cote et al., "Radical cystectomy in the treatment of invasive bladder cancer: long-term results in 1,054 patients," *Journal of Clinical Oncology*, vol. 19, no. 3, pp. 666–675, 2001.

[8] P. L. Liu, J. R. Tsai, A. L. Charles et al., "Resveratrol inhibits human lung adenocarcinoma cell metastasis by suppressing heme oxygenase 1-mediated nuclear factor-κB pathway and subsequently downregulating expression of matrix metalloproteinases," *Molecular Nutrition and Food Research*, vol. 54, supplement 2, pp. S196–S204, 2010.

[9] G. Christofori, "New signals from the invasive front," *Nature*, vol. 441, no. 7092, pp. 444–450, 2006.

[10] A. R. Folgueras, A. M. Pendas, L. M. Sanchez, and C. Lopez-Otin, "Matrix metalloproteinases in cancer: from new functions to improved inhibition strategies," *The International Journal of Developmental Biology*, vol. 48, no. 5-6, pp. 411–424, 2004.

[11] K. Kessenbrock, V. Plaks, and Z. Werb, "Matrix metalloproteinases: regulators of the tumor microenvironment," *Cell*, vol. 141, no. 1, pp. 52–67, 2010.

[12] L. M. Coussens, B. Fingleton, and L. M. Matrisian, "Matrix metalloproteinase inhibitors and cancer: trials and tribulations," *Science*, vol. 295, no. 5564, pp. 2387–2392, 2002.

[13] W. Li, L. Xie, Z. Chen et al., "Cantharidin, a potent and selective PP2A inhibitor, induces an oxidative stress-independent growth inhibition of pancreatic cancer cells through G2/M cell-cycle arrest and apoptosis," *Cancer Science*, vol. 101, no. 5, pp. 1226–1233, 2010.

[14] A. McCluskey, S. P. Ackland, M. C. Bowyer et al., "Cantharidin analogues: synthesis and evaluation of growth inhibition in a panel of selected tumour cell lines," *Bioorganic Chemistry*, vol. 31, no. 1, pp. 68–79, 2003.

[15] R. E. Honkanen, "Cantharidin, another natural toxin that inhibits the activity of serine/threonine protein phosphatases types 1 and 2A," *FEBS Letters*, vol. 330, no. 3, pp. 283–286, 1993.

[16] P. R. Clarke, I. Hoffmann, G. Draetta, and E. Karsenti, "Dephosphorylation of cdc25-C by a type-2A protein phosphatase: specific regulation during the cell cycle in Xenopus egg extracts," *Molecular Biology of the Cell*, vol. 4, no. 4, pp. 397–411, 1993.

[17] Y. Ishida, Y. Furukawa, J. A. Decaprio, M. Saito, and J. D. Griffin, "Treatment of myeloid leukemia cells with the phosphatase inhibitor okadaic acid induces cell cycle arrest at either G1/S or G2/M depending on dose," *Journal of Cellular Physiology*, vol. 150, no. 3, pp. 484–492, 1992.

[18] Y. N. Chen, J. C. Chen, S. C. Yin et al., "Effector mechanisms of norcantharidin-induced mitotic arrest and apoptosis in human hepatoma cells," *International Journal of Cancer*, vol. 100, no. 2, pp. 158–165, 2002.

[19] H. S. Kang, B. S. Lee, Y. Yang et al., "Roles of protein phosphatase 1 and 2A in an IL-6-mediated autocrine growth loop of human myeloma cells," *Cellular Immunology*, vol. 168, no. 2, pp. 174–183, 1996.

[20] S. H. Kok, S. J. Cheng, C. Y. Hong et al., "Norcantharidin-induced apoptosis in oral cancer cells is associated with an increase of proapoptotic to antiapoptotic protein ratio," *Cancer Letters*, vol. 217, no. 1, pp. 43–52, 2005.

[21] D. C. Dorn, C. A. Kou, K. J. Png, and M. A. S. Moore, "The effect of cantharidins on leukemic stem cells," *International Journal of Cancer*, vol. 124, no. 9, pp. 2186–2199, 2009.

[22] S. Yi, J. Wass, P. Vincent, and H. Iland, "Inhibitory effect of norcantharidin on K562 human myeloid leukemia cells in vitro," *Leukemia Research*, vol. 15, no. 10, pp. 883–886, 1991.

[23] R. M. Ray, S. Bhattacharya, and L. R. Johnson, "Protein phosphatase 2A regulates apoptosis in intestinal epithelial cells," *Journal of Biological Chemistry*, vol. 280, no. 35, pp. 31091–31100, 2005.

[24] J. H. Kuo, Y. L. Chu, J. S. Yang et al., "Cantharidin induces apoptosis in human bladder cancer TSGH 8301 cells through mitochondria-dependent signal pathways," *International Journal of Oncology*, vol. 37, no. 5, pp. 1243–1250, 2010.

[25] W. W. Huang, S. W. Ko, H. Y. Tsai et al., "Cantharidin induces G2/M phase arrest and apoptosis in human colorectal cancer colo 205 cells through inhibition of CDK1 activity and caspase-dependent signaling pathways," *International Journal of Oncology*, vol. 38, no. 4, pp. 1067–1073, 2011.

[26] N. G. Chen, C. C. Lu, Y. H. Lin et al., "Proteomic approaches to study epigallocatechin gallate-provoked apoptosis of TSGH-8301 human urinary bladder carcinoma cells: roles of AKT and heat shock protein 27-modulated intrinsic apoptotic pathways," *Oncology Reports*, vol. 26, no. 4, pp. 939–947, 2011.

[27] C. C. Lu, J. S. Yang, J. H. Chiang et al., "Novel quinazolinone MJ-29 triggers endoplasmic reticulum stress and intrinsic apoptosis in murine leukemia WEHI-3 cells and inhibits leukemic mice," *PLoS ONE*, vol. 7, no. 5, article e36831, 2012.

[28] K. C. Liu, A. C. Huang, P. P. Wu et al., "Gallic acid suppresses the migration and invasion of PC-3 human prostate cancer cells via inhibition of matrix metalloproteinase-2 and -9 signaling pathways," *Oncology Reports*, vol. 26, no. 1, pp. 177–184, 2011.

[29] C. Y. Ma, W. T. Ji, F. S. Chueh et al., "Butein inhibits the migration and invasion of SK-HEP-1 human hepatocarcinoma cells through suppressing the ERK, JNK, p38, and uPA signaling multiple pathways," *Journal of Agricultural and Food Chemistry*, vol. 59, no. 16, pp. 9032–9038, 2011.

[30] C. L. Liao, K. C. Lai, A. C. Huang et al., "Gallic acid inhibits migration and invasion in human osteosarcoma U-2 OS cells through suppressing the matrix metalloproteinase-2/-9, protein kinase B (PKB) and PKC signaling pathways," *Food and Chemical Toxicology*, vol. 50, no. 5, pp. 1734–1740, 2012.

[31] Y. Y. Chen, S. Y. Chiang, J. G. Lin et al., "Emodin, aloe-emodin and rhein inhibit migration and invasion in human tongue cancer SCC-4 cells through the inhibition of gene expression of matrix metalloproteinase-9," *International Journal of Oncology*, vol. 36, no. 5, pp. 1113–1120, 2010.

[32] Y. T. Ho, J. S. Yang, T. C. Li et al., "Berberine suppresses in vitro migration and invasion of human SCC-4 tongue squamous cancer cells through the inhibitions of FAK, IKK, NF-κB, u-PA and MMP-2 and -9," *Cancer Letters*, vol. 279, no. 2, pp. 155–162, 2009.

[33] J. H. Chiang, J. S. Yang, C. Y. Ma et al., "Danthron, an anthraquinone derivative, induces DNA damage and caspase cascades-mediated apoptosis in SNU-1 human gastric cancer cells through mitochondrial permeability transition pores and Bax-triggered pathways," *Chemical Research in Toxicology*, vol. 24, no. 1, pp. 20–29, 2011.

[34] C. C. Lu, J. S. Yang, A. C. Huang et al., "Chrysophanol induces necrosis through the production of ROS and alteration of ATP levels in J5 human liver cancer cells," *Molecular Nutrition and Food Research*, vol. 54, no. 7, pp. 967–976, 2010.

[35] C. C. Lu, J. S. Yang, J. H. Chiang et al., "Inhibition of invasion and migration by newly synthesized quinazolinone MJ-29 in human oral cancer CAL 27 cells through suppression of MMP-2/9 expression and combined down-regulation of MAPK and AKT signaling," *Anticancer Research*, vol. 32, no. 7, pp. 2895–2903, 2012.

[36] K. C. Lai, A. N. C. Huang, S. C. Hsu et al., "Benzyl Lsothiocyanate (BITC) inhibits migration and invasion of human colon cancer HT29 cells by inhibiting matrix metalloproteinase-2/-9 and urokinase plasminogen (uPA) through PKC and MAPK signaling pathway," *Journal of Agricultural and Food Chemistry*, vol. 58, no. 5, pp. 2935–2942, 2010.

[37] S. F. Yang, M. K. Chen, Y. S. Hsieh et al., "Antimetastatic effects of Terminalia catappa L. on oral cancer via a down-regulation of metastasis-associated proteases," *Food and Chemical Toxicology*, vol. 48, no. 4, pp. 1052–1058, 2010.

[38] C. Gialeli, A. D. Theocharis, and N. K. Karamanos, "Roles of matrix metalloproteinases in cancer progression and their pharmacological targeting," *The FEBS Journal*, vol. 278, no. 1, pp. 16–27, 2011.

[39] P. N. Chen, Y. S. Hsieh, H. L. Chiou, and S. C. Chu, "Silibinin inhibits cell invasion through inactivation of both PI3K-Akt and MAPK signaling pathways," *Chemico-Biological Interactions*, vol. 156, no. 2-3, pp. 141–150, 2005.

[40] Y. C. Hsiao, W. H. Kuo, P. N. Chen et al., "Flavanone and 2′-OH flavanone inhibit metastasis of lung cancer cells via down-regulation of proteinases activities and MAPK pathway," *Chemico-Biological Interactions*, vol. 167, no. 3, pp. 193–206, 2007.

[41] J. S. Rao, "Molecular mechanisms of glioma invasiveness: the role of proteases," *Nature Reviews Cancer*, vol. 3, no. 7, pp. 489–501, 2003.

[42] J. Westermarck and V. M. Kähäri, "Regulation of matrix metalloproteinase expression in tumor invasion," *The FASEB Journal*, vol. 13, no. 8, pp. 781–792, 1999.

Hindawi Publishing Corporation
Evidence-Based Complementary and Alternative Medicine
Volume 2013, Article ID 836179, 8 pages
http://dx.doi.org/10.1155/2013/836179

Research Article

A Metabolomics-Based Strategy for the Quality Control of Traditional Chinese Medicine: Shengmai Injection as a Case Study

Xiaodong Li,[1,2] Huiyuan Chen,[2] Wei Jia,[2] and Guoxiang Xie[2]

[1] *College of Pharmacy, Fujian University of Traditional Chinese Medicine, Fuzhou, Fujian 350108, China*
[2] *Center for Translational Biomedical Research, University of North Carolina at Greensboro, North Carolina Research Campus, Kannapolis, NC 28081, USA*

Correspondence should be addressed to Guoxiang Xie; g_xie@uncg.edu

Received 6 December 2012; Accepted 19 December 2012

Academic Editor: Aiping Lu

Quality control of traditional Chinese medicines (TCMs) used clinically is becoming a challenge and has limited the development of TCM due to the high variability in concentration levels of active ingredients and markers as well as the lack of well-established criteria. Using Shengmai injection, which is a well-established TCM, as an example, we developed an integrated profiling approach that simultaneously captures the entire spectrum of ingredients and quantitatively determines the levels of seven key ingredients in the TCM product. A multivariate statistical model was constructed to establish a "seven-marker-" based quality standard that qualified the majority of samples in this study. This newly developed strategy showed that a panel of key ingredients or markers in the TCM product were relatively consistent within a statistically acceptable range. Therefore, this metabolomics-based approach will complement the current quality control standard using the concentration of several key ingredients or their total content and help improve the consistency and clinic efficacy of TCM products.

1. Introduction

Traditional Chinese medicine (TCM) is gaining greater acceptance throughout the world, especially in western countries, for improving health and preventing or healing diseases. Recently, a traditional herbal medicinal product manufactured in China called Diao Xin Xue Kang, used for treating myocardial ischemia, has been approved for sale in Europe [1]. TCMs are composed of more than one herb, and the quality and content of the herbs are highly variable depending on geographical origins, climate, cultivation, and the growth stage when harvested [2]. The therapeutic effect of TCM is based on the synergic effect of its complex components, which is different from that of western medicine [3–6]. However, there is currently insufficient data on TCM due to the lack of modern and scientific approaches for standardization. Traditional methods for determining the quality and authenticity of a complex herbal medicine or preparation are to assess a defined number of bioactive components or pharmacological constituents [7]. Quality-control of TCMs continues to be a challenge and restricts the development of TCM throughout the world. Current criteria listed in pharmacopeia or other criteria issued by the Ministry of Health of China usually use the concentration of several key ingredients or their total content to control the quality and ensure reproducible clinical efficacy. Although the concentration of each bioactive component or the total concentration of all components may meet the requirements of the criteria, there is often variation in the concentration of each of these bioactive components between batches. Furthermore, in some cases one or more of the bioactive components may be absent from a preparation, but the total content can still meet the criteria stipulated. It is worth noting that different concentrations of the proportion of mass constituents in herbal medicine may result in different therapeutic effects [8]. For example, EGb761, a *Ginkgo* biloba extract produced by Schwabe Pharmaceuticals, was standardized on the basis of the presence of 24% (w/w) "*Ginkgo* flavone" glycosides and 6% (w/w) terpene lactones. However, *Ginkgo* extracts from other manufacturers easily met this standard, but were clearly distinct from EGb761 [9]. Xie [6] reported that it was difficult to distinguish between

the EGb761 standard and other preparations of *Ginkgo* extracts containing rutin. Therefore, it is challenging to obtain well-quality-controlled herbal drugs and preparations with current criteria/standards.

Over the past several decades, the chromatographic fingerprint technique has been used as a more accurate approach for controlling the quality of herbal medicines or their products due to the systemic characterization of compositions of samples and focusing on identifying and assessing the stability of the plants. The fingerprint analysis technique has been introduced and accepted by the World Health Organization (WHO) [10], Food and Drug Administration (FDA) [4], and European Medicines Agency (EMEA) [5] as a strategy for assessing consistency between batches of botanical drugs. In 2004, the State Food and Drug Administration (SFDA) of China also required that all injections made from herbal medicines or their raw materials should be standardized by chromatographic fingerprinting [11]. However, a validated fingerprint method has not been accepted in general quality control standards of herbal medicines until now. One of the main difficulties is the lack of an analytical method for scientifically evaluating the complex chromatograms of herbal medicines [9]. The technique uses the traditional concept of pharmaceutical analysis and combines it with an analysis of chromatographic peaks. However, the current fingerprint analysis technique does not correct for chromatographic shifts among different runs or from different experimental conditions and cannot compare the fingerprints of TCMs from different species of herbs, grown at different locations, from different harvesting seasons, or extracted and processed using different methods. Therefore, an effective quality control method for TCMs or herbal medicines should be developed in order to further develop their standardization and modernization.

Metabolomics, or metabonomics, which aims to identify and quantify the full complement of low molecular weight (<1,000 Da), soluble metabolites in actively metabolizing tissues [12, 13], has garnered extensive awareness and interest in the research community, especially in botanical studies for the quality control of plants [14–17], metabolic phenotyping [18, 19], and the pharmacological effects of TCMs [20, 21]. A metabolomics approach is uniquely suited for developing a new and effective method for the quality control of the processing and manufacturing of TCMs. The central goal of our strategy is to ensure that representative bioactive components in one preparation are consistent, that the content of each bioactive component meets the stipulated standards, and that concentration proportions of mass constituents are within a reasonable range. Here, we reported a quality control method by integrating the metabolic profiling approach together with the multivariate statistical analysis on the study of a well-quality-controlled injection, Shengmai [22], prepared from *Radix Ginseng*, *Radix Ophiopogonis,* and *Schisandra chinensis*. A total of 22 Shengmai injections obtained from 4 different manufacturers in China were analyzed by liquid chromatography/time-of-flight mass spectrometry (LC-TOF-MS) to obtain a metabolic profile. Saponins from the principal herb (Jun Yao in Chinese) under the theory of TCM, *Radix Ginseng*, were quantitatively measured to determine whether a given batch met established acceptance criteria or our newly established standard as well as the content variation among different batches. Eight ginsenosides, namely, Rb_2, Rd, Rf, Rg_2, Rg_1, Rb_1, Rc, and Re, were analyzed according to the method described in our previous study [17].

2. Materials and Methods

2.1. Chemicals and Materials. HPLC grade acetonitrile, methanol, and formic acid were obtained from Sigma Aldrich (St. Louis, MO, USA). Ultrapure water was prepared using a Milli-Q system (18.2 MΩ, Milford, MA, USA). Shengmai injection samples were obtained from four different manufacturers from China (sample A, B, C, and D with several batches of each; Table 2). Ginsenoside Re, Rb1, Rc, Rb2, Rd, Rg2, Rg1, and Rf standards were obtained from ChromaDex (Irvine, CA, USA).

Individual stock solutions (1.0 mg/mL) of eight standard ginsenosides were prepared in methanol for LC-TOF-MS analysis.

Working standards (5, 10, 20, 50, 100, 200, 500, 1000, 2000, 5000, and 10000 ng/mL) were prepared by diluting the corresponding stock solution with methanol for the LC-TOF-MS analysis. All stock solutions were stored under refrigerated conditions (4°C).

2.2. Sample Preparation. A 10 μL sample of each batch of Shengmai injection was diluted to 1 mL in ultrapure water. The solutions were then vortexed for 30 s, filtered through a syringe filter membrane (0.20 μm), and then injected directly into the LC-TOF-MS system.

2.3. HPLC-TOFMS Analysis. An Agilent HPLC 1200 system equipped with a binary solvent delivery manager and a sample manager (Agilent Corporation, Santa Clara, CA, USA) was used with chromatographic separations performed on a 4.6 × 150 mm 5 μm Agilent ZORBAX Eclipse XDB-C18 chromatography column. The LC elution conditions were optimized as follows: isocratic at 1% B (0–0.5 min), linear gradient from 1% to 20% B (0.5–9.0 min), 20%–75% B (9.0–15.0 min), 75%–100% B (15.0–18.0 min), isocratic at 100% B (18–19.5 min); linear gradient from 100% to 1% B (19.5–20.0 min) and isocratic at 1% B (20.0–25.0 min). Here, A = water with 0.1% formic acid and B = acetonitrile with 0.1% formic acid. The column was maintained at 30°C. A 5 μL aliquot sample was then injected onto the column. Mass spectrometry was performed using an Agilent model 6220 MSD TOF mass spectrometer equipped with a dual sprayer electrospray ionization source (Agilent Corporation, Santa Clara, CA, USA). The system was tuned for optimum sensitivity and resolution using an Agilent ESI-L low concentration tuning mix in both positive (ES+) and negative (ES−) electrospray ionization modes. The Agilent API-TOF reference mass solution kit was used to obtain accurate mass TOF data in both positive and negative mode operations. The TOF mass spectrometer was operated with the following optimized conditions: (1) ES+ mode, capillary voltage 3500 V, nebulizer 45 psig, drying gas temperature 325°C, drying gas flow 11 L/min, and (2) ES− mode, similar conditions as the

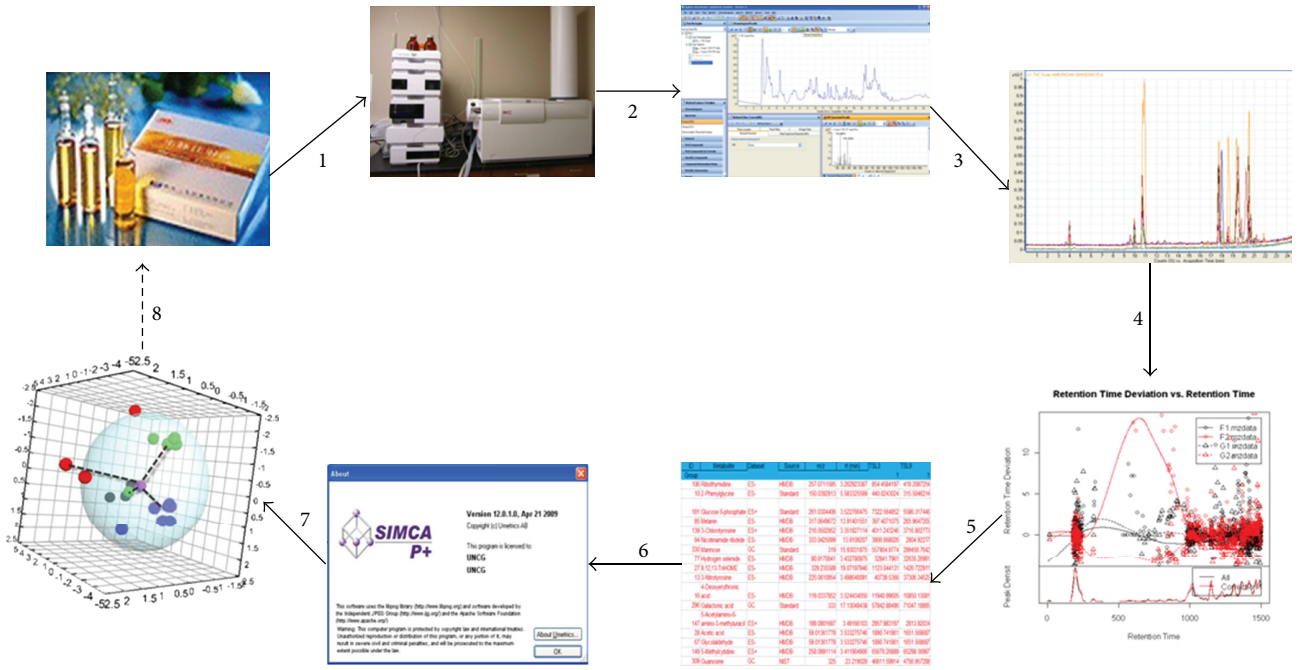

Figure 1: Schematic diagram of the strategy used for the quality control of traditional Chinese medicine (TCM). (1) LC-TOF-MS analysis of TCM; (2) Pretreatment data obtained from the LC-TOF-MS analysis; (3) Data export using software; (4) Exported.xml data files are analyzed using the open source XCMS package to pick, align, and quantify features; (5) The resulting 3D matrix contains arbitrarily assigned peak index, retention time, and abundance value (.xls file); (6) The .xls data files are then exported to SIMCA-P software 12.0 (Umetrics, Umeå, Sweden) for multivariate statistical analysis; (7) A quality control standard is then established; (8) The established standard is used for quality control of TCM.

ES+ mode except that the capillary voltage was adjusted to 3000 V. The TOF mass spectrometer was calibrated routinely in ES+ and ES− modes using the Agilent ESI-L low concentration tuning mix. During metabolite profiling experiments, both plot and centroid data were acquired for each sample from 50 to 1,000 Da over a 25 min analysis time.

2.4. Data Analysis. The resulting.d files were centroided, deisotoped, and converted to mzData xml files using the MassHunter Qualitative Analysis Program (vB.03.01) (Agilent). Following conversion, xml files were analyzed using the open source XCMS package (v1.24.1) (http://metlin.scripps.edu/), which runs in the statistical package R (v.2.12.1) (http://www.r-project.org/), to pick, align, and quantify features (chromatographic events corresponding to specific *m/z* values and retention times). The software was used with default settings as described (http://metlin.scripps.edu/) except for xset (bw = 5) and rector (plottype = "m", family = "s"). The created.tsv file was opened using Excel software and saved as an .xls file. The resulting 3D matrix containing arbitrarily assigned peak index, retention time, and abundance value (.xls file) were then exported to SIMCA-P software 12.0 (Umetrics, Umeå, Sweden) for multivariate statistical analysis. Mean-centered and par-scaled (scaled to square root of SD) mathematical methods were performed to pretreat the datasets that were obtained from the previous samples. Principal component analysis (PCA) was used to visualize general clustering, trends, and outliers among the observations.

2.5. Strategy for Quality Control. An integrated metabolomics and multivariate statistical analysis was conducted according to the process as proposed in Figure 1. Representative Shengmai injections were used as a model TCM for analysis and characterization. LC-TOF-MS was used to measure the global metabolite pool of the samples and quantify the bioactive ginsenosides.

The metabolome of the herbal medicine was obtained from the metabolomics analysis. The metabolite similarities were visualized from the PCA analysis. Quantitative analysis of the reported key ingredients was performed, and the concentration of each key ingredient had to meet the requirements of the criteria. Furthermore, the concentration proportion of each key ingredient had to be within a reasonable range to maintain consistency in pharmacological effects and clinical efficacy between batches. The spatial distance away from the standard center also had to be within a reasonable range to ensure the quality, and the range was set logically based on the data. For example, if the concentration was within a range of 85%–115% of the standard concentration, then the sample dot would be within the sphere and identified as qualified product. However, if the concentration was out of range from the standard concentration, then the red dots would be outside of the sphere and the preparation would be considered as an unqualified product. The standard locus of a TCM can be dotted using SIMCA-P software by importing data obtained from a sample made from the standard herbs using the preparative procedure. As evident in Figure 1, the violet dot represents the standard criteria, and

Table 1: Calibration curves of eight ginsenosides[a].

Compound	Rt (min)	Linearity			LOD (ng/mL)	LOQ (ng/mL)	*S/N*
		Range (ng/mL)	Calibration curves	R^2			
Rg2	18.72	185.55–5834.39	$A = 35.65C + 4737.90$	0.9971	46.39	92.78	>25
Rf	18.41	92.78–5863.20	$A = 207.73C + 19139.65$	0.9990	23.20	46.39	>19
Rd	18.57	88.18–5977.96	$A = 68.68C - 2068.57$	0.9997	23.20	56.18	>10
Rc	18.17	46.39–5937.50	$A = 138.13C + 1677.32$	0.9997	11.6	23.14	>11
Re	17.59	185.55–5720.31	$A = 27.08 + 10884.83$	0.9884	46.00	93.01	>12
Rb1	18.04	46.39–5916.00	$A = 128.06C + 3291.30$	0.9994	11.58	23.20	>19
Rb2	18.24	92.78–5874.07	$A = 149.19C + 7256.20$	0.9989	23.20	46.39	>18
Rg1	17.59	185.54–5937.3	$A = 707.444C + 113373.52$	0.9929	46.38	92.77	>30

[a]Calibration curves were constructed based on the peak area (A) versus concentration (C). R^2: linearity correction coefficient within the linear range of the sample concentration.

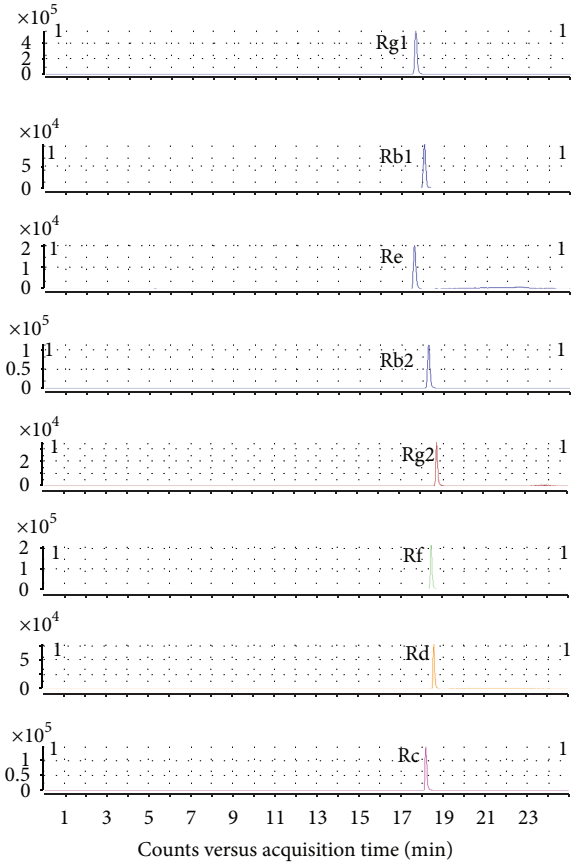

Figure 2: Extracted ion chromatograms of eight ginsenosides, including Rg1, Rb1, Re, Rb2, Rg2, Rf, Rd, and Rc.

the group/products expressed as green, black, and blue dots are within the scope of acceptable quality. In contrast, the red dots represent samples not meeting the quality criteria.

3. Results and Discussion

3.1. Method Validation. Extracted ion chromatograms of eight ginsenosides, including Re, Rb1, Rc, Rb2, Rd, Rg2, Rg1, and Rf, are shown in Figure 2. Calibration curves of peak area (y) versus concentration (x) were constructed. These curves showed good linearity over the concentration range listed in Table 1 with correlation coefficients from 0.9971 to 0.9997, respectively. The limit of detection (LOD) and limit of quantitation (LOQ) were determined using the signal-to-noise ratio (*S/N*) provided by MassHunter quantitative analysis software (Ver. B.01.04), and all of the *S/N* values were greater than 10.0, which allowed for the individual calculation of each compound's quantification limit. The reproducibility was investigated using the spiked standard solution. After correction with the internal standard, the relative standard deviations (RSDs) of the peak area for each spiked standard were comparable, with RSDs below 10%. In addition, the stability assay was evaluated using the aforementioned spiked standards. For most spiked compounds, the RSDs were less than 6.5% within 24 h and less than 10% within 36 h. To further validate our methodology for analyzing complex endogenous metabolites, each 20 μL aliquot of 0.5, 1, and 2 μg/mL of the spiked standard solution was mixed with a 20 μL aliquot of diluted Shengmai injection. Recovery was calculated using the aforementioned calibration curves, and the mean recoveries of all these compounds ranged from 90% to 110%, with RSDs better than 15%.

3.2. LC-TOF-MS Analysis of Shengmai Samples. LC-TOF-MS analysis was then performed for 22 Shengmai samples obtained from four manufacturers. Typical LC-TOF-MS chromatograms of the samples are shown in Figure 3, where similar characteristic peaks were observed, with the exception of some minor peaks. This finding may indicate that the components of each injection manufactured by different factories are similar, except for the quantity of the components contained within each. In particular, the peaks located between 17 and 19 min, which corresponded to the saponins in the principal herb, *Radix Ginseng*, showed very similar profiles.

3.3. Quantitative Analysis of Ginsenosides in Shengmai Samples. Using our optimized LC-TOF-MS method, a high regression coefficient ($r > 0.99$) value for each calibration curve from the eight spiked standards was obtained, indicating good linearity in this study (Table 1). The quantitative analysis results of ginsenosides in different batches of one

Table 2: Quantitative analysis results of 7 ginsenosides in Shengmai samples obtained from different manufacturers.

Manufacturer	Batch	Rf (μg/mL)		Rd (μg/mL)		Rc (μg/mL)		Re (μg/mL)		Rb1 (μg/mL)		Rb2 (μg/mL)		Rg1 (μg/mL)	
		Content	Mean	Content	Mean	Content	Mean	Content	Mean	Content	Mean	Content	Mean	Content	Mean
A	1	31.44	31.21	47.17	49.60	159.18	155.96	98.82	92.63	196.81	190.23	145.08	142.12	148.203	145.922
		31.95		47.67		155.86		90.08		186.46		142.04		146.519	
		30.24		53.95		152.83		89.00		187.43		139.24		143.045	
	2	36.14	36.40	59.00	60.15	170.96	174.31	82.60	86.51	228.21	233.92	155.92	159.17	165.648	169.609
		35.27		60.24		178.04		84.86		237.07		162.44		171.297	
		37.80		61.20		173.92		92.06		236.49		159.16		171.881	
	3	38.89	41.11	50.96	58.05	189.40	195.35	117.60	124.82	206.99	217.00	172.90	178.63	158.711	167.618
		42.08		68.24		192.80		124.60		217.83		176.81		167.248	
		42.36		54.94		203.84		132.27		226.18		186.18		176.894	
B	1	37.89	37.89	76.92	76.92	199.80	199.80	84.00	84.00	338.82	338.82	182.46	182.46	148.997	148.997
	2	34.27	34.27	63.96	63.96	209.33	209.33	118.07	118.07	448.86	448.86	192.31	192.31	122.846	122.846
	3	41.94	42.20	67.33	70.24	248.78	259.36	115.49	122.86	311.92	330.06	227.53	237.27	185.855	190.272
		42.45		73.14		269.95		130.23		348.21		247.01		194.69	
	4	27.48	29.03	60.70	61.29	170.33	175.27	89.37	87.84	305.55	306.64	155.35	159.90	120.291	124.315
		30.87		61.27		179.75		88.26		312.04		164.01		125.437	
		28.74		61.89		175.74		85.88		302.32		160.33		127.219	
C	1	43.17	44.27	70.33	69.79	241.48	244.37	115.49	124.36	357.08	355.17	220.81	223.62	197.394	204.205
		44.74		71.95		245.26		136.14		351.39		225.08		211.019	
		44.89		67.09		246.38		121.44		357.05		224.98		204.203	
D	1	43.09	43.83	66.41	71.18	188.39	197.72	121.00	121.13	253.69	264.56	172.48	180.72	129.588	133.091
		40.79		69.18		200.84		116.26		262.77		183.42		130.592	
		47.61		77.95		203.94		126.12		277.22		186.27		139.092	

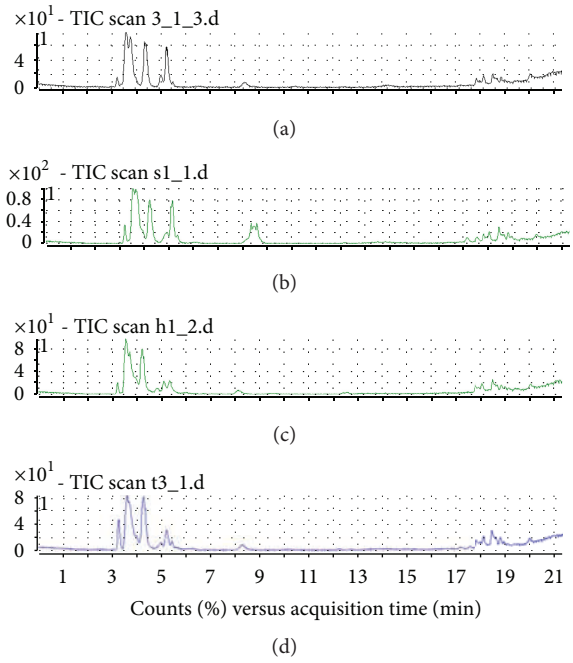

Figure 3: Total ion current (TIC) chromatograms of four Shengmai injection samples.

manufacturer and from different manufacturers are listed in Table 2. The content of Rg2 was relatively low in the injections and below the LOQ, and therefore only seven ginsenosides were quantified (Table 2). The levels of the seven ginsenosides from all samples were comparable and met the criteria requirements issued by the Ministry of Health of China, which stipulates that the level of Rg1 should be higher than 80 ng/mL and the Re level should be at least 40 ng/mL [22]. However, the concentrations of Rg1 and Re were significantly different between several batches form one manufacturer as well as between different manufacturers, though they all meet the criteria for clinical use. However, due to the differences in ginsenoside concentrations in preparations from the four manufacturers, differences in clinical efficacy would be expected. Furthermore, the variations in concentration between batches were large, indicating that the reproducibility of the product was poor. Because the preparative procedure was standardized, the differences may be a result of variability in the raw materials used. Therefore, it is very important to control the quality consistency between factories, and particularly among the different batches, to ensure satisfactory quality and comparable efficacy between batches.

3.4. Principal Component Analysis. Chemometrics, the science of extracting information from chemical measurement systems with mathematics and statistics, can be employed to the multicomponent metabolic profile patterns to ascertain consistency/variations in multiple batches of herbal medicines. Application of chemometrics methods to multiple commercial batch metabolic profile data is a big leap forward in the quality assurance of medicinal herb preparations which

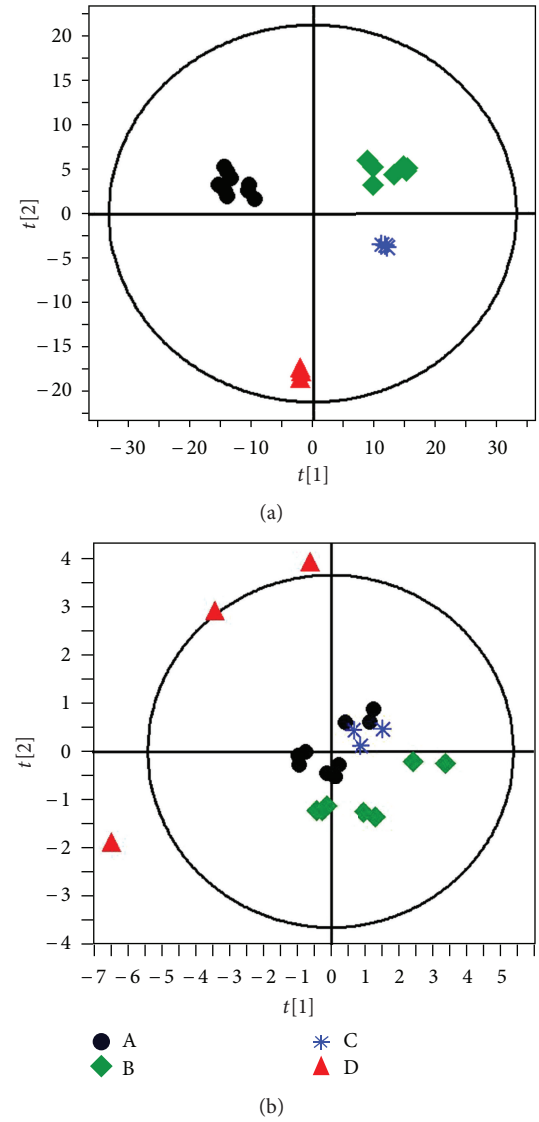

Figure 4: PCA sores plot of (a) metabolic profile of 22 Shengmai injection samples using all of the data and (b) metabolic profile of 22 Shengmai injection samples using the ginsenoside quantitative data.

provides information on batch consistency, "outlier" batches, and possible "contaminants." One impressive example of exploratory data analysis is the PCA which is a "workhorse" in chemometrics [23]. PCA, unsupervised clustering method requiring little prior knowledge of the dataset, acts to reduce the dimensionality of multivariate data without losing important information [24], and supervised orthogonal partial least-squares-discriminant analysis (OPLS-DA) of the metabolomics data has been extensively used for the holistic quality inconsistencies of herbal medicines [21, 25]. In this study, both UV-scaled (scaled to the standard deviation) and par-scaled (scaled to the square root of the standard deviation) mathematical methods were performed to pretreat the datasets obtained from 22 batches of injections. In order to explain the difference and the consistency of Shengmai

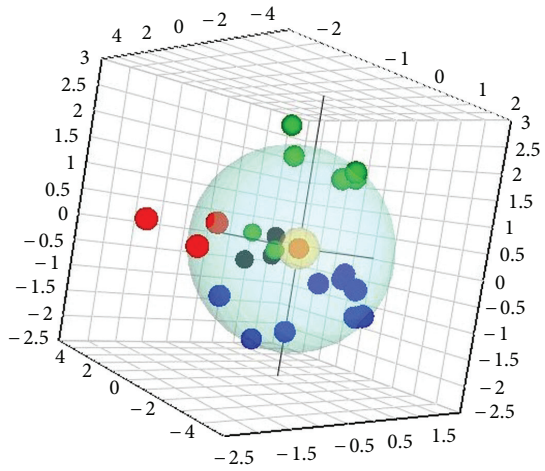

Figure 5: PCA scores plot of the ginsenoside metabolite profile of 22 Shengmai injection samples obtained from four different manufacturers. Blue dot: sample A; green dot: sample B; black dot: sample C; red dot: sample D.

samples from 4 different manufacturers, the data obtained from all metabolites and the quantitative concentration of Shengmai samples shown in Table 2 were imported to SIMCA P 12.0 software to obtain the PCA scores plot. Clear separation of the four different samples was observed in the PCA scores plot of all data (Figure 4(a)) and quantitative ginsenoside data (Figure 4(b)), where each coordinate represents one sample. Using the quantitative analysis data, the red dots were derived from other samples and represent outliers; thus, they are considered to be unqualified products.

3.5. Quality Control of Shengmai Injection. Using the established approach, the quantitative analysis results of 22 batches of Shengmai samples (Table 2) were imported into SIMCA P 12.0 software to determine the quality control results. Using the standard compound concentration (the average concentration of seven ginsenosides of 22 batches of Shengmai samples) as the center, all of the qualified products would fall within the range of the spatial sphere (Figure 5) and the unqualified products would be outside the sphere. Sample C (black dots) met all of the requirements, sample A (blue dots) met most of the requirements, and samples B and D (green and red dots, resp.) were outside of the established standard. This clearly indicates that there were differences among products obtained from different manufacturers as well as different batches of product generated by one manufacturer. Using the established standard, some samples were found to be unqualified products, though they all met the current standard. Therefore, these data indicate that this method will help to guarantee the quality, reproducibility, and efficacy of the products made from natural herbs.

4. Conclusion

For complicated herbal products, it is easy to control the concentration of several key ingredients to achieve a standard level; however, it is difficult to keep the concentration proportion of different key ingredients in a comparable range. Different concentration proportions of mass constituents may result in different therapeutic effects of herbal medicines and subsequent variability in clinical efficacy. Our strategy proposed in this study will enable us to measure the global metabolite profile of preparations and simultaneously quantify the key ingredients in order to ascertain treatment efficacy and minimize probable side effects, which will greatly enhance pharmacological evaluation. We believe that this approach will help to prefect the current quality control method used for complicated herbal materials or medicines, improve the quality of TCMs, and ensure the efficacy of the products used in the clinic.

Acknowledgment

This study was financially supported by the Fumin Foundation of Fujian Province in China.

References

[1] N. Gilbert, *Chinese Herbal Medicine Breaks into EU Market*, 2012.

[2] G. B. Mahady, H. S. Fong, and N. R. Farnsworth, *Botanical Dietary Supplements: Quality, Safety, and Efficacy*, Swets & Zeitlinger, Amsterdam, The Netherlands, 2001.

[3] X. Di, K. K. C. Chan, H. W. Leung, and C. W. Huie, "Fingerprint profiling of acid hydrolyzates of polysaccharides extracted from the fruiting bodies and spores of Lingzhi by high-performance thin-layer chromatography," *Journal of Chromatography A*, vol. 1018, no. 1, pp. 85–95, 2003.

[4] *FDA Guidance for Industry—Botanical Drug Products (Draft Guidance)*, US Food and Drug Administration, Rockville, Md, USA, 2000.

[5] *Note for Guidance on Quality, of Herbal Medicinal Products*, European Medicines Agency, London, UK, 2001.

[6] P. S. Xie, "A feasible strategy for applying chromatography fingerprint to assess quality of Chinese herbal medicine," in *Proceedings of the International Symposium on Quality of TCM with Chromatographic Fingerprint*, Guangzhou, China, 2001.

[7] R. Capasso, A. A. Izzo, L. Pinto, T. Bifulco, C. Vitobello, and N. Mascolo, "Phytotherapy and quality of herbal medicines," *Fitoterapia*, vol. 71, no. 1, pp. S58–S65, 2000.

[8] L. W. Yang, D. H. Wu, X. Tang et al., "Fingerprint quality control of Tianjihuang by high-performance liquid chromatography-photodiode array detection," *Journal of Chromatography A*, vol. 1070, no. 1-2, pp. 35–42, 2005.

[9] O. Sticher, "Quality of Ginkgo preparations," *Planta Medica*, vol. 59, no. 1, pp. 2–11, 1993.

[10] WHO, *Guidelines for the Assessment of Herbal Medicines*, World Health Organization, Munich, Germany, 1991.

[11] *State Food and Drug Administration of China, Note for Studying Fingerprint of Traditional Chinese Medicine Injections (Draft)*, Shanghai, China , 2000.

[12] O. Fiehn, "Metabolomics—the link between genotypes and phenotypes," *Plant Molecular Biology*, vol. 48, no. 1-2, pp. 155–171, 2002.

[13] S. Rochfort, "Metabolomics reviewed: a new "omics" platform technology for systems biology and implications for natural

products research," *Journal of Natural Products*, vol. 68, no. 12, pp. 1813–1820, 2005.

[14] K. Lan and W. Jia, "An Integrated metabolomics and pharmacokinetics strategy for multi-component drugs evaluation," *Current Drug Metabolism*, vol. 11, no. 1, pp. 105–114, 2010.

[15] E. C. Y. Chan, S. L. Yap, A. J. Lau, P. C. Leow, D. F. Toh, and H. L. Koh, "Ultra-performance liquid chromatography/time-of-flight mass spectrometry based metabolomics of raw and steamed Panax notoginseng," *Rapid Communications in Mass Spectrometry*, vol. 21, no. 4, pp. 519–528, 2007.

[16] J. L. Wolfender, G. Glauser, J. Boccard, and S. Rudaz, "MS-based plant metabolomic approaches for biomarker discovery," *Natural Product Communications*, vol. 4, no. 10, pp. 1417–1430, 2009.

[17] G. Xie, R. Plumb, M. Su et al., "Ultra-performance LC/TOF MS analysis of medicinal Panax herbs for metabolomic research," *Journal of Separation Science*, vol. 31, no. 6-7, pp. 1015–1026, 2008.

[18] H. Dai, C. Xiao, H. Liu, and H. Tang, "Combined NMR and LC-MS analysis reveals the metabonomic changes in salvia miltiorrhiza bunge induced by water depletion," *Journal of Proteome Research*, vol. 9, no. 3, pp. 1460–1475, 2010.

[19] H. Dai, C. Xiao, H. Liu, F. Hao, and H. Tang, "Combined NMR and LC-DAD-MS analysis reveals comprehensive metabonomic variations for three phenotypic cultivars of salvia miltiorrhiza bunge," *Journal of Proteome Research*, vol. 9, no. 3, pp. 1565–1578, 2010.

[20] X. Liang, X. Chen, Q. Liang et al., "Metabonomic study of Chinese Medicine Shuanglong Formula as an effective treatment for myocardial infarction in rats," *Journal of Proteome Research*, vol. 10, no. 2, pp. 790–799, 2011.

[21] H. M. Zhang, S. L. Li, H. Zhang et al., "Holistic quality evaluation of commercial white and red ginseng using a UPLC-QTOF-MS/MS-based metabolomics approach," *Journal of Pharmaceutical and Biomedical Analysis*, vol. 62, pp. 258–273, 2012.

[22] Traditional Chinese Drug standards of Ministry of Health of the People's Republic of China, *Shengmai Zhusheye (Injection) Quality Standard*, Ministry of Health, Beijing, China, 1998.

[23] J. E. Jackson, *A Users Guide to Principal Components*, Wiley, New York, NY, USA, 1991.

[24] L. Eriksson, E. Johansson, N. Kettaneh-Wold, and S. Wold, *Multi- and Megavariate Data Analysis*, Umetrics Academy, Umea, Sweden, 2001.

[25] S. S. Zeng, L. Wang, T. Chen et al., "Direct analysis in real time mass spectrometry and multivariate data analysis: a novel approach to rapid identification of analytical markers for quality control of traditional Chinese medicine preparation," *Analytica Chimica Acta*, vol. 733, pp. 38–47, 2012.